TP 10517E

PHASE CENTRE DETERMINATION OF MLS ANTENNA SYSTEMS - PHASE I

CA1
DTC800-
90
P31

446261

41.D

by

H. Moheb A. Sebak
A. Helaly L. Shafai

Department of Electrical & Computer Engineering
University of Manitoba
Winnipeg, Manitoba, Canada R3T 2N2

for

Transportation Development Centre
Policy and Coordination Group
Transport Canada

Library and Information Centre / Centre de documentation (GSLA)
RECEIVED / REÇU LE
SEP 4 1990
Transport Canada / Transports Canada

June 1990

446261

DSW 446259

92-01927/

The contents of this report reflect the views of the authors and not necessarily the official view or opinions of the Transportation Development Centre of Transport Canada.

Un sommaire en français de ce rapport est inclus avant la table des matières.

Transport Canada / Transports Canada

PUBLICATION DATA FORM

1. Transport Canada Publication No.	2. Project No.	3. Recipient's Catalogue No.
TP10517E	7327	

4. Title and Subtitle	5. Publication Date
Phase Centre Determination of MLS Antenna Systems - Phase I	June 1990
	6. Performing Organization Document No.

7. Author(s)	8. Transport Canada File No.
H. Moheb, A. Helaly, A. Sebak, L. Shafai	ZCD1455-153-8

9. Performing Organization Name and Address	10. DSS File No.
Department of Electrical and Computer Engineering University of Manitoba Winnipeg, Manitoba, R3T 2N2	16 SD.T8200-9-9513
	11. DSS or Transport Canada Contract No. T8200-9-9513/01-SD

12. Sponsoring Agency Name and Address	13. Type of Publication and Period Covered
Transportation Development Centre (TDC) 200 René Lévesque Blvd. West Suite 601, West Tower Montreal, Quebec H2Z 1X4	Final (July 89/June 90)
	14. Project Officer Micha Avni

15. Supplementary Notes (Funding programs, titles of related publications, etc.)

16. Abstract

This study is undertaken to determine the location and uniqueness of the phase centre for MLS azimuth antennas. Initially, a general mathematical model is developed that enables one to locate the phase centre of any antenna. The model is then applied to investigation of the MLS azimuth antenna phase centre and its movement due to beam scanning and various design or operational errors. It is shown that for an ideal antenna (error free case), its phase centre coincides with its geometrical centre. However, any deviation from the ideal conditions, due to design, fabrication or operational errors, such as phase shifter quantization or scan algorithm, etc., causes its non-uniqueness and movement from the antenna's geometrical centre.

The proposed method is also used to study the effects of ground reflections on the phase centre movement. The ground effect is included by adding multipath signal interference. Geometrical optics is used to determine the reflected rays, and the Fresnel reflection coefficient for vertical polarization is employed to compute their amplitude. Both ground and range parameters are then varied and their effect on the phase centre location and movement is studied.

17. Key Words	18. Distribution Statement
Microwave Landing System, MLS, Azimuth Antenna Phase Centre, Beam Deviation, Sidelobe, Ground Reflection.	Limited number of copies available from the Transportation Development Centre on request

19. Security Classification (of this publication)	20. Security Classification (of this page)	21. Declassification (date)	22. No. of Pages	23. Price
Unclassified	Unclassified	—	292	—

TDC/CDT 79-005
Rev 88

Canada

Transports Canada Transport Canada

FORMULE DE DONNÉES POUR PUBLICATION

1. N° de la publication de Transports Canada	2. N° de l'étude	3. N° de catalogue du destinataire
TP10517E	7327	

4. Titre et sous-titre	5. Date de la publication
Phase Centre Determination of MLS Antenna Systems - Phase I	**Juin 1990**
	6. N° du document de l'organisme exécutant

7. Auteur(s)	8. N° de dossier — Transports Canada
H. Moheb, A. Helaly, A. Sebak, L. Shafai	ZCD1455-153-8

9. Nom et adresse de l'organisme exécutant	10. N° de dossier — ASC
Department of Electrical and Computer Engineering University of Manitoba Winnipeg (Manitoba) R3T 2N2	16SD.T8200-9-9513
	11. N° de contrat — ASC ou Transports Canada T8200-9-9513/01-SD

12. Nom et adresse de l'organisme parrain	13. Genre de publication et période visée
Centre de développement des transports 200 ouest, boul. René Lévesque Tour ouest, suite 601 Montréal (Québec) H2Z 1X4	Final (Juillet 89/Juin 90)
	14. Agent de projet Micha Avni

15. Remarques additionnelles (Programmes de financement, titres de publications connexes, etc.)

16. Résumé

Cette recherche a concerné la localisation et les déplacements d'un point caractéristique des antennes d'azimut MLS appelé centre de phase. Les chercheurs cnt commencé par élaborer un modèle mathématique général permettant de localiser le centre de phase d'une antenne quelconque. Ce même modèle a été ensuite utilisé à l'égard d'une antenne d'azimut MLS dans le but de repérer les diverses positions que son centre de phase peut occuper soit lors du balayage de l'espace par le faisceau, soit en raison de défauts ou d'erreurs de conception ou d'exploitation. Il est démontré que dans une antenne parfaite, le centre de phase et le centre géométrique coïncident. Cependant, un écart quelconque par rapport à cette situation et dû à une erreur attribuable à la conception, à la fabrication ou à l'exploitation de l'antenne (ex. quantification du déphaseur, algorithme de balayage angulaire, etc.) entraîne une perte de coïncidence, causant ainsi la séparation des centres.

Le modèle proposé est ensuite élargi à l'influence de la réflexion du faisceau par le sol sur les déplacements du centre de phase. Cette influence est égale à la somme vectorielle des trajectoires multiples suivies par les signaux. Les modèles de calcul utilisés, inspirés des lois de l'optique géométrique, permettent de calculer l'effet sol ainsi que le facteur de réflexion de Fresnel pour la polarisation verticale représentant l'amplitude des trajectoires multiples. En faisant varier les paramètres sol et distances, les chercheurs ont déterminé leur influence sur l'emplacement du centre de phase et ses déplacements.

17. Mots clés	18. Diffusion
Système d'atterrissage hyperfréquences, MLS, centre de phase d'antenne d'azimut, déviation du faisceau, lobes secondaires	Le Centre de développement des transports dispose d'un nombre limitée d'exemplaires.

19. Classification de sécurité (de cette publication)	20. Classification de sécurité (de cette page)	21. Déclassification (date)	22. Nombre de pages	23. Prix
Non classifiée	Non classifiée	--	292	--

CDT/TDC 79-005
Rev 88

Canada

Acknowledgements

The authors would like to acknowledge the contributions and financial assistance provided by Transport Canada, especially Mr. M. Avni of Transportation Development Centre, Policy and Coordination Group and Mr. G. Einarsson and Dr. M. Elgamal of Microwave Landing System Project, Aviation Group.

Summary

A study is undertaken to investigate the location and uniqueness of the phase centre for *MLS* azimuth antennas. Initially, a general mathematical model is developed that enables one to locate the phase centre of any antenna. The model is then applied for investigation of the *MLS* azimuth antenna phase centre and its movement due to beam scanning and various design or operational errors. It is shown that, for an ideal antenna (error-free case), its phase centre coincides with its geometrical centre. However, any deviation from the ideal conditions, due to design, fabrication or operational errors, such as phase shifter quantization, or scan angle algorithm, causes its non-uniqueness and movement from the antenna's geometrical centre.

The proposed formulation is then extended to treat the effects of ground reflection on the phase centre movement. A model is developed to determine the errors caused by the multipath effect, due to interaction of the direct signal and the signal reflected by the ground. The developed model which is based on the geometrical optics, computes the ground effect due to the specular reflection. The multipath amplitude is taken to be the Fresnel reflection coefficient for the vertical polarization, which depends on the ground characteristics. The developed model is subsequently used to determine the variation of the phase centre location, due to the receiver position, the range between the transmitter and receiver, and also ground characteristics.

Next, the effect of thermal expansion and/or contraction on the performance of the *MLS* array is studied. A relatively simple model is proposed to relate the uniform spatial variation of antenna elements to that of temperature variation across the array. We expect the thermal effect to be far more significant on the slotted waveguide field distribution than its phase centre movement. However, this is outside the scope of the present study and is not included in computations.

Finally, numerical simulations are performed to study the effect of various error types on the antenna performance, such as pointing angle, $3dB$ beam-width, and the peak sidelobe power level.

Sommaire

Une recherche a été lancée sur la localisation et la coïncidence d'un point caractéristique des antennes d'azimut MLS appelé centre de phase. Les chercheurs ont commencé par élaborer un modèle mathématique général permettant de localiser le centre de phase d'une antenne quelconque. Ce même modèle est ensuite utilisé à l'égard d'une antenne d'azimuth MLS dans le but de repérer les diverses positions que son centre de phase peut occuper soit lors du balayage de l'espace par le faisceau, soit en raison de défauts ou d'erreurs de conception ou d'exploitation. Il est démontré que, dans une antenne parfaite, le centre de phase et le centre géométrique coïncident. Cependant, un écart quelconque par rapport à cette situation et dû à une erreur attribuable à la conception, à la fabrication ou à l'exploitation de l'antenne (ex. quantification du déphaseur, algorithme de balayage angulaire, etc.) entraîne une perte de coïncidence, causant ainsi la séparation des centres.

Le modèle proposé est ensuite élargi à l'influence de la réflexion du faisceau par le sol sur les déplacements du centre de phase. Le modèle mis au point a permis de mettre en évidence les erreurs occasionnées par l'effet des trajectoires multiples, dû à l'interaction des ondes directes et celles réfléchies par le son. Ce modèle, s'inspirant des lois de l'optique géométrique, permet de calculer l'effet sol dû à la réflexion spéculaire. Quant à l'amplitude des trajectoires multiples, elle est tenue pour être le facteur de réflexion de Fresnel pour la polarisation verticale, lequel dépend des caractéristiques du sol. Le modèle est ensuite utilisé pour cerner les déplacements du centre de phase, dus à la position du récepteur, à la distance entre celui-ci et l'émetteur et aux caractéristiques du sol.

La recherche passe ensuite à l'étude de l'effet thermique (dilation ou contraction) sur le rendement du réseau MLS. Un modèle assez simple est proposé montrant les variations spatiales uniformes des éléments rayonnants en fonction des variations de température le

long du réseau. Il est possible que cet effet ait beaucoup plus d'influence sur la distribution du champ du guide d'onde à fente que sur le déplacement de son centre de phase. Mais, comme la recherche sur cet effet n'entrait pas dans le cadre du mandat confié, il n'a donc pas été pris en compte.

Enfin, des simulations numériques ont été faites dans le but de déterminer l'effet de certaines erreurs sur le rendement de l'antenne, telles que l'angle de braquage, la largeur angulaire à mi-puissance et la puissance maximale des lobes secondaires.

TABLE OF CONTENTS

Chapter 1: Introduction 1

1.1 Background 1

1.2 Outline of the report 3

Chapter 2: Determination of the phase centre 5

2.1 Introduction 5

2.2 Method of solution 5

2.3 Simple array geometries 7

2.3.1 2-Element array 7

2.3.2 2 by 2 planar array 9

2.4 Extension of the method to large arrays 10

2.5 56-Element linear array 12

2.6 Discussion 12

Chapter 3: Microstrip linear array 17

3.1 Introduction 17

3.2 A rectangular microstrip patch 17

3.3 Mutual coupling effect 19

3.3.1 Mutual admittance of two patches 20

3.3.2 Self admittance 23

3.4 Numerical results 24

3.5 Discussion 25

Chapter 4: Slotted waveguide array 63

4.1 Introduction 63

4.2 Random error 64

4.3 Element failure 64

4.3.1 Amplitude failure 65

4.3.2 Phase failure 65

Chapter 5: Phase centre of two-dimensional array 141
5.1 Introduction 141
5.2 Two-dimensional array 141
5.3 Ground reflection 146
5.4 Numerical results 149

Chapter 6: Thermal Expansion/Contraction 197

Chapter 7: Array Performance 207
7.1 Introduction 207
7.2 Beam/HPBW deviations 208
7.2.1 Element failure 208
7.2.2 Amplitude/phase errors 209
7.2.3 Thermal expansion/contraction 209
7.3 Sidelobe/peak power levels 210
7.3 Discussion 210

Chapter 8: Conclusions and discussion 241
8.1 Conclusions 241
8.2 Experimental procedure 243

References 245

Appendix : Application to MLS antenna A-1
1 Introduction A-1
2 Phase centre movement A-1
3 Pointing errors A-1

List of principal symbols

Unless otherwise stated, the symbols most commonly used in this report have the following meaning :

α	approach angle
α_{xn}	phase excitation of the n-th element in the x-coordinate
α_{yn}	phase excitation of the n-th element in the y-coordinate
β	rotation angle
δ	delta function
ε_e, μ_e	permittivity and permeability of the exterior region
γ	rotation angle
λ	wavelength in free space
μ	permeability of medium
ω	radian frequency
σ_a	amplitude random error
σ_p	phase random error
Ψ	phase distribution of the radiated field
ψ	grazing angle
θ_s	scan angle
ρ_s	reflection coefficient of the smooth surface
r, θ, ϕ	spherical coordinates system
d	element spacing
E	far-zone electric field
$f(\theta, \phi)$	element pattern
h	substrate thickness
h_r	receiver height
h_t	transmitter height
IMSL	International Mathematical and Statistical Library
k_o	free space propagation constant
l_t	expanded length at $T°$ C.
LU	Lower and Upper triangular decomposition technique
m	mean
M	equivalent magnetic current
MLS	Microwave Landing System

N_x	number of array element in the x-direction
N_y	number of array element in the y-direction
R	range between the transmitter and the receiver
R_s	reflection coefficient of the rough surface
T	temperature
V_n	amplitude excitation of the n-th element
x, y, z	Cartesian coordinates system
x_a, y_a, z_a	antenna coordinates system
x_b, y_b, z_b	beam coordinates system
Y_{ij}	mutual admittance

LIST OF FIGURES

Figure	page
Fig. 2.1 : Phase centre geometry	7
Fig. 2.2 : Two elements array	8
Fig. 2.3 : Four elements array	9
Fig. 2.4 : Eight elements array	11
Fig. 2.5 : 56-elements array	12
Fig. 2.6 : Antenna phase centre coord., for error free case	14
Fig. 3.1 : Coordinate system of rectangular patch antenna	18
Fig. 3.2 : An array of N-elements, with its equivalent...	20
Fig. 3.3 : Two identical rectangular patches with coordinate...	22
Fig. 4.1 : Plot of uniform random numbers, seed no. 235912749	67
Fig. 4.2 : Plot of uniform random numbers, seed no. 176329845	68
Fig. 4.3 : Plot of uniform random numbers, seed no. 123456789	69
Fig. 4.4 : Plot of uniform random numbers, seed no. 987654321	70
Fig. 4.5 : Plot of uniform random numbers, seed no. 555558888	71
Fig. 4.6 : Normalized version of Fig. 4.1	72
Fig. 4.7 : Normalized version of Fig. 4.2	73
Fig. 4.8 : Normalized version of Fig. 4.3	74
Fig. 4.9 : Normalized version of Fig. 4.4	75
Fig. 4.10 : Normalized version of Fig. 4.5	76
Fig. 4.11 : Phase centre movement due to the phase random errors, σ_p = 5 degrees, seed no. 235912749	77
Fig. 4.12 : Phase centre movement due to the phase random errors, σ_p = 5 degrees, seed no. 176329845	78
Fig. 4.13 : Phase centre movement due to the phase random errors, σ_p = 5 degrees, seed no. 123456789	79
Fig. 4.14 : Phase centre movement due to the phase random errors, σ_p = 5 degrees, seed no. 987654321	80
Fig. 4.15 : Phase centre movement due to the phase random errors, σ_p = 5 degrees, seed no. 555558888	81
Fig. 4.16 : Phase centre movement due to the random amplitude errors, σ_a = 5%, seed no. 235912749	82
Fig. 4.17 : Phase centre movement due to the random amplitude errors, σ_a = 5%, seed no. 176329845	83

Fig. 4.18 : Phase centre movement due to the random amplitude errors, σ_a = 5%, seed no. 123456789 84
Fig. 4.19 : Phase centre movement due to the random amplitude errors, σ_a = 5%, seed no. 987654321 85
Fig. 4.20 : Phase centre movement due to the random amplitude errors, σ_a = 5%, seed no. 555558888 86
Fig. 4.21 : Phase centre movement due to the amplitude failures, θ_s = –40° 87
Fig. 4.22 : Phase centre movement due to the amplitude failures, θ_s = –20° 88
Fig. 4.23 : Phase centre movement due to the amplitude failures, θ_s = 0.0° 89
Fig. 4.24 : Phase centre movement due to the amplitude failures, θ_s = 20° 90
Fig. 4.25 : Phase centre movement due to the amplitude failures, θ_s = 40° 91
Fig. 4.26 : Phase centre movement due to the amplitude failures, element no. 1 & 56 92
Fig. 4.27 : Phase centre movement due to the amplitude failures, element no. 16 & 40 93
Fig. 4.28 : Phase centre movement due to the amplitude failures, element no. 28 & 29 94
Fig. 4.29 : Phase centre movement due to the amplitude failures, element no. 10 & 46 95
Fig. 4.30 : Phase centre movement due to the amplitude failures, element no. 1 to 5 96
Fig. 4.31 : Phase centre movement due to the amplitude failures, element no. 6 to 10 97
Fig. 4.32 : Phase centre movement due to the amplitude failures, element no. 11 to 15 98
Fig. 4.33 : Phase centre movement due to the amplitude failures, element no. 16 to 20 99
Fig. 4.34 : Phase centre movement due to the amplitude failures, element no. 21 to 25 100
Fig. 4.35 : Phase centre movement due to the amplitude failures, element no. 26 to 30 101
Fig. 4.36 : Phase centre movement due to the amplitude failures, element no. 31 to 35 102
Fig. 4.37 : Phase centre movement due to the amplitude failures, element no. 36 to 40 103
Fig. 4.38 : Phase centre movement due to the amplitude failures, element

no. 41 to 45 104
Fig. 4.39 : Phase centre movement due to the amplitude failures, element no. 46 to 50 105
Fig. 4.40 : Phase centre movement due to the amplitude failures, element no. 51 to 56 106
Fig. 4.41 : Phase centre movement due to a pre-determined error of 0.05 added to each element, $\theta_s = -40°$ 107
Fig. 4.42 : Phase centre movement due to a pre-determined error of 0.05 added to each element, $\theta_s = -20°$ 108
Fig. 4.43 : Phase centre movement due to a pre-determined error of 0.05 added to each element, $\theta_s = 0°$ 109
Fig. 4.44 : Phase centre movement due to a pre-determined error of 0.05 added to each element, $\theta_s = 20°$ 110
Fig. 4.45 : Phase centre movement due to a pre-determined error of 0.05 added to each element, $\theta_s = 40°$ 111
Fig. 4.46 : Phase centre movement due to the phase shifter failures, $\theta_s = -40°$ 112
Fig. 4.47 : Phase centre movement due to the phase shifter failures, $\theta_s = -20°$ 113
Fig. 4.48 : Phase centre movement due to the phase shifter failures, $\theta_s = 0°$ 114
Fig. 4.49 : Phase centre movement due to the phase shifter failures, $\theta_s = 20°$ 115
Fig. 4.50 : Phase centre movement due to the phase shifter failures, $\theta_s = 40°$ 116
Fig. 4.51 : Phase centre movement due to the phase shifter failures, element no. 1 & 56 117
Fig. 4.52 : Phase centre movement due to the phase shifter failures, element no. 10 & 47 118
Fig. 4.53 : Phase centre movement due to the phase shifter failures, element no. 28 & 29 119
Fig. 4.54 : Phase centre movement due to the phase shifter failures, element no. 10 & 46 120
Fig. 4.55 : Phase centre movement due to the phase shifter failures, element no. 16 & 40 121
Fig. 4.56 : Phase centre movement due to the phase shifter failures,

element no. 1 to 5 122
Fig. 4.57 : Phase centre movement due to the phase shifter failures, element no. 6 to 10 123
Fig. 4.58 : Phase centre movement due to the phase shifter failures, element no. 11 to 15 124
Fig. 4.59 : Phase centre movement due to the phase shifter failures, element no. 16 to 20 125
Fig. 4.60 : Phase centre movement due to the phase shifter failures, element no. 21 to 25 126
Fig. 4.61 : Phase centre movement due to the phase shifter failures, element no. 26 to 30 127
Fig. 4.62 : Phase centre movement due to the phase shifter failures, element no. 31 to 35 128
Fig. 4.63 : Phase centre movement due to the phase shifter failures, element no. 36 to 40 129
Fig. 4.64 : Phase centre movement due to the phase shifter failures, element no. 41 to 45 130
Fig. 4.65 : Phase centre movement due to the phase shifter failures, element no. 46 to 50 131
Fig. 4.66 : Phase centre movement due to the phase shifter failures, element no. 51 to 56 132
Fig. 4.67 : Phase centre movement due to a pre-determined error of 5° added to each phase shifter, $\theta_s = -40°$ 133
Fig. 4.68 : Phase centre movement due to a pre-determined error of 5° added to each phase shifter, $\theta_s = -20°$ 134
Fig. 4.69 : Phase centre movement due to a pre-determined error of 5° added to each phase shifter, $\theta_s = 0°$ 135
Fig. 4.70 : Phase centre movement due to a pre-determined error of 5° added to each phase shifter, $\theta_s = 20°$ 136
Fig. 4.71 : Phase centre movement due to a pre-determined error of 5° added to each phase shifter, $\theta_s = 40°$ 137
Fig. 4.72 : Phase centre movement due to a pre-determined error of 5° added to each phase shifter 138
Fig. 4.73 : Phase centre movement due to a pre-determined error of 10° added to each phase shifter 139
Fig. 5.1 : Array geometry 142

Fig. 5.2 : Antenna radiation pattern, $\phi = 0.0°$ 143
Fig. 5.3 : Antenna radiation pattern, $\phi = 90.0°$ 144
Fig. 5.4 : Specular reflection 148
Fig. 5.5 : Random phase error, $\sigma_p = 5°$, seed no. 235912749 151
Fig. 5.6 : Random phase error, $\sigma_p = 5°$, seed no. 176329845 152
Fig. 5.7 : Random phase error, $\sigma_p = 5°$, seed no. 123456789 153
Fig. 5.8 : Random phase error, $\sigma_p = 5°$, seed no. 987654321 154
Fig. 5.9 : Random phase error, $\sigma_p = 5°$, seed no. 555558888 155
Fig. 5.10 : Amplitude failures, $\theta_s = -40°$ 156
Fig. 5.11 : Amplitude failures, $\theta_s = -20°$ 157
Fig. 5.12 : Amplitude failures, $\theta_s = 0°$ 158
Fig. 5.13 : Amplitude failures, $\theta_s = 20°$ 159
Fig. 5.14 : Amplitude failures, $\theta_s = 40°$ 160
Fig. 5.15 : Phase shifter failures, $\theta_s = -40°$ 161
Fig. 5.16 : Phase shifter failures, $\theta_s = -20°$ 162
Fig. 5.17 : Phase shifter failures, $\theta_s = 0°$ 163
Fig. 5.18 : Phase shifter failures, $\theta_s = 20°$ 164
Fig. 5.19 : Phase shifter failures, $\theta_s = 40°$ 165
Fig. 5.20 : Magnitude of reflection coefficient 166
Fig. 5.21 : Phase of reflection coefficient 167
Fig. 5.22 : Variation of grazing angle vs range 168
Fig. 5.23 : Variation of grazing angle vs receiver height 169
Fig. 5.24 : Multipath reflection from the wet ground 170
Fig. 5.25 : Multipath reflection from the dry ground 171
Fig. 5.26 : Multipath reflection from the concrete 172
Fig. 5.27 : Multipath reflection from the wet ground, $R = 37km$ 173
Fig. 5.28 : Multipath reflection from the dry ground, $R = 37km$ 174
Fig. 5.29 : Multipath reflection from the concrete, $R = 37km$ 175
Fig. 5.30 : Multipath reflection from the wet ground, $R = 50km$ 176
Fig. 5.31 : Multipath reflection from the dry ground, $R = 50km$ 177
Fig. 5.32 : Multipath reflection from the concrete, $R = 50km$ 178
Fig. 5.33 : $R = 50.0km$, $\Delta\theta_e = 1.0$ deg., $\alpha = 3.0$ deg., concrete 179
Fig. 5.34 : $R = 50.0km$, $\Delta\theta_e = 1.0$ deg., $\alpha = 3.0$ deg., dry ground 180
Fig. 5.35 : $R = 50.0km$, $\Delta\theta_e = 1.0$ deg., $\alpha = 3.0$ deg., wet ground 181
Fig. 5.36 : $R = 50.0km$, $\Delta\theta_e = 1.0$ deg., $h_r = 6km$, concrete 182
Fig. 5.37 : $R = 50.0km$, $\Delta\theta_e = 1.0$ deg., $h_r = 6km$, dry ground 183

Fig. 5.38 : R = 50.0km, $\Delta\theta_c$ = 1.0 deg., h_r = 6km, wet ground 184
Fig. 5.39 : R = 50.0km, $\Delta\theta_c$ = 1.0 deg., h_r = 6km, wet ground 185
Fig. 5.40 : R = 50.0km, $\Delta\theta_c$ = 1.0 deg., h_r = 6km, dry ground 186
Fig. 5.41 : R = 50.0km, $\Delta\theta_c$ = 1.0 deg., h_r = 6km, concrete 187
Fig. 5.42 : R = 396m, h_r = 56.82m, h_t = 21.34m, dry ground, for DFL lab 188
Fig. 5.43 : R = 396m, h_r = 56.82m, h_t = 21.34m, concrete, for DFL lab 189
Fig. 5.44 : R = 396m, h_r = 56.82m, h_t = 21.34m, wet ground, for DFL lab 190
Fig. 5.45 : R = 396m, h_r = 56.82m, h_t = 21.34m, dry ground, for DFL lab 191
Fig. 5.46 : R = 396m, h_r = 56.82m, h_t = 21.34m, concrete, for DFL lab 192
Fig. 5.47 : R = 396m, h_r = 56.82m, h_t = 21.34m, wet ground, for DFL lab 193
Fig. 5.48 : R = 396m, h_r = 56.82m, h_t = 21.34m, concrete, for DFL lab 194
Fig. 5.49 : R = 396m, h_r = 56.82m, h_t = 21.34m, dry ground, for DFL lab 195
Fig. 5.50 : R = 396m, h_r = 56.82m, h_t = 21.34m, wet ground, for DFL lab 196
Fig. 6.1 : Thermal expansion of the horizontal arrays, copper (T = 60° C) 199
Fig. 6.2 : Thermal contraction of the horizontal arrays, copper (T = –60° C) 200
Fig. 6.3 : Thermal expansion of the vertical arrays, copper (T = 60° C) 201
Fig. 6.4 : Thermal contraction of the vertical arrays, copper (T = –60° C) 202
Fig. 6.5 : Thermal expansion of the horizontal arrays, aluminum (T = 60° C) 203
Fig. 6.6 : Thermal contraction of the horizontal arrays, aluminum (T = –60° C) 204
Fig. 6.7 : Thermal expansion of the vertical arrays, aluminum (T = 60° C) 205
Fig. 6.8 : Thermal contraction of the vertical arrays, aluminum (T = –60° C) 206
Fig. 7.1 : Radiation pattern of a 56-element array, 0 deg. scan 210
Fig. 7.2 : Radiation pattern of a 56-element array, 40 deg. scan 211
Fig. 7.3 : Effect of one phase shifter failure (#22) 212
Fig. 7.4 : Effect of two symmetrical phase shifters failure 213
Fig. 7.5 : Pointing and beam width errors due to a single phase shifter failure, θ_s = 20 degree 214
Fig. 7.6 : Pointing and beam width errors due to a single phase shifter failure, θ_s = 40 degree 215
Fig. 7.7 : Pointing and beam width errors due to amplitude failure, θ_s = 20 degree 216
Fig. 7.8 : Pointing and beam width errors due to amplitude failure, θ_s = 40 degree 217

Fig. 7.9 : Pointing and beam width errors due to two symmetrical phase shifters failure, θ_s = 20 degree 218
Fig. 7.10 : Pointing and beam width errors due to two symmetrical phase shifters failure, θ_s = 40 degree 219
Fig. 7.11 : Pointing and beam width errors due to two symmetrical amplitude failure, θ_s = 20 degree 220
Fig. 7.12 : Pointing and beam width errors due to two symmetrical amplitude failure, θ_s = 40 degree 221
Fig. 7.13 : Pointing and beam width errors due to a 10 deg. phase error added to each element, θ_s = 20 degree 222
Fig. 7.14 : Pointing and beam width errors due to a 10% amplitude error added to each element, θ_s = 20 degree 223
Fig. 7.15 : Pointing and beam width errors due to a 10 deg. phase error added to each element, θ_s = 40 degree 224
Fig. 7.16 : Pointing and beam width errors due to a 10% amplitude error added to each element, θ_s = 40 degree 225
Fig. 7.17 : Pointing and beam width errors due to random phase errors, with rms = 10 degree 226
Fig. 7.18 : Same as in Fig. 7.17, but with another set of random phase errors, with rms = 10 degree 227
Fig. 7.19 : Pointing and beam width errors due to combined random phase rms = 10 degree 228
Fig. 7.20 : Same as in Fig. 7.19, but with another set of combined random phase rms = 10 degree 229
Fig. 7.21 : Pointing and beam width errors due to a uniform thermal expansion of 0.01 mm per element spacing 230
Fig. 7.22 : Pointing and beam width errors due to a uniform thermal contraction of 0.01 mm per element spacing 231
Fig. 7.23 : Pointing and beam width errors due to a uniform thermal expansion of 0.05 mm per element spacing 232
Fig. 7.24 : Pointing and beam width errors due to a uniform thermal contraction of 0.05 mm per element spacing 233
Fig. 7.25 : Pointing and beam width errors due to a uniform thermal expansion of 0.1 mm per element spacing 234
Fig. 7.26 : The increase in the peak sidelobe and decrease in the maximum radiated power levels 235

Fig. 7.27 : The increase in the peak sidelobe and decrease in the maximum radiated power levels 236
Fig. 7.28 : The increase in the peak sidelobe and decrease in the maximum radiated power levels 237
Fig. 7.29 : The increase in the peak sidelobe and decrease in the maximum radiated power levels 238
Fig. A.1 : Phase centre movement for the selected scan angles, error-free case A-3
Fig. A.2 : Phase centre movement for the selected scan angles, error-free case A-4
Fig. A.3 : Phase centre movement for the selected scan angles, random error added A-5
Fig. A.4 : Phase centre movement for the selected scan angles, random error added A-6
Fig. A.5 : Phase centre movement due to amplitude failure, θ_s = 10 degree A-7
Fig. A.6 : Phase centre movement due to amplitude failure, θ_s = 30.014 degree A-8
Fig. A.7 : Phase centre movement due to phase shifters failure, θ_s = 10 degree A-9
Fig. A.8 : Phase centre movement due to phase shifters failure, θ_s = 30.014 degree A-10
Fig. A.9: Pointing and beam width errors due to a single phase shifter failure, θ_s = 30.014 degree A-11
Fig. A.10: Pointing and beam width errors due to a single phase shifter failure, θ_s = 30.016 degree A-12
Fig. A.11: Pointing and beam width errors due to a single phase shifter failure, θ_s = 30.212 degree A-13
Fig. A.12: Pointing and beam width errors due to a single phase shifter failure, θ_s = 30.313 degree A-14
Fig. A.13: Pointing and beam width errors due to a single phase shifter failure, θ_s = 30.405 degree A-15
Fig. A.14: Pointing and beam width errors due to a single phase shifter failure, θ_s = 30.504 degree A-16
Fig. A.15: Pointing and beam width errors due to a single phase shifter failure, θ_s = 30.014 deg. for Micronav A-17

Fig. A.16: Pointing and beam width errors due to a single phase shifter failure, θ_s = 30.106 deg. for Micronav A-18
Fig. A.17: Pointing and beam width errors due to a single phase shifter failure, θ_s = 30.212 deg. for Micronav A-19
Fig. A.18: Pointing and beam width errors due to a single phase shifter failure, θ_s = 30.313 deg. for Micronav A-20
Fig. A.19: Pointing and beam width errors due to a single phase shifter failure, θ_s = 30.405 deg. for Micronav A-21
Fig. A.20: Pointing and beam width errors due to a single phase shifter failure, θ_s = 30.504 deg. for Micronav A-22

Chapter 1
Introduction

1.1 Background

The work presented in this report is a summary of efforts made to develop a mathematical model to determine the uniqueness of the phase centre for the azimuth antenna of Microwave Landing Systems (*MLS*). It is shown that for an ideal antenna the phase centre is located at its geometrical centre. However, any deviation from the ideal conditions, due to the scan angle algorithm, phase shifter quantization and *rms* errors, design or implementation errors in array amplitude taper, etc., results in the movement of the phase centre from geometrical centre and causes its non-uniqueness. Under various design and operational conditions, therefore, the *MLS* antenna has an apparent phase centre that generally moves with its beam scan. This report initially provides a mathematical model for locating the phase centre of any given antenna or arrays and then utilizes it for investigating the effect of different antenna parameters on its uniqueness. The model is then extended to investigate the effects of secondary parameters such as ground reflection and thermal expansion and/or contraction on the phase centre movement. This section summarizes the background work on the phase centre studies and outlines the aims and achievements of the remaining sections.

The phase centre is defined as the centre of a sphere surrounding the antenna on which the measured or calculated phase is constant. The field radiated by such an antenna can then be assumed to be spherical waves with spherical equi-phase surfaces, i.e., the phase centre can be considered as the apparent source of radiation. The phase centre of an antenna plays a fundamental role in all those systems where the information contained in the phase of a received (or transmitted) electromagnetic field is of primary importance. This class of systems includes those systems developed for satellite geodetic applications [1] and UHF radio positioning systems [2]. Also, a knowledge of the feed phase centre is important for designing a reflector antenna system, since it determines the location of the feed relative to the focal point of the reflector. In such systems, it is desirable to design the antenna so that it can behave as

a single point source, representing its phase centre.

In recent years several theoretical and experimental methods have been developed to find the location of the antenna phase centre. Dyson [3] has summarized the theoretical and experimental techniques for determining the phase centre location. Also, he has discussed experimental methods of measuring the complete phase pattern of an antenna. Hu [4] introduced a graphical method to locate the phase centre of any radiating system from the expression of its radiation field. However, the developed method is applied only to a special case of radiating systems with an axially symmetric radiation pattern, i.e., its radiation field is independent of the angle ϕ. Vol'pert [5] and Gething [6] established the general analytical shape of the phase distribution in which antennas must have a phase centre from which the co-ordinates of the phase centre are defined. This method was applied to discrete and linear array antennas, which can be used for more complicated structures. A more practical definition of the phase centre has been given by Rusch and Potter [7] as the phase centre of the best nearly constant phase spheres. Although the definition given by Rusch and Potter is general enough to obtain combined E- and H- plane phase centres within a given solid angle, practical formulas were given only for numerical calculation of a phase centre in a single principal plane.

A more useful location of the phase centre for reflector antennas was defined recently by Kildal [8] as a point that maximizes the reflector gain. This definition is quite general, but the expression provided by Kildal enables one to locate the phase centre close to a trial point that causes small aperture-phase errors. For wide-angle patterns estimating the approximate location of the phase centre is quite difficult. Rao and Shafai [9] pointed out that the analysis given by Kildal is valid only for small phase errors. Hence they introduced a more general method, valid for small as well as large phase error values, for determining the optimum phase centre location of feed antennas used in prime-focus or dual reflector systems.

Although it can be said that most complex antenna structures do not have a phase centre, many of them have a phase reference point that can be considered as the apparent phase centre for the limited observation angle. The concept of an "apparent phase centre" is a useful parameter in the practical applications of these antennas. Since it has been observed that the movement of this phase reference point, as the angle of observation is changed, may be very small in terms of the wavelength. An apparent phase centre must, however, be specified in terms of the polarization of the incident field, the plane of the observation, and a range of angular co-ordinates associated with that plane.

The purpose of this study is to develop a simple model, yet reliable, for determining the location of the phase centre. Furthermore, we intend to incorporate the effects of design errors, element or phase failures, and the effects of ground reflection and thermal expansion and/or contraction on the antenna phase centre movement. The objective is to develop a practical model to investigate and understand the phase centre movement due to all these effects, so that a better measurement procedure can be developed, and/or the measurement data can be analyzed to provide correct beam and pattern data for a given measurement setup. The presented results can also be used to improve the antenna locating schemes during actual operational modes.

Existing scattering models in the literature are usually intended for quantitative assessment of specific *MLS* systems and techniques. These models are applicable to certain representative airport sites and include those objects, structures, or terrain features which causes significant effect on the performance of a *MLS* profile. Here, due to the nature of the problem under investigation such a detail analysis is not carried out, and a simplified model, neglecting secondary effects is used for computer simulation.

The task of modeling the ground reflection is simplified by assuming an infinite ground plane and utilization of ray optics properties and ray tracing. The complicated finite ground representation which uses the Kirchoff-Fresnel integral to compute the ground reflection coefficient has been carried out by MIT Lincoln Lab [10]. However, its use requires excessive computer time. As a result, in their follow up report [11], they have replaced their complex model by a simplified one which is similar to that used in this report.

1.2 Outline of the report

In the remainder of this chapter a brief overview of the remaining chapters is presented.

In chapter 2, the formulation for the phase centre determination is given. In order to illustrate the feasibility and accuracy of the formulation, several simple array geometries are analytically solved and a closed form solution for the phase centre is obtained. Next, the extension of the model to more complicated planar arrays is discussed and a numerical technique is recommended to determine the antenna phase centre position.

In chapter 3, the developed method is applied to microstrip array antennas. The antenna phase centre movement is studied due to the presence of mutual coupling between the array elements. A model is presented to describe the mutual coupling between the array elements, and is subsequently applied to arrays to determine the phase centre movement, due to element failures.

In chapter 4, the proposed method is applied to one dimensional slotted waveguide arrays. The antenna phase centre is determined and the effect of random and pre-determined errors on the phase centre is investigated.

In chapter 5, the formulation is extended to treat the ground reflection. A model for the multipath reflection is developed to investigate signal variation and the performance of the antenna phase centre due to the specular reflection by the ground.

In chapter 6, a simple model for determining the linear thermal expansion/contraction of the materials is recommended. The method is subsequently used to compute the phase centre movement due to the thermal expansion and/or contraction of the antenna.

In chapter 7, the effects of different errors on the antenna performance is discussed. Important parameters such as beam deviation, 3 *dB* beam width, and sidelobe level due to element failures, random errors and also pre-determined errors, added to each antenna element are investigated.

Finally, conclusions of the work presented herein are drawn and the overall assessment of *MLS* array phase centre is presented. A brief discussion on the experimental procedure is also included.

Chapter 2
Determination of the phase centre

2.1 Introduction

It is the purpose of this chapter to define the phase centre of a radiating system and determine it from the radiation far field data. Initially, the far field components of the antenna are expressed in a convenient form to isolate their phase variation. Then the phase centre is defined as a unique point in space, from which a point source radiates a similar field. Since a point source radiates spherical waves, then the phase fronts are spherical surfaces and the phase centre is their origin. Consequently, for a given antenna one may determine the phase centre by locating the centre of a sphere over which the radiation field of the antenna has a constant phase [12], [13]. In section 2.2, the proposed method of solution is described and its validity is subsequently illustrated by its application to simple array geometries. The extension of the method to more complex array geometries is described in section 2.4. Finally, a 56-element linear array is considered and some numerical results are presented.

2.2 Method of solution

Suppose we have an antenna occupying a certain volume in space and that, the point O is an arbitrary origin as shown in Fig. 2.1. We assume that the observation point is sufficiently far from the origin, so that all the rays received from different points of the antenna can be regarded as parallel. The expression for the components of the far-zone electric field vector $\overline{E}$ at the point of observation can be expressed as

$$E = f(\theta, \phi) \frac{e^{-jk_0R}}{R} e^{j\psi(\theta, \phi)} \tag{2.1}$$

where $f(\theta, \phi)$ is the amplitude pattern, k_0 is the free space propagation constant and $\psi(\theta, \phi)$ is the phase distribution of the radiated field.

The problem of determining an apparent phase centre of the field is that of finding a point O' which is the centre of a sphere of radius r upon which the field has a constant or nearly constant phase. If R and r are much greater than r_0, then the position vector of O' is related to that of O by

$$R = r + |Op| \tag{2.2}$$

Here, $\overline{Op}$ is along $\overline{R}$ and perpendicular to a plane passing by $O'(x_0, y_0, z_0)$. Then $|\overline{Op}|$ can be written as,

$$|\overline{Op}| = \overline{r}_0 \cdot \hat{R} \tag{2.3.a}$$

with

$$\overline{r}_0 = x_0 \hat{x} + y_0 \hat{y} + z_0 \hat{z} \tag{2.3.b}$$

$$\hat{R} = \sin\theta \cos\phi \hat{x} + \sin\theta \cos\phi \hat{y} + \cos\theta \hat{z} \tag{2.3.c}$$

where $\hat{x}$, $\hat{y}$, $\hat{z}$ are unit vectors along $x-$, $y-$ and $z-$ axes, and $\hat{R}$ is a unit vector along $\overline{R}$. Substituting the above equations in (2.2) will result in the following expression for the spatial distance R.

$$R = r + x_0 \sin\theta \cos\phi + y_0 \sin\theta \sin\phi + z_0 \cos\theta \tag{2.4}$$

Next, utilizing (2.1) and (2.4), the expression for the phase can take the following form,

$$\psi(\theta, \phi) - k_0 (x_0 \sin\theta \cos\phi + y_0 \sin\theta \sin\phi + z_0 \cos\theta) - k_0 r \tag{2.5}$$

If the antenna has a phase centre, we can then find a point $O'(x_0, y_o, z_0)$ for which the above phase term is independent of θ and ϕ. That is,

$$\psi(\theta, \phi) - k_0 (x_0 \sin\theta \cos\phi + y_0 \sin\theta \sin\phi + z_0 \cos\theta) = q \tag{2.6}$$

where q is a constant which is independent of θ and ϕ. Consequently, in this case $k_0 r$ in equation (2.5) has a constant value and the selected point $O'(x_0, y_0, z_0)$ is the phase centre. To satisfy the relationship (2.6), we require a definite analytical form for the phase distribution $\psi(\theta, \phi)$. It can be seen from the structure of this relationship that it still holds, when the general expression for the phase distribution is in the form [5],

$$\psi(\theta, \phi) = A \sin\theta \cos\phi + B \sin\theta \sin\phi + C \cos\theta + D \tag{2.7}$$

where A, B, C and D are constants independent of θ and ϕ.

Hence, the expression for the phase distribution given by (2.7) is the general condition for the existence of a phase centre. Comparing this condition with (2.6), the coordinates of the phase centre and the constant q can be found in a general form as a function of the coefficients of the general expression for the phase distribution, i.e.,

$$x_0 = \frac{A}{k_0} \; ; \qquad y_0 = \frac{B}{k_0} \; ; \quad z_0 = \frac{C}{k_0} \; ; \qquad q = D \tag{2.8}$$

Therefore, if the radiated field phase distribution of an antenna is given in an analytical form similar to (2.7), one can determine the location of the associated phase centre.

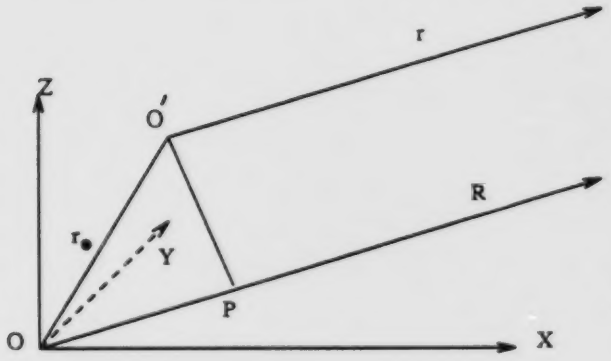

Fig. 2.1 : Phase centre geometry.

2.3 Simple array geometries

In this section, special cases are considered for which the phase of the far field can be derived in a closed form. several examples are discussed to validate the proposed formulation.

2.3.1 2-Element array

Consider the array geometry of Fig. 2.2, where we have two elements located on the x-axis and excited uniformly by I_0. The components of the far electric field can be expressed as

$$E(\theta, \phi) = E^{(1)}(\theta, \phi) + E^{(2)}(\theta, \phi) \tag{2.9.a}$$

$$= f(\theta, \phi)\ \frac{e^{-jk_0R}}{R}\ (A.F.) \tag{2.9.b}$$

where $f(\theta, \phi)$ is the element pattern and $(A.F.)$ is the array factor, which can be written, in the $\phi = 0^o$ -plane, as

$$A.F. = I_0\ (\ 1 + e^{jk_0d\sin\theta}\ ) \tag{2.10.a}$$

$$= 2\ I_0\ \cos(\frac{k_0\ d\ \sin\theta}{2}\ )\ e^{j\frac{k_0d\sin\theta}{2}} \tag{2.10.b}$$

where, the phase $\psi(\theta, \phi)$ is given by

$$\psi(\theta, \phi) = k_0\ (\frac{d}{2})\ \sin\theta \tag{2.11.a}$$

Comparing (2.11.a) with (2.7), it can be seen that the array does have a phase centre. That is,

$$A = k_0(\frac{d}{2})\ ,\ B = 0\ ,\ C = 0\ ,\ D = 0 \tag{2.11.b}$$

Comparing (2.11.b) with equation (2.8), one can obtain

$$x_0 = \frac{d}{2}\ ,\ y_0 = 0\ ,\ z_0 = 0 \tag{2.11.d}$$

or the phase centre is at $(\frac{d}{2}, 0, 0)$, as one would expect.

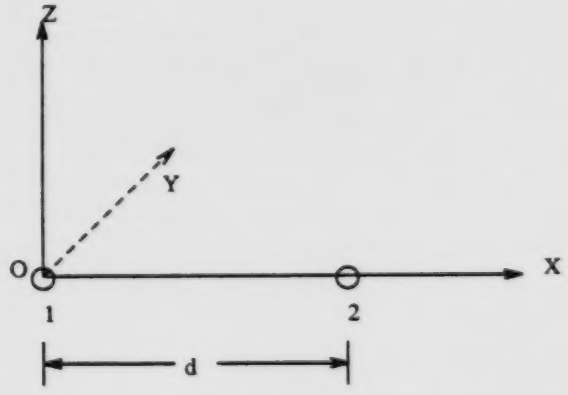

Fig. 2.2 : Two elements array.

2.3.2 2 × 2 planar array

In this example, we have 4 elements forming a planar array in the $x-y$ plane as shown in Fig. 2.3. The elements are equally excited by I_0 and the array factor, in this case, can be defined as

$$A.F. = I_0 \sum_{i=1}^{4} e^{jk_0 r_i (\cos\theta \cos\theta_i + \sin\theta \sin\theta_i \cos(\phi - \phi_i))} \tag{2.12}$$

where r_i, θ_i, ϕ_i are the spherical coordinates of the i^{th} element. Considering that the array elements are in the $x-y$ plane, i.e., $\theta_i = 0^o$, after some mathematical manipulations, the $A.F.$ can be written as

$$A.F. = 4\, I_0 \cos(k_0 \frac{d}{2} \sin\theta\cos\phi) \cos(k_0 \frac{d}{2} \sin\theta\sin\phi) \cdot e^{j\,(k_0 \frac{d}{2} \sin\theta\cos\phi + k_0 \frac{d}{2} \sin\theta\sin\phi)} \tag{2.13}$$

where, the phase of the array is given by,

$$\psi(\theta, \phi) = k_0(\frac{d}{2})\, \sin\theta\cos\phi + k_0(\frac{d}{2})\, \sin\theta\sin\phi \tag{2.14.a}$$

Again, comparing (2.14.a) with (2.7), we have

$$A = k_0(\frac{d}{2}),\ B = k_0(\frac{d}{2}),\ C = 0,\ D = 0 \tag{2.14.b}$$

or,

$$x_0 = \frac{d}{2},\ y_0 = \frac{d}{2},\ z_0 = 0 \tag{2.14.c}$$

Hence, the point $(\frac{d}{2}, \frac{d}{2}, 0)$ is the phase centre of the array at hand.

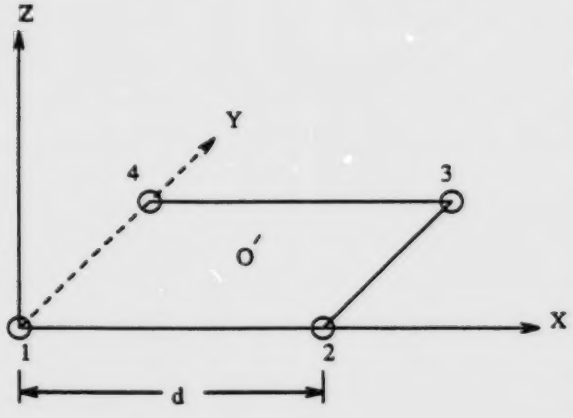

Fig. 2.3 : Four elements array.

2.4. Extension of the method to large array

The previous examples illustrated the simplicity of the method, as applied to simple antennas. The method becomes straightforward when there is a possibility of a closed form solution for the phase of the radiating system. In reality, it is difficult to express the array phase in a closed form. Some of the difficulties can be summarized as;

1) existence of a large number of elements forming the array,
2) non-uniform excitation of elements,
3) random errors in the excitation coefficients,
4) mutual coupling effect, etc.

Therefore, it is important to modify the method described previously, in order to define the phase centre of any radiating system under different operational conditions. This modification can be done in the following steps,

i) The phase centre can be obtained in the $\phi = 0^o$ plane (H-plane). As a result, the equation (2.7) takes the form,

$$\psi(\theta, 0^o) = A \sin\theta + C \cos\theta + D \tag{2.15}$$

which is valid for all values of θ and has three unknowns, { A, C, D }. A substitution of three different values of θ will result in three equations in three unknowns, which can be solved for the constants, A, C and D.

ii) Similarly, the phase centre can be computed in $\phi = 90^o$ plane (E-plane). Here, the equation (2.7) simplifies to,

$$\psi(\theta, 90^o) = B \sin\theta + C \cos\theta + D \tag{2.16}$$

Proceeding as in the previous step, the unknowns B, C and D can be found.

The phase centre in the E- or H-plane means that if the arbitrary origin is taken at that phase centre, the computed phase of the system will be constant (or nearly constant) at each point in that plane, on a circle centred at the phase centre. If it is desired to define a unique phase centre in whole space, the phase centres of E- and H-planes should be combined. A simple approach, but not necessarily general, is to define the global phase centre as the intersection point of two lines drawn from phase centre in each plane, normal to that plane. This is shown in Fig. 2.4 for an eight element array. The following example will illustrate the procedure.

Consider the array geometry given in Fig. 2.4. The elements are excited by $I_i\ e^{j\alpha_i}$ and the space between them in the $x-$, $y-$ and $z-$ directions are equal. The array factor $A.F.$ can be written as

ray factor $A.F.$ can be written as

$$A.F. = \sum_{i=1}^{8} I_i \, e^{jk_0 r_i \, (\cos\theta\cos\theta_i + \sin\theta\sin\theta_i\cos(\phi-\phi_i) + \alpha_i)} \tag{2.17}$$

where (r_i, θ_i, ϕ_i) are the spherical coordinates of the i-th element, and α_i can be arbitrarily adjusted, so that the main beam points along the (θ_0, ϕ_0) direction. In this case, α_i is defined by

$$\alpha_i = -k_0 r_i \left[\cos\theta_0\cos\theta_i + \sin\theta_0\sin\theta_i\cos(\phi_0-\phi_i) \right] \tag{2.18}$$

The formulation was programmed and numerical results generated for the following operating parameters : $I_i = 1$, $f = 5.06\ GHz$ and $d = 0.56\ \lambda$. The phase centres in the $H-$ and $E-$ Planes are shown in Tables 2.1a and 2.1b, respectively. The uncertainties in determining the phase centre are defined by Dx, Dy and Dz and tabulated in the same tables. In all cases, the uncertainties of finding the phase centre in each plane are very small. The location of the global phase centre was determined for different values of θ on the main beam, and the scanned angle of 0^o. The computed phase centre coordinates were found to be, $(0.837\lambda, 0.838\lambda, 0.287\lambda)$, corresponding to the exact location of $(0.84\lambda, 0.84\lambda, 0.28\lambda)$ which represents the centre of the cube.

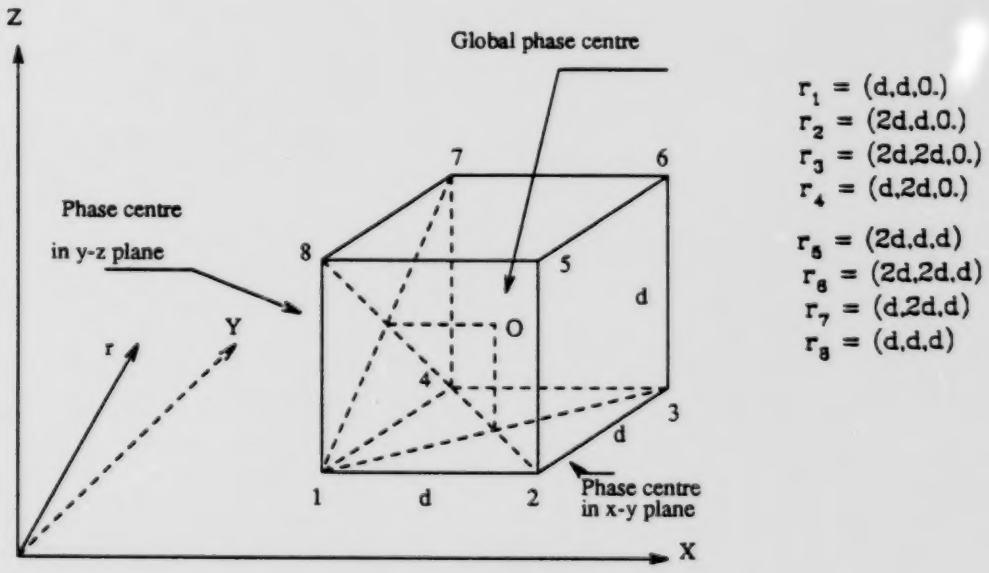

Fig 2.4 : Eight elements array.

2.5. 56-Element linear array

The method just described in the previous section was applied to a large linear array shown in Fig. 2.5. In this example, the amplitude distribution is assumed to be -30 dB Taylor distribution with 56 elements. The interelement spacing d is 0.56 λ at the centre frequency of 5.06 GHz, and the corresponding half-power beam width ($HPBW$) is about 2.03°. The numerical results, for the coordinates of the phase centre, under different scan conditions θ_s are shown in Fig. 2.6. The generated result is for the perfect array with exclusion of all random or pre-determined errors. From this figure, one can observe that, for all scan angles the phase centre coordinates coincide with the antenna physical centre. This is partly due to the symmetric excitation of the array, and partly due to the lack of errors, i.e., a perfect operating condition of the antenna.

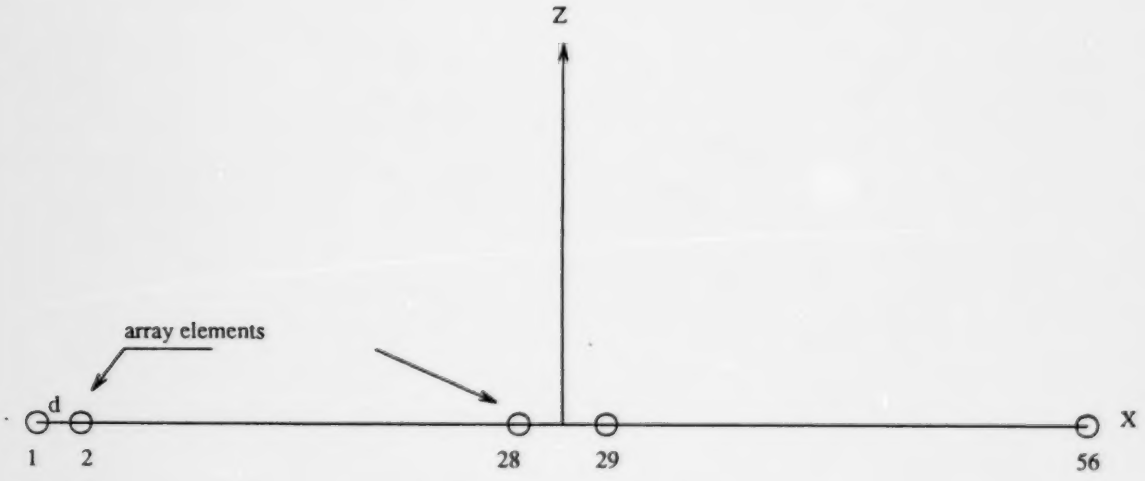

Fig. 2.5 : 56-elements linear array.

2.6. Discussion

A method was proposed to determine the phase centre location of any planar array antenna. Several simple examples were selected to analytically verify the formulation. The model was based on selecting a minimum of three points on the main beam, and solving a system of linear equations for three unknowns. The LU decomposition method was used to solve the system of linear equations numerically.

Data for computer validations were presented for a one dimensional array antenna. In addition, comparisons were made of the computed data with the analytical results. The generated results indicated the reliability and also the efficiency of the technique in locating the antenna phase centre. It was found that the recommended formulation is computationally efficient and requires minimum computer time for performing the calculations. It should be noted that the determination of the phase centre coordinates was also investigated by an alternative approach of using a least square algorithm applied to equation (2.6). While it may be more stable than the proposed method, it generally requires more computer time. For large arrays, such as the *MLS* one, the computer time requirements are excessive and consequently the method was not adopted.

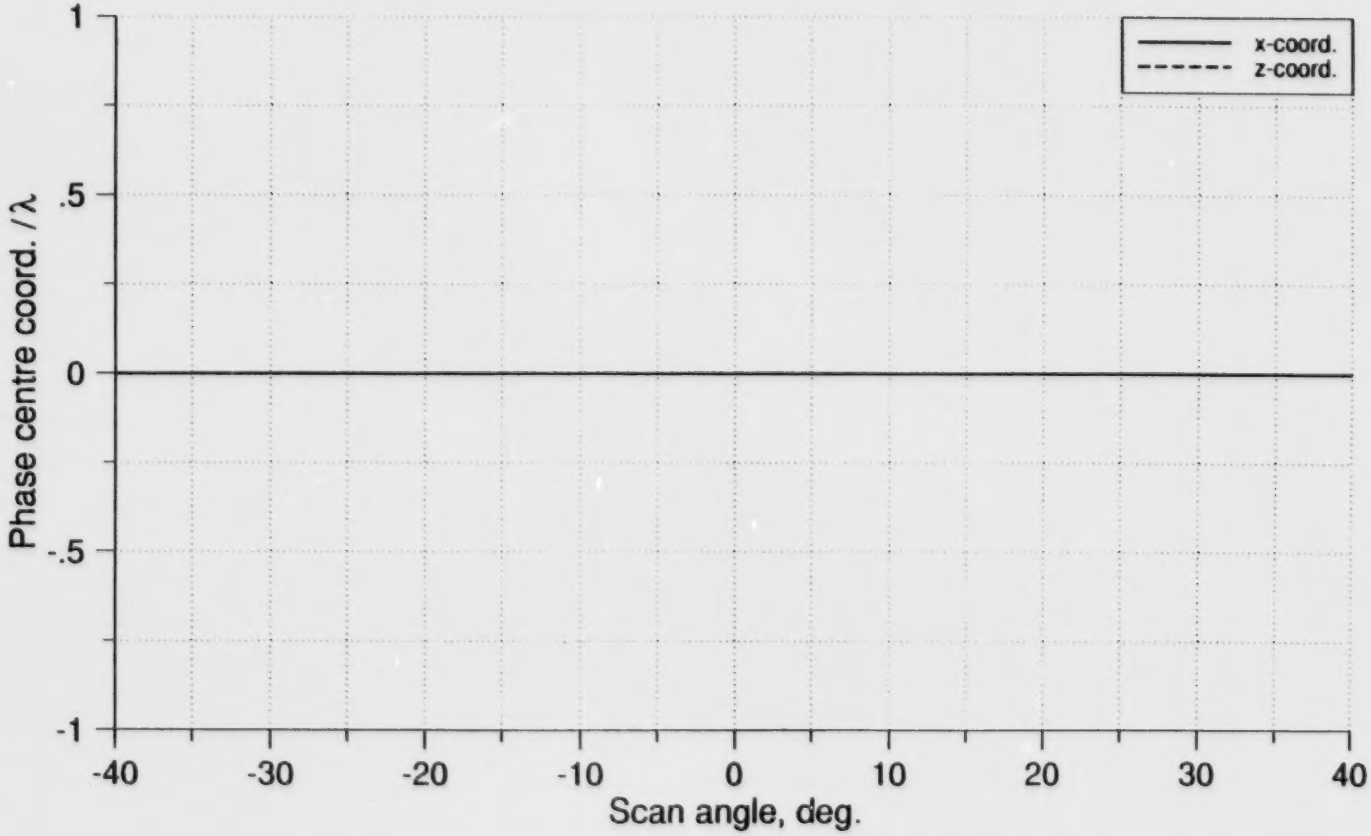

Fig. 2.6 : Antenna phase centre coord., for error free case.

Table 2.1a

Phase center (x0,y0,z0) in H- Plane
Exact phase center is at (0.84λ,0.0,0.28λ)

Set no.	Theta, deg.	x0/λ	z0/λ	Dx/λ	Dz/λ
1	-21.0, -20.0, -19.0	0.83664	0.28927	-0.00336	0.00927
2	-18.0, -17.0, -16.0	0.83676	0.28889	-0.00324	0.00889
3	-15.0, -14.0, -13.0	0.83690	0.28839	-0.00310	0.00839
4	-12.0, -11.0, -10.0	0.83702	0.28785	-0.00298	0.00785
5	-9.0, -8.0, -7.0	0.83711	0.28733	-0.00289	0.00733
6	-6.0, -5.0, -4.0	0.83716	0.28692	-0.00284	0.00692
7	-3.0, -2.0, -1.0	0.83717	0.28670	-0.00283	0.00670
8	0.0, 1.0, 2.0	0.83717	0.28673	-0.00283	0.00673
9	3.0, 4.0, 5.0	0.83719	0.28712	-0.00281	0.00712
10	6.0, 7.0, 8.0	0.83727	0.28796	-0.00273	0.00796
11	9.0, 10.0, 11.0	0.83749	0.28940	-0.00251	0.00940
12	12.0, 13.0, 14.0	0.83794	0.29160	-0.00206	0.01160
13	15.0, 16.0, 17.0	0.83878	0.29480	-0.00122	0.01480
14	18.0, 19.0, 20.0	0.84021	0.29934	0.00021	0.01934

Table 2.1b

Phase center (x0,y0,z0) in E- Plane
Exact phase center is at (0.0,0.84 λ,0.28 λ)

Set no.	Theta, deg.	y0/λ	z0/λ	Dy/λ	Dz/λ
1	-21.0, -20.0, -19.0	0.83811	0.28802	-0.00189	0.00802
2	-18.0, -17.0, -16.0	0.83844	0.28706	-0.00156	0.00706
3	-15.0, -14.0, -13.0	0.83857	0.28658	-0.00143	0.00658
4	-12.0, -11.0, -10.0	0.83861	0.28642	-0.00139	0.00642
5	-9.0, -8.0, -7.0	0.83861	0.28645	-0.00139	0.00645
6	-6.0, -5.0, -4.0	0.83859	0.28656	-0.00141	0.00656
7	-3.0, -2.0, -1.0	0.83859	0.28666	-0.00141	0.00666
8	0.0, 1.0, 2.0	0.83859	0.28666	-0.00141	0.00666
9	1.0, 2.0, 3.0	0.83858	0.28662	-0.00142	0.00662
10	4.0, 5.0, 6.0	0.83857	0.28633	-0.00143	0.00633
11	7.0, 8.0, 9.0	0.83849	0.28569	-0.00151	0.00569
12	11.0, 12.0, 13.0	0.83819	0.28403	-0.00181	0.00403
13	14.0, 15.0, 16.0	0.83769	0.28195	-0.00231	0.00195
14	17.0, 18.0, 19.0	0.83676	0.27884	-0.00324	-0.00116

Chapter 3
Microstrip linear array

3.1 Introduction

This chapter aims at investigating the effect of mutual coupling between the array elements on the phase centre movement under different scan conditions. The mutual coupling between the elements is derived, utilizing the reaction theorem, and the modal expansion technique. The formulation is subsequently applied to study the phase centre movement, due to element failures with and without the mutual coupling. Also, computer simulation tests are performed to generate numerical results, due to random errors representing the material and environmental tolerances, and the excitation errors. The reason for selecting a microstrip antenna array in this chapter is the fact that, their mutual coupling can be computed more accurately. This enables us to investigate precisely the mutual coupling effects on the phase centre movement.

3.2 A rectangular microstrip patch

In this section we first present the necessary relations for the radiation patterns of rectangular microstrip antennas. The derivation of mutual coupling is presented in the next section. Consider the geometry shown in Fig. 3.1, the radiation pattern of the patch for the dominant mode (e.g. m =0 , n = 1) is given by [14]

$$E_\theta = j \frac{4 V^a}{\lambda_0} \left(\frac{e^{-jk_0R}}{R}\right) \cdot \sin\left(\frac{k_0 a}{2} \cos\phi \sin\theta\right) \cos\phi \sin\theta \cdot \left\{ \frac{1}{k_0^2 \cos^2\phi \sin^2\theta} + \frac{1}{k_0^2 \sin^2\phi \sin^2\theta - \left(\frac{\pi}{b}\right)^2} \right\} \tag{3.1}$$

$$E_\phi = j \frac{4 V^a}{\lambda_0} \left(\frac{e^{-jk_0 R}}{R}\right) \cdot \sin\left(\frac{k_0 a}{2} \cos\phi \sin\theta\right) \cos\theta \cdot \left\{ \frac{1}{k_0^2 \sin^2\theta} - \frac{\sin^2\phi}{k_0^2 \sin^2\phi \sin^2\theta - \left(\frac{\pi}{b}\right)^2} \right\} \tag{3.2}$$

where a , b are the patch dimensions, y_0 is feed point location, k_0 is free space propagation constant, and V^a is the aperture voltage defined as

$$V^a = V^s / \cos(\pi y_0 / b) \tag{3.3}$$

with V^s representing the voltage at the source location.

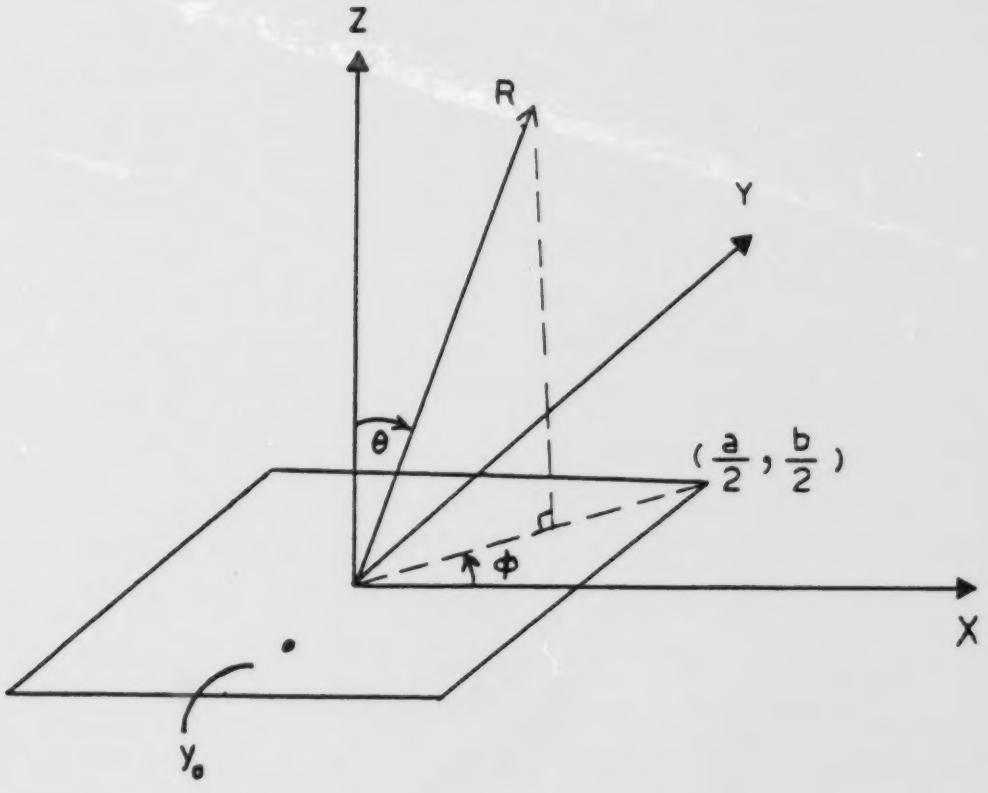

Fig. 3.1 coordinate system of rectangular patch antenna.

3.3 Mutual coupling effect

When an element radiates in the environment of some other neighboring radiating sources, its performance is affected considerably, due to the mutual coupling effect between them. The effective voltage at the antenna input, responsible for radiation, depends upon the active input impedance of the antenna. This is due to the fact that, the applied voltage is shared by the source internal impedance and the active input impedance of the antenna. Hence, developing expressions for the effective voltage, and active input impedance of each element, in the array becomes essential.

To formulate the problem, each element is considered to be excited separately with a non ideal voltage source, to assess the beam steering capability. Each element is modeled as a lumped load connected in series with the source internal resistance as shown in Fig. 3.2. The lumped loads represent the input impedance of the elements. Let I_i^a represent the current supplied by the source voltage V_i^s, whose internal impedance is Z_i^s, at the i^{th} radiating element. Also, V_i^a be the effective voltage at the input terminal of the i^{th} element. The current I_i^a is linearly related to the effective voltage V_j^a by

$$I_i^a = Y_{i1}\, V_1^a + \cdots + Y_{iN}\, V_N^a \qquad , \; i = 1, 2, \cdots N \tag{3.4}$$

where Y_{ij} is the mutual admittance. Equation (3.4) is a matrix equation which can be rewritten as,

$$\left[I_i^a \right] = \left[Y_{ij} \right] \left[V_j^a \right] \quad , \; j = 1, 2, ..., N \tag{3.5}$$

here, $\left[I_i^a \right]$ and $\left[V_j^a \right]$ are column matrices with N rows, and $\left[Y_{ij} \right]$ is an $N \times N$ square matrix. From Fig. 3.2, V_i^s , V_i^a and I_i^a are related by Kirchoff's law as,

$$I_i^a = \frac{V_i^s - V_i^a}{Z_i^s} \tag{3.6}$$

A substitution of (3.6) in (3.5) results in a matrix equation of the form,

$$\left[V_i^s \right] = \left[Y_{ij}\, Z_i^s + \delta_{ij} \right] \left[V_i^a \right] \tag{3.7}$$

or,

$$\left[V^a \right] = \left[B \right]^{-1} \left[V^s \right] \tag{3.8.a)}$$

where

$$B = \left[Y_{ij}\, Z_i^s + \delta_{ij} \right] \qquad (3.8.b)$$

$$\delta_{ij} = 1 \quad , \; i = j \qquad (3.8.c)$$

$$= 0 \quad , \; i = j \qquad (3.8.d)$$

Equation (3.8) is a system of linear equation which can be solved numerically. However, one needs first to find a proper relation for the admittances, Y_{ij}. In the next section a procedure is outlined to accomplish this task.

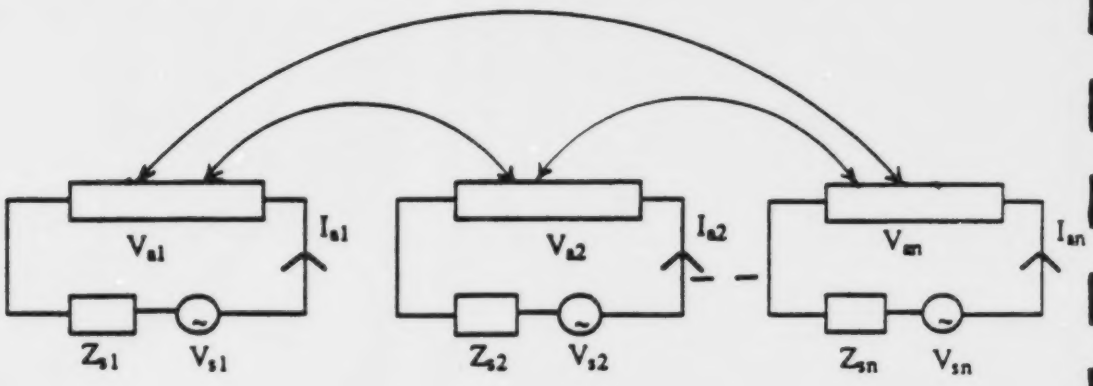

Fig. 3.2 : An array of N-elements, with its equivalent circuit representation.

3.3.1 Mutual admittance of two patches (off diagonal elements)

Two identical rectangular patches i and j are shown in Fig. 3.3. The physical dimensions of each patch are $a \times b$. The feed points for i and j patches are located at distances y_{oi} and y_{0j} from the edges, respectively. According to the cavity model the patch is considered to be a cavity with a magnetic wall near its periphery. The magnetic wall is placed a small distance away from the physical contour of the patch, so that the effective dimension of the rectangular cavity becomes $a_e \times b_e$ where,

$$a_e = a + 2\,\Delta l_1 \qquad , \; b_e = b + 2\,\Delta l_2 \tag{3.9.a)}$$

and Δl_1 is defined as [15]

$$\Delta l_1 = 0.41\, h\, \frac{(\varepsilon_e + 0.3)\,(\frac{b}{h} + 0.264)}{(\varepsilon_e - 0.258)(\frac{b}{h} + 0.8)} \tag{3.9.b}$$

with

$$\varepsilon_e = \frac{\varepsilon_r + 1}{2} + \frac{\varepsilon_r - 1}{2}\,(1.0 + \frac{12h}{b})^{\frac{-1}{2}} \tag{3.9.c}$$

In the above, h is the substrate thickness and ε_r is the relative dielectric constant of the substrate. A similar expression for Δl_2 can be obtained by replacing b with a.

By virtue of the reaction concept, the mutual admittance between the two patches can be defined by [16]

$$Y_{ij} = \frac{1}{2}\,\frac{< i\ ,\ j >}{V_i\ V_j} \tag{3.10}$$

where $< i\ ,\ j >$ is the mutual reaction normalized with respect to the aperture voltage. It is defined by the following reaction integral,

$$< i\ ,\ j > = -\int_{c_j} \overline{H_{ij}} \cdot \overline{M_j}\ dl_j \tag{3.11}$$

where, $\overline{H_{ij}}$ is the magnetic field produced by the i^{th} antenna near the location of j^{th} antenna, $\overline{M_j}$ is the equivalent magnetic current at the j^{th} antenna which takes the form of

$$\overline{M_j} = m_{jx}(x', y')\,\hat{x} + m_{jy}(x', y')\,\hat{y} \tag{3.12}$$

and m_{jx} , m_{jy} are the x- and y- directed magnetic line currents on the aperture of the j^{th} antenna. After some mathematical manipulations, the reaction integral simplifies as,

$$\begin{aligned} < i\ ,\ j > = \frac{-1}{4\pi\ j\ \omega\ \mu_0} \int_{l_j}\int_{l_i} \Big\{ & m_{ix}\ m_{jx}\ \Delta_{xx} \\ & + m_{iy}\ m_{jx}\ \Delta_{xy} + m_{ix}\ m_{jx}\ (k_0^2\ \frac{e^{-jk_0 r_1}}{r_1}) \\ & + m_{ix}\ m_{jy}\ \Delta_{xy} + m_{iy}\ m_{jy}\ \Delta_{yy} \end{aligned}$$

$$+ m_{iy}\, m_{jy} \left(k_0^2 \frac{e^{-jk_0 r_1}}{r_1} \right) \Big] \, dl_i \, dl_j \qquad (3.13.a)$$

where

$$r_1^2 = | \, \bar{r} - \bar{r}' \, |^2 \qquad (3.13.b)$$

and

$$\Delta_{xx} = -\frac{e^{-jk_0 r_1}}{r_1^5} (k_o^2 r_1^2 - 3jk_o r_1 - 3)(x_i - x_j)^2 + r_1^2 \, (1 + jk_0 r_1) \qquad (3.13.c)$$

$$\Delta_{yy} = -\frac{e^{-jk_0 r_1}}{r_1^5} (k_o^2 r_1^2 - 3jk_o r_1 - 3)(y_i - y_j)^2 + r_1^2 \, (1 + jk_0 r_1) \qquad (3.13.d)$$

$$\Delta_{xy} = -\frac{e^{-jk_0 r_1}}{r_1^5} (k_o^2 r_1^2 - 3jk_o r_1 - 3)(x_i - x_j) \, (y_i - y_j) \qquad (3.13.e)$$

Equation (3.13) together with (3.10) give the mutual admittance between two patches.

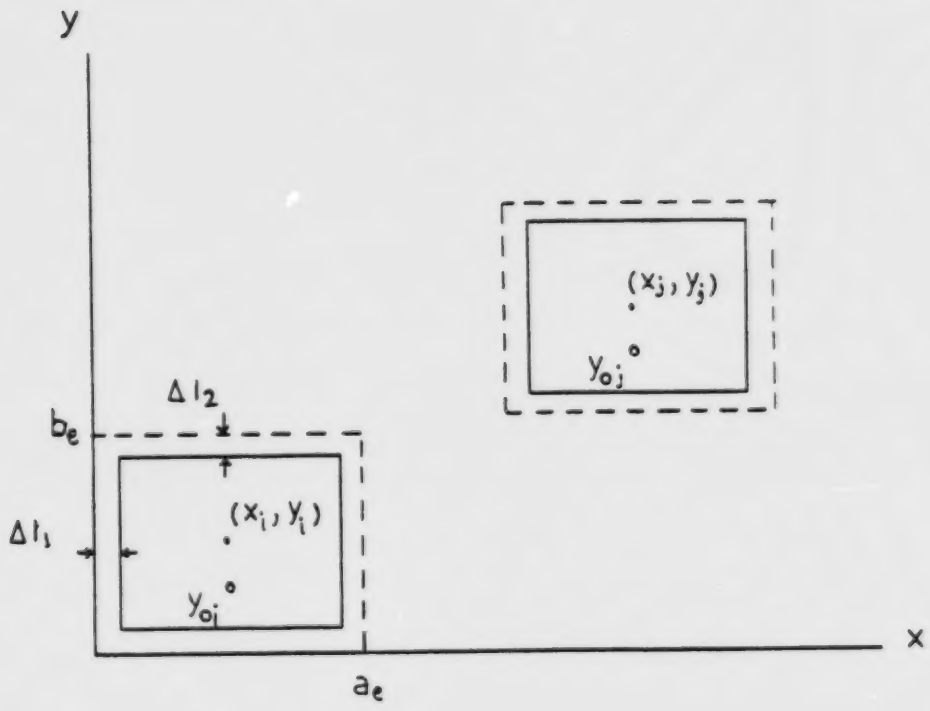

Fig. 3.3 : two identical rectangular patches with coordinate systems.

3.3.2 Self admittance (diagonal elements)

Expressions for the off diagonal terms of the matrix $[Y_{ij}]$ in equation (3.5) was derived in the previous section. The diagonal terms Y_{ji}, also known as the self admittance, is considered in this section. The self admittance of a rectangular patch can be obtained from (3.13) by setting $x_j = x_i$ and $y_j = y_i$. It should be noted that under such a condition, the value of r_1 approaches zero, which result in a singular integrand. For this type of the singularity, the integrand can be separated into real and imaginary parts, with the removable singularity of the real part, utilizing the *L'Hopital's* rule. However, for the imaginary part, the singularity is not removable and results in an undetermined value. This is due to the fact that, an infinitely thin magnetic current source (line current) was used in deriving $<i, j>$ reaction integral. In reality, the magnetic current is a surface current of width h, the thickness of substrate, which results in a finite susceptance.

Next, the modal expansion method is used to obtain an expression for the imaginary part of the integrand, i.e., B. The electric field inside the cavity ($a_e \times b_e$) can be expressed as a summation of several eigen-functions, which satisfy magnetic wall boundary conditions at $x = 0$, a_e and $y = 0$, b_e, or

$$E_z(x, y) = \sum_m \sum_n A_{mn} \cos(\frac{m\pi x}{a_e}) \cos(\frac{n\pi y}{b_e}) \tag{3.14}$$

where A_{mn} are unknown coefficients to be determined. Suppose the patch is excited at a point (x_0, y_0) with the excitation current given by

$$J_z = I_0 \, \delta(x - x_0) \, \delta(y - y_0) \tag{3.15}$$

Here, I_0 represents the excitation, and δ is the delta function defining the position of the source. The electric field E_z should satisfies the Helmholtz equation,

$$\frac{\partial^2 E_z}{\partial x^2} + \frac{\partial^2 E_z}{\partial y^2} + k_1^2 \, E_z = j\omega\mu_0 J_z^2 \tag{3.16}$$

where $k_1^2 = \omega^2 \mu_0 \varepsilon_0 \varepsilon_r$. After some mathematical manipulation, one can obtain the unknown coefficients from,

$$A_{mn} = \frac{4 \, j\omega \, \mu_0 \, I_0 \cos(\frac{m\pi x_0}{a_e}) \cos(\frac{m\pi y_0}{b_e})}{\sigma_m \sigma_n a_e b_e \, [\, k_1^2 - (\frac{m\pi}{a_e})^2 - (\frac{n\pi}{b_e})^2 \,]} \tag{3.17}$$

with

$$\sigma_0 = 0 \quad , \quad \sigma_m = 1; \; m = 0$$

For the operating frequency near the eigen frequency, the electric field given by (3.15) becomes undefined. In such cases, E_z can be approximated by,

$$E_z = \frac{2\, j\omega\, \mu_0\, I_0}{a_e\, b_e} \; \frac{\cos(\frac{\pi\, x_0}{a_e})\, \cos(\frac{\pi\, x}{a_e})}{[\, k_1^2 - (\frac{\pi}{a_e})^2\,]} \tag{3.18}$$

where, the impedance seen by the source I_0 is defined as,

$$\frac{1}{j\, B} = Z_{cavity} = \frac{-\, h\; E_z(x_0, y_0)}{I_0} \tag{3.19.a}$$

$$= \frac{-\, 2\, j\omega\, \mu_0\, h}{a_e\, b_e} \; \frac{\cos^2(\frac{\pi x_0}{a_e})}{[\, k_1^2 - (\frac{\pi}{a_e})^2\,]} \tag{3.19.b}$$

Since the cavity is assumed lossless, the impedance becomes purely reactive, as it is expected. The patch, however, radiates energy and the input impedance should have a real part which accounts for the radiation loss. In order to incorporate the radiation loss, a conductance is added in parallel with the susceptance jB. Its value is proportional to the radiation conductance of the aperture and can be obtained by determining the self reaction of the aperture. Hence,

$$G = \frac{Real\langle i, j\rangle}{2\, \cos^2(\frac{\pi x_0}{a_e})} \tag{3.20}$$

and $\langle i, j\rangle$ represents the self reaction of the aperture normalized to the feed voltage as defined before.

3.4 Numerical results

Consider the linear array of microstrip patches shown in Fig. 2.5. Here, the amplitude distribution is assumed to be $-30\ dB$ Taylor distribution with 56 rectangular microstrip patches ($\varepsilon_r = 2.33$). The interelement spacing d is 0.593 λ at the centre frequency of 5.06 GHz. The feed point is located at the patch edge. The phase centre is calculated in the $xz-plane$ ($\phi = 0^o$), for different scan angles ranging from -40^o to

+40°. Both the phase centre cartesian coordinates (x_o, z_o) and the polar ones (r_o, δ) are recorded for convenience. Also, the phase has been calculated with respect to the computed phase centre and shown to be nearly constant with variations represented by Dp, in the provided tables.

Several computer simulation runs are performed to investigate the effect of mutual coupling between the elements. First, an *IMSL* routine is used to generate random numbers, for different scan angles, θ_s. The details are provided in the next chapter. Second, several antenna elements are considered to have zero amplitude or phase, portraying the case of total amplitude or phase shifter failure.

The generated results are tabulated in table 3.1 to 3.17. In the case of amplitude failure, the phase centre is moved about 0.4 λ for a failure in elements number 1 to 4, and about 0.84 λ, for a failure in elements 13 to 16 at a scan angle of 23 degrees.

From table 3.13 to 3.18 one can observe that the phase shifter failure has more drastic effects on the phase centre displacement from the antenna physical centre. It is about 8.0 λ for failure in elements 25 to 28 at a scan angle of 13 degrees, and 5.82 λ for failure in elements 1 to 4 at a scan angle of 14 degrees.

The effect of mutual coupling is quite insignificant where, the generated results indicate that, the contribution of coupling between the elements result in a fractional change in the phase centre location. For the simulated cases presented here, the addition of mutual coupling results in a change in the location of phase centre by less than 2.0% at different scan angles.

3.5 Discussion

A relation for the mutual coupling between the elements of microstrip patches was derived. The formulation was based on reaction concept, to obtain the mutual admittances of adjacent patches. A mode matching technique was used to remove the singularity for the self admittances. The technique was subsequently applied to investigate the contribution of mutual coupling by introducing random errors, and amplitude and phase shifter failures. It was found that the contribution of mutual coupling is insignificant and for all the cases presented, the difference in the phase centre movement was generally less than 2.0%, when the coupling was included.

Table 3.1

Phase centre and phase variation (Dp-deg.) of a 56-element linear array in H-plane for different scan angles. Random error in amplitude excitation with standard deviation 5%, Mutual coupling between array elements is not included.

Scan Angle	Cartezian coords.		polar coords.		Dp, deg.	
(deg.)	x0/λ	z0/λ	r0/λ	delta-deg.	Min.	Max.
-40.	-0.0817	0.0081	0.0821	174.3380	-0.0140 :	0.0144
-39.	-0.1327	0.0157	0.1336	173.2569	-0.0278 :	0.0286
-38.	0.0417	-0.0108	0.0431	-14.5419	-0.0198 :	0.0193
-37.	0.0465	-0.0048	0.0467	-5.9046	-0.0088 :	0.0086
-36.	-0.1176	0.0063	0.1178	176.9213	-0.0122 :	0.0125
-35.	-0.0300	0.0016	0.0301	176.9643	-0.0030 :	0.0031
-34.	-0.1122	0.0091	0.1126	175.3745	-0.0181 :	0.0185
-33.	-0.0517	0.0074	0.0522	171.8114	-0.0154 :	0.0157
-32.	0.0017	0.0053	0.0055	71.7459	-0.0103 :	0.0106
-31.	0.0383	-0.0007	0.0383	-0.9972	-0.0015 :	0.0015
-30.	0.0139	-0.0079	0.0160	-29.6729	-0.0176 :	0.0173
-29.	0.0210	0.0013	0.0210	3.6344	-0.0026 :	0.0026
-28.	0.0755	-0.0033	0.0756	-2.4867	-0.0082 :	0.0080
-27.	0.0972	-0.0067	0.0974	-3.9175	-0.0168 :	0.0165
-26.	-0.0358	0.0038	0.0360	173.9482	-0.0091 :	0.0093
-25.	0.0391	-0.0008	0.0391	-1.1316	-0.0018 :	0.0018
-24.	0.1078	-0.0145	0.1088	-7.6781	-0.0393 :	0.0387
-23.	-0.0237	-0.0026	0.0239	-173.7017	-0.0074 :	0.0073
-22.	-0.0612	0.0001	0.0612	179.8992	-0.0003 :	0.0003
-21.	0.0261	-0.0131	0.0292	-26.6440	-0.0398 :	0.0393
-20.	-0.0373	-0.0026	0.0374	-175.9698	-0.0075 :	0.0074
-19.	0.0445	-0.0041	0.0446	-5.2112	-0.0132 :	0.0130
-18.	-0.0357	0.0019	0.0358	176.9306	-0.0065 :	0.0066
-17.	0.0228	0.0037	0.0231	9.2353	-0.0128 :	0.0130
-16.	-0.0134	0.0056	0.0146	157.2417	-0.0213 :	0.0216
-15.	-0.0744	0.0120	0.0754	170.8724	-0.0487 :	0.0492
-14.	-0.0099	0.0009	0.0100	174.6329	-0.0047 :	0.0048
-13.	0.0720	-0.0024	0.0720	-1.9167	-0.0124 :	0.0123
-12.	-0.0023	-0.0019	0.0030	-141.0363	-0.0103 :	0.0102
-11.	-0.0370	-0.0035	0.0372	-174.5694	-0.0182 :	0.0181
-10.	-0.0407	0.0026	0.0408	176.3248	-0.0159 :	0.0160
-9.	-0.0158	-0.0021	0.0159	-172.6064	-0.0135 :	0.0134
-8.	-0.0366	0.0061	0.0371	170.4638	-0.0463 :	0.0465
-7.	0.0274	0.0020	0.0275	4.1747	-0.0161 :	0.0162
-6.	0.0127	0.0013	0.0128	5.8331	-0.0140 :	0.0141
-5.	0.0392	-0.0025	0.0393	-3.7097	-0.0315 :	0.0314
-4.	0.0065	-0.0015	0.0066	-13.0268	-0.0227 :	0.0226
-3.	-0.0791	0.0013	0.0791	179.0227	-0.0275 :	0.0276
-2.	0.0154	-0.0015	0.0155	-5.4524	-0.0437 :	0.0436
-1.	0.0546	-0.0002	0.0546	-0.1736	-0.0099 :	0.0099

Table 3.1 - Cont.

Scan Angle	Cartezian coords.		polar coords.		Dp, deg.	
(deg.)	x0/λ	z0/λ	r0/λ	delta-deg.	Min.	Max.
0.	-0.1388	-0.0000	0.1388	-180.0000	-0.0772 :	0.0772
1.	0.0443	0.0002	0.0443	0.3069	-0.0148 :	0.0148
2.	0.0102	0.0004	0.0102	2.4221	-0.0121 :	0.0121
3.	0.0386	0.0012	0.0386	1.7170	-0.0238 :	0.0239
4.	-0.0652	-0.0017	0.0652	-178.4993	-0.0263 :	0.0262
5.	-0.0619	-0.0027	0.0619	-177.5010	-0.0340 :	0.0339
6.	-0.0718	-0.0003	0.0718	-179.7414	-0.0036 :	0.0036
7.	-0.0780	-0.0033	0.0780	-177.5741	-0.0299 :	0.0298
8.	0.0685	0.0024	0.0685	1.9850	-0.0179 :	0.0180
9.	-0.0083	0.0023	0.0086	164.6102	-0.0152 :	0.0152
10.	-0.0856	-0.0040	0.0857	-177.3563	-0.0252 :	0.0251
11.	0.0504	-0.0007	0.0504	-0.7966	-0.0028 :	0.0028
12.	0.0130	0.0007	0.0130	3.2167	-0.0036 :	0.0036
13.	0.0795	0.0040	0.0796	2.8498	-0.0192 :	0.0193
14.	-0.0336	-0.0001	0.0336	-179.7753	-0.0009 :	0.0009
15.	0.0460	0.0063	0.0464	7.7926	-0.0260 :	0.0263
16.	-0.0754	-0.0033	0.0754	-177.4762	-0.0134 :	0.0133
17.	0.0380	0.0011	0.0380	1.6882	-0.0040 :	0.0040
18.	0.0895	0.0085	0.0899	5.4089	-0.0303 :	0.0307
19.	0.0246	0.0042	0.0250	9.5731	-0.0139 :	0.0141
20.	-0.0221	-0.0053	0.0227	-166.4819	-0.0167 :	0.0165
21.	-0.0122	0.0058	0.0135	154.5919	-0.0171 :	0.0173
22.	0.0231	0.0073	0.0242	17.5237	-0.0208 :	0.0211
23.	-0.0421	-0.0076	0.0428	-169.7937	-0.0218 :	0.0215
24.	-0.0886	-0.0082	0.0890	-174.6874	-0.0217 :	0.0214
25.	-0.0208	0.0008	0.0208	177.6643	-0.0020 :	0.0020
26.	-0.0086	0.0050	0.0100	149.6384	-0.0126 :	0.0128
27.	-0.0078	0.0034	0.0085	156.8526	-0.0079 :	0.0081
28.	0.0297	0.0140	0.0328	25.3272	-0.0323 :	0.0329
29.	0.0313	-0.0006	0.0314	-1.1405	-0.0009 :	0.0009
30.	0.0647	0.0071	0.0651	6.3057	-0.0158 :	0.0161
31.	-0.0239	-0.0086	0.0254	-160.0911	-0.0185 :	0.0181
32.	-0.0554	-0.0053	0.0556	-174.5305	-0.0112 :	0.0109
33.	0.0274	-0.0023	0.0275	-4.7528	-0.0045 :	0.0044
34.	-0.0712	-0.0056	0.0714	-175.5172	-0.0114 :	0.0111
35.	0.0001	0.0044	0.0044	88.5190	-0.0085 :	0.0087
36.	-0.0050	-0.0003	0.0050	-176.3319	-0.0005 :	0.0005
37.	0.0281	0.0088	0.0294	17.3528	-0.0159 :	0.0164
38.	0.0178	0.0060	0.0188	18.5388	-0.0108 :	0.0111
39.	-0.0028	0.0010	0.0030	161.0297	-0.0019 :	0.0019
40.	-0.0817	-0.0140	0.0829	-170.2938	-0.0249 :	0.0242

Table 3.2 - Cont.

Scan Angle	Cartezian coords.		polar coords.		Dp, deg.	
(deg.)	x0/λ	z0/λ	r0/λ	delta-deg.	Min.	Max.
0.	-0.1387	0.0078	0.1389	176.7621	-0.0772 :	0.0772
1.	0.0443	0.0121	0.0459	15.2963	-0.0149 :	0.0150
2.	0.0094	-0.0182	0.0204	-62.7434	-0.0122 :	0.0122
3.	0.0381	-0.0115	0.0398	-16.8611	-0.0238 :	0.0238
4.	-0.0640	0.0154	0.0658	166.4985	-0.0263 :	0.0262
5.	-0.0618	0.0011	0.0618	179.0152	-0.0338 :	0.0338
6.	-0.0740	-0.0205	0.0768	-164.5046	-0.0035 :	0.0035
7.	-0.0777	-0.0024	0.0777	-178.2054	-0.0300 :	0.0299
8.	0.0712	0.0226	0.0747	17.5902	-0.0179 :	0.0181
9.	-0.0094	-0.0029	0.0098	-162.7013	-0.0153 :	0.0154
10.	-0.0883	-0.0196	0.0905	-167.4752	-0.0252 :	0.0251
11.	0.0529	0.0116	0.0542	12.3828	-0.0029 :	0.0029
12.	0.0165	0.0185	0.0248	48.1630	-0.0037 :	0.0038
13.	0.0769	-0.0065	0.0772	-4.8323	-0.0193 :	0.0194
14.	-0.0356	-0.0084	0.0366	-166.6811	-0.0009 :	0.0009
15.	0.0513	0.0261	0.0576	26.9219	-0.0260 :	0.0263
16.	-0.0719	0.0097	0.0726	172.3096	-0.0133 :	0.0132
17.	0.0342	-0.0105	0.0358	-17.0322	-0.0040 :	0.0041
18.	0.0892	0.0073	0.0895	4.6550	-0.0302 :	0.0306
19.	0.0323	0.0268	0.0420	39.6805	-0.0139 :	0.0141
20.	-0.0192	0.0037	0.0196	168.9578	-0.0166 :	0.0164
21.	-0.0165	-0.0048	0.0172	-163.6812	-0.0171 :	0.0173
22.	0.0245	0.0109	0.0268	23.8941	-0.0207 :	0.0210
23.	-0.0332	0.0139	0.0360	157.2385	-0.0218 :	0.0215
24.	-0.0862	-0.0016	0.0862	-178.9350	-0.0217 :	0.0213
25.	-0.0257	-0.0091	0.0273	-160.6127	-0.0020 :	0.0020
26.	-0.0070	0.0087	0.0111	128.9112	-0.0125 :	0.0127
27.	0.0014	0.0222	0.0223	86.3173	-0.0079 :	0.0081
28.	0.0329	0.0213	0.0392	32.9465	-0.0323 :	0.0330
29.	0.0261	-0.0092	0.0277	-19.3011	-0.0010 :	0.0009
30.	0.0650	0.0081	0.0655	7.0664	-0.0157 :	0.0160
31.	-0.0147	0.0072	0.0164	153.7643	-0.0186 :	0.0182
32.	-0.0497	0.0048	0.0499	174.5150	-0.0111 :	0.0109
33.	0.0229	-0.0084	0.0244	-20.0660	-0.0045 :	0.0044
34.	-0.0747	-0.0104	0.0754	-172.0434	-0.0114 :	0.0112
35.	0.0067	0.0142	0.0157	64.6876	-0.0084 :	0.0086
36.	0.0032	0.0117	0.0121	74.6029	-0.0005 :	0.0005
37.	0.0271	0.0084	0.0284	17.1576	-0.0159 :	0.0164
38.	0.0114	-0.0017	0.0116	-8.3588	-0.0108 :	0.0111
39.	-0.0025	0.0016	0.0029	147.5853	-0.0018 :	0.0018
40.	-0.0735	-0.0039	0.0736	-176.9986	-0.0249 :	0.0242

Table 3.2

Phase centre and phase variation (Dp-deg.) of a 56-element linear array in H-plane for different scan angles. Random error in ampliude excitation with standard deviation 5%. Mutual coupling between array elements is included.

Scan Angle	Cartezian coords.		polar coords.		Dp, deg.	
(deg.)	x0/λ	z0/λ	r0/λ	delta-deg.	Min.	Max.
-40.	-0.0797	0.0066	0.0799	175.2848	-0.0140 :	0.0144
-39.	-0.1383	0.0233	0.1403	170.4268	-0.0278 :	0.0286
-38.	0.0389	-0.0069	0.0395	-10.0833	-0.0199 :	0.0193
-37.	0.0537	-0.0140	0.0555	-14.6025	-0.0089 :	0.0087
-36.	-0.1099	-0.0035	0.1099	-178.1773	-0.0123 :	0.0125
-35.	-0.0323	0.0058	0.0328	169.7960	-0.0031 :	0.0031
-34.	-0.1177	0.0179	0.1190	171.3669	-0.0180 :	0.0184
-33.	-0.0488	0.0034	0.0489	176.0535	-0.0153 :	0.0156
-32.	0.0105	-0.0080	0.0132	-37.2919	-0.0103 :	0.0105
-31.	0.0399	-0.0023	0.0400	-3.2452	-0.0015 :	0.0015
-30.	0.0076	0.0038	0.0085	26.9033	-0.0176 :	0.0173
-29.	0.0208	0.0021	0.0209	5.6368	-0.0025 :	0.0025
-28.	0.0842	-0.0190	0.0864	-12.7337	-0.0082 :	0.0081
-27.	0.1003	-0.0117	0.1010	-6.6509	-0.0167 :	0.0164
-26.	-0.0417	0.0167	0.0449	158.1704	-0.0091 :	0.0093
-25.	0.0378	0.0021	0.0379	3.2258	-0.0019 :	0.0019
-24.	0.1153	-0.0309	0.1194	-15.0181	-0.0393 :	0.0387
-23.	-0.0204	-0.0092	0.0224	-155.6852	-0.0073 :	0.0072
-22.	-0.0663	0.0136	0.0677	168.4031	-0.0003 :	0.0003
-21.	0.0258	-0.0122	0.0285	-25.3946	-0.0399 :	0.0394
-20.	-0.0303	-0.0214	0.0371	-144.8321	-0.0076 :	0.0074
-19.	0.0468	-0.0097	0.0478	-11.7278	-0.0131 :	0.0129
-18.	-0.0401	0.0160	0.0432	158.3297	-0.0065 :	0.0066
-17.	0.0236	0.0009	0.0236	2.0768	-0.0127 :	0.0129
-16.	-0.0074	-0.0149	0.0167	-116.5713	-0.0213 :	0.0215
-15.	-0.0739	0.0110	0.0747	171.5177	-0.0488 :	0.0493
-14.	-0.0137	0.0160	0.0210	130.5927	-0.0047 :	0.0048
-13.	0.0742	-0.0128	0.0753	-9.7731	-0.0125 :	0.0124
-12.	0.0022	-0.0227	0.0228	-84.5057	-0.0102 :	0.0101
-11.	-0.0382	0.0034	0.0384	174.9248	-0.0181 :	0.0180
-10.	-0.0428	0.0133	0.0448	162.7130	-0.0158 :	0.0160
-9.	-0.0131	-0.0206	0.0244	-122.3492	-0.0136 :	0.0135
-8.	-0.0342	-0.0101	0.0357	-163.4785	-0.0464 :	0.0466
-7.	0.0258	0.0151	0.0300	30.3626	-0.0161 :	0.0162
-6.	0.0123	0.0030	0.0126	13.7869	-0.0139 :	0.0140
-5.	0.0413	-0.0274	0.0496	-33.5790	-0.0315 :	0.0314
-4.	0.0069	-0.0062	0.0093	-41.9045	-0.0226 :	0.0226
-3.	-0.0800	0.0177	0.0819	167.5558	-0.0274 :	0.0275
-2.	0.0155	-0.0116	0.0193	-36.7222	-0.0438 :	0.0438
-1.	0.0550	-0.0226	0.0595	-22.3353	-0.0099 :	0.0099

Table 3.3

Phase centre and phase variation (Dp-deg.) of a 56-element linear array in H-plane for different scan angles.
Random error in phase excitation with standard deviation 5 degrees,
Mutual coupling between array elements is not included.

Scan Angle	Cartezian coords.		polar coords.		Dp, deg.	
(deg.)	x0/λ	z0/λ	r0/λ	delta-deg.	Min.	Max.
-40.	0.8284	-0.9852	1.2872	-49.9432	-0.0018 :	0.0000
-39.	-0.4668	0.5848	0.7482	128.5958	-0.0020 :	0.0004
-38.	-1.0366	1.3176	1.6765	128.1946	-0.0019 :	0.0037
-37.	-2.7360	3.6328	4.5479	126.9844	-0.0001 :	0.0054
-36.	1.0542	-1.4625	1.8029	-54.2161	-0.0042 :	0.0004
-35.	-0.4632	0.6673	0.8123	124.7659	-0.0002 :	0.0040
-34.	-1.5681	2.3157	2.7966	124.1044	-0.0032 :	0.0025
-33.	-1.8424	2.8341	3.3804	123.0274	-0.0000 :	0.0054
-32.	-0.0985	0.1555	0.1840	122.3434	-0.0026 :	0.0003
-31.	0.7769	-1.2951	1.5103	-59.0410	-0.0043 :	0.0012
-30.	-0.9532	1.6642	1.9179	119.8022	-0.0003 :	0.0085
-29.	0.2636	-0.4573	0.5278	-60.0368	-0.0004 :	0.0057
-28.	0.5736	-1.0771	1.2203	-61.9609	-0.0058 :	0.0000
-27.	0.2949	-0.5901	0.6597	-63.4439	-0.0073 :	0.0000
-26.	1.8872	-3.8867	4.3207	-64.1005	-0.0048 :	0.0001
-25.	-0.3464	0.7519	0.8279	114.7328	-0.0001 :	0.0046
-24.	2.5485	-5.7387	6.2791	-66.0546	-0.0174 :	0.0000
-23.	-0.1684	0.3887	0.4236	113.4247	-0.0001 :	0.0064
-22.	-1.0761	2.6480	2.8583	112.1168	-0.0001 :	0.0140
-21.	2.8318	-7.3853	7.9096	-69.0216	-0.0171 :	0.0002
-20.	0.4366	-1.1905	1.2681	-69.8609	-0.0028 :	0.0000
-19.	1.0817	-3.1460	3.3268	-71.0255	-0.0092 :	0.0000
-18.	0.1165	-0.3476	0.3667	-71.4684	-0.0026 :	0.0035
-17.	-1.2020	3.9268	4.1067	107.0189	-0.0008 :	0.0103
-16.	-2.4293	8.4744	8.8157	105.9959	-0.0001 :	0.0206
-15.	-0.3934	1.4702	1.5219	104.9813	-0.0004 :	0.0132
-14.	2.4785	-9.9486	10.2527	-76.0109	-0.0337 :	0.0000
-13.	-1.1641	5.0332	5.1661	103.0229	-0.0000 :	0.0135
-12.	-0.9605	4.5106	4.6117	102.0218	-0.0002 :	0.0229
-11.	-0.3222	1.6717	1.7024	100.9091	-0.0004 :	0.0084
-10.	0.2076	-1.1841	1.2021	-80.0555	-0.0001 :	0.0025
-9.	-0.7076	4.4358	4.4919	99.0632	-0.0001 :	0.0129
-8.	0.9387	-6.7743	6.8390	-82.1105	-0.0214 :	0.0008
-7.	-0.6619	5.4883	5.5280	96.8771	-0.0014 :	0.0165
-6.	0.7988	-7.6101	7.6519	-84.0079	-0.0254 :	0.0000
-5.	0.4670	-5.3485	5.3688	-85.0096	-0.0163 :	0.0000
-4.	-0.0799	1.1125	1.1154	94.1072	-0.0000 :	0.0072
-3.	0.0595	-1.0898	1.0914	-86.8755	-0.0052 :	0.0020
-2.	-0.0469	1.3527	1.3535	91.9849	-0.0000 :	0.0063
-1.	0.1545	-8.5410	8.5424	-88.9635	-0.0223 :	0.0000

Table 3.3 - Cont.

Scan Angle	Cartezian coords.		polar coords.		Dp, deg.	
(deg.)	x0/λ	z0/λ	r0/λ	delta-deg.	Min.	Max.
0.	0.0014	-1.1328	1.1328	-89.9278	-0.0039 :	0.0004
1.	-0.0694	-4.2456	4.2462	-90.9370	-0.0138 :	0.0005
2.	0.5647	16.3139	16.3237	88.0175	-0.0000 :	0.0468
3.	-0.6004	-11.3002	11.3162	-93.0413	-0.0175 :	0.0002
4.	0.1871	2.6632	2.6698	85.9810	-0.0000 :	0.0076
5.	0.4575	5.2670	5.2868	85.0361	-0.0002 :	0.0220
6.	-0.2387	-2.1615	2.1747	-96.3028	-0.0035 :	0.0033
7.	0.6328	5.1442	5.1830	82.9869	-0.0000 :	0.0151
8.	0.1982	1.3889	1.4030	81.8770	-0.0001 :	0.0069
9.	0.0005	0.0437	0.0437	89.3331	-0.0022 :	0.0026
10.	-0.8742	-4.9970	5.0729	-99.9234	-0.0129 :	0.0000
11.	-1.8875	-9.7207	9.9023	-100.9886	-0.0262 :	0.0000
12.	0.0066	0.0799	0.0802	85.2723	-0.0027 :	0.0006
13.	-1.2006	-5.1665	5.3041	-103.0821	-0.0076 :	0.0011
14.	-0.3425	-1.3784	1.4204	-103.9548	-0.0024 :	0.0000
15.	-2.6400	-9.8801	10.2267	-104.9601	-0.0240 :	0.0000
16.	1.1593	4.0494	4.2121	74.0241	-0.0000 :	0.0191
17.	0.3656	1.1743	1.2299	72.7049	-0.0000 :	0.0152
18.	0.4501	1.3813	1.4527	71.9519	-0.0002 :	0.0047
19.	1.7799	5.1893	5.4861	71.0686	-0.0003 :	0.0155
20.	-1.1164	-3.0651	3.2621	-110.0138	-0.0086 :	0.0000
21.	0.4170	1.0780	1.1558	68.8527	-0.0027 :	0.0023
22.	0.1780	0.4301	0.4655	67.5164	-0.0080 :	0.0008
23.	3.5732	8.4078	9.1355	66.9753	-0.0000 :	0.0175
24.	0.4716	1.0536	1.1543	65.8867	-0.0009 :	0.0012
25.	-0.0317	-0.0586	0.0667	-118.4149	-0.0009 :	0.0062
26.	0.1501	0.3169	0.3506	64.6470	-0.0031 :	0.0021
27.	-0.1073	-0.2268	0.2509	-115.3331	-0.0004 :	0.0097
28.	0.0384	0.1042	0.1111	69.7890	-0.0037 :	0.0062
29.	1.9297	3.4800	3.9792	60.9913	-0.0002 :	0.0135
30.	1.7661	3.0719	3.5434	60.1045	-0.0001 :	0.0084
31.	0.5668	0.9272	1.0868	58.5633	-0.0008 :	0.0067
32.	-1.0859	-1.7480	2.0579	-121.8494	-0.0066 :	0.0000
33.	-1.2999	-1.9971	2.3829	-123.0595	-0.0055 :	0.0001
34.	-1.0792	-1.5980	1.9283	-124.0325	-0.0000 :	0.0018
35.	-1.0855	-1.5431	1.8867	-125.1234	-0.0085 :	0.0013
36.	-0.2992	-0.4128	0.5099	-125.9376	-0.0016 :	0.0000
37.	-4.0106	-5.3199	6.6623	-127.0124	-0.0133 :	0.0000
38.	-0.2760	-0.3509	0.4464	-128.1865	-0.0006 :	0.0001
39.	0.2642	0.3243	0.4183	50.8395	-0.0000 :	0.0012
40.	-0.5965	-0.7042	0.9229	-130.2664	-0.0033 :	0.0010

Table 3.4

Phase centre and phase variation (Dp-deg.) of a 56-element linear array in H-plane for different scan angles. Random error in phase excitation with standard deviation 5 degrees, Mutual coupling between array elements is included.

Scan Angle	Cartezian coords.		polar coords.		Dp, deg.	
(deg.)	x0/λ	z0/λ	r0/λ	delta-deg.	Min.	Max.
-40.	0.8298	-0.9860	1.2887	-49.9196	-0.0018 :	0.0000
-39.	-0.4718	0.5917	0.7567	128.5671	-0.0019 :	0.0006
-38.	-1.0391	1.3211	1.6807	128.1861	-0.0018 :	0.0036
-37.	-2.7290	3.6240	4.5366	126.9808	-0.0000 :	0.0054
-36.	1.0622	-1.4727	1.8158	-54.1980	-0.0042 :	0.0003
-35.	-0.4654	0.6715	0.8170	124.7276	-0.0001 :	0.0041
-34.	-1.5735	2.3243	2.8069	124.0967	-0.0032 :	0.0024
-33.	-1.8403	2.8313	3.3768	123.0236	-0.0000 :	0.0055
-32.	-0.0892	0.1414	0.1672	122.2326	-0.0026 :	0.0003
-31.	0.7785	-1.2966	1.5124	-59.0186	-0.0043 :	0.0012
-30.	-0.9594	1.6758	1.9310	119.7914	-0.0004 :	0.0084
-29.	0.2637	-0.4570	0.5276	-60.0165	-0.0004 :	0.0058
-28.	0.5822	-1.0926	1.2380	-61.9469	-0.0058 :	0.0000
-27.	0.2987	-0.5963	0.6670	-63.3919	-0.0073 :	0.0000
-26.	1.8818	-3.8747	4.3075	-64.0957	-0.0047 :	0.0001
-25.	-0.3477	0.7551	0.8313	114.7263	-0.0002 :	0.0044
-24.	2.5562	-5.7555	6.2977	-66.0525	-0.0173 :	0.0000
-23.	-0.1653	0.3824	0.4166	113.3707	-0.0002 :	0.0065
-22.	-1.0814	2.6618	2.8731	112.1106	-0.0000 :	0.0140
-21.	2.8314	-7.3843	7.9085	-69.0215	-0.0171 :	0.0001
-20.	0.4435	-1.2091	1.2879	-69.8572	-0.0029 :	0.0000
-19.	1.0839	-3.1514	3.3326	-71.0194	-0.0093 :	0.0000
-18.	0.1119	-0.3328	0.3511	-71.4220	-0.0026 :	0.0035
-17.	-1.2010	3.9234	4.1031	107.0205	-0.0008 :	0.0102
-16.	-2.4232	8.4533	8.7938	105.9954	-0.0001 :	0.0206
-15.	-0.3928	1.4688	1.5204	104.9719	-0.0004 :	0.0131
-14.	2.4748	-9.9340	10.2376	-76.0110	-0.0336 :	0.0000
-13.	-1.1617	5.0220	5.1546	103.0251	-0.0000 :	0.0136
-12.	-0.9560	4.4898	4.5904	102.0209	-0.0002 :	0.0229
-11.	-0.3232	1.6776	1.7084	100.9046	-0.0004 :	0.0083
-10.	0.2056	-1.1738	1.1917	-80.0646	-0.0001 :	0.0026
-9.	-0.7049	4.4178	4.4737	99.0660	-0.0001 :	0.0128
-8.	0.9411	-6.7902	6.8552	-82.1093	-0.0217 :	0.0006
-7.	-0.6636	5.5024	5.5423	96.8771	-0.0014 :	0.0165
-6.	0.7982	-7.6075	7.6492	-84.0100	-0.0255 :	0.0000
-5.	0.4691	-5.3734	5.3938	-85.0107	-0.0162 :	0.0000
-4.	-0.0793	1.1060	1.1088	94.1002	-0.0000 :	0.0072
-3.	0.0585	-1.0723	1.0739	-86.8786	-0.0052 :	0.0020
-2.	-0.0468	1.3435	1.3443	91.9961	-0.0000 :	0.0062
-1.	0.1550	-8.5646	8.5660	-88.9634	-0.0223 :	0.0000

Table 3.4 - Cont.

Scan Angle	Cartezian coords.		polar coords.		Dp, deg.	
(deg.)	x0/λ	z0/λ	r0/λ	delta-deg.	Min.	Max.
0.	0.0016	-1.1254	1.1254	-89.9206	-0.0040 :	0.0004
1.	-0.0694	-4.2310	4.2315	-90.9394	-0.0139 :	0.0005
2.	0.5639	16.2960	16.3058	88.0181	-0.0000 :	0.0467
3.	-0.6009	-11.3135	11.3294	-93.0405	-0.0175 :	0.0003
4.	0.1883	2.6798	2.6865	85.9800	-0.0000 :	0.0076
5.	0.4576	5.2714	5.2912	85.0387	-0.0002 :	0.0219
6.	-0.2408	-2.1807	2.1940	-96.3014	-0.0035 :	0.0032
7.	0.6330	5.1441	5.1829	82.9849	-0.0000 :	0.0152
8.	0.2009	1.4083	1.4225	81.8811	-0.0001 :	0.0069
9.	-0.0008	0.0369	0.0369	91.2497	-0.0021 :	0.0024
10.	-0.8770	-5.0129	5.0890	-99.9231	-0.0129 :	0.0000
11.	-1.8850	-9.7087	9.8900	-100.9878	-0.0261 :	0.0000
12.	0.0101	0.0972	0.0978	84.0726	-0.0026 :	0.0006
13.	-1.2036	-5.1786	5.3166	-103.0842	-0.0075 :	0.0010
14.	-0.3446	-1.3870	1.4292	-103.9518	-0.0025 :	0.0000
15.	-2.6349	-9.8611	10.2071	-104.9599	-0.0239 :	0.0000
16.	1.1624	4.0613	4.2244	74.0282	-0.0000 :	0.0192
17.	0.3620	1.1631	1.2181	72.7127	-0.0000 :	0.0152
18.	0.4498	1.3802	1.4517	71.9504	-0.0001 :	0.0046
19.	1.7872	5.2109	5.5089	71.0696	-0.0003 :	0.0156
20.	-1.1135	-3.0559	3.2524	-110.0210	-0.0086 :	0.0000
21.	0.4124	1.0667	1.1436	68.8643	-0.0027 :	0.0023
22.	0.1793	0.4335	0.4691	67.5259	-0.0079 :	0.0007
23.	3.5823	8.4299	9.1595	66.9769	-0.0000 :	0.0176
24.	0.4741	1.0605	1.1617	65.9115	-0.0008 :	0.0012
25.	-0.0365	-0.0681	0.0773	-118.1879	-0.0009 :	0.0062
26.	0.1520	0.3209	0.3551	64.6582	-0.0032 :	0.0022
27.	-0.0979	-0.2077	0.2296	-115.2518	-0.0004 :	0.0097
28.	0.0416	0.1113	0.1188	69.5357	-0.0036 :	0.0061
29.	1.9243	3.4711	3.9688	60.9971	-0.0002 :	0.0135
30.	1.7657	3.0715	3.5429	60.1074	-0.0001 :	0.0084
31.	0.5761	0.9433	1.1054	58.5854	-0.0008 :	0.0067
32.	-1.0804	-1.7383	2.0467	-121.8636	-0.0066 :	0.0000
33.	-1.3037	-2.0021	2.3891	-123.0711	-0.0055 :	0.0001
34.	-1.0829	-1.6031	1.9346	-124.0389	0.0000 :	0.0019
35.	-1.0792	-1.5338	1.8754	-125.1306	-0.0086 :	0.0014
36.	-0.2908	-0.4005	0.4949	-125.9866	-0.0016 :	0.0000
37.	-4.0118	-5.3206	6.6636	-127.0168	-0.0133 :	0.0000
38.	-0.2827	-0.3589	0.4569	-128.2217	-0.0005 :	0.0001
39.	0.2654	0.3261	0.4205	50.8591	-0.0000 :	0.0012
40.	-0.5879	-0.6936	0.9093	-130.2857	-0.0033 :	0.0011

Table 3.5

Phase centre and phase variation (Dp-deg.) of a 56-element linear array in H-plane for different scan angles.
Random error in amplitude ext. with st. deviation 5% and in phase ext. with st. deviation 5 degs.
Mutual coupling between array elements is not included.

Scan Angle	Cartezian coords.		polar coords.		Dp, deg.	
(deg.)	x0/λ	z0/λ	r0/λ	delta-deg.	Min.	Max.
-40.	0.6805	-0.8982	1.1269	-52.8501	-0.0153 :	0.0128
-39.	-0.6279	0.6354	0.8933	134.6600	-0.0274 :	0.0267
-38.	-1.1884	1.5550	1.9571	127.3893	-0.0157 :	0.0180
-37.	-2.7410	3.6963	4.6017	126.5589	-0.0041 :	0.0120
-36.	0.9141	-1.4248	1.6929	-57.3166	-0.0132 :	0.0085
-35.	-0.4359	0.5868	0.7310	126.6095	-0.0010 :	0.0072
-34.	-1.6225	2.2387	2.7648	125.9332	-0.0217 :	0.0207
-33.	-1.7984	2.6938	3.2390	123.7266	-0.0114 :	0.0200
-32.	-0.1083	0.1793	0.2095	121.1357	-0.0131 :	0.0103
-31.	0.8579	-1.3670	1.6139	-57.8879	-0.0060 :	0.0025
-30.	-0.9729	1.7151	1.9718	119.5638	-0.0140 :	0.0255
-29.	0.3224	-0.5240	0.6152	-58.3952	0.0000 :	0.0046
-28.	0.5747	-0.9404	1.1021	-58.5696	-0.0130 :	0.0041
-27.	0.3831	-0.5781	0.6935	-56.4700	-0.0236 :	0.0123
-26.	1.9780	-4.1423	4.5904	-64.4751	-0.0124 :	0.0047
-25.	-0.2142	0.5510	0.5912	111.2461	-0.0002 :	0.0053
-24.	2.7772	-6.0257	6.6349	-65.2553	-0.0526 :	0.0235
-23.	[illegible]	0.5785	0.6400	115.3150	-0.0024 :	0.0112
-22.	[illegible]	2.9435	3.2006	113.1224	-0.0000 :	0.0153
-21.	[illegible]	-7.0941	7.6054	-68.8724	-0.0527 :	0.0258
-20.	0.4597	-1.3584	1.4341	-71.3040	-0.0108 :	0.0048
-19.	1.1896	-3.3340	3.5398	-70.3633	-0.0212 :	0.0058
-18.	0.0846	-0.3583	0.3682	-76.7221	-0.0032 :	0.0042
-17.	-1.1380	3.7960	3.9629	106.6887	-0.0110 :	0.0229
-16.	-2.6045	9.0450	9.4125	106.0635	-0.0100 :	0.0428
-15.	-0.6196	2.0468	2.1385	106.8422	-0.0354 :	0.0569
-14.	2.5159	-10.1376	10.4452	-76.0622	-0.0385 :	0.0007
-13.	-1.1648	5.3443	5.4697	102.2954	-0.0054 :	0.0262
-12.	-0.9791	4.5845	4.6879	102.0553	-0.0009 :	0.0251
-11.	-0.3070	1.3995	1.4328	102.3740	-0.0161 :	0.0253
-10.	0.2201	-1.4820	1.4983	-81.5524	-0.0143 :	0.0160
-9.	-0.7434	4.5608	4.6210	99.2574	-0.0040 :	0.0229
-8.	0.9437	-7.0692	7.1319	-82.3961	-0.0686 :	0.0359
-7.	-0.6193	5.3685	5.4041	96.5806	-0.0030 :	0.0199
-6.	0.7900	-7.4031	7.4451	-83.9089	-0.0348 :	0.0028
-5.	0.5811	-6.2022	6.2294	-84.6475	-0.0449 :	0.0167
-4.	-0.0737	1.1157	1.1181	93.7795	-0.0164 :	0.0276
-3.	-0.0308	-0.8732	0.8737	-92.0170	-0.0253 :	0.0224
-2.	-0.0154	0.8961	0.8963	90.9824	-0.0395 :	0.0481
-1.	0.2058	-8.3466	8.3491	-88.5874	-0.0312 :	0.0031

Table 3.5 - Cont.

Scan Angle	Cartezian coords.		polar coords.		Dp, deg.	
(deg.)	x0/λ	z0/λ	r0/λ	delta-deg.	Min.	Max.
0.	-0.1371	-1.2139	1.2217	-96.4452	-0.0812 :	0.0759
1.	-0.0240	-4.1989	4.1989	-90.3282	-0.0285 :	0.0102
2.	0.5800	16.4660	16.4762	87.9825	-0.0006 :	0.0555
3.	-0.5776	-11.6006	11.6149	-92.8507	-0.0357 :	0.0093
4.	0.1555	3.1412	3.1450	87.1652	-0.0194 :	0.0347
5.	0.3903	5.2026	5.2172	85.7096	-0.0228 :	0.0540
6.	-0.2965	-2.0325	2.0541	-98.3006	-0.0064 :	0.0068
7.	0.5216	4.8721	4.9000	83.8889	-0.0186 :	0.0427
8.	0.2484	1.2626	1.2868	78.8687	-0.0120 :	0.0210
9.	-0.0288	-0.0856	0.0903	-108.6151	-0.0129 :	0.0124
10.	-0.8537	-4.3985	4.4806	-100.9836	-0.0354 :	0.0168
11.	-1.7596	-9.3195	9.4842	-100.6918	-0.0274 :	0.0000
12.	-0.0172	-0.0934	0.0950	-100.4230	-0.0042 :	0.0009
13.	-1.2845	-5.8679	6.0069	-102.3475	-0.0208 :	0.0103
14.	-0.3659	-1.3370	1.3861	-105.3064	-0.0033 :	0.0004
15.	-2.4086	-9.1826	9.4932	-104.6979	-0.0468 :	0.0134
16.	0.9754	3.6682	3.7957	75.1093	-0.0037 :	0.0299
17.	0.4281	1.2573	1.3282	71.1951	-0.0006 :	0.0188
18.	0.5818	1.5193	1.6269	69.0452	-0.0278 :	0.0358
19.	1.8754	5.4005	5.7168	70.8495	-0.0035 :	0.0234
20.	-1.0406	-2.8016	2.9886	-110.3762	-0.0229 :	0.0102
21.	0.3870	1.0387	1.1084	69.5661	-0.0198 :	0.0193
22.	0.1610	0.3378	0.3742	64.5241	-0.0286 :	0.0195
23.	3.6112	8.5884	9.3168	67.1944	-0.0088 :	0.0360
24.	0.4764	1.2554	1.3427	69.2184	-0.0221 :	0.0230
25.	-0.0716	-0.0981	0.1215	-126.0996	-0.0001 :	0.0044
26.	0.1058	0.2487	0.2703	66.9606	-0.0107 :	0.0095
27.	-0.0460	-0.0881	0.0994	-117.5683	-0.0052 :	0.0175
28.	0.0336	0.0543	0.0639	58.2356	-0.0266 :	0.0290
29.	1.8915	3.3543	3.8509	60.5811	-0.0002 :	0.0124
30.	2.1052	3.5538	4.1305	59.3582	-0.0081 :	0.0226
31.	0.5103	0.8649	1.0042	59.4581	-0.0126 :	0.0185
32.	-1.2436	-1.9169	2.2850	-122.9735	-0.0164 :	0.0055
33.	-1.2480	-1.9616	2.3249	-122.4646	-0.0099 :	0.0025
34.	-1.1014	-1.5307	1.8858	-125.7351	-0.0093 :	0.0125
35.	-1.0035	-1.4223	1.7407	-125.2052	-0.0093 :	0.0020
36.	-0.4070	-0.5540	0.6875	-126.3031	-0.0022 :	0.0000
37.	-4.0562	-5.4088	6.7607	-126.8671	-0.0259 :	0.0065
38.	-0.2859	-0.3807	0.4761	-126.9040	-0.0116 :	0.0111
39.	0.2701	0.3365	0.4315	51.2418	-0.0010 :	0.0028
40.	-0.5828	-0.6044	0.8396	-133.9614	-0.0279 :	0.0251

Table 3.6

Phase centre and phase variation (Dp-deg.) of a 56-element linear array in H-plane for different scan angles.
Random error in amplitude ext. with st. deviation 5% and in phase ext. with st. deviation 5 degs.
. Mutual coupling between array elements is included.

Scan Angle	Cartezian coords.		polar coords.		Dp, deg.	
(deg.)	x0/λ	z0/λ	r0/λ	delta-deg.	Min.	Max.
-40.	0.6818	-0.8989	1.1283	-52.8197	-0.0153 :	0.0128
-39.	-0.6327	0.6420	0.9014	134.5813	-0.0274 :	0.0267
-38.	-1.1910	1.5587	1.9616	127.3838	-0.0159 :	0.0179
-37.	-2.7338	3.6872	4.5901	126.5544	-0.0042 :	0.0121
-36.	0.9222	-1.4351	1.7059	-57.2737	-0.0132 :	0.0085
-35.	-0.4384	0.5913	0.7361	126.5542	-0.0011 :	0.0071
-34.	-1.6275	2.2467	2.7742	125.9193	-0.0217 :	0.0206
-33.	-1.7962	2.6909	3.2353	123.7235	-0.0113 :	0.0199
-32.	-0.0994	0.1658	0.1933	120.9365	-0.0131 :	0.0103
-31.	0.8594	-1.3684	1.6159	-57.8684	-0.0059 :	0.0025
-30.	-0.9792	1.7269	1.9852	119.5549	-0.0140 :	0.0255
-29.	0.3224	-0.5236	0.6149	-58.3769	0.0000 :	0.0045
-28.	0.5835	-0.9563	1.1202	-58.6091	-0.0131 :	0.0041
-27.	0.3866	-0.5838	0.7001	-56.4875	-0.0235 :	0.0122
-26.	1.9723	-4.1297	4.5765	-64.4716	-0.0123 :	0.0047
-25.	-0.2156	0.5542	0.5947	111.2574	-0.0003 :	0.0054
-24.	2.7848	-6.0422	6.6531	-65.2555	-0.0527 :	0.0235
-23.	-0.2706	0.5725	0.6333	115.2990	-0.0023 :	0.0112
-22.	-1.2621	2.9573	3.2153	113.1122	-0.0000 :	0.0153
-21.	2.7413	-7.0942	7.6054	-68.8724	-0.0528 :	0.0259
-20.	0.4665	-1.3767	1.4536	-71.2813	-0.0108 :	0.0048
-19.	1.1919	-3.3397	3.5460	-70.3588	-0.0211 :	0.0058
-18.	0.0801	-0.3443	0.3535	-76.8961	-0.0032 :	0.0042
-17.	-1.1370	3.7922	3.9590	106.6899	-0.0111 :	0.0227
-16.	-2.5985	9.0247	9.3913	106.0631	-0.0100 :	0.0428
-15.	-0.6189	2.0450	2.1366	106.8371	-0.0355 :	0.0570
-14.	2.5122	-10.1228	10.4298	-76.0624	-0.0385 :	0.0006
-13.	-1.1624	5.3330	5.4582	102.2959	-0.0055 :	0.0263
-12.	-0.9746	4.5639	4.6668	102.0546	-0.0009 :	0.0251
-11.	-0.3081	1.4055	1.4389	102.3623	-0.0160 :	0.0252
-10.	0.2182	-1.4721	1.4882	-81.5702	-0.0142 :	0.0159
-9.	-0.7408	4.5432	4.6032	99.2609	-0.0041 :	0.0230
-8.	0.9462	-7.0859	7.1488	-82.3943	-0.0687 :	0.0360
-7.	-0.6209	5.3820	5.4177	96.5814	-0.0031 :	0.0199
-6.	0.7895	-7.4010	7.4430	-83.9110	-0.0347 :	0.0027
-5.	0.5832	-6.2276	6.2548	-84.6499	-0.0450 :	0.0167
-4.	-0.0731	1.1092	1.1116	93.7708	-0.0163 :	0.0276
-3.	-0.0318	-0.8560	0.8566	-92.1244	-0.0251 :	0.0225
-2.	-0.0153	0.8860	0.8862	90.9888	-0.0398 :	0.0481
-1.	0.2063	-8.3701	8.3727	-88.5883	-0.0312 :	0.0031

Table 3.6 - Cont.

Scan Angle	Cartezian coords.		polar coords.		Dp, deg.	
(deg.)	x0/λ	z0/λ	r0/λ	delta-deg.	Min.	Max.
0.	-0.1370	-1.2066	1.2144	-96.4775	-0.0812 :	0.0760
1.	-0.0240	-4.1849	4.1850	-90.3287	-0.0285 :	0.0103
2.	0.5792	16.4478	16.4580	87.9831	-0.0006 :	0.0556
3.	-0.5782	-11.6137	11.6281	-92.8501	-0.0356 :	0.0092
4.	0.1567	3.1575	3.1614	87.1583	-0.0194 :	0.0347
5.	0.3904	5.2068	5.2214	85.7117	-0.0226 :	0.0539
6.	-0.2985	-2.0510	2.0726	-98.2814	-0.0064 :	0.0068
7.	0.5218	4.8721	4.9000	83.8867	-0.0187 :	0.0427
8.	0.2511	1.2819	1.3062	78.9180	-0.0120 :	0.0211
9.	-0.0302	-0.0926	0.0974	-108.0441	-0.0130 :	0.0125
10.	-0.8563	-4.4137	4.4960	-100.9796	-0.0355 :	0.0168
11.	-1.7571	-9.3079	9.4723	-100.6906	-0.0274 :	0.0000
12.	-0.0137	-0.0759	0.0772	-100.1988	-0.0042 :	0.0010
13.	-1.2875	-5.8801	6.0194	-102.3508	-0.0209 :	0.0104
14.	-0.3680	-1.3456	1.3950	-105.2947	-0.0034 :	0.0005
15.	-2.4035	-9.1633	9.4733	-104.6972	-0.0467 :	0.0134
16.	0.9785	3.6802	3.8081	75.1103	-0.0036 :	0.0299
17.	0.4246	1.2464	1.3167	71.1891	-0.0006 :	0.0189
18.	0.5814	1.5179	1.6254	69.0415	-0.0277 :	0.0358
19.	1.8830	5.4229	5.7405	70.8513	-0.0033 :	0.0235
20.	-1.0376	-2.7922	2.9788	-110.3852	-0.0228 :	0.0101
21.	0.3825	1.0278	1.0967	69.5859	-0.0198 :	0.0193
22.	0.1624	0.3416	0.3783	64.5690	-0.0285 :	0.0194
23.	3.6205	8.6108	9.3410	67.1954	-0.0088 :	0.0361
24.	0.4787	1.2618	1.3496	69.2229	-0.0221 :	0.0229
25.	-0.0764	-0.1077	0.1321	-125.3433	-0.0001 :	0.0044
26.	0.1078	0.2531	0.2751	66.9341	-0.0106 :	0.0094
27.	-0.0367	-0.0693	0.0784	-117.9376	-0.0052 :	0.0175
28.	0.0367	0.0612	0.0713	59.0599	-0.0266 :	0.0290
29.	1.8861	3.3454	3.8404	60.5860	-0.0002 :	0.0125
30.	2.1052	3.5541	4.1308	59.3607	-0.0081 :	0.0226
31.	0.5197	0.8810	1.0228	59.4657	-0.0126 :	0.0186
32.	-1.2380	-1.9070	2.2736	-122.9920	-0.0164 :	0.0054
33.	-1.2518	-1.9666	2.3313	-122.4782	-0.0099 :	0.0025
34.	-1.1052	-1.5360	1.8923	-125.7357	-0.0095 :	0.0125
35.	-0.9972	-1.4129	1.7294	-125.2136	-0.0093 :	0.0020
36.	-0.3988	-0.5419	0.6728	-126.3474	-0.0022 :	0.0000
37.	-4.0573	-5.4095	6.7620	-126.8715	-0.0259 :	0.0065
38.	-0.2927	-0.3889	0.4867	-126.9646	-0.0116 :	0.0111
39.	0.2712	0.3380	0.4334	51.2585	-0.0009 :	0.0027
40.	-0.5743	-0.5938	0.8261	-134.0435	-0.0280 :	0.0250

Table 3.7

Phase centre and phase variation (Dp-deg.) of a 56-element linear array in H-plane for different scan angles.
Complete amplitude ext. failure in elements no. 1 to 4,
Mutual coupling between array elements is not included.

Scan Angle	Cartezian coords.		polar coords.		Dp, deg.	
(deg.)	x0/λ	z0/λ	r0/λ	delta-deg.	Min.	Max.
-40.	0.4088	0.0533	0.4123	7.4301	-0.0938 :	0.0966
-39.	0.4076	0.0548	0.4113	7.6528	-0.0984 :	0.1011
-38.	0.4065	0.0562	0.4104	7.8652	-0.1029 :	0.1057
-37.	0.4056	0.0573	0.4096	8.0483	-0.1075 :	0.1103
-36.	0.4047	0.0585	0.4089	8.2282	-0.1122 :	0.1150
-35.	0.4040	0.0595	0.4083	8.3844	-0.1169 :	0.1197
-34.	0.4033	0.0605	0.4078	8.5378	-0.1216 :	0.1244
-33.	0.4028	0.0612	0.4075	8.6447	-0.1263 :	0.1292
-32.	0.4023	0.0620	0.4071	8.7638	-0.1310 :	0.1339
-31.	0.4020	0.0625	0.4069	8.8365	-0.1358 :	0.1386
-30.	0.4018	0.0628	0.4067	8.8874	-0.1405 :	0.1433
-29.	0.4017	0.0631	0.4066	8.9239	-0.1452 :	0.1480
-28.	0.4017	0.0630	0.4066	8.9155	-0.1499 :	0.1526
-27.	0.4017	0.0630	0.4066	8.9140	-0.1545 :	0.1572
-26.	0.4020	0.0625	0.4068	8.8405	-0.1591 :	0.1618
-25.	0.4022	0.0621	0.4069	8.7783	-0.1636 :	0.1662
-24.	0.4025	0.0613	0.4072	8.6549	-0.1680 :	0.1706
-23.	0.4029	0.0605	0.4074	8.5381	-0.1724 :	0.1749
-22.	0.4032	0.0596	0.4076	8.4116	-0.1766 :	0.1791
-21.	0.4038	0.0583	0.4080	8.2097	-0.1808 :	0.1832
-20.	0.4043	0.0569	0.4083	8.0131	-0.1848 :	0.1872
-19.	0.4048	0.0554	0.4086	7.7940	-0.1888 :	0.1911
-18.	0.4054	0.0536	0.4089	7.5375	-0.1926 :	0.1948
-17.	0.4060	0.0517	0.4093	7.2622	-0.1962 :	0.1984
-16.	0.4066	0.0496	0.4096	6.9596	-0.1997 :	0.2018
-15.	0.4072	0.0475	0.4099	6.6582	-0.2031 :	0.2050
-14.	0.4078	0.0450	0.4103	6.2942	-0.2063 :	0.2081
-13.	0.4085	0.0423	0.4107	5.9087	-0.2093 :	0.2110
-12.	0.4090	0.0397	0.4110	5.5395	-0.2121 :	0.2137
-11.	0.4096	0.0370	0.4113	5.1549	-0.2147 :	0.2162
-10.	0.4101	0.0339	0.4115	4.7297	-0.2172 :	0.2185
-9.	0.4106	0.0310	0.4118	4.3134	-0.2194 :	0.2206
-8.	0.4111	0.0279	0.4120	3.8782	-0.2214 :	0.2225
-7.	0.4115	0.0245	0.4123	3.4137	-0.2232 :	0.2242
-6.	0.4119	0.0213	0.4125	2.9550	-0.2248 :	0.2256
-5.	0.4122	0.0178	0.4126	2.4705	-0.2261 :	0.2268
-4.	0.4125	0.0143	0.4128	1.9850	-0.2273 :	0.2278
-3.	0.4127	0.0108	0.4129	1.5052	-0.2282 :	0.2286
-2.	0.4129	0.0073	0.4129	1.0067	-0.2288 :	0.2291
-1.	0.4130	0.0036	0.4130	0.5037	-0.2293 :	0.2294

Table 3.7 - Cont.

Scan Angle	Cartezian coords.		polar coords.		Dp, deg.	
(deg.)	x0/λ	z0/λ	r0/λ	delta-deg.	Min.	Max.
0.	0.4130	-0.0000	0.4130	-0.0000	-0.2295 :	0.2295
1.	0.4130	-0.0036	0.4130	-0.5037	-0.2294 :	0.2293
2.	0.4129	-0.0073	0.4129	-1.0067	-0.2291 :	0.2288
3.	0.4127	-0.0108	0.4129	-1.5052	-0.2286 :	0.2282
4.	0.4125	-0.0143	0.4128	-1.9850	-0.2278 :	0.2273
5.	0.4122	-0.0178	0.4126	-2.4705	-0.2268 :	0.2261
6.	0.4119	-0.0213	0.4125	-2.9550	-0.2256 :	0.2248
7.	0.4115	-0.0245	0.4123	-3.4137	-0.2242 :	0.2232
8.	0.4111	-0.0279	0.4120	-3.8782	-0.2225 :	0.2214
9.	0.4106	-0.0310	0.4118	-4.3134	-0.2206 :	0.2194
10.	0.4101	-0.0339	0.4115	-4.7297	-0.2185 :	0.2172
11.	0.4096	-0.0370	0.4113	-5.1549	-0.2162 :	0.2147
12.	0.4090	-0.0397	0.4110	-5.5395	-0.2137 :	0.2121
13.	0.4085	-0.0423	0.4107	-5.9087	-0.2110 :	0.2093
14.	0.4078	-0.0450	0.4103	-6.2942	-0.2081 :	0.2063
15.	0.4072	-0.0475	0.4099	-6.6582	-0.2050 :	0.2031
16.	0.4066	-0.0496	0.4096	-6.9596	-0.2018 :	0.1997
17.	0.4060	-0.0517	0.4093	-7.2622	-0.1984 :	0.1962
18.	0.4054	-0.0536	0.4089	-7.5375	-0.1948 :	0.1926
19.	0.4048	-0.0554	0.4086	-7.7940	-0.1911 :	0.1888
20.	0.4043	-0.0569	0.4083	-8.0131	-0.1872 :	0.1848
21.	0.4038	-0.0583	0.4080	-8.2097	-0.1832 :	0.1808
22.	0.4032	-0.0596	0.4076	-8.4116	-0.1791 :	0.1766
23.	0.4029	-0.0605	0.4074	-8.5381	-0.1749 :	0.1724
24.	0.4025	-0.0613	0.4072	-8.6549	-0.1706 :	0.1680
25.	0.4022	-0.0621	0.4069	-8.7783	-0.1662 :	0.1636
26.	0.4020	-0.0625	0.4068	-8.8405	-0.1618 :	0.1591
27.	0.4017	-0.0630	0.4066	-8.9140	-0.1572 :	0.1545
28.	0.4017	-0.0630	0.4066	-8.9155	-0.1526 :	0.1499
29.	0.4017	-0.0631	0.4066	-8.9239	-0.1480 :	0.1452
30.	0.4018	-0.0628	0.4067	-8.8874	-0.1433 :	0.1405
31.	0.4020	-0.0625	0.4069	-8.8365	-0.1386 :	0.1358
32.	0.4023	-0.0620	0.4071	-8.7638	-0.1339 :	0.1310
33.	0.4028	-0.0612	0.4075	-8.6447	-0.1292 :	0.1263
34.	0.4033	-0.0605	0.4078	-8.5378	-0.1244 :	0.1216
35.	0.4040	-0.0595	0.4083	-8.3844	-0.1197 :	0.1169
36.	0.4047	-0.0585	0.4089	-8.2282	-0.1150 :	0.1122
37.	0.4056	-0.0573	0.4096	-8.0483	-0.1103 :	0.1075
38.	0.4065	-0.0562	0.4104	-7.8652	-0.1057 :	0.1029
39.	0.4076	-0.0548	0.4113	-7.6528	-0.1011 :	0.0984
40.	0.4088	-0.0533	0.4123	-7.4301	-0.0966 :	0.0938

Table 3.8

Phase centre and phase variation (Dp-deg.) of a 56-element linear array in H-plane for different scan angles. Complete amplitude ext. failure in elements no. 1 to 4, Mutual coupling between array elements is included.

Scan Angle	Cartezian coords.		polar coords.		Dp, deg.	
(deg.)	x0/λ	z0/λ	r0/λ	delta-deg.	Min.	Max.
-40.	0.4132	0.0489	0.4161	6.7449	-0.0939 :	0.0966
-39.	0.4032	0.0609	0.4077	8.5884	-0.0984 :	0.1011
-38.	0.4055	0.0578	0.4096	8.1056	-0.1028 :	0.1056
-37.	0.4151	0.0451	0.4176	6.2031	-0.1075 :	0.1102
-36.	0.4147	0.0456	0.4172	6.2723	-0.1122 :	0.1150
-35.	0.4031	0.0618	0.4078	8.7225	-0.1169 :	0.1198
-34.	0.3979	0.0692	0.4038	9.8646	-0.1215 :	0.1244
-33.	0.4068	0.0554	0.4106	7.7596	-0.1262 :	0.1290
-32.	0.4131	0.0456	0.4156	6.3064	-0.1310 :	0.1339
-31.	0.4044	0.0597	0.4088	8.4049	-0.1358 :	0.1387
-30.	0.3953	0.0749	0.4024	10.7324	-0.1405 :	0.1433
-29.	0.4016	0.0636	0.4066	8.9970	-0.1451 :	0.1479
-28.	0.4109	0.0464	0.4135	6.4447	-0.1498 :	0.1526
-27.	0.4051	0.0575	0.4092	8.0775	-0.1546 :	0.1573
-26.	0.3954	0.0770	0.4028	11.0174	-0.1591 :	0.1618
-25.	0.4003	0.0665	0.4057	9.4348	-0.1634 :	0.1661
-24.	0.4102	0.0447	0.4126	6.2250	-0.1679 :	0.1706
-23.	0.4056	0.0552	0.4094	7.7429	-0.1725 :	0.1751
-22.	0.3966	0.0769	0.4040	10.9682	-0.1766 :	0.1792
-21.	0.4019	0.0632	0.4068	8.9397	-0.1807 :	0.1831
-20.	0.4108	0.0394	0.4127	5.4833	-0.1848 :	0.1872
-19.	0.4059	0.0533	0.4094	7.4768	-0.1889 :	0.1912
-18.	0.3990	0.0737	0.4058	10.4631	-0.1926 :	0.1948
-17.	0.4055	0.0532	0.4089	7.4698	-0.1961 :	0.1982
-16.	0.4121	0.0309	0.4132	4.2897	-0.1997 :	0.2018
-15.	0.4064	0.0516	0.4096	7.2416	-0.2032 :	0.2052
-14.	0.4026	0.0658	0.4080	9.2875	-0.2062 :	0.2081
-13.	0.4097	0.0362	0.4113	5.0429	-0.2091 :	0.2109
-12.	0.4129	0.0219	0.4135	3.0369	-0.2122 :	0.2138
-11.	0.4074	0.0494	0.4103	6.9174	-0.2149 :	0.2164
-10.	0.4070	0.0509	0.4102	7.1304	-0.2171 :	0.2185
-9.	0.4129	0.0156	0.4132	2.1662	-0.2193 :	0.2206
-8.	0.4129	0.0161	0.4132	2.2273	-0.2216 :	0.2227
-7.	0.4092	0.0445	0.4116	6.2058	-0.2233 :	0.2243
-6.	0.4109	0.0286	0.4119	3.9775	-0.2247 :	0.2255
-5.	0.4141	-0.0037	0.4141	-0.5161	-0.2262 :	0.2269
-4.	0.4127	0.0138	0.4130	1.9182	-0.2275 :	0.2280
-3.	0.4115	0.0332	0.4129	4.6156	-0.2282 :	0.2286
-2.	0.4129	0.0017	0.4129	0.2315	-0.2287 :	0.2290
-1.	0.4134	-0.0163	0.4137	-2.2625	-0.2294 :	0.2295

Table 3.8 - Cont.

Scan Angle	Cartezian coords.		polar coords.		Dp, deg.	
(deg.)	x0/λ	z0/λ	r0/λ	delta-deg.	Min.	Max.
0.	0.4132	0.0128	0.4134	1.7677	-0.2296 :	0.2296
1.	0.4132	0.0140	0.4134	1.9378	-0.2293 :	0.2292
2.	0.4122	-0.0233	0.4129	-3.2282	-0.2291 :	0.2288
3.	0.4124	-0.0209	0.4130	-2.8945	-0.2288 :	0.2283
4.	0.4142	0.0081	0.4143	1.1203	-0.2279 :	0.2274
5.	0.4128	-0.0100	0.4129	-1.3932	-0.2267 :	0.2260
6.	0.4099	-0.0403	0.4119	-5.6174	-0.2256 :	0.2248
7.	0.4123	-0.0204	0.4128	-2.8308	-0.2244 :	0.2234
8.	0.4147	-0.0027	0.4147	-0.3678	-0.2225 :	0.2214
9.	0.4101	-0.0331	0.4115	-4.6204	-0.2205 :	0.2193
10.	0.4077	-0.0483	0.4106	-6.7618	-0.2186 :	0.2173
11.	0.4131	-0.0203	0.4136	-2.8071	-0.2164 :	0.2149
12.	0.4137	-0.0175	0.4140	-2.4178	-0.2136 :	0.2120
13.	0.4064	-0.0506	0.4096	-7.0904	-0.2109 :	0.2092
14.	0.4065	-0.0509	0.4097	-7.1360	-0.2082 :	0.2064
15.	0.4137	-0.0234	0.4144	-3.2424	-0.2051 :	0.2032
16.	0.4112	-0.0328	0.4125	-4.5573	-0.2017 :	0.1997
17.	0.4027	-0.0618	0.4074	-8.7294	-0.1983 :	0.1962
18.	0.4060	-0.0519	0.4093	-7.2864	-0.1949 :	0.1927
19.	0.4138	-0.0291	0.4148	-4.0211	-0.1911 :	0.1888
20.	0.4083	-0.0447	0.4108	-6.2514	-0.1871 :	0.1848
21.	0.3998	-0.0680	0.4055	-9.6487	-0.1832 :	0.1808
22.	0.4055	-0.0541	0.4091	-7.5952	-0.1793 :	0.1768
23.	0.4133	-0.0353	0.4148	-4.8819	-0.1750 :	0.1724
24.	0.4063	-0.0517	0.4096	-7.2535	-0.1705 :	0.1679
25.	0.3976	-0.0712	0.4039	-10.1549	-0.1662 :	0.1636
26.	0.4043	-0.0576	0.4083	-8.1033	-0.1619 :	0.1592
27.	0.4127	-0.0408	0.4147	-5.6450	-0.1573 :	0.1545
28.	0.4060	-0.0538	0.4096	-7.5430	-0.1525 :	0.1498
29.	0.3964	-0.0718	0.4028	-10.2600	-0.1480 :	0.1452
30.	0.4019	-0.0622	0.4067	-8.8017	-0.1434 :	0.1406
31.	0.4122	-0.0449	0.4147	-6.2194	-0.1387 :	0.1358
32.	0.4085	-0.0511	0.4116	-7.1348	-0.1338 :	0.1310
33.	0.3977	-0.0682	0.4035	-9.7236	-0.1291 :	0.1263
34.	0.3992	-0.0662	0.4046	-9.4122	-0.1245 :	0.1216
35.	0.4107	-0.0495	0.4137	-6.8652	-0.1198 :	0.1169
36.	0.4132	-0.0460	0.4158	-6.3455	-0.1150 :	0.1121
37.	0.4036	-0.0590	0.4079	-8.3183	-0.1103 :	0.1075
38.	0.3985	-0.0657	0.4039	-9.3653	-0.1057 :	0.1029
39.	0.4070	-0.0553	0.4107	-7.7316	-0.1012 :	0.0984
40.	0.4166	-0.0435	0.4189	-5.9677	-0.0966 :	0.0939

Table 3.9

Phase centre and phase variation (Dp-deg.) of a 56-element linear array in H-plane for different scan angles.
Complete amplitude ext. failure in elements no. 13 to 16,
Mutual coupling between array elements is not included.

Scan Angle	Cartezian coords.		polar coords.		Dp, deg.	
(deg.)	x0/λ	z0/λ	r0/λ	delta-deg.	Min.	Max.
-40.	0.8206	-0.0946	0.8260	-6.5771	-0.1711 :	0.1664
-39.	0.8227	-0.0972	0.8284	-6.7369	-0.1792 :	0.1744
-38.	0.8246	-0.0996	0.8306	-6.8878	-0.1874 :	0.1825
-37.	0.8264	-0.1019	0.8326	-7.0281	-0.1956 :	0.1907
-36.	0.8279	-0.1039	0.8344	-7.1550	-0.2039 :	0.1989
-35.	0.8292	-0.1057	0.8359	-7.2655	-0.2123 :	0.2073
-34.	0.8303	-0.1074	0.8372	-7.3680	-0.2207 :	0.2157
-33.	0.8312	-0.1088	0.8383	-7.4537	-0.2291 :	0.2241
-32.	0.8320	-0.1100	0.8393	-7.5298	-0.2375 :	0.2325
-31.	0.8325	-0.1108	0.8399	-7.5812	-0.2459 :	0.2409
-30.	0.8329	-0.1113	0.8403	-7.6129	-0.2543 :	0.2493
-29.	0.8331	-0.1118	0.8406	-7.6448	-0.2626 :	0.2576
-28.	0.8331	-0.1117	0.8406	-7.6398	-0.2709 :	0.2659
-27.	0.8331	-0.1116	0.8405	-7.6325	-0.2790 :	0.2742
-26.	0.8327	-0.1110	0.8401	-7.5902	-0.2871 :	0.2823
-25.	0.8324	-0.1102	0.8396	-7.5393	-0.2950 :	0.2903
-24.	0.8318	-0.1089	0.8389	-7.4575	-0.3029 :	0.2982
-23.	0.8312	-0.1074	0.8381	-7.3645	-0.3105 :	0.3060
-22.	0.8305	-0.1057	0.8372	-7.2567	-0.3180 :	0.3135
-21.	0.8296	-0.1035	0.8360	-7.1109	-0.3253 :	0.3209
-20.	0.8287	-0.1011	0.8349	-6.9580	-0.3323 :	0.3281
-19.	0.8277	-0.0984	0.8336	-6.7778	-0.3392 :	0.3351
-18.	0.8267	-0.0954	0.8322	-6.5797	-0.3458 :	0.3419
-17.	0.8256	-0.0919	0.8307	-6.3482	-0.3521 :	0.3484
-16.	0.8246	-0.0882	0.8293	-6.1041	-0.3582 :	0.3546
-15.	0.8235	-0.0843	0.8278	-5.8455	-0.3640 :	0.3606
-14.	0.8224	-0.0800	0.8263	-5.5529	-0.3694 :	0.3662
-13.	0.8213	-0.0754	0.8248	-5.2465	-0.3746 :	0.3716
-12.	0.8203	-0.0707	0.8233	-4.9272	-0.3794 :	0.3766
-11.	0.8193	-0.0658	0.8219	-4.5947	-0.3839 :	0.3812
-10.	0.8183	-0.0606	0.8205	-4.2319	-0.3880 :	0.3856
-9.	0.8174	-0.0551	0.8193	-3.8593	-0.3917 :	0.3895
-8.	0.8166	-0.0494	0.8181	-3.4636	-0.3950 :	0.3931
-7.	0.8158	-0.0436	0.8170	-3.0561	-0.3980 :	0.3963
-6.	0.8151	-0.0377	0.8160	-2.6470	-0.4006 :	0.3991
-5.	0.8145	-0.0315	0.8151	-2.2167	-0.4027 :	0.4015
-4.	0.8141	-0.0254	0.8145	-1.7837	-0.4045 :	0.4035
-3.	0.8137	-0.0192	0.8139	-1.3543	-0.4059 :	0.4051
-2.	0.8134	-0.0129	0.8135	-0.9060	-0.4068 :	0.4063
-1.	0.8132	-0.0064	0.8133	-0.4537	-0.4073 :	0.4070

Table 3.9 - Cont.

Scan Angle	Cartezian coords.		polar coords.		Dp. deg.	
(deg.)	x0/λ	z0/λ	r0/λ	delta-deg.	Min.	Max.
0.	0.8132	-0.0000	0.8132	-0.0000	-0.4074	0.4074
1.	0.8132	0.0064	0.8133	0.4537	-0.4070	0.4073
2.	0.8134	0.0129	0.8135	0.9060	-0.4063	0.4068
3.	0.8137	0.0192	0.8139	1.3543	-0.4051	0.4059
4.	0.8141	0.0254	0.8145	1.7837	-0.4035	0.4045
5.	0.8145	0.0315	0.8151	2.2167	-0.4015	0.4027
6.	0.8151	0.0377	0.8160	2.6470	-0.3991	0.4006
7.	0.8158	0.0436	0.8170	3.0561	-0.3963	0.3980
8.	0.8166	0.0494	0.8181	3.4636	-0.3931	0.3950
9.	0.8174	0.0551	0.8193	3.8593	-0.3895	0.3917
10.	0.8183	0.0606	0.8205	4.2319	-0.3856	0.3880
11.	0.8193	0.0658	0.8219	4.5947	-0.3812	0.3839
12.	0.8203	0.0707	0.8233	4.9272	-0.3766	0.3794
13.	0.8213	0.0754	0.8248	5.2465	-0.3716	0.3746
14.	0.8224	0.0800	0.8263	5.5529	-0.3662	0.3694
15.	0.8235	0.0843	0.8278	5.8455	-0.3606	0.3640
16.	0.8246	0.0882	0.8293	6.1041	-0.3546	0.3582
17.	0.8256	0.0919	0.8307	6.3482	-0.3484	0.3521
18.	0.8267	0.0954	0.8322	6.5797	-0.3419	0.3458
19.	0.8277	0.0984	0.8336	6.7778	-0.3351	0.3392
20.	0.8287	0.1011	0.8349	6.9580	-0.3281	0.3323
21.	0.8296	0.1035	0.8360	7.1109	-0.3209	0.3253
22.	0.8305	0.1057	0.8372	7.2567	-0.3135	0.3180
23.	0.8312	0.1074	0.8381	7.3645	-0.3060	0.3105
24.	0.8318	0.1089	0.8389	7.4575	-0.2982	0.3029
25.	0.8324	0.1102	0.8396	7.5393	-0.2903	0.2950
26.	0.8327	0.1110	0.8401	7.5902	-0.2823	0.2871
27.	0.8331	0.1116	0.8405	7.6325	-0.2742	0.2790
28.	0.8331	0.1117	0.8406	7.6398	-0.2659	0.2709
29.	0.8331	0.1118	0.8406	7.6448	-0.2576	0.2626
30.	0.8329	0.1113	0.8403	7.6129	-0.2493	0.2543
31.	0.8325	0.1108	0.8399	7.5812	-0.2409	0.2459
32.	0.8320	0.1100	0.8393	7.5298	-0.2325	0.2375
33.	0.8312	0.1088	0.8383	7.4537	-0.2241	0.2291
34.	0.8303	0.1074	0.8372	7.3680	-0.2157	0.2207
35.	0.8292	0.1057	0.8359	7.2655	-0.2073	0.2123
36.	0.8279	0.1039	0.8344	7.1550	-0.1989	0.2039
37.	0.8264	0.1019	0.8326	7.0281	-0.1907	0.1956
38.	0.8246	0.0996	0.8306	6.8878	-0.1825	0.1874
39.	0.8227	0.0972	0.8284	6.7369	-0.1744	0.1792
40.	0.8206	0.0946	0.8260	6.5771	-0.1664	0.1711

Table 3.10

Phase centre and phase variation (Dp-deg.) of a 56-element linear array in H-plane for different scan angles. Complete amplitude ext. failure in elements no. 13 to 16, Mutual coupling between array elements is included.

Scan Angle	Cartezian coords.		polar coords.		Dp, deg.	
(deg.)	x0/λ	z0/λ	r0/λ	delta-deg.	Min.	Max.
-40.	0.8223	-0.0958	0.8279	-6.6459	-0.1711 :	0.1663
-39.	0.8150	-0.0870	0.8197	-6.0954	-0.1792 :	0.1744
-38.	0.8209	-0.0945	0.8263	-6.5637	-0.1875 :	0.1826
-37.	0.8342	-0.1118	0.8417	-7.6355	-0.1957 :	0.1907
-36.	0.8365	-0.1148	0.8443	-7.8176	-0.2039 :	0.1989
-35.	0.8261	-0.1003	0.8322	-6.9251	-0.2122 :	0.2072
-34.	0.8226	-0.0954	0.8281	-6.6127	-0.2207 :	0.2157
-33.	0.8341	-0.1127	0.8417	-7.6974	-0.2292 :	0.2242
-32.	0.8424	-0.1258	0.8518	-8.4931	-0.2375 :	0.2325
-31.	0.8341	-0.1122	0.8416	-7.6601	-0.2458 :	0.2408
-30.	0.8250	-0.0969	0.8307	-6.7010	-0.2543 :	0.2493
-29.	0.8326	-0.1105	0.8399	-7.5587	-0.2627 :	0.2578
-28.	0.8429	-0.1295	0.8528	-8.7357	-0.2709 :	0.2660
-27.	0.8368	-0.1178	0.8451	-8.0121	-0.2790 :	0.2741
-26.	0.8258	-0.0958	0.8313	-6.6172	-0.2871 :	0.2823
-25.	0.8307	-0.1064	0.8375	-7.3019	-0.2952 :	0.2905
-24.	0.8408	-0.1286	0.8505	-8.6930	-0.3029 :	0.2983
-23.	0.8350	-0.1153	0.8429	-7.8637	-0.3104 :	0.3059
-22.	0.8242	-0.0894	0.8290	-6.1926	-0.3179 :	0.3135
-21.	0.8286	-0.1011	0.8348	-6.9529	-0.3254 :	0.3211
-20.	0.8371	-0.1237	0.8461	-8.4066	-0.3324 :	0.3282
-19.	0.8302	-0.1045	0.8368	-7.1761	-0.3391 :	0.3350
-18.	0.8211	-0.0775	0.8247	-5.3951	-0.3458 :	0.3419
-17.	0.8264	-0.0948	0.8318	-6.5441	-0.3523 :	0.3485
-16.	0.8319	-0.1135	0.8396	-7.7707	-0.3582 :	0.3546
-15.	0.8239	-0.0848	0.8282	-5.8783	-0.3638 :	0.3604
-14.	0.8179	-0.0623	0.8203	-4.3531	-0.3694 :	0.3663
-13.	0.8239	-0.0875	0.8285	-6.0639	-0.3747 :	0.3717
-12.	0.8256	-0.0957	0.8312	-6.6130	-0.3793 :	0.3765
-11.	0.8178	-0.0577	0.8199	-4.0337	-0.3837 :	0.3811
-10.	0.8158	-0.0474	0.8172	-3.3280	-0.3880 :	0.3857
-9.	0.8207	-0.0776	0.8244	-5.4001	-0.3918 :	0.3896
-8.	0.8193	-0.0679	0.8221	-4.7401	-0.3949 :	0.3930
-7.	0.8138	-0.0270	0.8142	-1.9031	-0.3979 :	0.3963
-6.	0.8145	-0.0350	0.8153	-2.4591	-0.4007 :	0.3993
-5.	0.8169	-0.0604	0.8192	-4.2314	-0.4028 :	0.4015
-4.	0.8146	-0.0310	0.8152	-2.1778	-0.4044 :	0.4034
-3.	0.8125	0.0004	0.8125	0.0309	-0.4059 :	0.4052
-2.	0.8135	-0.0239	0.8138	-1.6806	-0.4070 :	0.4065
-1.	0.8137	-0.0332	0.8144	-2.3334	-0.4073 :	0.4070

Table 3.10 - Cont.

Scan Angle	Cartezian coords.		polar coords.		Dp, deg.	
(deg.)	x0/λ	z0/λ	r0/λ	delta-deg.	Min.	Max.
0.	0.8133	0.0094	0.8133	0.6641	-0.4073 :	0.4073
1.	0.8133	0.0213	0.8136	1.5015	-0.4072 :	0.4074
2.	0.8124	-0.0092	0.8125	-0.6476	-0.4064 :	0.4069
3.	0.8130	0.0038	0.8130	0.2710	-0.4050 :	0.4057
4.	0.8155	0.0457	0.8168	3.2067	-0.4035 :	0.4045
5.	0.8146	0.0358	0.8154	2.5140	-0.4017 :	0.4029
6.	0.8124	0.0124	0.8125	0.8764	-0.3992 :	0.4006
7.	0.8160	0.0438	0.8172	3.0758	-0.3962 :	0.3979
8.	0.8198	0.0729	0.8230	5.0795	-0.3931 :	0.3951
9.	0.8161	0.0484	0.8175	3.3950	-0.3897 :	0.3919
10.	0.8148	0.0403	0.8158	2.8335	-0.3855 :	0.3879
11.	0.8221	0.0798	0.8260	5.5431	-0.3811 :	0.3838
12.	0.8243	0.0907	0.8293	6.2774	-0.3767 :	0.3795
13.	0.8179	0.0618	0.8202	4.3236	-0.3717 :	0.3747
14.	0.8197	0.0689	0.8226	4.8078	-0.3661 :	0.3693
15.	0.8294	0.1063	0.8362	7.3004	-0.3605 :	0.3639
16.	0.8282	0.1022	0.8345	7.0337	-0.3547 :	0.3584
17.	0.8206	0.0763	0.8242	5.3122	-0.3485 :	0.3522
18.	0.8260	0.0928	0.8312	6.4132	-0.3417 :	0.3457
19.	0.8361	0.1229	0.8450	8.3639	-0.3351 :	0.3392
20.	0.8316	0.1103	0.8389	7.5543	-0.3283 :	0.3325
21.	0.8237	0.0888	0.8284	6.1536	-0.3210 :	0.3253
22.	0.8313	0.1080	0.8383	7.3995	-0.3134 :	0.3179
23.	0.8410	0.1313	0.8512	8.8743	-0.3059 :	0.3105
24.	0.8344	0.1159	0.8424	7.9086	-0.2983 :	0.3030
25.	0.8259	0.0971	0.8316	6.7022	-0.2903 :	0.2950
26.	0.8339	0.1135	0.8415	7.7516	-0.2822 :	0.2870
27.	0.8438	0.1333	0.8542	8.9777	-0.2741 :	0.2790
28.	0.8367	0.1196	0.8452	8.1354	-0.2660 :	0.2710
29.	0.8264	0.1005	0.8325	6.9312	-0.2576 :	0.2626
30.	0.8321	0.1104	0.8394	7.5571	-0.2492 :	0.2542
31.	0.8430	0.1287	0.8527	8.6808	-0.2408 :	0.2459
32.	0.8382	0.1209	0.8469	8.2104	-0.2325 :	0.2376
33.	0.8254	0.1007	0.8316	6.9560	-0.2241 :	0.2291
34.	0.8258	0.1011	0.8320	6.9769	-0.2156 :	0.2206
35.	0.8367	0.1168	0.8448	7.9453	-0.2072 :	0.2122
36.	0.8376	0.1180	0.8458	8.0170	-0.1990 :	0.2039
37.	0.8249	0.1008	0.8310	6.9655	-0.1907 :	0.1957
38.	0.8169	0.0902	0.8219	6.3020	-0.1825 :	0.1873
39.	0.8231	0.0979	0.8289	6.7805	-0.1743 :	0.1791
40.	0.8303	0.1066	0.8371	7.3138	-0.1663 :	0.1711

Table 3.11

Phase centre and phase variation (Dp-deg.) of a 56-element linear array in H-plane for different scan angles. Complete amplitude ext. failure in elements no. 25 to 28, Mutual coupling between array elements is not included.

Scan Angle	Cartezian coords.		polar coords.		Dp, deg.	
(deg.)	x0/λ	z0/λ	r0/λ	delta-deg.	Min.	Max.
-40.	0.2240	-0.0459	0.2286	-11.5690	-0.0789 :	0.0765
-39.	0.2252	-0.0473	0.2301	-11.8650	-0.0829 :	0.0805
-38.	0.2264	-0.0488	0.2315	-12.1549	-0.0869 :	0.0845
-37.	0.2274	-0.0501	0.2328	-12.4232	-0.0911 :	0.0886
-36.	0.2283	-0.0514	0.2340	-12.6792	-0.0952 :	0.0927
-35.	0.2291	-0.0525	0.2351	-12.9050	-0.0995 :	0.0969
-34.	0.2299	-0.0536	0.2361	-13.1224	-0.1037 :	0.1012
-33.	0.2305	-0.0545	0.2369	-13.3099	-0.1080 :	0.1055
-32.	0.2311	-0.0554	0.2376	-13.4850	-0.1123 :	0.1098
-31.	0.2315	-0.0561	0.2382	-13.6219	-0.1167 :	0.1141
-30.	0.2318	-0.0566	0.2387	-13.7293	-0.1210 :	0.1184
-29.	0.2321	-0.0571	0.2391	-13.8300	-0.1254 :	0.1228
-28.	0.2322	-0.0574	0.2392	-13.8728	-0.1297 :	0.1271
-27.	0.2323	-0.0575	0.2394	-13.9118	-0.1340 :	0.1314
-26.	0.2323	-0.0575	0.2393	-13.8950	-0.1382 :	0.1357
-25.	0.2322	-0.0573	0.2392	-13.8596	-0.1425 :	0.1399
-24.	0.2320	-0.0569	0.2389	-13.7716	-0.1466 :	0.1442
-23.	0.2318	-0.0563	0.2385	-13.6554	-0.1507 :	0.1483
-22.	0.2315	-0.0556	0.2381	-13.5145	-0.1547 :	0.1524
-21.	0.2311	-0.0547	0.2375	-13.3057	-0.1587 :	0.1564
-20.	0.2308	-0.0536	0.2369	-13.0771	-0.1625 :	0.1603
-19.	0.2303	-0.0523	0.2362	-12.8023	-0.1662 :	0.1640
-18.	0.2298	-0.0509	0.2354	-12.4936	-0.1699 :	0.1677
-17.	0.2293	-0.0492	0.2345	-12.1174	-0.1733 :	0.1713
-16.	0.2288	-0.0474	0.2336	-11.7069	-0.1767 :	0.1747
-15.	0.2282	-0.0455	0.2327	-11.2634	-0.1798 :	0.1780
-14.	0.2277	-0.0432	0.2317	-10.7469	-0.1829 :	0.1811
-13.	0.2271	-0.0409	0.2308	-10.2076	-0.1857 :	0.1841
-12.	0.2266	-0.0384	0.2298	-9.6253	-0.1884 :	0.1868
-11.	0.2260	-0.0358	0.2289	-9.0105	-0.1909 :	0.1894
-10.	0.2255	-0.0330	0.2279	-8.3342	-0.1932 :	0.1918
-9.	0.2250	-0.0301	0.2270	-7.6238	-0.1953 :	0.1941
-8.	0.2246	-0.0270	0.2262	-6.8652	-0.1972 :	0.1961
-7.	0.2242	-0.0239	0.2254	-6.0802	-0.1988 :	0.1979
-6.	0.2238	-0.0207	0.2248	-5.2826	-0.2003 :	0.1994
-5.	0.2235	-0.0173	0.2242	-4.4327	-0.2015 :	0.2008
-4.	0.2232	-0.0139	0.2237	-3.5748	-0.2025 :	0.2019
-3.	0.2230	-0.0106	0.2233	-2.7182	-0.2033 :	0.2028
-2.	0.2229	-0.0071	0.2230	-1.8203	-0.2038 :	0.2035
-1.	0.2228	-0.0035	0.2228	-0.9125	-0.2041 :	0.2039

Table 3.11 - Cont.

Scan Angle	Cartezian coords.		polar coords.		Dp, deg.	
(deg.)	x0/λ	z0/λ	r0/λ	delta-deg.	Min.	Max.
0.	0.2227	-0.0000	0.2227	-0.0000	-0.2041 :	0.2041
1.	0.2228	0.0035	0.2228	0.9125	-0.2039 :	0.2041
2.	0.2229	0.0071	0.2230	1.8203	-0.2035 :	0.2038
3.	0.2230	0.0106	0.2233	2.7182	-0.2028 :	0.2033
4.	0.2232	0.0139	0.2237	3.5748	-0.2019 :	0.2025
5.	0.2235	0.0173	0.2242	4.4327	-0.2008 :	0.2015
6.	0.2238	0.0207	0.2248	5.2826	-0.1994 :	0.2003
7.	0.2242	0.0239	0.2254	6.0802	-0.1979 :	0.1988
8.	0.2246	0.0270	0.2262	6.8652	-0.1961 :	0.1972
9.	0.2250	0.0301	0.2270	7.6238	-0.1941 :	0.1953
10.	0.2255	0.0330	0.2279	8.3342	-0.1918 :	0.1932
11.	0.2260	0.0358	0.2289	9.0105	-0.1894 :	0.1909
12.	0.2266	0.0384	0.2298	9.6253	-0.1868 :	0.1884
13.	0.2271	0.0409	0.2308	10.2076	-0.1841 :	0.1857
14.	0.2277	0.0432	0.2317	10.7469	-0.1811 :	0.1829
15.	0.2282	0.0455	0.2327	11.2634	-0.1780 :	0.1798
16.	0.2288	0.0474	0.2336	11.7069	-0.1747 :	0.1767
17.	0.2293	0.0492	0.2345	12.1174	-0.1713 :	0.1733
18.	0.2298	0.0509	0.2354	12.4936	-0.1677 :	0.1699
19.	0.2303	0.0523	0.2362	12.8023	-0.1640 :	0.1662
20.	0.2308	0.0536	0.2369	13.0771	-0.1603 :	0.1625
21.	0.2311	0.0547	0.2375	13.3057	-0.1564 :	0.1587
22.	0.2315	0.0556	0.2381	13.5145	-0.1524 :	0.1547
23.	0.2318	0.0563	0.2385	13.6554	-0.1483 :	0.1507
24.	0.2320	0.0569	0.2389	13.7716	-0.1442 :	0.1466
25.	0.2322	0.0573	0.2392	13.8596	-0.1399 :	0.1425
26.	0.2323	0.0575	0.2393	13.8950	-0.1357 :	0.1382
27.	0.2323	0.0575	0.2394	13.9118	-0.1314 :	0.1340
28.	0.2322	0.0574	0.2392	13.8728	-0.1271 :	0.1297
29.	0.2321	0.0571	0.2391	13.8300	-0.1228 :	0.1254
30.	0.2318	0.0566	0.2387	13.7293	-0.1184 :	0.1210
31.	0.2315	0.0561	0.2382	13.6219	-0.1141 :	0.1167
32.	0.2311	0.0554	0.2376	13.4850	-0.1098 :	0.1123
33.	0.2305	0.0545	0.2369	13.3099	-0.1055 :	0.1080
34.	0.2299	0.0536	0.2361	13.1224	-0.1012 :	0.1037
35.	0.2291	0.0525	0.2351	12.9050	-0.0969 :	0.0995
36.	0.2283	0.0514	0.2340	12.6792	-0.0927 :	0.0952
37.	0.2274	0.0501	0.2328	12.4232	-0.0886 :	0.0911
38.	0.2264	0.0488	0.2315	12.1549	-0.0845 :	0.0869
39.	0.2252	0.0473	0.2301	11.8650	-0.0805 :	0.0829
40.	0.2240	0.0459	0.2286	11.5690	-0.0765 :	0.0789

Table 3.12

Phase centre and phase variation (Dp-deg.) of a 56-element linear array in H-plane for different scan angles. Complete amplitude ext. failure in elements no. 25 to 28, Mutual coupling between array elements is included.

Scan Angle	Cartezian coords.		polar coords.		Dp, deg.	
(deg.)	x0/λ	z0/λ	r0/λ	delta-deg.	Min.	Max.
-40.	0.2276	-0.0493	0.2329	-12.2108	-0.0789 :	0.0765
-39.	0.2201	-0.0403	0.2237	-10.3742	-0.0829 :	0.0805
-38.	0.2251	-0.0468	0.2299	-11.7551	-0.0870 :	0.0846
-37.	0.2375	-0.0631	0.2457	-14.8731	-0.0911 :	0.0886
-36.	0.2395	-0.0658	0.2484	-15.3640	-0.0953 :	0.0927
-35.	0.2294	-0.0518	0.2352	-12.7314	-0.0994 :	0.0969
-34.	0.2258	-0.0470	0.2307	-11.7499	-0.1038 :	0.1012
-33.	0.2367	-0.0637	0.2451	-15.0610	-0.1081 :	0.1055
-32.	0.2447	-0.0765	0.2564	-17.3524	-0.1124 :	0.1097
-31.	0.2368	-0.0638	0.2453	-15.0690	-0.1167 :	0.1140
-30.	0.2282	-0.0495	0.2335	-12.2402	-0.1210 :	0.1184
-29.	0.2355	-0.0629	0.2438	-14.9634	-0.1255 :	0.1228
-28.	0.2457	-0.0821	0.2591	-18.4658	-0.1298 :	0.1271
-27.	0.2400	-0.0714	0.2504	-16.5663	-0.1340 :	0.1314
-26.	0.2296	-0.0509	0.2351	-12.5104	-0.1382 :	0.1357
-25.	0.2345	-0.0621	0.2426	-14.8231	-0.1426 :	0.1400
-24.	0.2446	-0.0846	0.2588	-19.0742	-0.1467 :	0.1441
-23.	0.2393	-0.0728	0.2501	-16.9152	-0.1507 :	0.1482
-22.	0.2290	-0.0486	0.2341	-11.9826	-0.1547 :	0.1524
-21.	0.2336	-0.0611	0.2415	-14.6650	-0.1588 :	0.1564
-20.	0.2421	-0.0844	0.2564	-19.2264	-0.1626 :	0.1602
-19.	0.2358	-0.0671	0.2451	-15.8815	-0.1662 :	0.1639
-18.	0.2271	-0.0421	0.2310	-10.4992	-0.1698 :	0.1677
-17.	0.2326	-0.0605	0.2403	-14.5707	-0.1734 :	0.1713
-16.	0.2383	-0.0803	0.2514	-18.6209	-0.1767 :	0.1746
-15.	0.2307	-0.0537	0.2369	-13.1088	-0.1798 :	0.1779
-14.	0.2251	-0.0333	0.2276	-8.4082	-0.1829 :	0.1811
-13.	0.2312	-0.0598	0.2388	-14.4898	-0.1858 :	0.1841
-12.	0.2333	-0.0695	0.2434	-16.5937	-0.1884 :	0.1867
-11.	0.2258	-0.0339	0.2284	-8.5417	-0.1908 :	0.1894
-10.	0.2240	-0.0258	0.2255	-6.5606	-0.1932 :	0.1919
-9.	0.2291	-0.0573	0.2362	-14.0347	-0.1954 :	0.1941
-8.	0.2279	-0.0498	0.2333	-12.3323	-0.1971 :	0.1960
-7.	0.2227	-0.0117	0.2230	-3.0155	-0.1988 :	0.1978
-6.	0.2236	-0.0216	0.2246	-5.5235	-0.2004 :	0.1995
-5.	0.2261	-0.0489	0.2313	-12.1953	-0.2016 :	0.2008
-4.	0.2240	-0.0221	0.2251	-5.6410	-0.2024 :	0.2018
-3.	0.2220	0.0066	0.2221	1.7031	-0.2032 :	0.2029
-2.	0.2230	-0.0196	0.2238	-5.0358	-0.2039 :	0.2036
-1.	0.2233	-0.0312	0.2255	-7.9541	-0.2041 :	0.2039

Table 3.12 - Cont.

Scan Angle	Cartezian coords.		polar coords.		Dp, deg.	
(deg.)	x0/λ	z0/λ	r0/λ	delta-deg.	Min.	Max.
0.	0.2229	0.0083	0.2230	2.1332	-0.2040 :	0.2041
1.	0.2228	0.0176	0.2235	4.5116	-0.2040 :	0.2042
2.	0.2219	-0.0149	0.2224	-3.8468	-0.2036 :	0.2038
3.	0.2224	-0.0046	0.2224	-1.1783	-0.2028 :	0.2032
4.	0.2247	0.0342	0.2273	8.6668	-0.2019 :	0.2025
5.	0.2236	0.0220	0.2247	5.6315	-0.2009 :	0.2016
6.	0.2212	-0.0034	0.2212	-0.8742	-0.1995 :	0.2003
7.	0.2245	0.0252	0.2259	6.3980	-0.1978 :	0.1988
8.	0.2279	0.0513	0.2336	12.6914	-0.1961 :	0.1973
9.	0.2239	0.0250	0.2253	6.3591	-0.1942 :	0.1954
10.	0.2224	0.0148	0.2229	3.8150	-0.1919 :	0.1931
11.	0.2292	0.0514	0.2349	12.6406	-0.1893 :	0.1909
12.	0.2309	0.0601	0.2386	14.5837	-0.1869 :	0.1885
13.	0.2243	0.0299	0.2263	7.5843	-0.1841 :	0.1858
14.	0.2257	0.0349	0.2284	8.8013	-0.1810 :	0.1828
15.	0.2347	0.0697	0.2449	16.5322	-0.1779 :	0.1799
16.	0.2332	0.0641	0.2418	15.3598	-0.1747 :	0.1768
17.	0.2254	0.0372	0.2284	9.3761	-0.1713 :	0.1734
18.	0.2302	0.0519	0.2360	12.7060	-0.1676 :	0.1698
19.	0.2397	0.0799	0.2527	18.4437	-0.1640 :	0.1663
20.	0.2349	0.0664	0.2441	15.7782	-0.1603 :	0.1626
21.	0.2269	0.0445	0.2313	11.0899	-0.1564 :	0.1587
22.	0.2341	0.0622	0.2423	14.8668	-0.1523 :	0.1547
23.	0.2433	0.0841	0.2574	19.0588	-0.1482 :	0.1508
24.	0.2366	0.0684	0.2463	16.1254	-0.1442 :	0.1467
25.	0.2282	0.0495	0.2335	12.2383	-0.1399 :	0.1425
26.	0.2359	0.0650	0.2447	15.4087	-0.1356 :	0.1382
27.	0.2453	0.0837	0.2592	18.8375	-0.1313 :	0.1340
28.	0.2384	0.0702	0.2486	16.4119	-0.1271 :	0.1297
29.	0.2286	0.0516	0.2343	12.7136	-0.1227 :	0.1254
30.	0.2343	0.0612	0.2422	14.6391	-0.1183 :	0.1209
31.	0.2448	0.0788	0.2572	17.8374	-0.1140 :	0.1167
32.	0.2404	0.0714	0.2508	16.5400	-0.1098 :	0.1124
33.	0.2284	0.0522	0.2343	12.8780	-0.1054 :	0.1080
34.	0.2292	0.0529	0.2352	12.9961	-0.1011 :	0.1037
35.	0.2400	0.0683	0.2496	15.8943	-0.0968 :	0.0994
36.	0.2413	0.0699	0.2512	16.1622	-0.0927 :	0.0953
37.	0.2297	0.0540	0.2360	13.2359	-0.0886 :	0.0911
38.	0.2227	0.0446	0.2272	11.3235	-0.0845 :	0.0869
39.	0.2294	0.0526	0.2353	12.9159	-0.0804 :	0.0828
40.	0.2370	0.0617	0.2449	14.5854	-0.0765 :	0.0789

Table 3.13

Phase centre and phase variation (Dp-deg.) of a 56-element linear array in H-plane for different scan angles.
Complete phase ext. failure in elements no. 1 to 4,
Mutual coupling between array elements is not included.

Scan Angle	Cartezian coords.		polar coords.		Dp, deg.	
(deg.)	x0/λ	z0/λ	r0/λ	delta-deg.	Min.	Max.
-40.	-1.7300	2.7261	3.2287	122.3985	-0.1234 :	0.1274
-39.	-3.7457	5.1369	6.3575	126.0984	-0.0892 :	0.0936
-38.	0.5153	-0.2420	0.5693	-25.1564	-0.0695 :	0.0713
-37.	4.6737	-5.6348	7.3208	-50.3263	-0.0998 :	0.1005
-36.	2.0663	-2.0741	2.9277	-45.1079	-0.1491 :	0.1521
-35.	-3.1846	5.2758	6.1624	121.1161	-0.1347 :	0.1374
-34.	-2.2072	3.8105	4.4036	120.0815	-0.0888 :	0.0948
-33.	2.8161	-3.7834	4.7164	-53.3384	-0.1012 :	0.1038
-32.	3.3477	-4.5771	5.6708	-53.8180	-0.1574 :	0.1585
-31.	-1.0923	2.6853	2.8989	112.1348	-0.1659 :	0.1645
-30.	-2.1204	4.3986	4.8830	115.7369	-0.1160 :	0.1213
-29.	1.2353	-1.5555	1.9863	-51.5433	-0.1191 :	0.1273
-28.	2.1360	-3.1945	3.8428	-56.2320	-0.1717 :	0.1743
-27.	-0.1958	1.3056	1.3202	98.5289	-0.1753 :	0.1700
-26.	-0.3005	1.5101	1.5397	101.2525	-0.1339 :	0.1356
-25.	1.0775	-1.3897	1.7585	-52.2123	-0.1537 :	0.1662
-24.	-0.0382	1.0480	1.0487	92.0863	-0.1985 :	0.2042
-23.	-0.5169	2.1421	2.2036	103.5653	-0.1672 :	0.1585
-22.	2.0270	-3.9705	4.4580	-62.9548	-0.1389 :	0.1352
-21.	1.5673	-2.7717	3.1841	-60.5140	-0.2070 :	0.2236
-20.	-2.4016	7.7906	8.1523	107.1330	-0.2273 :	0.2356
-19.	-0.8202	3.2619	3.3634	104.1150	-0.1396 :	0.1290
-18.	4.2953	-11.9386	12.6877	-70.2122	-0.1435 :	0.1346
-17.	1.4199	-2.7221	3.0701	-62.4520	-0.2835 :	0.3043
-16.	-4.3864	16.7417	17.3068	104.6819	-0.2322 :	0.2418
-15.	-0.0711	1.0468	1.0492	93.8877	-0.0968 :	0.0825
-14.	5.8232	-21.5266	22.3003	-74.8631	-0.1714 :	0.1630
-13.	-0.0319	3.0179	3.0180	90.6060	-0.3745 :	0.3929
-12.	-4.9992	25.1020	25.5950	101.2635	-0.1833 :	0.1997
-11.	1.6453	-7.7291	7.9022	-77.9824	-0.0609 :	0.0344
-10.	5.6102	-28.6334	29.1779	-78.9144	-0.2496 :	0.2563
-9.	-1.9250	16.5233	16.6351	96.6452	-0.4297 :	0.4320
-8.	-3.5887	26.9621	27.1999	97.5815	-0.0898 :	0.1200
-7.	2.9218	-22.5259	22.7146	-82.6095	-0.0612 :	0.0169
-6.	3.4676	-26.3085	26.5361	-82.4914	-0.3853 :	0.4132
-5.	-2.2584	32.9580	33.0353	93.9200	-0.3745 :	0.3667
-4.	-1.1840	17.7988	17.8381	93.8057	-0.0152 :	0.0429
-3.	2.2161	-37.0002	37.0665	-86.5724	-0.1146 :	0.0671
-2.	1.1864	-10.9162	10.9805	-83.7972	-0.5195 :	0.5381
-1.	-0.2666	41.8668	41.8676	90.3649	-0.2147 :	0.2309

Table 3.13 - Cont.

Scan Angle	Cartezian coords.		polar coords.		Dp, deg.	
(deg.)	x0/λ	z0/λ	r0/λ	delta-deg.	Min.	Max.
0.	-0.0000	-0.0000	0.0000	-91.4997	-0.0000 :	0.0000
1.	-0.2666	-41.8668	41.8676	-90.3649	-0.2309 :	0.2147
2.	1.1864	10.9162	10.9805	83.7972	-0.5381 :	0.5195
3.	2.2161	37.0002	37.0665	86.5724	-0.0671 :	0.1146
4.	-1.1840	-17.7988	17.8381	-93.8057	-0.0429 :	0.0152
5.	-2.2584	-32.9580	33.0353	-93.9200	-0.3667 :	0.3745
6.	3.4676	26.3085	26.5361	82.4914	-0.4132 :	0.3853
7.	2.9218	22.5259	22.7146	82.6095	-0.0169 :	0.0612
8.	-3.5887	-26.9621	27.1999	-97.5815	-0.1200 :	0.0898
9.	-1.9250	-16.5233	16.6351	-96.6452	-0.4320 :	0.4297
10.	5.6102	28.6334	29.1779	78.9144	-0.2563 :	0.2496
11.	1.6453	7.7291	7.9022	77.9824	-0.0344 :	0.0609
12.	-4.9992	-25.1020	25.5950	-101.2635	-0.1997 :	0.1833
13.	-0.0319	-3.0179	3.0180	-90.6060	-0.3929 :	0.3745
14.	5.8232	21.5266	22.3003	74.8631	-0.1630 :	0.1714
15.	-0.0711	-1.0468	1.0492	-93.8877	-0.0825 :	0.0968
16.	-4.3864	-16.7417	17.3068	-104.6819	-0.2418 :	0.2322
17.	1.4199	2.7221	3.0701	62.4520	-0.3043 :	0.2835
18.	4.2953	11.9386	12.6877	70.2122	-0.1346 :	0.1435
19.	-0.8202	-3.2619	3.3634	-104.1150	-0.1290 :	0.1396
20.	-2.4016	-7.7906	8.1523	-107.1330	-0.2356 :	0.2273
21.	1.5673	2.7717	3.1841	60.5140	-0.2236 :	0.2070
22.	2.0270	3.9705	4.4580	62.9548	-0.1352 :	0.1389
23.	-0.5169	-2.1421	2.2036	-103.5653	-0.1585 :	0.1672
24.	-0.0382	-1.0480	1.0487	-92.0863	-0.2042 :	0.1985
25.	1.0775	1.3897	1.7585	52.2123	-0.1662 :	0.1537
26.	-0.3005	-1.5101	1.5397	-101.2525	-0.1356 :	0.1339
27.	-0.1958	-1.3056	1.3202	-98.5289	-0.1700 :	0.1753
28.	2.1360	3.1945	3.8428	56.2320	-0.1743 :	0.1717
29.	1.2353	1.5555	1.9863	51.5433	-0.1273 :	0.1191
30.	-2.1204	-4.3986	4.8830	-115.7369	-0.1213 :	0.1160
31.	-1.0923	-2.6853	2.8989	-112.1348	-0.1645 :	0.1659
32.	3.3477	4.5771	5.6708	53.8180	-0.1585 :	0.1574
33.	2.8161	3.7834	4.7164	53.3384	-0.1038 :	0.1012
34.	-2.2072	-3.8105	4.4036	-120.0815	-0.0948 :	0.0888
35.	-3.1846	-5.2758	6.1624	-121.1161	-0.1374 :	0.1347
36.	2.0663	2.0741	2.9277	45.1079	-0.1521 :	0.1491
37.	4.6737	5.6348	7.3208	50.3263	-0.1005 :	0.0998
38.	0.5153	0.2420	0.5693	25.1564	-0.0713 :	0.0695
39.	-3.7457	-5.1369	6.3575	-126.0984	-0.0936 :	0.0892
40.	-1.7300	-2.7261	3.2287	-122.3985	-0.1274 :	0.1234

Table 3.14

Phase centre and phase variation (Dp-deg.) of a 56-element linear array in H-plane for different scan angles.
Complete phase ext. failure in elements no. 1 to 4,
Mutual coupling between array elements is included.

Scan Angle	Cartezian coords.		polar coords.		Dp, deg.	
(deg.)	x0/λ	z0/λ	r0/λ	delta-deg.	Min.	Max.
-40.	-1.7235	2.7191	3.2193	122.3680	-0.1235 :	0.1274
-39.	-3.7475	5.1398	6.3610	126.0962	-0.0893 :	0.0936
-38.	0.5135	-0.2393	0.5665	-24.9828	-0.0695 :	0.0712
-37.	4.6804	-5.6433	7.3317	-50.3284	-0.0997 :	0.1004
-36.	2.0766	-2.0875	2.9445	-45.1502	-0.1489 :	0.1523
-35.	-3.1835	5.2752	6.1614	121.1103	-0.1347 :	0.1375
-34.	-2.2121	3.8184	4.4129	120.0849	-0.0888 :	0.0948
-33.	2.8184	-3.7865	4.7202	-53.3387	-0.1011 :	0.1037
-32.	3.3579	-4.5927	5.6893	-53.8278	-0.1573 :	0.1585
-31.	-1.0889	2.6807	2.8934	112.1064	-0.1660 :	0.1645
-30.	-2.1263	4.4096	4.8955	115.7429	-0.1160 :	0.1213
-29.	1.2347	-1.5539	1.9847	-51.5296	-0.1190 :	0.1271
-28.	2.1446	-3.2102	3.8606	-56.2540	-0.1717 :	0.1741
-27.	-0.1922	1.2998	1.3139	98.4135	-0.1754 :	0.1701
-26.	-0.3067	1.5238	1.5544	101.3800	-0.1340 :	0.1356
-25.	1.0759	-1.3859	1.7545	-52.1782	-0.1536 :	0.1661
-24.	-0.0309	1.0322	1.0327	91.7137	-0.1984 :	0.2042
-23.	-0.5148	2.1383	2.1994	103.5354	-0.1673 :	0.1587
-22.	2.0208	-3.9543	4.4407	-62.9315	-0.1389 :	0.1353
-21.	1.5663	-2.7690	3.1813	-60.5057	-0.2068 :	0.2235
-20.	-2.3955	7.7745	8.1352	107.1257	-0.2273 :	0.2356
-19.	-0.8202	3.2628	3.3643	104.1103	-0.1397 :	0.1291
-18.	4.2896	-11.9208	12.6691	-70.2090	-0.1435 :	0.1346
-17.	1.4205	-2.7241	3.0722	-62.4601	-0.2834 :	0.3042
-16.	-4.3820	16.7266	17.2911	104.6802	-0.2323 :	0.2418
-15.	-0.0728	1.0538	1.0563	93.9503	-0.0969 :	0.0827
-14.	5.8191	-21.5102	22.2834	-74.8623	-0.1714 :	0.1630
-13.	-0.0300	3.0089	3.0091	90.5704	-0.3745 :	0.3928
-12.	-4.9968	25.0912	25.5839	101.2629	-0.1834 :	0.1998
-11.	1.6431	-7.7168	7.8898	-77.9799	-0.0609 :	0.0346
-10.	5.6082	-28.6226	29.1669	-78.9142	-0.2495 :	0.2563
-9.	-1.9228	16.5088	16.6204	96.6434	-0.4296 :	0.4320
-8.	-3.5880	26.9584	27.1961	97.5812	-0.0899 :	0.1201
-7.	2.9201	-22.5114	22.7000	-82.6092	-0.0613 :	0.0169
-6.	3.4672	-26.3064	26.5339	-82.4916	-0.3852 :	0.4131
-5.	-2.2571	32.9432	33.0204	93.9196	-0.3746 :	0.3668
-4.	-1.1841	17.8020	17.8413	93.8053	-0.0151 :	0.0432
-3.	2.2154	-36.9870	37.0532	-86.5723	-0.1146 :	0.0672
-2.	1.1865	-10.9218	10.9860	-83.7999	-0.5194 :	0.5380
-1.	-0.2663	41.8567	41.8576	90.3646	-0.2148 :	0.2310

Table 3.14 - Cont.

Scan Angle	Cartezian coords.		polar coords.		Dp, deg.	
(deg.)	x0/λ	z0/λ	r0/λ	delta-deg.	Min.	Max.
0.	0.0001	0.0080	0.0080	89.0811	-0.0001 :	0.0001
1.	-0.2665	-41.8566	41.8574	-90.3648	-0.2309 :	0.2148
2.	1.1861	10.9071	10.9714	83.7939	-0.5382 :	0.5193
3.	2.2161	36.9962	37.0625	86.5721	-0.0672 :	0.1147
4.	-1.1830	-17.7873	17.8266	-93.8052	-0.0429 :	0.0153
5.	-2.2578	-32.9504	33.0277	-93.9199	-0.3667 :	0.3745
6.	3.4667	26.2991	26.5266	82.4908	-0.4132 :	0.3853
7.	2.9222	22.5275	22.7163	82.6090	-0.0170 :	0.0613
8.	-3.5864	-26.9465	27.1841	-97.5812	-0.1200 :	0.0899
9.	-1.9243	-16.5184	16.6301	-96.6447	-0.4319 :	0.4296
10.	5.6088	28.6248	29.1692	78.9139	-0.2564 :	0.2497
11.	1.6471	7.7373	7.9106	77.9822	-0.0345 :	0.0610
12.	-4.9951	-25.0824	25.5749	-101.2630	-0.1997 :	0.1834
13.	-0.0320	-3.0175	3.0176	-90.6068	-0.3928 :	0.3744
14.	5.8217	21.5203	22.2939	74.8626	-0.1631 :	0.1715
15.	-0.0667	-1.0308	1.0329	-93.7042	-0.0826 :	0.0969
16.	-4.3808	-16.7215	17.2859	-104.6808	-0.2417 :	0.2322
17.	1.4183	2.7173	3.0652	62.4384	-0.3042 :	0.2835
18.	4.2947	11.9366	12.6857	70.2117	-0.1347 :	0.1436
19.	-0.8126	-3.2396	3.3399	-104.0812	-0.1291 :	0.1397
20.	-2.3959	-7.7740	8.1348	-107.1292	-0.2355 :	0.2272
21.	1.5639	2.7636	3.1754	60.4952	-0.2235 :	0.2070
22.	2.0280	3.9729	4.4605	62.9581	-0.1354 :	0.1391
23.	-0.5066	-2.1176	2.1773	-103.4557	-0.1586 :	0.1673
24.	-0.0334	-1.0362	1.0367	-91.8466	-0.2040 :	0.1985
25.	1.0728	1.3804	1.7482	52.1470	-0.1662 :	0.1537
26.	-0.2987	-1.5062	1.5355	-101.2162	-0.1357 :	0.1341
27.	-0.1844	-1.2826	1.2958	-98.1829	-0.1701 :	0.1754
28.	2.1400	3.2034	3.8525	56.2547	-0.1742 :	0.1715
29.	1.2297	1.5461	1.9755	51.5033	-0.1273 :	0.1190
30.	-2.1196	-4.3969	4.8811	-115.7376	-0.1213 :	0.1162
31.	-1.0814	-2.6664	2.8774	-112.0749	-0.1646 :	0.1659
32.	3.3524	4.5857	5.6805	53.8311	-0.1584 :	0.1573
33.	2.8102	3.7752	4.7063	53.3366	-0.1038 :	0.1012
34.	-2.2096	-3.8136	4.4074	-120.0883	-0.0949 :	0.0889
35.	-3.1765	-5.2637	6.1479	-121.1098	-0.1375 :	0.1347
36.	2.0729	2.0841	2.9394	45.1541	-0.1522 :	0.1489
37.	4.6695	5.6301	7.3145	50.3283	-0.1004 :	0.0997
38.	0.5094	0.2350	0.5610	24.7620	-0.0713 :	0.0695
39.	-3.7436	-5.1339	6.3538	-126.0990	-0.0937 :	0.0893
40.	-1.7231	-2.7174	3.2176	-122.3788	-0.1274 :	0.1234

Table 3.15

Phase centre and phase variation (Dp-deg.) of a 56-element linear array in H-plane for different scan angles.
Complete phase ext. failure in elements no. 13 to 16,
Mutual coupling between array elements is not included.

Scan Angle	Cartezian coords.		polar coords.		Dp, deg.	
(deg.)	x0/λ	z0/λ	r0/λ	delta-deg.	Min.	Max.
-40.	1.7111	-1.2865	2.1408	-36.9391	-0.1559 :	0.1394
-39.	2.3556	-1.9521	3.0593	-39.6484	-0.1976 :	0.1752
-38.	2.0960	-1.5149	2.5862	-35.8587	-0.2334 :	0.2144
-37.	0.9016	0.0880	0.9059	5.5724	-0.2474 :	0.2421
-36.	-0.3282	1.6998	1.7312	100.9284	-0.2364 :	0.2463
-35.	-0.6423	2.0137	2.1136	107.6899	-0.2094 :	0.2251
-34.	0.0039	0.9348	0.9348	89.7610	-0.1841 :	0.1931
-33.	1.0337	-0.7009	1.2490	-34.1398	-0.1783 :	0.1739
-32.	1.8564	-1.9737	2.7096	-46.7548	-0.1989 :	0.1815
-31.	1.9898	-2.0878	2.8841	-46.3768	-0.2364 :	0.2137
-30.	1.2341	-0.6751	1.4067	-28.6811	-0.2727 :	0.2558
-29.	0.1210	1.3792	1.3845	84.9871	-0.2939 :	0.2912
-28.	-0.3291	2.2182	2.2425	98.4392	-0.2995 :	0.3065
-27.	0.3133	0.9357	0.9867	71.4868	-0.2982 :	0.3022
-26.	1.4648	-1.4378	2.0526	-44.4675	-0.2998 :	0.2927
-25.	2.1085	-2.8436	3.5401	-53.4436	-0.3024 :	0.2885
-24.	1.5827	-1.7509	2.3602	-47.8892	-0.2936 :	0.2872
-23.	0.2314	1.2750	1.2959	79.7138	-0.2718 :	0.2811
-22.	-0.7777	3.6409	3.7231	102.0571	-0.2528 :	0.2704
-21.	-0.5388	3.0640	3.1110	99.9739	-0.2642 :	0.2693
-20.	0.9658	-0.7533	1.2248	-37.9526	-0.3304 :	0.3033
-19.	2.7923	-5.5686	6.2294	-63.3693	-0.4348 :	0.3776
-18.	3.1321	-6.3308	7.0632	-63.6763	-0.4930 :	0.4501
-17.	1.2148	-0.3795	1.2727	-17.3466	-0.4428 :	0.4627
-16.	-0.9350	6.2863	6.3554	98.4598	-0.3192 :	0.3896
-15.	-1.5054	7.6072	7.7548	101.1936	-0.1922 :	0.2581
-14.	-0.7282	4.2840	4.3455	99.6469	-0.1490 :	0.1683
-13.	1.1019	-2.8073	3.0158	-68.5705	-0.2690 :	0.2122
-12.	3.4568	-12.1170	12.6005	-74.0776	-0.5317 :	0.3944
-11.	3.7162	-12.1284	12.6850	-72.9647	-0.6943 :	0.5901
-10.	0.7849	3.6654	3.7485	77.9132	-0.6033 :	0.6633
-9.	-1.2457	14.0231	14.0784	95.0764	-0.3784 :	0.5345
-8.	-1.0458	10.1928	10.2463	95.8582	-0.1381 :	0.2417
-7.	-0.3020	3.2436	3.2577	95.3198	-0.0384 :	0.0579
-6.	0.8837	-5.7361	5.8037	-81.2423	-0.2061 :	0.1225
-5.	2.4866	-18.0416	18.2121	-82.1526	-0.6028 :	0.3974
-4.	2.6168	-14.9258	15.1535	-80.0560	-0.8200 :	0.6793
-3.	1.0616	10.6209	10.6738	84.2918	-0.6898 :	0.8039
-2.	0.2971	19.4047	19.4069	89.1229	-0.4043 :	0.6202
-1.	0.1127	9.0631	9.0638	89.2875	-0.1013 :	0.2069

Table 3.15 - Cont.

Scan Angle	Cartezian coords.		polar coords.		Dp, deg.	
(deg.)	x0/λ	z0/λ	r0/λ	delta-deg.	Min.	Max.
0.	-0.0000	-0.0000	0.0000	-91.4997	-0.0000 :	0.0000
1.	0.1127	-9.0631	9.0638	-89.2875	-0.2069 :	0.1013
2.	0.2971	-19.4047	19.4069	-89.1229	-0.6202 :	0.4043
3.	1.0616	-10.6209	10.6738	-84.2918	-0.8039 :	0.6898
4.	2.6168	14.9258	15.1535	80.0560	-0.6793 :	0.8200
5.	2.4866	18.0416	18.2121	82.1526	-0.3974 :	0.6028
6.	0.8837	5.7361	5.8037	81.2423	-0.1225 :	0.2061
7.	-0.3020	-3.2436	3.2577	-95.3198	-0.0579 :	0.0384
8.	-1.0458	-10.1928	10.2463	-95.8582	-0.2417 :	0.1381
9.	-1.2457	-14.0231	14.0784	-95.0764	-0.5345 :	0.3784
10.	0.7849	-3.6654	3.7485	-77.9132	-0.6633 :	0.6033
11.	3.7162	12.1284	12.6850	72.9647	-0.5901 :	0.6943
12.	3.4568	12.1170	12.6005	74.0776	-0.3944 :	0.5317
13.	1.1019	2.8073	3.0158	68.5705	-0.2122 :	0.2690
14.	-0.7282	-4.2840	4.3455	-99.6469	-0.1683 :	0.1490
15.	-1.5054	-7.6072	7.7548	-101.1936	-0.2581 :	0.1922
16.	-0.9350	-6.2863	6.3554	-98.4598	-0.3896 :	0.3192
17.	1.2148	0.3795	1.2727	17.3466	-0.4627 :	0.4428
18.	3.1321	6.3308	7.0632	63.6763	-0.4501 :	0.4930
19.	2.7923	5.5686	6.2294	63.3693	-0.3776 :	0.4348
20.	0.9658	0.7533	1.2248	37.9526	-0.3033 :	0.3304
21.	-0.5388	-3.0640	3.1110	-99.9739	-0.2693 :	0.2642
22.	-0.7777	-3.6409	3.7231	-102.0571	-0.2704 :	0.2528
23.	0.2314	-1.2750	1.2959	-79.7138	-0.2811 :	0.2718
24.	1.5827	1.7509	2.3602	47.8892	-0.2872 :	0.2936
25.	2.1085	2.8436	3.5401	53.4436	-0.2885 :	0.3024
26.	1.4648	1.4378	2.0526	44.4675	-0.2927 :	0.2998
27.	0.3133	-0.9357	0.9867	-71.4868	-0.3022 :	0.2982
28.	-0.3291	-2.2182	2.2425	-98.4392	-0.3065 :	0.2995
29.	0.1210	-1.3792	1.3845	-84.9871	-0.2912 :	0.2939
30.	1.2341	0.6751	1.4067	28.6811	-0.2558 :	0.2727
31.	1.9898	2.0878	2.8841	46.3768	-0.2137 :	0.2364
32.	1.8564	1.9737	2.7096	46.7548	-0.1815 :	0.1989
33.	1.0337	0.7009	1.2490	34.1398	-0.1739 :	0.1783
34.	0.0039	-0.9348	0.9348	-89.7610	-0.1931 :	0.1841
35.	-0.6423	-2.0137	2.1136	-107.6899	-0.2251 :	0.2094
36.	-0.3282	-1.6998	1.7312	-100.9284	-0.2463 :	0.2364
37.	0.9016	-0.0880	0.9059	-5.5724	-0.2421 :	0.2474
38.	2.0960	1.5149	2.5862	35.8587	-0.2144 :	0.2334
39.	2.3556	1.9521	3.0593	39.6484	-0.1752 :	0.1976
40.	1.7111	1.2865	2.1408	36.9391	-0.1394 :	0.1559

Table 3.16

Phase centre and phase variation (Dp-deg.) of a 56-element linear array in H-plane for different scan angles.
Complete phase ext. failure in elements no. 13 to 16,
Mutual coupling between array elements is included.

Scan Angle	Cartezian coords.		polar coords.		Dp, deg.	
(deg.)	x0/λ	z0/λ	r0/λ	delta-deg.	Min.	Max.
-40.	1.7133	-1.2883	2.1436	-36.9411	-0.1559 :	0.1394
-39.	2.3481	-1.9421	3.0472	-39.5938	-0.1977 :	0.1752
-38.	2.0917	-1.5091	2.5793	-35.8092	-0.2335 :	0.2145
-37.	0.9096	0.0777	0.9130	4.8824	-0.2475 :	0.2422
-36.	-0.3196	1.6889	1.7189	100.7167	-0.2364 :	0.2463
-35.	-0.6457	2.0196	2.1203	107.7299	-0.2094 :	0.2250
-34.	-0.0034	0.9462	0.9462	90.2043	-0.1843 :	0.1930
-33.	1.0366	-0.7050	1.2536	-34.2195	-0.1784 :	0.1740
-32.	1.8665	-1.9892	2.7278	-46.8217	-0.1930 :	0.1815
-31.	1.9916	-2.0897	2.8867	-46.3762	-0.2364 :	0.2135
-30.	1.2261	-0.6605	1.3927	-28.3105	-0.2727 :	0.2558
-29.	0.1203	1.3807	1.3860	85.0208	-0.2941 :	0.2913
-28.	-0.3191	2.2001	2.2231	98.2533	-0.2995 :	0.3066
-27.	0.3170	0.9297	0.9823	71.1754	-0.2982 :	0.3021
-26.	1.4578	-1.4226	2.0369	-44.2999	-0.2998 :	0.2927
-25.	2.1069	-2.8400	3.5362	-53.4291	-0.3025 :	0.2887
-24.	1.5917	-1.7707	2.3809	-48.0471	-0.2937 :	0.2872
-23.	0.2351	1.2674	1.2890	79.4890	-0.2717 :	0.2810
-22.	-0.7838	3.6568	3.7399	102.0980	-0.2528 :	0.2704
-21.	-0.5398	3.0665	3.1136	99.9837	-0.2643 :	0.2695
-20.	0.9739	-0.7752	1.2447	-38.5179	-0.3305 :	0.3033
-19.	2.7950	-5.5756	6.2369	-63.3754	-0.4346 :	0.3775
-18.	3.1261	-6.3117	7.0434	-63.6519	-0.4930 :	0.4500
-17.	1.2159	-0.3836	1.2750	-17.5084	-0.4430 :	0.4628
-16.	-0.9275	6.2605	6.3288	98.4273	-0.3191 :	0.3896
-15.	-1.5053	7.6079	7.7553	101.1920	-0.1921 :	0.2580
-14.	-0.7322	4.3000	4.3619	99.6637	-0.1490 :	0.1683
-13.	1.1038	-2.8167	3.0253	-68.6012	-0.2691 :	0.2123
-12.	3.4623	-12.1430	12.6269	-74.0856	-0.5316 :	0.3943
-11.	3.7147	-12.1200	12.6765	-72.9601	-0.6941 :	0.5900
-10.	0.7823	3.6787	3.7610	77.9945	-0.6034 :	0.6635
-9.	-1.2418	13.9970	14.0520	95.0699	-0.3785 :	0.5346
-8.	-1.0435	10.1775	10.2309	95.8544	-0.1380 :	0.2416
-7.	-0.3037	3.2578	3.2719	95.3266	-0.0384 :	0.0579
-6.	0.8828	-5.7307	5.7983	-81.2426	-0.2062 :	0.1227
-5.	2.4888	-18.0688	18.2394	-82.1573	-0.6029 :	0.3975
-4.	2.6174	-14.9335	15.1611	-80.0586	-0.8197 :	0.6791
-3.	1.0604	10.6425	10.6952	84.3102	-0.6898 :	0.8040
-2.	0.2974	19.3876	19.3899	89.1213	-0.4045 :	0.6204
-1.	0.1132	9.0397	9.0404	89.2829	-0.1013 :	0.2068

Table 3.16 - Cont.

Scan Angle	Cartezian coords.		polar coords.		Dp, deg.	
(deg.)	x0/λ	z0/λ	r0/λ	delta-deg.	Min.	Max.
0.	0.0001	0.0080	0.0080	89.0811	-0.0001	0.0007
1.	0.1128	-9.0467	9.0474	-89.2857	-0.2070	0.1014
2.	0.2962	-19.4225	19.4248	-89.1263	-0.6204	0.4044
3.	1.0608	-10.6397	10.6925	-84.3066	-0.8038	0.6896
4.	2.6184	14.9484	15.1760	80.0648	-0.6792	0.8200
5.	2.4862	18.0401	18.2106	82.1532	-0.3976	0.6830
6.	0.8811	5.7126	5.7802	81.2315	-0.1226	0.2061
7.	-0.3018	-3.2430	3.2570	-95.3162	-0.0579	0.0503
8.	-1.0426	-10.1695	10.2228	-95.8538	-0.2417	0.1501
9.	-1.2463	-14.0254	14.0806	-95.0782	-0.5347	0.3786
10.	0.7808	-3.6889	3.7706	-78.0495	-0.6633	0.6032
11.	3.7193	12.1436	12.7004	72.9715	-0.5900	0.6942
12.	3.4602	12.1345	12.6182	74.0841	-0.3945	0.5519
13.	1.0984	2.7934	3.0016	68.5347	-0.2129	0.2489
14.	-0.7304	-4.2933	4.3549	-99.6554	-0.1682	0.1409
15.	-1.4998	-7.5864	7.7332	-101.1830	-0.2579	0.1823
16.	-0.9307	-6.2702	6.3389	-98.4431	-0.3897	0.3193
17.	1.2095	0.3629	1.2628	16.7019	-0.4627	0.4430
18.	3.1312	6.3277	7.0601	63.6724	-0.4498	0.4930
19.	2.8007	5.5935	6.2555	63.4026	-0.3776	0.4340
20.	0.9684	0.7617	1.2320	38.1852	-0.3034	0.3386
21.	-0.5445	-3.0779	3.1257	-100.0315	-0.2693	0.2642
22.	-0.7769	-3.6388	3.7208	-102.0517	-0.2702	0.2927
23.	0.2412	-1.2513	1.2744	-79.0903	-0.2811	0.2718
24.	1.5853	1.7580	2.3672	47.9577	-0.2872	0.2837
25.	2.1020	2.8305	3.5257	53.4012	-0.2885	0.3024
26.	1.4659	1.4403	2.0551	44.4951	-0.2924	0.2996
27.	0.3241	-0.9139	0.9697	-70.4773	-0.3021	0.2982
28.	-0.3255	-2.2102	2.2340	-98.3770	-0.3066	0.2998
29.	0.1140	-1.3910	1.3957	-85.3167	-0.2912	0.2939
30.	1.2336	0.6746	1.4060	28.6712	-0.2596	0.2725
31.	2.0003	2.1059	2.9045	46.4725	-0.2135	0.2364
32.	1.8624	1.9843	2.7214	46.8158	-0.1815	0.1990
33.	1.0283	0.6934	1.2402	33.9941	-0.1739	0.1783
34.	-0.0008	-0.9413	0.9413	-90.0463	-0.1930	0.1840
35.	-0.6352	-2.0033	2.1016	-107.5932	-0.2250	0.2193
36.	-0.3182	-1.6854	1.7151	-100.6926	-0.2463	0.2384
37.	0.9000	-0.0892	0.9044	-5.6415	-0.2422	0.2479
38.	2.0881	1.5053	2.5742	35.7881	-0.2144	0.2333
39.	2.3567	1.9536	3.0611	39.6571	-0.1752	0.1979
40.	1.7209	1.2986	2.1559	37.0380	-0.1334	0.1555

Table 3.17

Phase centre and phase variation (Dp-deg.) of a 56-element linear array in H-plane for different scan angles. Complete phase ext. failure in elements no. 25 to 28, Mutual coupling between array elements is not included.

Scan Angle	Cartezian coords.		polar coords.		Dp, deg.	
(deg.)	x0/λ	z0/λ	r0/λ	delta-deg.	Min.	Max.
-40.	6.0608	-6.9873	9.2497	-49.0615	-0.1037 :	0.0664
-39.	6.1661	-7.3812	9.6178	-50.1256	-0.1043 :	0.0649
-38.	6.1516	-7.6437	9.8117	-51.1733	-0.1040 :	0.0634
-37.	6.0136	-7.7541	9.8127	-52.2049	-0.1030 :	0.0618
-36.	5.7543	-7.6973	9.6104	-53.2193	-0.1019 :	0.0603
-35.	5.3817	-7.4657	9.2032	-54.2136	-0.1004 :	0.0595
-34.	4.9104	-7.0606	8.6003	-55.1829	-0.0989 :	0.0595
-33.	4.3601	-6.4931	7.8212	-56.1185	-0.0976 :	0.0608
-32.	3.7563	-5.7853	6.8978	-57.0053	-0.0971 :	0.0633
-31.	3.1283	-4.9710	5.8734	-57.8172	-0.0978 :	0.0678
-30.	2.5096	-4.0964	4.8040	-58.5074	-0.0998 :	0.0742
-29.	1.9357	-3.2206	3.7575	-58.9918	-0.1039 :	0.0826
-28.	1.4436	-2.4145	2.8131	-59.1258	-0.1104 :	0.0930
-27.	1.0695	-1.7612	2.0605	-58.7310	-0.1200 :	0.1053
-26.	0.8474	-1.3527	1.5962	-57.9362	-0.1327 :	0.1196
-25.	0.8063	-1.2876	1.5192	-57.9454	-0.1492 :	0.1357
-24.	0.9676	-1.6646	1.9254	-59.8310	-0.1694 :	0.1530
-23.	1.3422	-2.5760	2.9047	-62.4783	-0.1936 :	0.1706
-22.	1.9271	-4.0970	4.5276	-64.8095	-0.2213 :	0.1875
-21.	2.7029	-6.2746	6.8320	-66.6948	-0.2513 :	0.2029
-20.	3.6328	-9.1154	9.8126	-68.2709	-0.2826 :	0.2149
-19.	4.6623	-12.5746	13.4111	-69.6568	-0.3131 :	0.2223
-18.	5.7223	-16.5495	17.5109	-70.9261	-0.3407 :	0.2236
-17.	6.7349	-20.8790	21.9384	-72.1220	-0.3631 :	0.2185
-16.	7.6205	-25.3520	26.4726	-73.2699	-0.3787 :	0.2080
-15.	8.3071	-29.7231	30.8621	-74.3853	-0.3860 :	0.1911
-14.	8.7383	-33.7346	34.8480	-75.4779	-0.3852 :	0.1682
-13.	8.8802	-37.1424	38.1892	-76.5538	-0.3755 :	0.1409
-12.	8.7241	-39.7373	40.6837	-77.6174	-0.3575 :	0.1157
-11.	8.2864	-41.3625	42.1844	-78.6716	-0.3326 :	0.0900
-10.	7.6047	-41.9220	42.6062	-79.7183	-0.3027 :	0.0669
-9.	6.7325	-41.3809	41.9250	-80.7592	-0.2693 :	0.0486
-8.	5.7326	-39.7587	40.1699	-81.7955	-0.2347 :	0.0321
-7.	4.6710	-37.1197	37.4124	-82.8279	-0.1995 :	0.0214
-6.	3.6118	-33.5602	33.7540	-83.8573	-0.1649 :	0.0130
-5.	2.6139	-29.1979	29.3146	-84.8844	-0.1319 :	0.0066
-4.	1.7279	-24.1626	24.2243	-85.9096	-0.1006 :	0.0036
-3.	0.9959	-18.5895	18.6162	-86.9334	-0.0716 :	0.0015
-2.	0.4502	-12.6148	12.6228	-87.9561	-0.0451 :	0.0002
-1.	0.1137	-6.3737	6.3747	-88.9782	-0.0211 :	0.0000

Table 3.17 - Cont.

Scan Angle	Cartezian coords.		polar coords.		Dp, deg.	
(deg.)	x0/λ	z0/λ	r0/λ	delta-deg.	Min.	Max.
0.	-0.0000	-0.0000	0.0000	-91.4997	-0.0000 :	0.0000
1.	0.1137	6.3737	6.3747	88.9782	-0.0000 :	0.0211
2.	0.4502	12.6148	12.6228	87.9561	-0.0002 :	0.0451
3.	0.9959	18.5895	18.6162	86.9334	-0.0015 :	0.0716
4.	1.7279	24.1626	24.2243	85.9096	-0.0036 :	0.1006
5.	2.6139	29.1979	29.3146	84.8844	-0.0066 :	0.1319
6.	3.6118	33.5602	33.7540	83.8573	-0.0130 :	0.1649
7.	4.6710	37.1197	37.4124	82.8279	-0.0214 :	0.1995
8.	5.7326	39.7587	40.1699	81.7955	-0.0321 :	0.2347
9.	6.7325	41.3809	41.9250	80.7592	-0.0486 :	0.2693
10.	7.6047	41.9220	42.6062	79.7183	-0.0669 :	0.3027
11.	8.2864	41.3625	42.1844	78.6716	-0.0900 :	0.3326
12.	8.7241	39.7373	40.6837	77.6174	-0.1157 :	0.3575
13.	8.8802	37.1424	38.1892	76.5538	-0.1409 :	0.3755
14.	8.7383	33.7346	34.8480	75.4779	-0.1682 :	0.3852
15.	8.3071	29.7231	30.8621	74.3853	-0.1911 :	0.3860
16.	7.6205	25.3520	26.4726	73.2699	-0.2080 :	0.3787
17.	6.7349	20.8790	21.9384	72.1220	-0.2185 :	0.3631
18.	5.7223	16.5495	17.5109	70.9261	-0.2236 :	0.3407
19.	4.6623	12.5746	13.4111	69.6568	-0.2223 :	0.3131
20.	3.6328	9.1154	9.8126	68.2709	-0.2149 :	0.2826
21.	2.7029	6.2746	6.8320	66.6948	-0.2029 :	0.2513
22.	1.9271	4.0970	4.5276	64.8095	-0.1875 :	0.2213
23.	1.3422	2.5760	2.9047	62.4783	-0.1706 :	0.1936
24.	0.9676	1.6646	1.9254	59.8310	-0.1530 :	0.1694
25.	0.8063	1.2876	1.5192	57.9454	-0.1357 :	0.1492
26.	0.8474	1.3527	1.5962	57.9362	-0.1196 :	0.1327
27.	1.0695	1.7612	2.0605	58.7310	-0.1053 :	0.1200
28.	1.4436	2.4145	2.8131	59.1258	-0.0930 :	0.1104
29.	1.9357	3.2206	3.7575	58.9918	-0.0826 :	0.1039
30.	2.5096	4.0964	4.8040	58.5074	-0.0742 :	0.0998
31.	3.1283	4.9710	5.8734	57.8172	-0.0678 :	0.0978
32.	3.7563	5.7853	6.8978	57.0053	-0.0633 :	0.0971
33.	4.3601	6.4931	7.8212	56.1185	-0.0608 :	0.0976
34.	4.9104	7.0606	8.6003	55.1829	-0.0595 :	0.0989
35.	5.3817	7.4657	9.2032	54.2136	-0.0595 :	0.1004
36.	5.7543	7.6973	9.6104	53.2193	-0.0603 :	0.1019
37.	6.0136	7.7541	9.8127	52.2049	-0.0618 :	0.1030
38.	6.1516	7.6437	9.8117	51.1733	-0.0634 :	0.1040
39.	6.1661	7.3812	9.6178	50.1256	-0.0649 :	0.1043
40.	6.0608	6.9873	9.2497	49.0615	-0.0664 :	0.1037

Table 3.18

Phase centre and phase variation (Dp-deg.) of a 56-element linear array in H-plane for different scan angles.
Complete phase ext. failure in elements no. 25 to 28,
Mutual coupling between array elements is included.

Scan Angle	Cartezian coords.		polar coords.		Dp, deg.	
(deg.)	x0/λ	z0/λ	r0/λ	delta-deg.	Min.	Max.
-40.	6.0604	-6.9859	9.2483	-49.0578	-0.1037 :	0.0664
-39.	6.1571	-7.3694	9.6030	-50.1217	-0.1042 :	0.0649
-38.	6.1468	-7.6374	9.8037	-51.1715	-0.1040 :	0.0634
-37.	6.0200	-7.7621	9.8230	-52.2042	-0.1031 :	0.0619
-36.	5.7613	-7.7060	9.6215	-53.2169	-0.1019 :	0.0603
-35.	5.3780	-7.4593	9.1958	-54.2093	-0.1003 :	0.0595
-34.	4.9028	-7.0487	8.5862	-55.1794	-0.0989 :	0.0596
-33.	4.3627	-6.4967	7.8256	-56.1175	-0.0977 :	0.0608
-32.	3.7660	-5.8000	6.9154	-57.0043	-0.0972 :	0.0633
-31.	3.1299	-4.9724	5.8755	-57.8116	-0.0976 :	0.0679
-30.	2.5026	-4.0835	4.7894	-58.4980	-0.0998 :	0.0743
-29.	1.9358	-3.2203	3.7573	-58.9893	-0.1040 :	0.0826
-28.	1.4536	-2.4327	2.8339	-59.1405	-0.1105 :	0.0929
-27.	1.0740	-1.7688	2.0694	-58.7336	-0.1199 :	0.1052
-26.	0.8417	-1.3401	1.5825	-57.8693	-0.1327 :	0.1197
-25.	0.8056	-1.2860	1.5175	-57.9344	-0.1493 :	0.1357
-24.	0.9774	-1.6861	1.9489	-59.8998	-0.1694 :	0.1530
-23.	1.3471	-2.5864	2.9162	-62.4868	-0.1936 :	0.1704
-22.	1.9218	-4.0833	4.5130	-64.7955	-0.2212 :	0.1875
-21.	2.7029	-6.2747	6.8321	-66.6953	-0.2512 :	0.2031
-20.	3.6422	-9.1407	9.8396	-68.2750	-0.2824 :	0.2151
-19.	4.6655	-12.5827	13.4198	-69.6560	-0.3130 :	0.2222
-18.	5.7172	-16.5334	17.4940	-70.9247	-0.3407 :	0.2237
-17.	6.7366	-20.8851	21.9447	-72.1227	-0.3631 :	0.2186
-16.	7.6285	-25.3795	26.5012	-73.2705	-0.3787 :	0.2080
-15.	8.3074	-29.7234	30.8625	-74.3848	-0.3859 :	0.1910
-14.	8.7342	-33.7187	34.8315	-75.4777	-0.3853 :	0.1682
-13.	8.8835	-37.1576	38.2048	-76.5544	-0.3756 :	0.1410
-12.	8.7294	-39.7614	40.7084	-77.6175	-0.3572 :	0.1158
-11.	8.2847	-41.3533	42.1750	-78.6713	-0.3325 :	0.0900
-10.	7.6027	-41.9121	42.5960	-79.7186	-0.3028 :	0.0669
-9.	6.7359	-41.4039	41.9483	-80.7596	-0.2696 :	0.0485
-8.	5.7348	-39.7739	40.1852	-81.7953	-0.2346 :	0.0320
-7.	4.6691	-37.1042	37.3968	-82.8278	-0.1994 :	0.0214
-6.	3.6115	-33.5601	33.7539	-83.8578	-0.1650 :	0.0131
-5.	2.6160	-29.2235	29.3404	-84.8847	-0.1319 :	0.0066
-4.	1.7283	-24.1661	24.2278	-85.9093	-0.1005 :	0.0036
-3.	0.9949	-18.5730	18.5996	-86.9336	-0.0716 :	0.0015
-2.	0.4503	-12.6249	12.6330	-87.9574	-0.0452 :	0.0002
-1.	0.1141	-6.3961	6.3971	-88.9780	-0.0211 :	0.0000

Table 3.18 - Cont.

Scan Angle	Cartezian coords.		polar coords.		Dp, deg.	
(deg.)	x0/λ	z0/λ	r0/λ	delta-deg.	Min.	Max.
0.	0.0001	0.0080	0.0080	89.0811	-0.0001 :	0.0001
1.	0.1137	6.3866	6.3876	88.9799	-0.0000 :	0.0213
2.	0.4494	12.5968	12.6048	87.9569	-0.0002 :	0.0452
3.	0.9953	18.5756	18.6022	86.9329	-0.0014 :	0.0716
4.	1.7292	24.1798	24.2415	85.9095	-0.0036 :	0.1007
5.	2.6141	29.2037	29.3204	84.8849	-0.0066 :	0.1320
6.	3.6095	33.5386	33.7322	83.8574	-0.0129 :	0.1650
7.	4.6709	37.1181	37.4108	82.8276	-0.0214 :	0.1994
8.	5.7356	39.7811	40.1924	81.7956	-0.0321 :	0.2348
9.	6.7317	41.3779	41.9219	80.7596	-0.0487 :	0.2695
10.	7.6013	41.9028	42.5867	79.7182	-0.0669 :	0.3027
11.	8.2889	41.3749	42.1970	78.6715	-0.0899 :	0.3326
12.	8.7287	39.7597	40.7066	77.6180	-0.1158 :	0.3575
13.	8.8776	37.1322	38.1787	76.5542	-0.1410 :	0.3756
14.	8.7357	33.7240	34.8371	75.4776	-0.1682 :	0.3851
15.	8.3134	29.7467	30.8866	74.3857	-0.1911 :	0.3859
16.	7.6253	25.3702	26.4914	73.2712	-0.2081 :	0.3788
17.	6.7308	20.8665	21.9252	72.1222	-0.2186 :	0.3631
18.	5.7224	16.5495	17.5109	70.9259	-0.2235 :	0.3407
19.	4.6719	12.6029	13.4410	69.6603	-0.2222 :	0.3131
20.	3.6371	9.1286	9.8265	68.2760	-0.2151 :	0.2825
21.	2.6985	6.2637	6.8202	66.6932	-0.2030 :	0.2512
22.	1.9296	4.1033	4.5344	64.8144	-0.1874 :	0.2212
23.	1.3537	2.6037	2.9346	62.5291	-0.1706 :	0.1936
24.	0.9719	1.6755	1.9370	59.8834	-0.1531 :	0.1694
25.	0.8020	1.2791	1.5098	57.9135	-0.1356 :	0.1492
26.	0.8507	1.3596	1.6038	57.9679	-0.1195 :	0.1327
27.	1.0819	1.7862	2.0883	58.7958	-0.1052 :	0.1200
28.	1.4491	2.4262	2.8260	59.1502	-0.0929 :	0.1105
29.	1.9317	3.2141	3.7499	58.9939	-0.0825 :	0.1039
30.	2.5113	4.0997	4.8077	58.5103	-0.0741 :	0.0998
31.	3.1405	4.9918	5.8975	57.8246	-0.0678 :	0.0977
32.	3.7647	5.7998	6.9145	57.0122	-0.0634 :	0.0971
33.	4.3573	6.4897	7.8168	56.1216	-0.0608 :	0.0975
34.	4.9085	7.0582	8.5972	55.1840	-0.0595 :	0.0988
35.	5.3911	7.4794	9.2199	54.2161	-0.0594 :	0.1003
36.	5.7660	7.7141	9.6309	53.2235	-0.0603 :	0.1019
37.	6.0149	7.7567	9.8156	52.2083	-0.0617 :	0.1031
38.	6.1466	7.6379	9.8040	51.1745	-0.0634 :	0.1039
39.	6.1685	7.3843	9.6217	50.1264	-0.0649 :	0.1042
40.	6.0723	7.0012	9.2677	49.0645	-0.0664 :	0.1037

Chapter 4
Slotted waveguide array

4.1 Introduction

In chapter 2, a method was presented to determine the apparent phase centre of any radiating system. The method was subsequently applied to a linear array of rectangular microstrip patch antennas to determine the effects of mutual coupling between the patches on the phase centre location. In the present chapter, the method is applied to a linear array of slotted waveguides. Again, the phase centre location is determined and its displacement due to random and pre-determined errors, as well as, amplifier and phase shifter failures is studied. The developed formulation is general and can be used also for determining the phase centre of other radiating structures.

Computer simulations are performed to understand the process of phase centre movement, due to different error types. Most of the generated results are statistical in nature. However, the generation of pseudo-random numbers to identify the source or magnitude of errors is not based on the actual physical processes. They are presented as sample examples, as requested by the contract.

The selected antenna is a linear array of 56 elements and its element excitation is a Taylor distribution with $-30\ dB$ side lobe level. The interelement spacing is selected to be 0.593 λ and array operates at 5.06 GHz.

For the above array a computer program is developed to simulate the effect of random errors and element failures on the *MLS* antenna phase centre location, and movement. The number of radiating elements, interelement spacing, and operating frequency, are the input parameters for the error free case. Other information as the types of errors and the number of failed amplifiers, number of failed phase shifters, and the seed number for pseudo-random generator are input data for the simulation program. The following section describes the results of various simulation runs.

4.2 Random error

As discussed earlier, the random errors represent the environmental effects, manufacturing tolerances, and excitation errors, etc. The effect of these errors is simulated by generating random numbers, normally distributed, then multiplying them by the specified standard deviation of amplitude and phase errors. The results are then added to the excitation coefficients. The *IMSL* routine (GGNML) is used to generate pseudo-random normal (0, 1) deviates, which transforms uniform deviates to normal deviates using the inverse normal routine. Given a seed number and the number of deviates, it generates specified uniform random numbers in the exclusive range (0, 1).

The output of the simulation run for different seed numbers are plotted in Figs. 4.1 to 4.5. These graphs correspond to the random errors introduced to each *MLS* antenna element. Random normal deviates with specified mean (m) and standard deviation (σ) may be obtained by normalizing the output according to the specified values of m, and σ. The normalized version of the same seed number plotted in Figs. 4.1 to 4.5 are shown in Figs. 4.6 to 4.10, with their respective m, and σ. Figs. 4.11 to 4.15 show the phase centre movement due to the phase random errors with σ = 5 degrees, for the same seed numbers. These results indicate that, the variation of the phase centre coordinates is in the range of 2.0 λ for the x-coordinate and 6.0 λ for the z-coordinate. The case of random errors in the amplitude for σ = 5% are shown in Figs. 4.16 to 4.20. Here, the results indicate the maximum coordinate variation of 0.07 λ for the x-coordinate and 0.01 λ variation for the z-coordinate. It is evident from these results that, errors in the excitation amplitude and phase of the antenna cause the phase centre movement from its physical centre. Phase errors are more important and displacements due to them are considerably larger than the displacements due to the amplitude errors.

4.3 Element failure

Our computer program is modified to simulate the phase centre movemen for a specified number of failures. Failures can occur on any amplifier or phase shifer that are attached to each radiating element. For each failed element, the program determines the displacement of the phase centre, if any, and computes the new phase centre coordinates.

4.3.1 Amplitude failure (amplitude is set to zero)

Initially, the number of failures is specified as an input parameter. For each failure, the program determines the location of antenna phase centre, if any. The output of the simulation runs at selected scan angles of –40°, –20°, 0.0°, 20°, and 40° are plotted in Figs. 4.21 to 4.25. These graphs correspond to amplitude failures, one at each time. The results for the selected scan angles indicate that, the movement of the phase centre is limited to 0.2 λ for the x-coordinate and to 0.05 λ for the z-coordinate. The case of two failed elements was also studied and the selected results are shown in Figs. 4.26 to 4.29. Here, due to symmetric failures the variations of the phase centre coordinates is negligible, except when the failed elements are 10 and 46 in which case the symmetry does not hold. For the cases presented here, the phase centre displacement is less than 0.0015 λ for the z-coordinate and 0.0025 λ for the x-coordinate. Figs 4.30 through 4.40 correspond to 5 failed elements when the location of the failures is moved from one end of the array to the other. It is clear that, the most severe displacement of the phase centre occurs when the intermediate elements are set to zero (short circuited), i.e. 16–20, and 36–40. The phase centre displacement is about 1.1 λ for the x-coordinate and 0.2 λ for the z-coordinate. A pre-determined error of 0.05 was also added to the amplitude of each element and the results for the selected scan angles are plotted in Figs. 4.41 to 4.45. Here, again the displacement is quite small and the maximum variation occurs at the scan angle of 40.0°. It is 0.0175 λ for the x- and 0.005 λ for the z-coordinate.

4.3.2 Phase shifter failure (phase is set to zero)

Similar to the amplitude failure case, in the simulation program, the number of failed phase shifter is specified as an input parameter. The program then computes the new location of the antenna phase centre. The simulated results of a single phase shifter failures and for the selected scan angles are shown in Figs 4.46 through 4.50. Comparing the results of Figs. (4.21)-(4.25) with the corresponding ones shown in Figs (4.46)-(4.50), one can observe that, the effect of phase shifter failures on the phase centre movement are more severe than those of amplitude failures. In addition, the variation in the phase centre coordinates is also scan angle dependent, and for the cases presented here, its location moves by as much as of 10.0 λ in the z–coordinate, and 5.0 λ in the x-coordinate. The movement is more pronounced for the intermediate failed phase shifters, i.e. in elements 16–20 and 36–40, and they have stronger effect on the phase centre movement, due to the type of excitation used in the analysis, i.e.,

$-30.0dB$ Taylor distribution. Figs. 4.51 to 4.55 illustrate the two element phase shifter failures. Similar to the amplitude failure cases, for symmetric failures the movement in the phase centre is negligible, and increases for unsymmetric ones (Figs. 4.54, and 4.55). The case of five failed phase shifters is also studied. The simulated results are plotted in Figs 4.56 through 4.66. In these cases, the phase centre displacements are considerable, and become even more significant for intermediate elements, as shown in table 4.1.

Table 4.1

Elem. No.	X_p / λ	θ_s^o	Z_p / λ	θ_s^o
1-5	5.2	-10.0	50.0	-2.0
6-10	5.6	-8.0	-41.0	-1.0
11-15	5.0	-10.0	36.8	-2.0
16-20	3.8	-14.0	11.14	-8.0
21-25	5.48	-33.0	53.0	-5.0
26-30	6.5	31.0	-13.4	-10.0
31-35	5.1	-28.0	59.0	-6.0
36-40	-4.0	-15.0	16.7	-2.0
41-45	-5.1	-4.0	31.67	2.0
46-50	-3.96	-33.0	39.15	1.0
51-56	-4.47	-29.0	-51.4	-3.0

Table 4.1. Variations in the phase centre coordinates due to five failed phase shifters.

Finally, the effect of pre-determined phase errors is investigated by adding a constant five degree error to each phase shifter. The simulated results are illustrated in Figs 4.67 through 4.71, for different elements, and in Figs. 4.72 and 4.73 for different scan angles. Here, the maximum phase centre displacement is about 1.2 λ in the z-coordinate for the 0.0 degree scan angle, and 0.4 λ in the x-coordinate for the 40.0 degree scan angle.

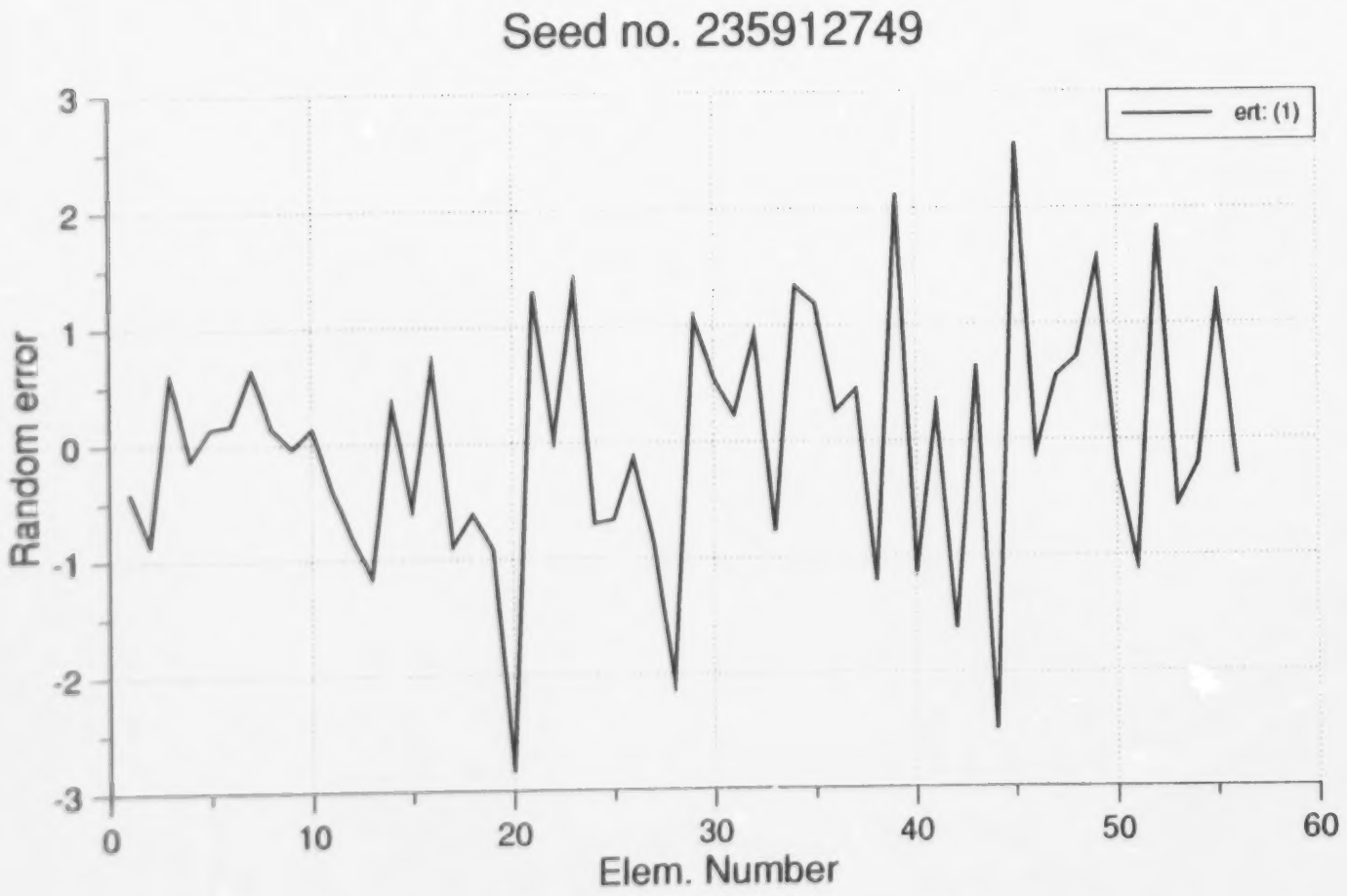

Fig. 4.1 : Plot of uniform random numbers, seed no. 235912749.

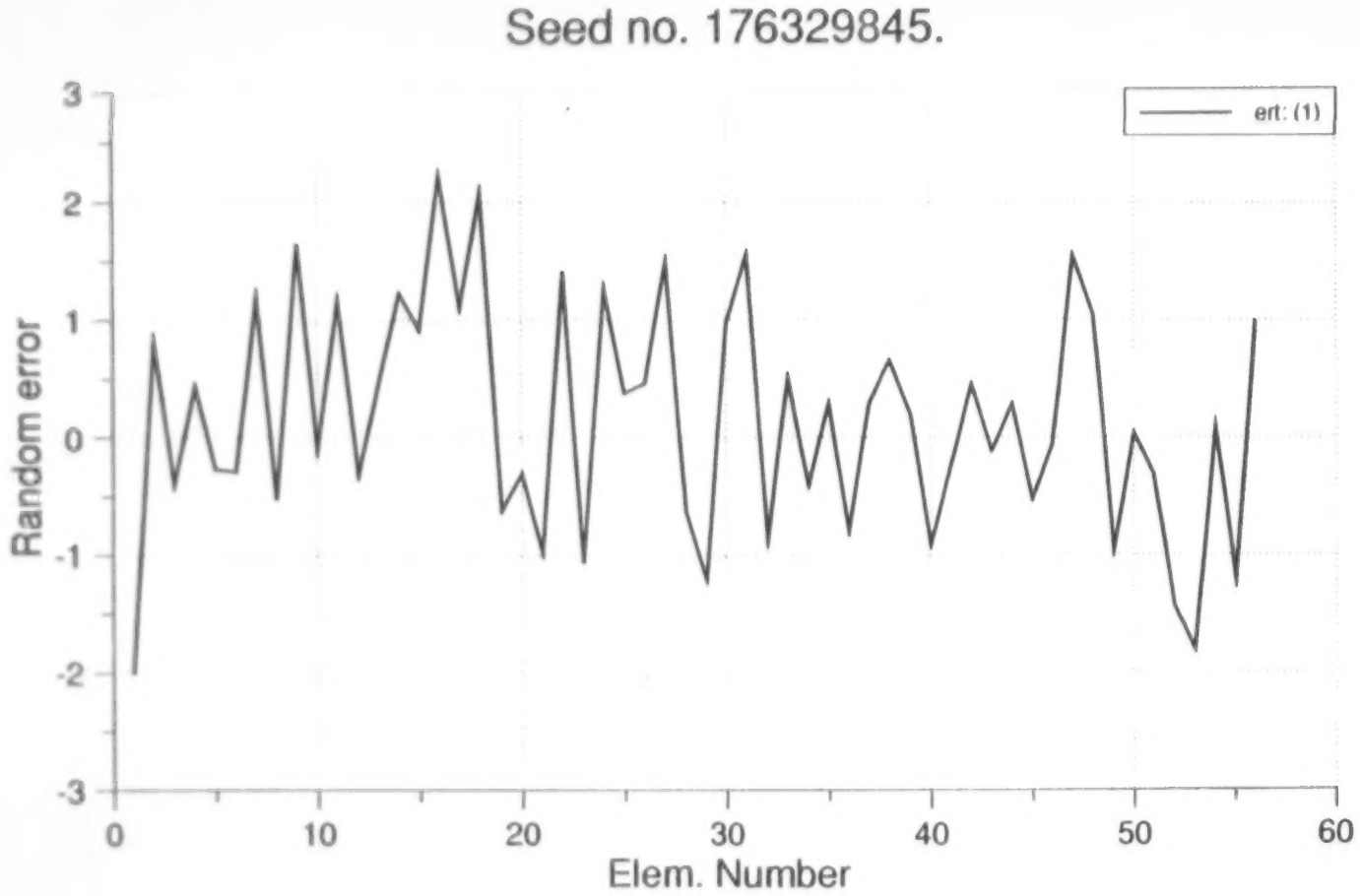

Fig. 4.2 : Plot of uniform random numbers, seed no. 176329845.

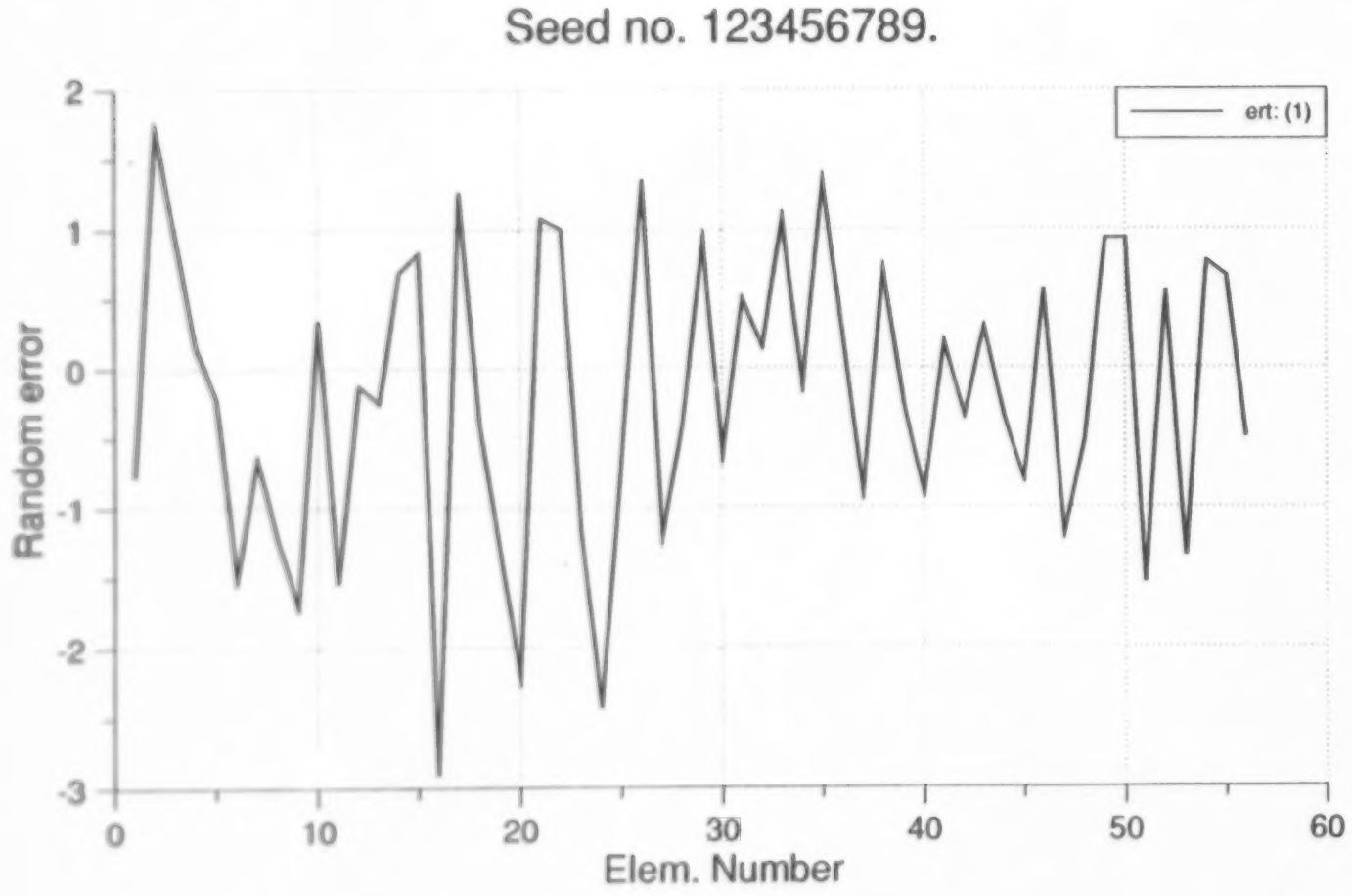

Fig. 4.3 : Plot of uniform random numbers, seed no. 123456789.

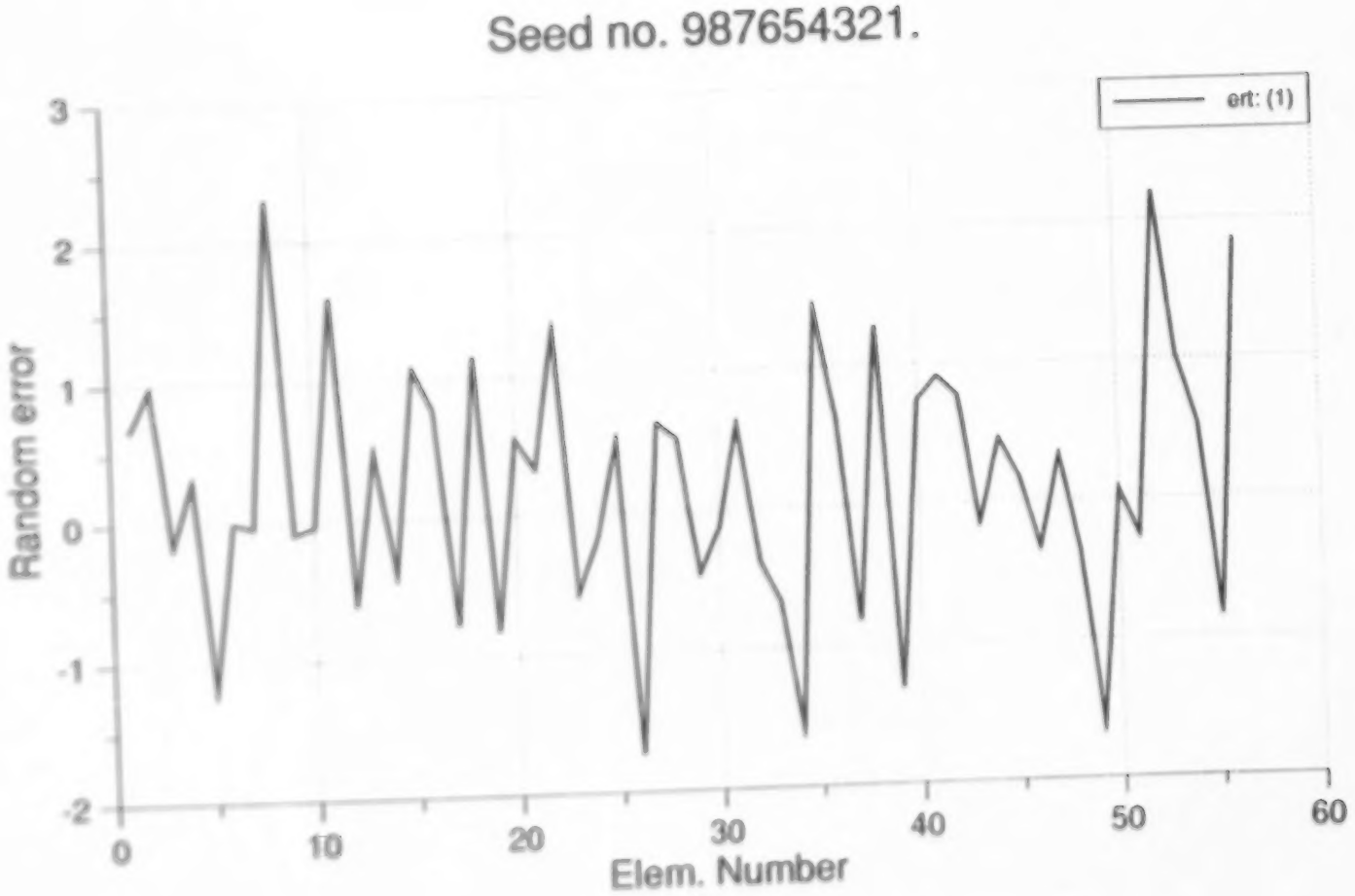

Fig. 4.4 : Plot of uniform random numbers, seed no. 987654321.

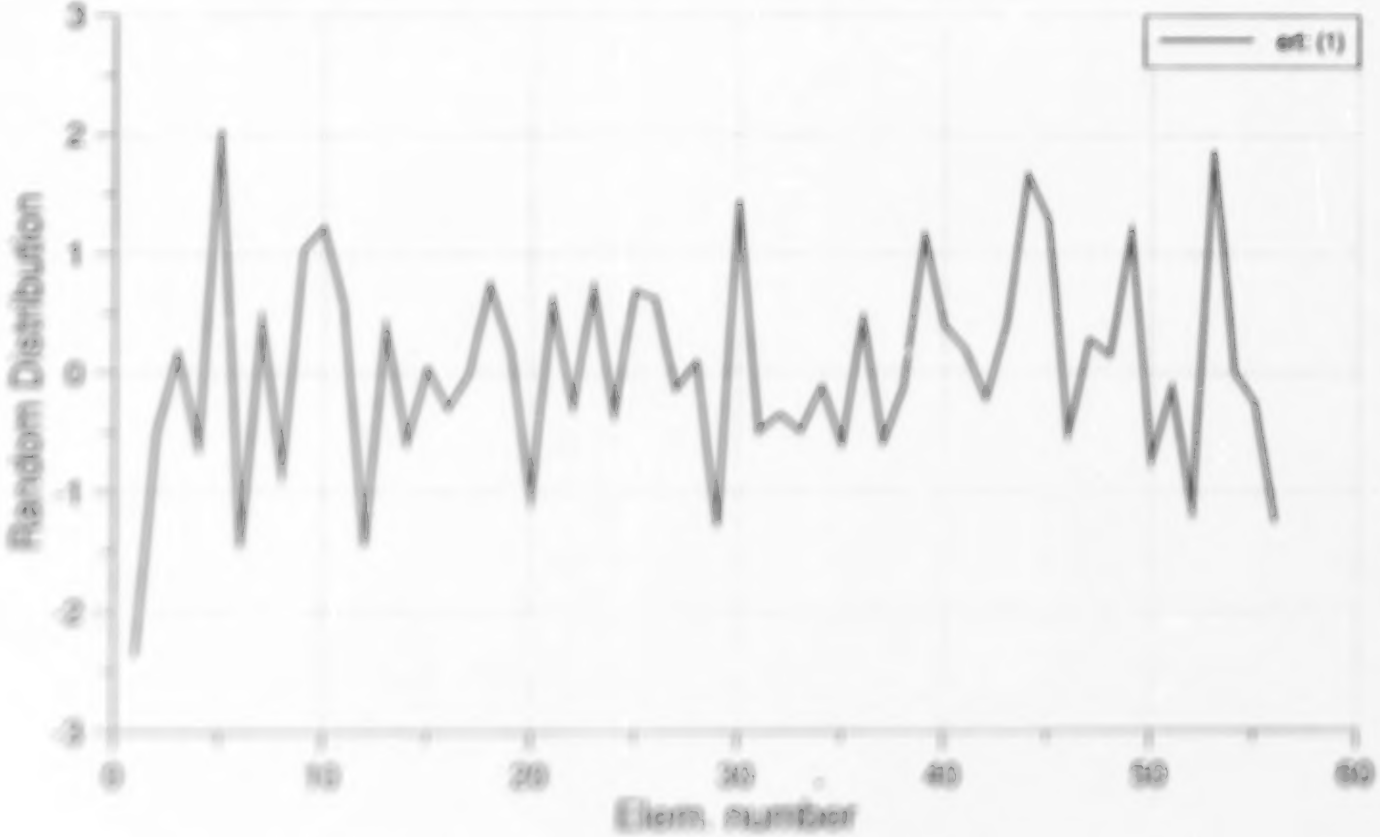

Fig. 4.3 : Plot of uniform random numbers, seed no. 555558888

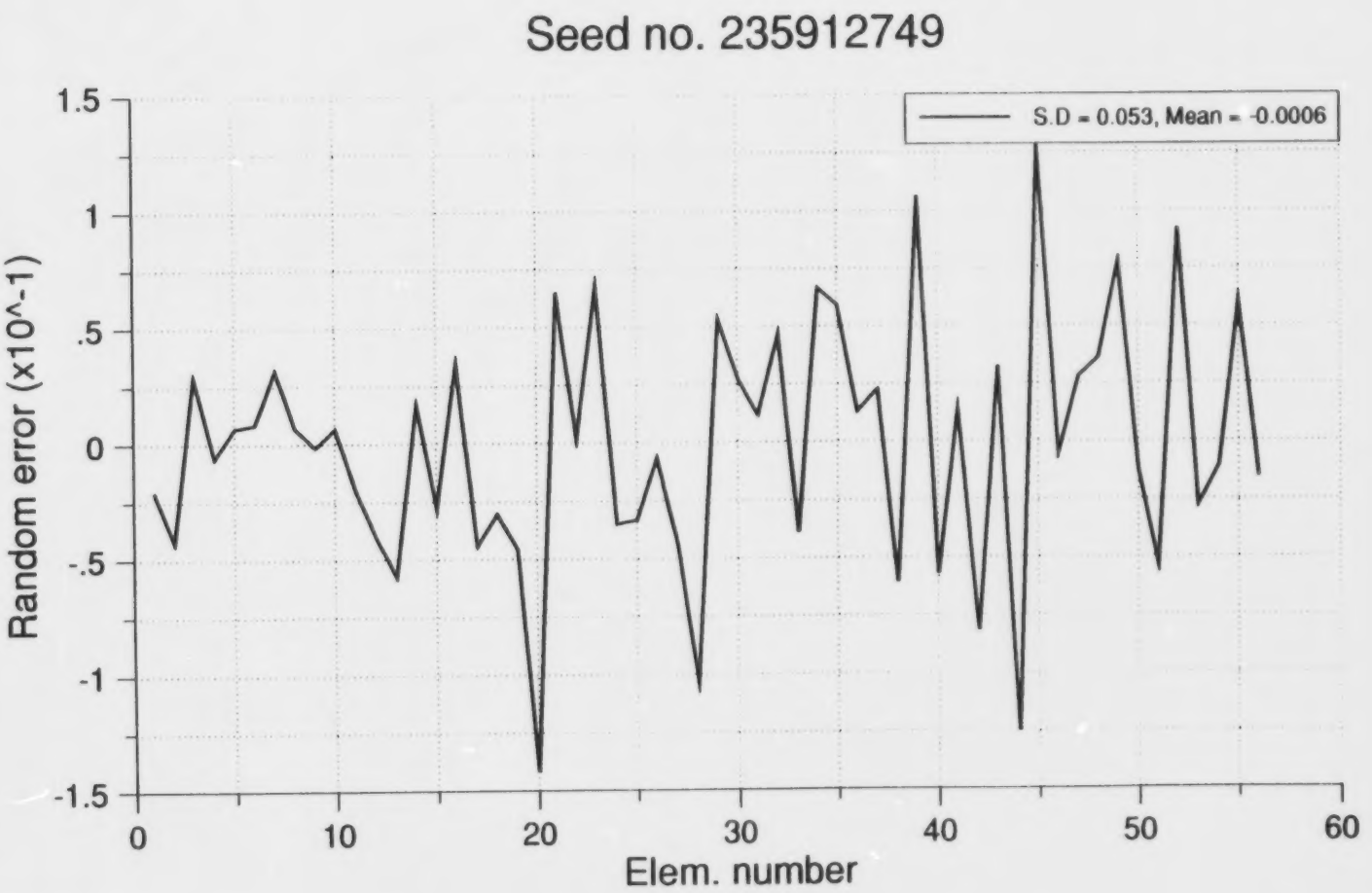

Fig. 4.6 : Normalized version of Fig. 4.1.

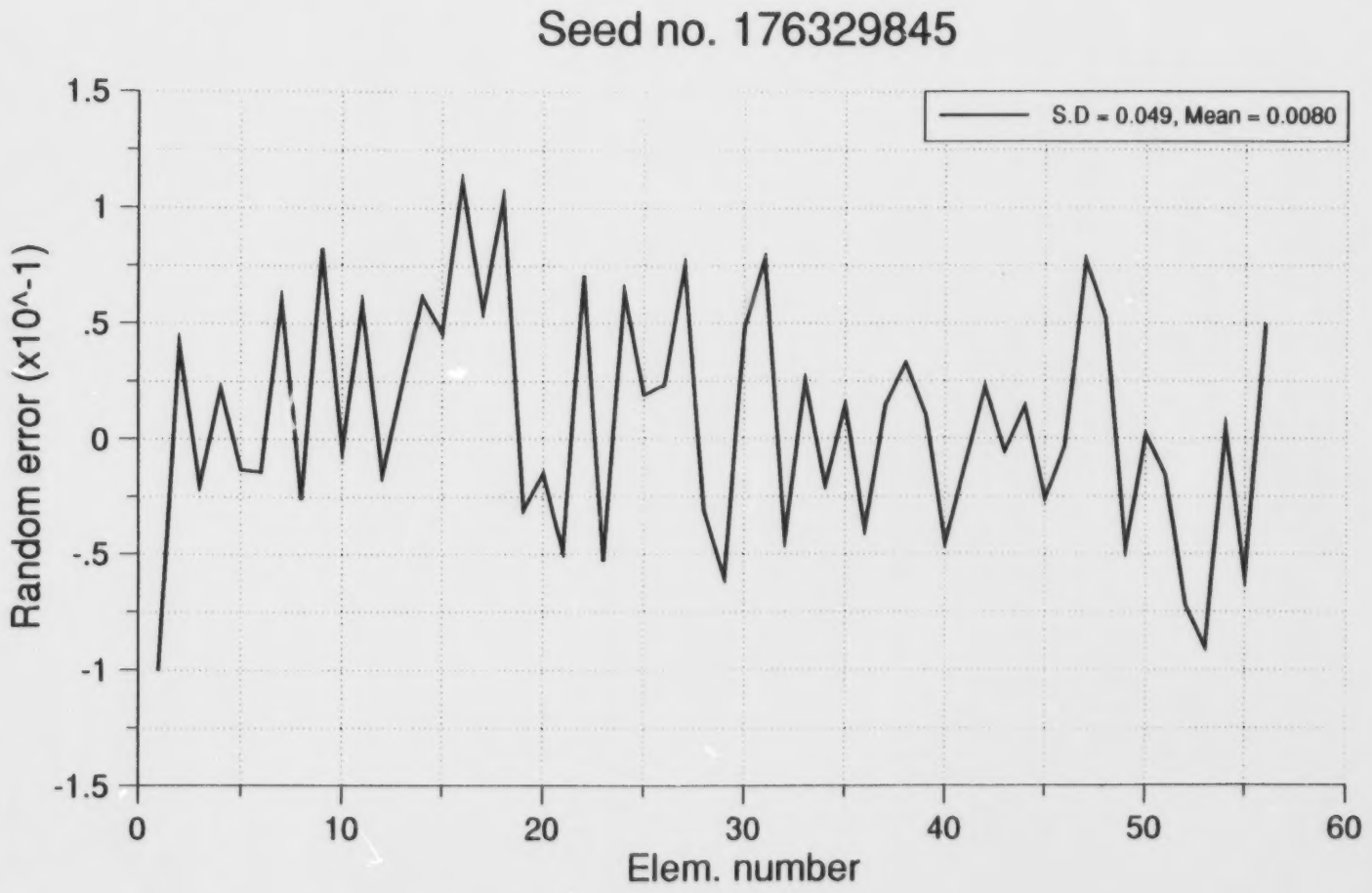

Fig. 4.7 : Normalized version of Fig. 4.2.

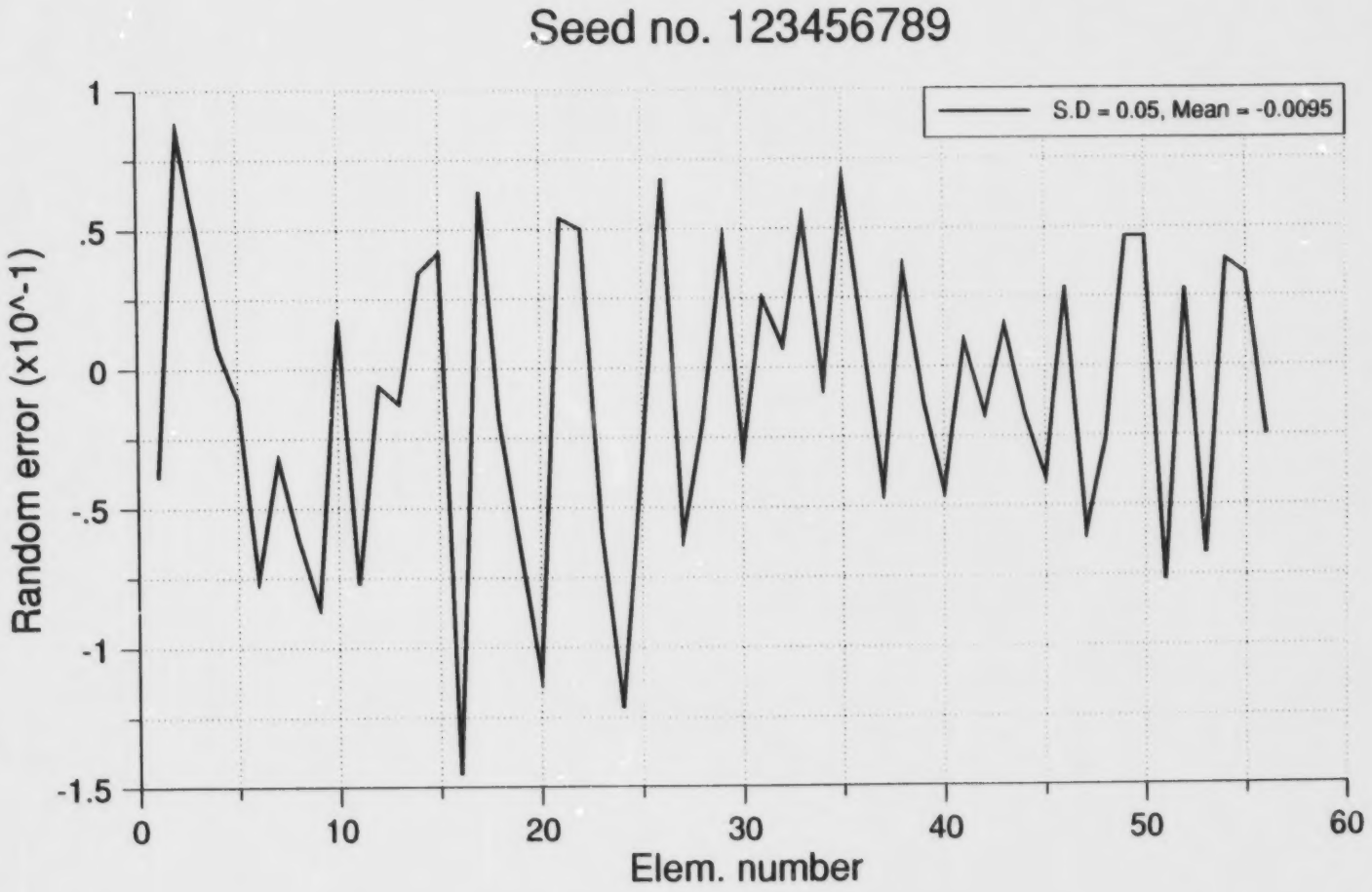

Fig. 4.8 : Normalized version of Fig. 4.3.

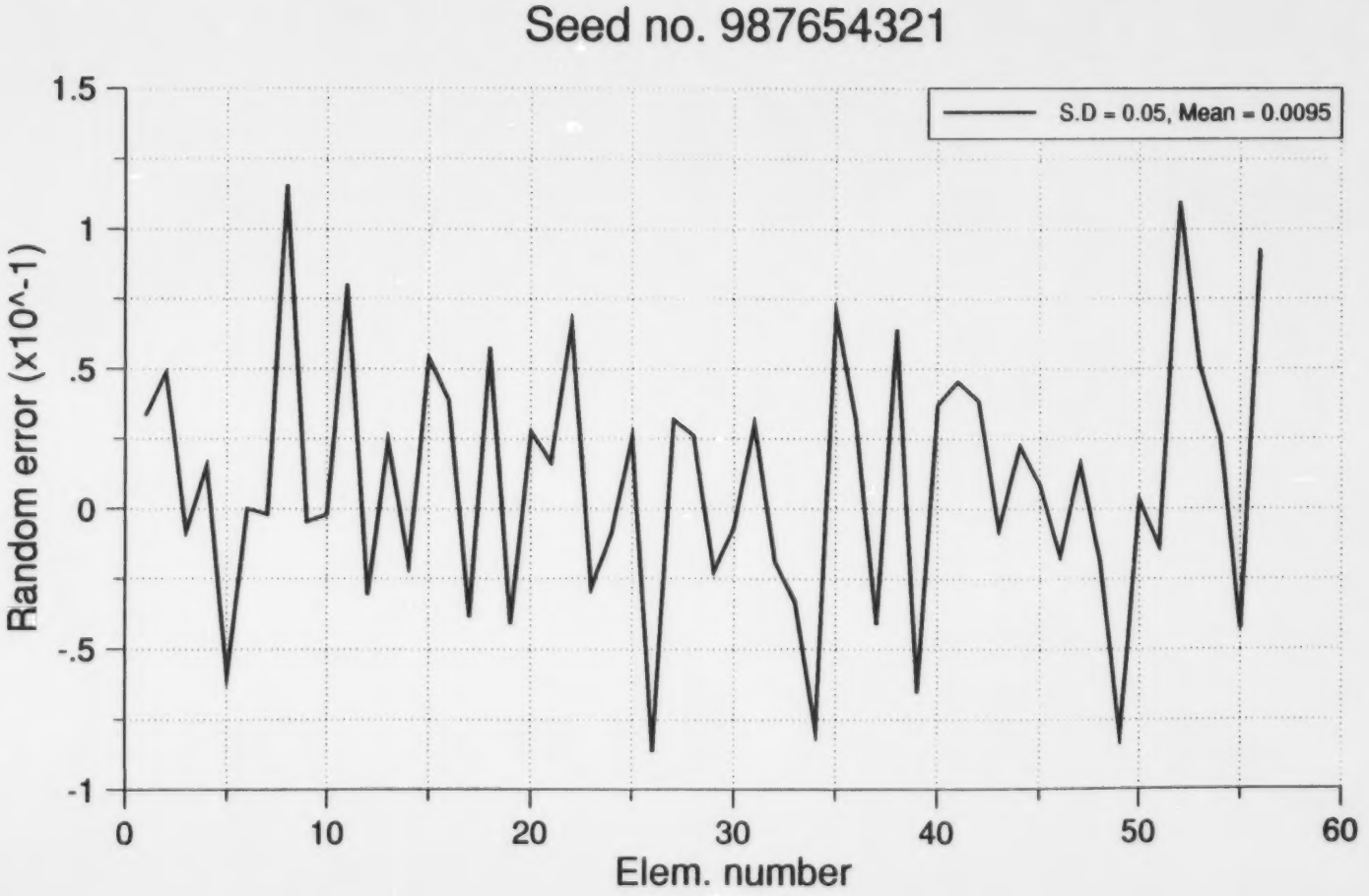

Fig. 4.9 : Normalized version of Fig. 4.4.

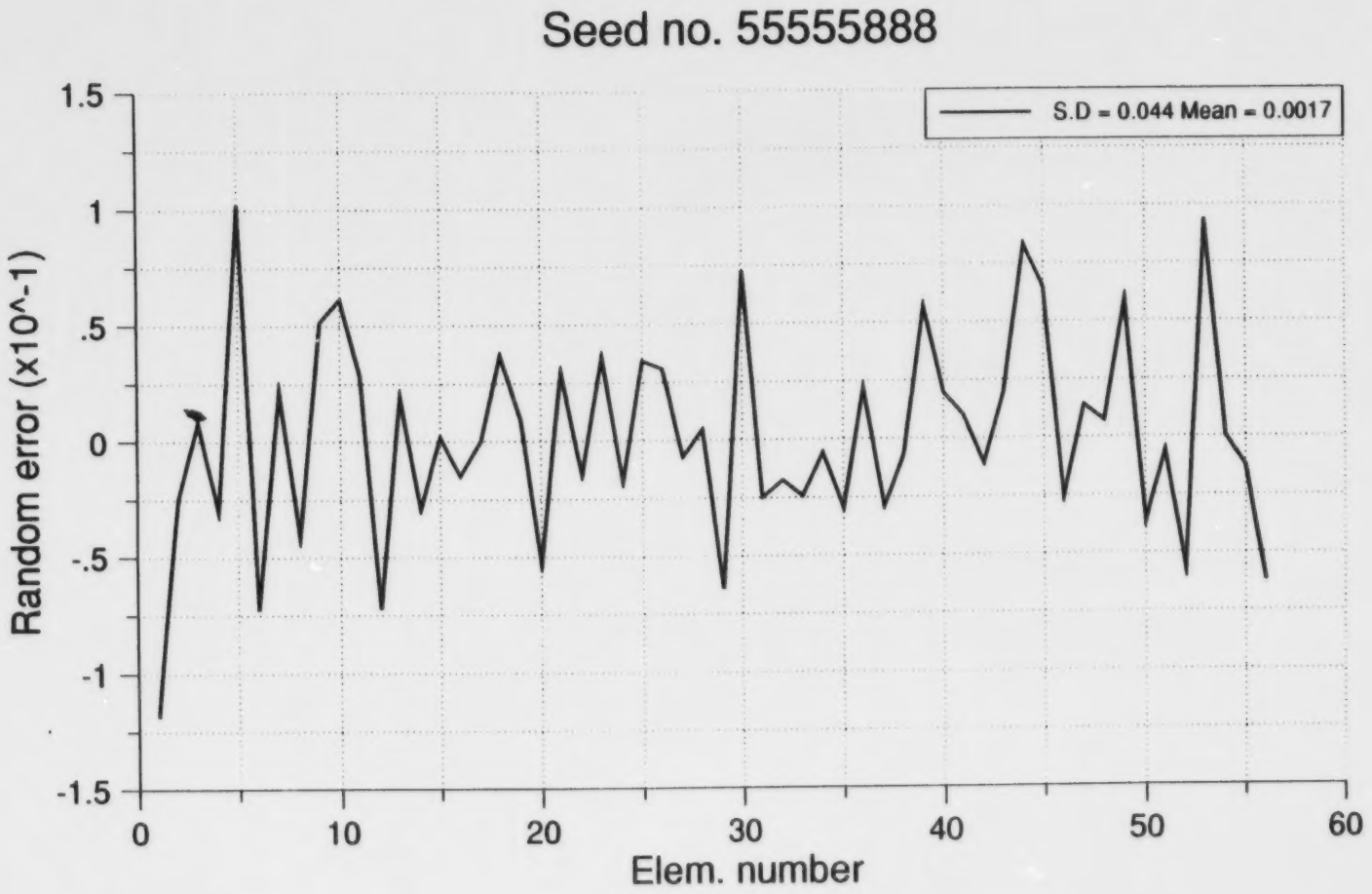

Fig. 4.10 : Normalized version of Fig. 4.5.

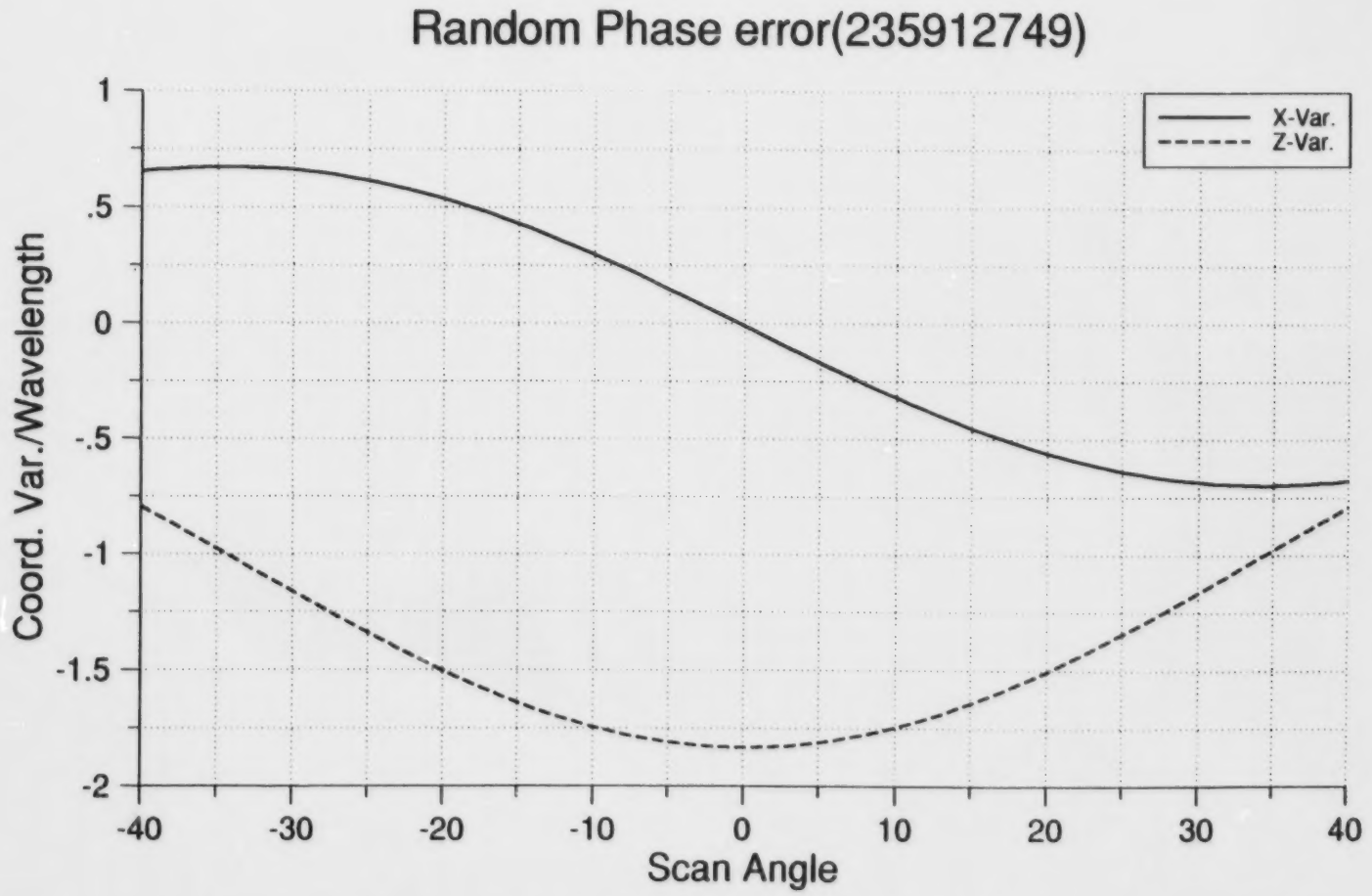

Fig. 4.11 : Phase centre movement due to the phase random errors, σ_p = 5 degrees, seed no. 235912749.

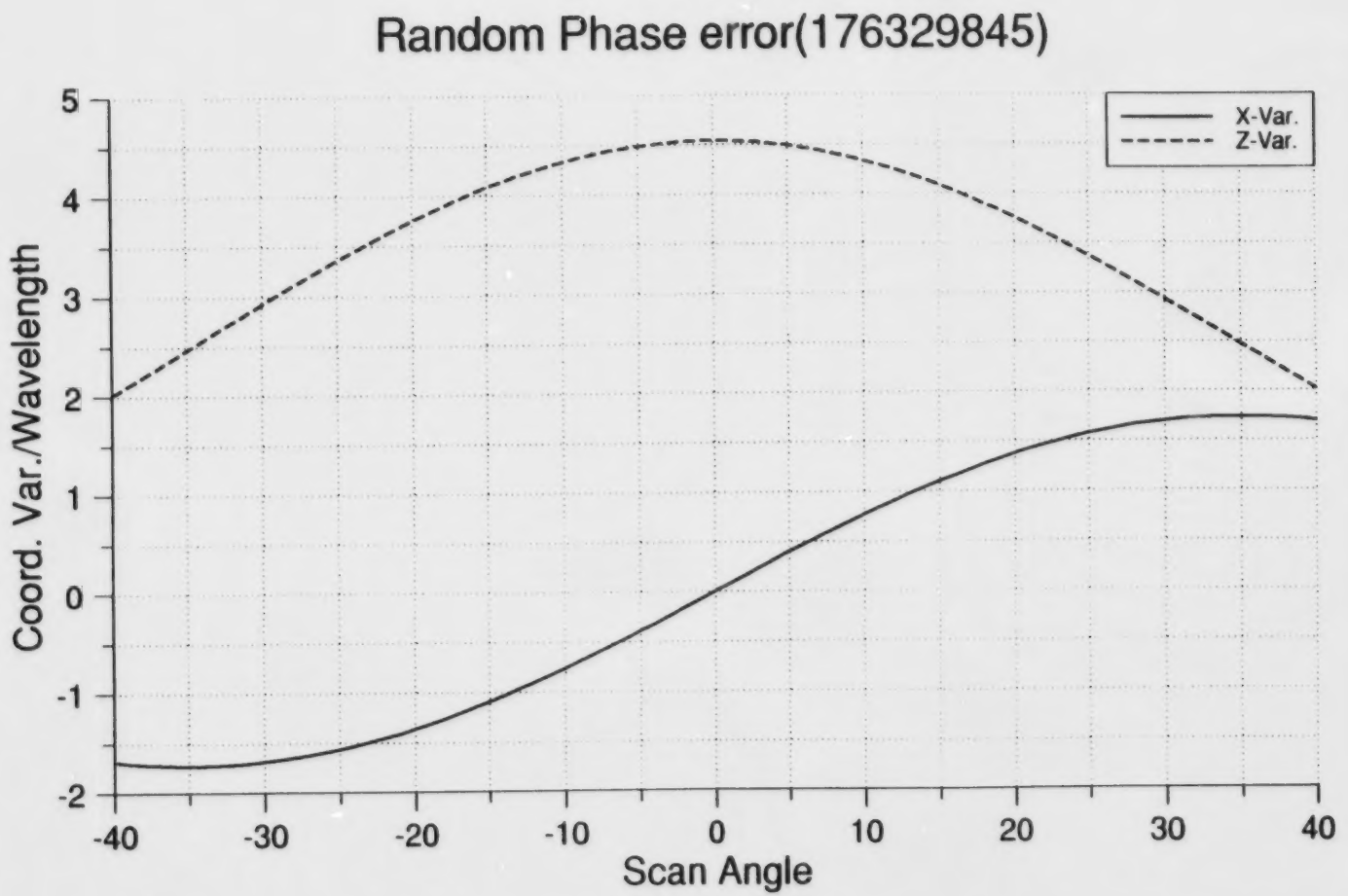

Fig. 4.12 : Phase centre movement due to the phase random errors, σ_p = 5 degrees, seed no. 176329845.

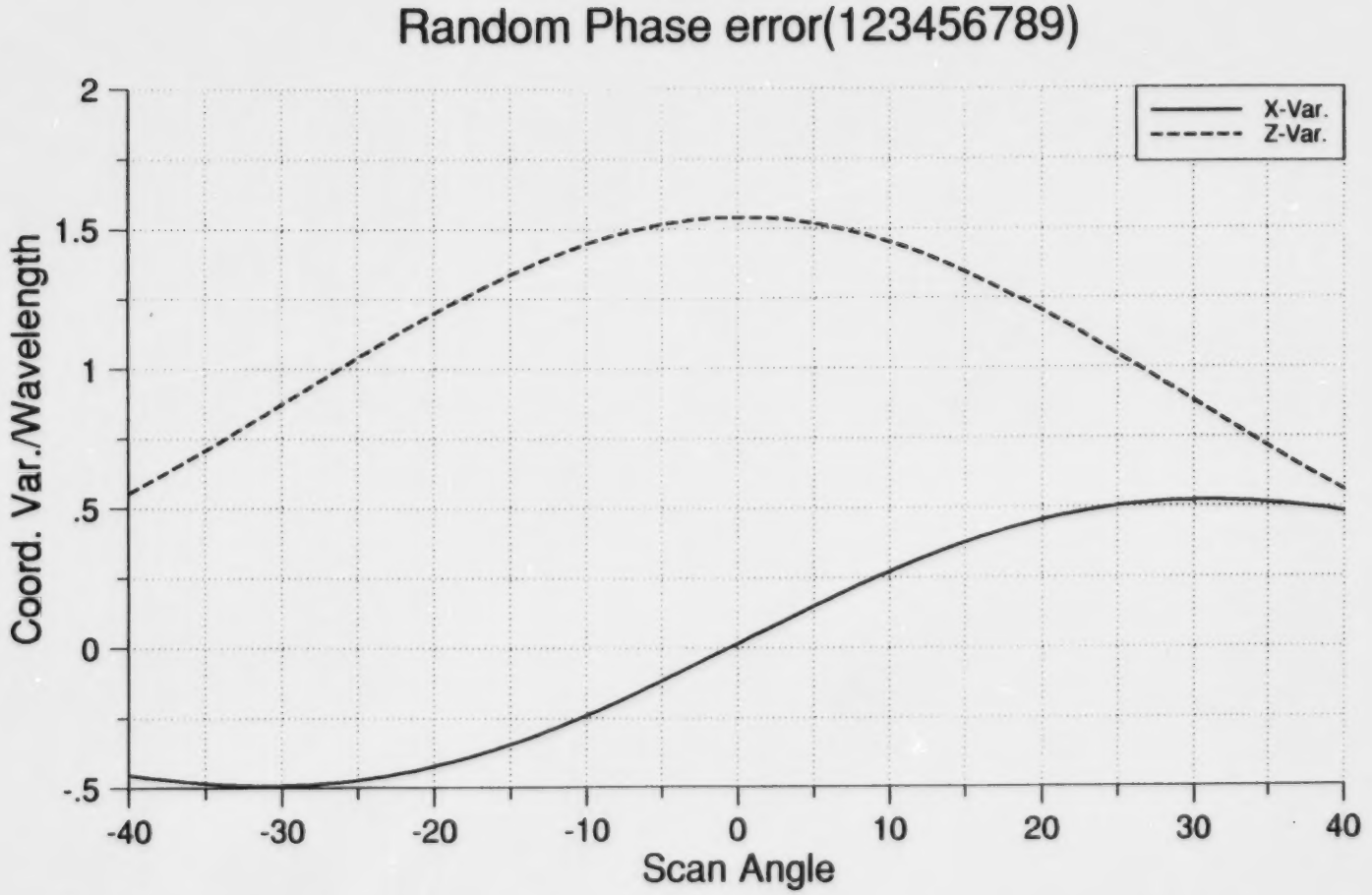

Fig. 4.13 : Phase centre movement due to the phase random errors, σ_p = 5 degrees, seed no. 123456789.

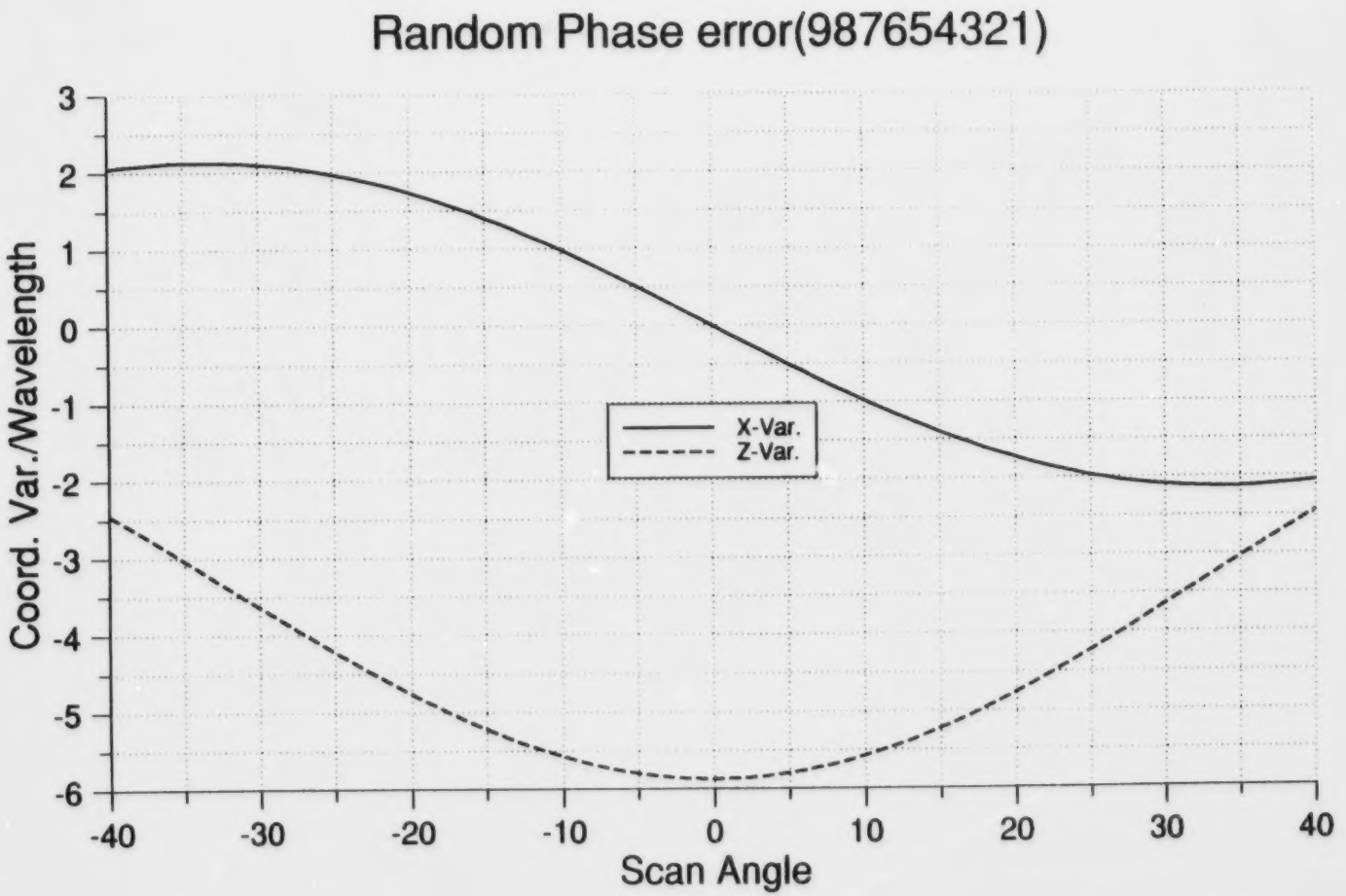

Fig. 4.14 : Phase centre movement due to the phase random errors, σ_p = 5 degrees, seed no. 987654321.

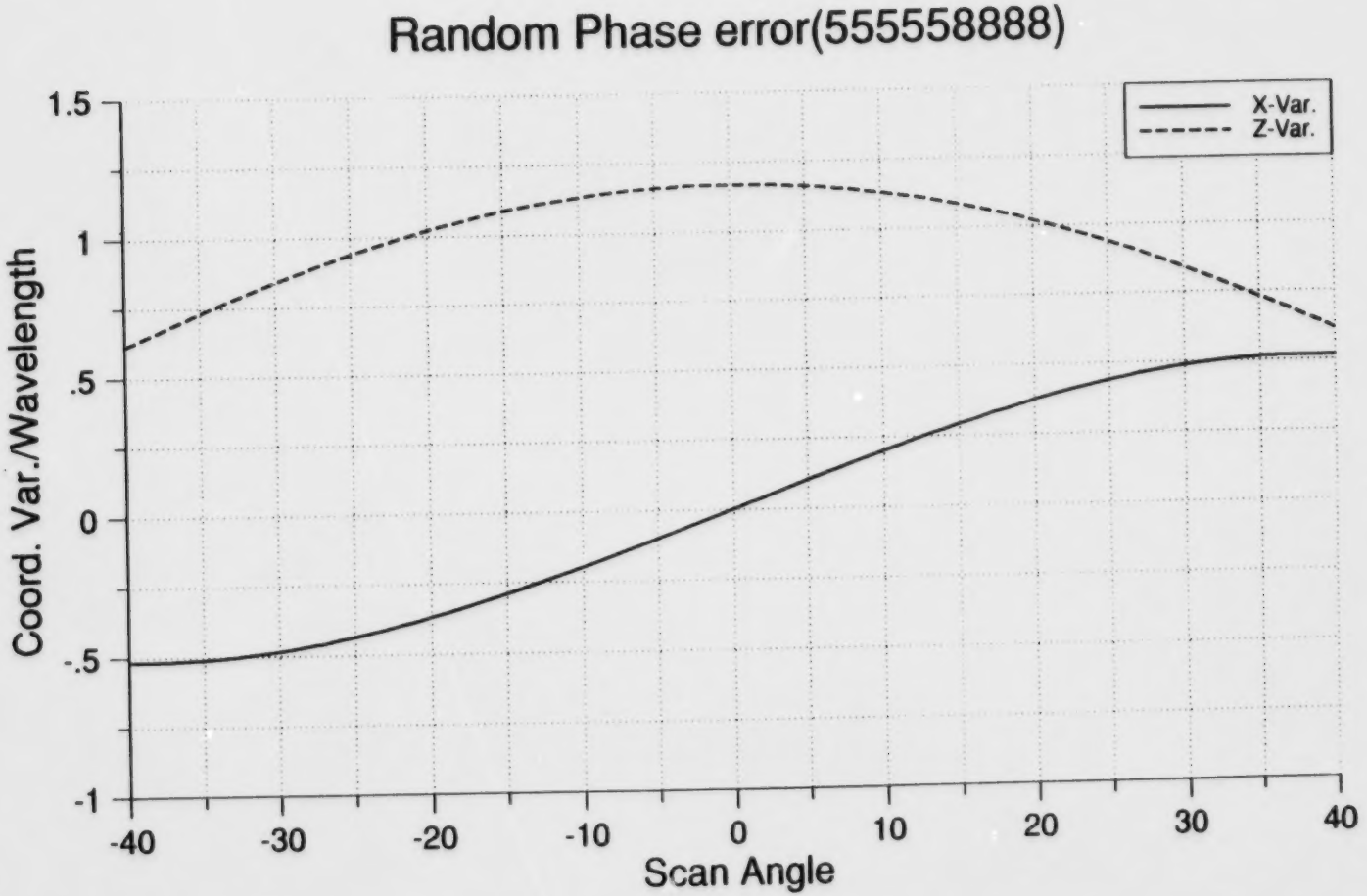

Fig. 4.15 : Phase centre movement due to the phase random errors, σ_p = 5 degrees, seed no. 555558888.

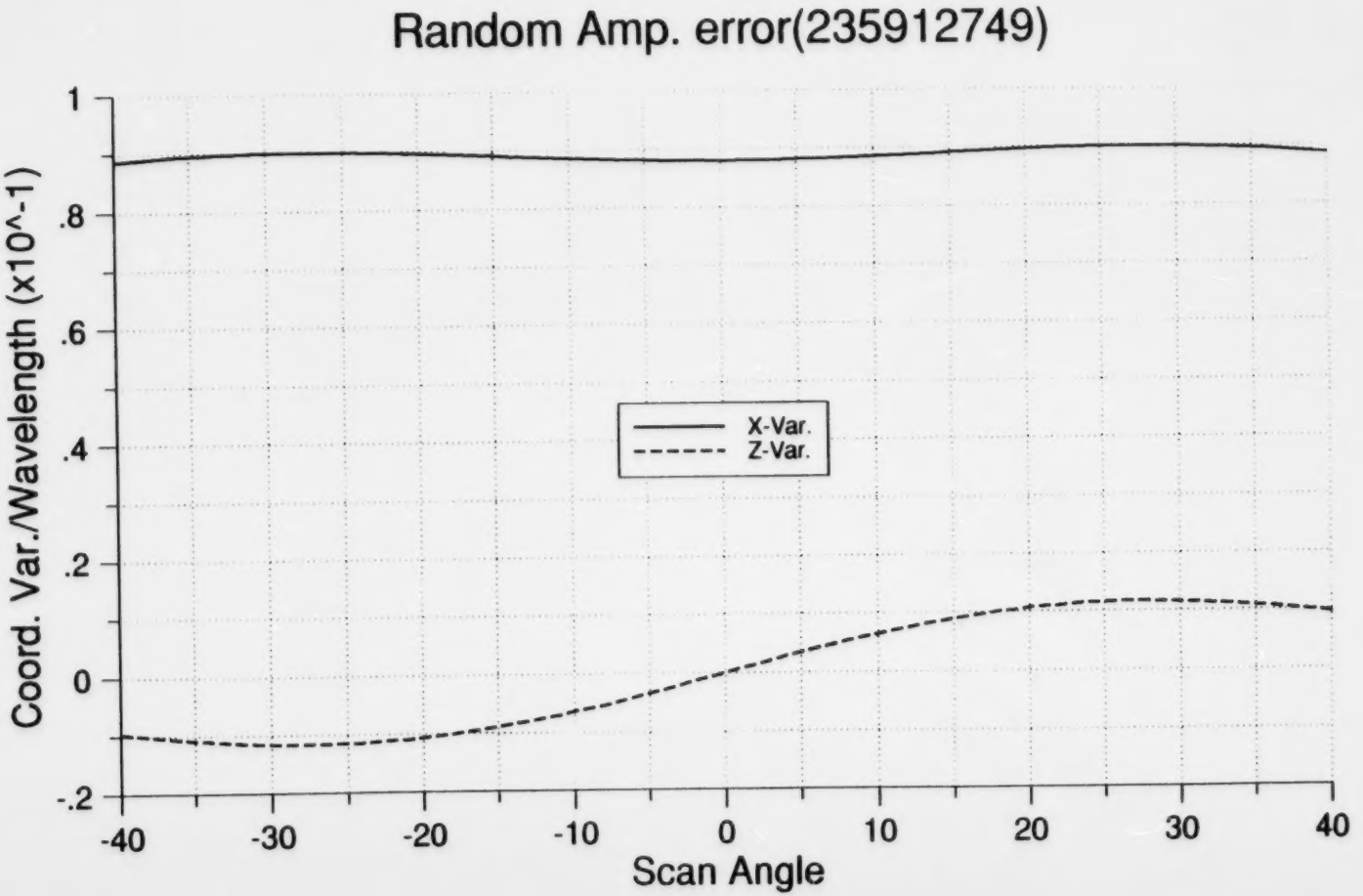

Fig. 4.16 : Phase centre movement due to the random amplitude errors, σ_a = 5%, seed no. 235912749.

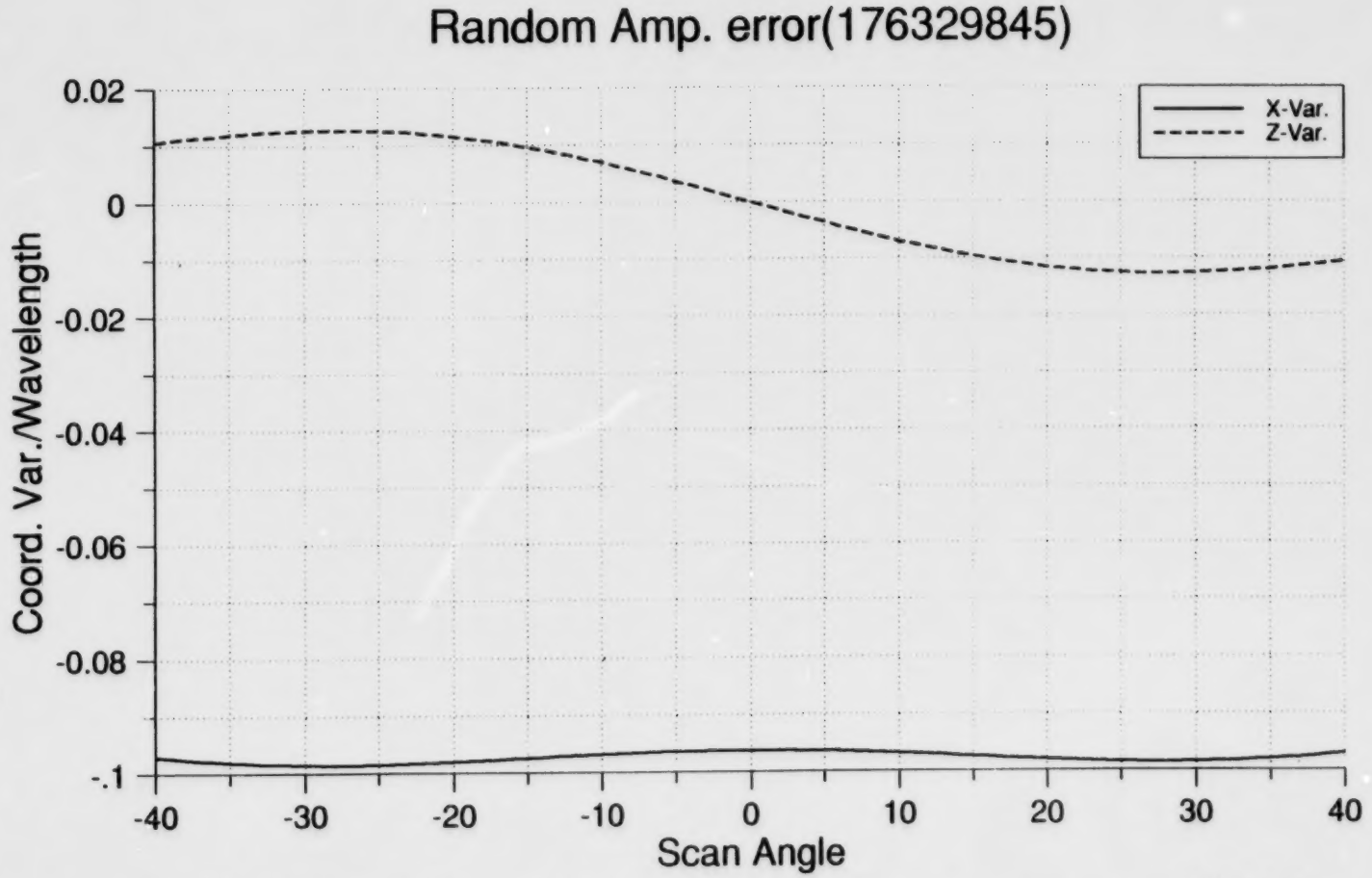

Fig. 4.17 : Phase centre movement due to the random amplitude errors, σ_a = 5%, seed no. 176329845.

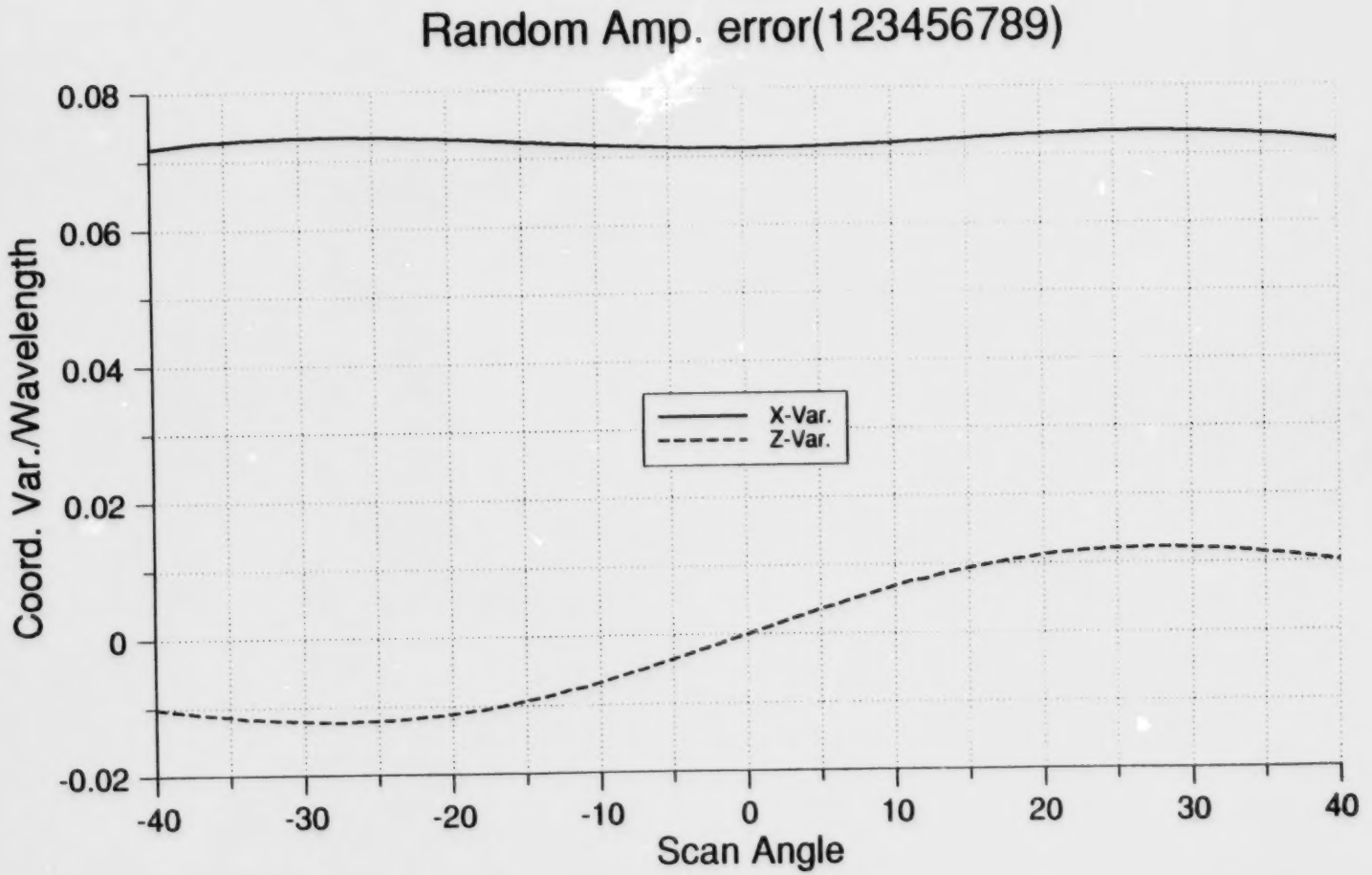

Fig. 4.18 : Phase centre movement due to the random amplitude errors, σ_a = 5%, seed no. 123456789.

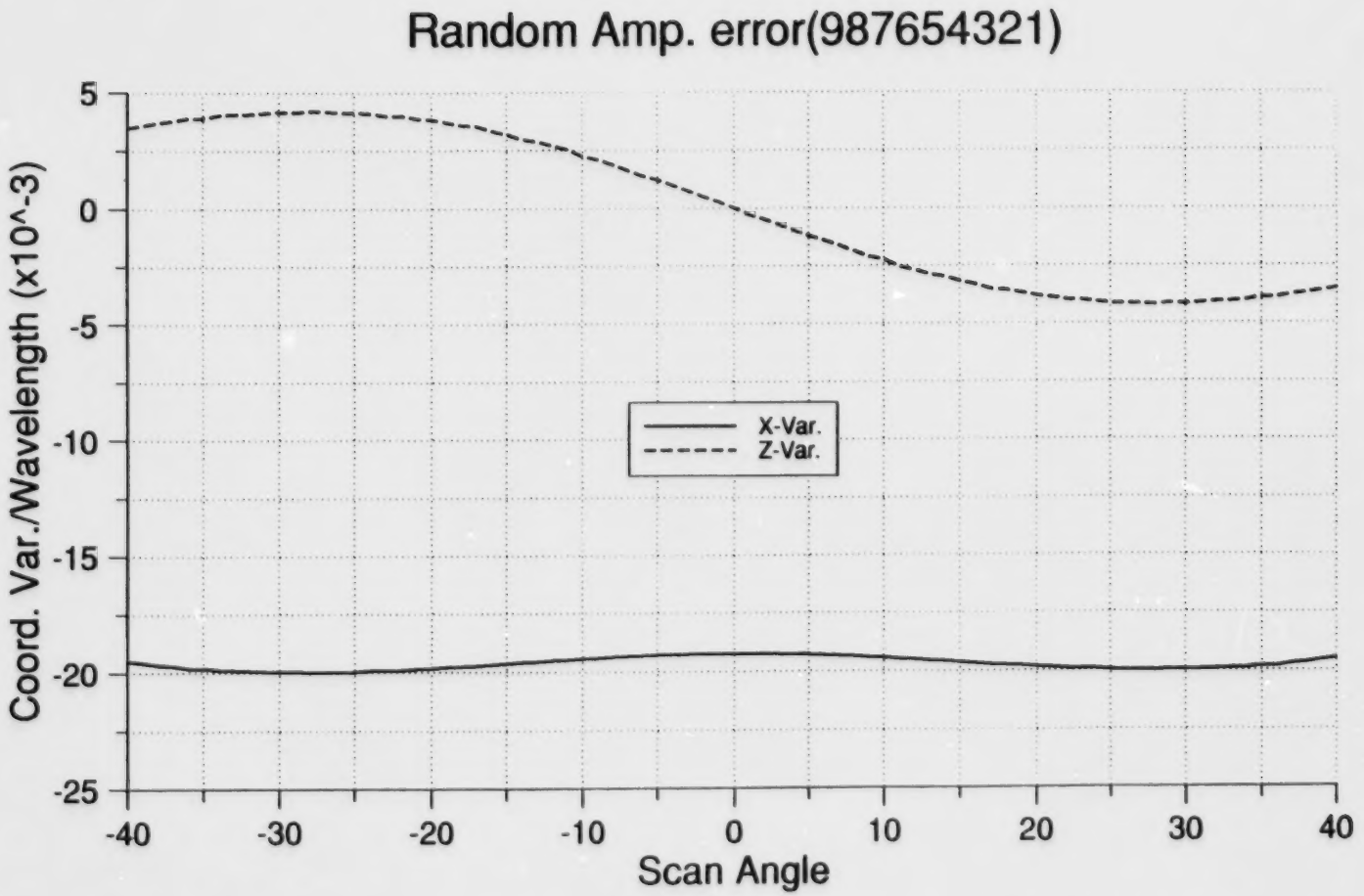

Fig. 4.19 : Phase centre movement due to the random amplitude errors, σ_a = 5%, seed no. 987654321.

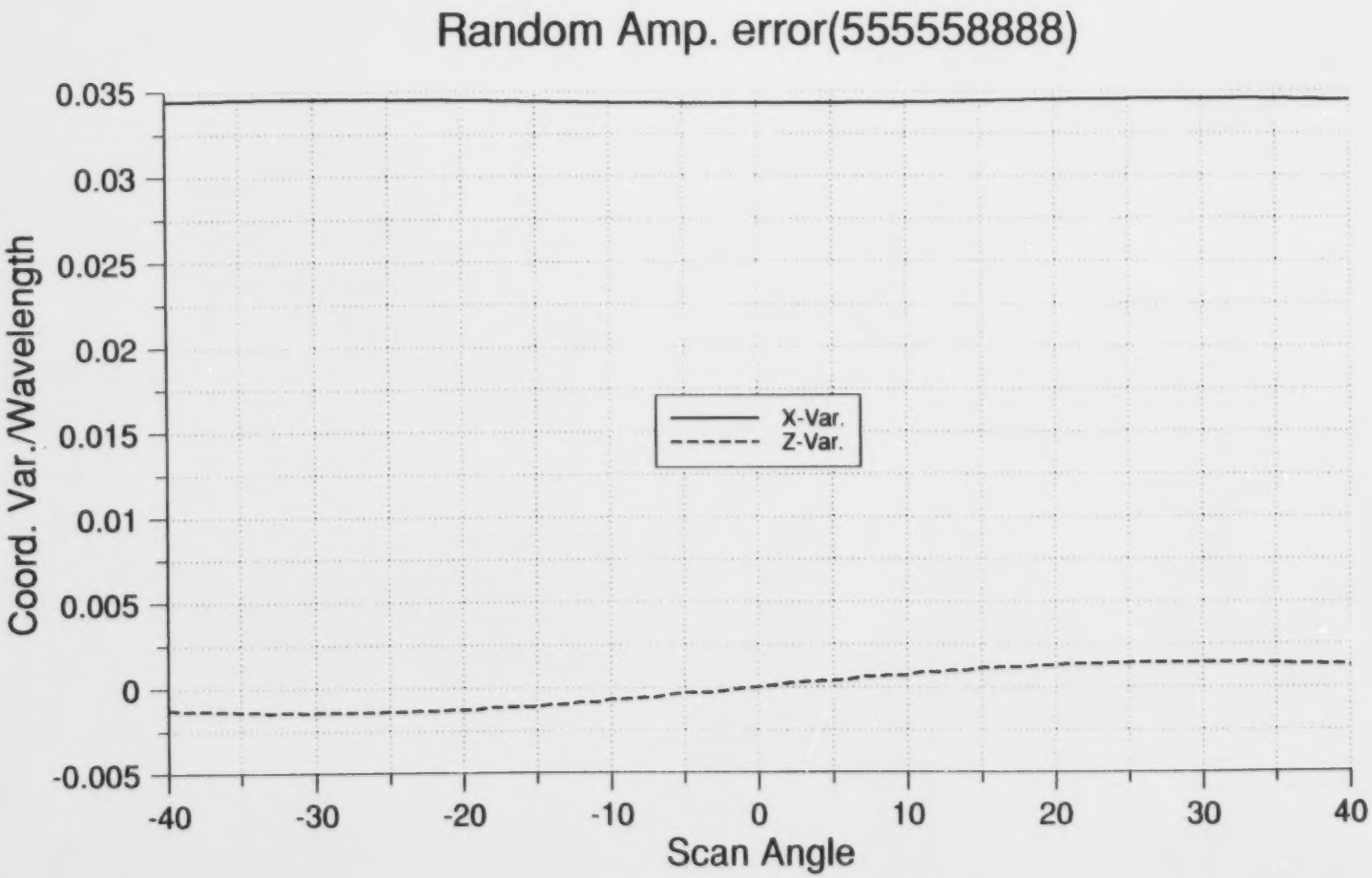

Fig. 4.20 : Phase centre movement due to the random amplitude errors, σ_a = 5%, seed no. 555558888.

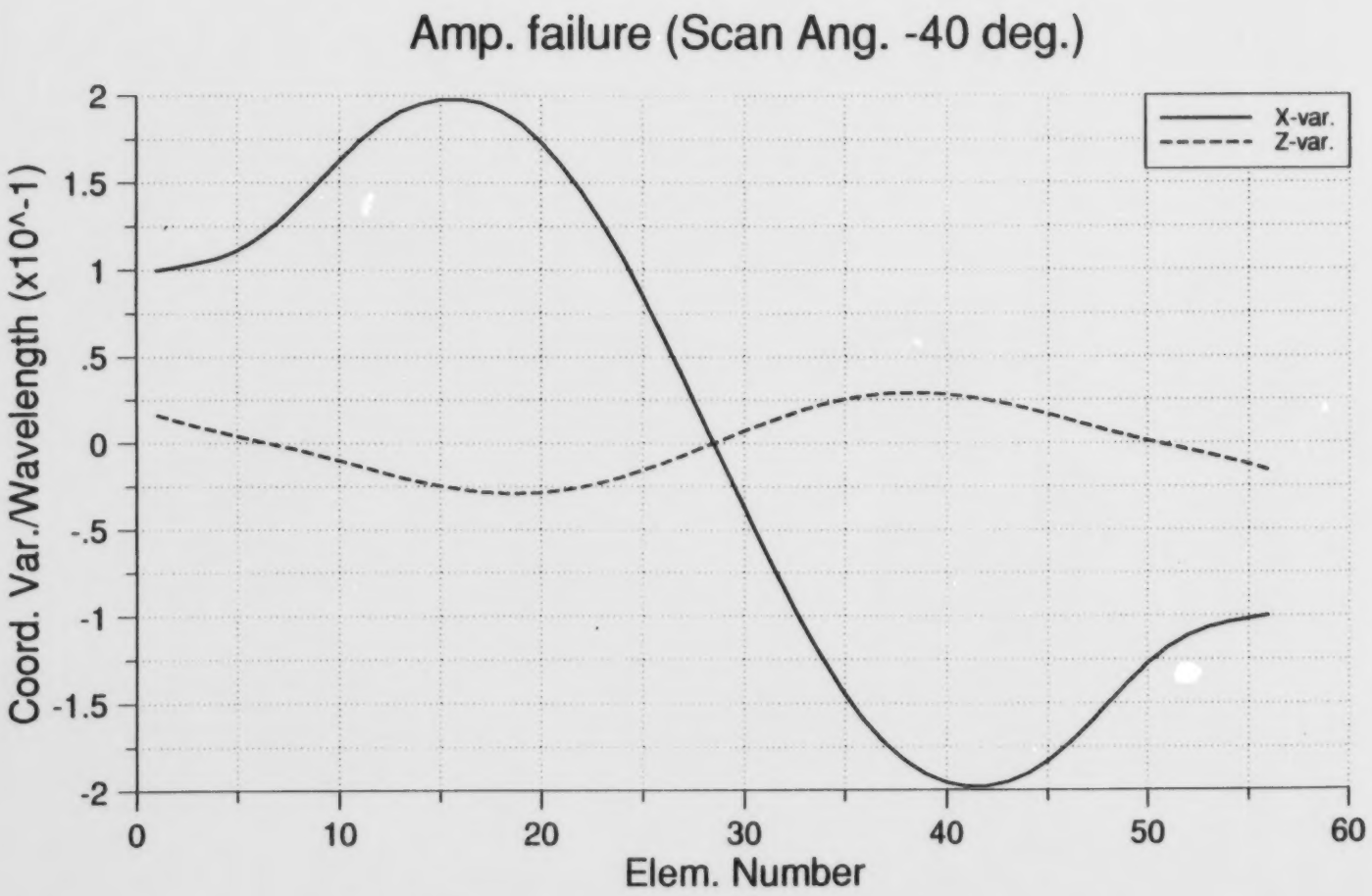

Fig. 4.21 : Phase centre movement due to the amplitude failures, $\theta_s = -40°$.

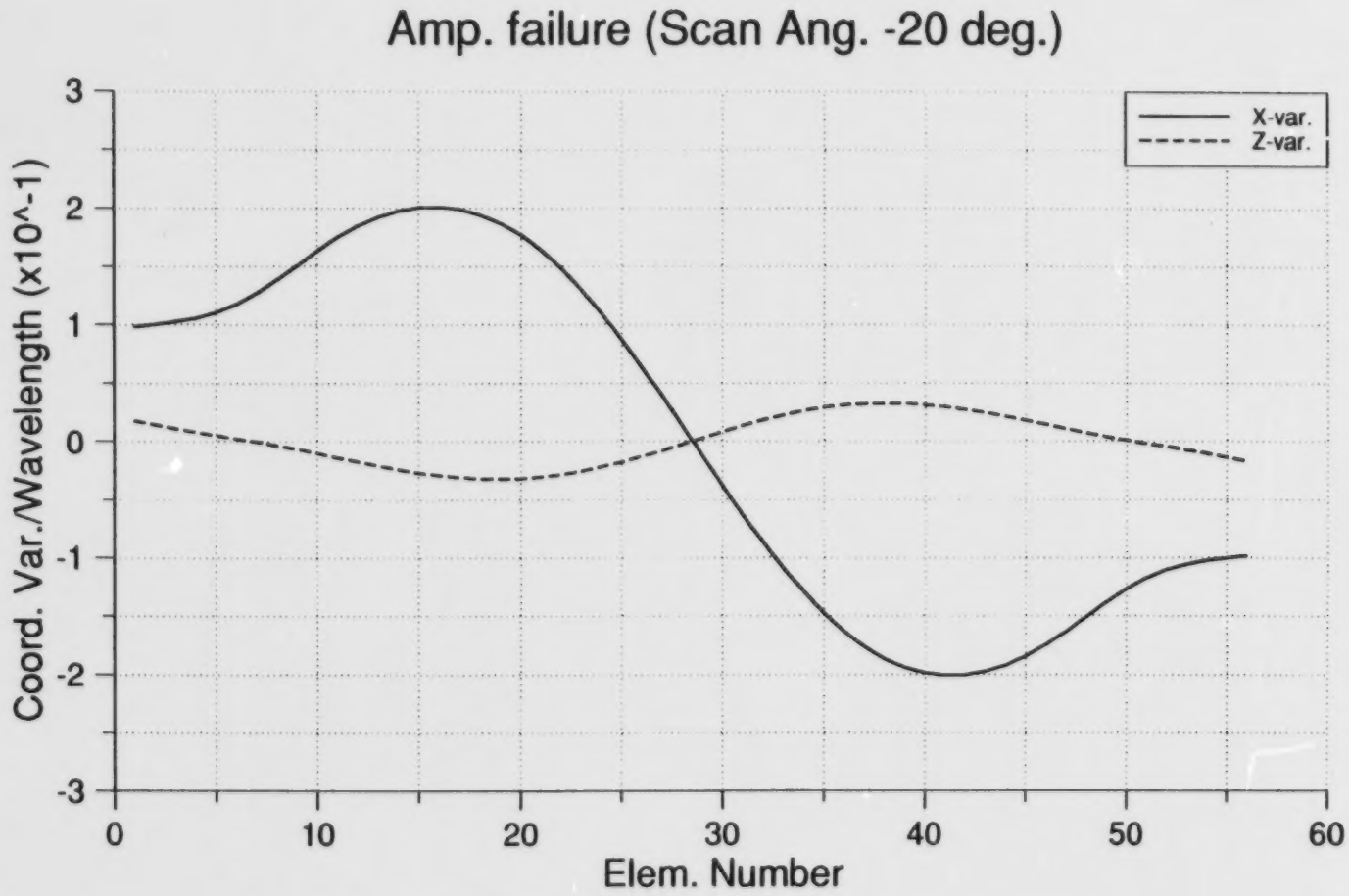

Fig. 4.22 : Phase centre movement due to the amplitude failures, $\theta_s = -20°$.

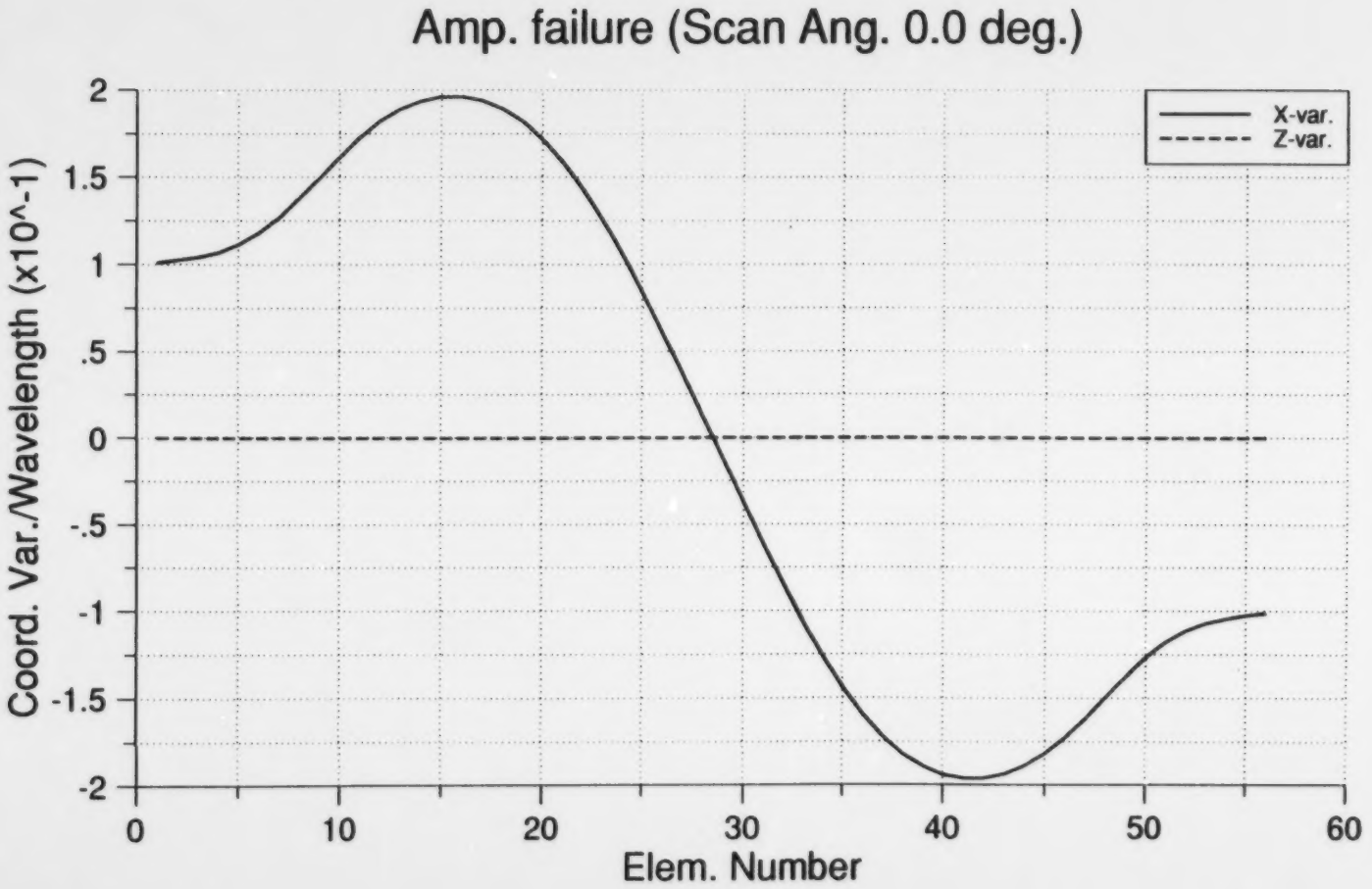

Fig. 4.23 : Phase centre movement due to the amplitude failures, θ_s = 0.0°.

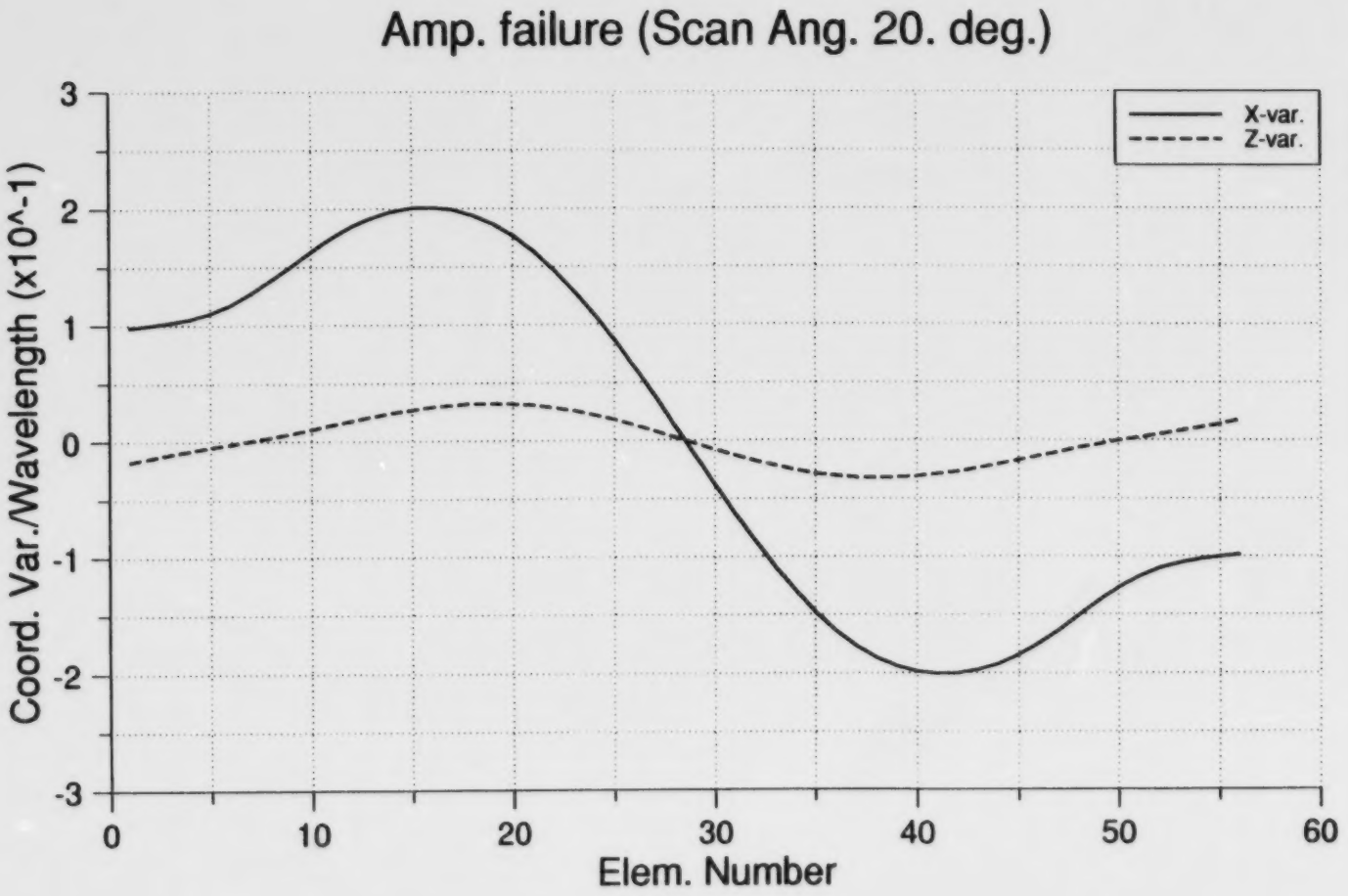

Fig. 4.24 : Phase centre movement due to the amplitude failures, θ_r = 20°.

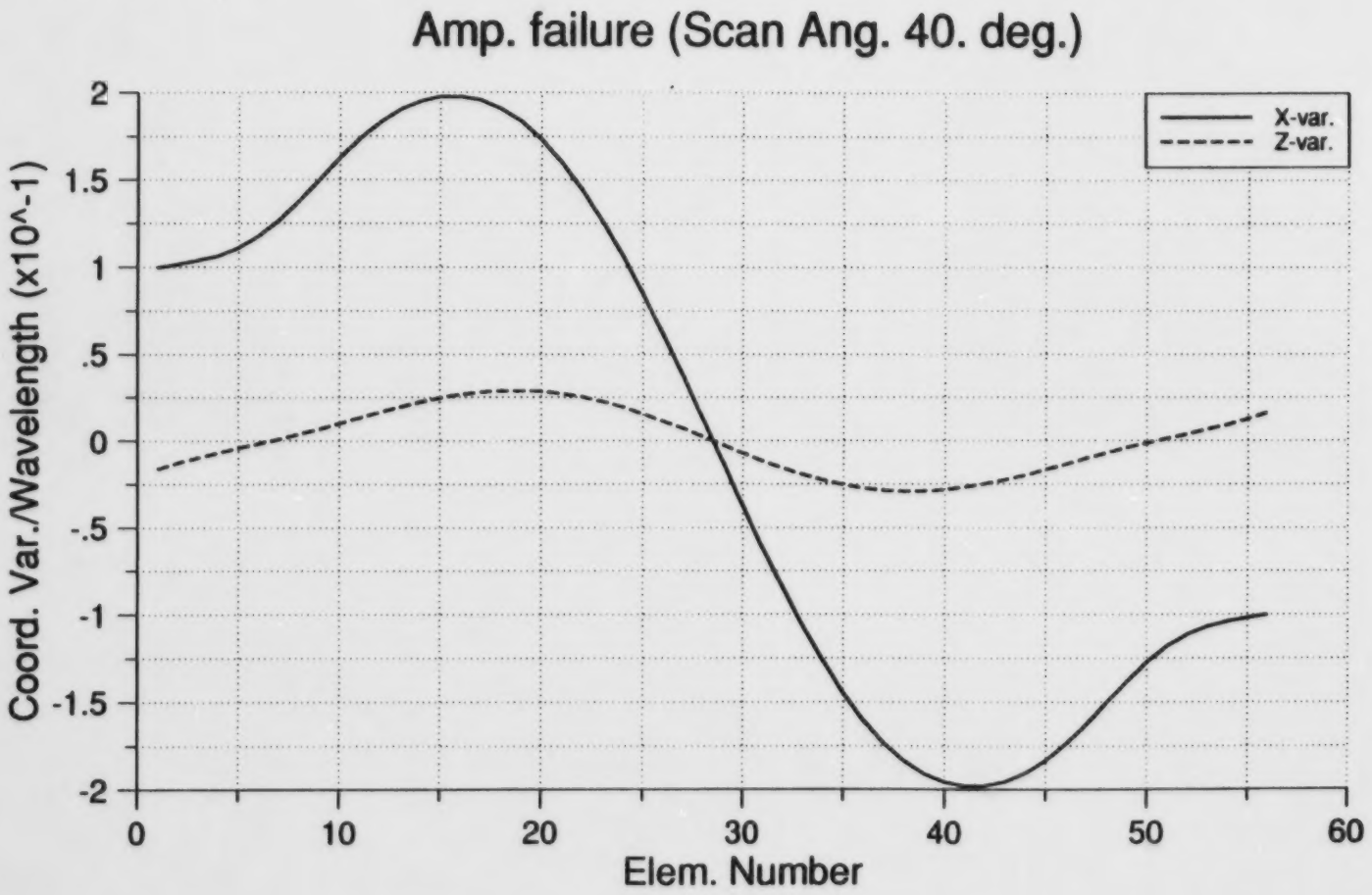

Fig. 4.25 : Phase centre movement due to the amplitude failures, $\theta_s = 40^o$.

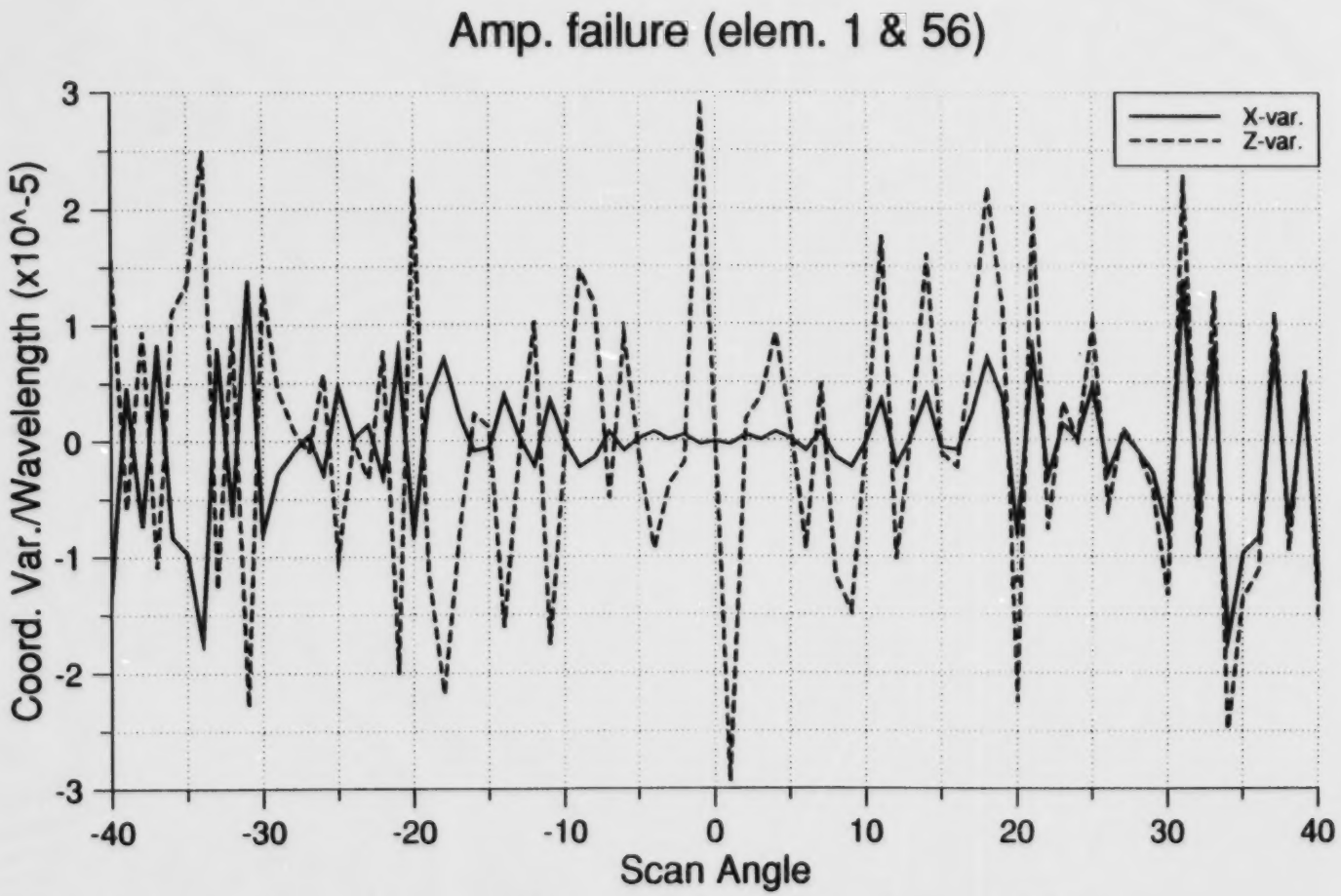

Fig. 4.26 : Phase centre movement due to the amplitude failures, element no. 1 & 56.

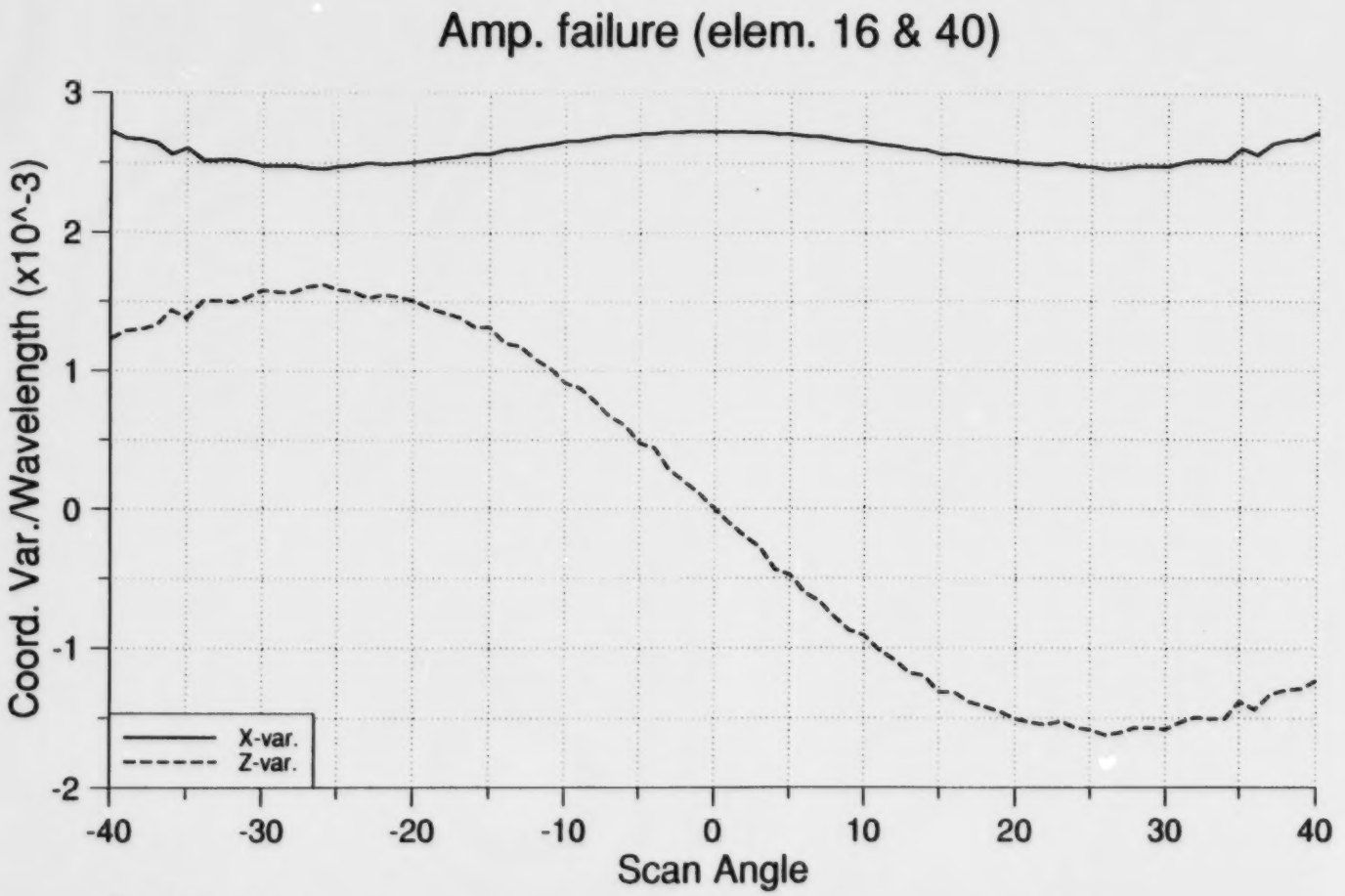

Fig. 4.27 : Phase centre movement due to the amplitude failures, element no. 16 & 40.

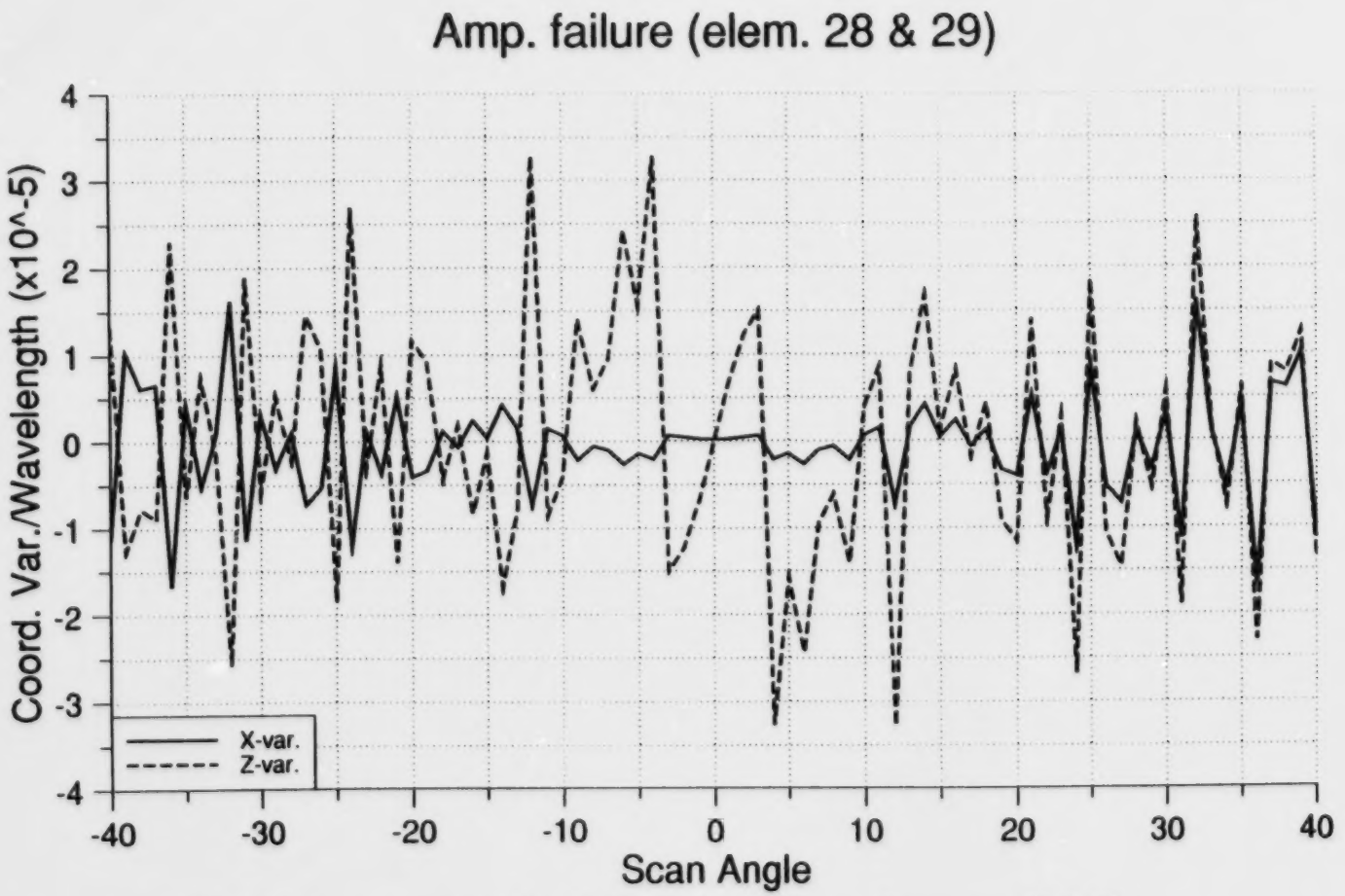

Fig. 4.28 : Phase centre movement due to the amplitude failures, element no. 28 & 29.

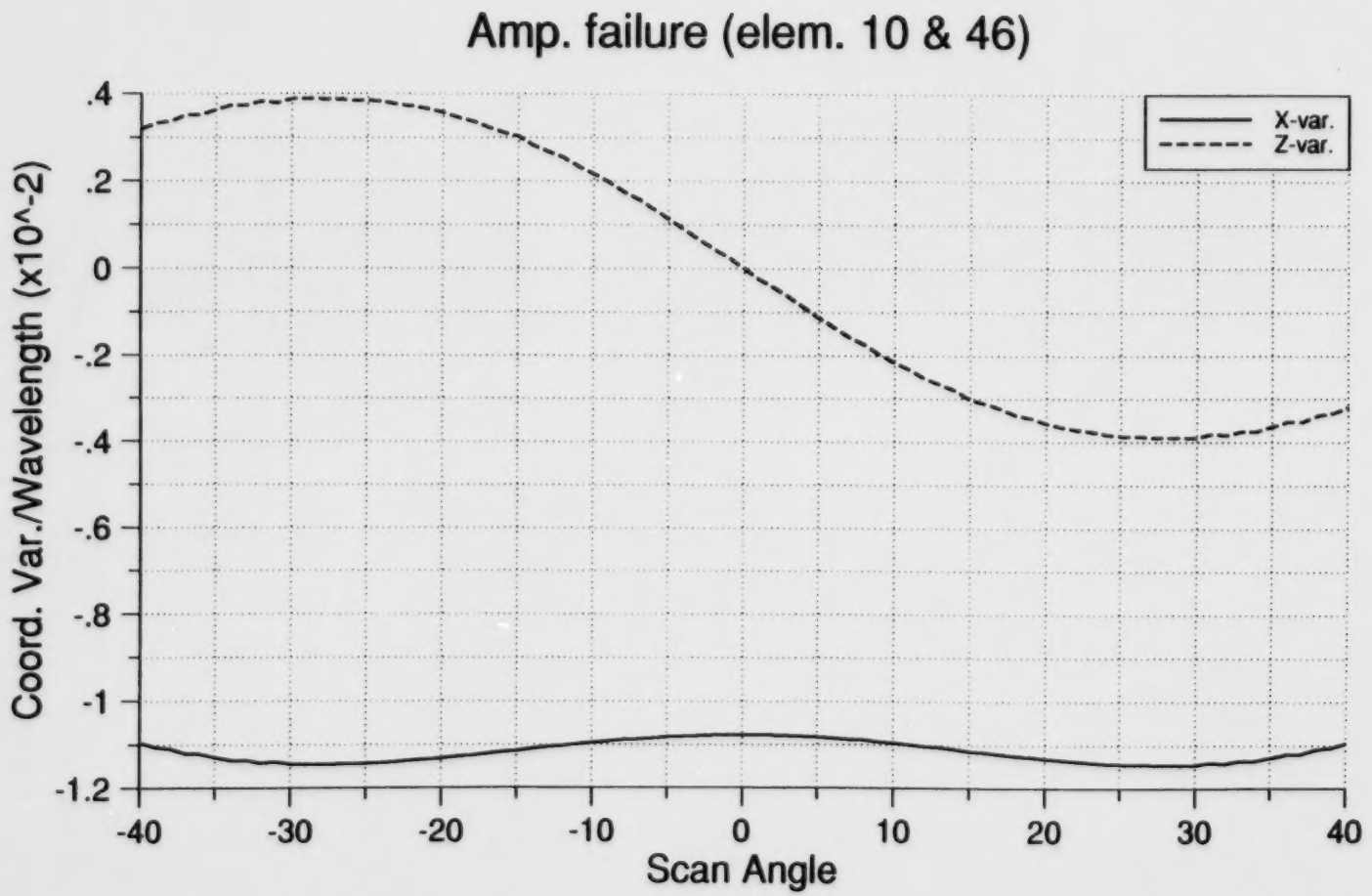

Fig. 4.29 : Phase centre movement due to the amplitude failures, element no. 10 & 46.

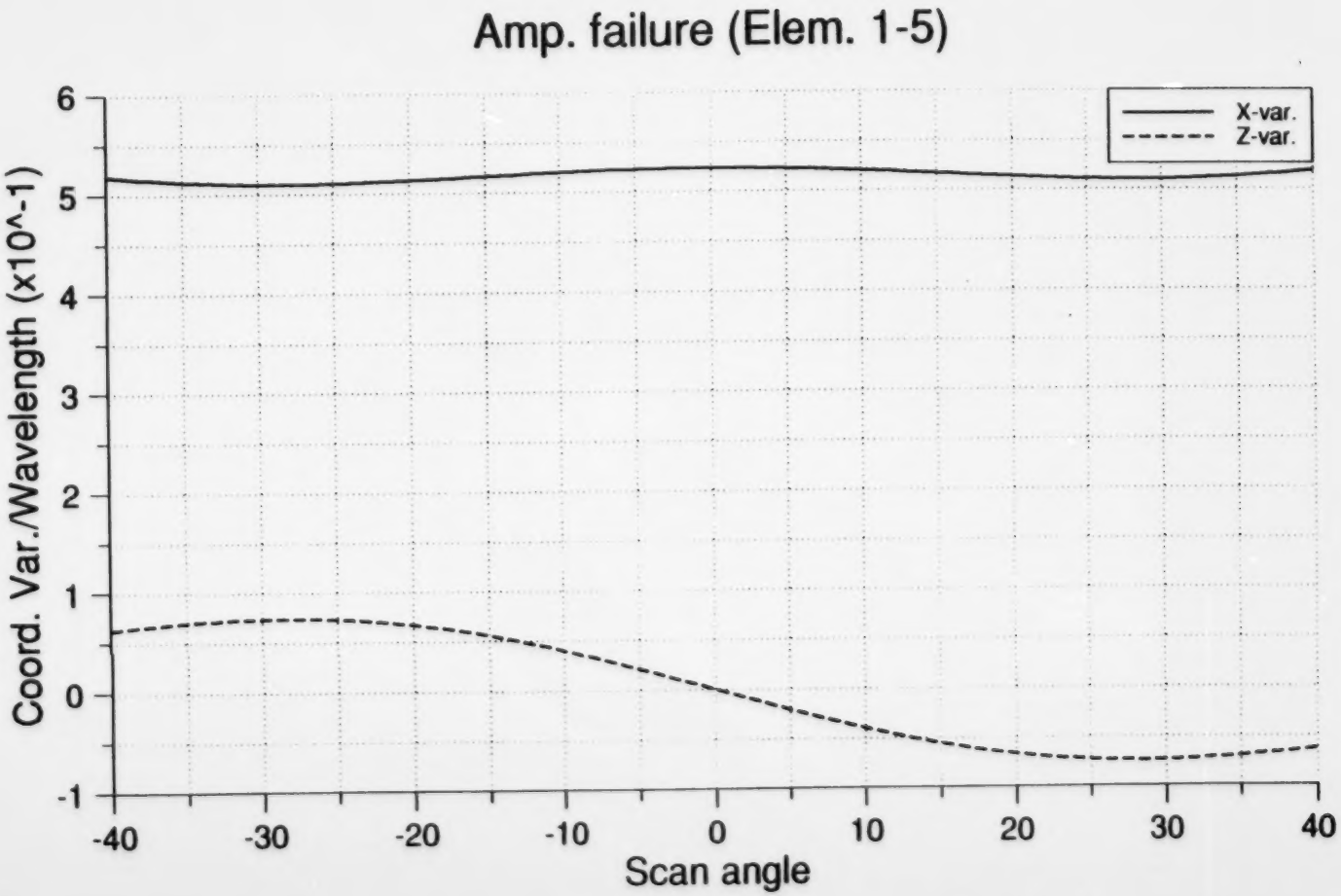

Fig. 4.30 : Phase centre movement due to the amplitude failures, element no. 1 to 5.

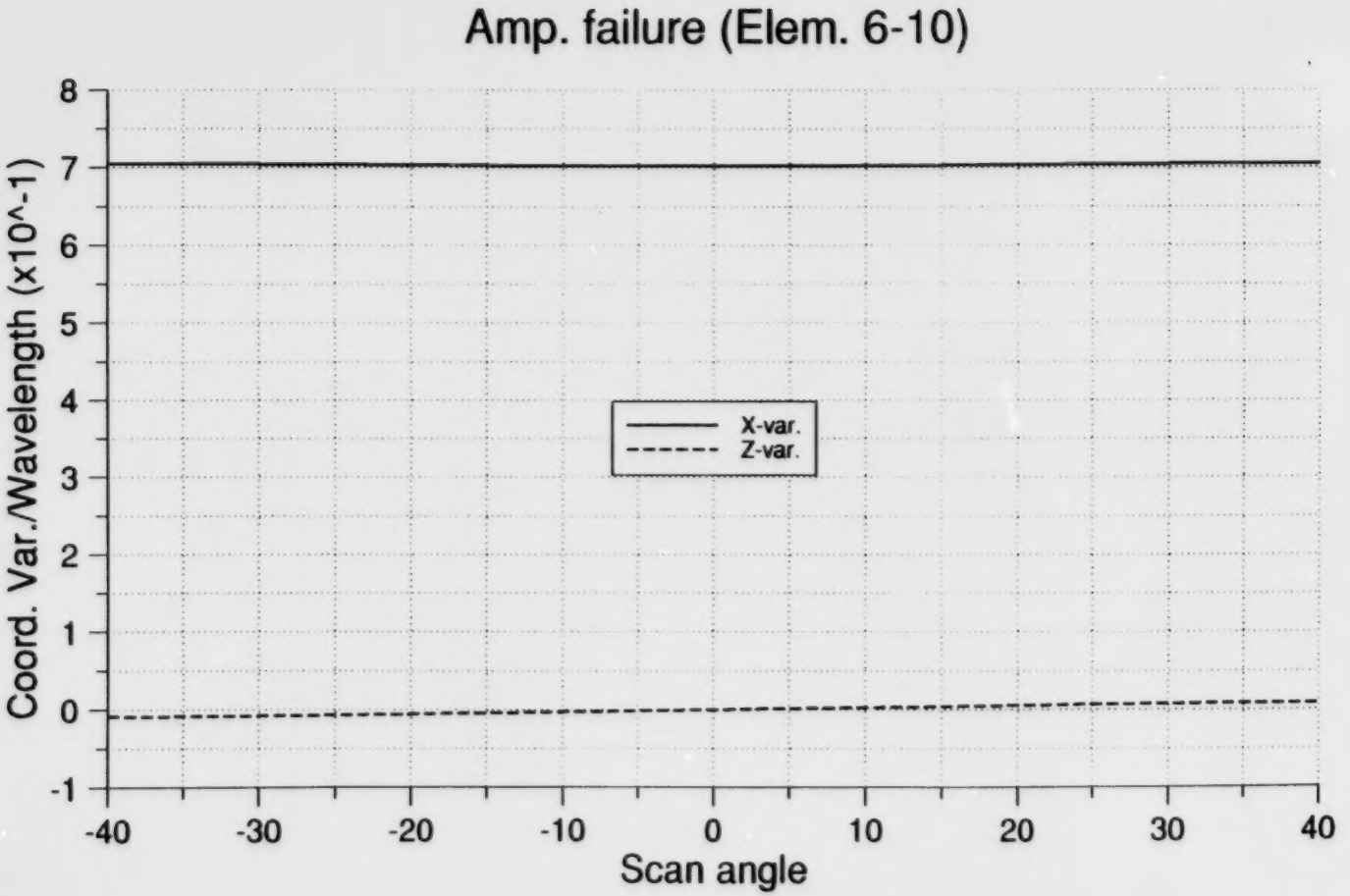

Fig. 4.31 : Phase centre movement due to the amplitude failures, element no. 6 to 10.

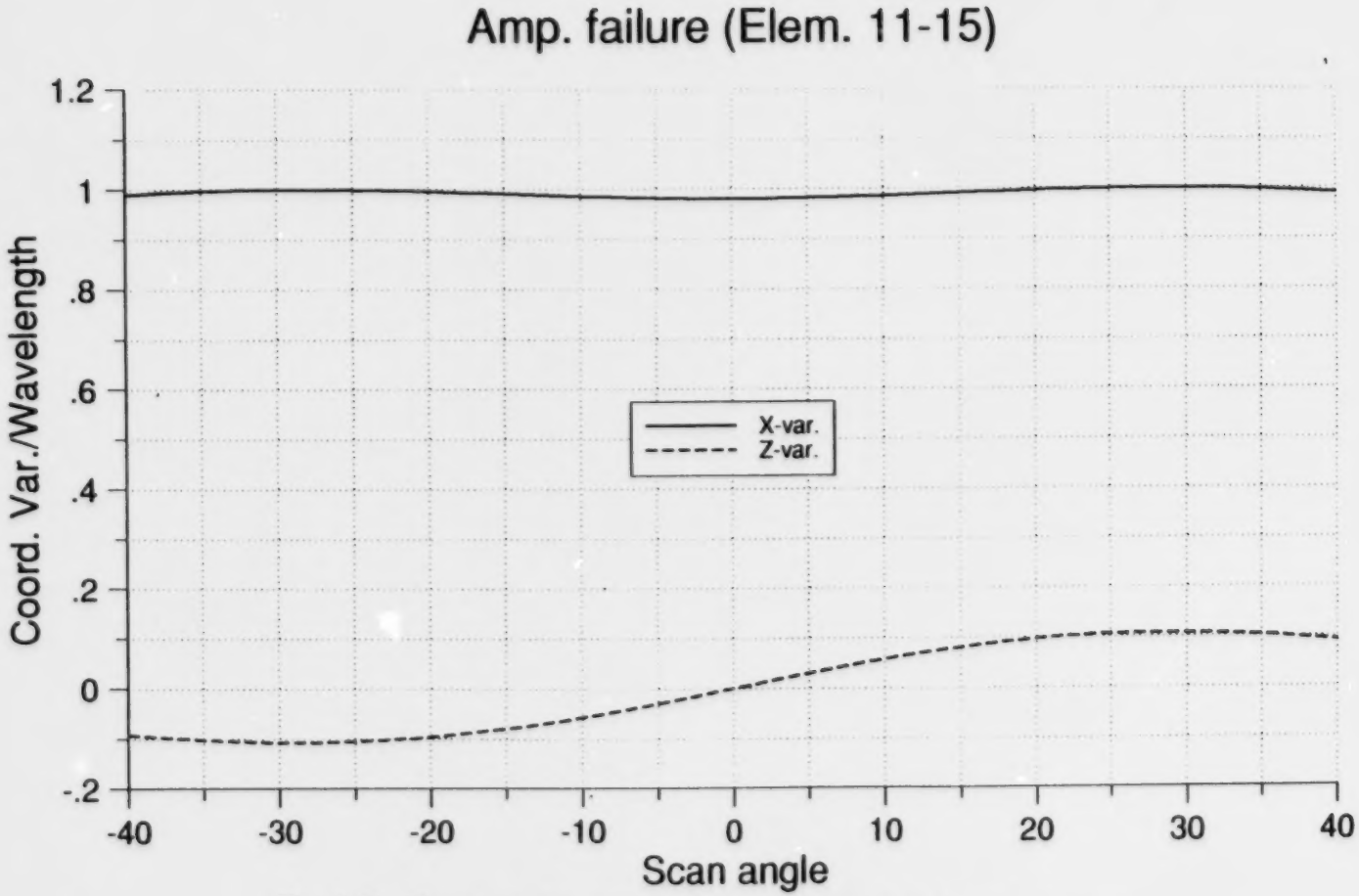

Fig. 4.32 : Phase centre movement due to the amplitude failures, element no. 11 to 15.

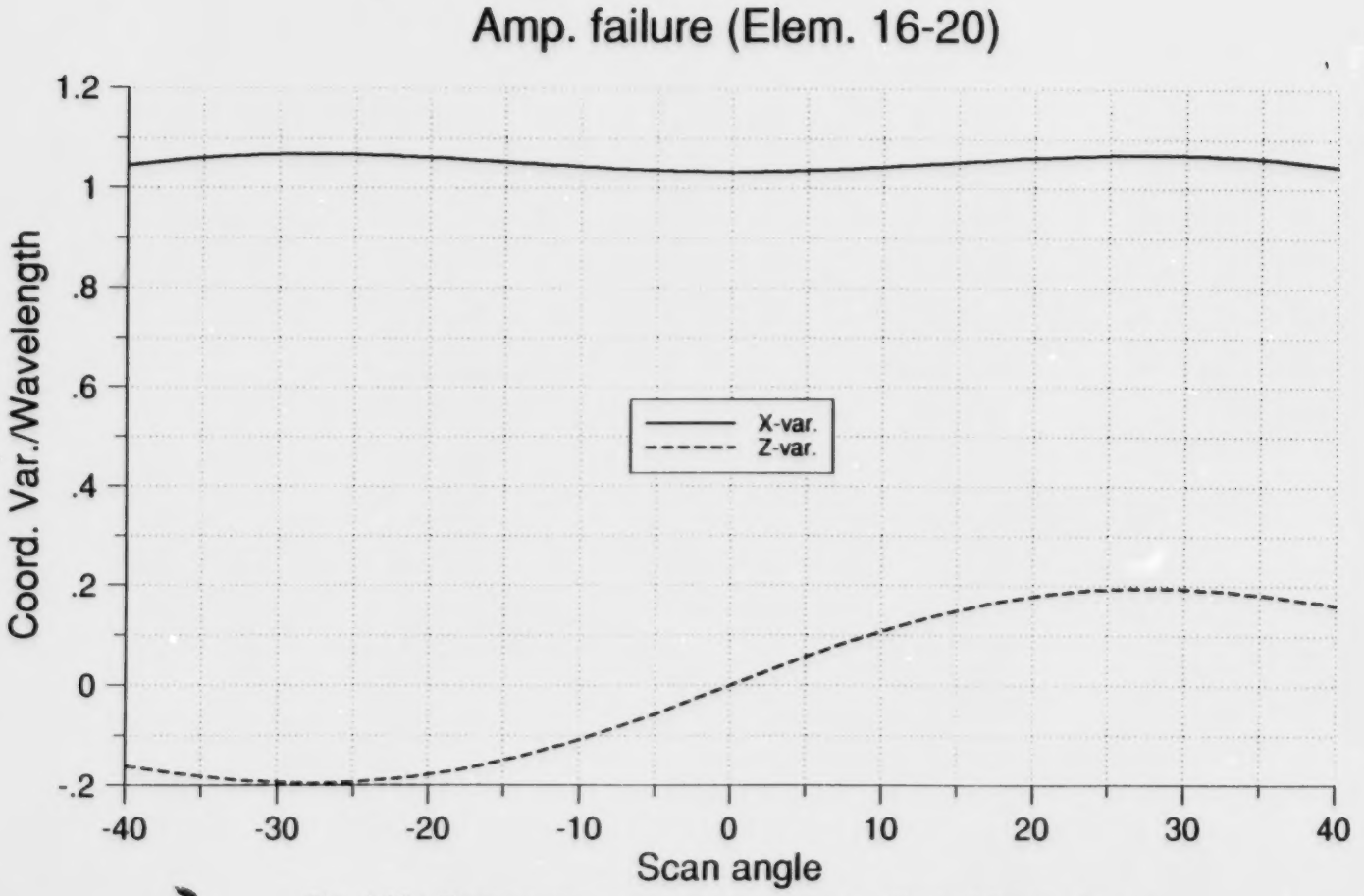

Fig. 4.33 : Phase centre movement due to the amplitude failures, element no. 16 to 20.

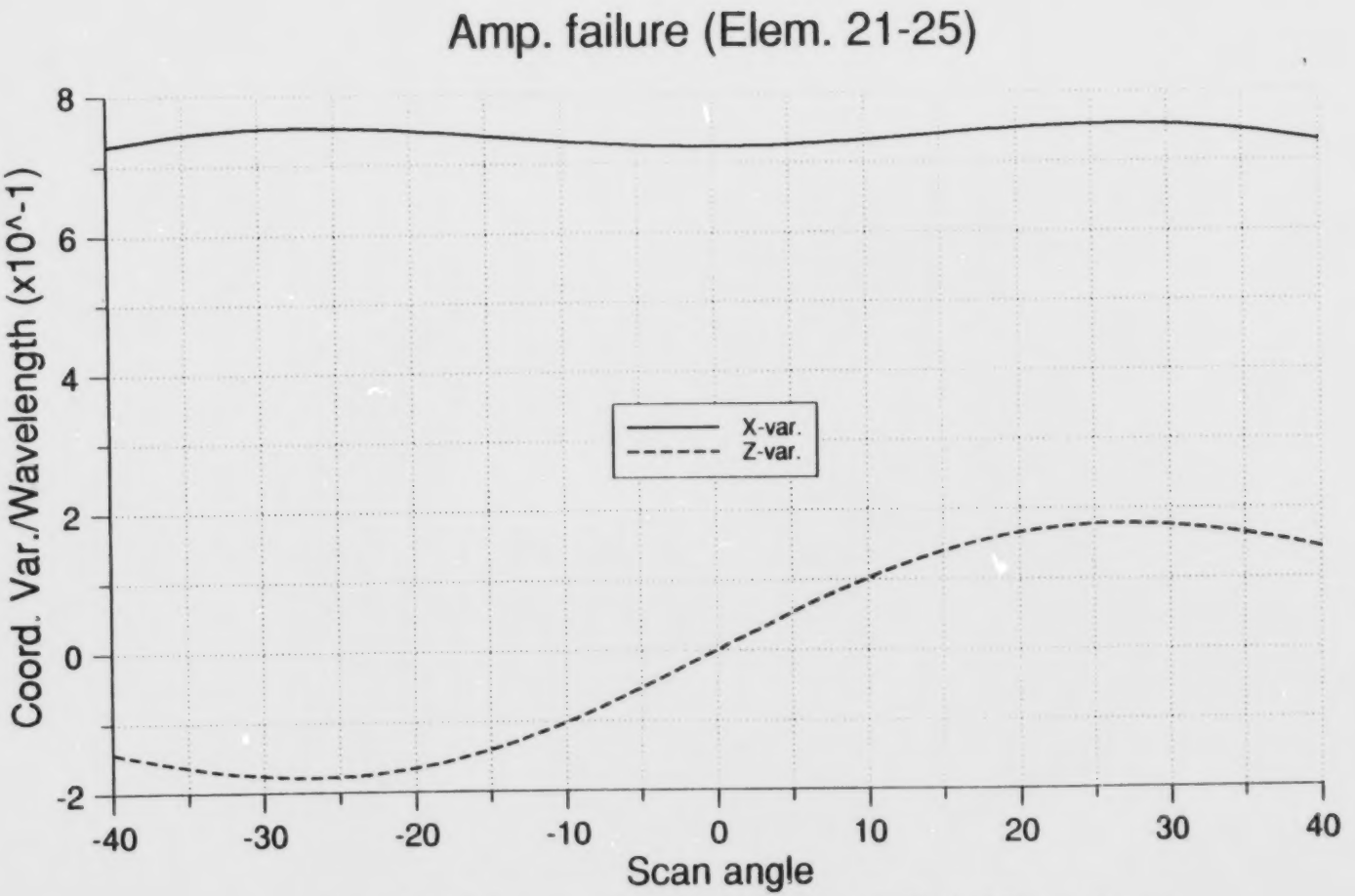

Fig. 4.34 : Phase centre movement due to the amplitude failures, element no. 21 to 25.

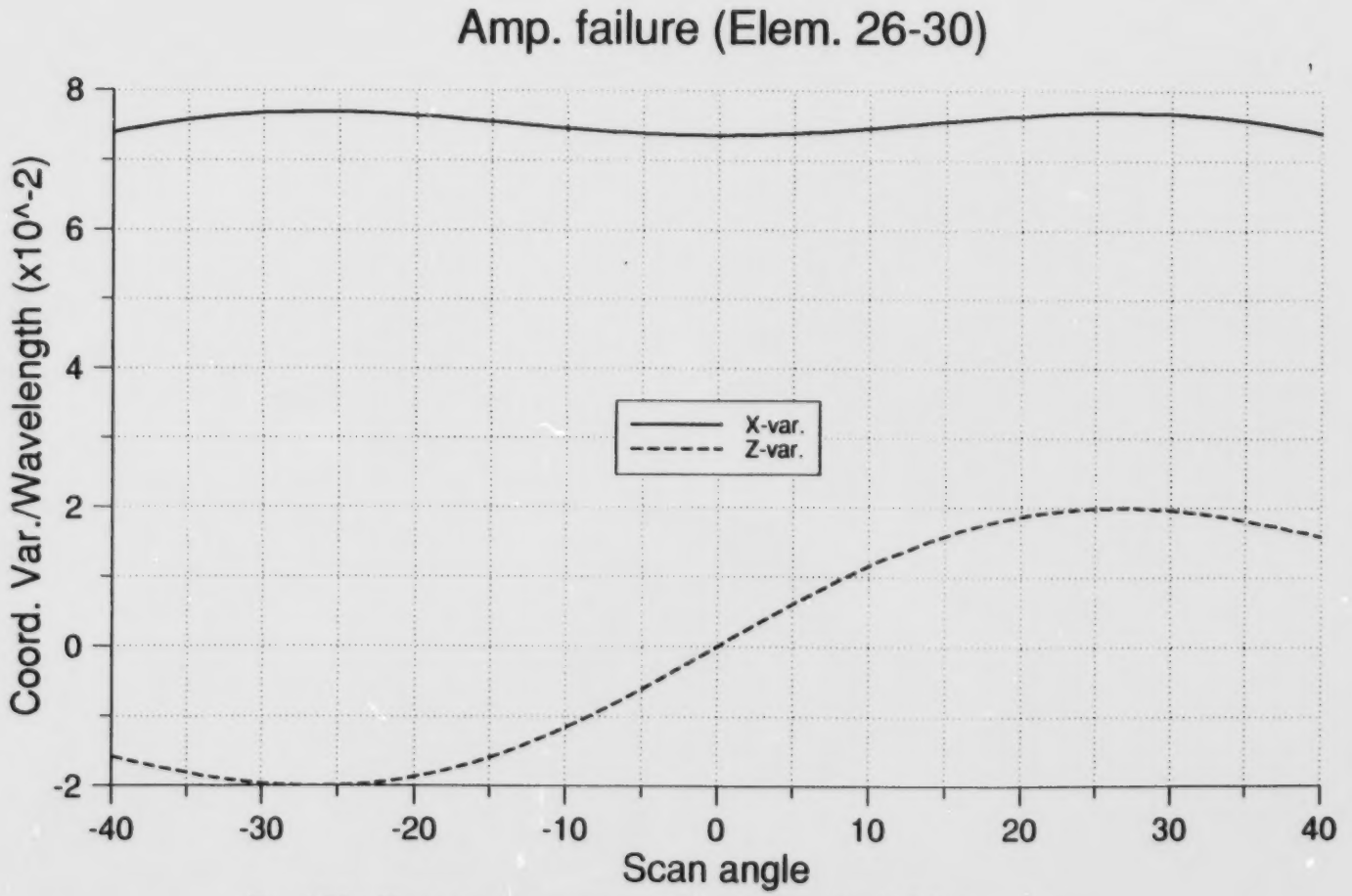

Fig. 4.35 : Phase centre movement due to the amplitude failures, element no. 26 to 30.

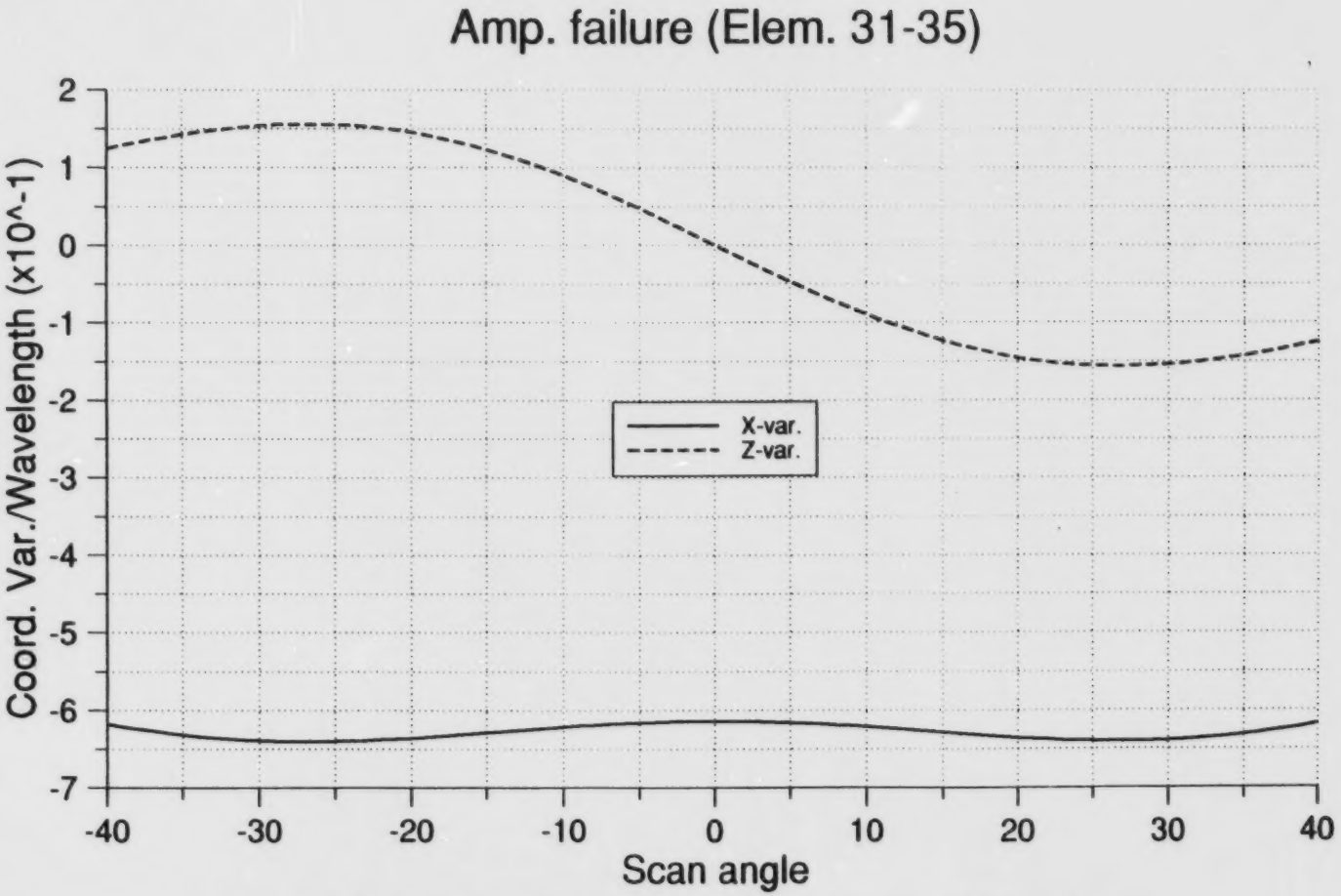

Fig. 4.36 : Phase centre movement due to the amplitude failures, element no. 31 to 35.

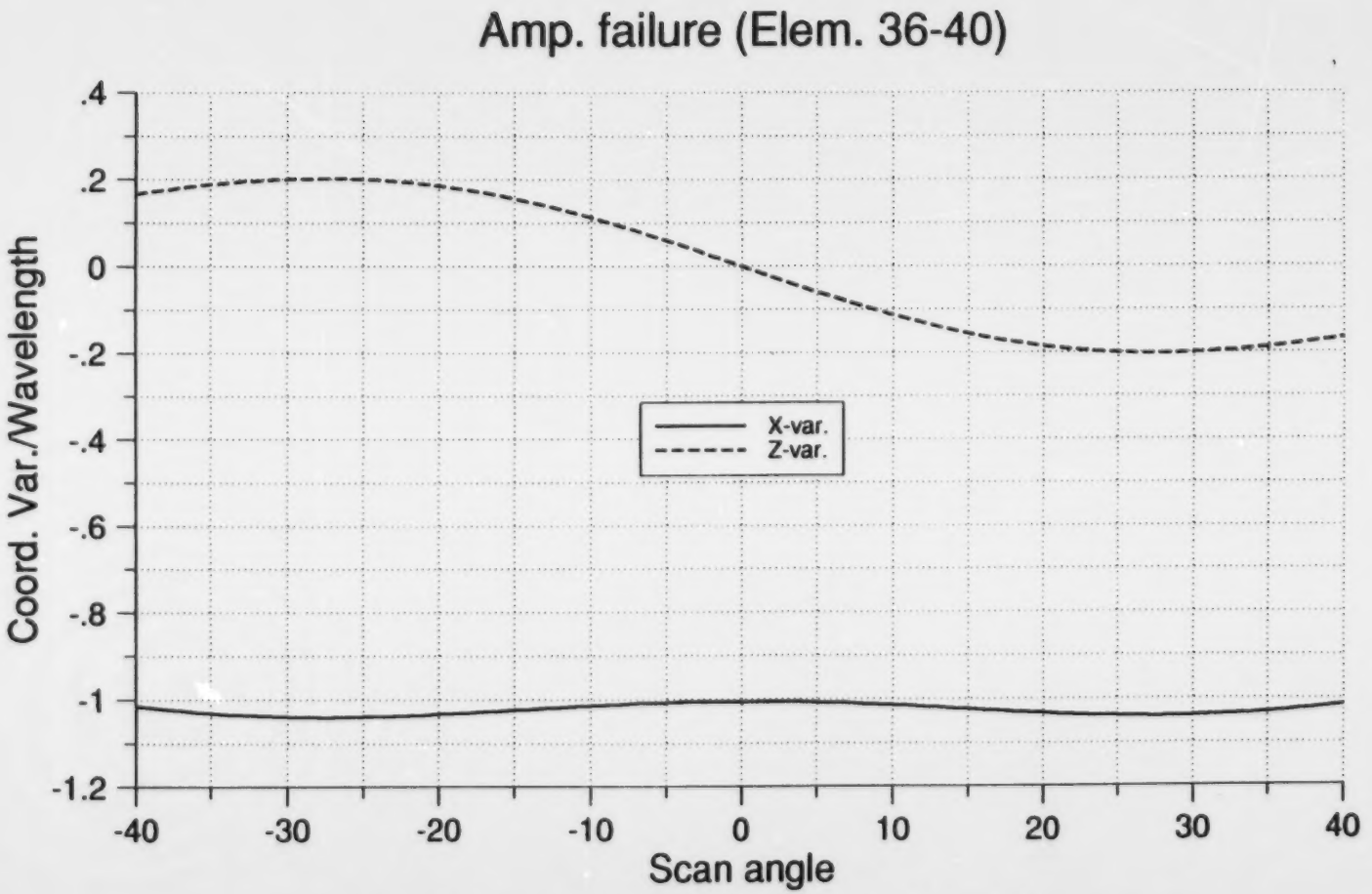

Fig. 4.37 : Phase centre movement due to the amplitude failures, element no. 36 to 40.

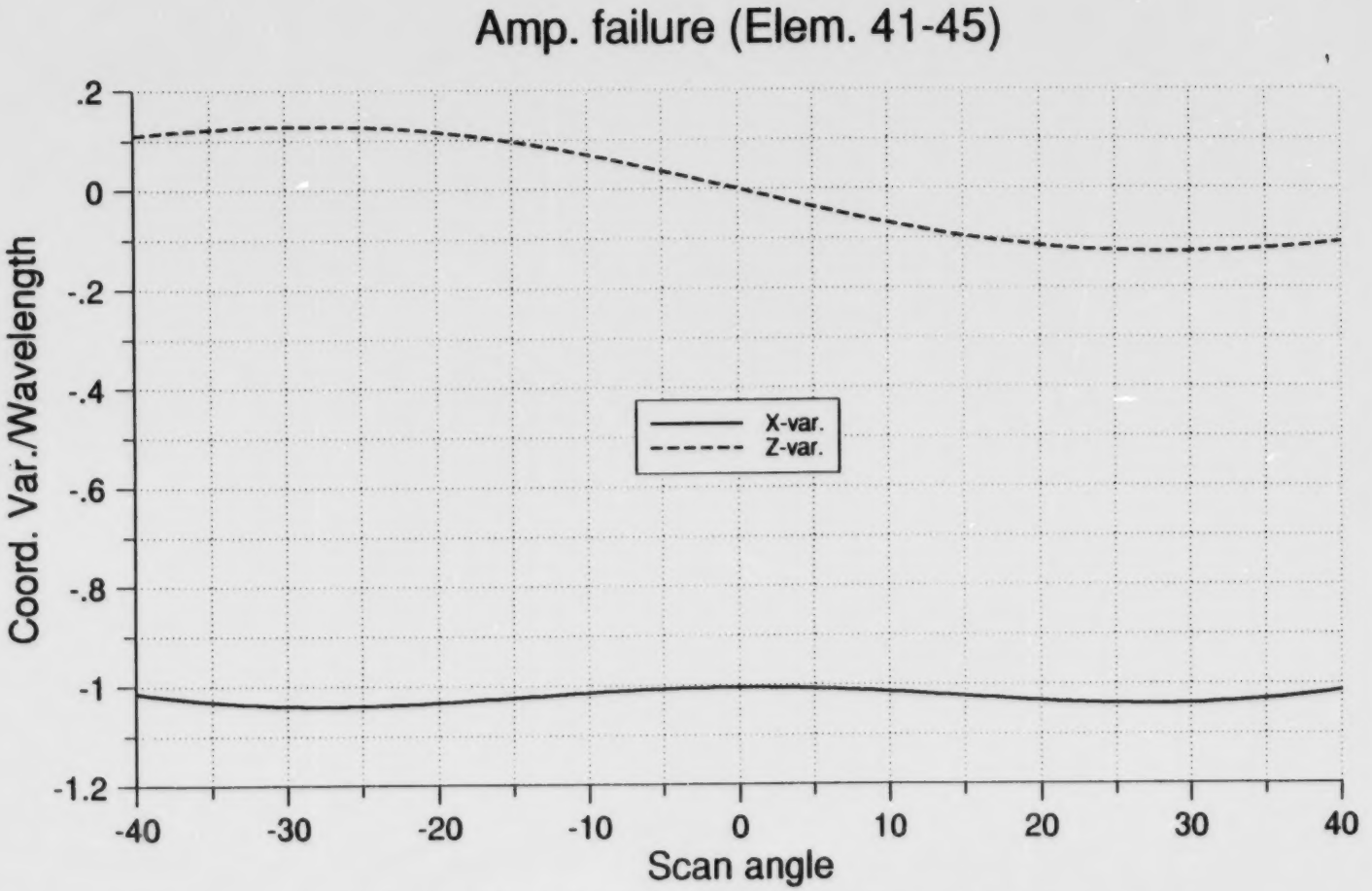

Fig. 4.38 : Phase centre movement due to the amplitude failures, element no. 41 to 45.

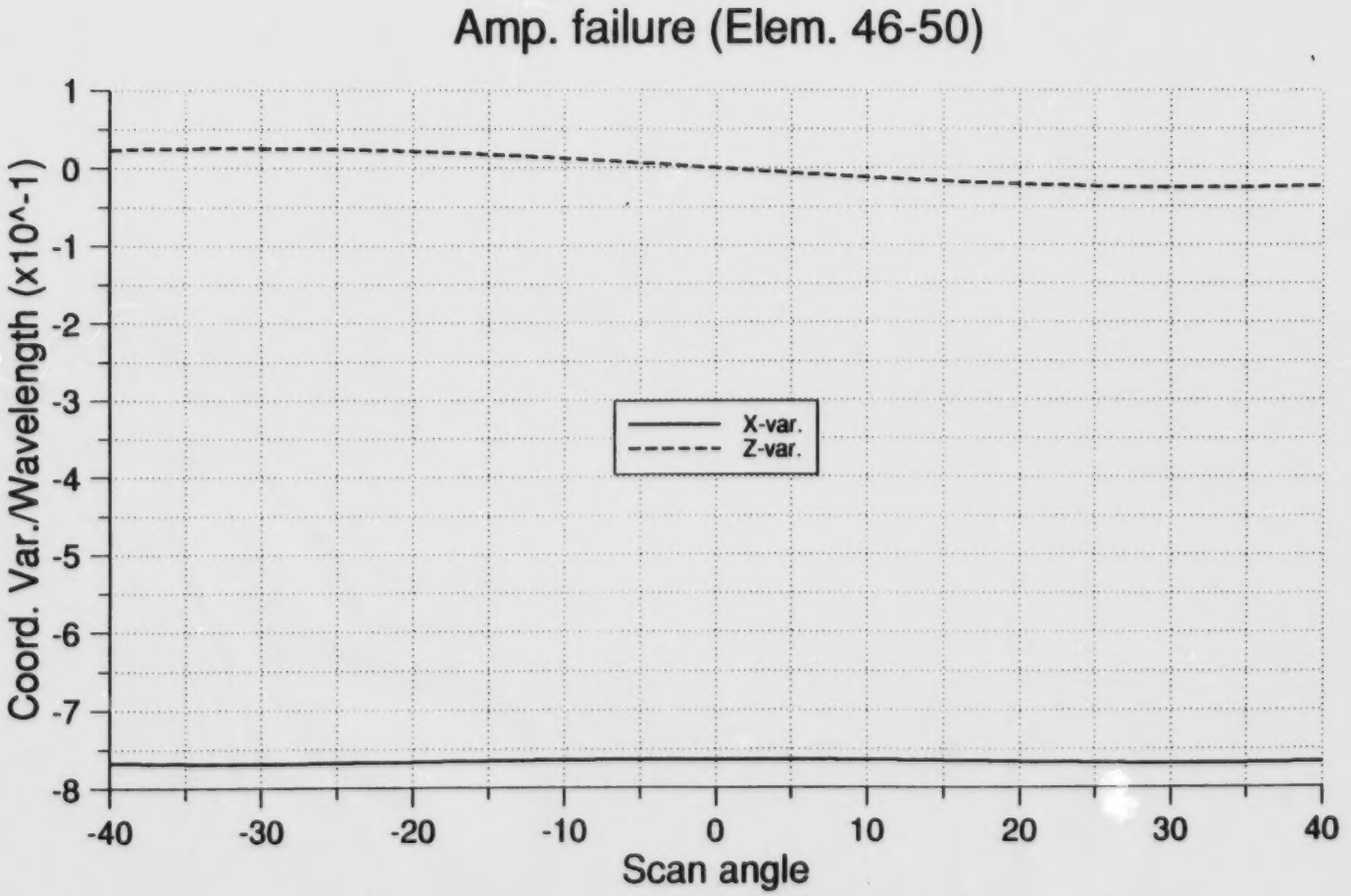

Fig. 4.39 : Phase centre movement due to the amplitude failures, element no. 46 to 50.

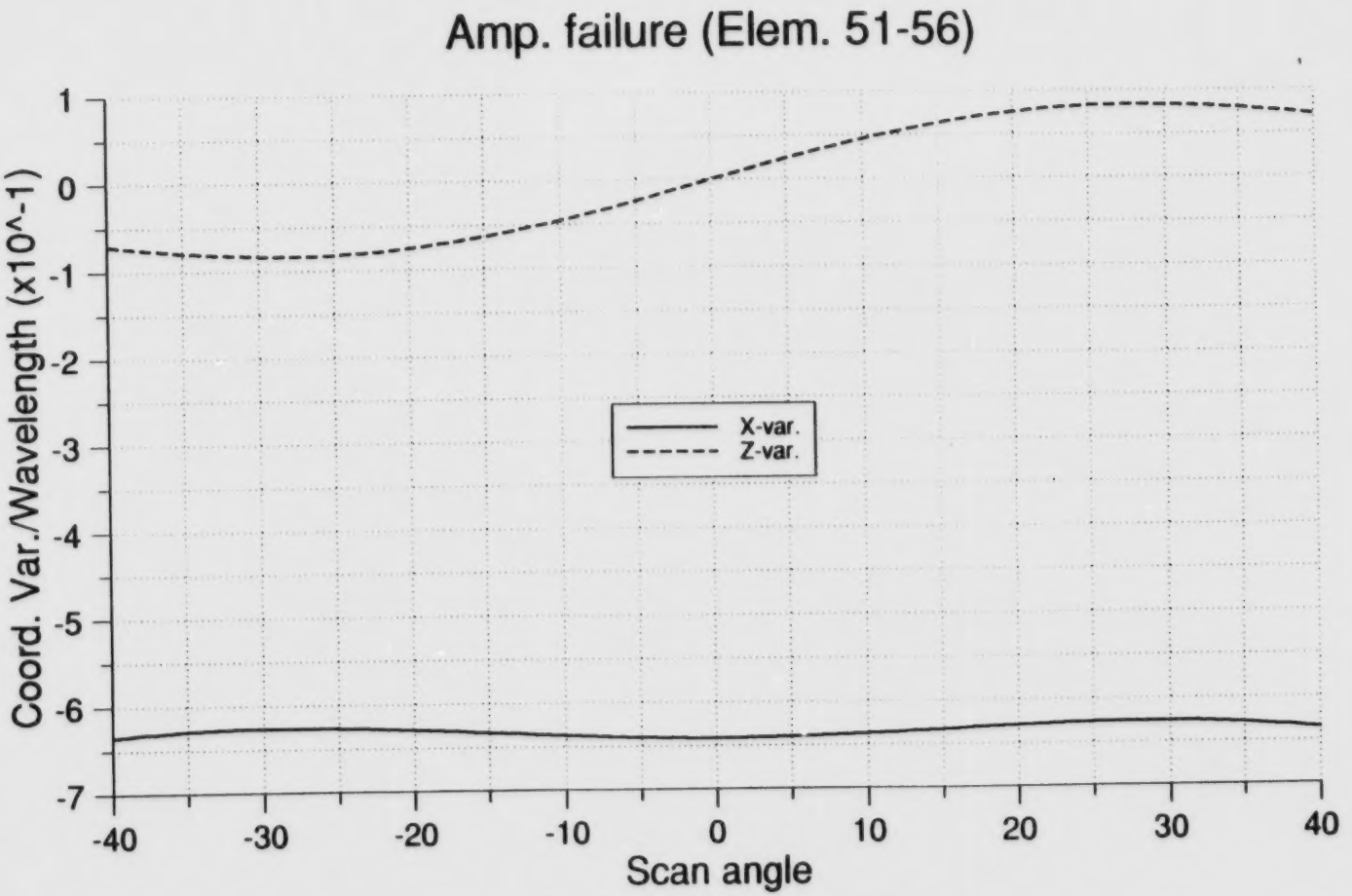

Fig. 4.40 : Phase centre movement due to the amplitude failures, element no. 51 to 56.

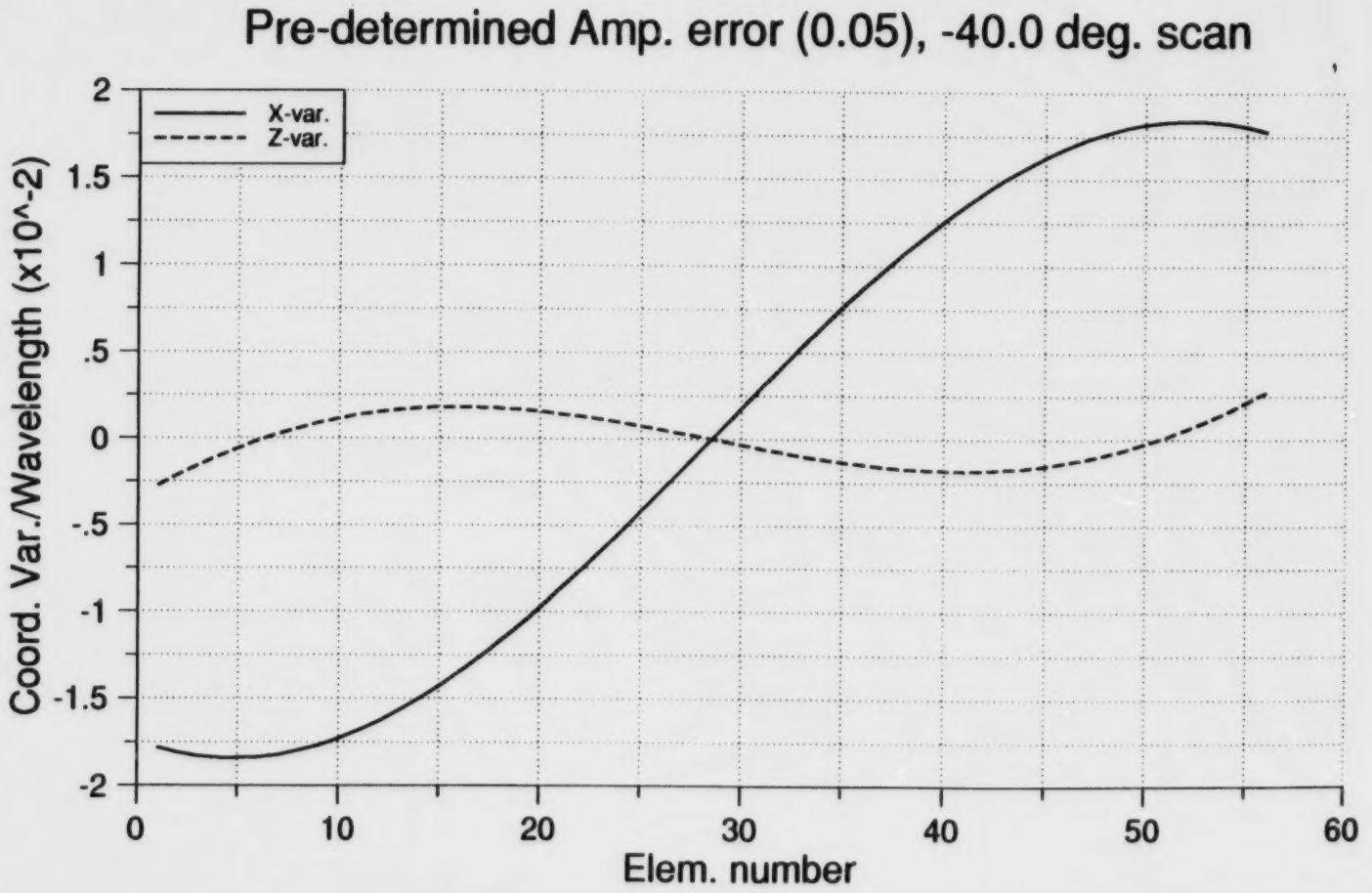

Fig. 4.41 : Phase centre movement due to a pre-determined error of 0.05 added to each element, $\theta_s = -40°$.

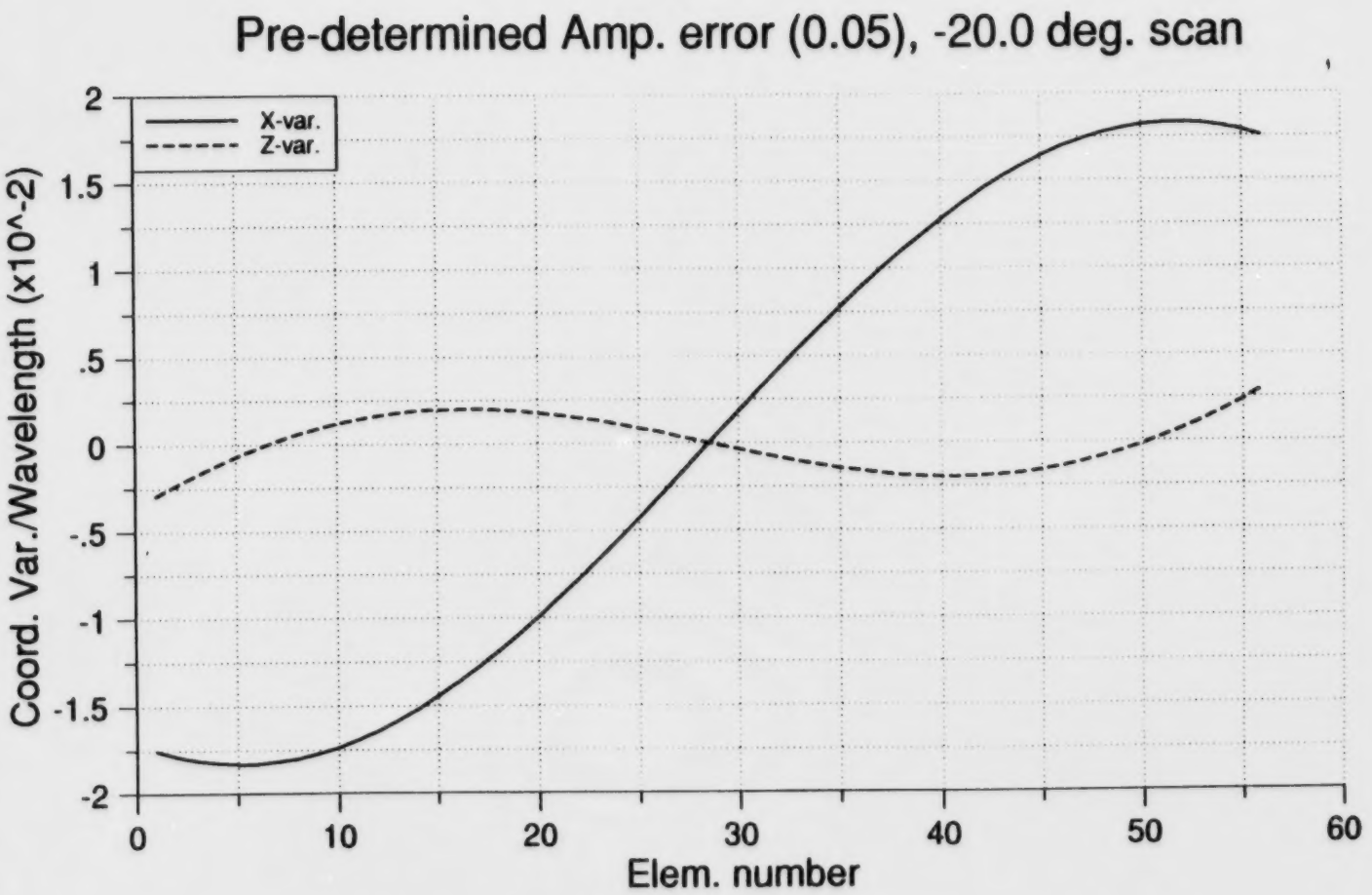

Fig. 4.42 : Phase centre movement due to a pre-determined error of 0.05 added to each element, $\theta_z = -20^\circ$.

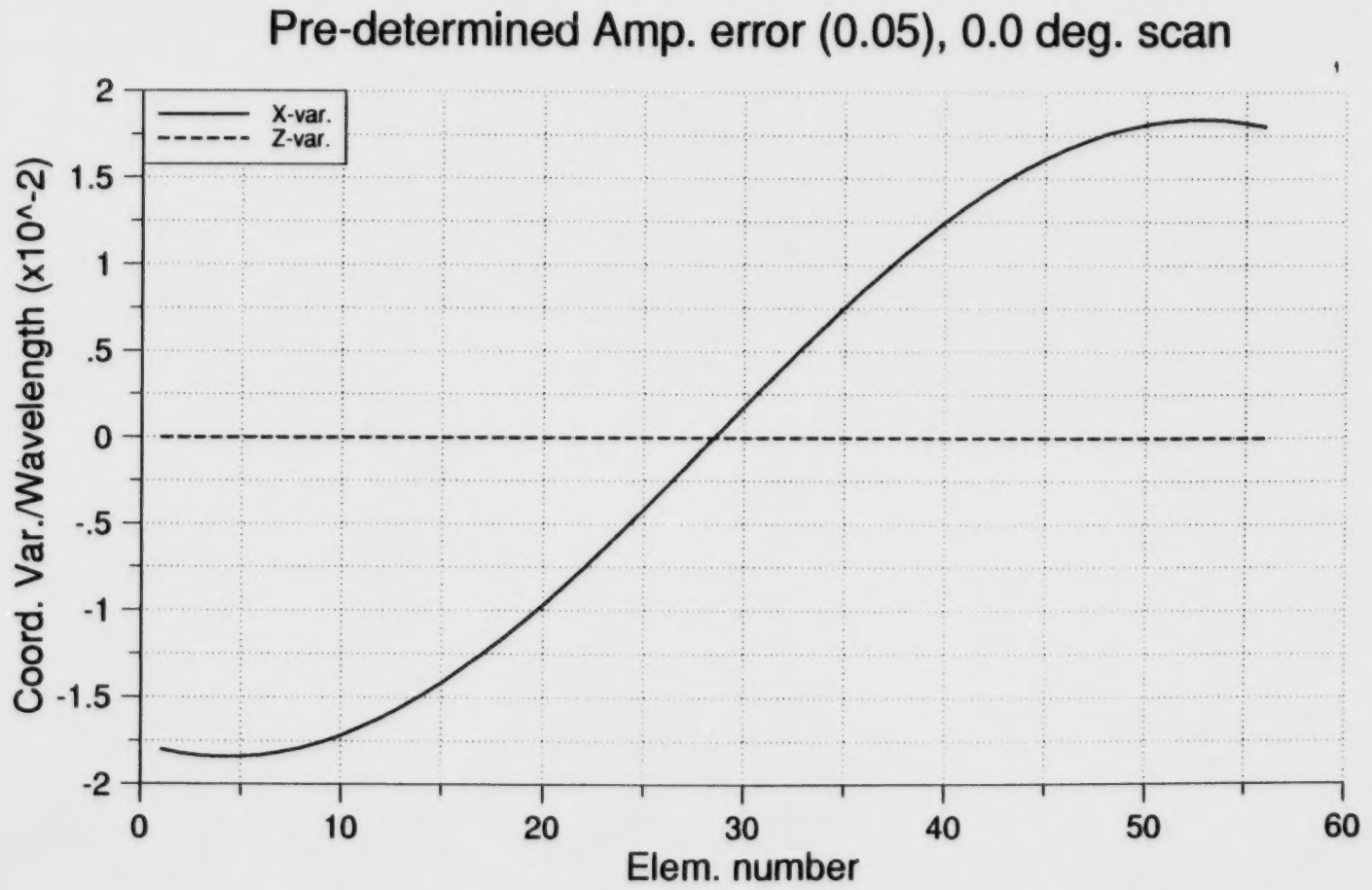

Fig. 4.43 : Phase centre movement due to a pre-determined error of 0.05 added to each element, $\theta_s = 0^o$.

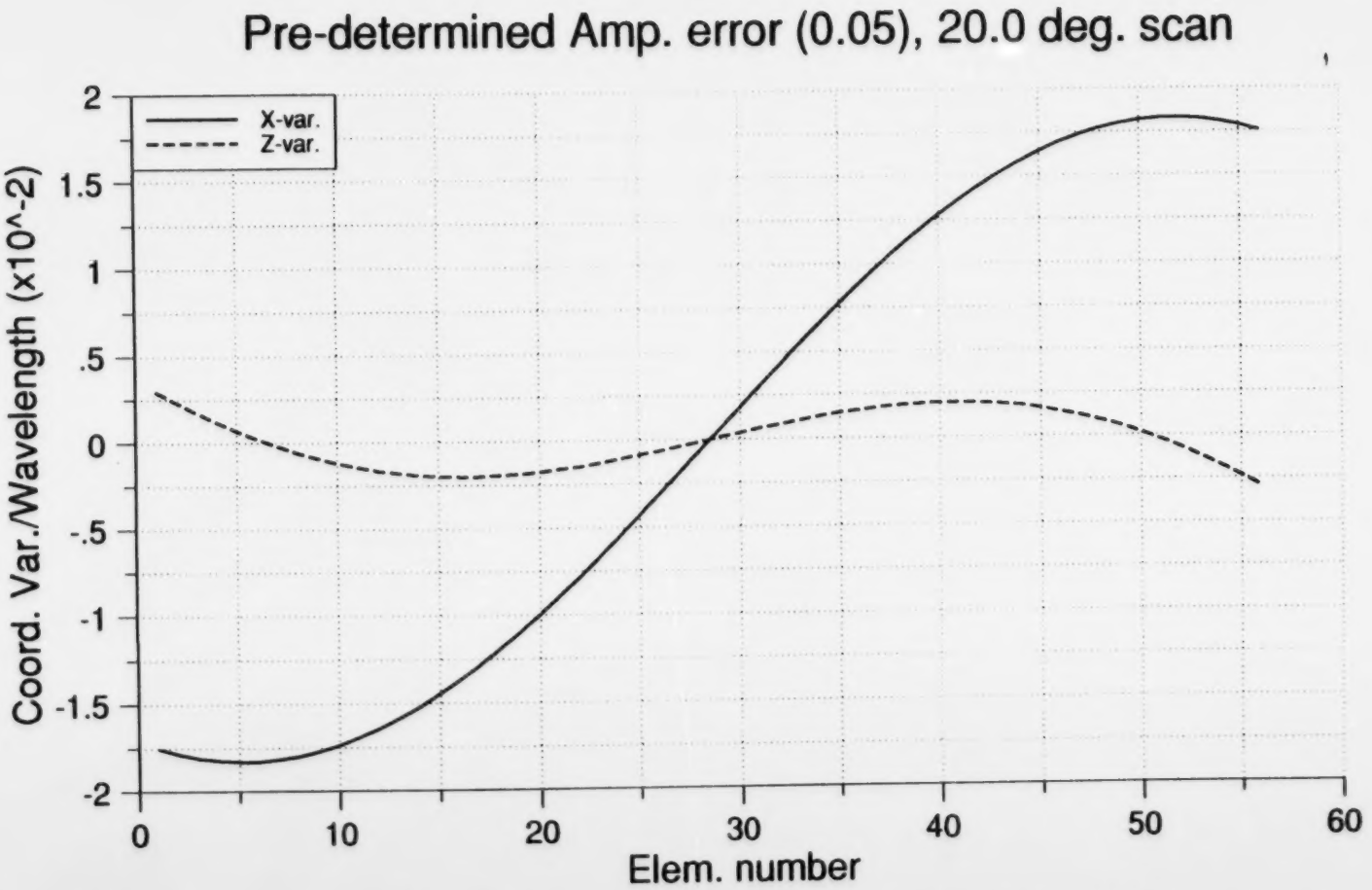

Fig. 4.44 : Phase centre movement due to a pre-determined error of 0.05 added to each element, $\theta_s = 20^o$.

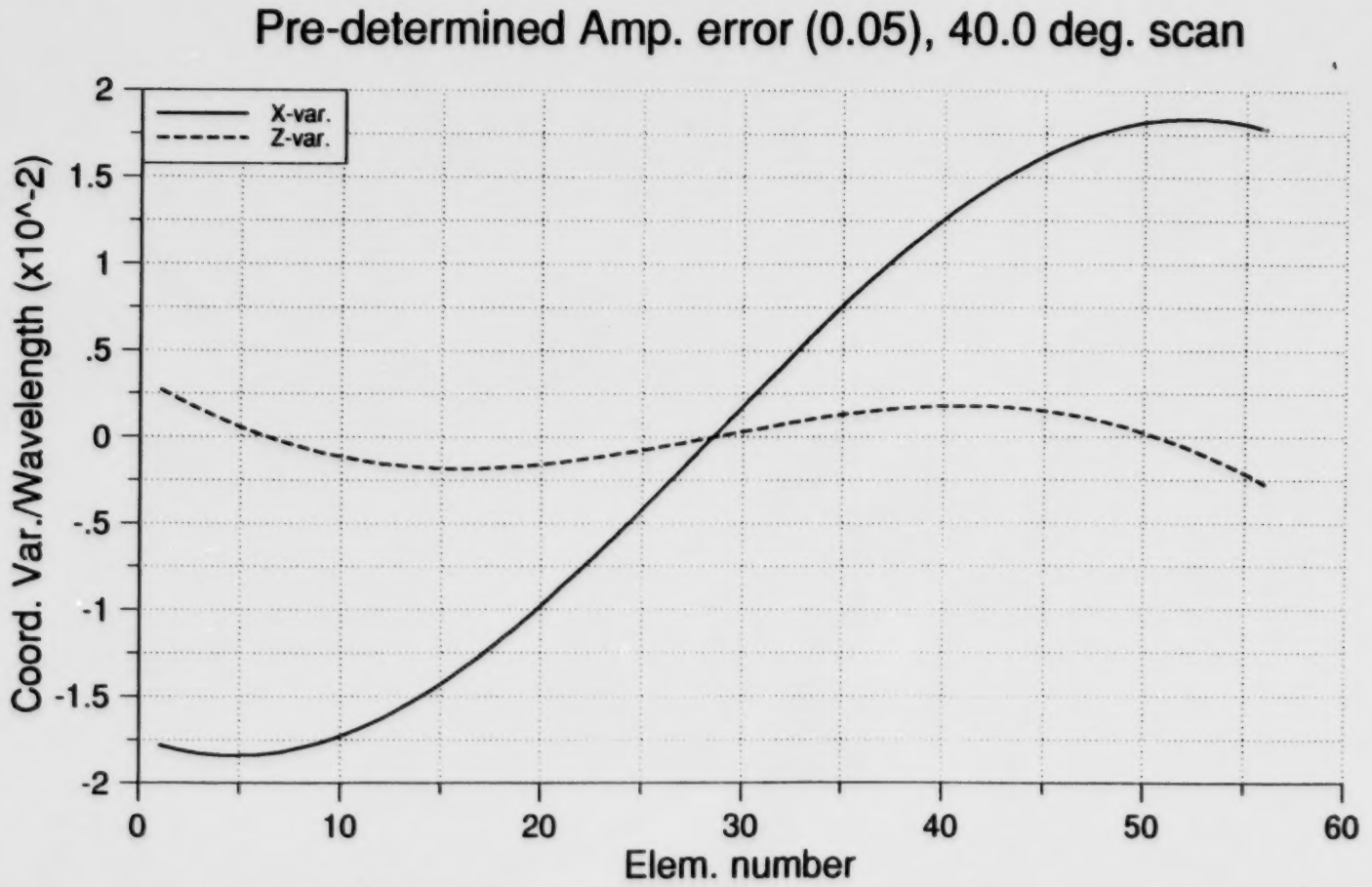

Fig. 4.45 : Phase centre movement due to a pre-determined error of 0.05 added to each element, $\theta_s = 40°$.

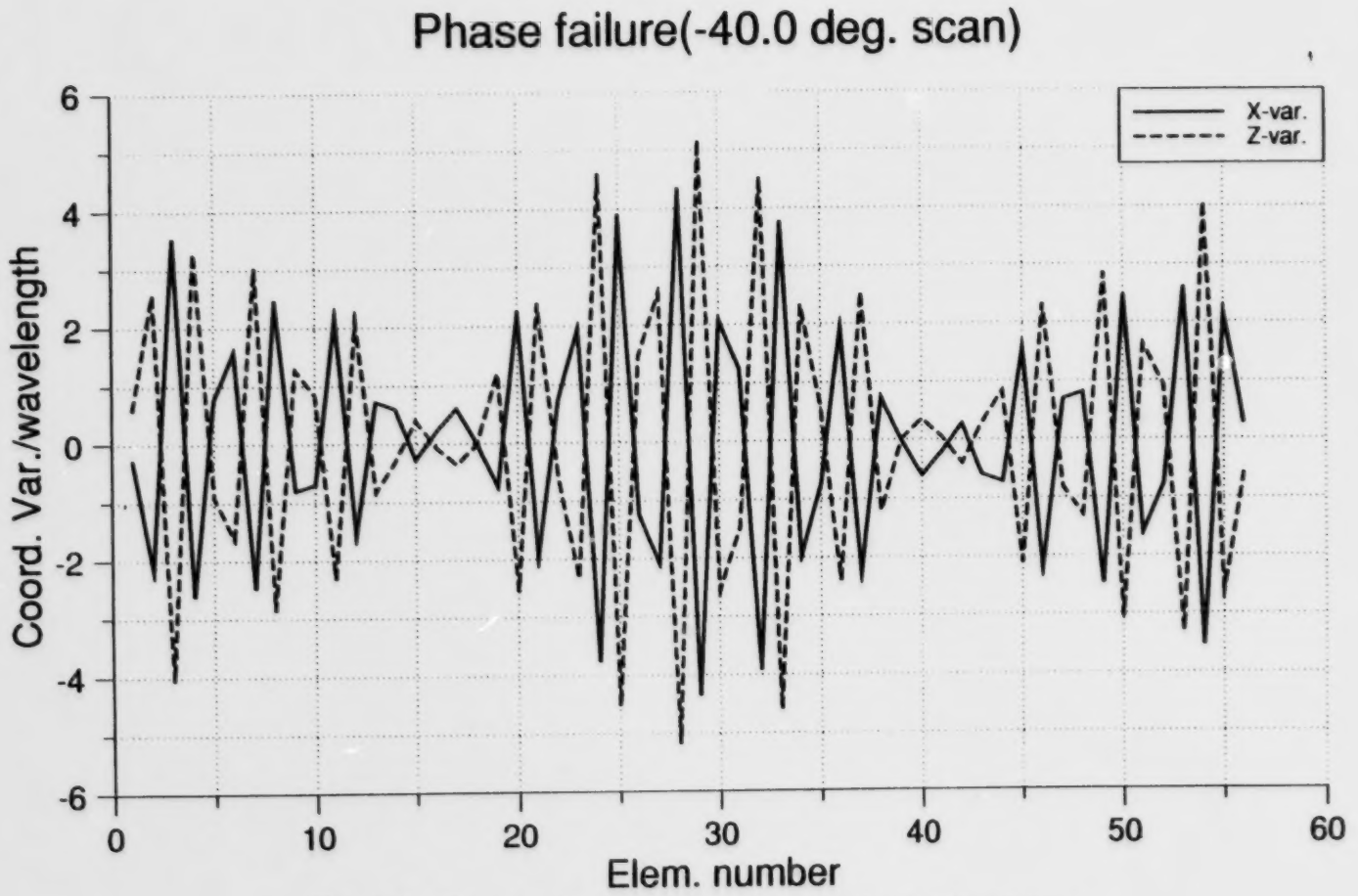

Fig. 4.46 : Phase centre movement due to the phase shifter failures, $\theta_s = -40^\circ$.

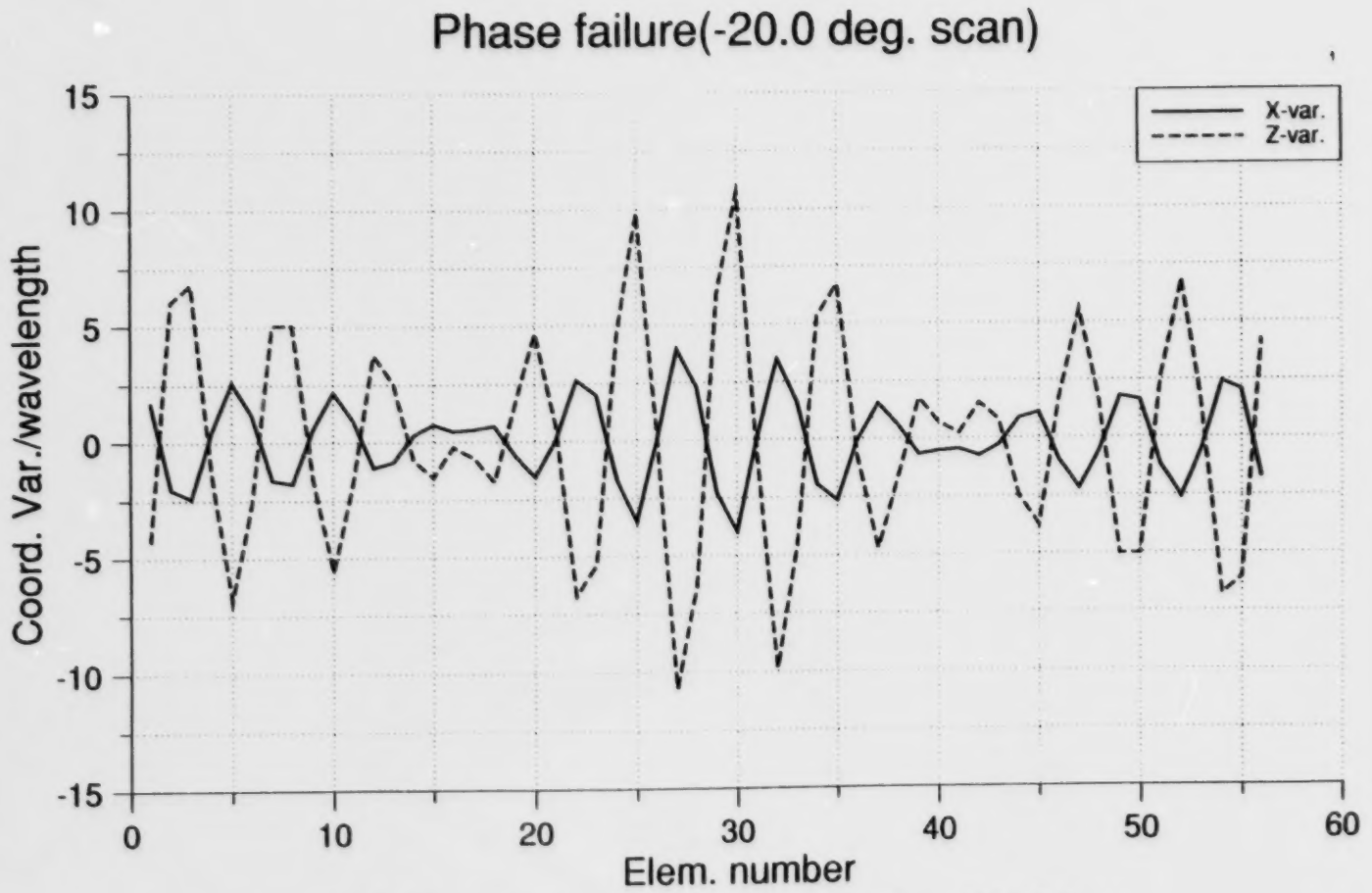

Fig. 4.47 : Phase centre movement due to the phase shifter failures, $\theta_s = -20°$.

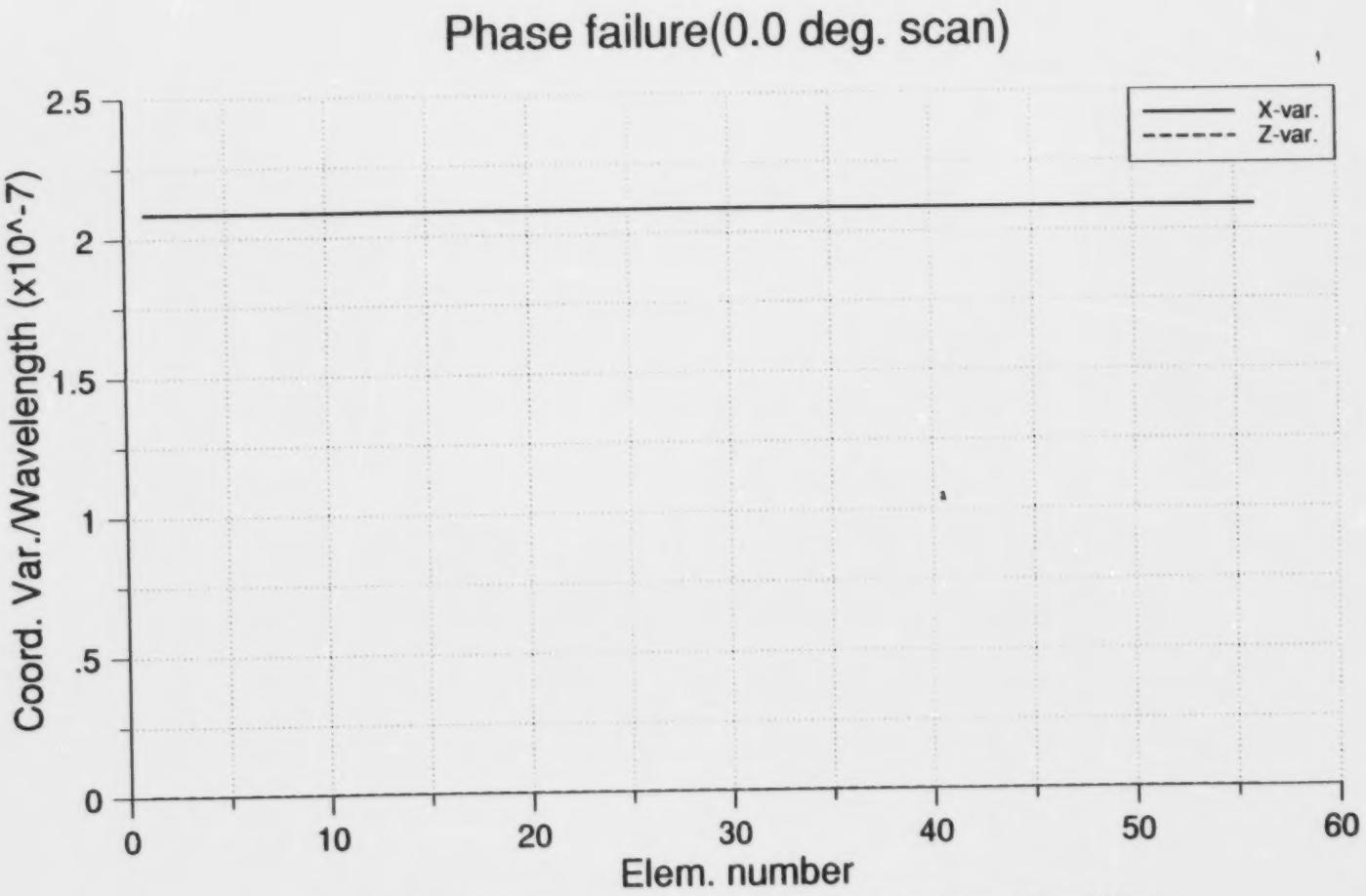

Fig. 4.48 : Phase centre movement due to the phase shifter failures, $\theta_s = 0^o$.

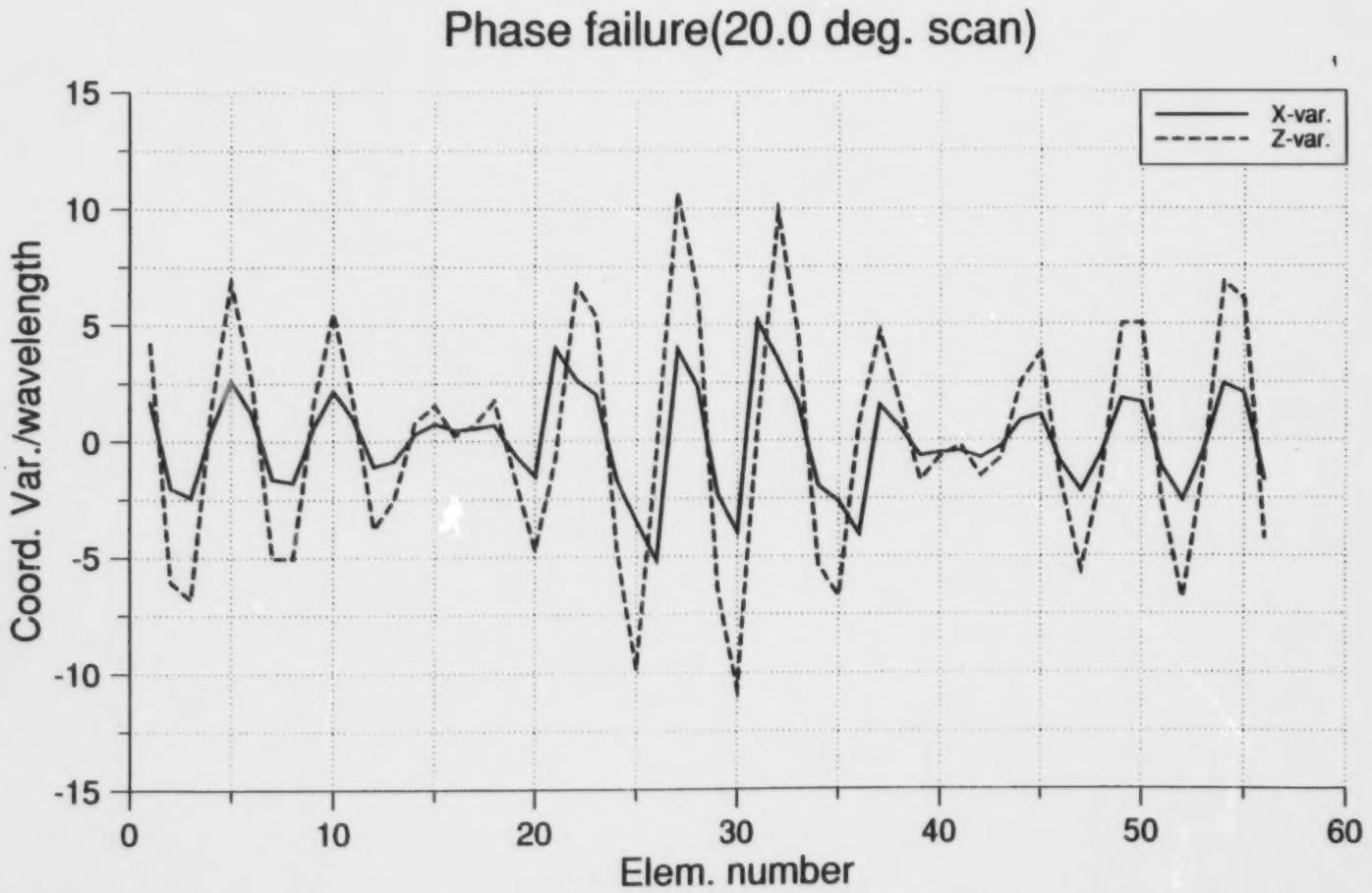

Fig. 4.49 : Phase centre movement due to the phase shifter failures, $\theta_s = 20°$.

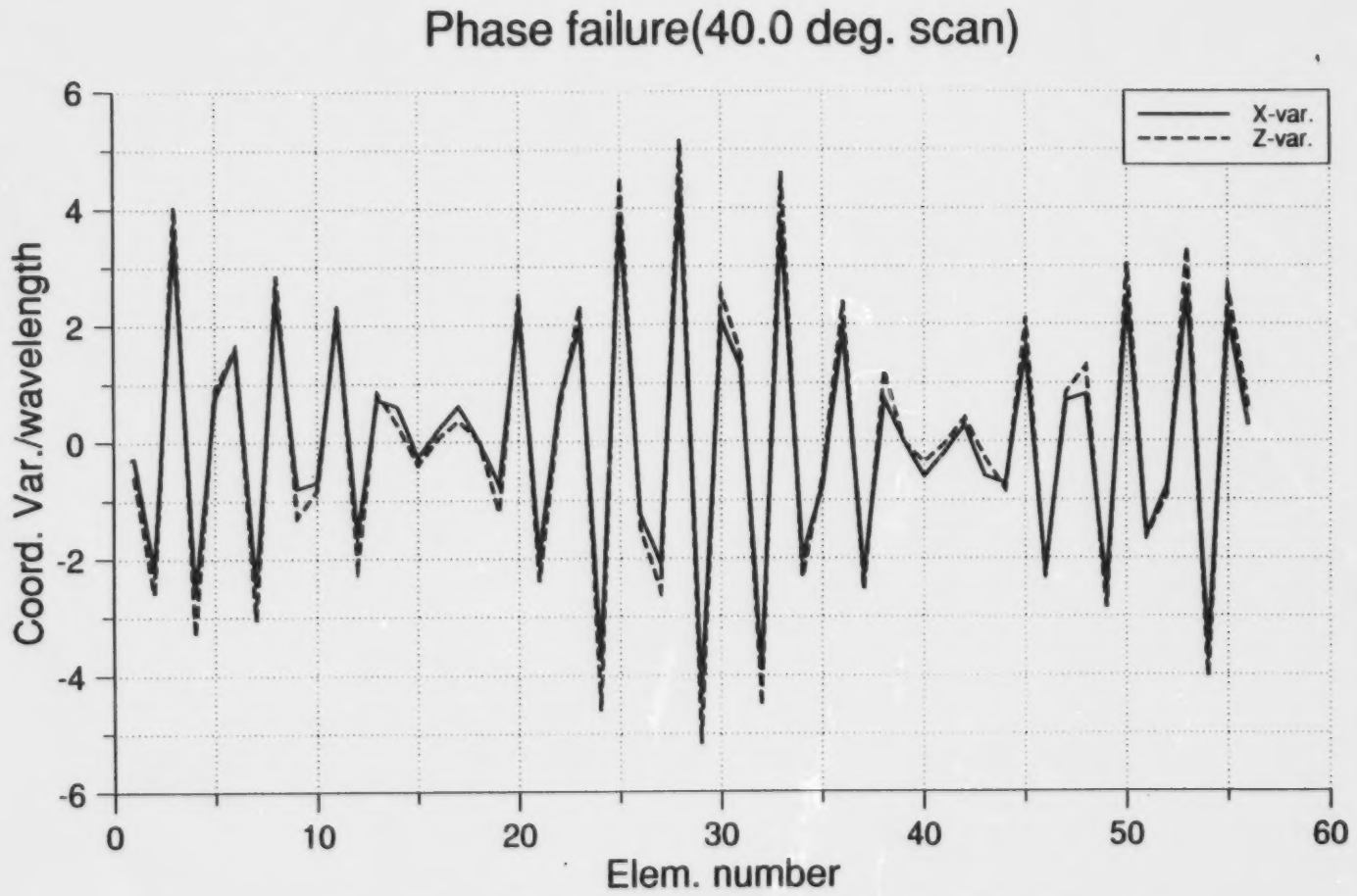

Fig. 4.50 : Phase centre movement due to the phase shifter failures, $\theta_s = 40^\circ$.

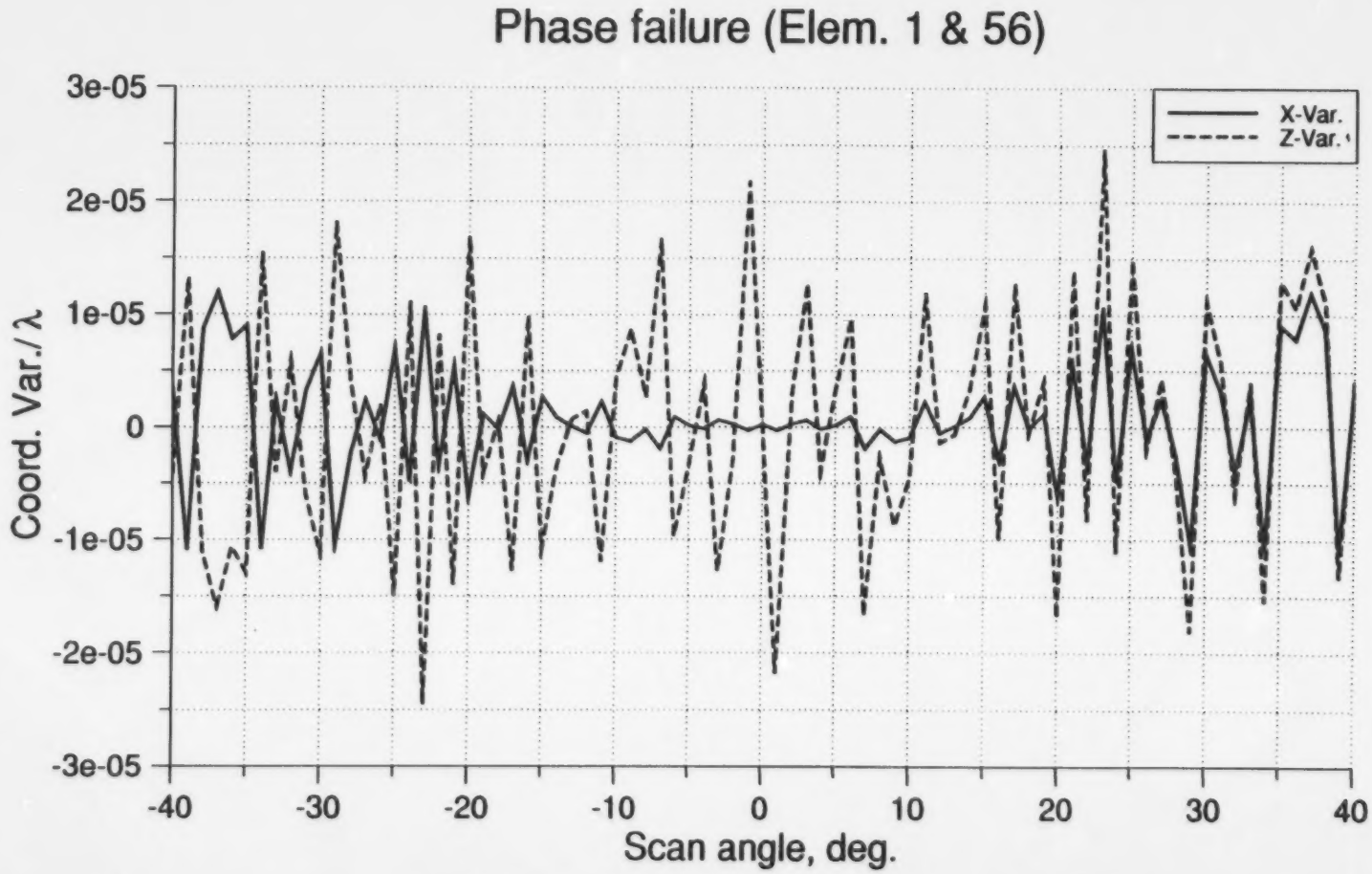

Fig. 4.51 : Phase centre movement due to the phase shifter failures, element no. 1 & 56.

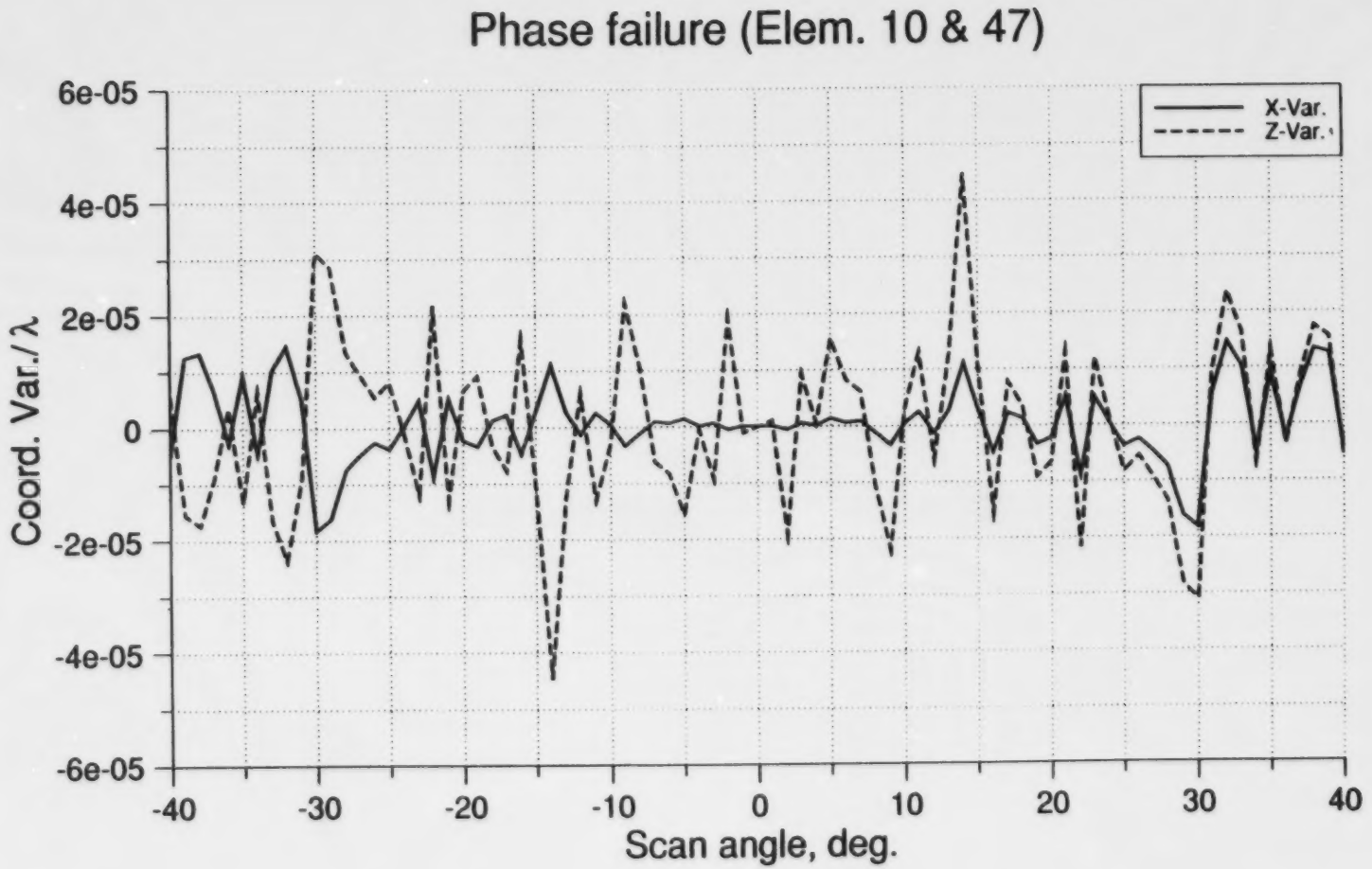

Fig. 4.52 : Phase centre movement due to the phase shifter failures, element no. 10 & 47.

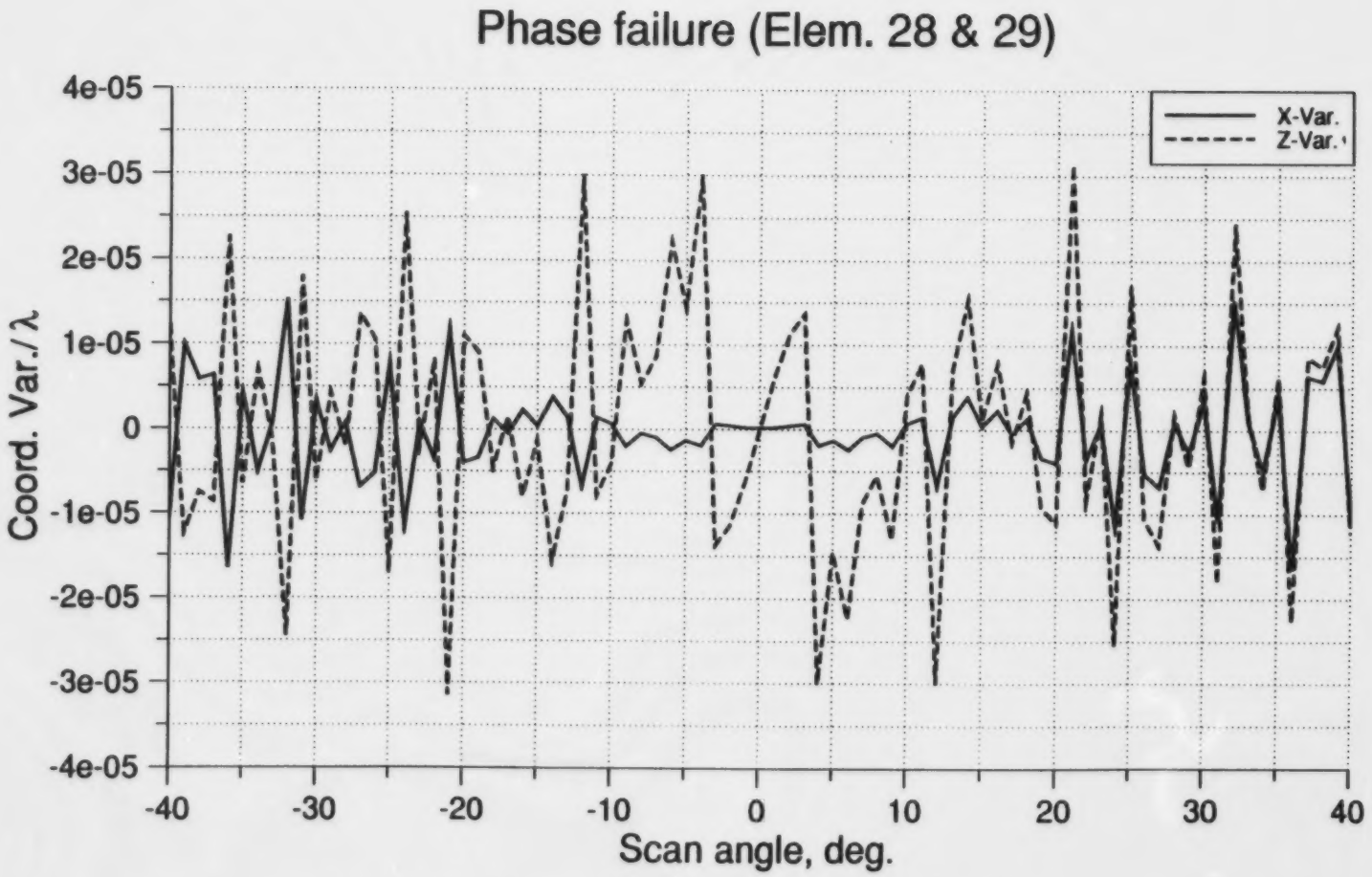

Fig. 4.53 : Phase centre movement due to the phase shifter failures, element no. 28 & 29.

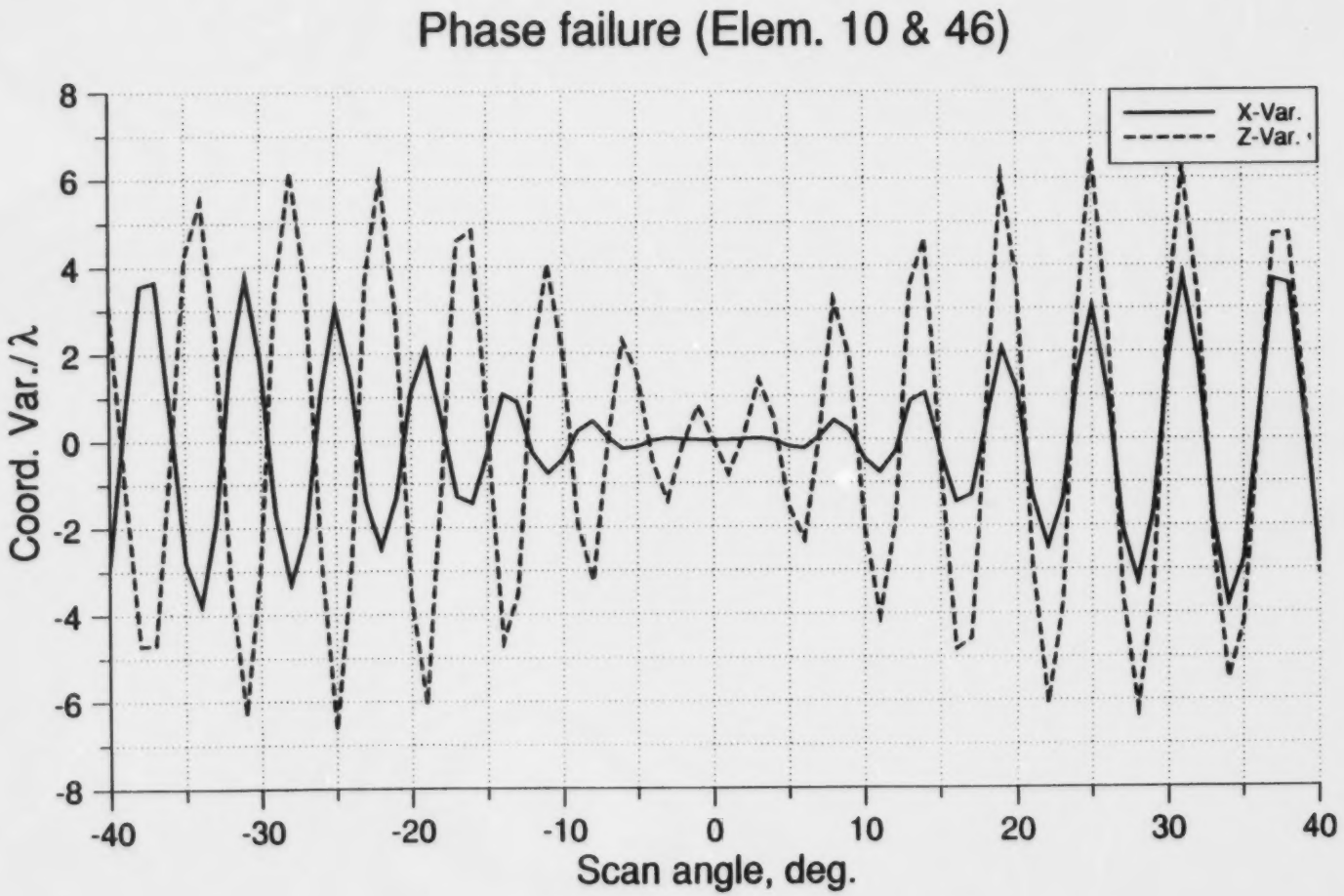

Fig. 4.54 : Phase centre movement due to the phase shifter failures, element no. 10 & 46.

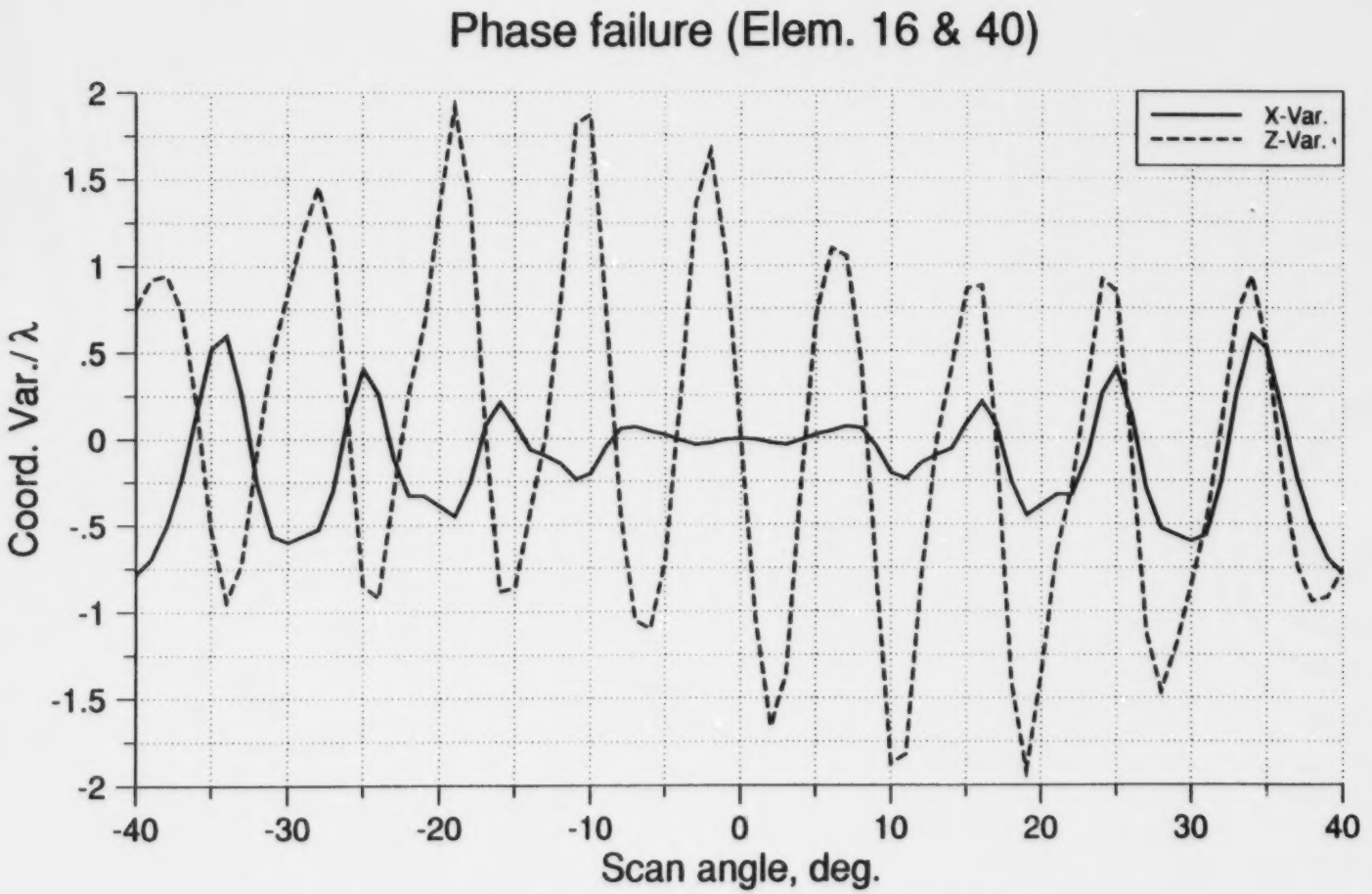

Fig. 4.55 : Phase centre movement due to the phase shifter failures, element no. 16 & 40.

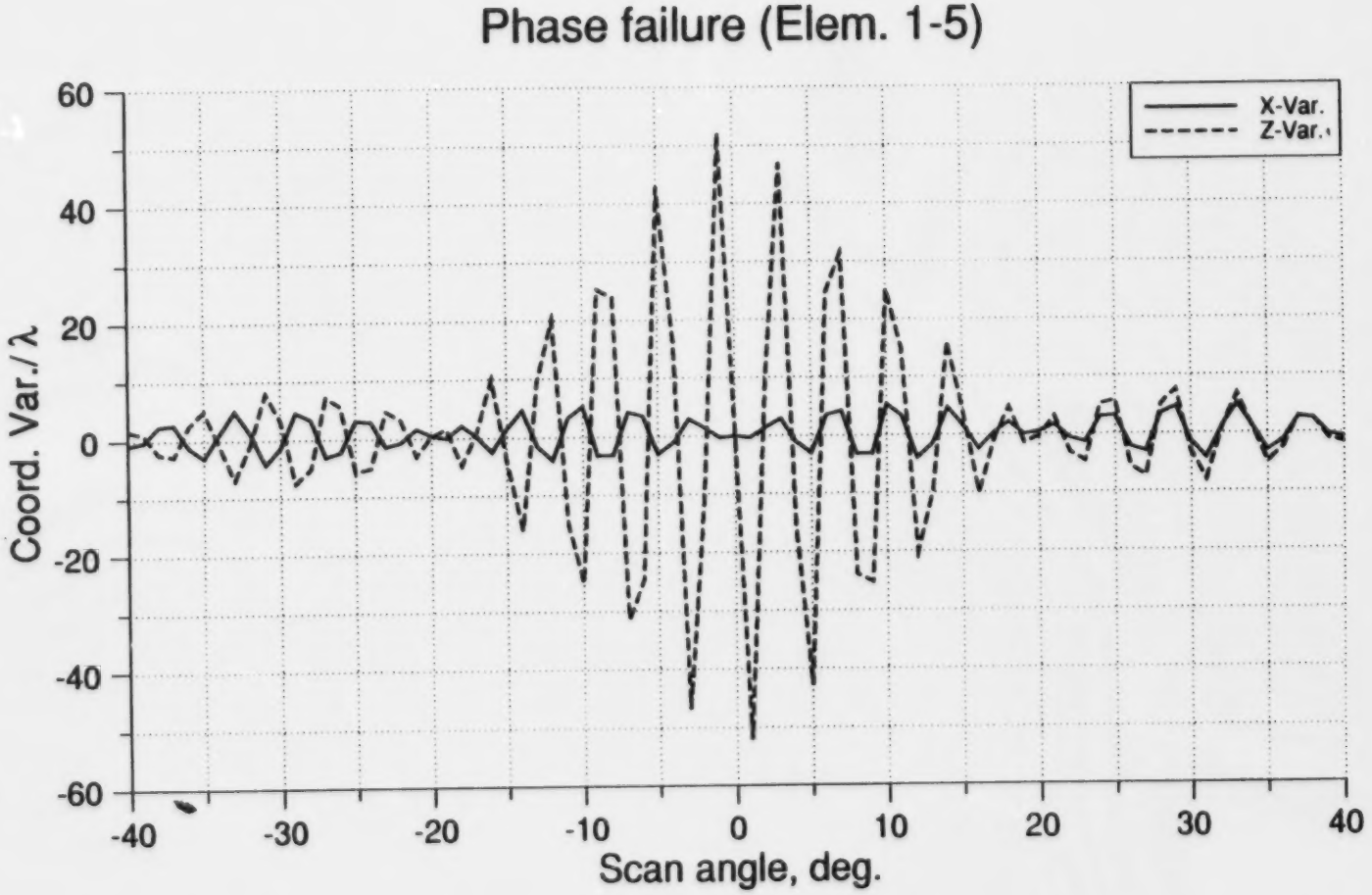

Fig. 4.56 : Phase centre movement due to the phase shifter failures, element no. 1 to 5.

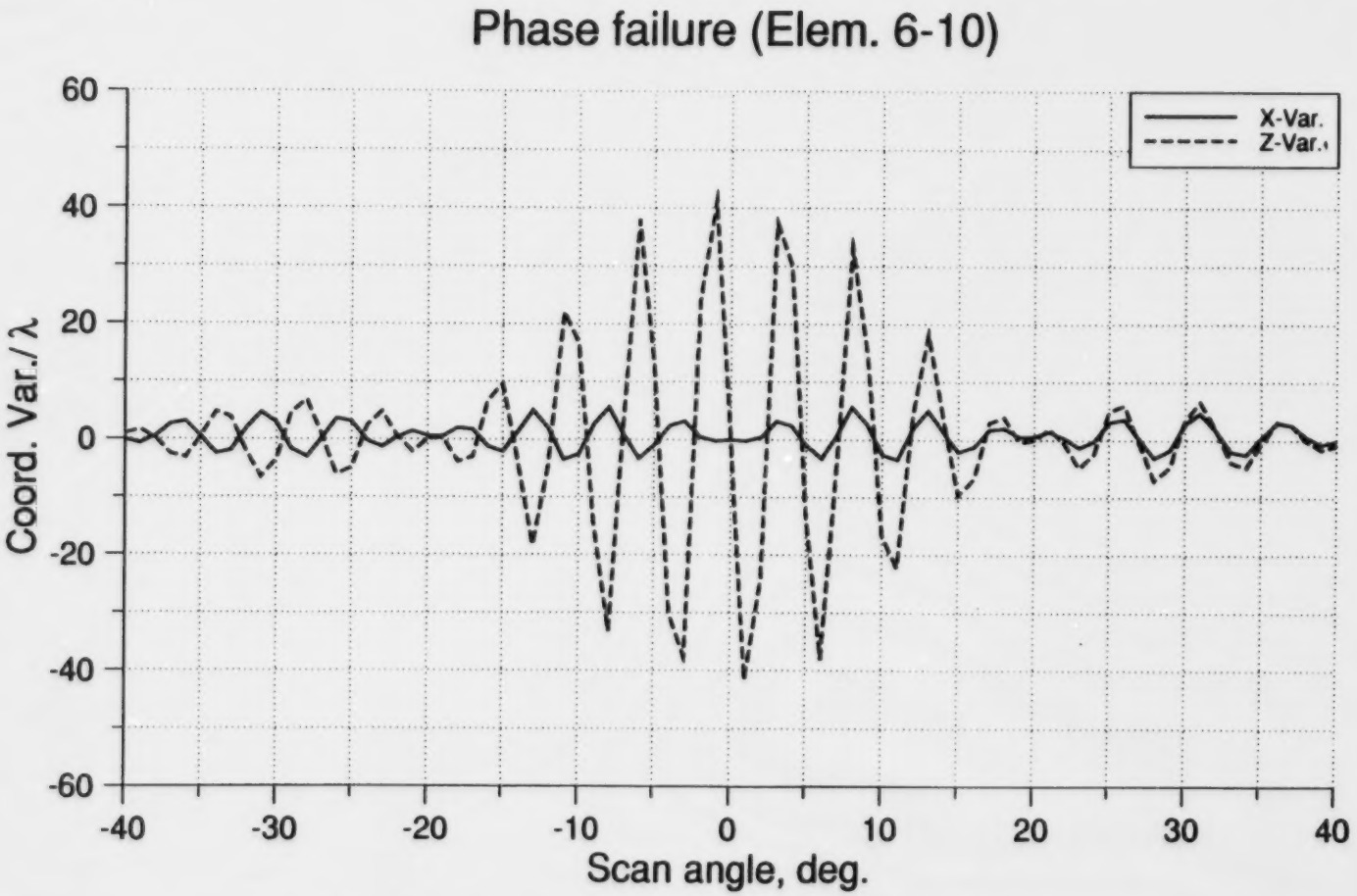

Fig. 4.57 : Phase centre movement due to the phase shifter failures, element no. 6 to 10.

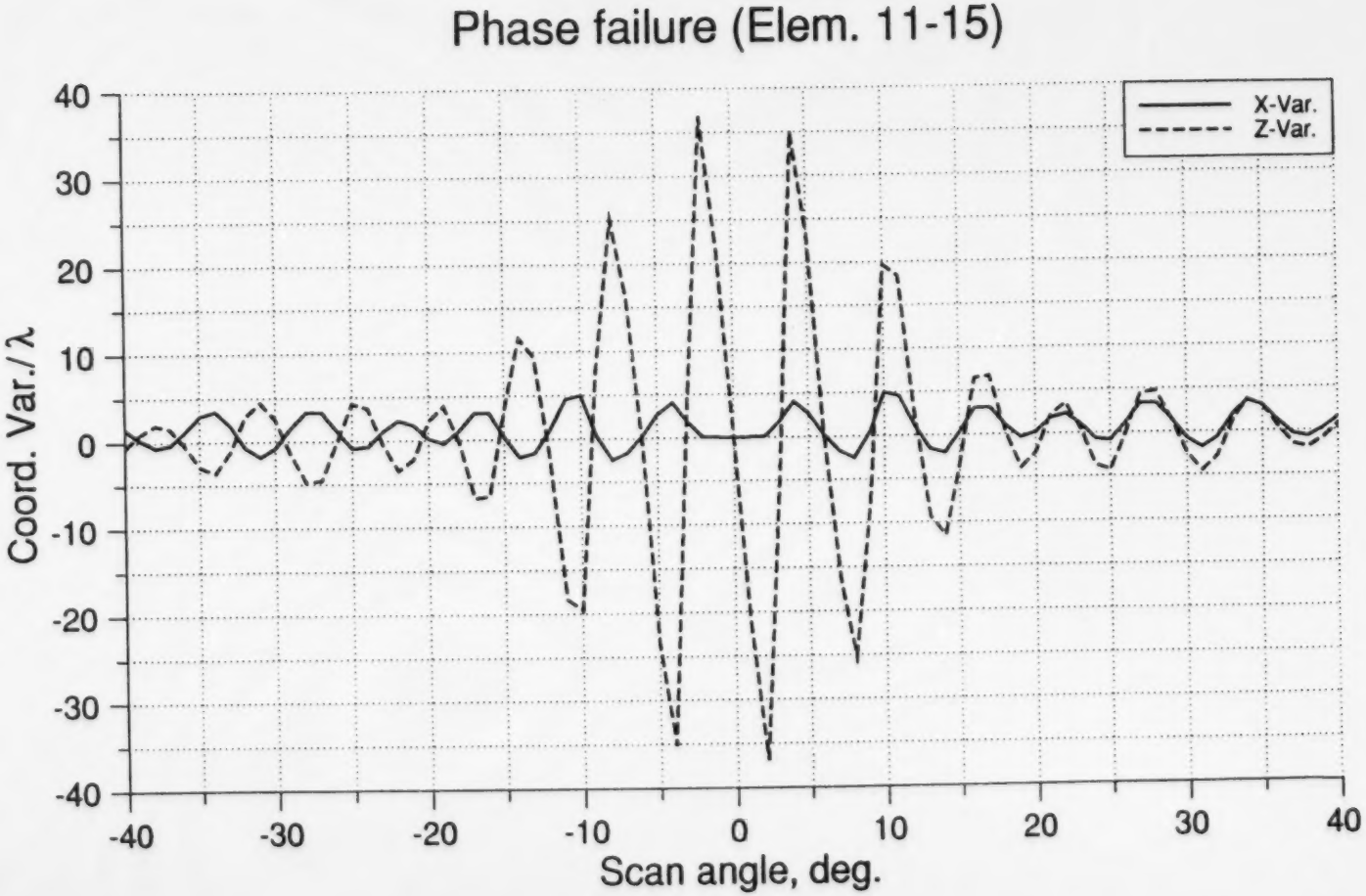

Fig. 4.58 : Phase centre movement due to the phase shifter failures, element no. 11 to 15.

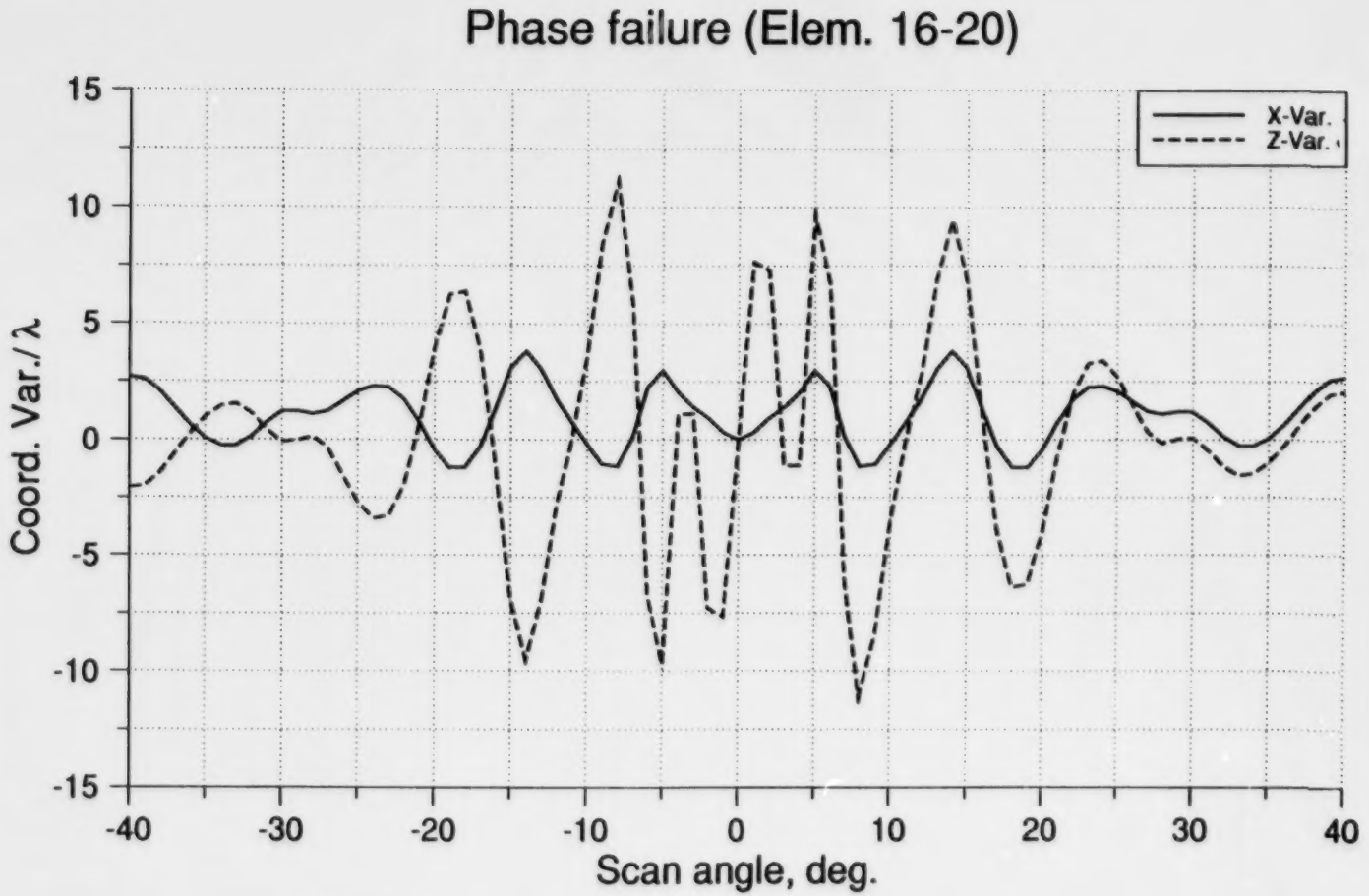

Fig. 4.59 : Phase centre movement due to the phase shifter failures, element no. 16 to 20.

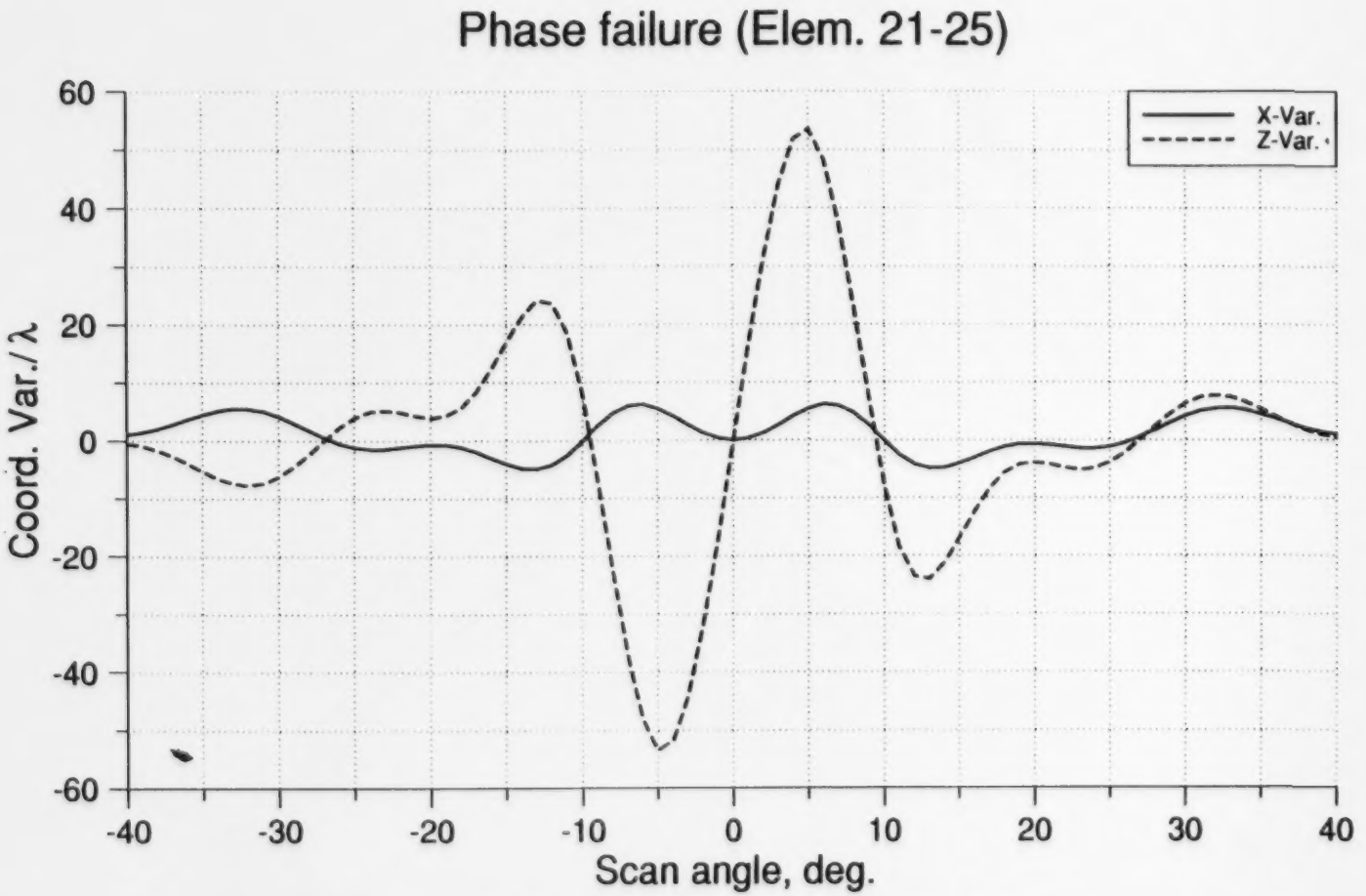

Fig. 4.60 : Phase centre movement due to the phase shifter failures, element no. 21 to 25.

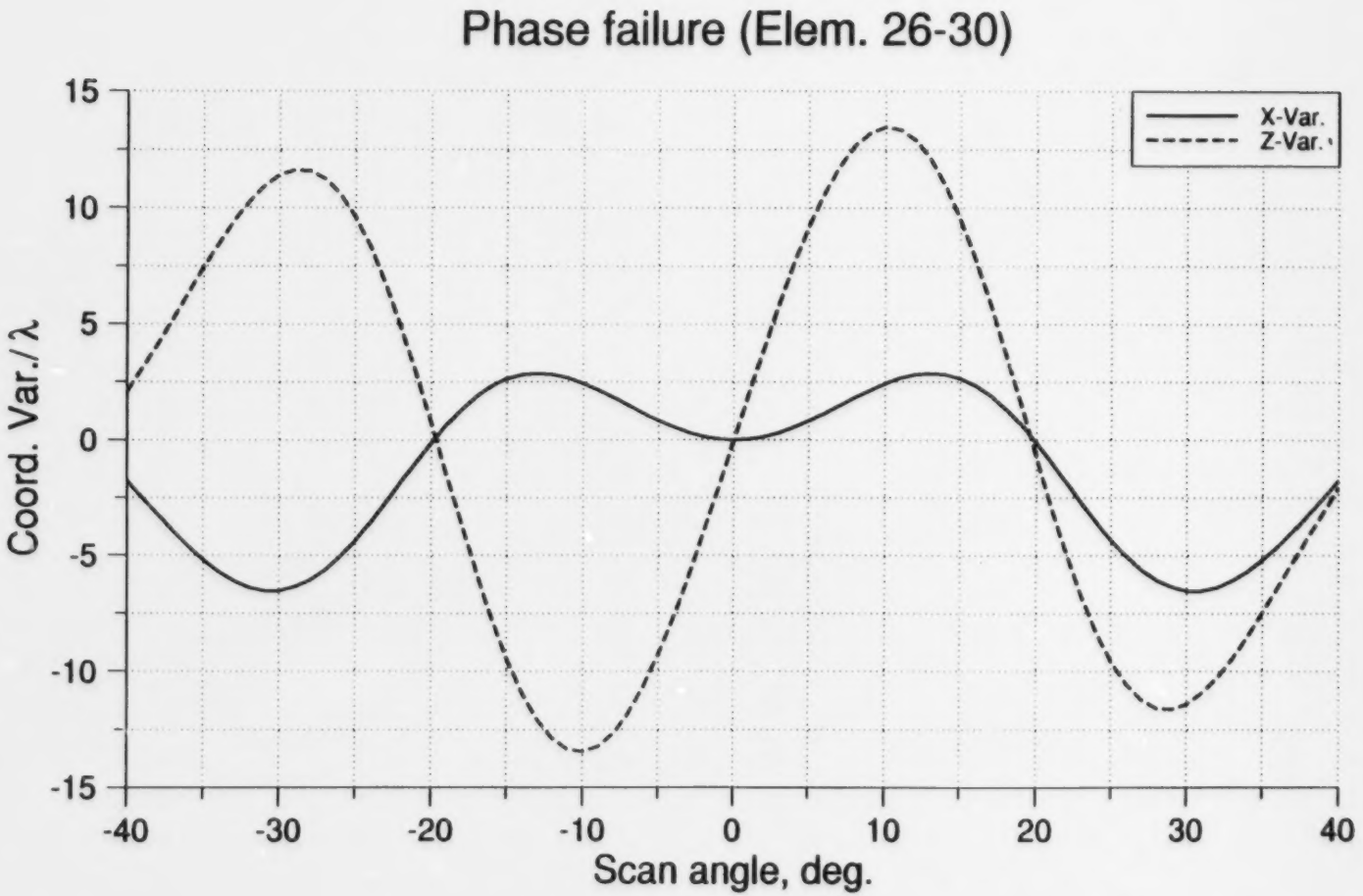

Fig. 4.61 : Phase centre movement due to the phase shifter failures, element no. 26 to 30.

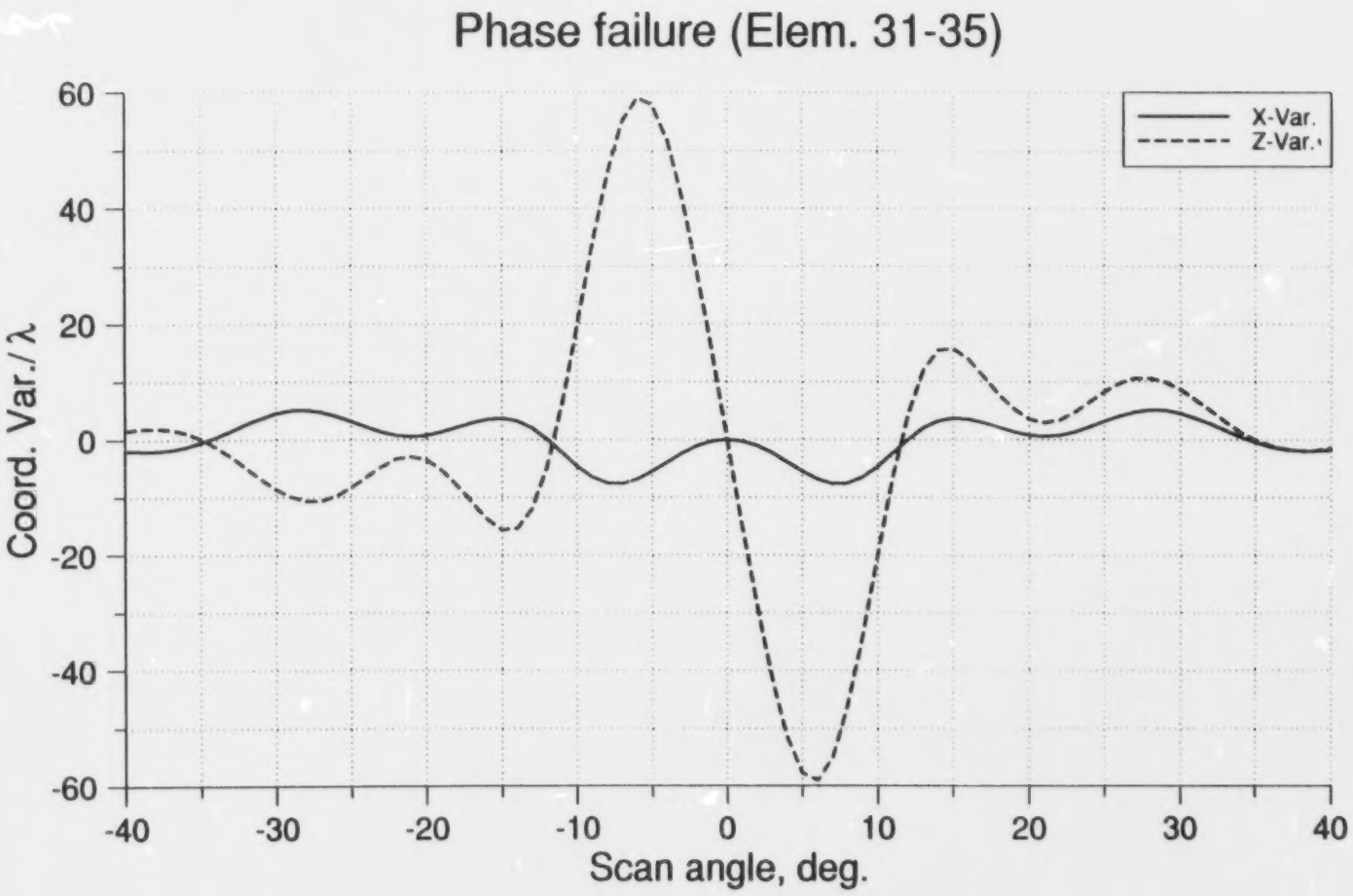

Fig. 4.62 : Phase centre movement due to the phase shifter failures, element no. 31 to 35.

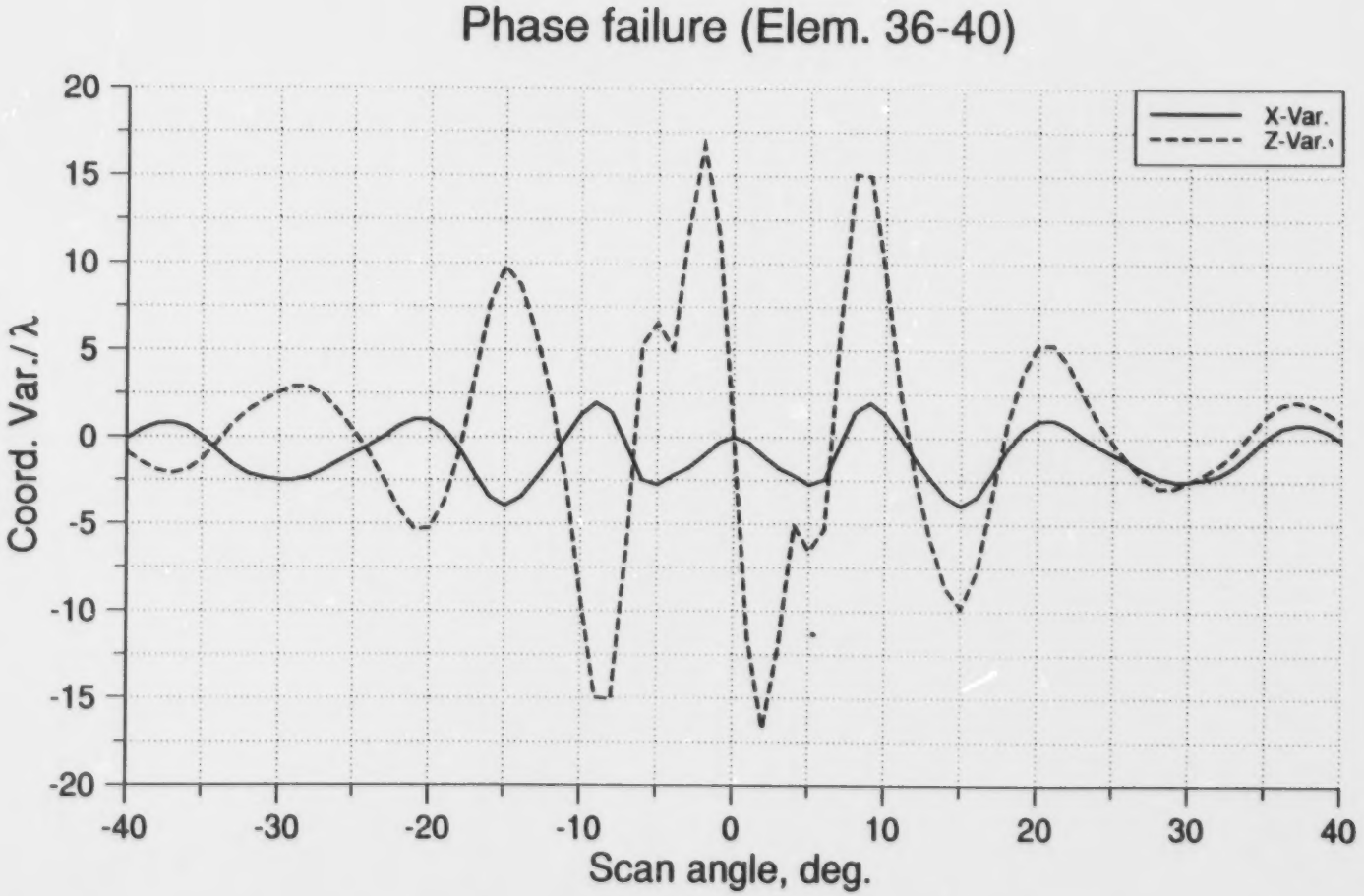

Fig. 4.63 : Phase centre movement due to the phase shifter failures, element no. 36 to 40.

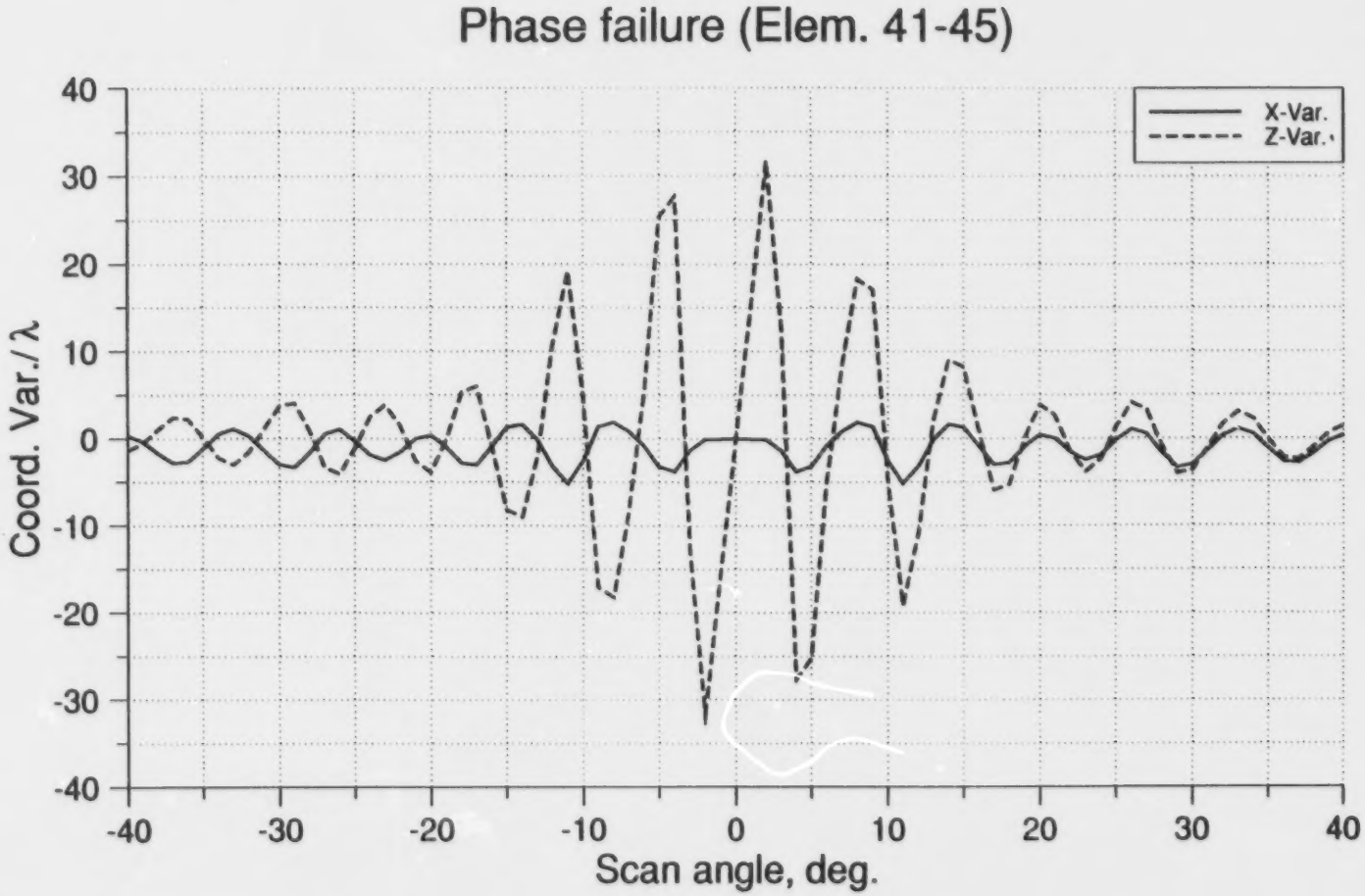

Fig. 4.64 : Phase centre movement due to the phase shifter failures, element no. 41 to 45.

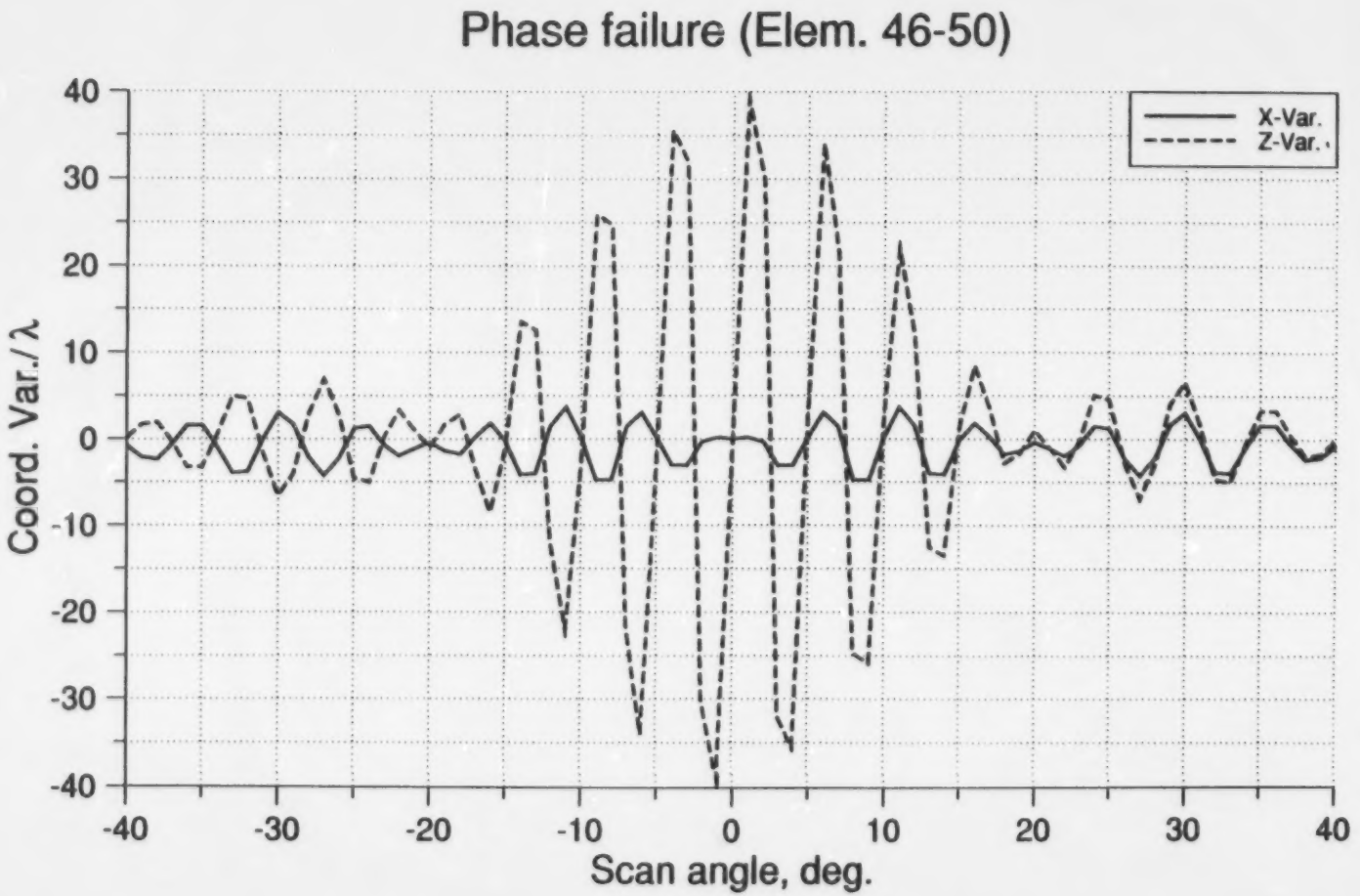

Fig. 4.65 : Phase centre movement due to the phase shifter failures, element no. 46 to 50.

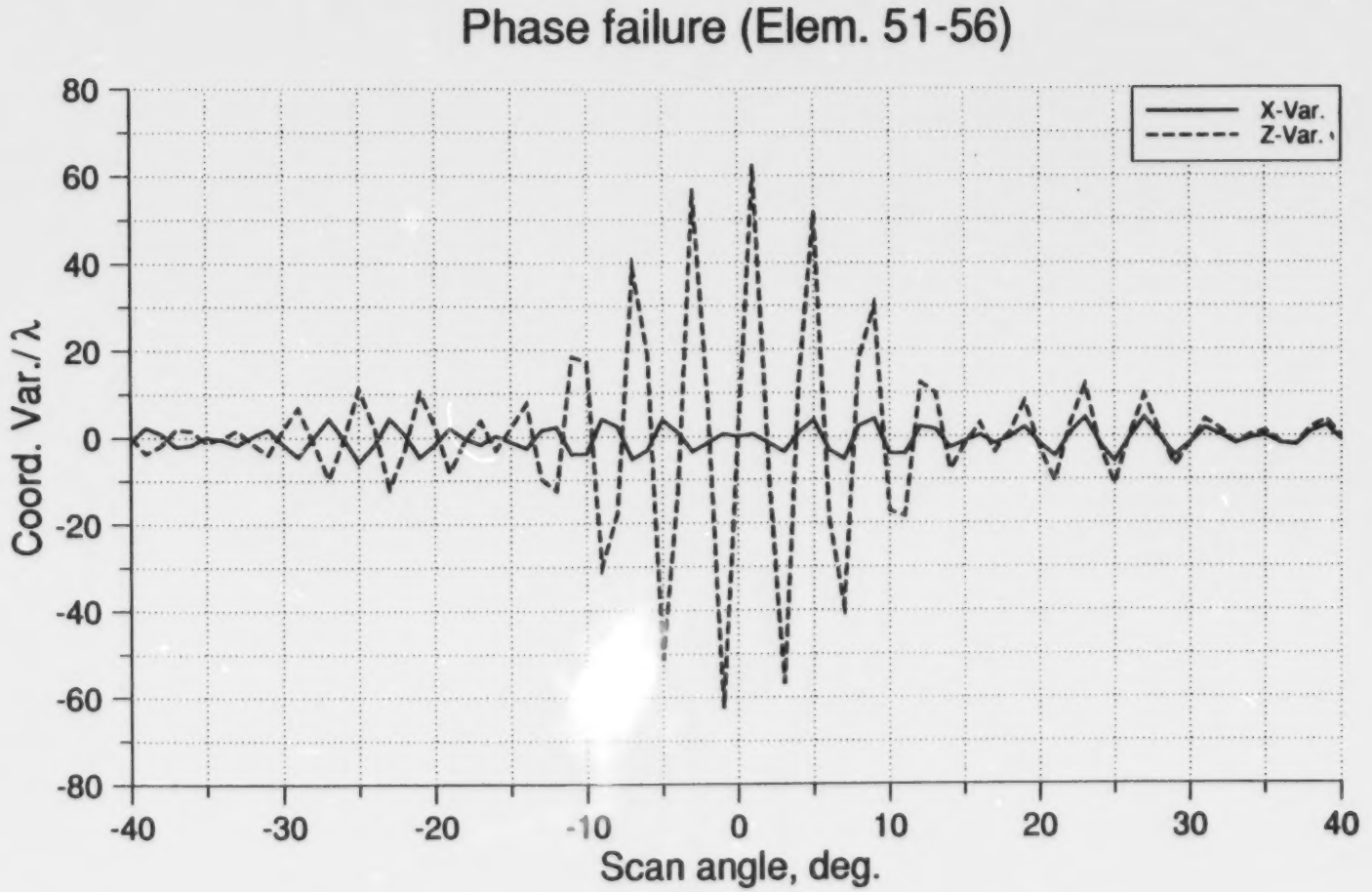

Fig. 4.66 : Phase centre movement due to the phase shifter failures, element no. 51 to 56.

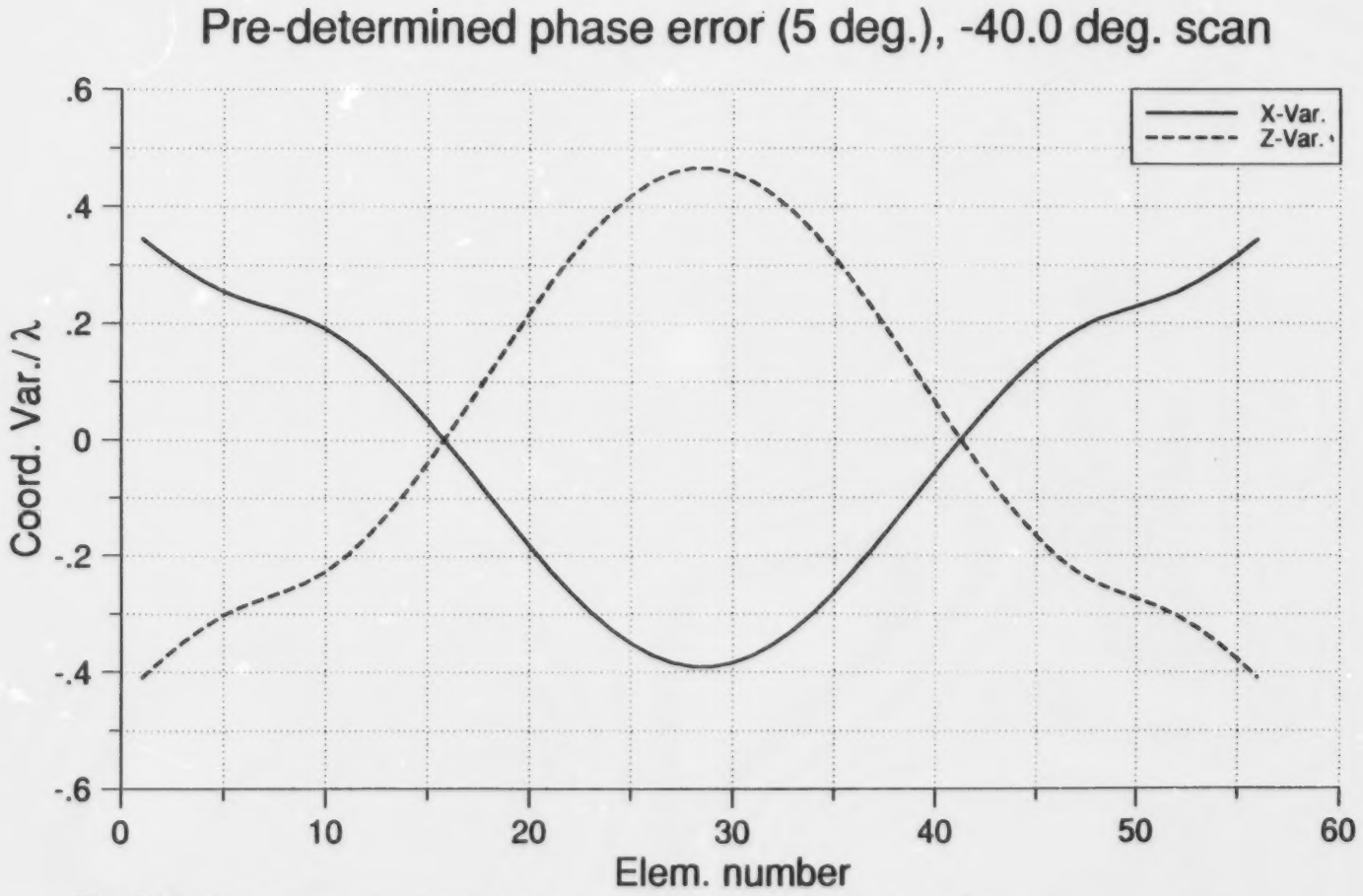

Fig. 4.67 : Phase centre movement due to a pre-determined error of 5° added to each phase shifter, $\theta_s = -40°$.

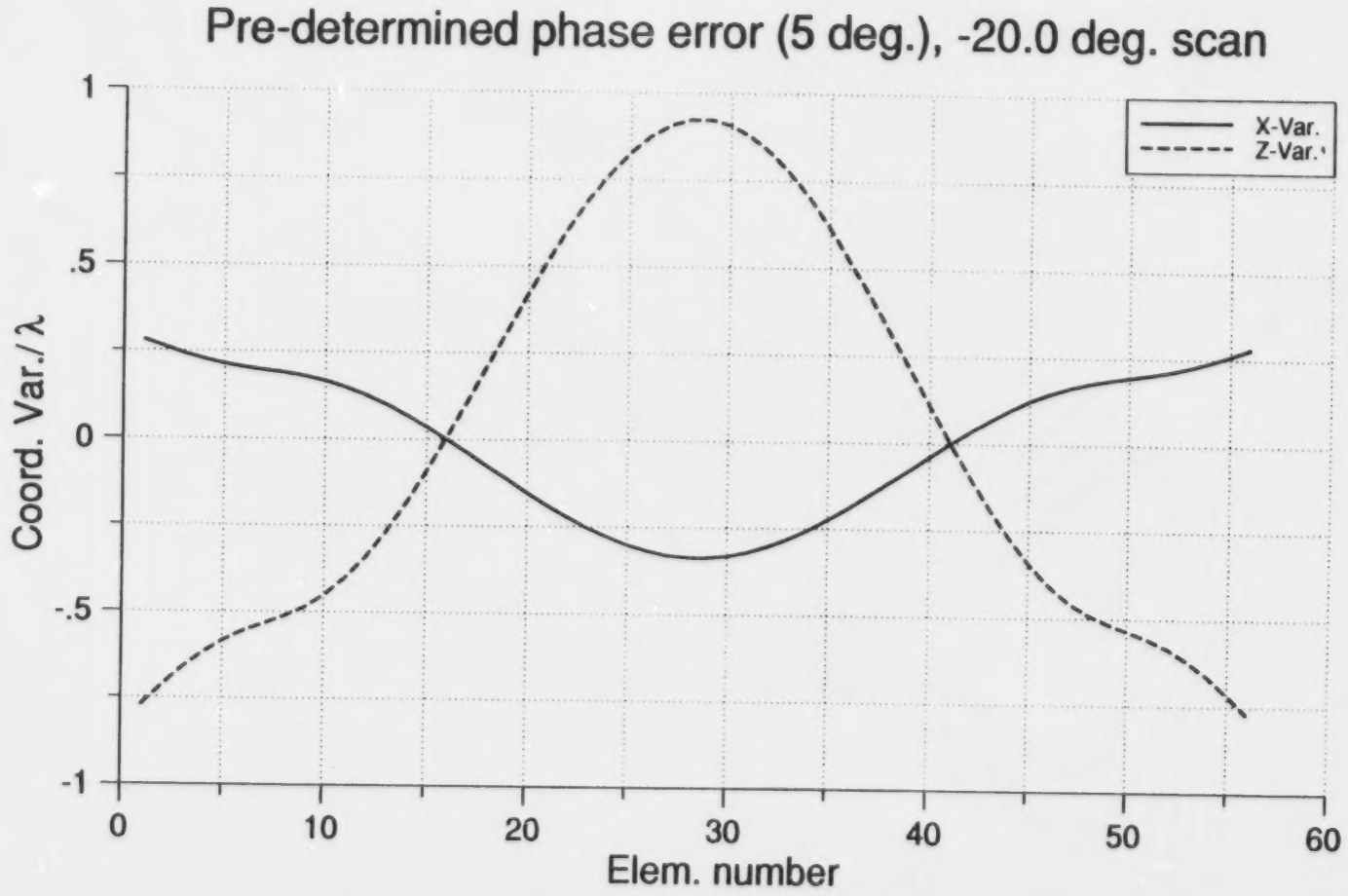

Fig. 4.68 : Phase centre movement due to a pre-determined error of 5° added to each phase shifter, $\theta_s = -20°$.

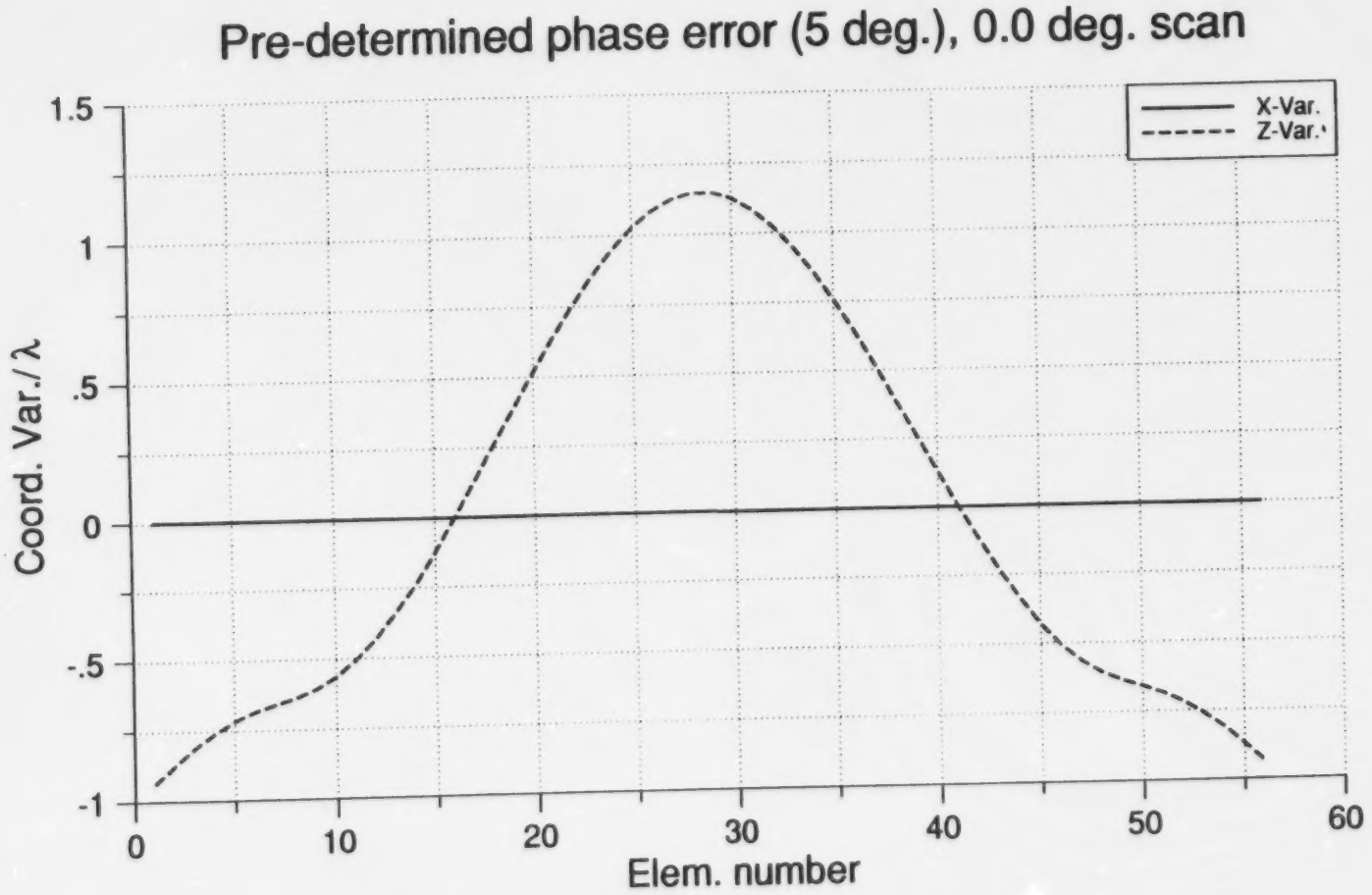

Fig. 4.69 : Phase centre movement due to a pre-determined error of 5° added to each phase shifter, $\theta_s = 0°$.

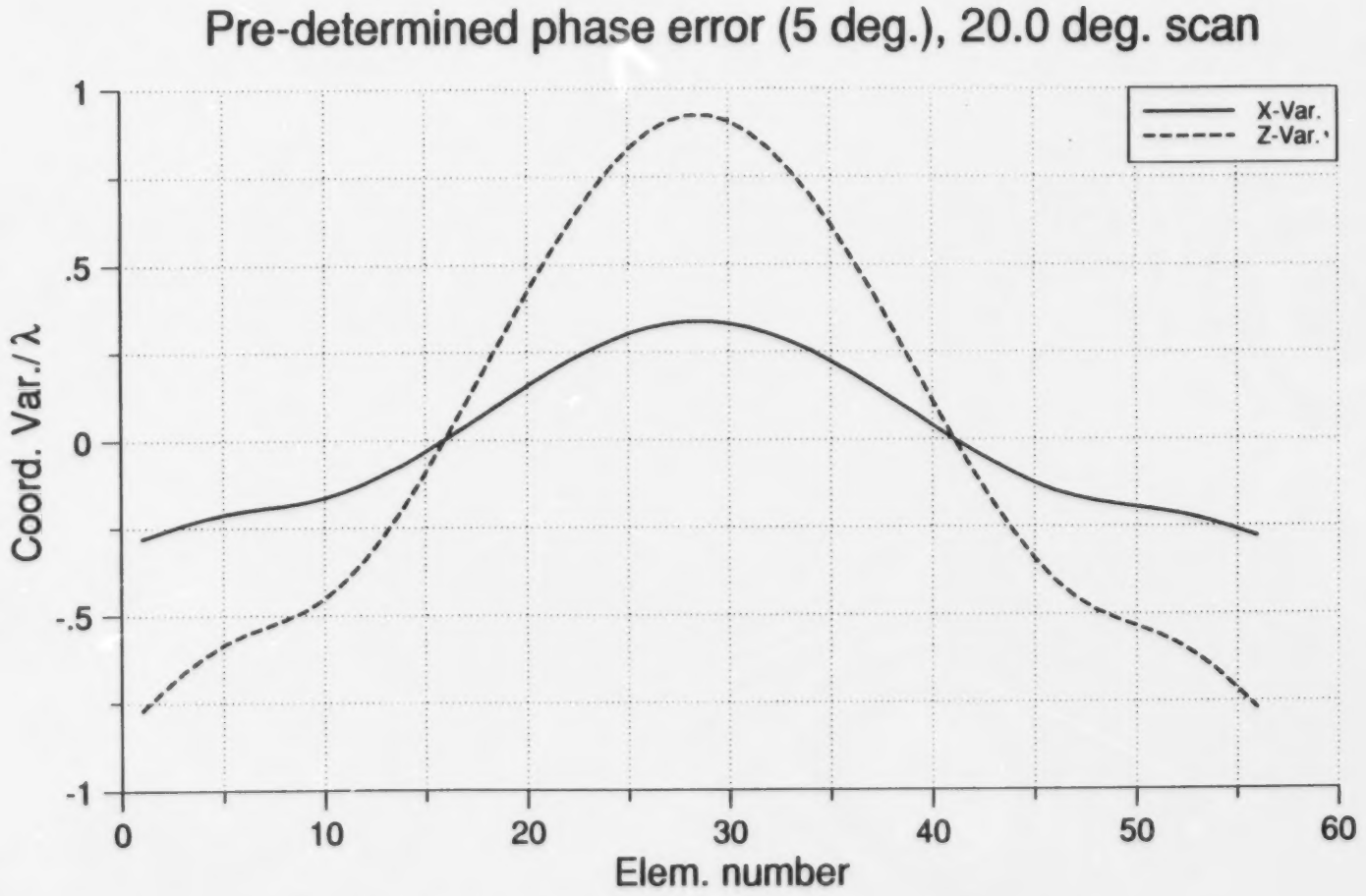

Fig. 4.70 : Phase centre movement due to a pre-determined error of 5° added to each phase shifter, $\theta_s = 20°$.

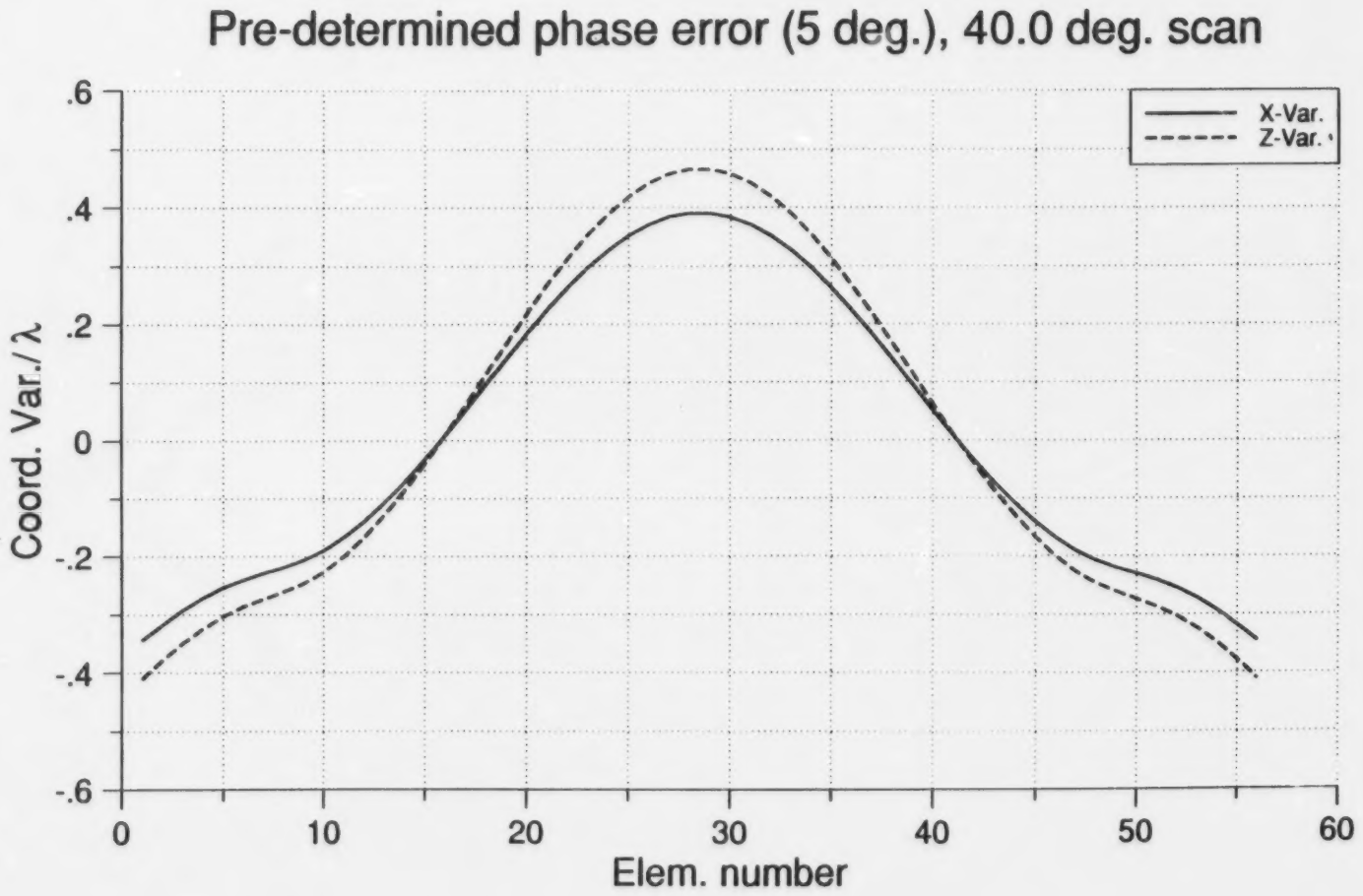

Fig. 4.71 : Phase centre movement due to a pre-determined error of 5° added to each phase shifter, $\theta_z = 40°$.

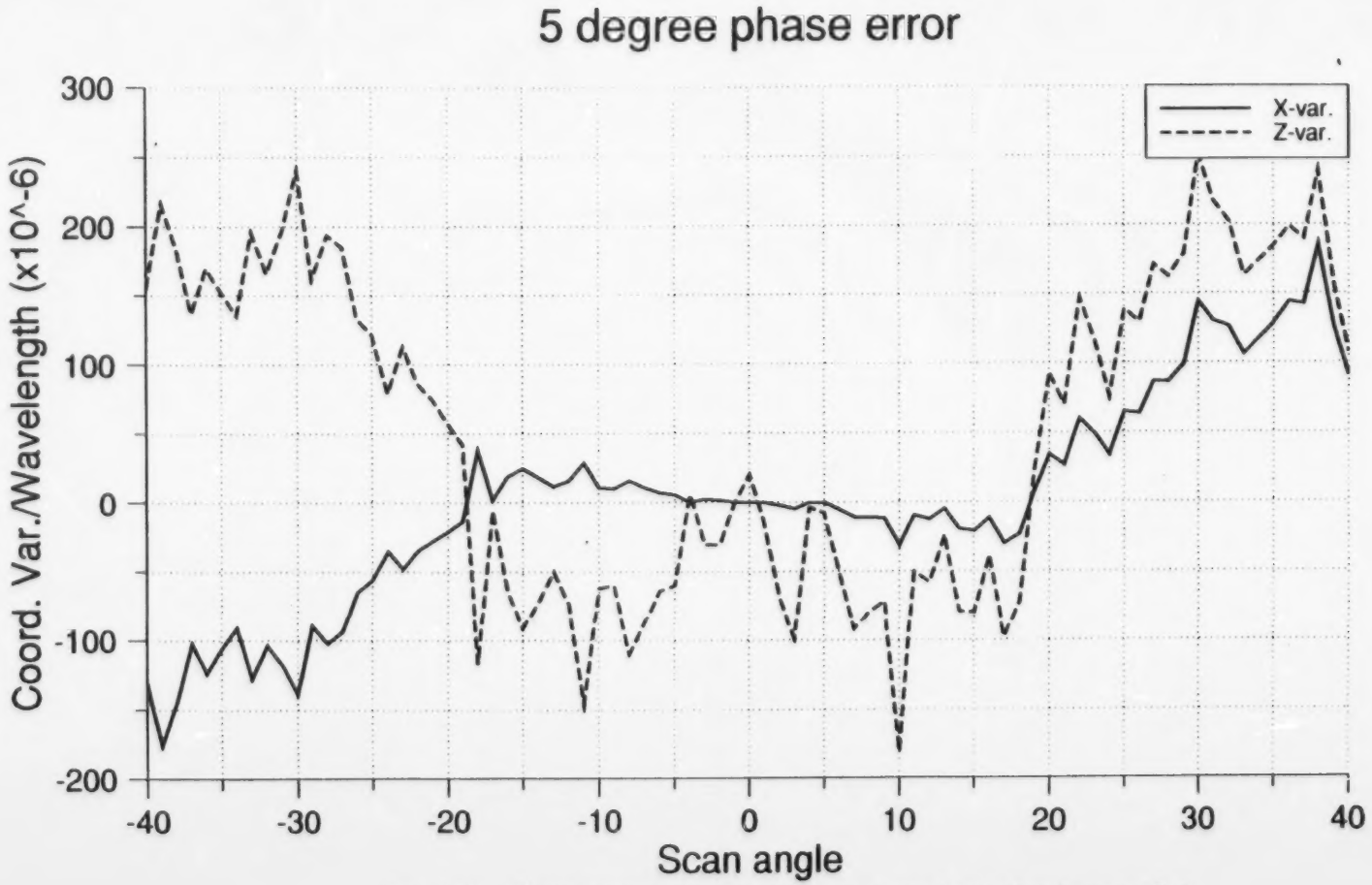

Fig. 4.72 : Phase centre movement due to a pre-determined error of 5° added to each phase shifter.

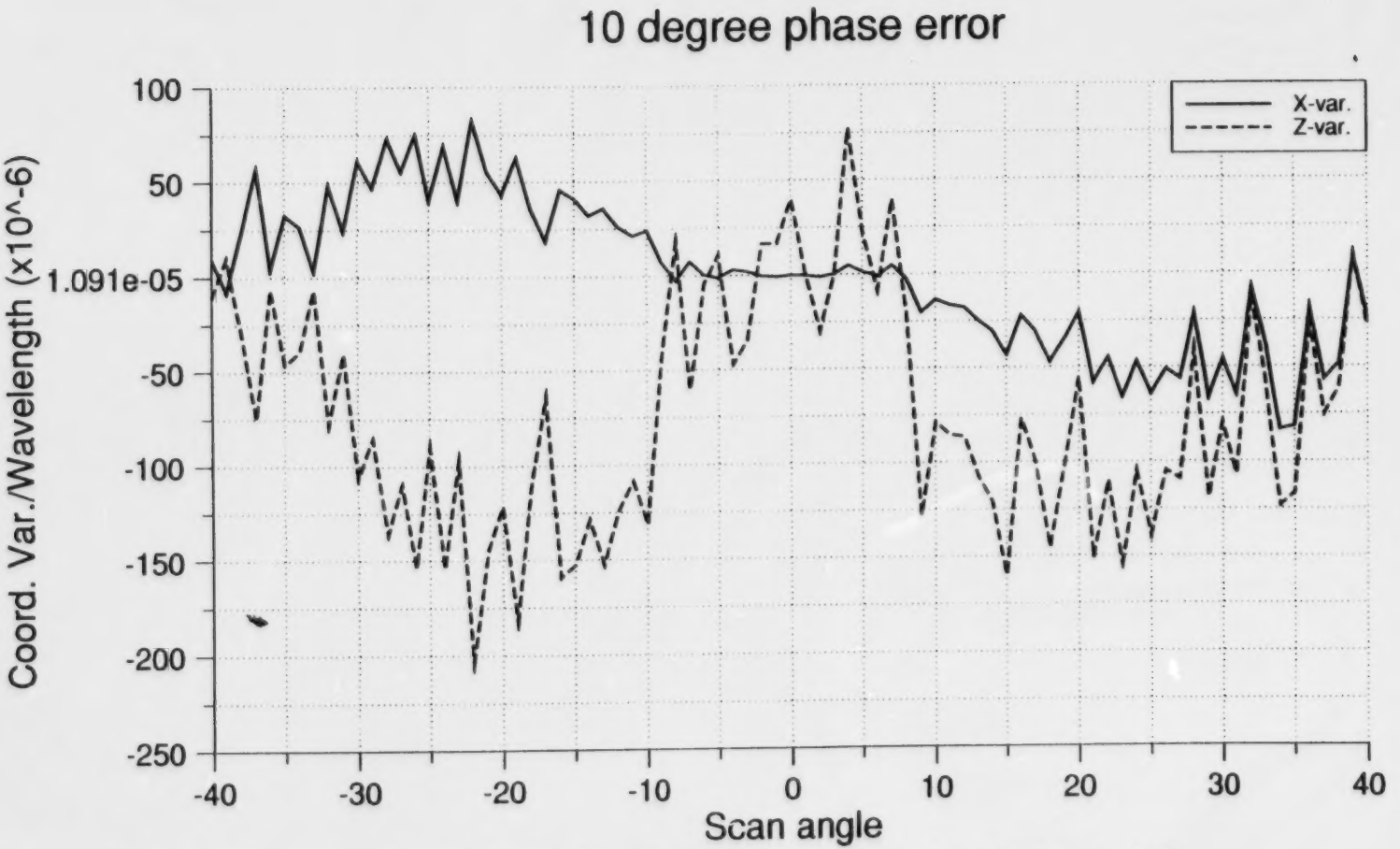

Fig. 4.73 : Phase centre movement due to a pre-determined error of 10° added to each phase shifter.

Chapter 5
Phase centre of two-dimensional array

5.1 Introduction

The purpose of this chapter is to extend the definition of phase centre of one-dimensional radiating system to the more general case of a two-dimensional one. Previous chapters dealt only with the phase centre movement of one-dimensional linear arrays. Here, the same formulation described in chapter two is applied to find a global phase centre of a two-dimensional linear array. The model is subsequently applied to investigate the effects of the ground reflection on the phase centre movement.

5.2 Two-dimensional array

Consider the array geometry shown in Fig. 5.1, where the elements of the array are positioned in the $x-y$ plane. The array has N_x elements with equal spacing d_x in each row parallel to the x-axis, and N_y elements of common spacing d_y, in each column parallel to the y-axis. The field, at a distant point p in free space, contributed by the array can be defined by [17],

$$E(\theta, \phi) = f(\theta, \phi) \sum_{m=1}^{N_x} \sum_{n=1}^{N_y} V_{xm}\, e^{j(k_0 x_m \sin\theta\cos\phi + \alpha_{xm})} \cdot V_{yn}\, e^{j(k_0 y_n \sin\theta \sin\phi + \alpha_{yn})} \quad (5.1)$$

where $f(\theta, \phi)$ is the element pattern, which in *MLS* case is the pattern of a slot on a waveguide, (V_{xm}, V_{yn}) and $(\alpha_{xm}, \alpha_{yn})$ may, respectively, be considered the total amplitude and phase excitations of the (m, n)-th element in the array, and k_0 is the free space propagation constant.

Equation (5.1) gives the general expression for the far field of a rectangular planar array. For the *MLS* array, the following specifications are required;
The array has $N_x = 56$ and $N_y = 35$ elements in the x- and y-coordinates, with the centre frequency of $f = 5.06\ GHz$ and the interelement spacing of $d_x = 0.593\ \lambda$ and

$d_y = 0.588\ \lambda$. The amplitude excitation V_{xm} is assumed to be a $-30dB$ Taylor distribution with a corresponding half-power beam width ($HPBW$) of 2.03°. The associated phase excitation α_{xm} is chosen such that the main beam points at (θ_s, ϕ_s). That is,

$$\alpha_{xm} = -k_o\ x_m\ \sin\theta_s\ \cos\phi_s \tag{5.2}$$

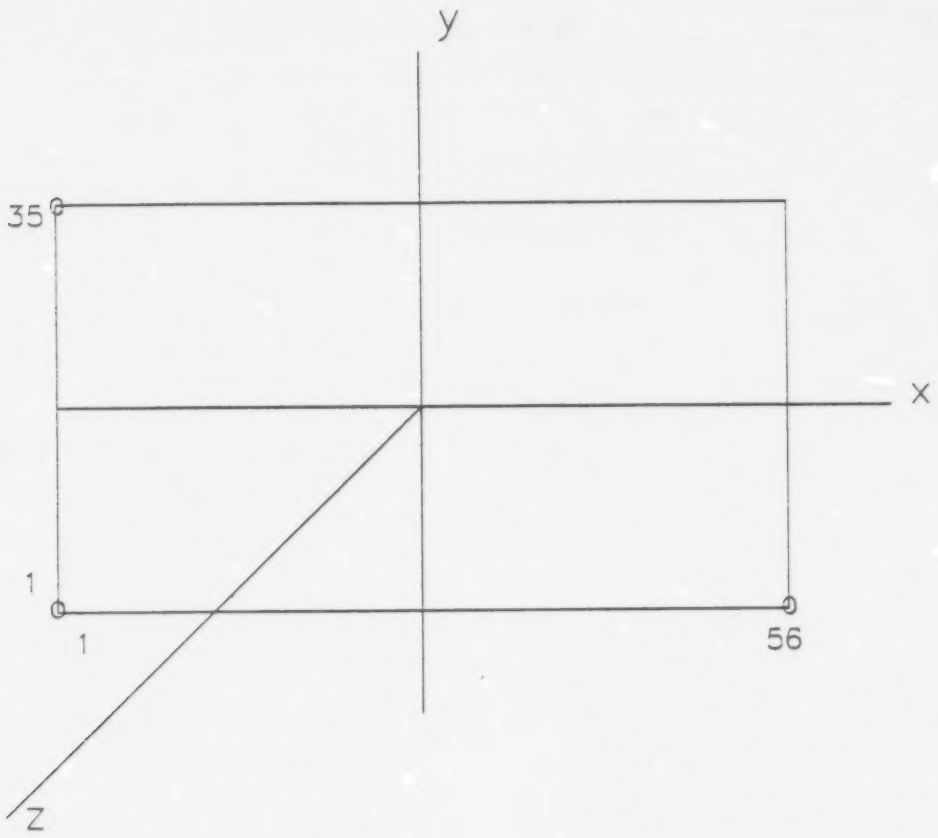

Fig. 5.1 : Array geometry, $N_x = 56$ elements, $N_y = 35$ elements.

Figs 5.2 and 5.3 show the radiation patterns of the antenna in the principal planes, i.e., $\phi = 0.0°$, and $90.0°$. The elevation pattern in the $\phi = 90°$ plane is similar to the one in [18] and shows a typical *MLS* antenna patterns. The field intensity around $\theta = 0.0°$, drops rapidly to minimize ground reflection. Unless otherwise specified, these radiation patterns are the base for computation of all phase centre coordinates in this report.

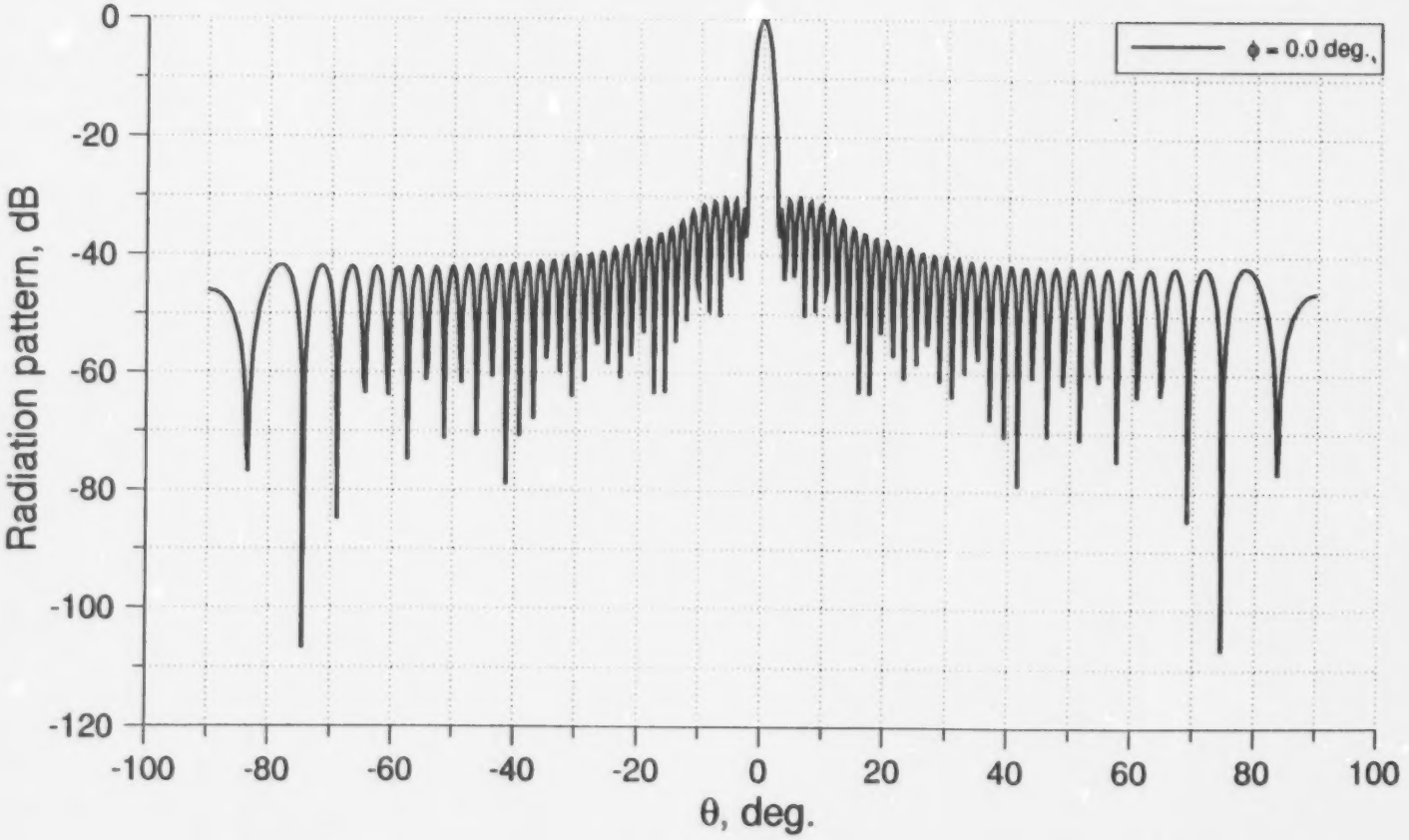

Fig. 5.2 : Antenna radiation pattern, $\phi = 0.0^{o}$

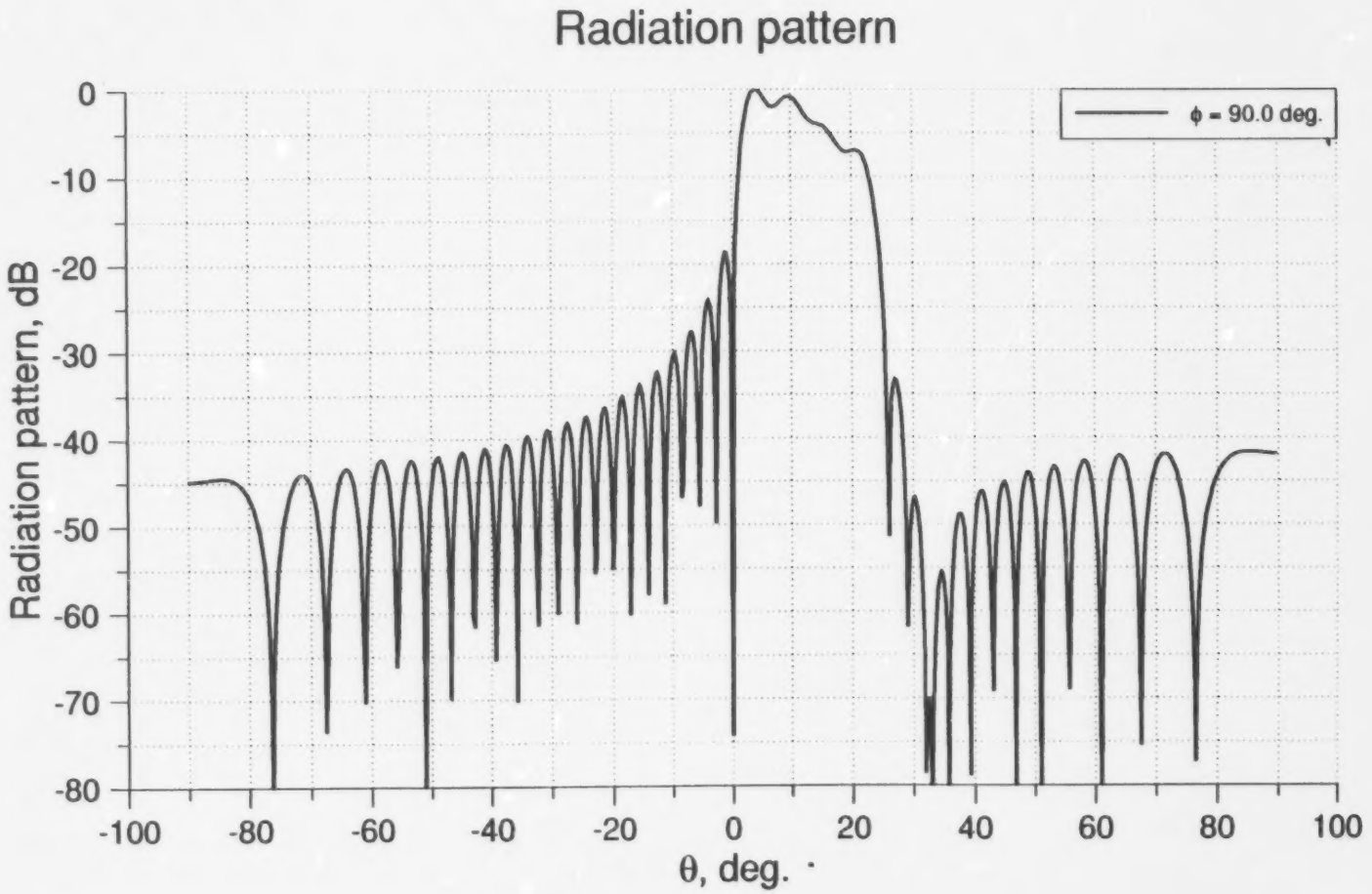

Fig. 5.3 : Antenna radiation pattern, $\phi = 90.0^{o}$

In order to determine the phase centre of the array, it is required to calculate the field in two orthogonal planes. For a two-dimensional array that radiates a pencil beam in the broadside direction, i.e. no scan condition, these orthogonal planes are the array principal-planes $\phi = 0^o$ and $\phi = 90^o$. However, when the array beam is scanned, its beam peak is no longer along the intersection of principal planes, i.e. $\phi = 0^o$. In addition, for *MLS* arrays the pattern is shaped in the elevation plane and the beam is no longer along $\theta = 0.^o$ direction as shown in Fig. 5.3. These complicate the computation of the array phase centre. To overcome these difficulties we define two separate coordinate systems. One is defined as the antenna coordinate system (x_a, y_a, z_a) and is identical to the global coordinates (x, y, z) shown in Fig. 5.1. The second system is defined as the beam coordinates (x_b, y_b, z_b) that shares the origin with the antenna coordinate system, but its $z-$axis pass through the beam peak, or intersects the beam peak along a certain selected elevation angle. This coordinate system can be obtained from the antenna coordinate system using two rotations, one about the y-axis by as much as the scan angle and the second one about the x-axis by a selected elevation angle. Mathematically, the coordinates in these two systems are related by

$$x_a = x_b \cos\beta + z_b \sin\beta \tag{5.3.a}$$

$$y_a = -x_b \sin\gamma \sin\beta + y_b \cos\gamma + z_b \sin\gamma \cos\beta \tag{5.3.b}$$

$$z_a = -x_b \sin\beta \cos\gamma - y_b \sin\gamma + z_b \cos\gamma \cos\beta \tag{5.3.c}$$

with

$$\rho_a = \sqrt{(x_a^2 + y_a^2)} \tag{5.3.d}$$

$$\theta_a = \tan^{-1}(\frac{\rho_a}{z_a}) \tag{5.3.e}$$

$$\phi_a = \tan^{-1}(\frac{y_a}{x_a}) \tag{5.3.f}$$

where, γ is the rotation angle about the x-axis in the $y-z$ plane and β is the rotation angle about the y-axis in the $x-z$ plane. Here, β takes the similar form as the scan angle, θ_s. Following the above procedure, the radiated field in the new coordinate system can be written as,

$$E(\theta_a, \phi_a) = f(\theta_a, \phi_a) \sum_{m=1}^{N_x} \sum_{n=1}^{N_y} V_{xm}\, e^{j(k_0 x_m \sin\theta_a \cos\phi_a + \alpha_{xm})} \cdot V_{yn}\, e^{j(k_0 y_n \sin\theta_a \sin\phi_a + \alpha_{yn})} \tag{5.4}$$

To determine the array phase centre, under any scan condition, we select the required points, on the pattern beam, in two principal planes in the beam coordinate system. Then using the transformations supplied in equations. 5.3.a to 5.3.f, we calculate the corresponding coordinates in the antenna coordinate system to be used in equation 5.4.

As discussed earlier in chapter two, the global phase centre of the planar array can be obtained by computing the phase centre in the principal planes, i.e., $x-z$ (x_1, 0., z_1), and $y-z$, (0., y_2, z_2). In the no-error case, z_1- and z_2-coordinates are equal, and the global phase centre is defined by

$$x_o = x_1 , \quad y_o = y_2 , \quad z_o = z_1 = z_2 \tag{5.5}$$

Once the error is introduced the z_1- and z_2-coordinates may become unequal. In such cases, first we determine the plane of the great circle which is given by $\phi_c = \tan^{-1}(\frac{y_o}{x_o})$. Then, by using the technique given in chapter two, the global phase centre in the plane $\phi = \phi_c$ is determined.

5.3 Ground reflection

In this section, the extension of the technique to include the multipath effect due to the ground reflection is discussed. A model for the multipath reflection is developed to investigate the received signal variation and its effect on the antenna phase centre location. A principal problem for the aircraft on a centre line approach is the errors caused by the multipath effect due to interaction of the direct signal and the indirect signals reflected by the ground [19]-[21]. The ground reflections encountered are usually divided into two categories, specular and diffuse. The specular reflection refers to the coherent part of the reflected signal, where the phase varies regularly with the position of the receiver or transmitter. It is a reflection of the same type as caused by a smooth surface, and obeys the geometrical optics principle. The diffuse reflection, on the other hand, refers to the incoherent part of the reflected signal, which varies randomly as the receiver or transmitter is moved. It has a small directivity, and its fluctuation has a large amplitude which is Rayleigh-distributed [22]. It is typically defined by a diffuse scattering coefficient ρ_d, where ρ_d^2 is the ratio of the diffuse power received by the aircraft to that of the direct signal. The diffuse reflection is a rather complicated function of the terrain characteristics, and antenna radiation pattern,

and is not included in the analysis.

Specular reflection is modeled by its reflection coefficient R_s which is defined as the ratio of the magnitude of the specular signal to that of the direct signal. The region of the surface where specular reflection is produced is often called the first Fresenl zone, where the phase of the reflected ray, and the form of the interference lobes are the same as if the reflecting surface is prefectly smooth. The reflection coefficient of the specular reflection is usually smaller than that of the smooth surface and is defined by [23],

$$R_s = \rho_s \; D \; R_r \tag{5.6}$$

where, R_s is the reflection coefficient for the specular reflection of the rough surface, ρ_s is the reflection coefficient of a plane smooth surface, D is a divergence factor ($0.0 < D < 1.0$), which takes into account the earth's curvature, and R_r is a factor ($0.0 < R_r < 1.0$), which describes the surface roughness. The following assumptions are made in the analysis :

1. The surface roughness is not included in the model, and ground is assumed to be flat with no random height variation, i.e., $R_r = 1.0$.
2. The multiple scattering effects are neglected.
3. The surface curvature is not included in the modeling, i.e., $D = 1.0$.

The multipath amplitude is taken to be the Fresnel reflection coefficient for the vertical polarization, which depends on the relative complex dielectric constant, and the conical incident angle relative to the earth's surface. The electrical parameters of the ground are assumed to be constant, specified by the relative dielectric constant.

Fig. 5.4 shows the characteristics of the ray geometry for the specular reflection from a plane earth. The receiving antenna is located at a range R and height h_r above the horizon, while the transmitter antenna is at a height h_t. The total electric field at a point P is given by the sum of the direct signal and reflected field. The reflected wave is related to the incident field intensity at the point of reflection by the complex Fresnel reflection coefficient of the ground

$$\frac{E^r}{E^i} = \rho_s e^{-j\phi} \tag{5.7}$$

where

$$\rho_s = \left| \frac{E^r}{E^i} \right| , \qquad \text{and} \qquad -\phi = arg\left(\frac{E^r}{E^i}\right) \tag{5.8}$$

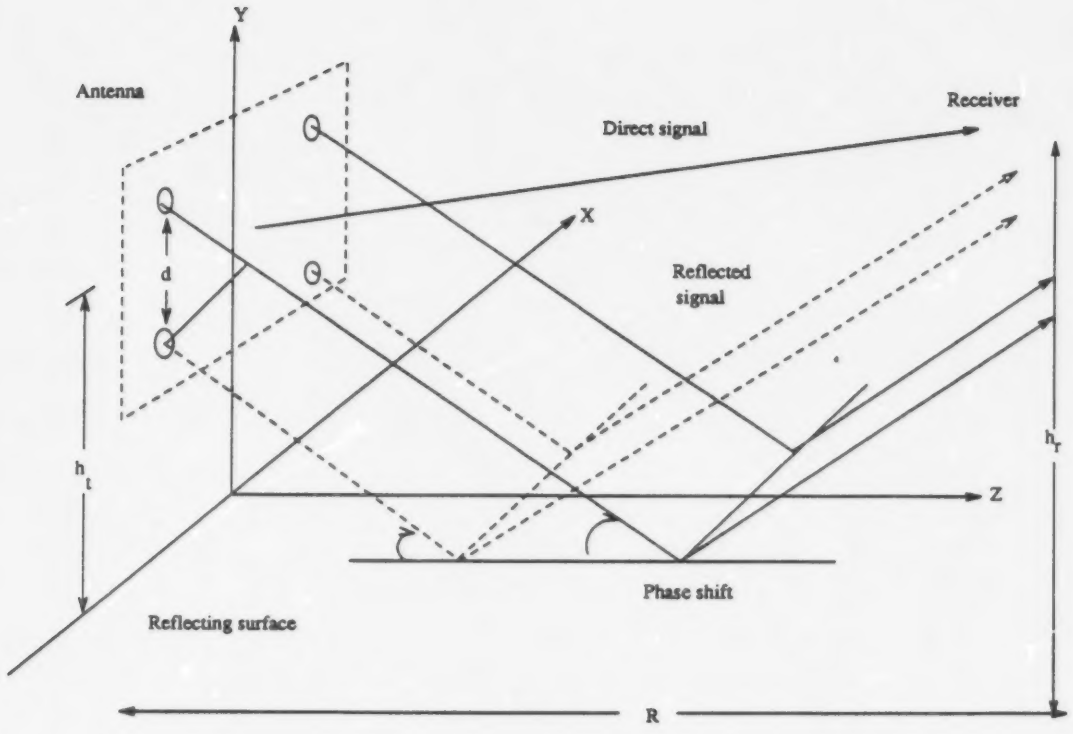

Fig. 5.4 : Specular reflection.

For the vertical polarization of the incident wave, it can be obtained from [24],

$$\rho_s = \frac{\varepsilon \sin\psi - (\varepsilon - \cos^2\psi)^{\frac{1}{2}}}{\varepsilon \sin\psi + (\varepsilon - \cos^2\psi)^{\frac{1}{2}}} \tag{5.9.a}$$

where ψ is measured perpendicular to the surface normal, and ε is the complex dielectric constant of the surface defined as

$$\varepsilon = \varepsilon' - j\varepsilon'' \tag{5.9.b}$$

Substituting (5.7) in (5.4) yields

$$E^t = E^i(1. + \rho_s e^{-j\gamma}) \quad , \qquad \gamma = \phi + \frac{2\pi}{\lambda}(L_1 - L) \tag{5.10}$$

where, E^t is the total field of the reflected and the direct fields, E^i is the incident field defined by (5.4), and $L_1 - L$ is the path length difference defined as,

$$L_1 - L = \frac{2\pi}{\lambda} \cdot \frac{4h_t h_r \cos\alpha \sin\psi}{\cos\alpha\,(h_r + h_t) + R \sin\psi} \tag{5.11}$$

Here, R is the range between the transmitter and the receiver, α is the approach angle, λ is the wavelength, and ψ is the incident angle measured from the earth's surface.

5.4 Numerical results

A computer programs is developed to simulate the effect of random errors and elements failures for the two-dimensional planar array. The input and output parameters of the program are similar to the one-dimensional case. The output of the simulated run for the selected seed numbers and the failed elements are presented in Figs. 5.5 to 5.19. These graphs show the effects of random errors and the failed elements, corresponding to their one-dimensional counterparts.

Next, the computer code was verified to simulate the phase centre movement, due to the ground reflection. Fig. 5.20 and 5.21 show the magnitude and the phase of the reflection coefficient for the selected dielectric constants. Fig. 5.22 and 5.23 illustrate the variation of the grazing angle for the selected range and the receiver height. Fig. 5.24 through 5.32 show the effect of the multipath reflection from the ground due to different dielectric constants, for the azimuth antenna located at $2.5m$ above the horizon. The ground illumination is assumed to be $10.0dB$ below the direct signal. The generated results are obtained initially for a case, where the aircraft height is kept con-

stant (6.0*km*), but the range is varied. In the second case, the range is kept at 37.0*km* and/or 50.0*km* and the altitude is varied. In both cases, the antenna phase centre moves in the $\phi = 90.0^{o}$ plane. The variation in the phase centre location, depends on the receiver position and also on the ground characteristics. It is evident that the maximum displacement of the phase centre occurs at 90.0*km* range and the height of 6.0*km*, for the dry ground. In this case, the grazing angle is about 3.8^{o}, which results in the highest reflection coefficient of about 0.55 (Fig. 5.20). The phase centre displacement is about 6.8 λ in the z-coordinate and 0.3 λ in the y-coordinate.

To further investigate the computation of the phase centre coordinates, and examine its uniqueness, one needs to consider different elevation cuts, i.e. approach angles. This procedure is necessary, because of broad and shaped elevation pattern in the $y-z$ plane. Hence, several elevation cut planes are selected to compute the antenna phase centre. The sampling points are positioned one degree apart, on either side of the cut plane.

Figs. 5.33 to 5.35 depict the existence of the phase centre, for selected input parameters. Figs. 5.36 to 5.41 illustrate the phase centre coordinates and the received signal phase centre variation as functions of α, the cut plane angle. These results indicate that, for the selected angular range of $\pm 1.0^{o}$, the variation of the signal phase as measured from the phase centre is quite small. However, beyond this range it varies rapidly.

Similar simulated run are performed for a range with parameters as : the transmitter to receiver distance of 396*m*, receiver height of 56.82*m*, and the transmitter height of 21.34*m* and results are shown in Figs. 5.42 through 5.50. These graphs correspond to the outdoor antenna range of the David Florida Laboratory (*DFL*).

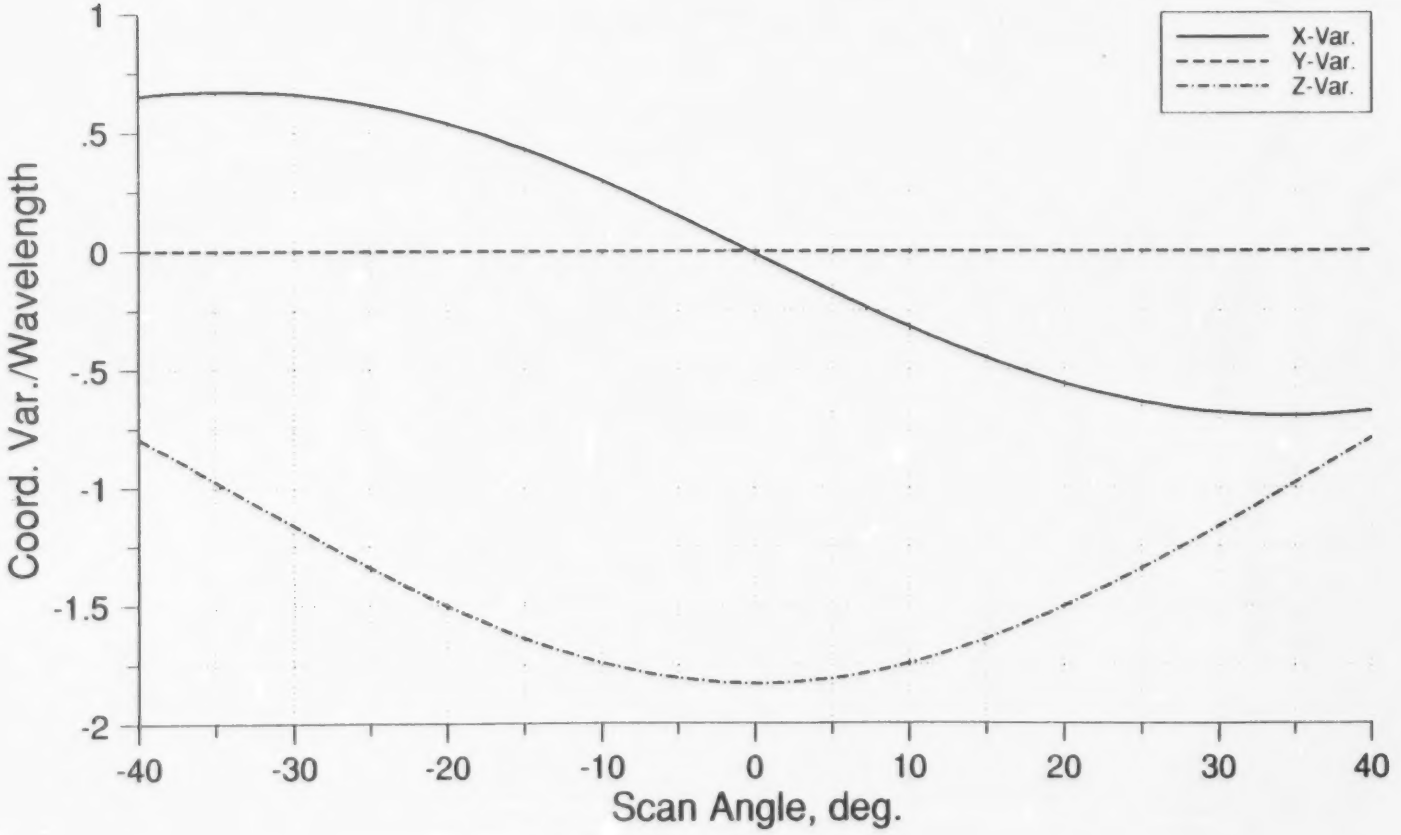

Fig. 5.5 : Random phase error, $\sigma_p = 5^o$, seed no. 235912749

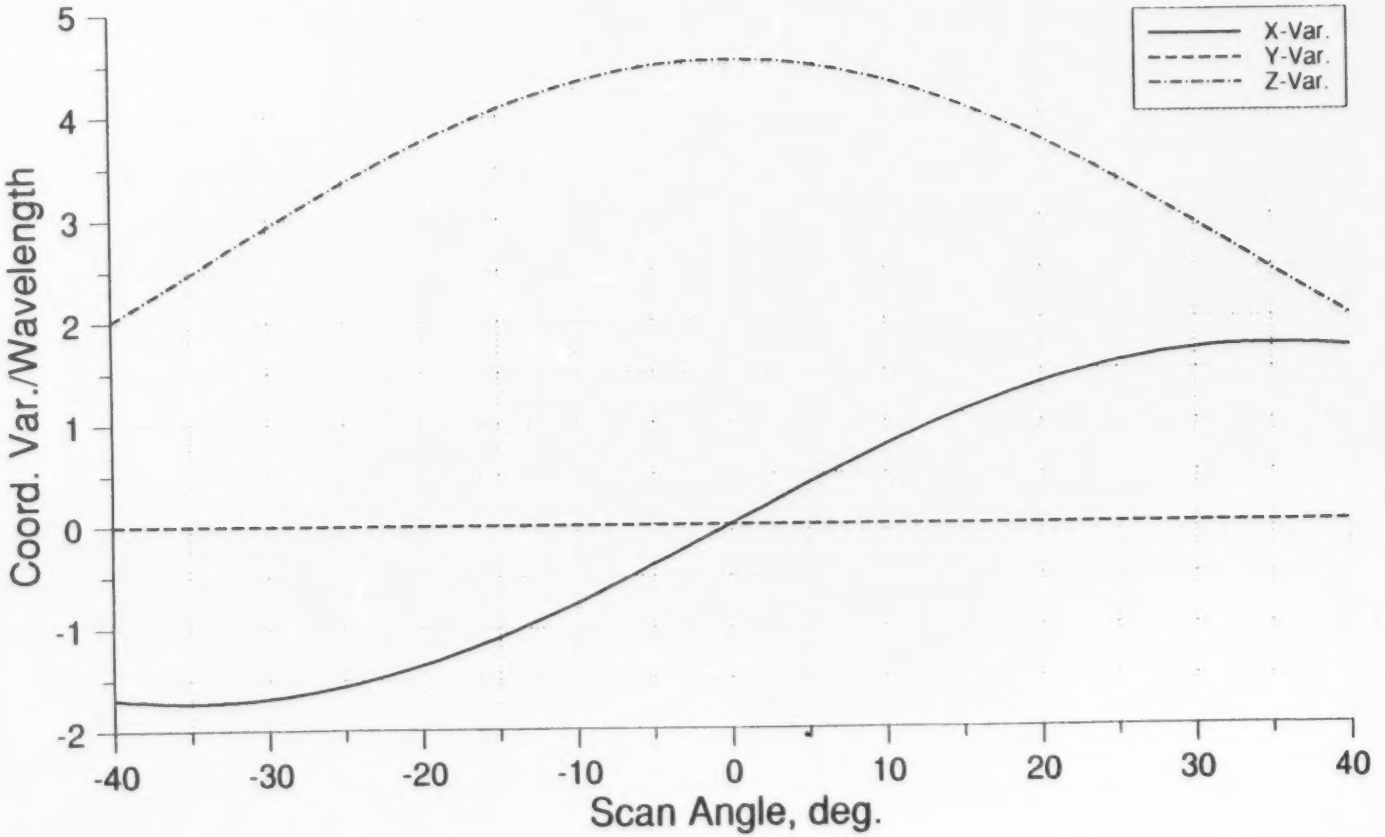

Fig. 5.6 : Random phase error, σ_p = 5°, seed no. 176329845

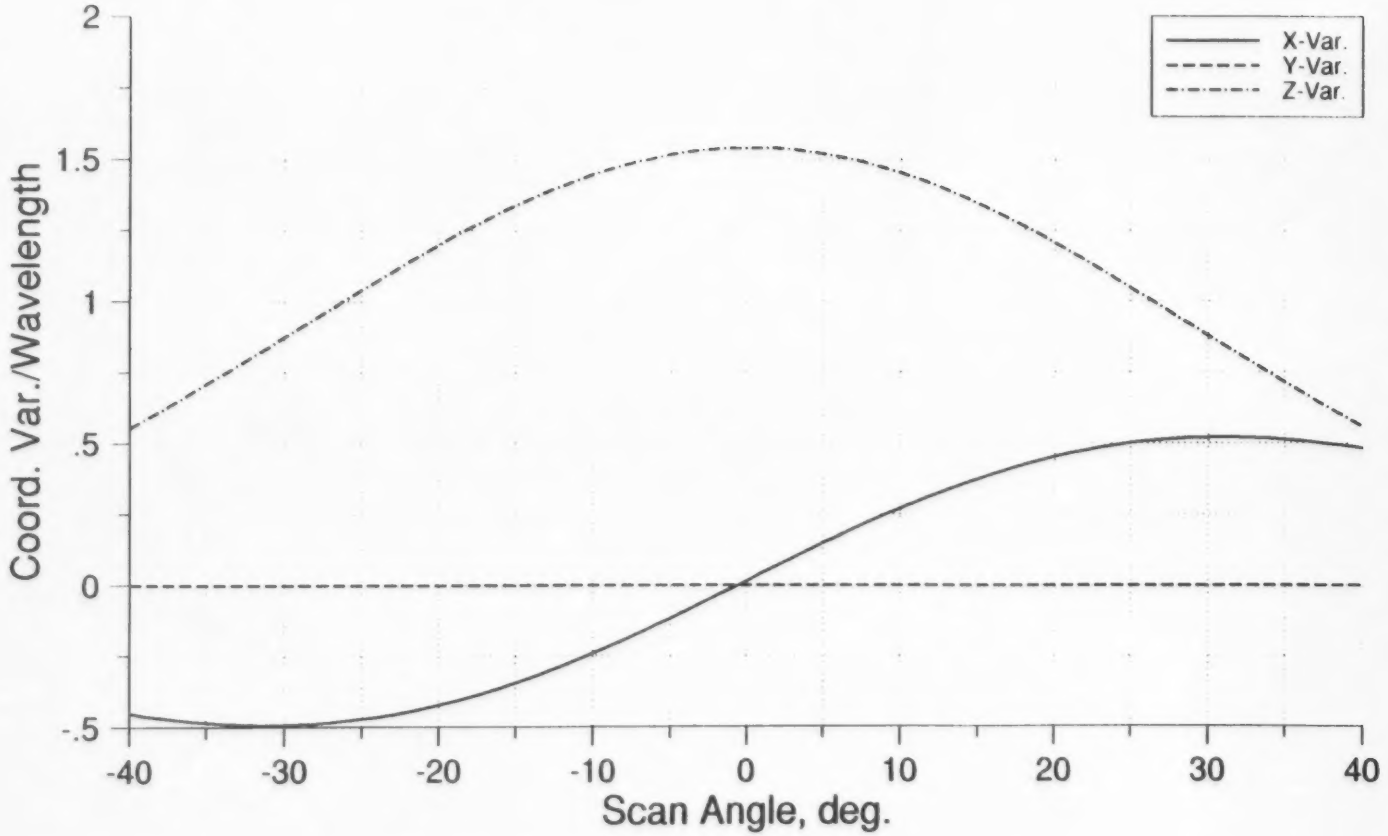

Fig. 5.7 : Random phase error, σ_p = 5°, seed no. 123456789

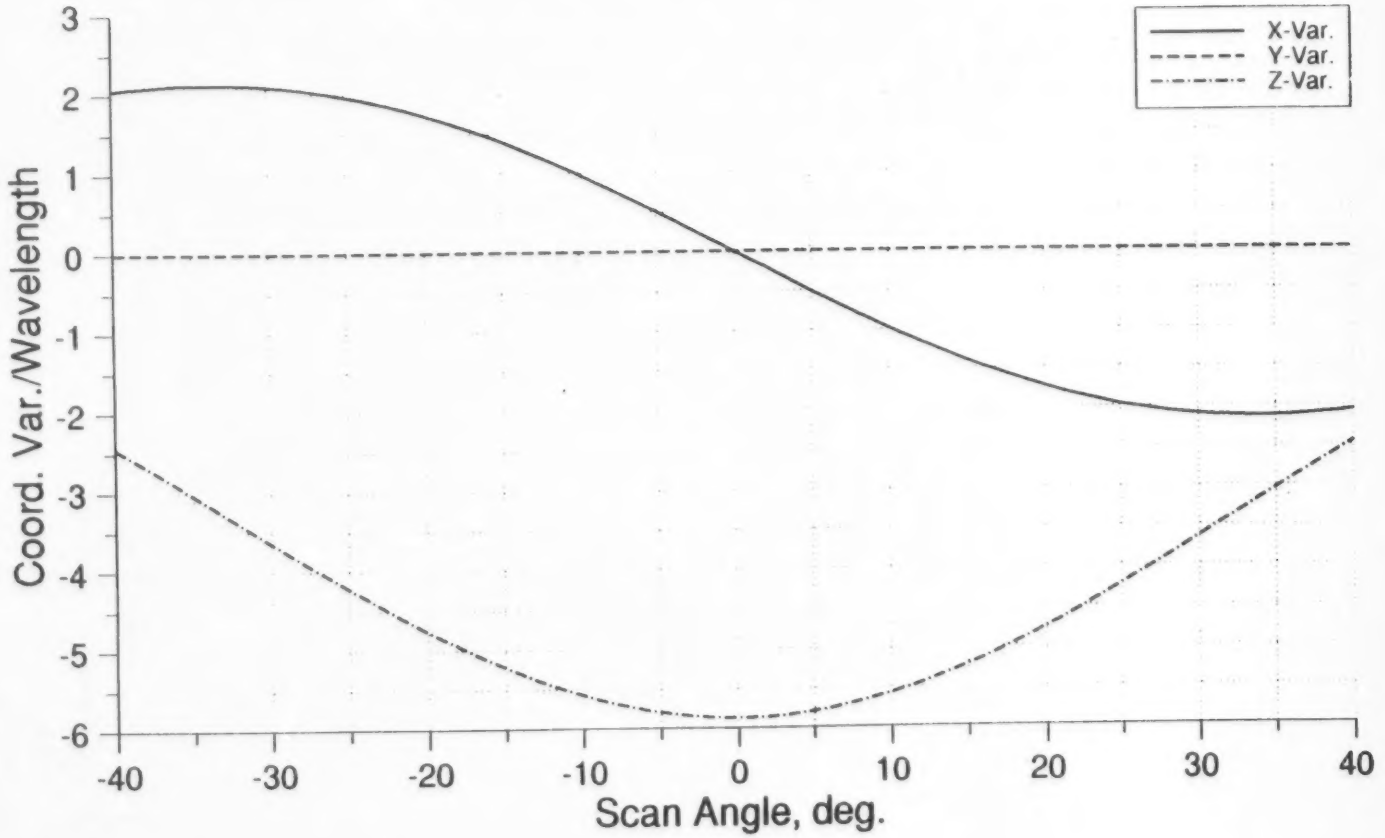

Fig. 5.8 : Random phase error, $\sigma_p = 5^o$, seed no. 987654321

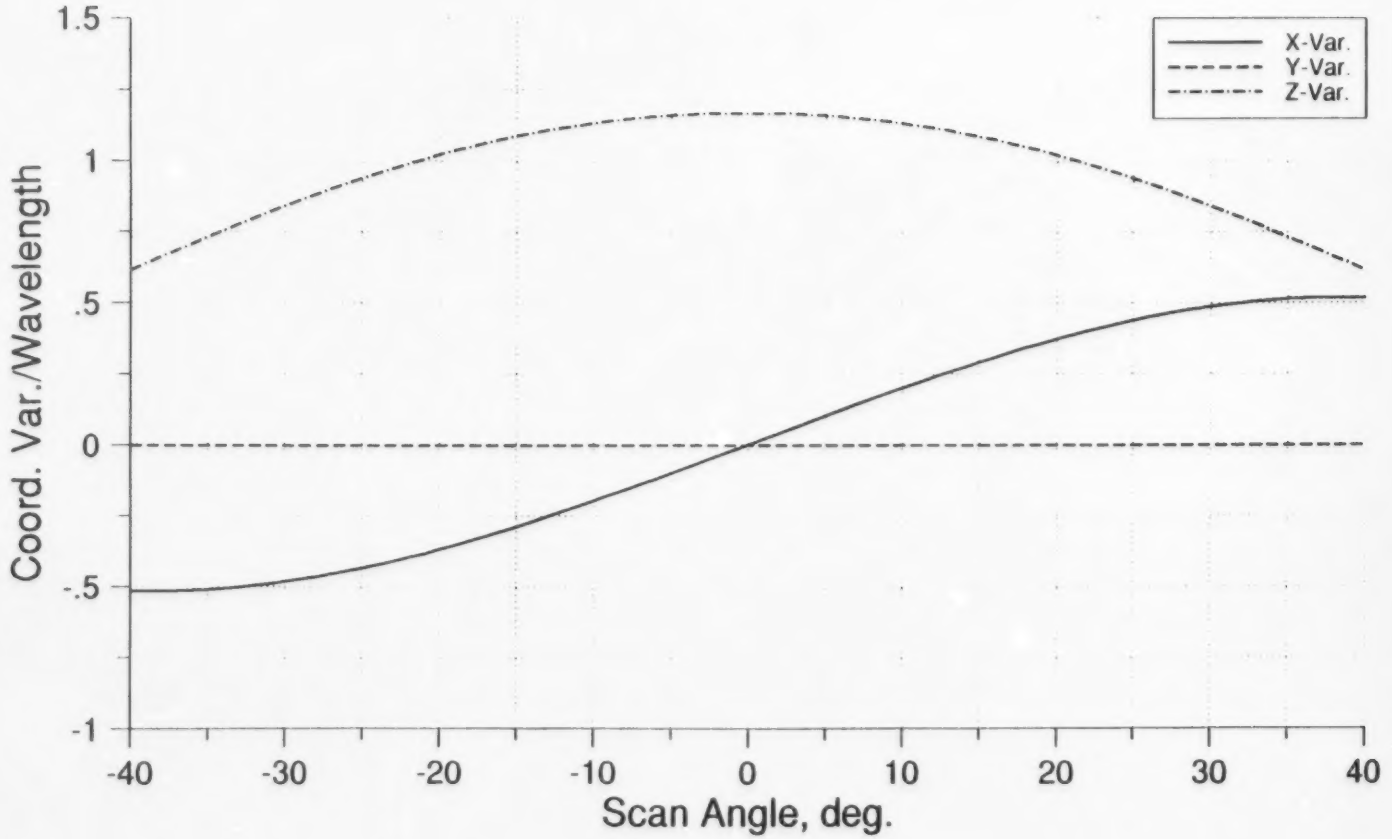

Fig. 5.9 : Random phase error, σ_p = 5°, seed no. 555558888

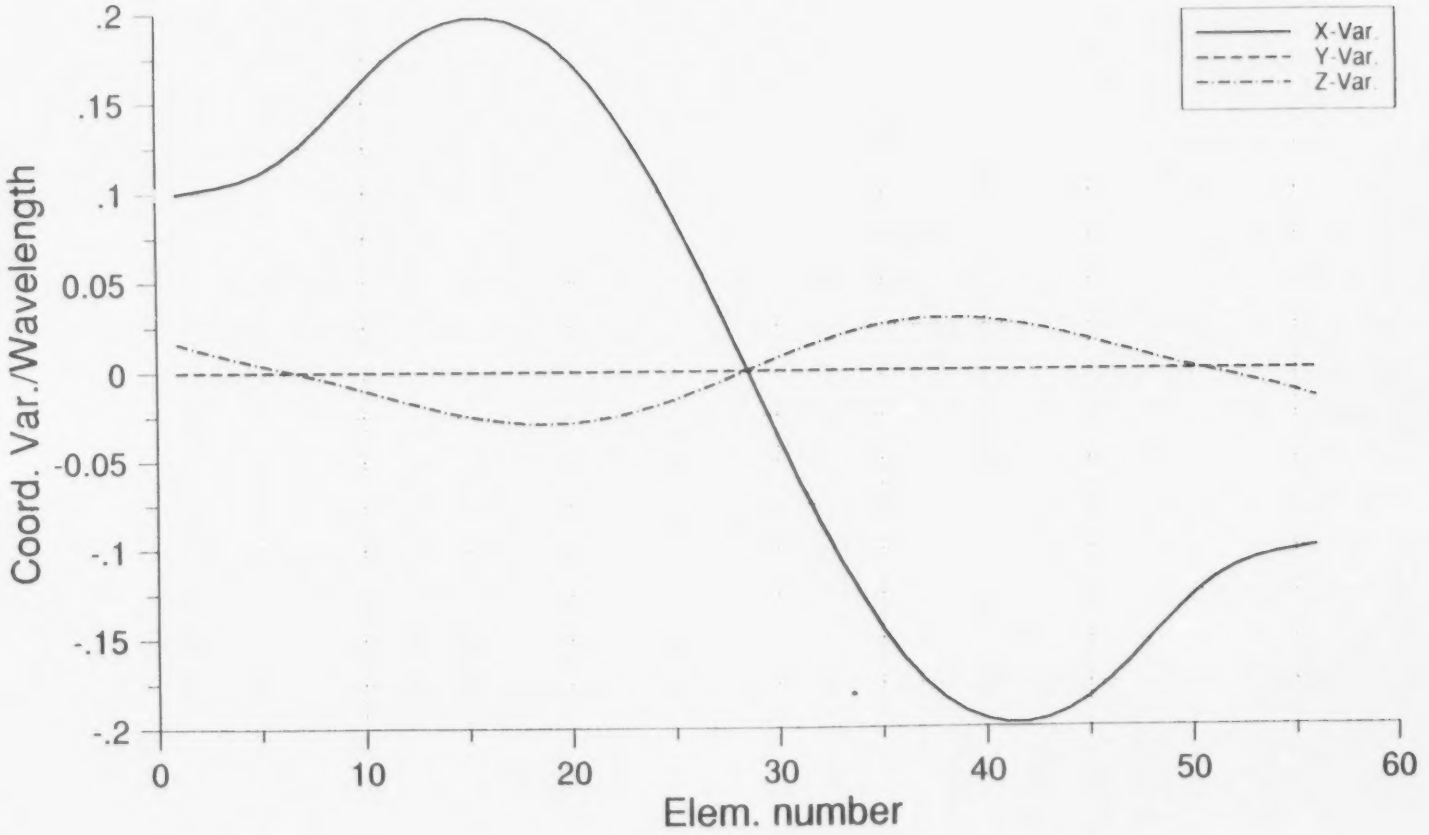

Fig. 5.10 : Amplitude failures, $\theta_s = -40^o$.

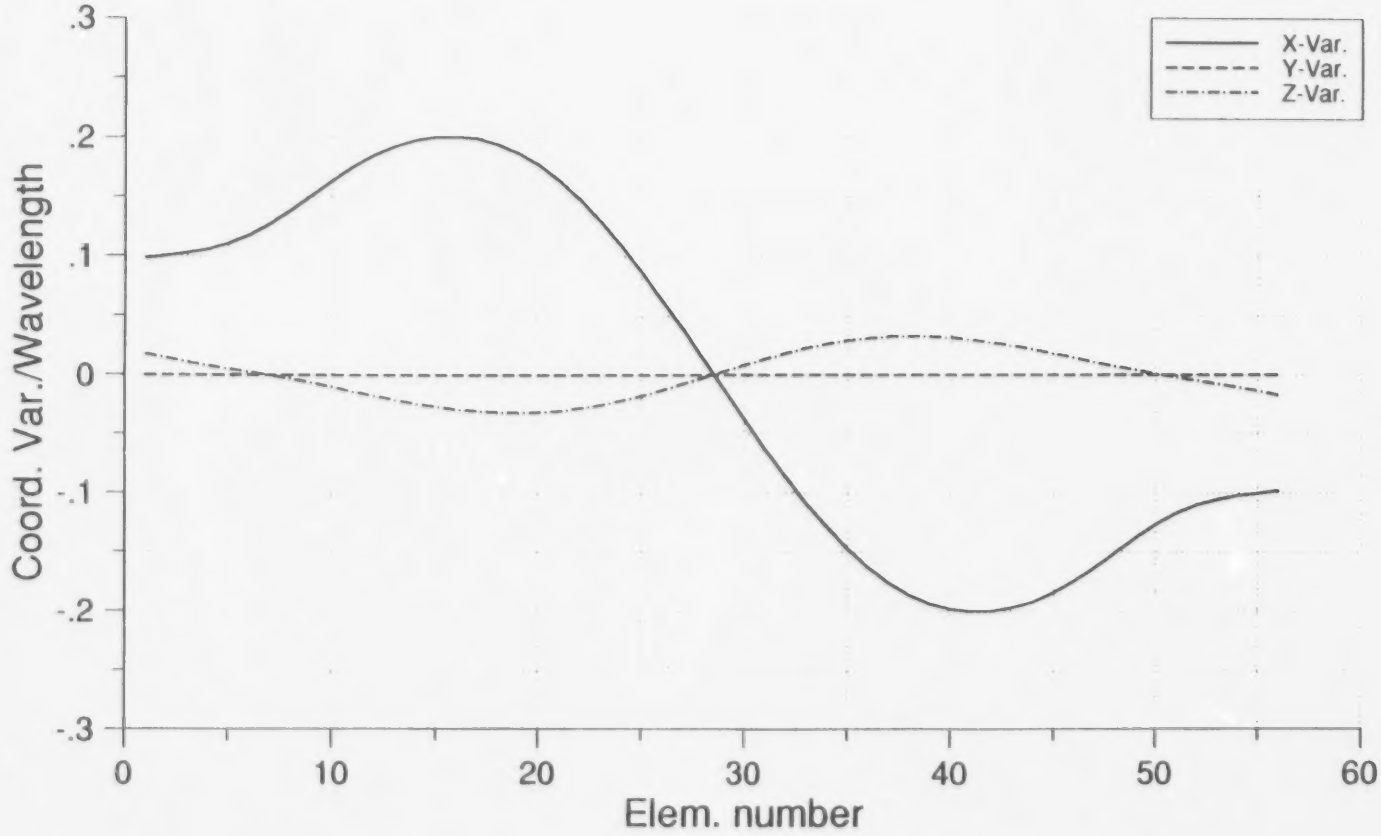

Fig. 5.11 : Amplitude failures, $\theta_z = -20°$.

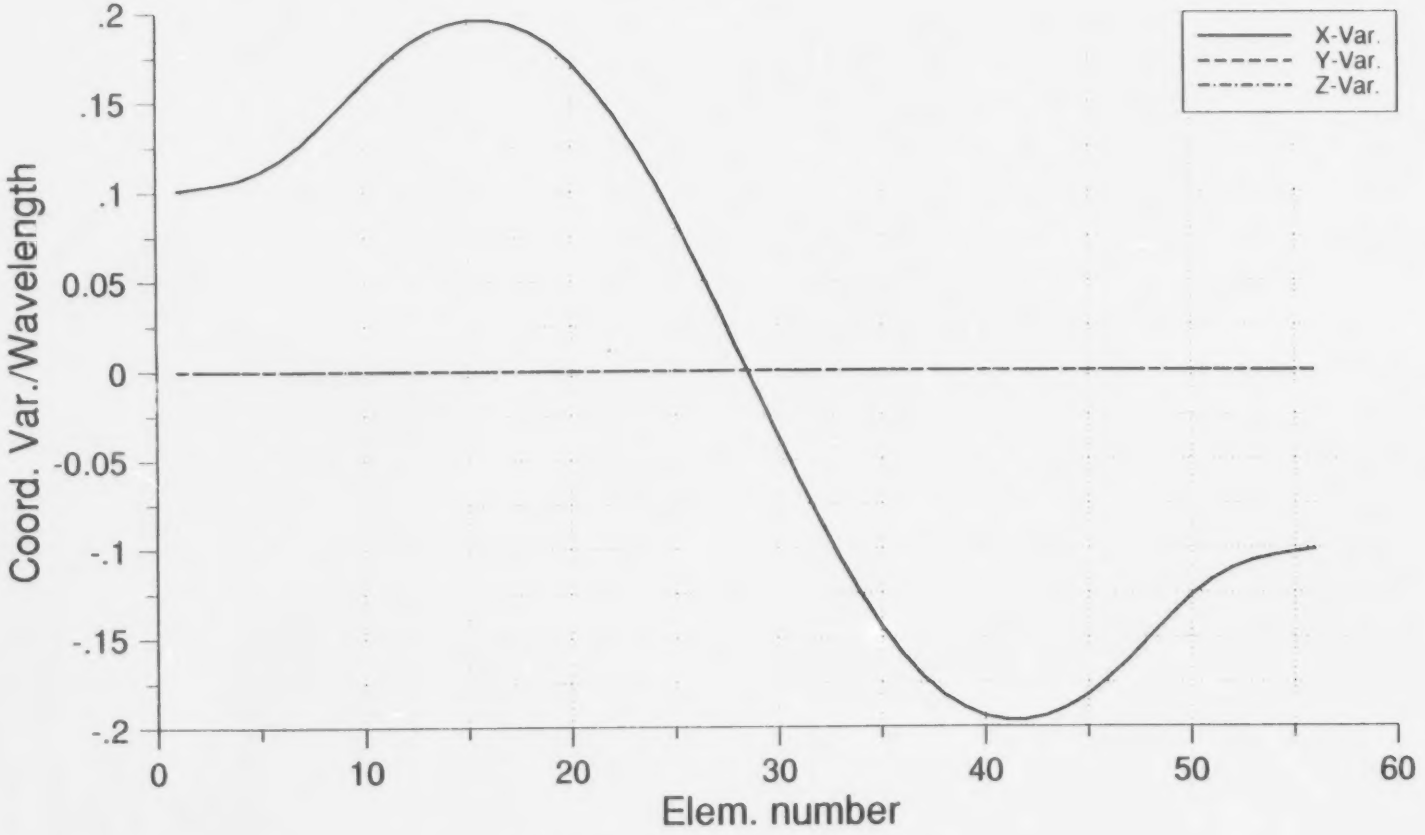

Fig. 5.12 : Amplitude failures, $\theta_z = 0^o$.

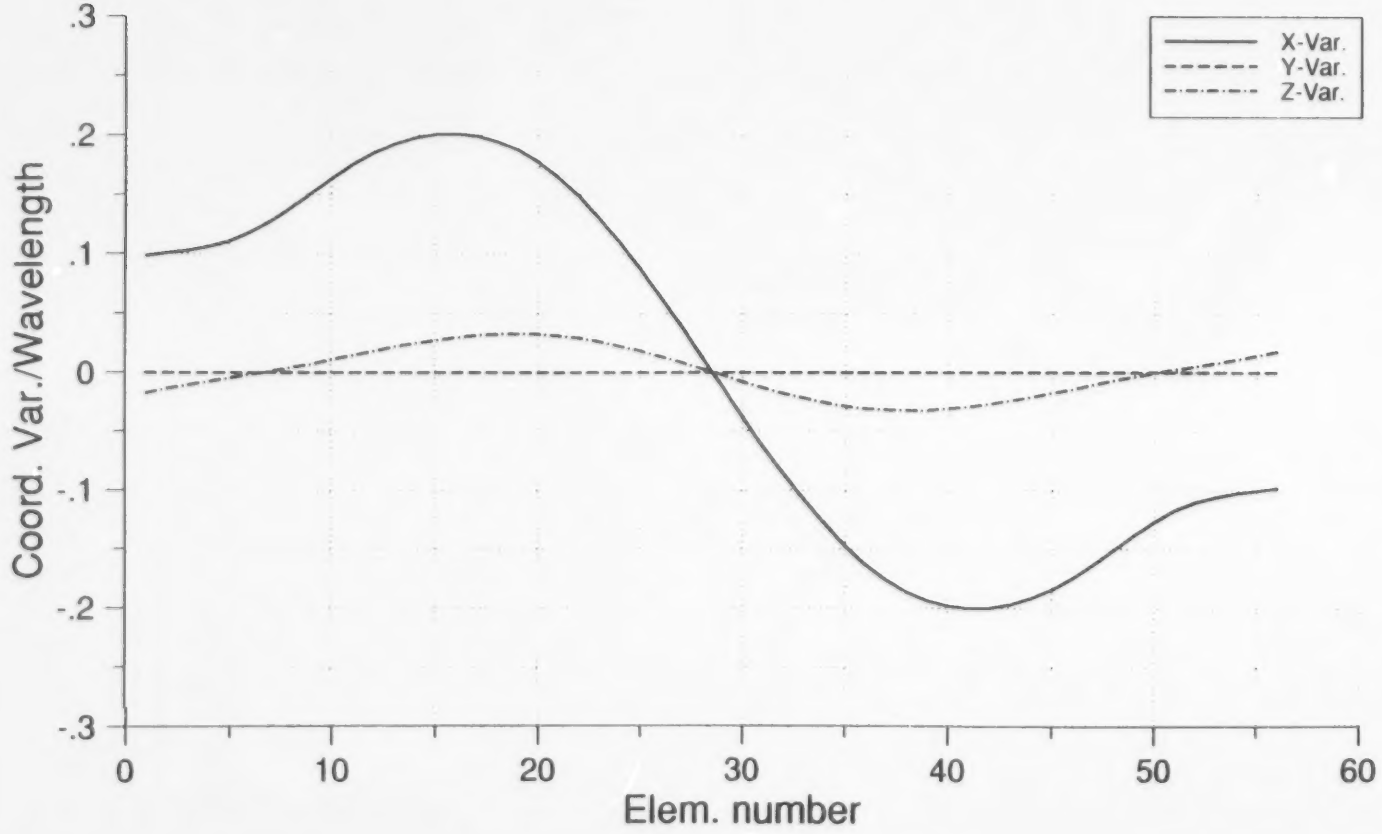

Fig. 5.13 : Amplitude failures, $\theta_z = 20°$.

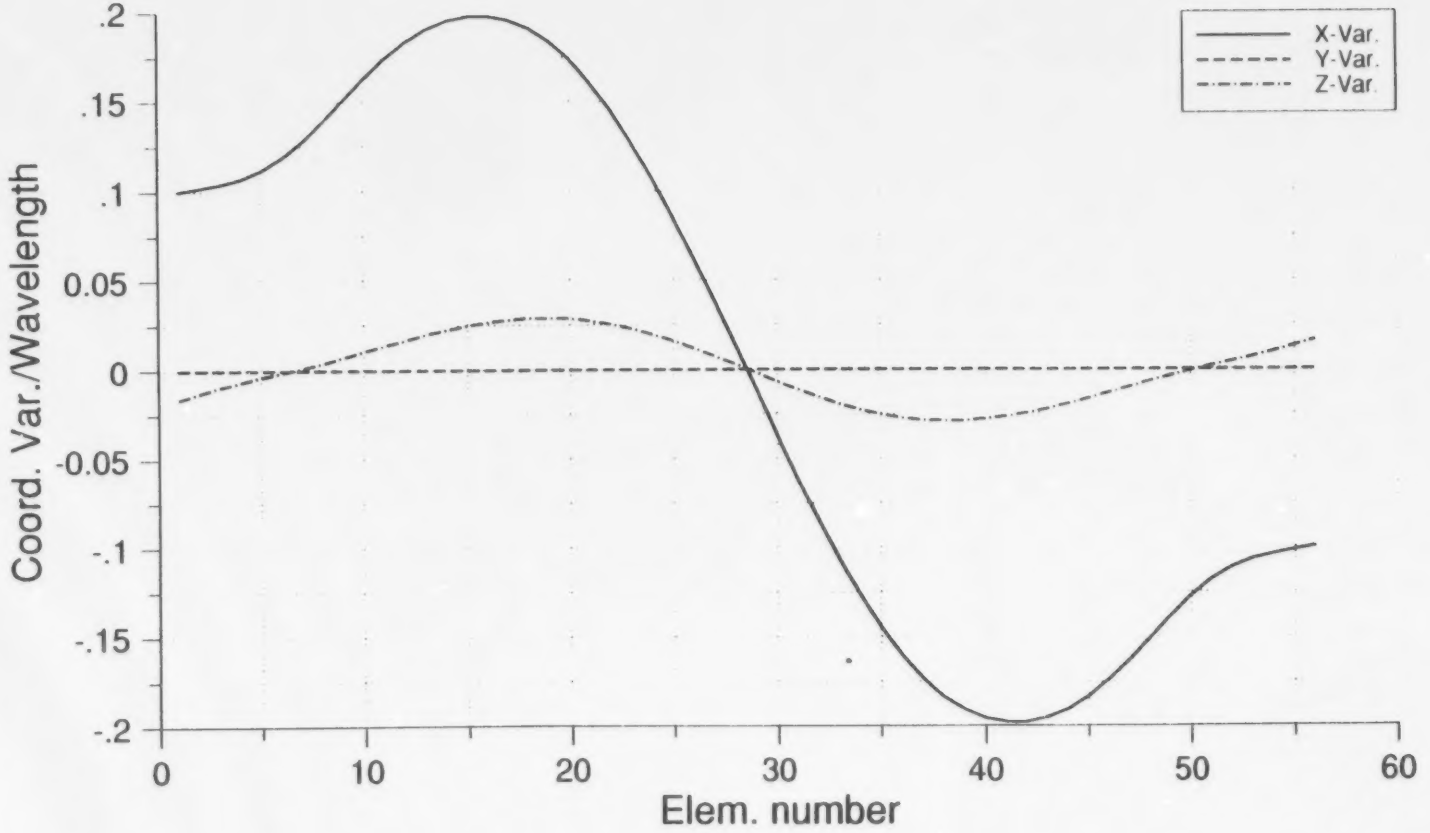

Fig. 5.14 : Amplitude failures, $\theta_z = 40^o$.

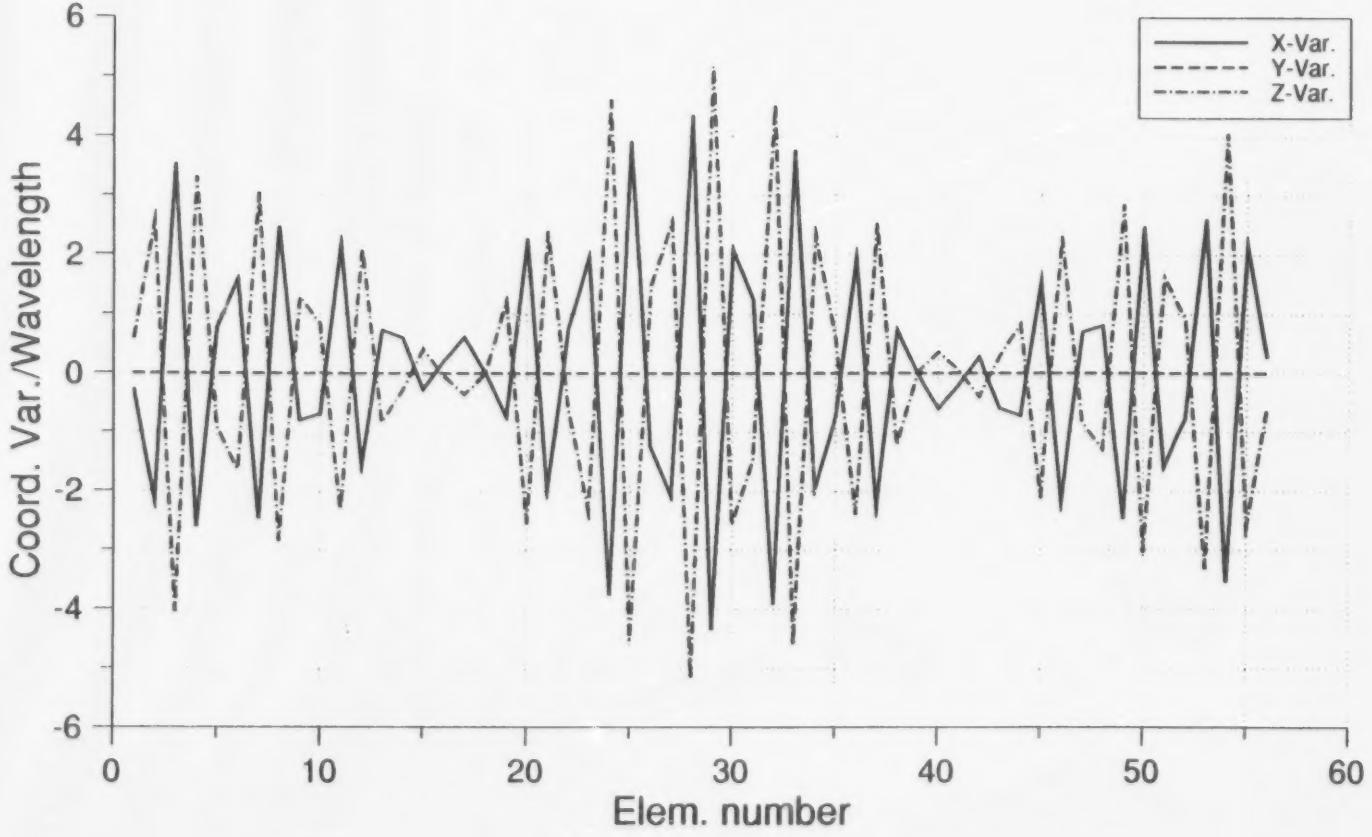

Fig. 5.15 : Phase shifter failures, $\theta_s = -40°$.

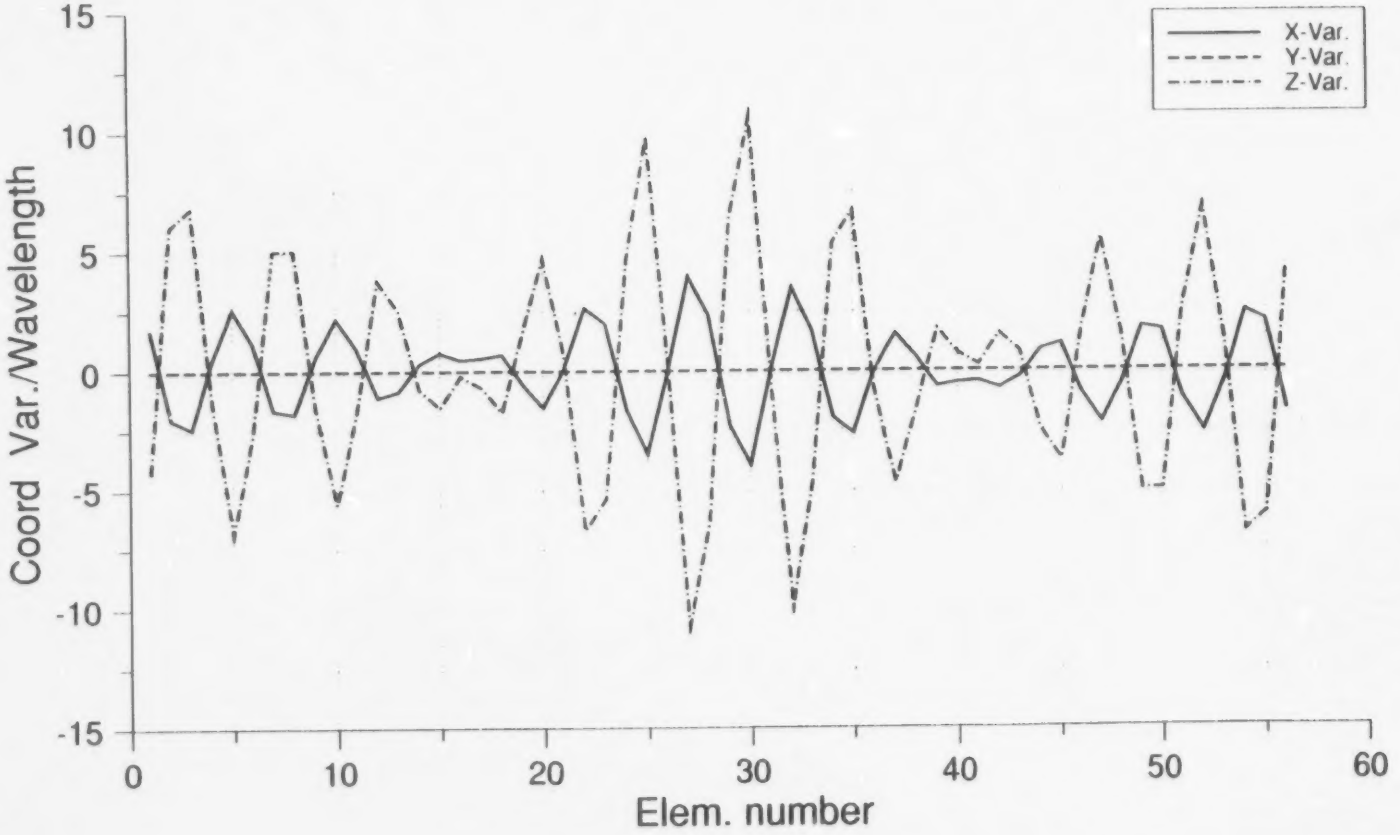

Fig. 5.16 : Phase shifter failures, $\theta_s = -20^{\circ}$.

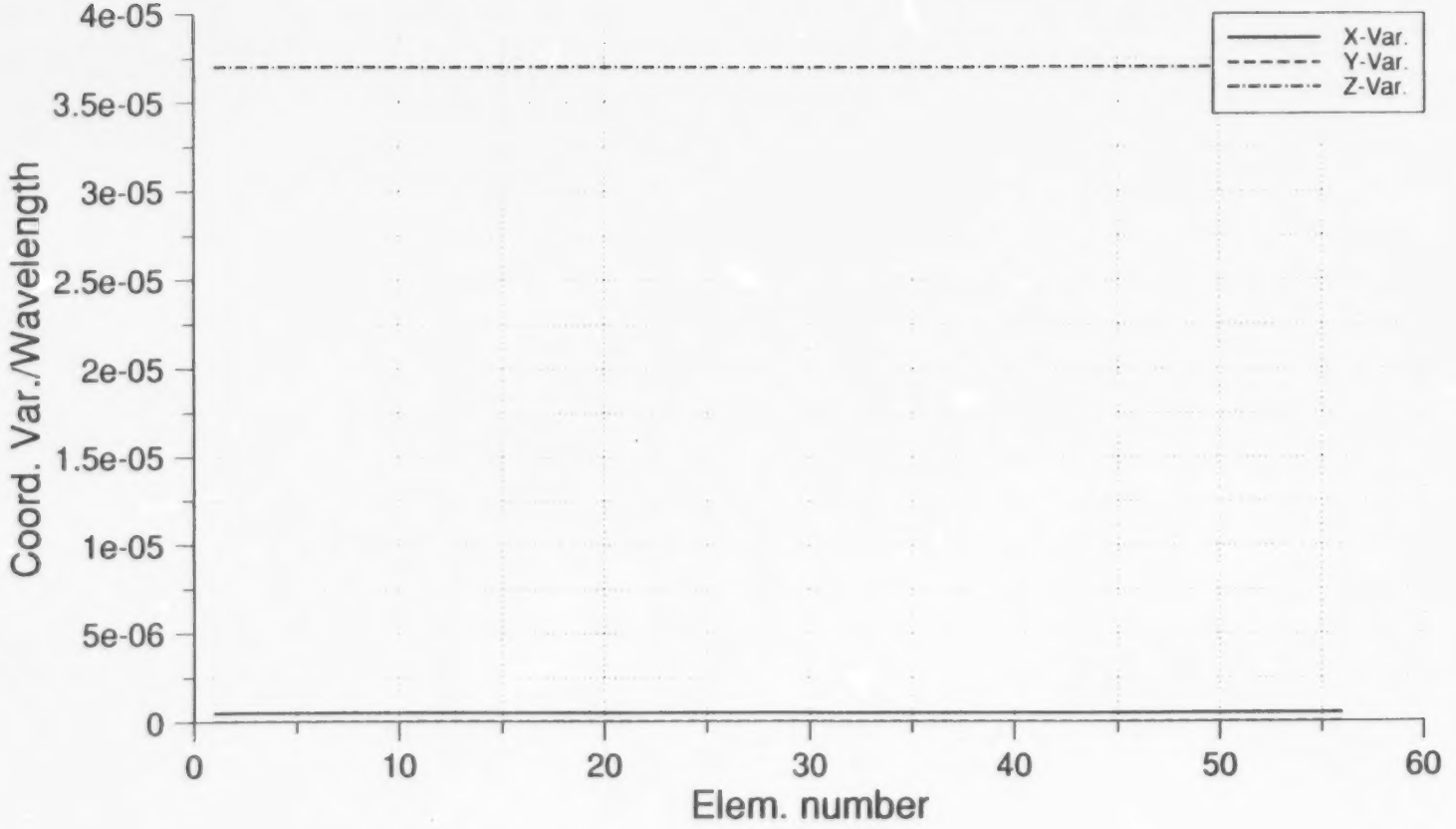

Fig. 5.17 : Phase shifter failures, $\theta_z = 0°$.

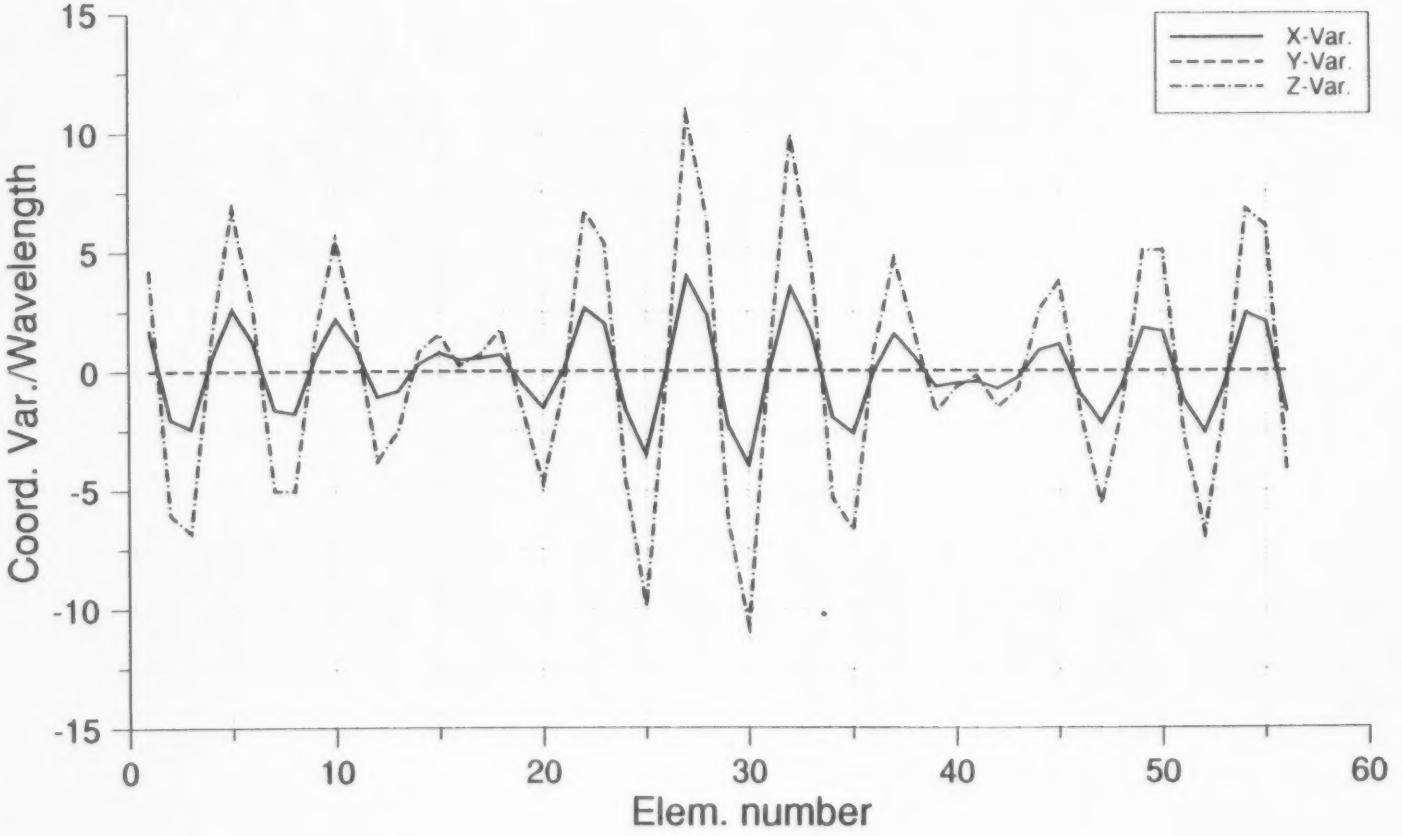

Fig. 5.18 : Phase shifter failures, $\theta_s = 20^o$.

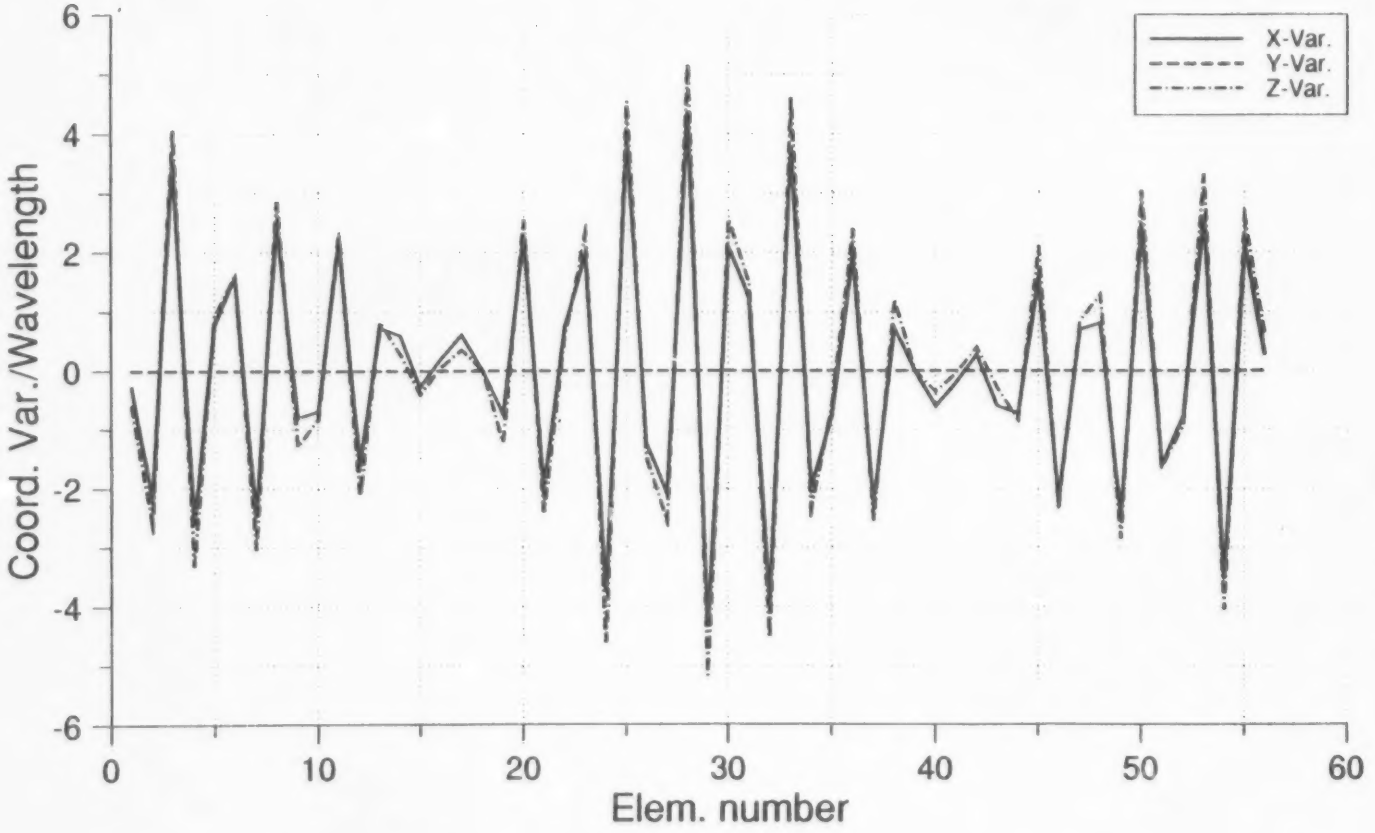

Fig. 5.19 : Phase shifter failures, $\theta_s = 40^o$.

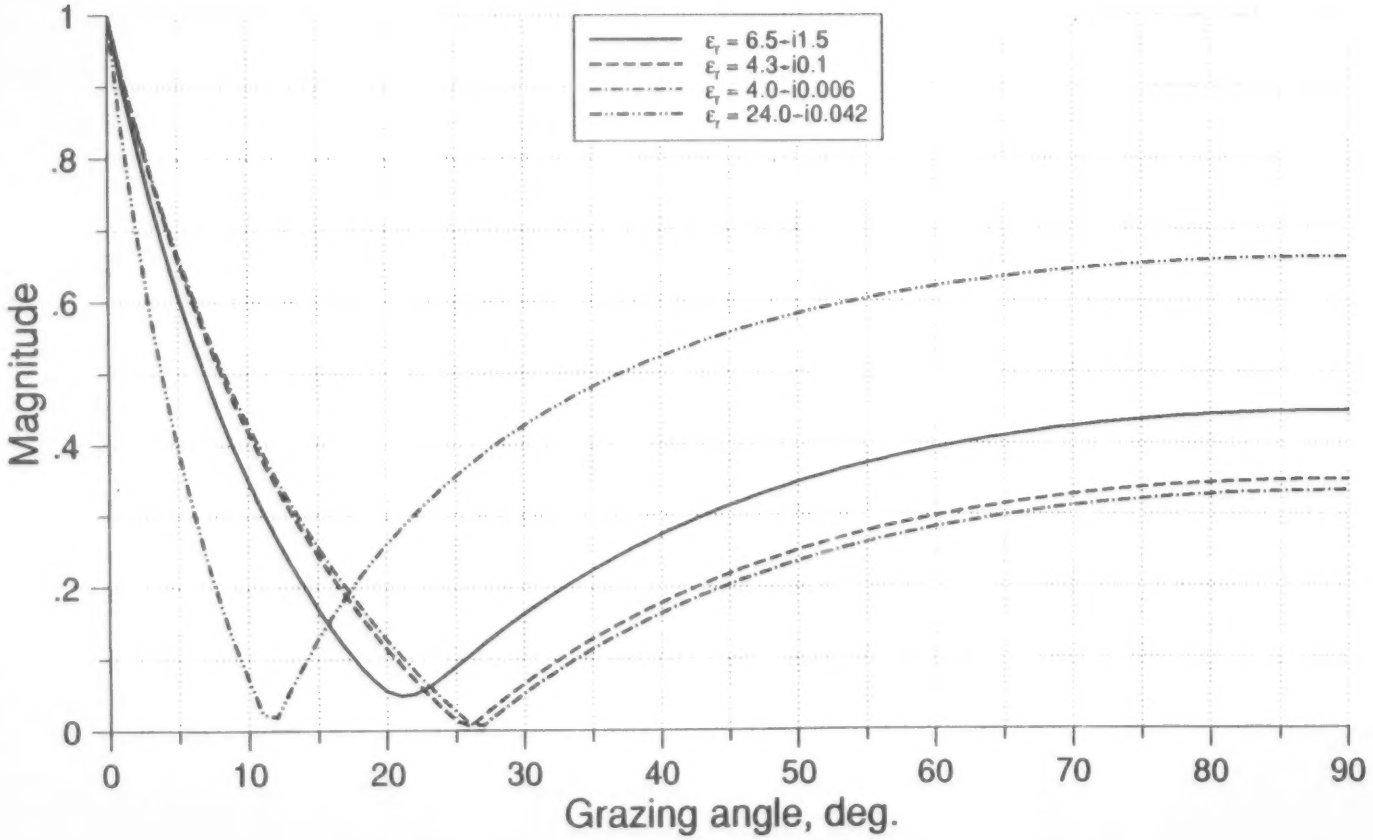

Fig. 5.20 : Magnitude of reflection coefficient.

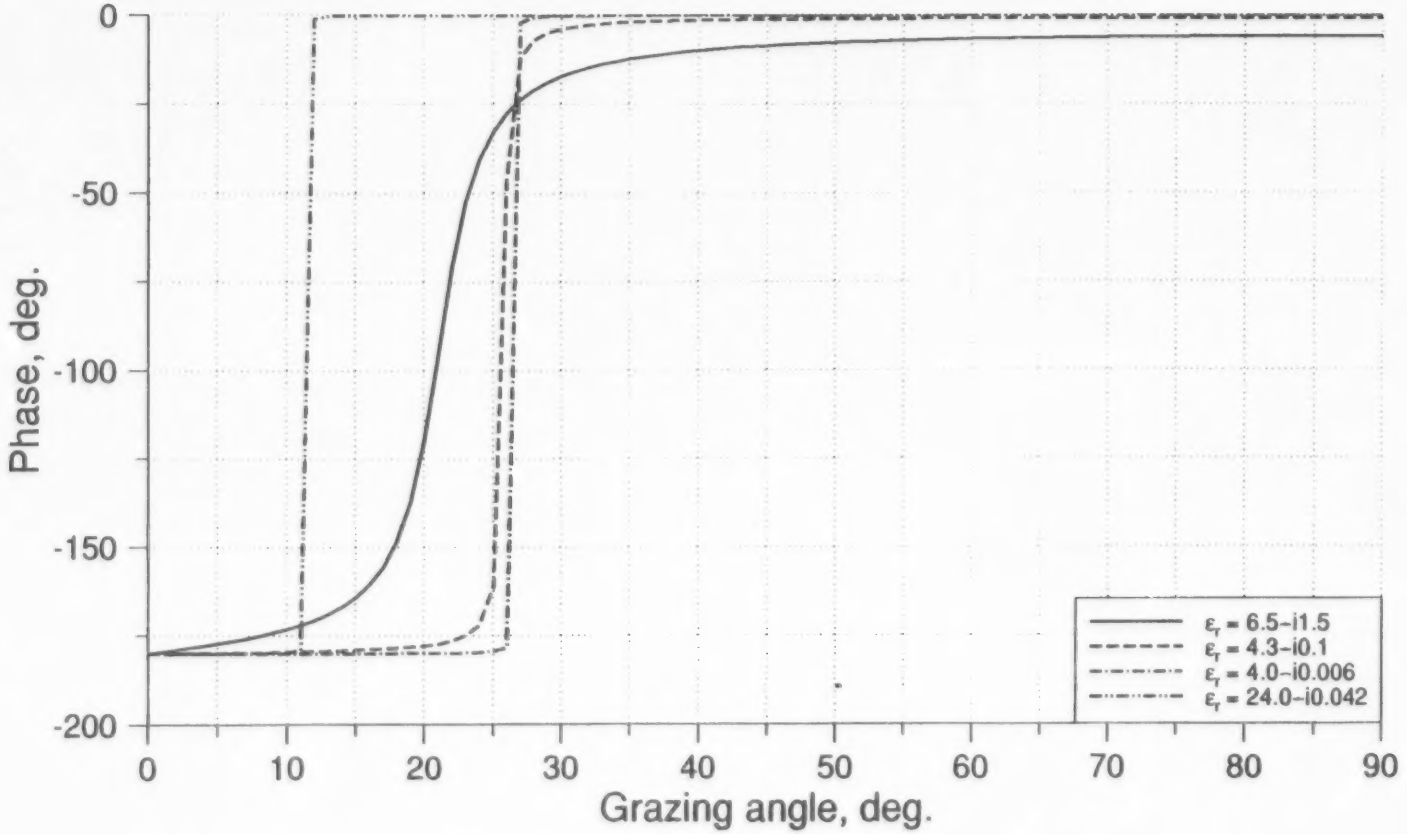

Fig. 5.21 : Phase of reflection coefficient.

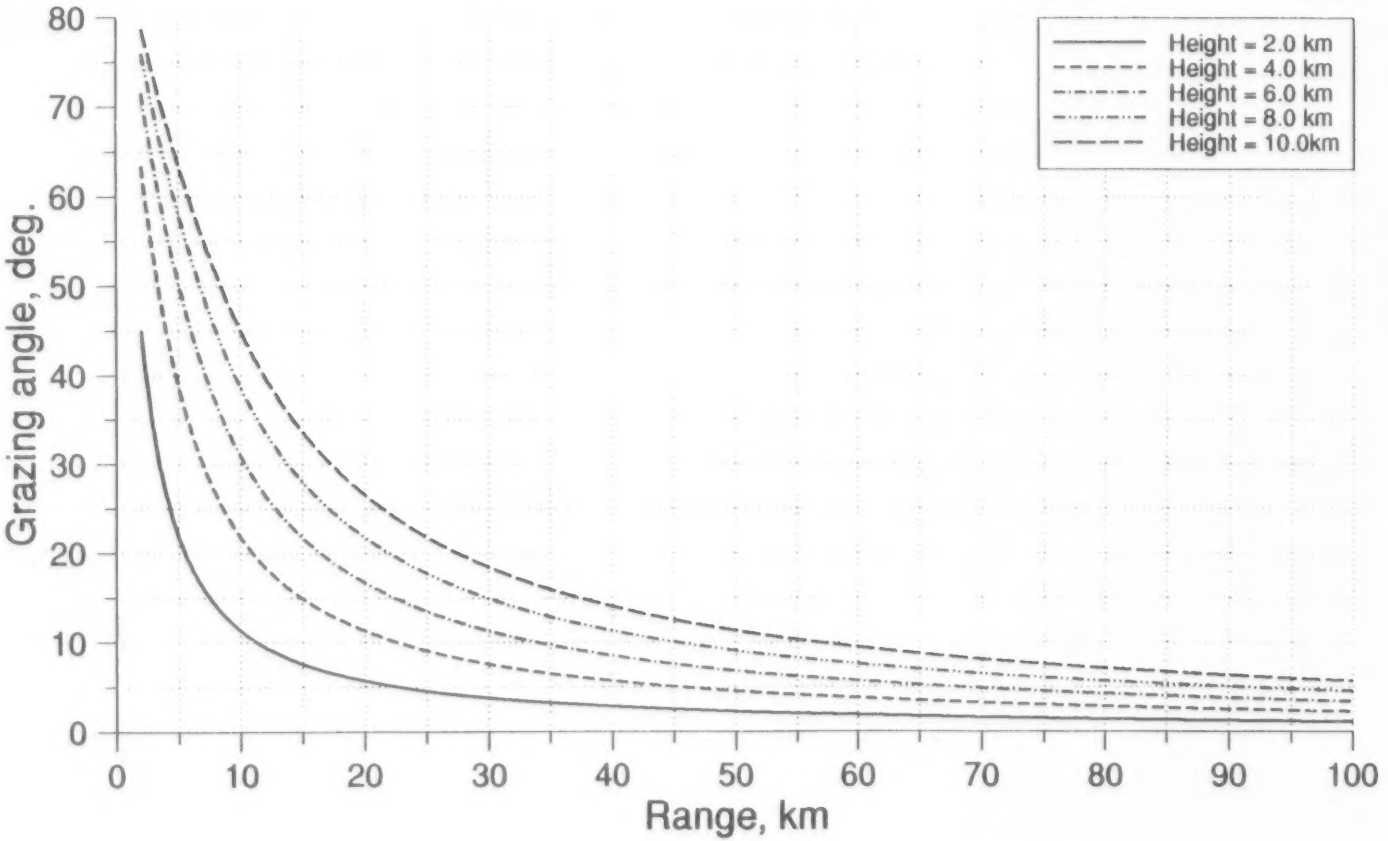

Fig. 5.22 : Variation of grazing angle vs range.

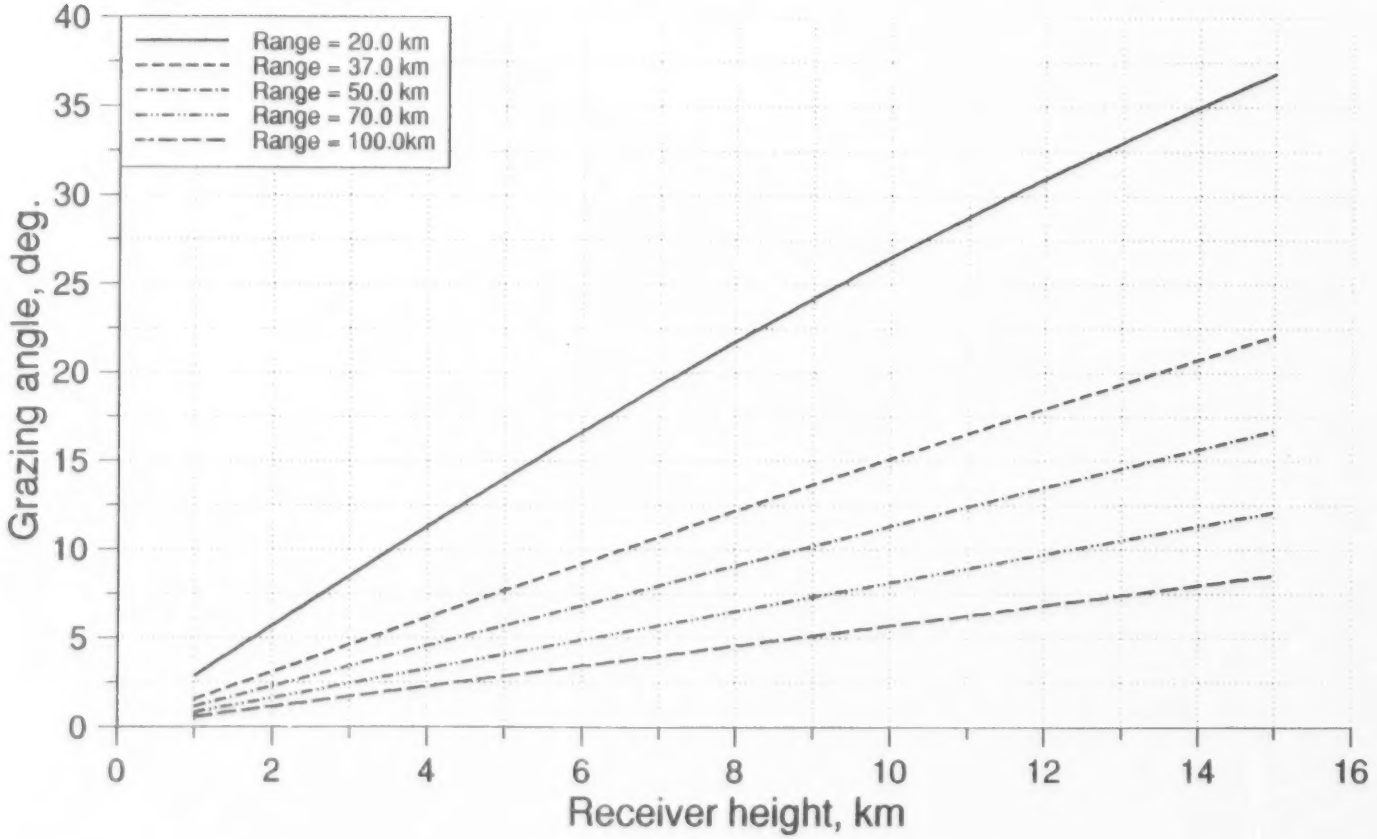

Fig. 5.23 : Variation of grazing angle vs receiver height.

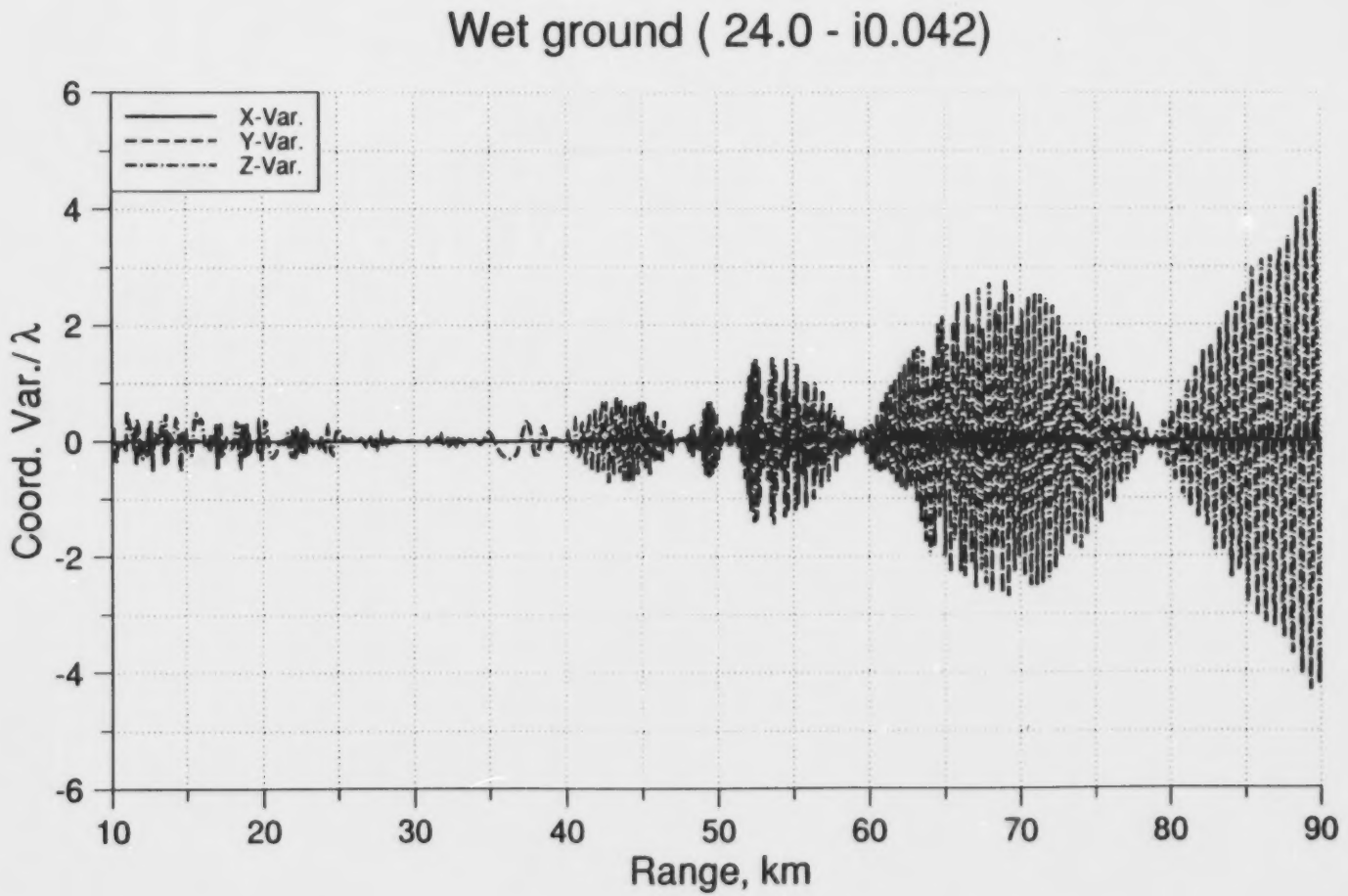

Fig. 5.24 : Multipath reflection from the wet ground.

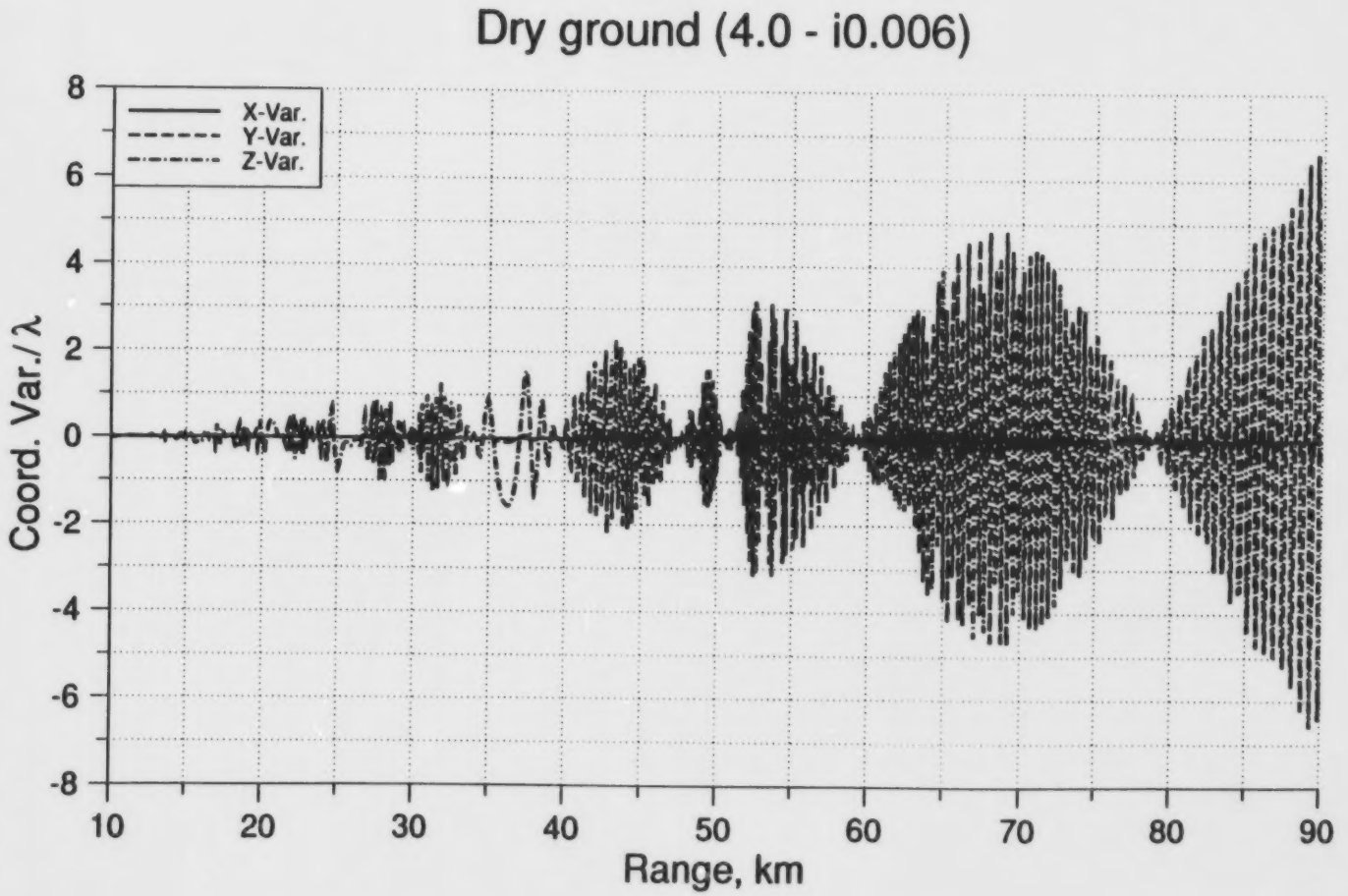

Fig. 5.25 : Multipath reflection from the dry ground.

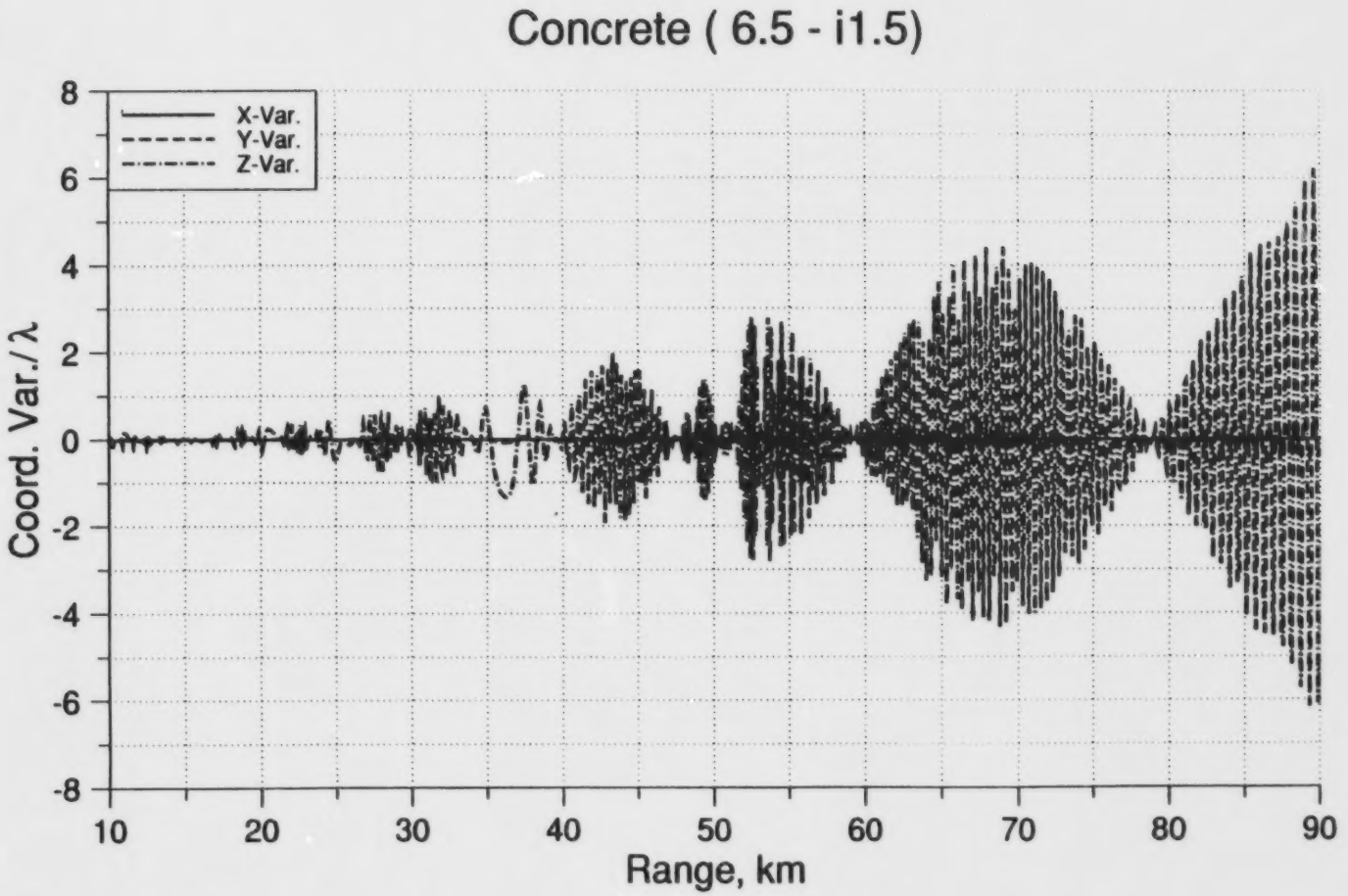

Fig. 5.26 : Multipath reflection from the concrete.

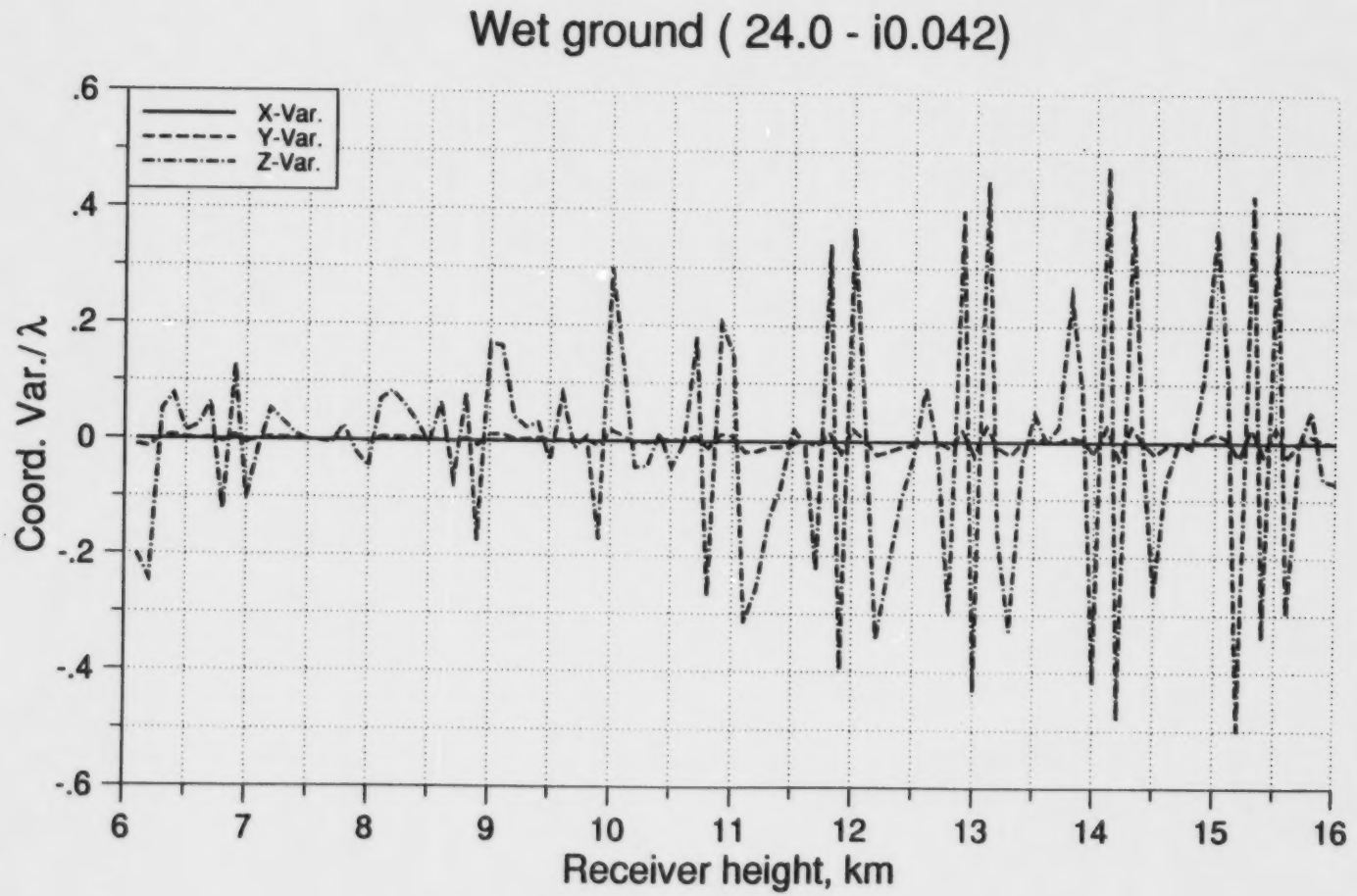

Fig. 5.27 : Multipath reflection from the wet ground, $R = 37km$.

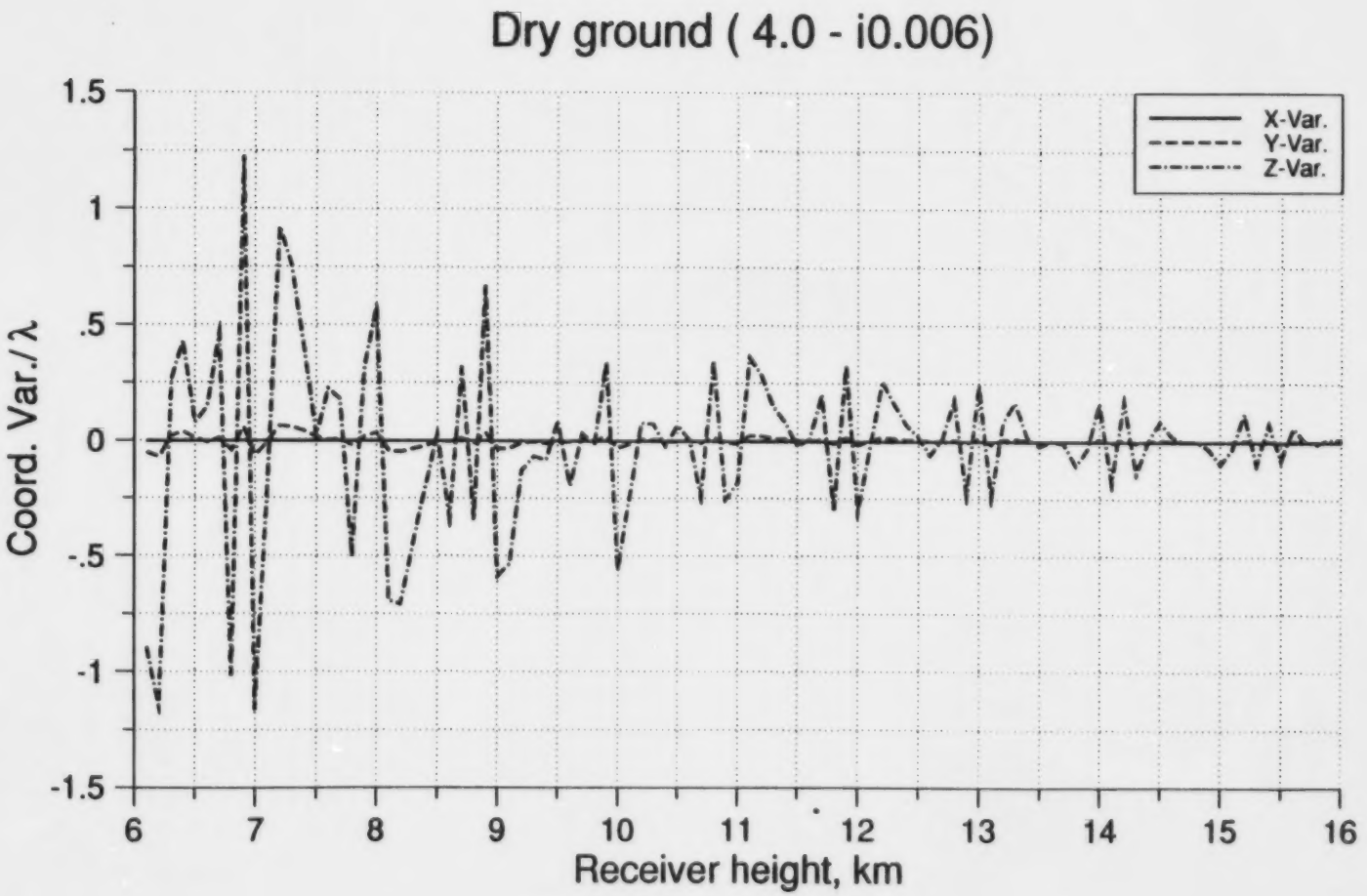

Fig. 5.28 : Multipath reflection from the dry ground, $R = 37km$.

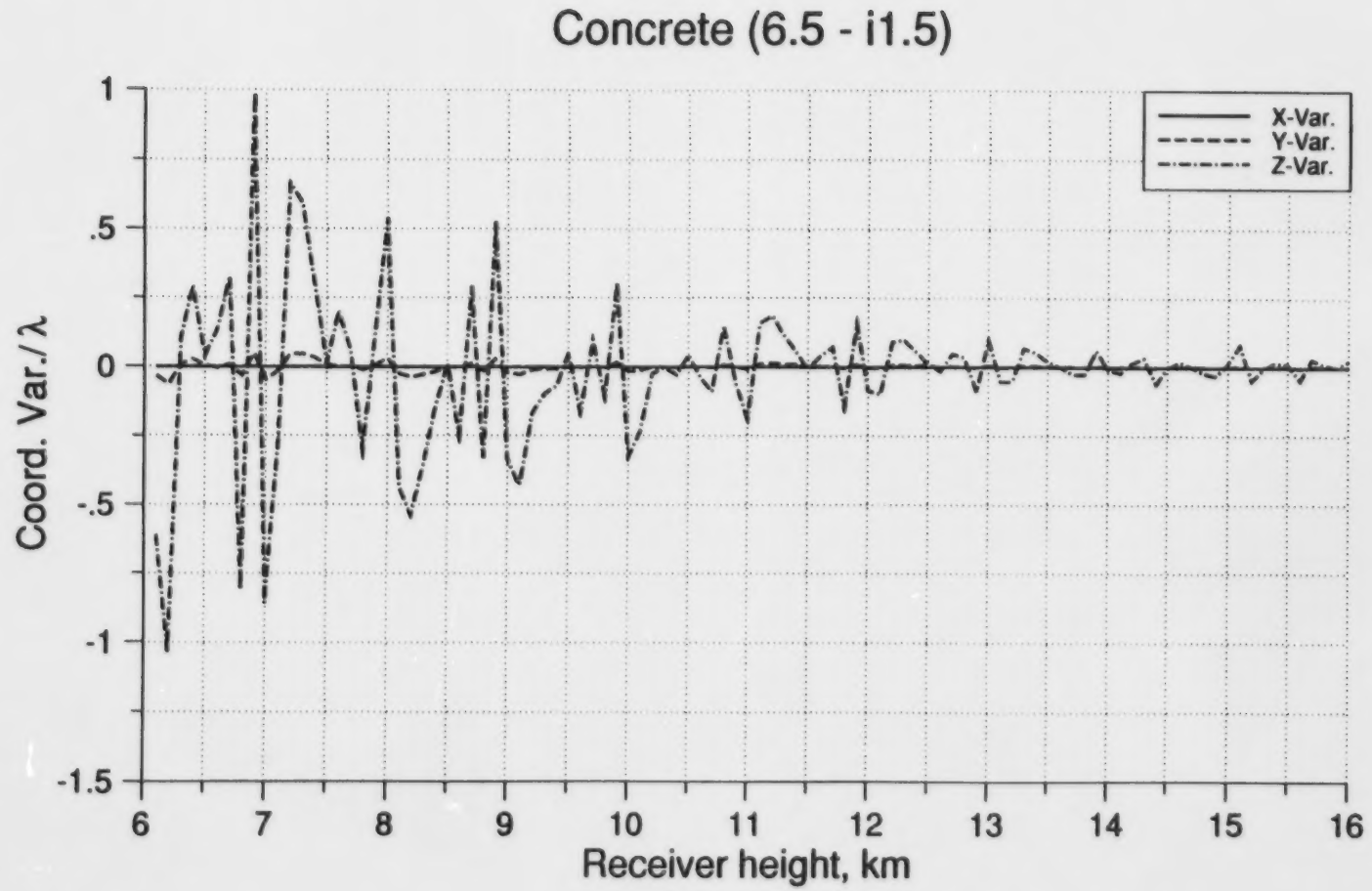

Fig. 5.29 : Multipath reflection from the concrete, $R = 37km$.

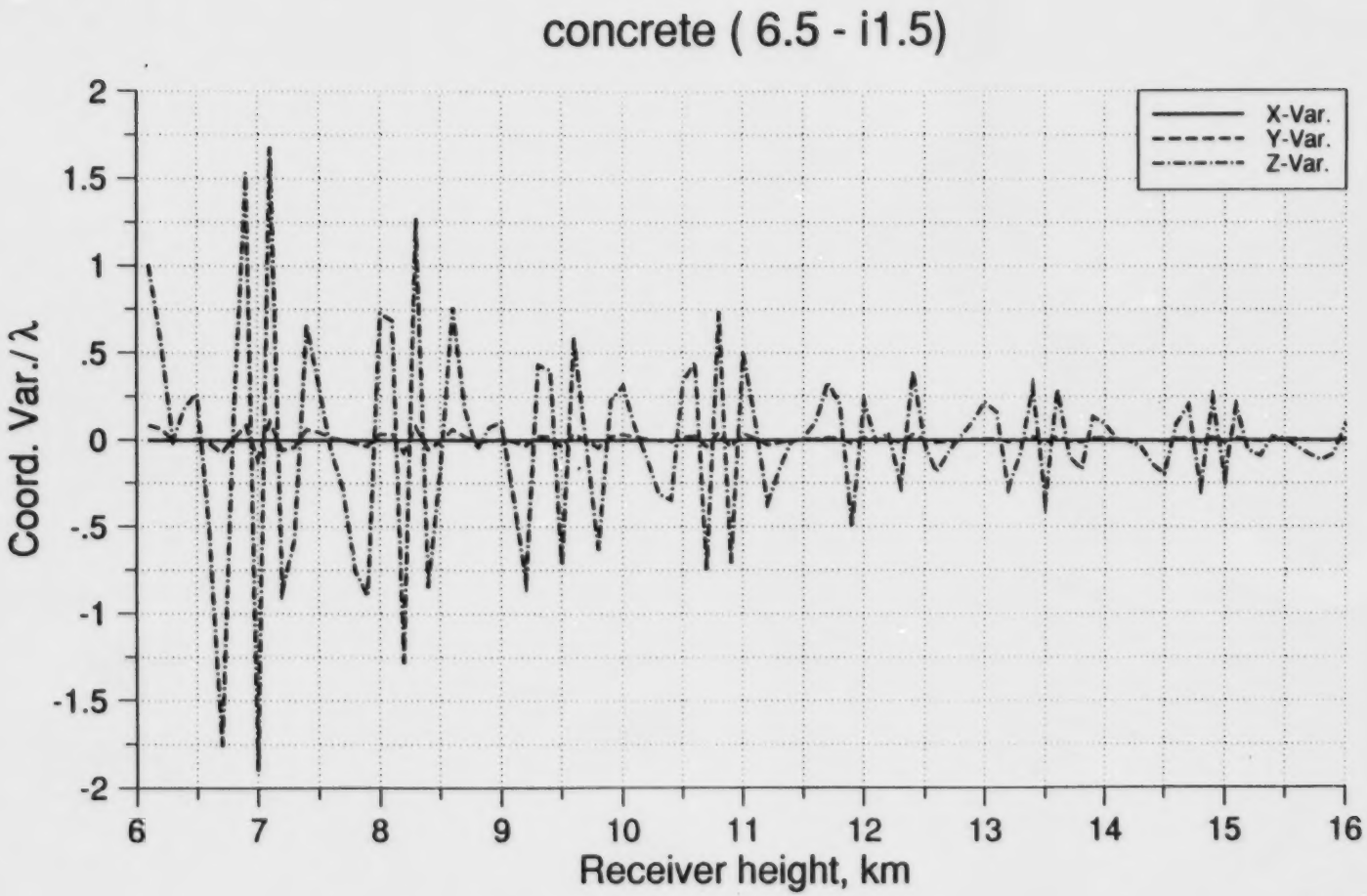

Fig. 5.30 : Multipath reflection from the wet ground, $R = 50km$.

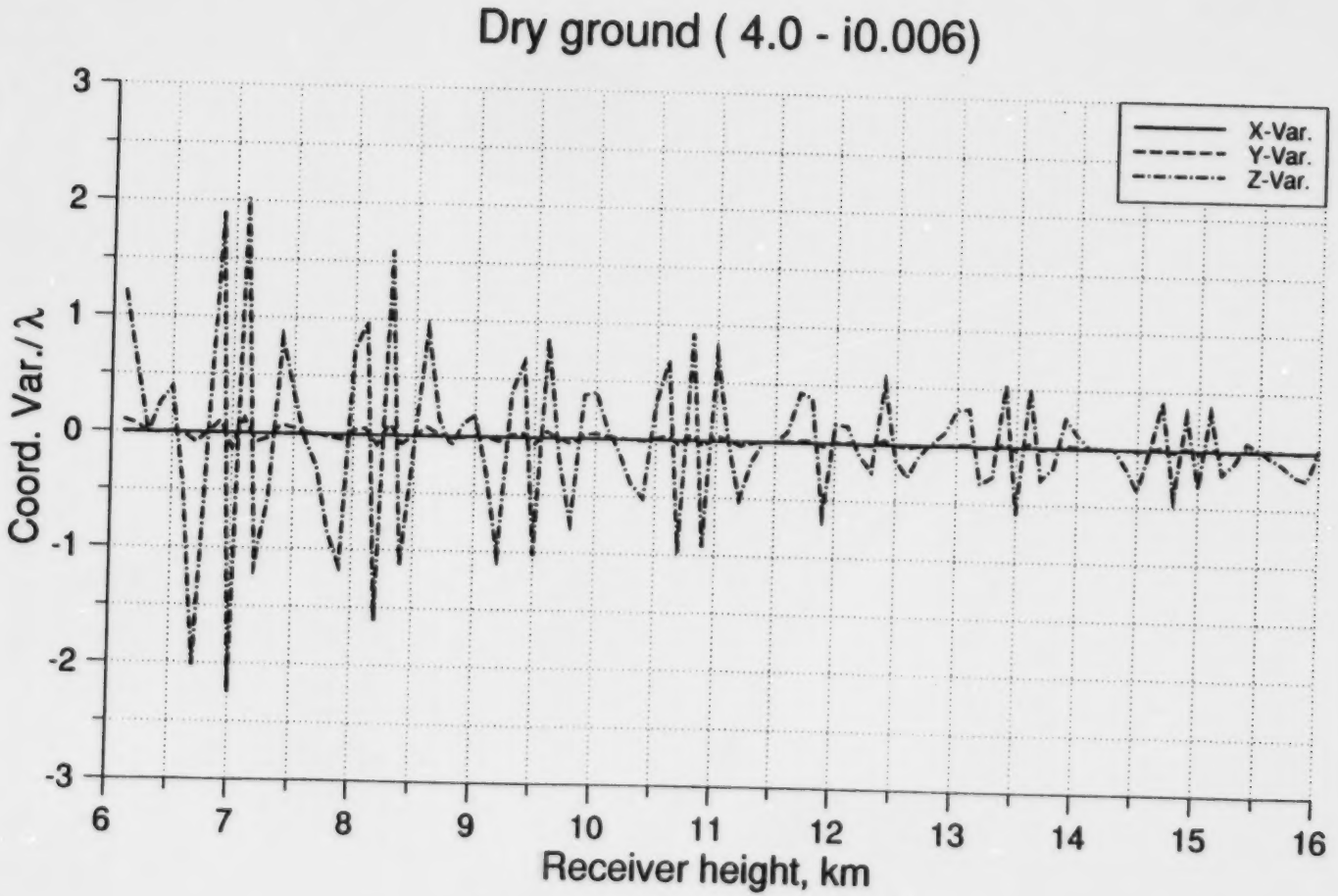

Fig. 5.31 : Multipath reflection from the dry ground, $R = 50km$.

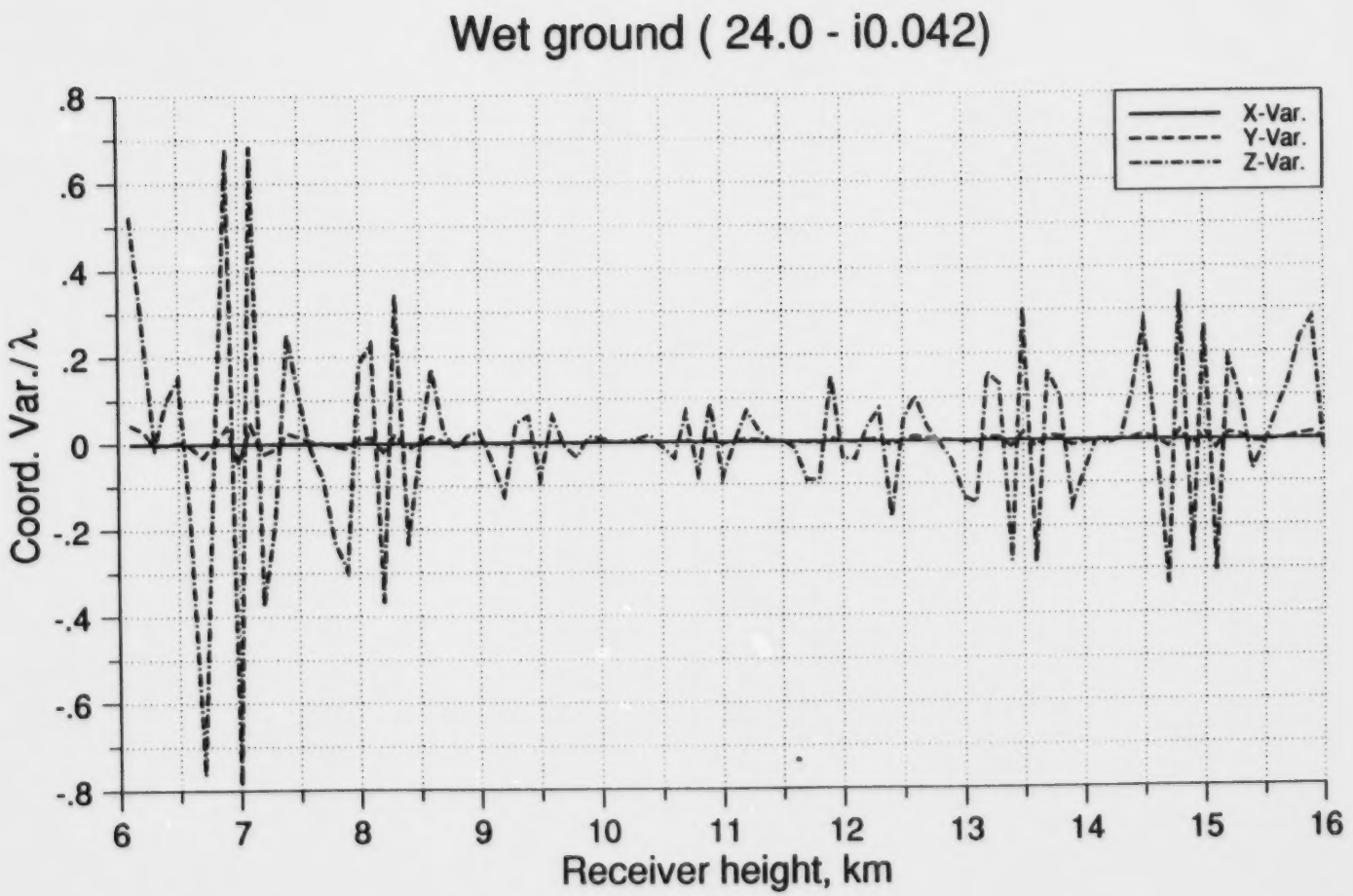

Fig. 5.32 : Multipath reflection from the concrete, $R = 50km$.

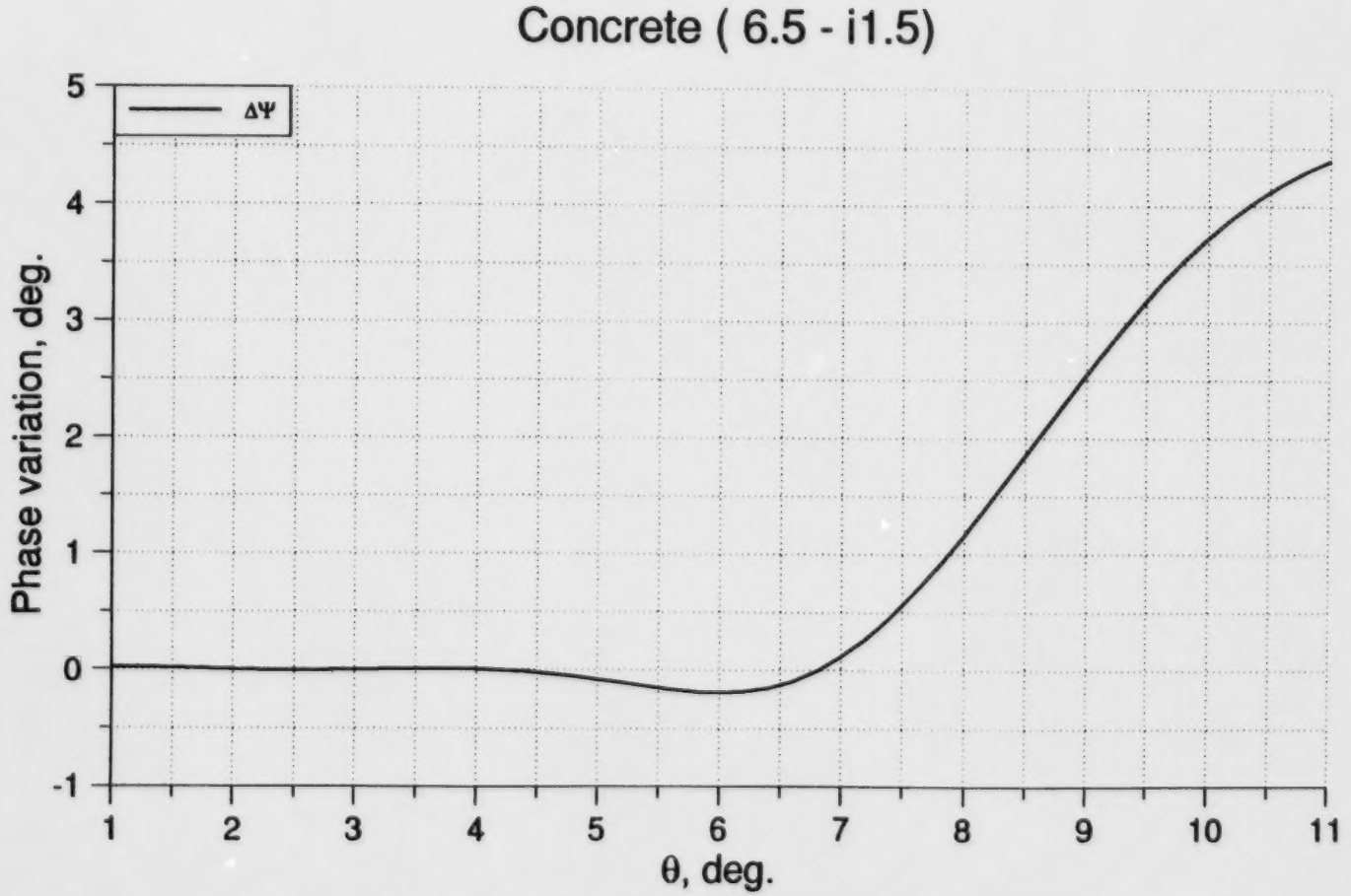

Fig. 5.33 : R = 50.0km, $\Delta\theta_c$ = 1.0 deg., α = 3.0 deg., concrete

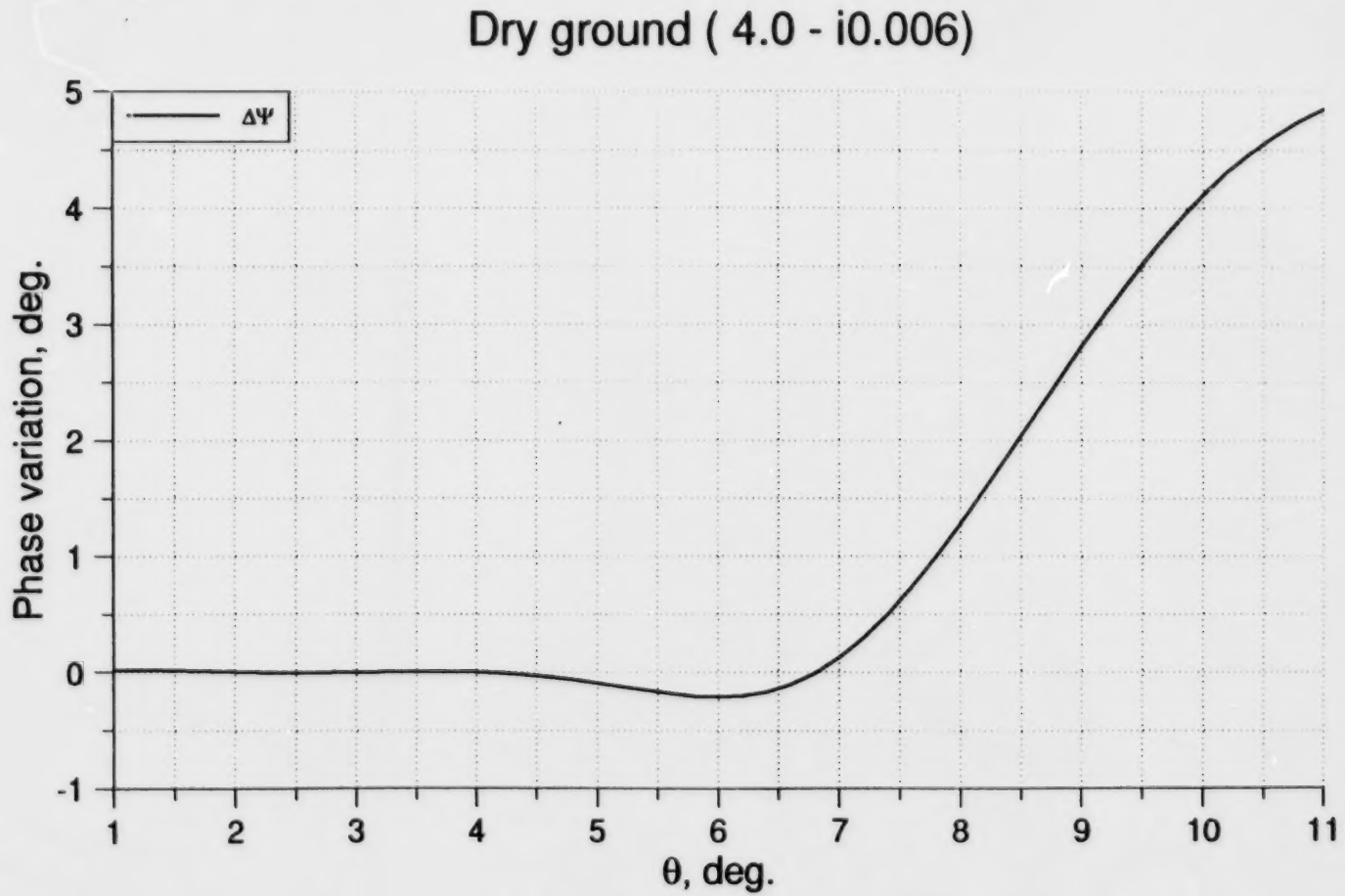

Fig. 5.34 : R = 50.0km, $\Delta\theta_c$ = 1.0 deg., α = 3.0 deg., dry ground.

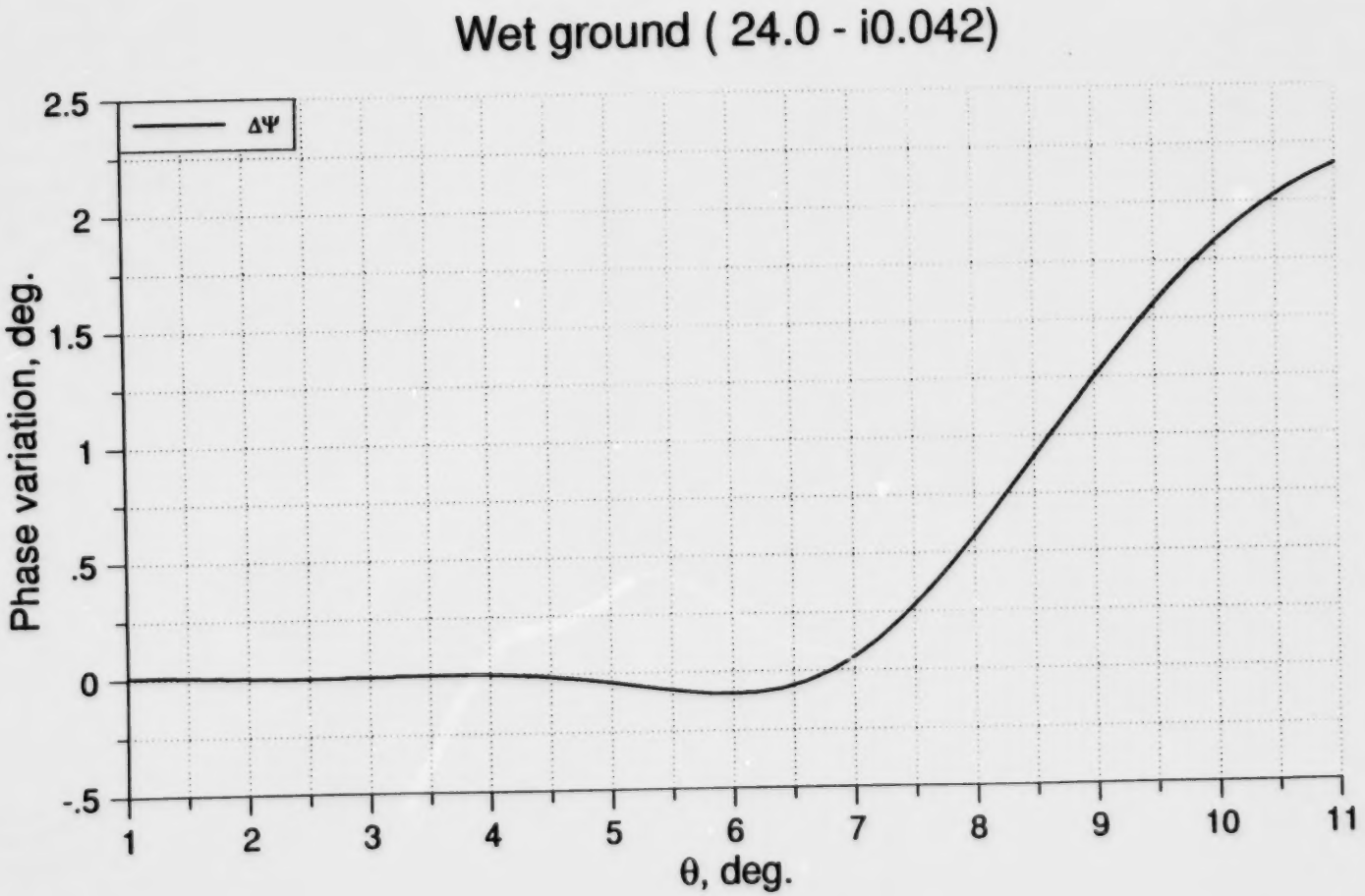

Fig. 5.35 : R = 50.0*km*, $\Delta\theta_c$ = 1.0 deg., α = 3.0 deg., wet ground.

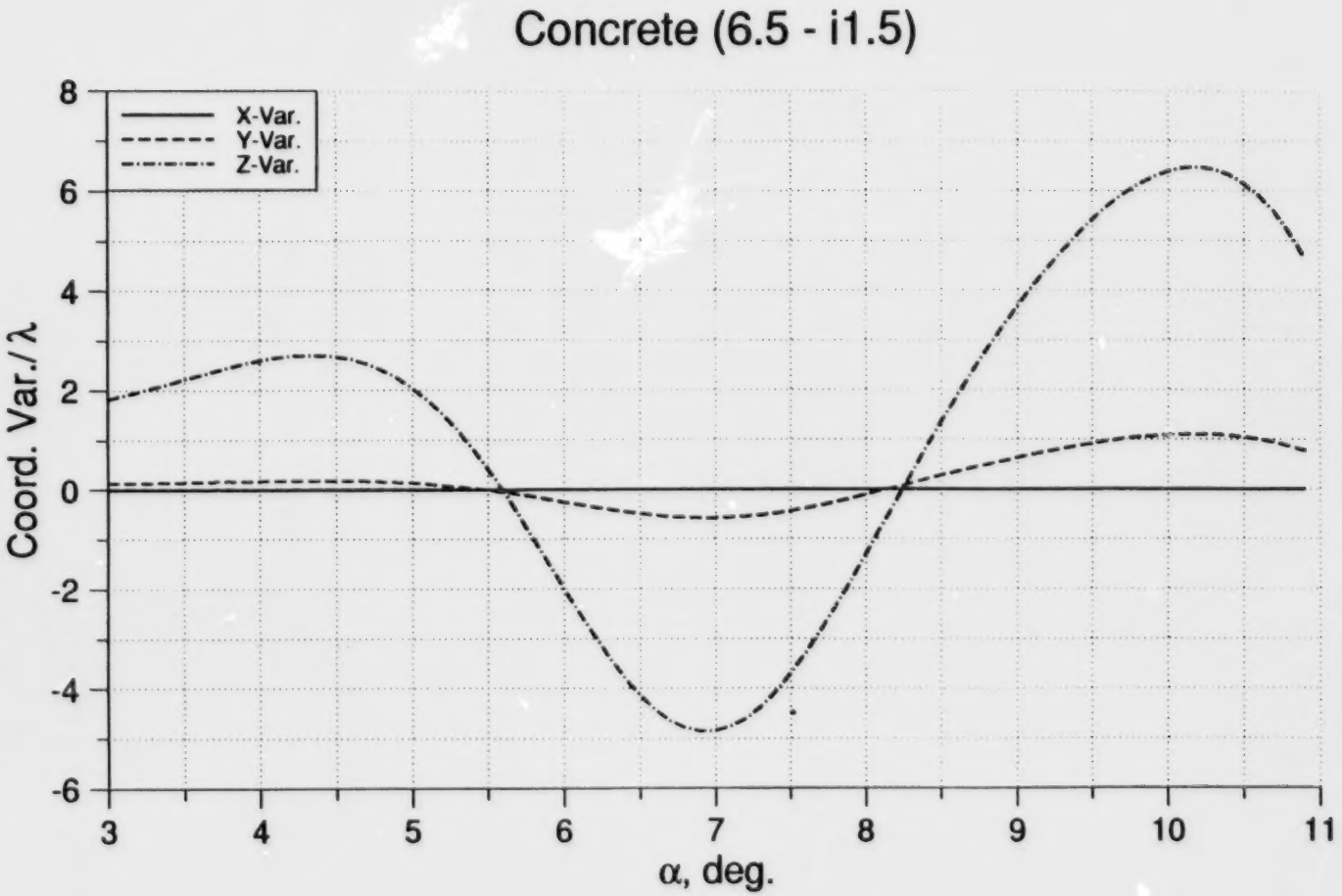

Fig. 5.36 : R = 50.0km, $\Delta\theta_c$ = 1.0 deg., h_r = 6km, concrete.

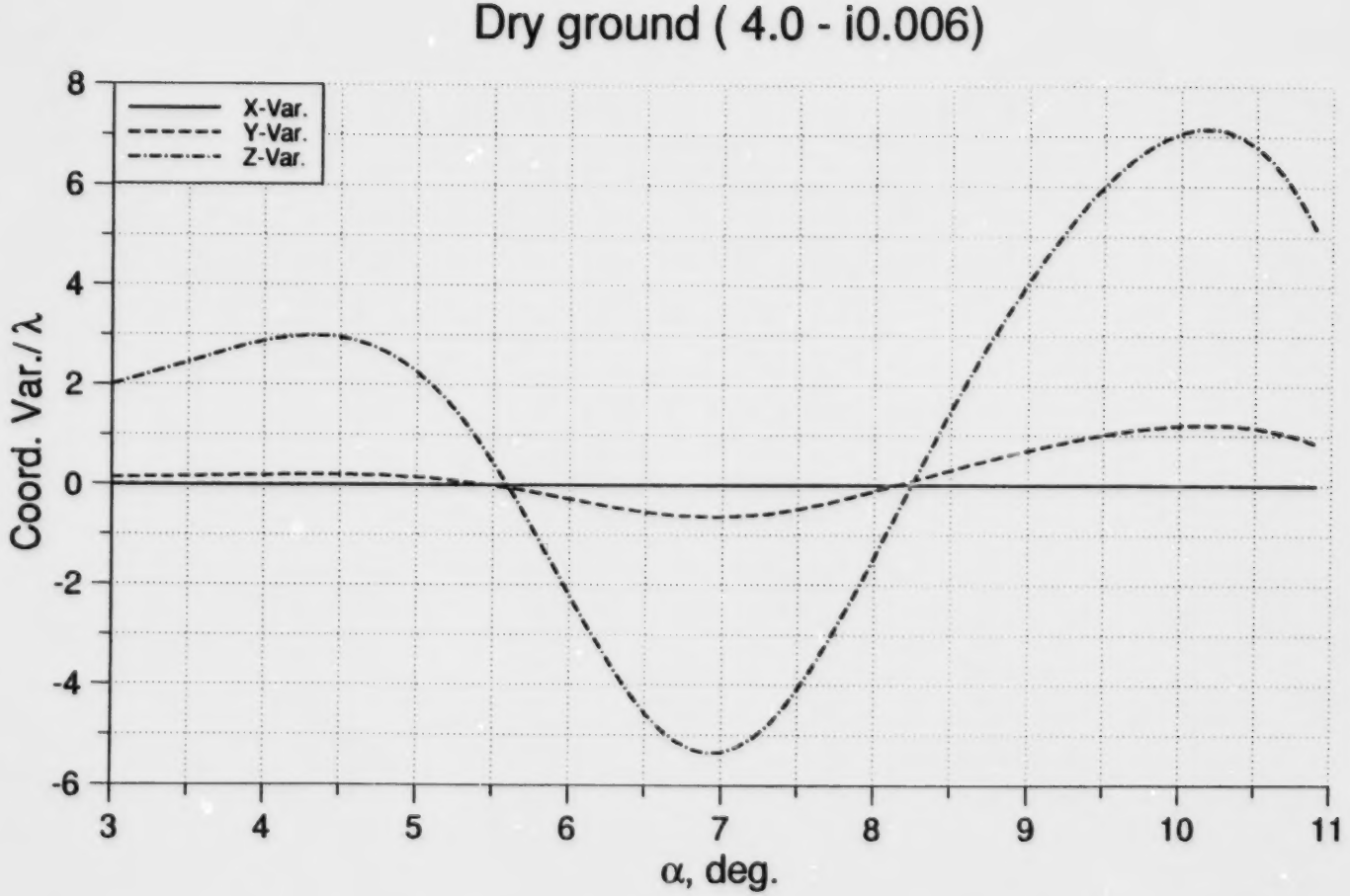

Fig. 5.37 : R = 50.0km, $\Delta\theta_c$ = 1.0 deg., h_r = 6km, dry ground.

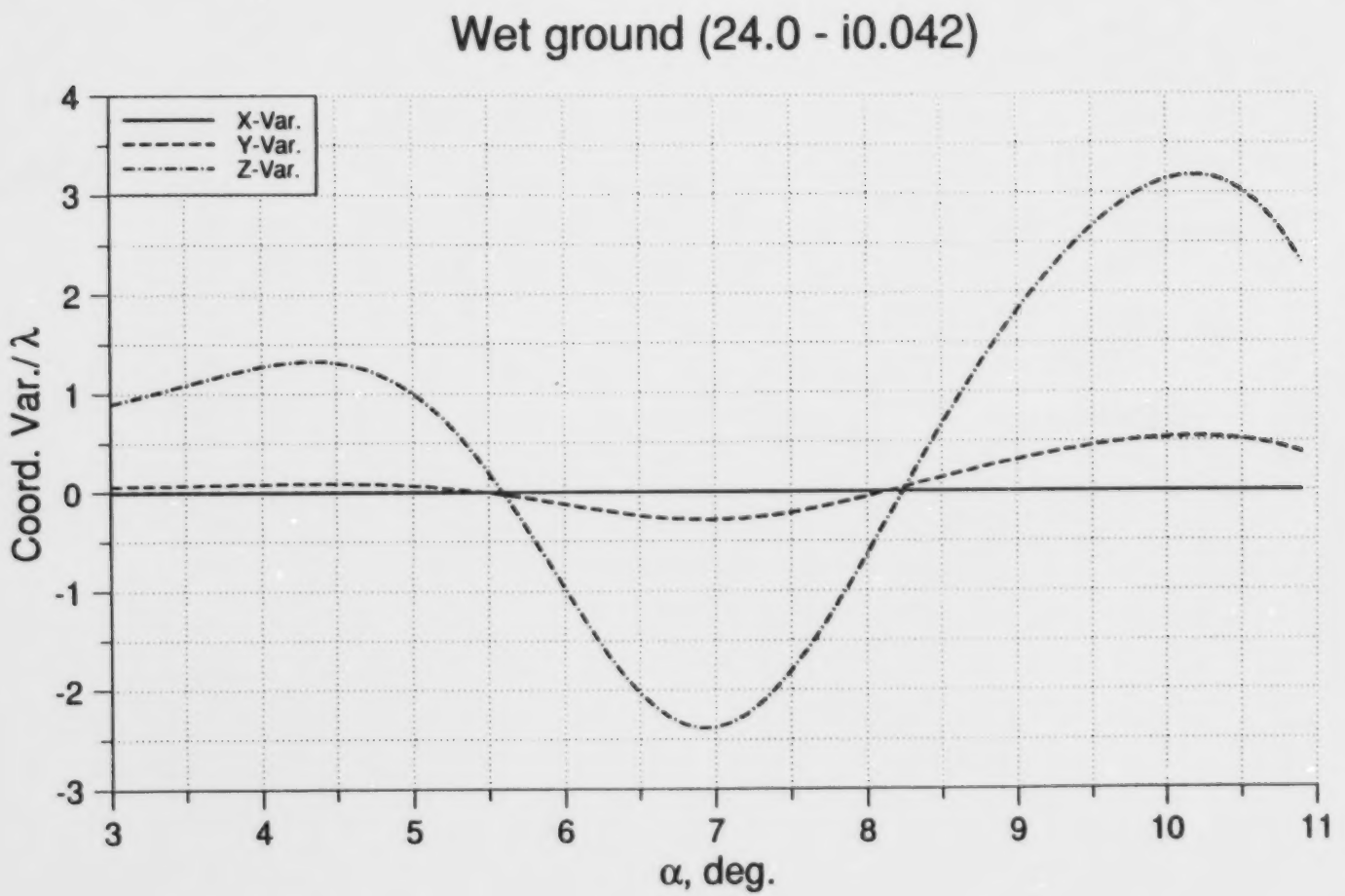

Fig. 5.38 : $R = 50.0km$, $\Delta\theta_c = 1.0$ deg., $h_r = 6km$, wet ground.

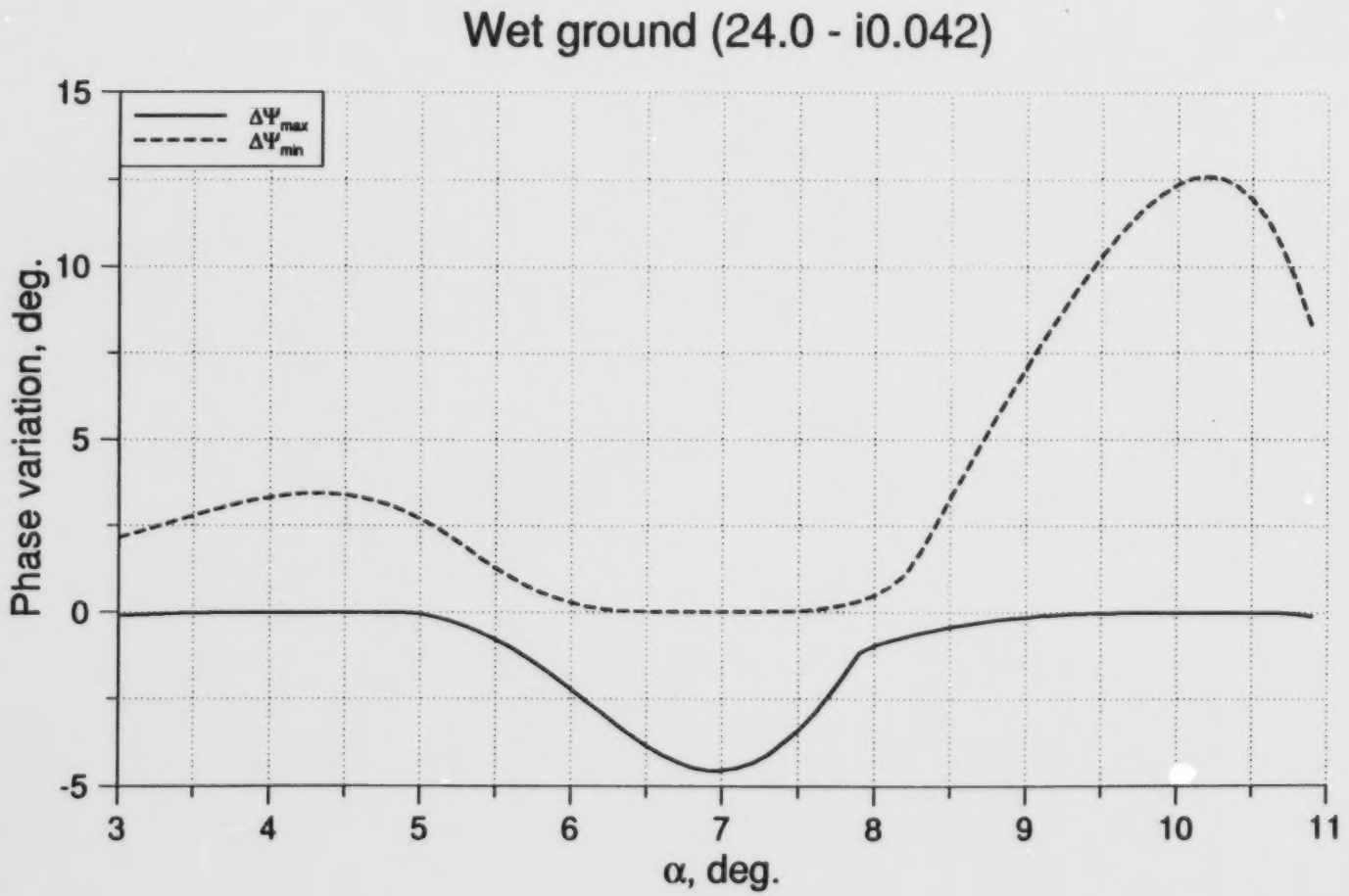

Fig. 5.39 : R = 50.0km, $\Delta\theta_c$ = 1.0 deg., h_r = 6km, wet ground.

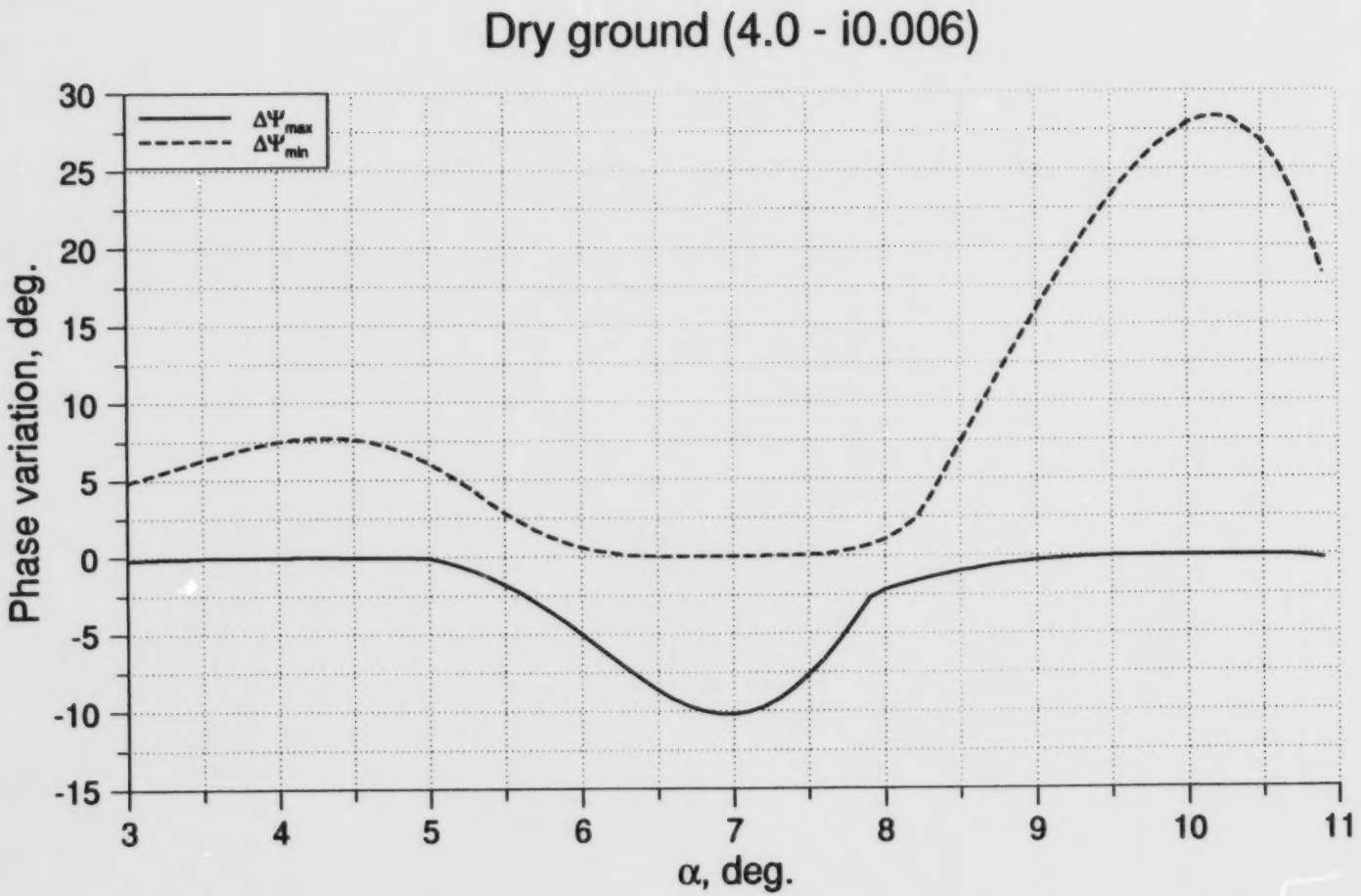

Fig. 5.40 : R = 50.0km, $\Delta\theta_c$ = 1.0 deg., h_r = 6km, dry ground.

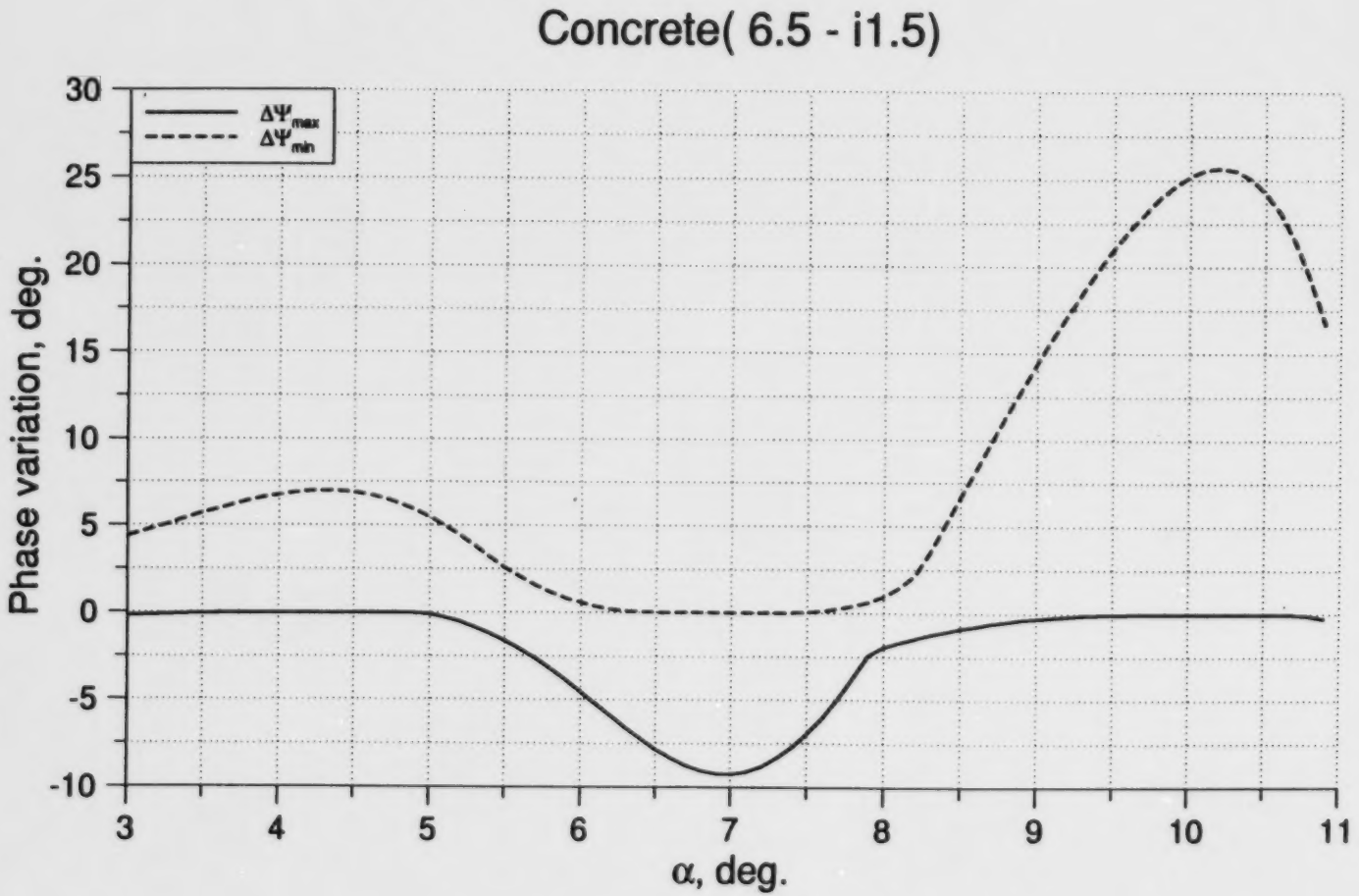

Fig. 5.41 : R = 50.0km, $\Delta\theta_c$ = 1.0 deg., h_r = 6km, concrete.

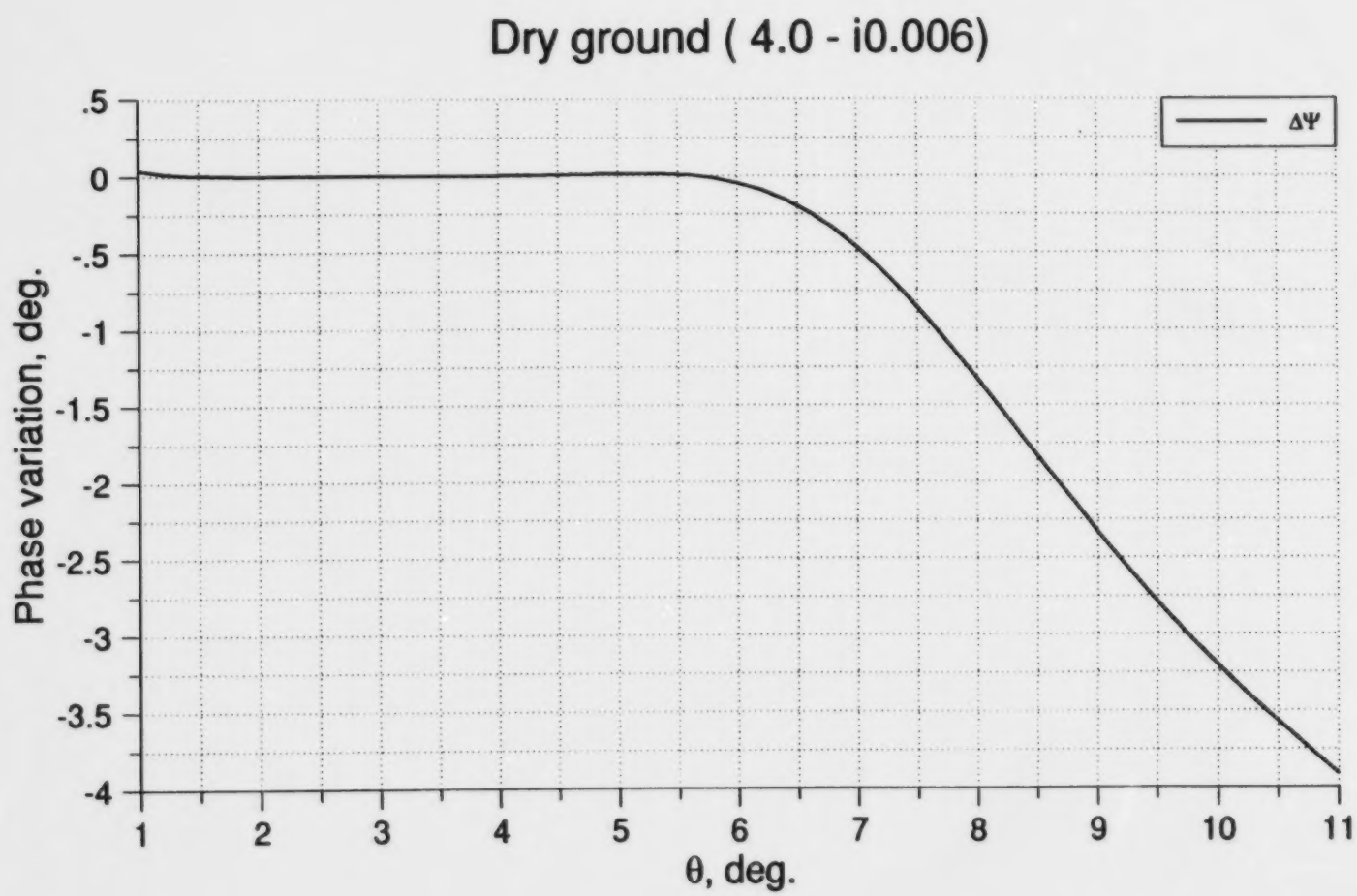

Fig. 5.42 : $R = 396m$, $h_r = 56.82m$, $h_t = 21.34m$, dry ground, for DFL lab.

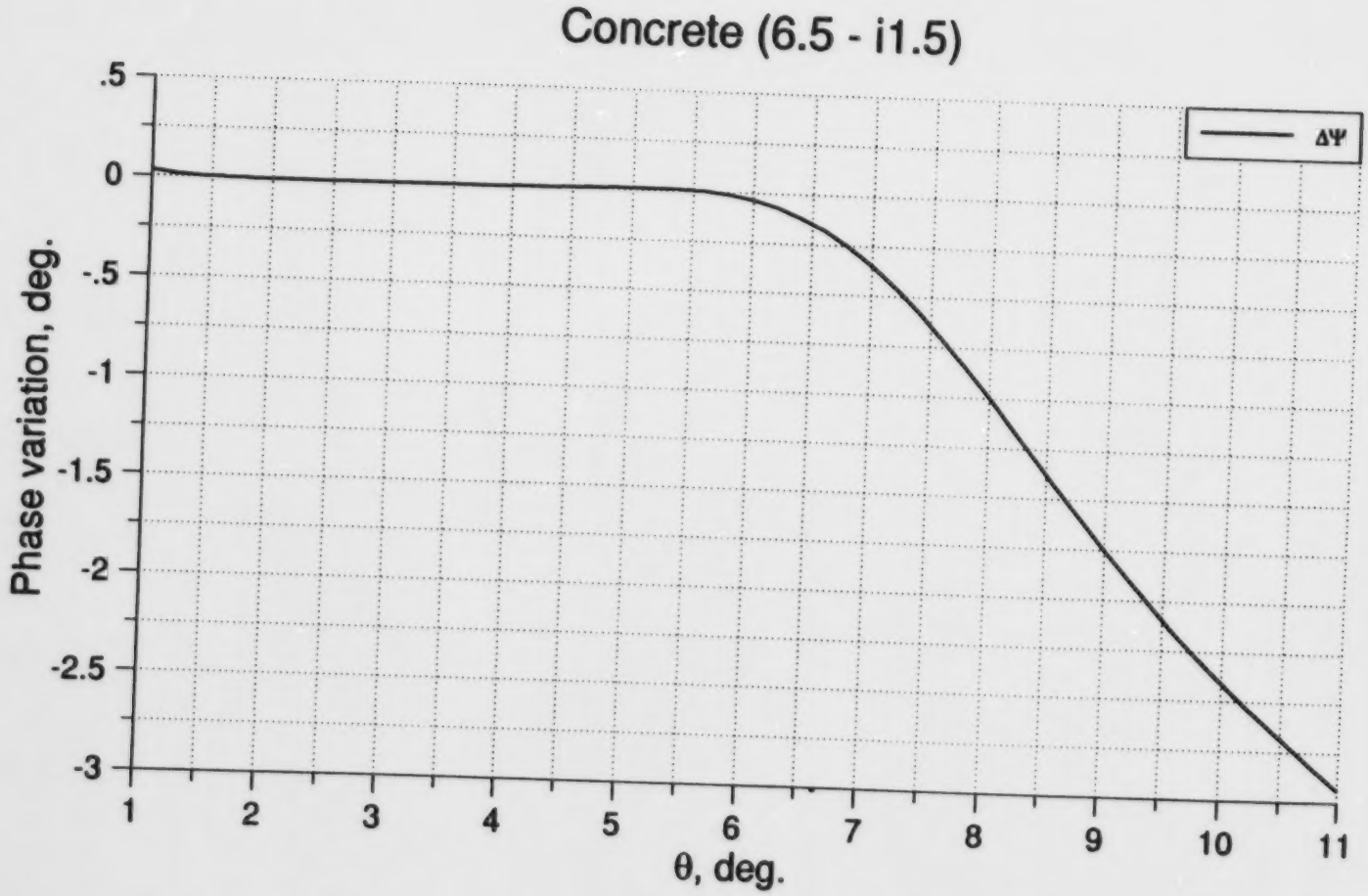

Fig. 5.43 : $R = 396m$, $h_r = 56.82m$, $h_t = 21.34m$, concrete, for DFL lab.

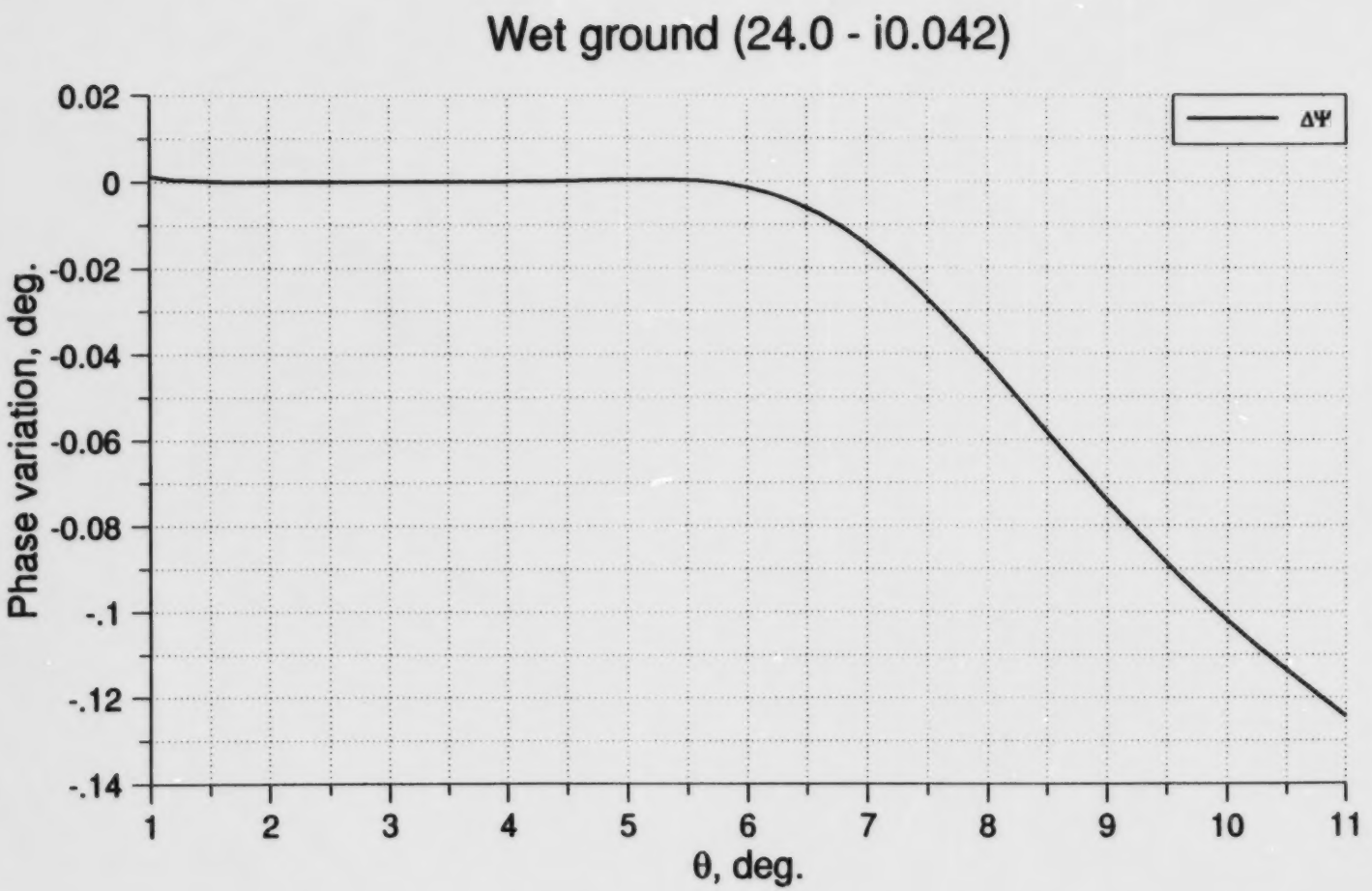

Fig. 5.44 : $R = 396m$, $h_r = 56.82m$, $h_t = 21.34m$, wet ground, for DFL lab.

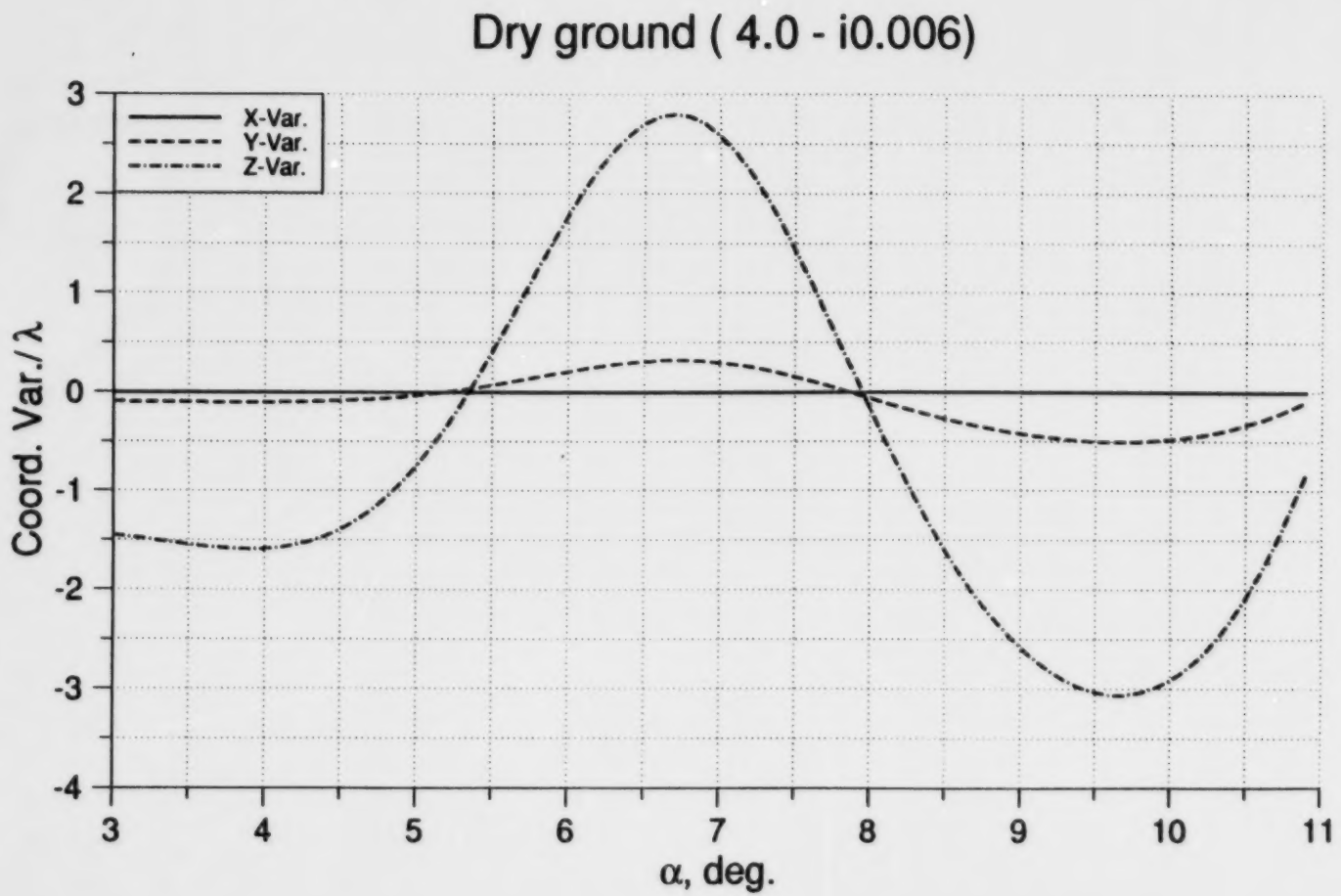

Fig. 5.45 : $R = 396m$, $h_r = 56.82m$, $h_t = 21.34m$, dry ground, for DFL lab.

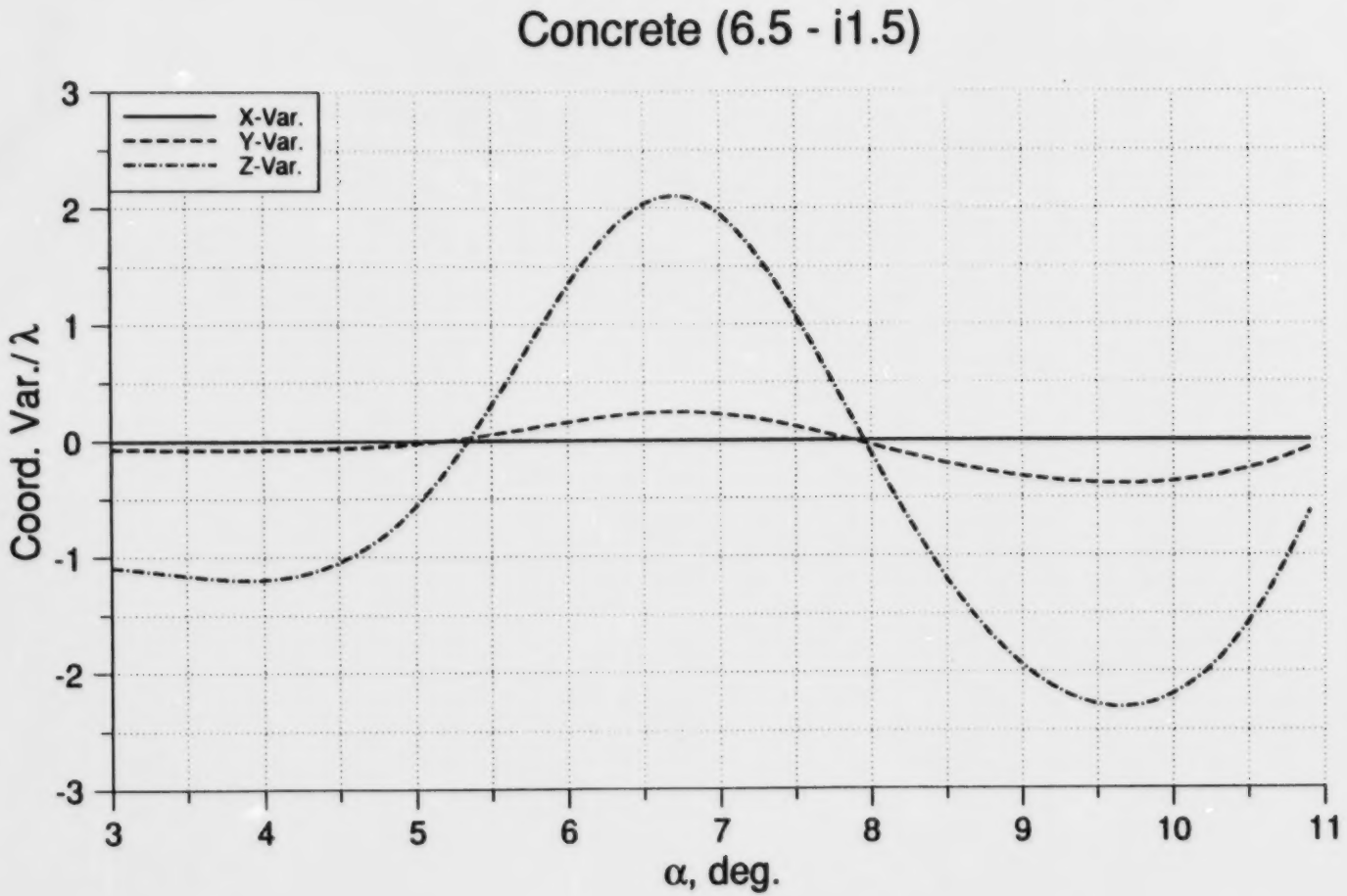

Fig. 5.46 : $R = 396m$, $h_r = 56.82m$, $h_t = 21.34m$, concrete, for DFL lab.

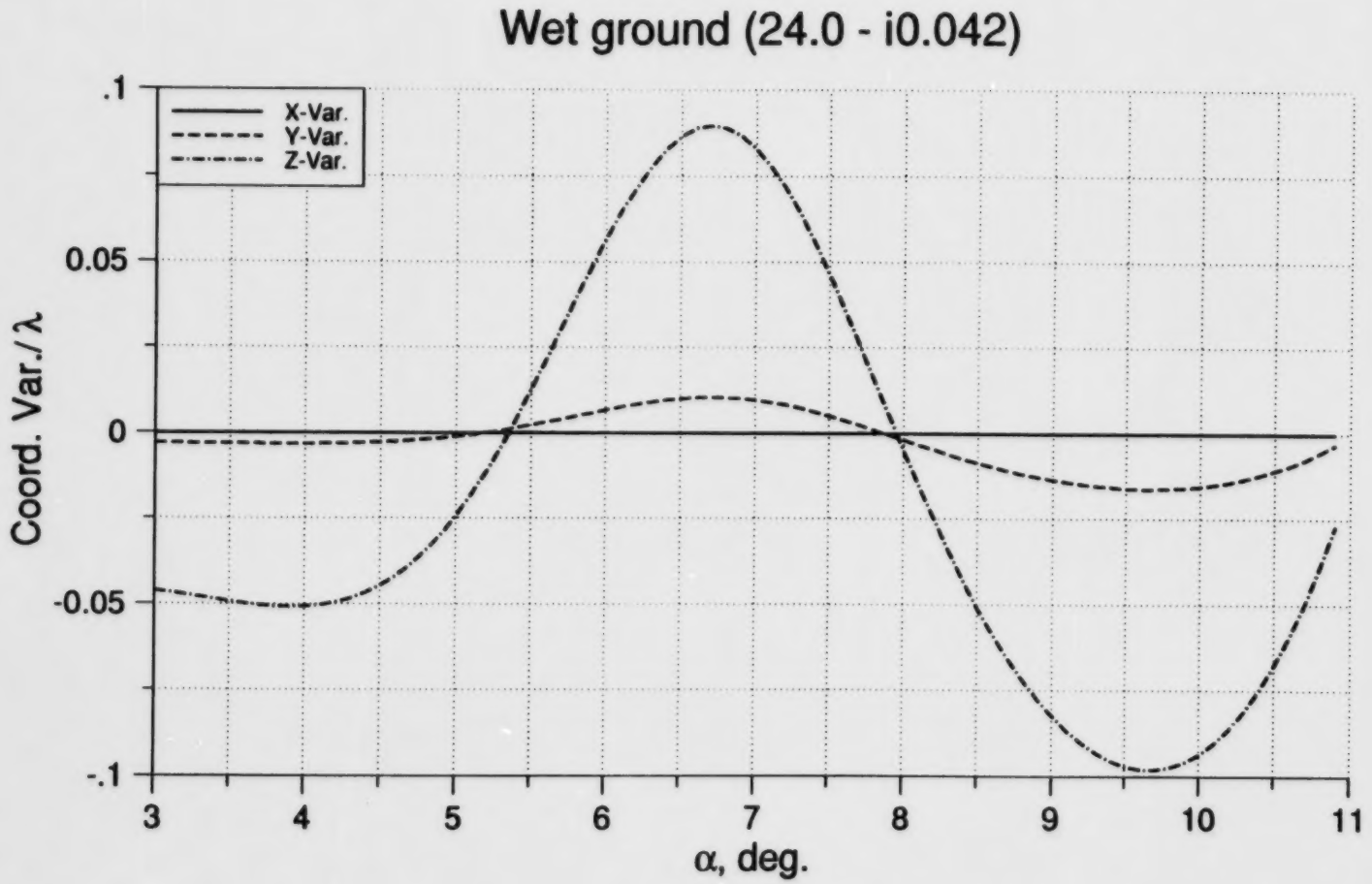

Fig. 5.47 : $R = 396m$, $h_r = 56.82m$, $h_t = 21.34m$, wet ground, for DFL lab.

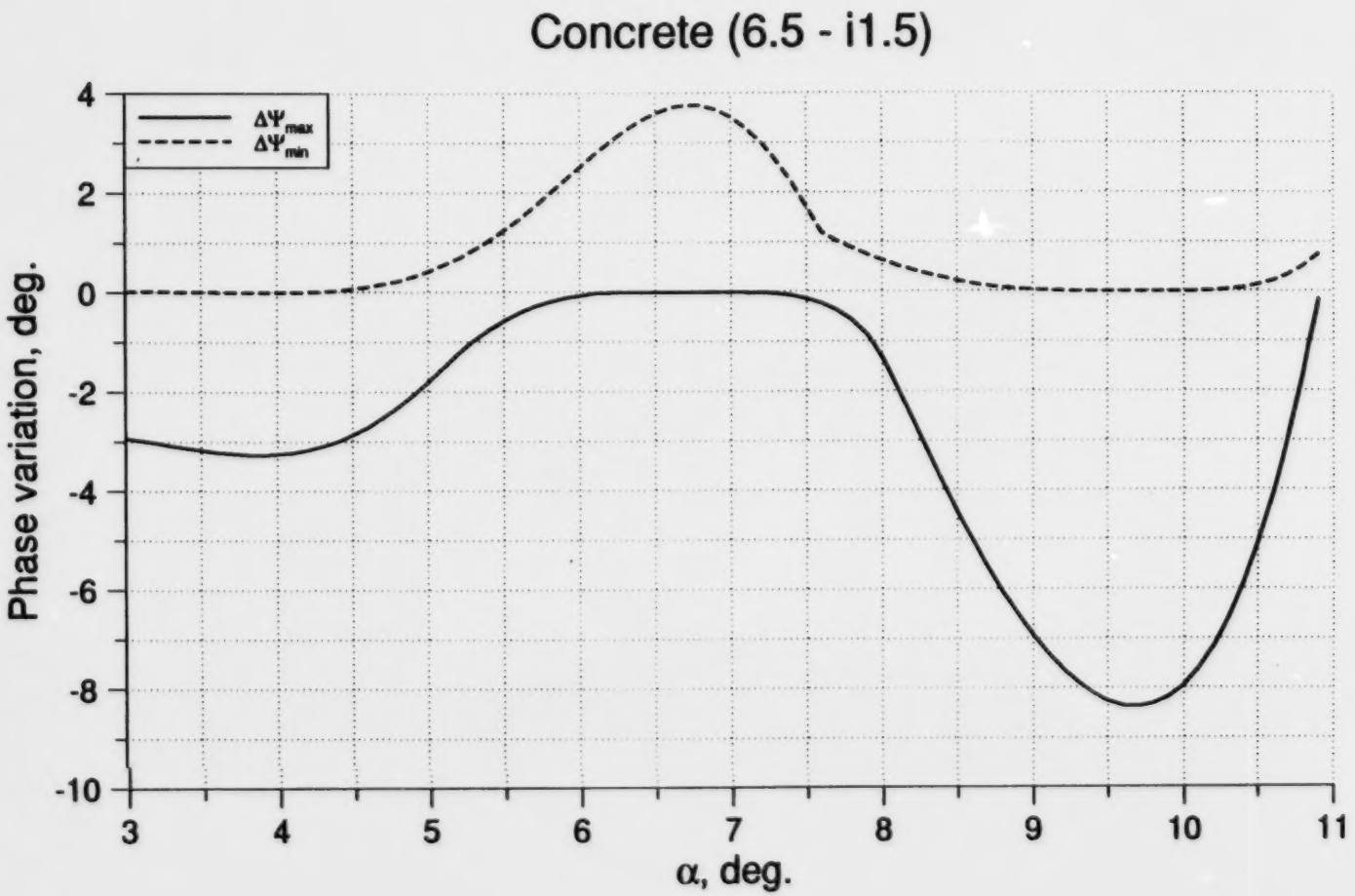

Fig. 5.48 : $R = 396m$, $h_r = 56.82m$, $h_t = 21.34m$, concrete, for DFL lab.

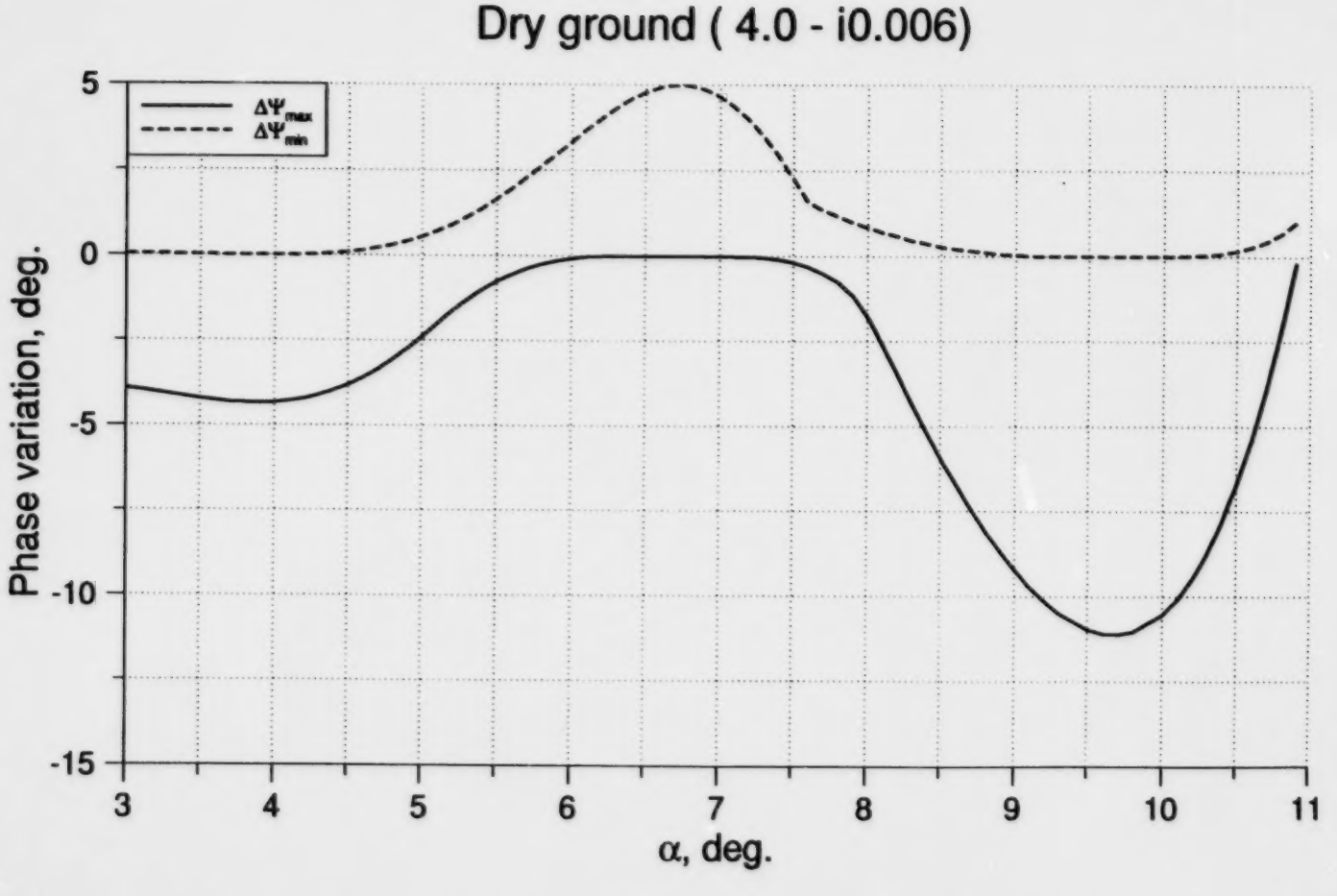

Fig. 5.49 : $R = 396m$, $h_r = 56.82m$, $h_t = 21.34m$, dry ground, for DFL lab.

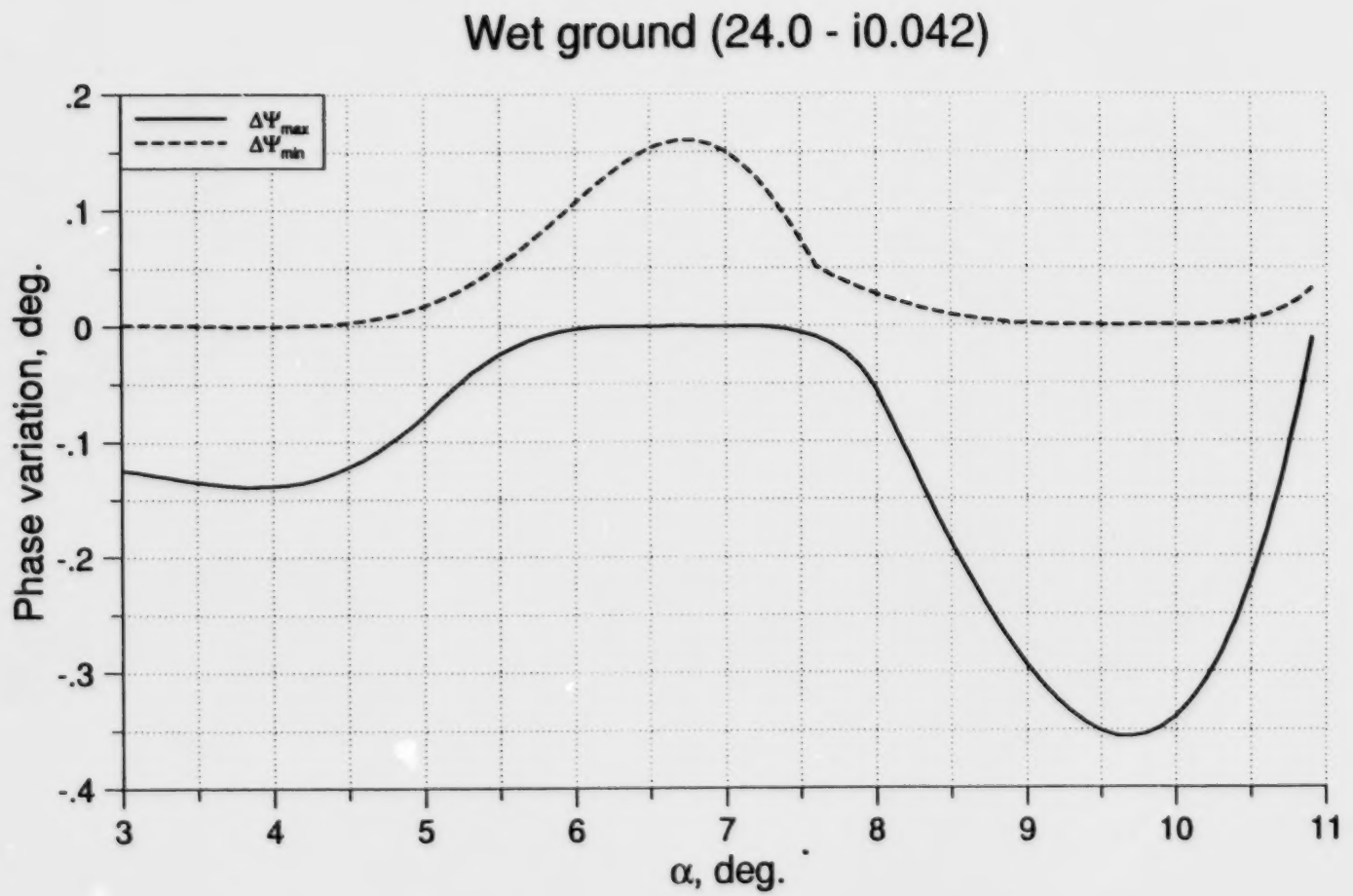

Fig. 5.50 : $R = 396m$, $h_r = 56.82m$, $h_t = 21.34m$, wet ground, for DFL lab.

Chapter 6
Thermal Expansion/Contraction

The issue of the thermal expansion and its effect on the performance of *MLS* array, or its phase centre movement is a complex one. Its effect depends on the thermal gradient over the array surface and, in turn, on the source of temperature variations. In the course of progress meetings, it was decided that, since the *MLS* antenna will operate inside an environmentally controlled radome, it is sufficient to investigate the case of uniform temperature variation over the array surface. Even in such a case, the thermal expansions or contractions will affect the propagation constant within the waveguide and consequently the slot excitation. The thermal effects are, therefore, expected to be far more serious on the elevation pattern than on the phase centre movement. Nevertheless, since this study involves only with the phase centre of the antenna, all other effects are neglected. The study, therefore, address as the effects of uniform temperature variations on the array phase centre location and its movement.

A model based on the linear expansion of materials is proposed to investigate the phase centre movement, due to the thermal expansion and/or contraction. Theoretically, the variation of the sample length due to the temperature change can be computed from

$$l_t = l_0 \, (1. + \alpha T) \tag{6.1}$$

where, α is the linear expansion coefficient, which is defined as the relative length change per degree centigrade (C), with respect to zero degree C, l_0 is the length at 0.0^oC, and l_t is the expanded length at T^oC. For copper and aluminum materials, α has the values of,

$$\alpha = 16.6 \times 10.0^{-6} \quad (^oC)^{-1} \quad \text{for } \textit{copper} \tag{6.2}$$

$$\alpha = 25.0 \times 10.0^{-6} \quad (^oC)^{-1} \quad \text{for } \textit{aluminum} \tag{6.3}$$

Hence, for a selected temperature variation, one can modify the element spacing by incorporating the spatial variation of the horizontal or vertical antenna elements.

Figs. 6.1 to 6.8 illustrate the phase centre coordinate variations, due to the thermal variations, for the copper and aluminum antenna materials. Uniform

contractions/expansions were assumed for all elements, and the interelemental spacing was modified to incorporate the thermal variation along the x-coordinate. A minor change in the phase centre coordinates is observed. The maximum phase centre displacement for the aluminum material is 0.0015 λ in the y–coordinate and 0.00005 λ in the z-coordinate. There is no variation of the phase centre in the x-coordinate. For the copper material, the displacement in the phase centre coordinate is virtually zero.

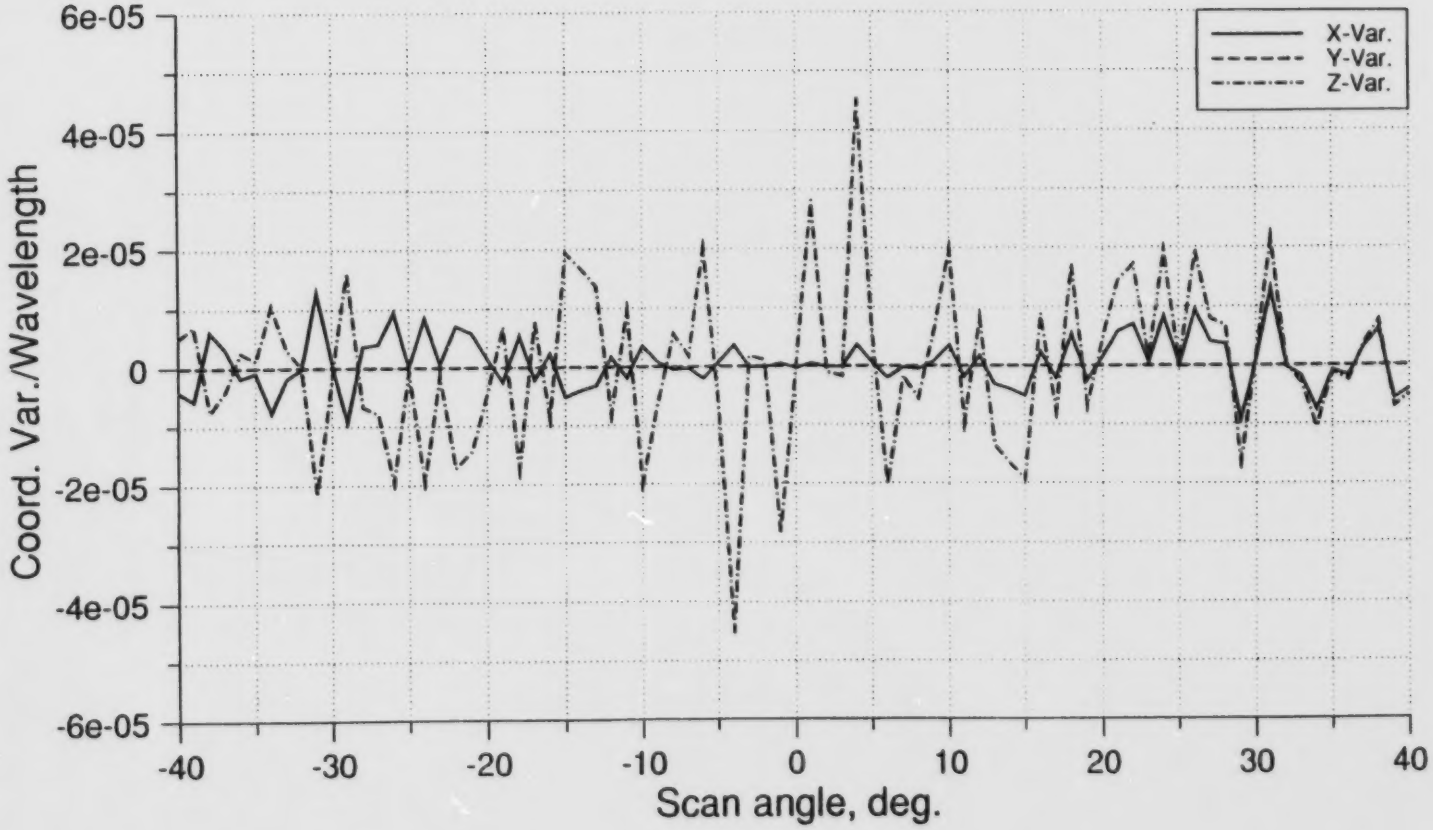

Fig. 6.1 : Thermal expansion of the horizontal arrays, copper ($T = 60° C$).

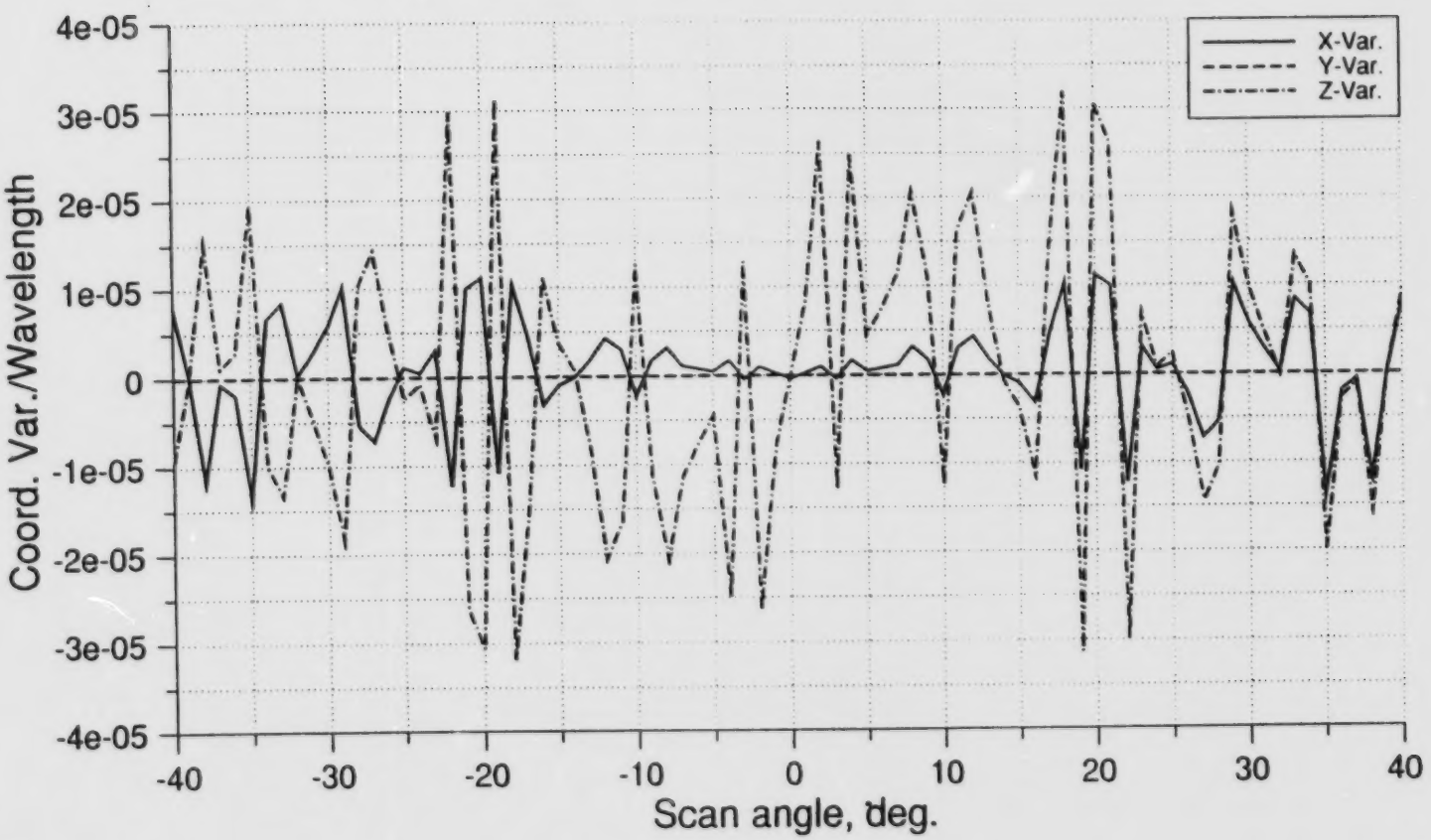

Fig. 6.2 : Thermal contraction of the horizontal arrays, copper (T = –60° C).

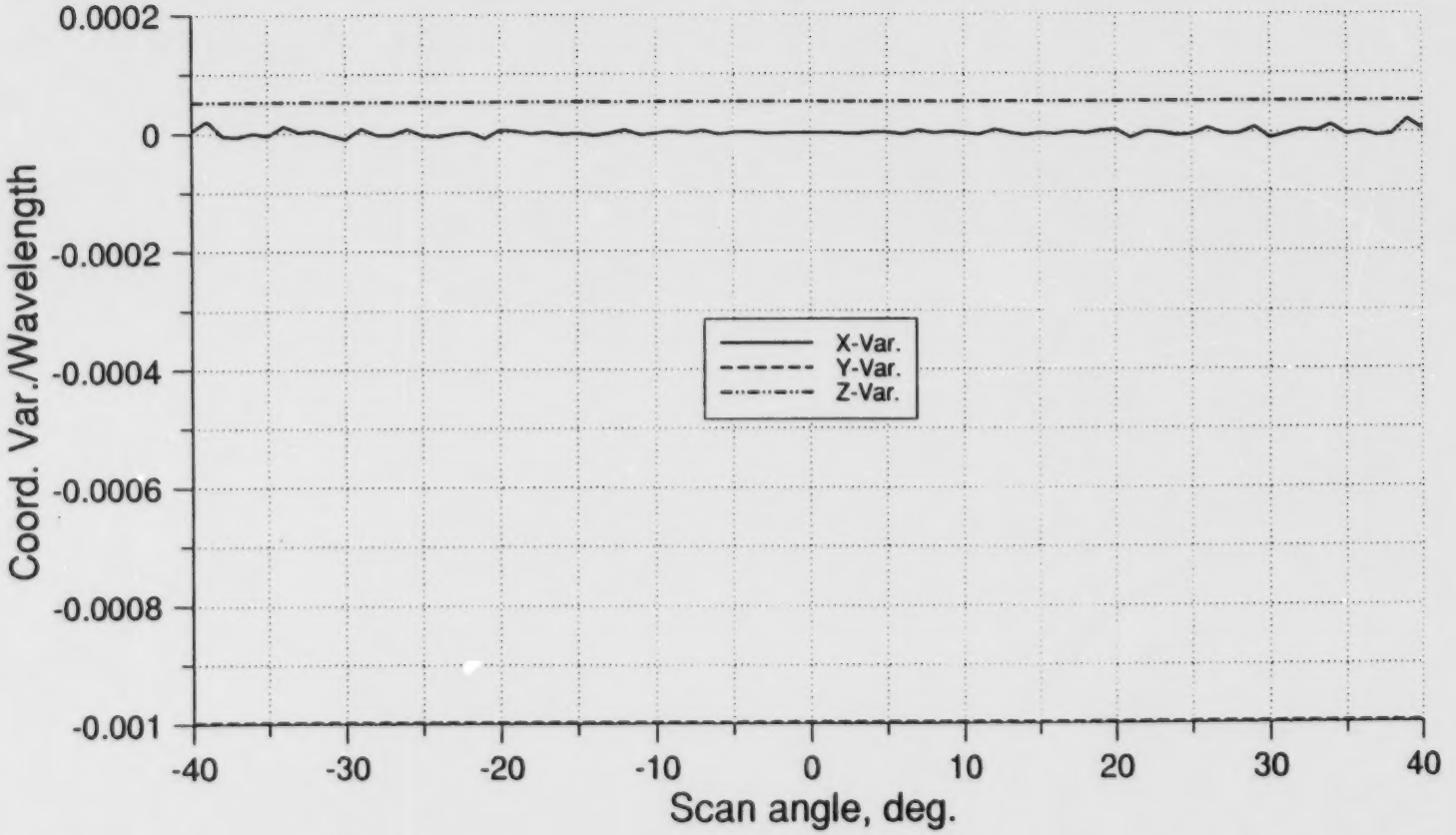

Fig. 6.3 : Thermal expansion of the vertical arrays, copper ($T = 60^{\circ} C$).

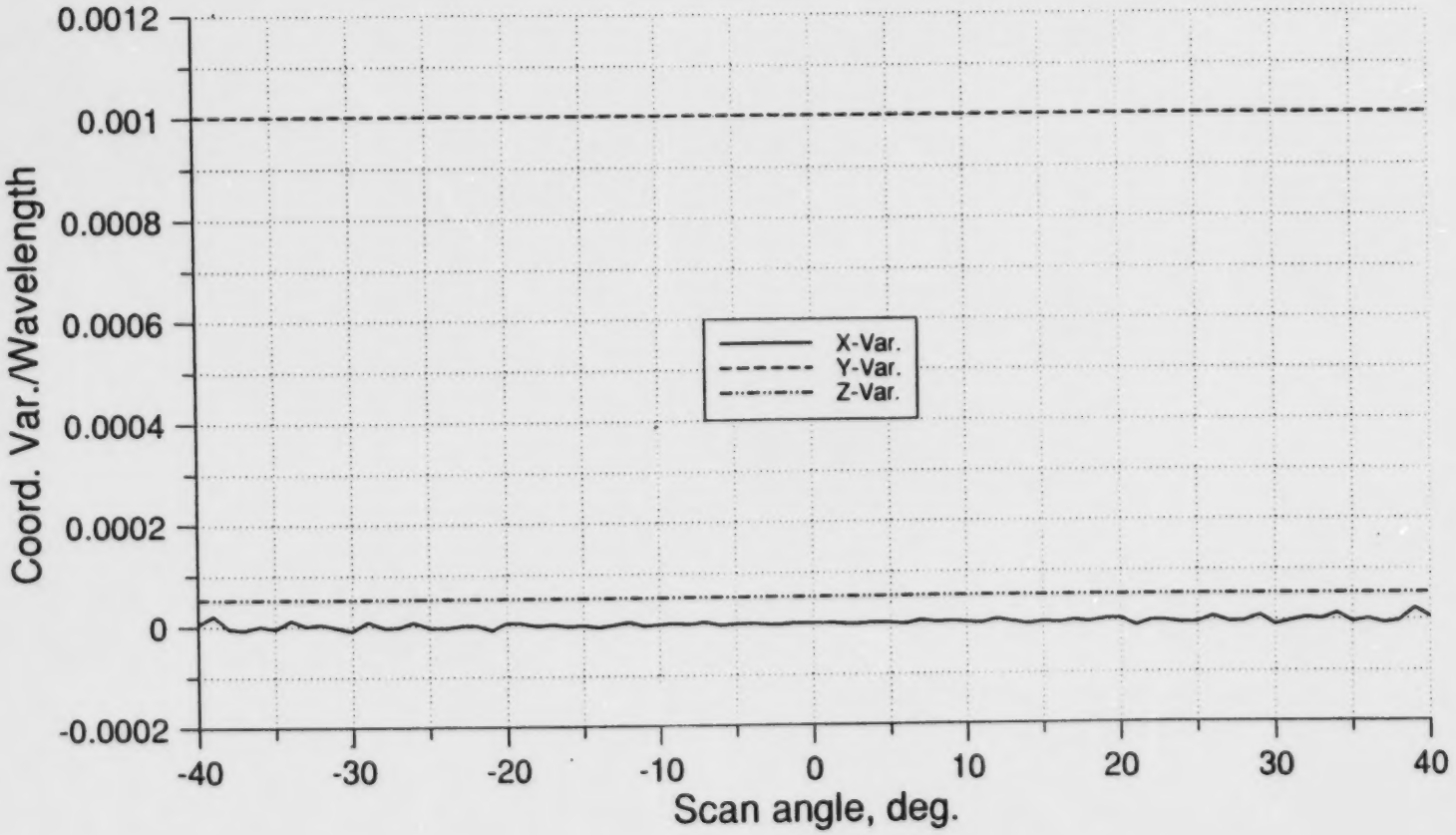

Fig. 6.4 : Thermal contraction of the vertical arrays, copper ($T = -60^{\circ} C$).

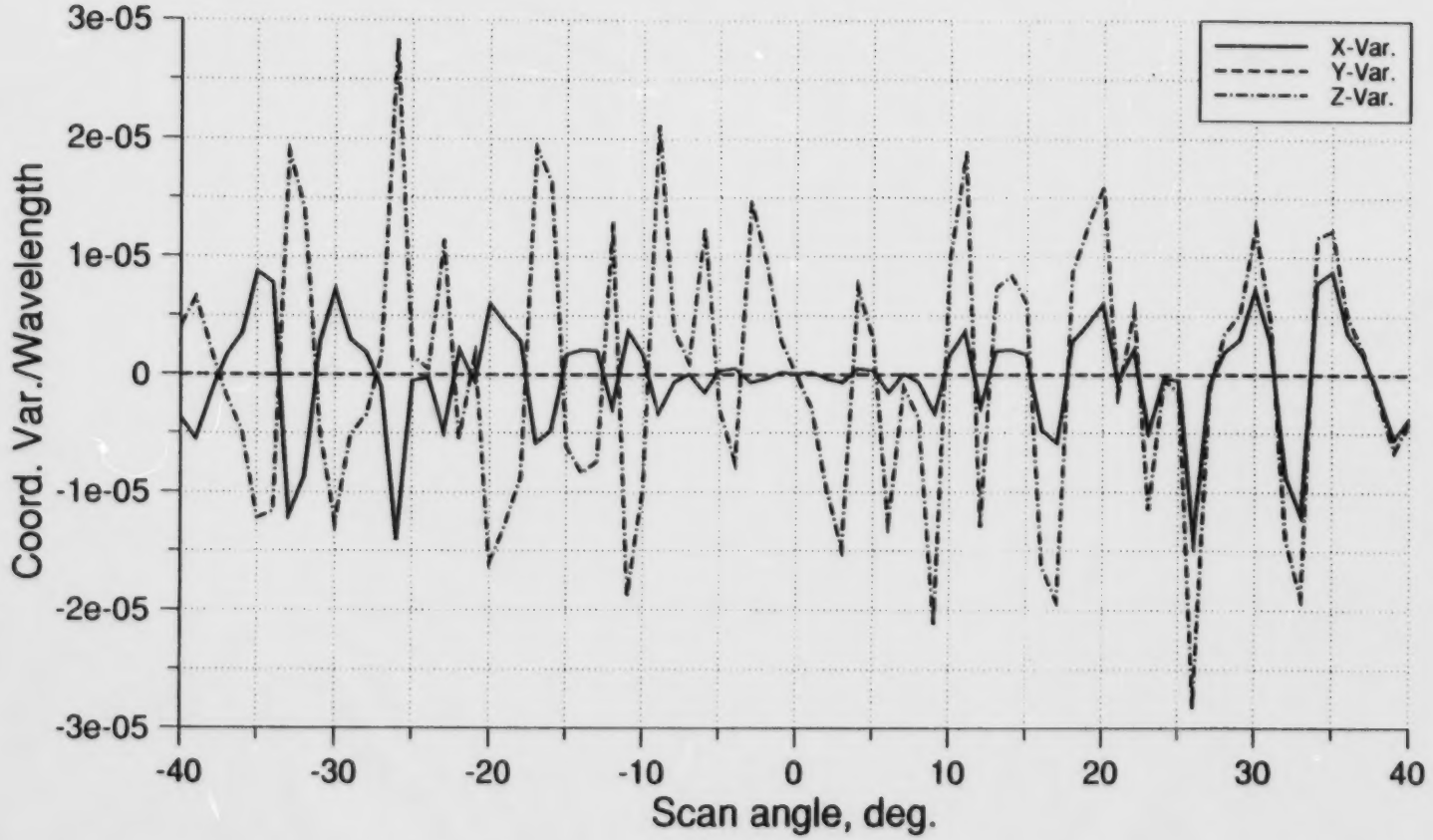

Fig. 6.5 : Thermal expansion of the horizontal arrays, aluminum ($T = 60^{o}\,C$).

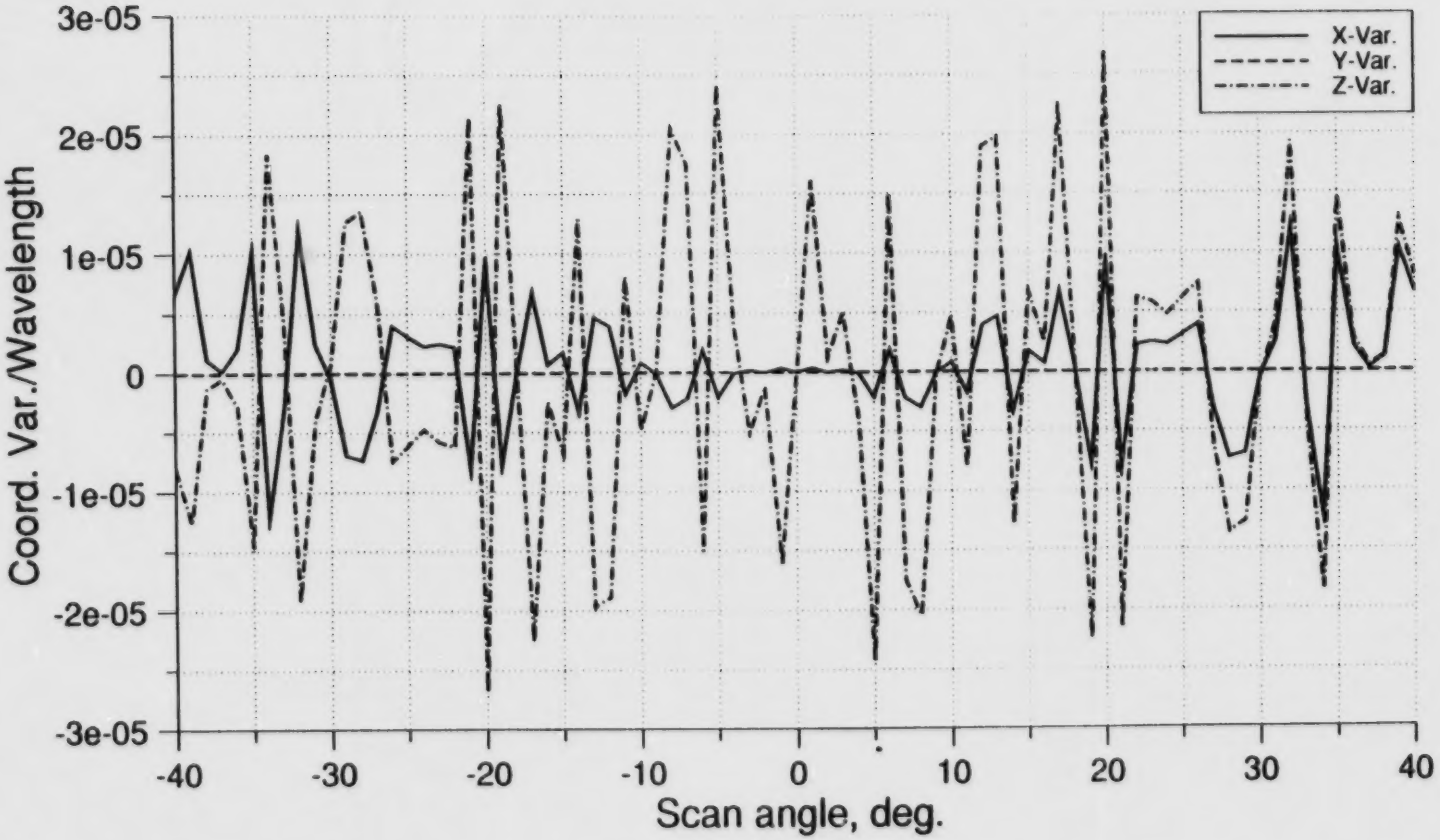

Fig. 6.6 : Thermal contraction of the horizontal arrays, aluminum ($T = -60^{\circ} C$).

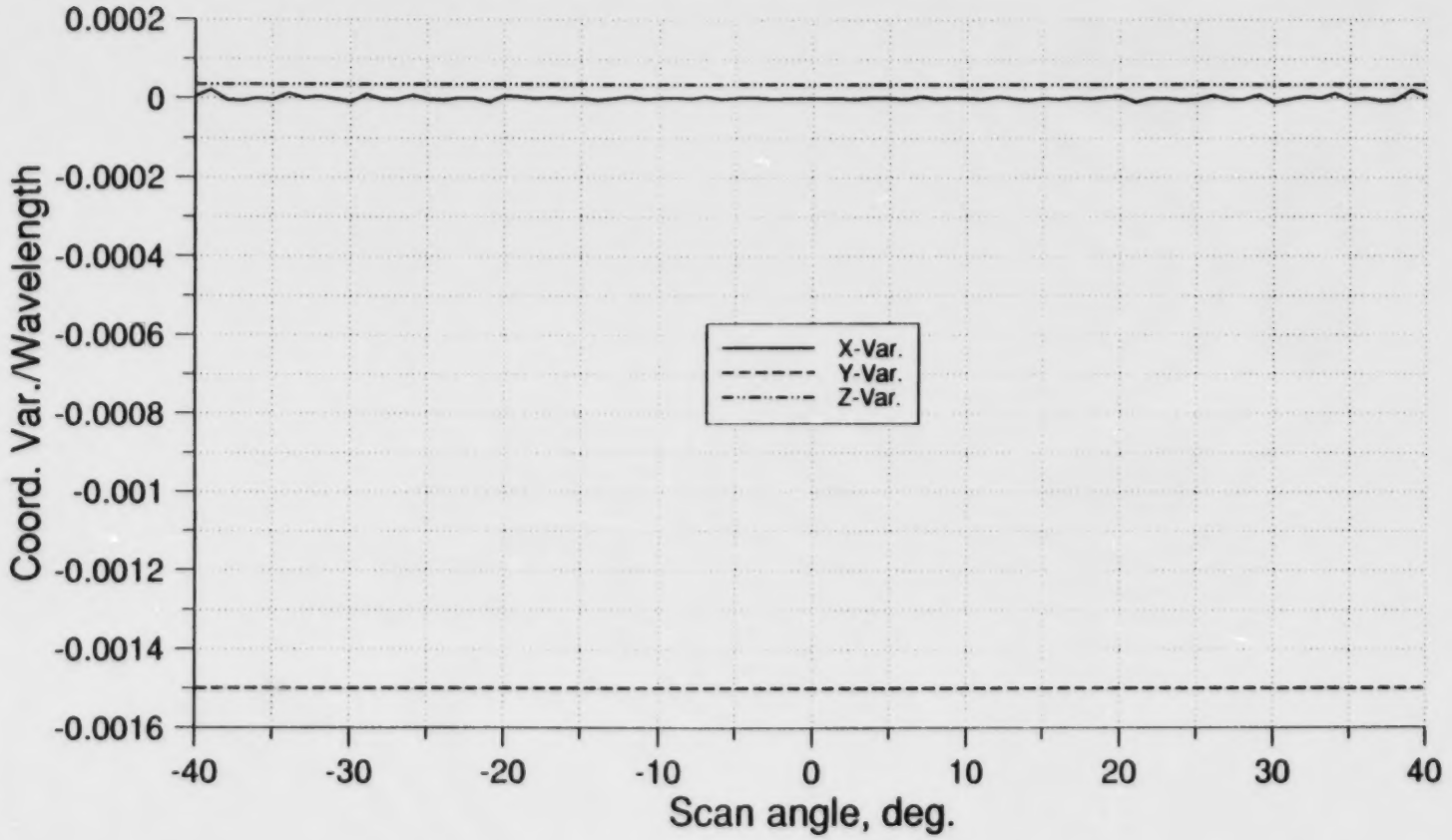

Fig. 6.7 : Thermal expansion of the vertical arrays, aluminum ($T = 60^{o}\,C$).

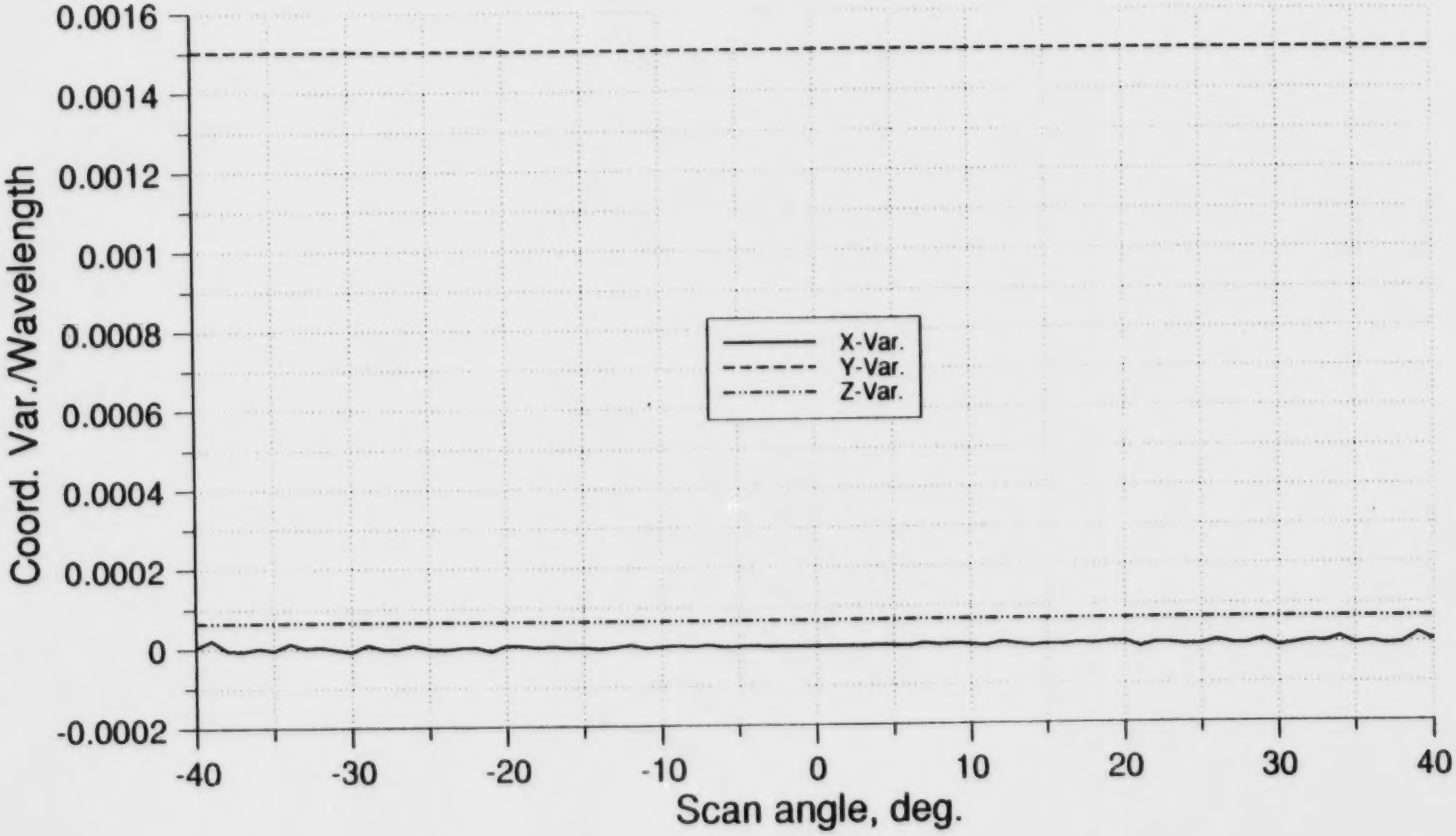

Fig. 6.8 : Thermal contraction of the vertical arrays, aluminum ($T = -60^{o}\,C$).

Chapter 7
Array performance

7.1 Introduction

Amplitude and phase errors as a result of manufacturing, material and environmental tolerances or elements failures may deteriorate the radiation pattern of an antenna. In this chapter we are simulating amplitude and phase errors distributed along an array and presenting their effects on the array radiation pattern. In addition, we are considering the effect of one or more radiating elements failures on an array of 56 elements with a -30 dB Taylor distribution and an interelement spacing d=0.593 λ. The numbering scheme is as follows: we start with number 1 for the far left element and end with element number 56 at the far right edge; the central elements are number 28 on the left side of the geometrical centre of the array and number 29 on the right side of it, as shown in Fig. 2.5. The effect of amplifiers and phase shifters failures on the radiation pattern is studied for two cases:

1) complete amplitude failure, i.e. a failed element receives no power, and

2) complete phase shifter failure, i.e. the phase of a failed element in this case is set to zero and keeping the element's power unaffected.

A computer program has been developed to simulate the effect of errors and elements failures on the performance of *MLS* antennas in terms of main beam power loss, shape, pointing accuracy and width as well as the peak sidelobe level. A linear array with a Taylor distribution is assumed. The number of radiating elements, interelement spacing, operating frequency, design sidelobe level, and the scan angle are input parameters for the error free case. On the other hand, the *rms* values for amplitude and phase errors, number of failed phase shifters and the type of failure as well as the steering algorithm are variable input data to the simulation program. Note that, unless otherwise stated, phase quantization errors due to use of digital phase shifters are not included in the following results.

7.2 Beam/HPBW deviations

A computer program to simulate the performance of an array with specified number of failures is written. Failures can occur on amplifier or phase shifter attached to the radiating element.

Initially the number of failures is specified as an input parameter. For each failed element, the program determines the type of failure, i.e. complete power failure or phase shifter failure, and then computes the corresponding radiation pattern. The results for the error free case are shown in Fig. 7.1 for scan angle $\theta_s = 0$ and in Fig. 7.2 for scan angle of 40^o.

The radiation pattern corresponding to a single and two symmetric elements phase failures are shown, respectively, in Figs. 7.3 and 7.4, for scan angle of 40^o. In both cases the peak sidelobe level deteriorates from the design theoretical value and the average values are higher for the two symmetrical elements failure. Another effect, due to elements failure, is that the beam peak will no longer be located at θ_s but instead will move to a point θ_s'. The angular error is thus defined by

$$\Delta\theta_s = \theta_s' - \theta_s \tag{7.1}$$

In addition, both the 3 dB beam width (HPBW) and the beam peak in the direction of the pointing angle are affected by such failures.

7.2.1 Element Failure

The results for selected cases of element by element failure, i.e. one at a time, are shown in Figs. 7.5-7.8. The case of a phase shifter failure is shown in Fig. 7.5 for $\theta_s = 20^o$ and in Fig. 7.6 for $\theta_s = 40^o$. The corresponding results for amplitude failures are shown in Figs. 7.7 and 7.8. It is clear from these figures that the most severe effect on the pointing angle corresponds to phase failures, in particular, when failures occur in the mid region (elements 12-16 or 40-44) of each side of the array. On the other hand, the effect of amplitude failure on the pointing angle is negligible.

The effect of simultaneous two symmetrical elements failure is shown in Figs. 7.9 and 7.10 for phase failures and in Figs. 7.11 and 7.12 for amplitude failures. It is clear from these figures that the effect of two symmetrical failures is stronger than the effect of a single failure.

7.2.2 Amplitude/Phase Errors

The effects of pre-determined phase (10^o) and amplitude (10%) errors which are introduced to individual elements are shown, respectively, in Figs. 7.13 and 7.14 for $\theta_s = 20^o$ and in Figs. 7.15 and 7.16 for $\theta_s = 40^o$. Again the effects of phase errors are more pronounced, but much less compared with phase failures as shown in Figs. 7.5 and 7.6.

Statistical analysis for the effect of random errors on the far-field radiation pattern of a phased array antenna was carried out in a previous study [25], where the mean values of the loss in the radiated power, the pointing error and the peak sidelobe level were given in terms of the variances of the amplitude and phase errors. Numerical results were also given to relate the allowable tolerances of errors to the desired pattern with a given probability. In this section, a simulation on the computer of both random amplitude and phase errors is given.

In the simulation program, the variances of the amplitude and phase errors across the array are input data. For each value(s), we calculate the corresponding radiation pattern. Initially, the optimal excitation distribution is determined. Next two sets (56 each) of normal random numbers are generated with zero means to be used to simulate the amplitude and phase errors. Each of these two sets is then multiplied by the corresponding *rms* σ (i.e., σ_a *or* σ_p) to yield the amplitude and phase errors of each radiating element. These random errors are then added to their respective excitation coefficients. The radiation pattern for each case is then computed and the pointing error is calculated. The results, as a function of the scan angle, are shown in Figs. 7.17 and 7.18 for two different sets of random numbers. It is clear that, for both cases, the magnitude of the error in the pointing angle is of the same order. This should not be considered a general conclusion. In fact, one should run few thousand cases to reach a reasonable conclusion. The effects of combined amplitude and phase random errors on the pointing angle and the 3 dB beam width are shown in Figs. 7.19 and 7.20. The error in the pointing angle is much larger compared with the phase only errors cases.

7.2.3 Thermal expansion/contraction

A model based on the linear expansion of metals has been presented in Chapter 6. Assuming a uniform spatial variation of antenna elements, for a selected temperature variation, one can modify the element spacing d by adding (for expansion) or subtracting (for contraction) a fixed amount Δd.

Figs. 7.21 and 7.22 show the variation in the pointing angle and HPBW due to a thermal expansion or contraction of 0.01 mm per element. This corresponds to a total expansion or contraction of 0.55 mm across the array which may result due to a temperature variation of about $60^{o}C$ from the operating temperature. Uniform expansions or contractions are assumed. The maximum error in the pointing angle occurs at $\pm 40^{o}$ and it is of order 0.015 deg. For a thermal expansion/contraction of 0.05 mm/element, the pointing error could be as large as 0.07 deg., as shown in Figs. 7.23 and 7.24. Finally, The results corresponding to a thermal expansion of 0.1 mm/element is shown in Fig. 7.25. It should be noted that the effect of thermal expansions/contractions on the phase centre coordinates and HPBW is minor compared with that on the pointing angle.

7.3 Sidelobe / peak power levels

The effect of element failures on the sidelobe (SL) and power level at the pointing angle (P_{max}) is shown in Fig. 7.26 for phase shifters failure and in Fig. 7.27 for amplitude failure. These figures show the increase in the sidelobe level ΔSL and the drop in the power level at the pointing angle from their respective optimal values. Again, the most severe effect is due to the phase failure and in particular when it occurs at central elements (where the input power is maximum). The peak sidelobe level, in both cases, is better than -20 dB.

Finally, the increase in the sidelobe and the drop in the maximum power levels corresponding to two simultaneous and symmetrical elements failures are given in Fig. 7.28 for phase failure and in Fig. 7.29 for amplitude failure. It can be seen that the peak sidelobe level exceeds -20 dB level when the failure occurs in two central elements. On the other hand, an amplitude failure for any two symmetrical elements results in a peak sidelobe level of better than -20 dB.

7.4 Discussion

In this chapter, a numerical simulation has been developed to investigate, theoretically, the effect of element failures and errors on the azimuth radiation pattern of the *MLS* antenna. Both amplifier and phase shifter failures together with amplitude and phase errors across the array were discussed. Quantization phase errors due to the use

of digital phase shifters were not included in this chapter, but their effects will be presented at the end of this report. Also presented was the effect of uniform thermal expansions/contractions on the pointing angle.

It was found that the shapes of the main beam and sidelobes as well as the pointing angle were significantly affected by the phase errors and phase shifter failures. Amplitude failures and/or errors did not have as much influence. It was also found that the pointing angle error was significantly affected by the thermal expansions/contractions.

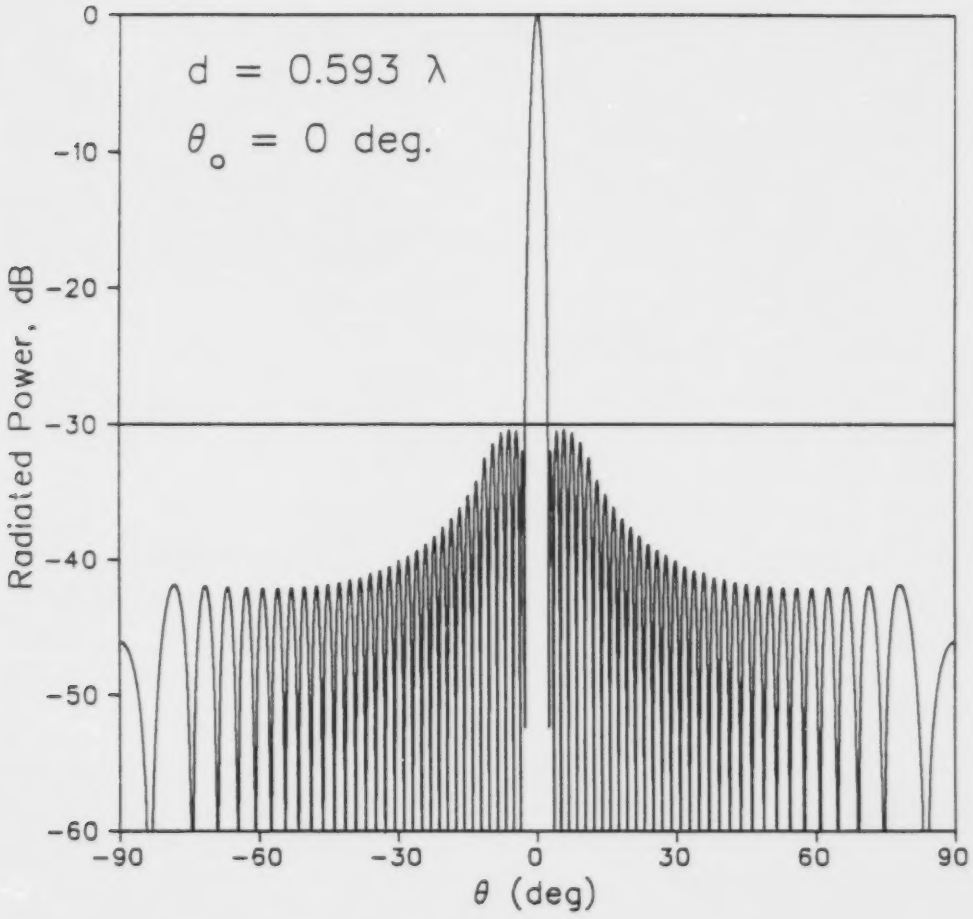

Fig. 7.1: Radiation pattern of a 56-element array with -30 dB Taylor distribution, 0 scan angle.

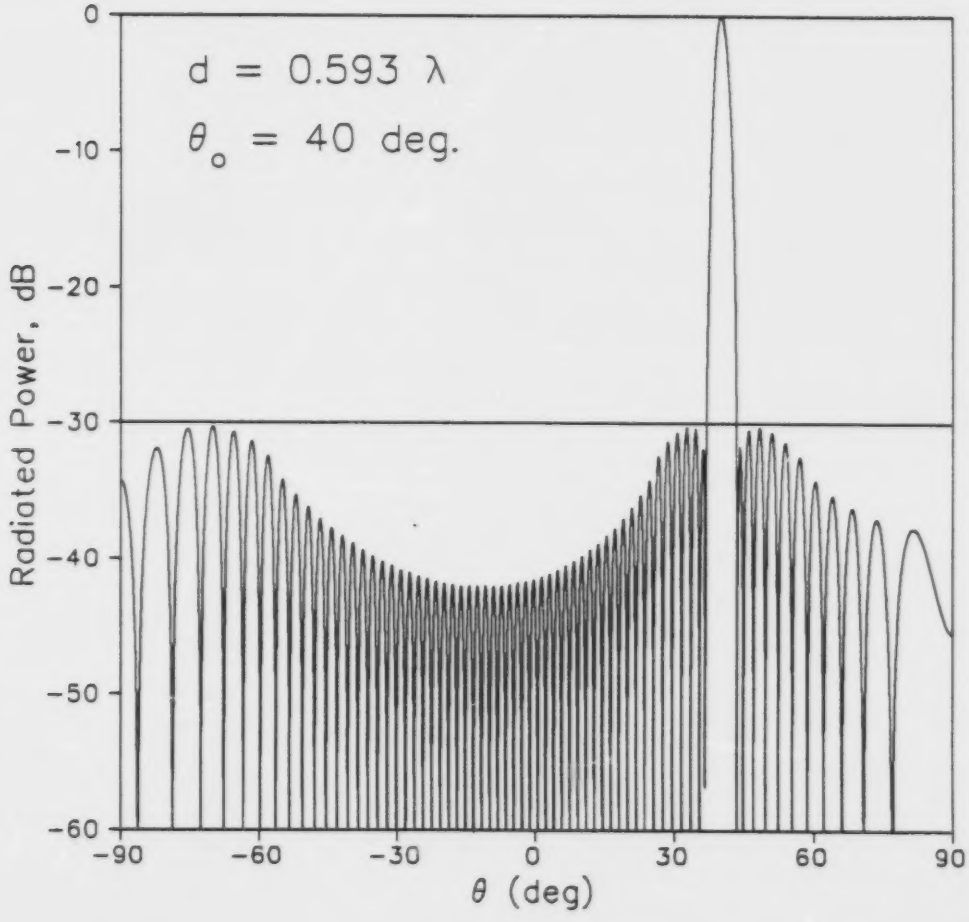

Fig. 7.2: Radiation pattern of a 56-element array with -30 dB Taylor distribution, 40 deg. scan angle.

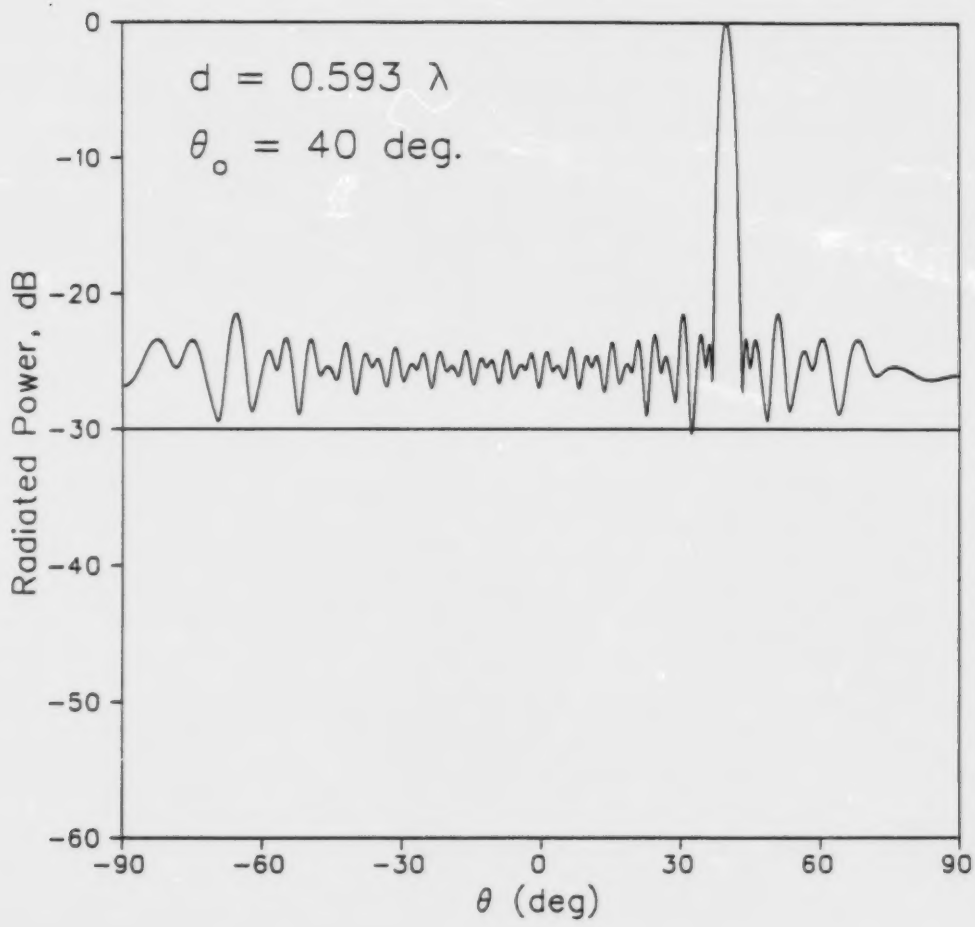

Fig. 7.3: Effect of one phase shifter failure (#22) on array pattern of Fig. (7.2).

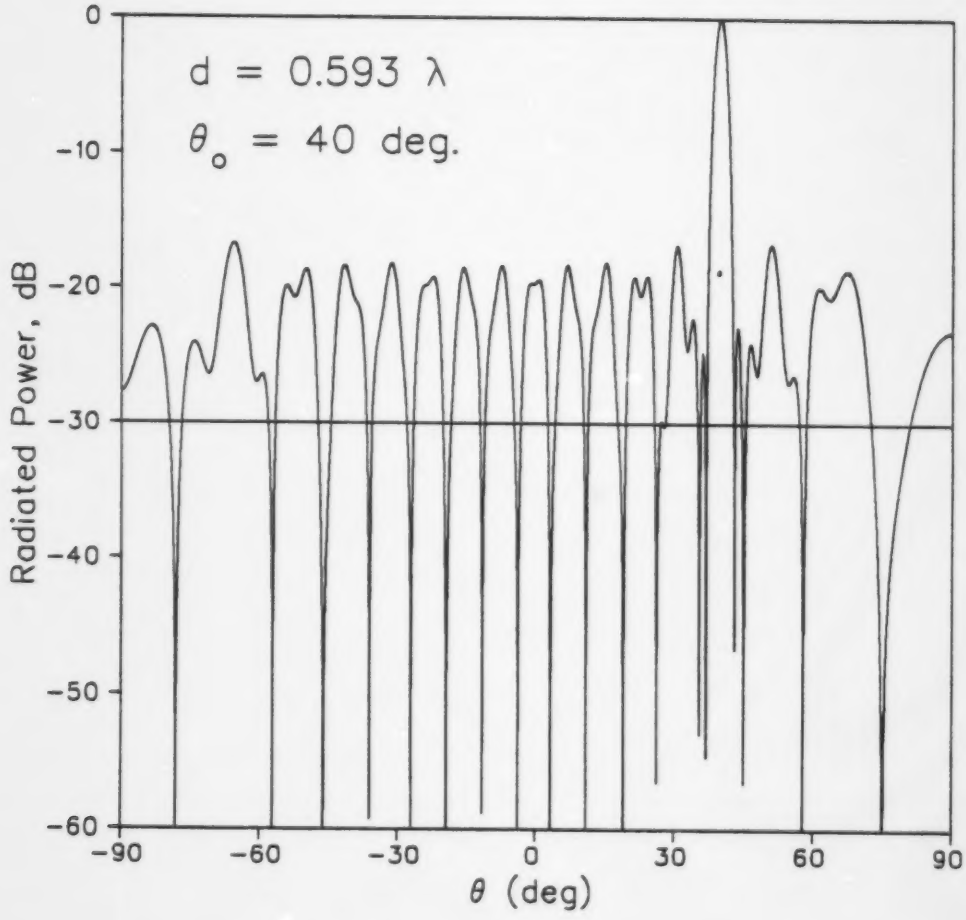

Fig. 7.4: Effect of two symmetrical phase shifters failure (# 22 & 35) on array pattern of Fig. 7.2.

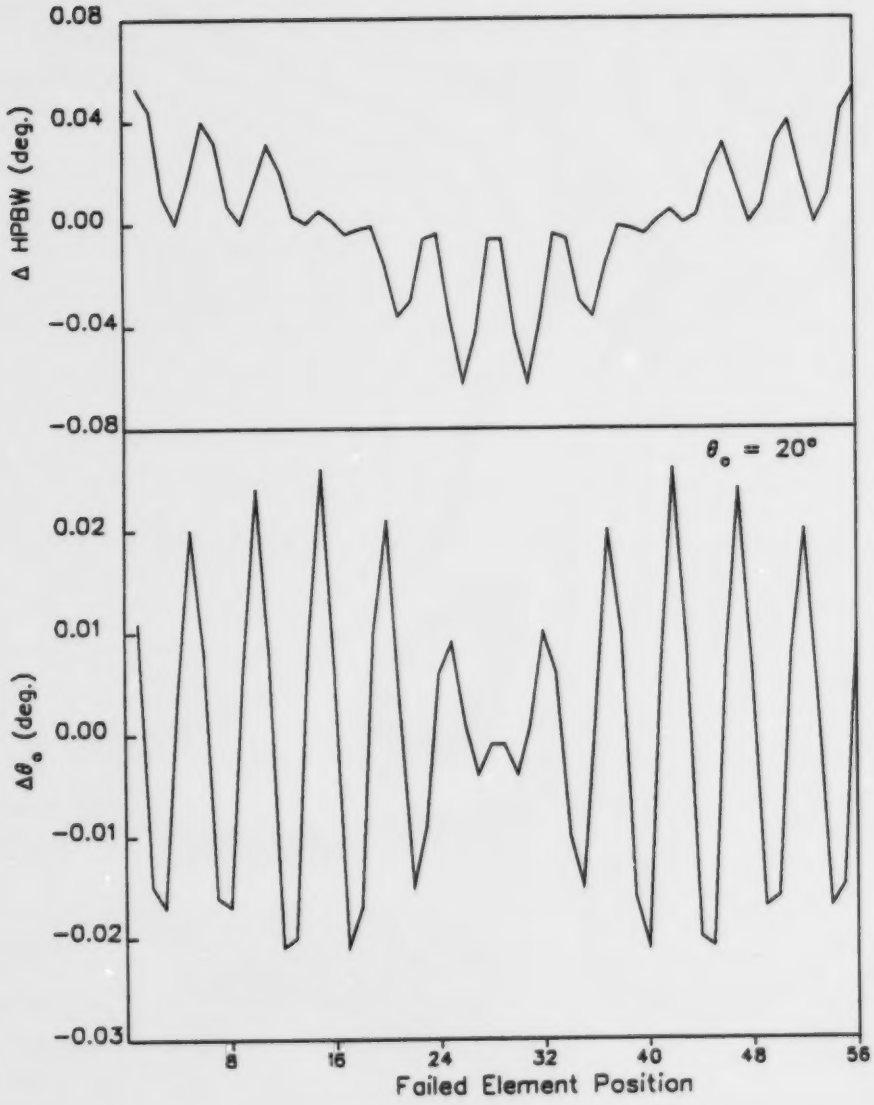

Fig. 7.5: Pointing and beam width errors due to a single phase shifter failure at 20 deg. scan angle.

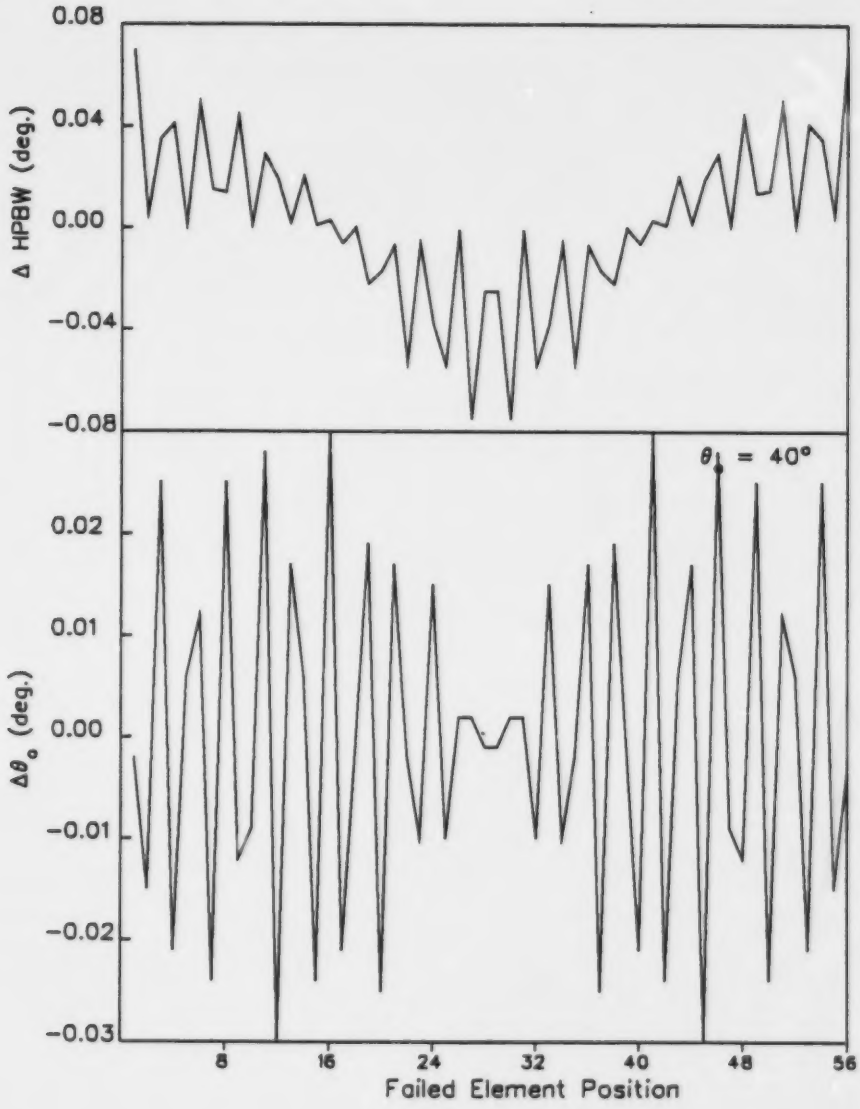

Fig. 7.6: Pointing and beam width errors due to a single phase shifter failure at 40 deg. scan angle.

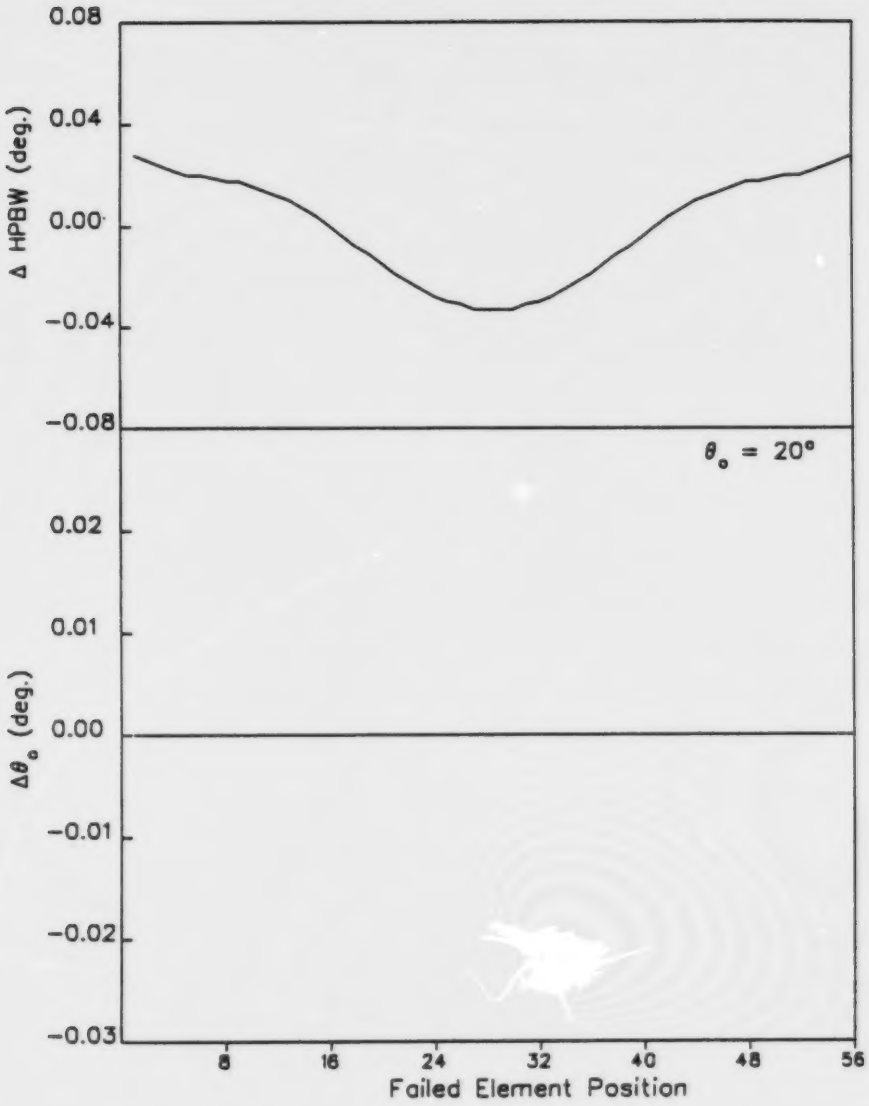

Fig. 7.7: Pointing and beam width errors due to a single amplifier failure at 20 deg. scan angle.

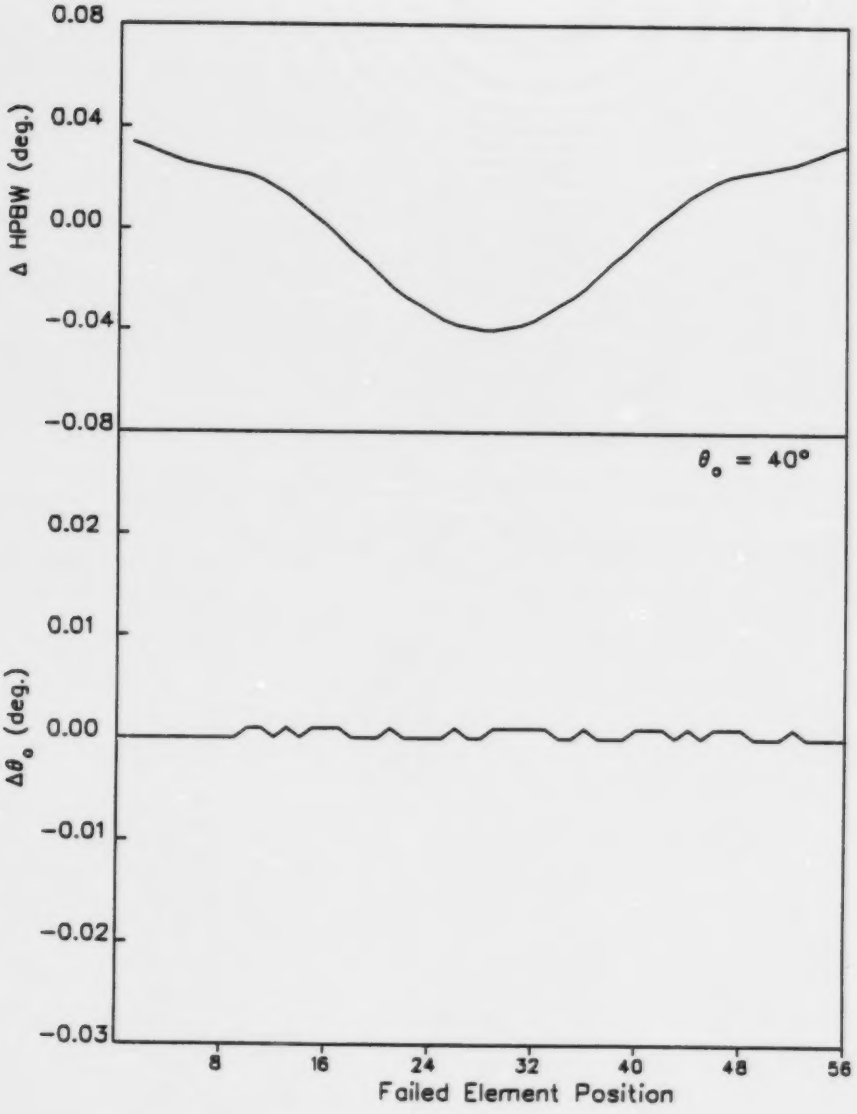

Fig. 7.8: Pointing and beam width errors due to a single amplifier failure at 40 deg. scan angle.

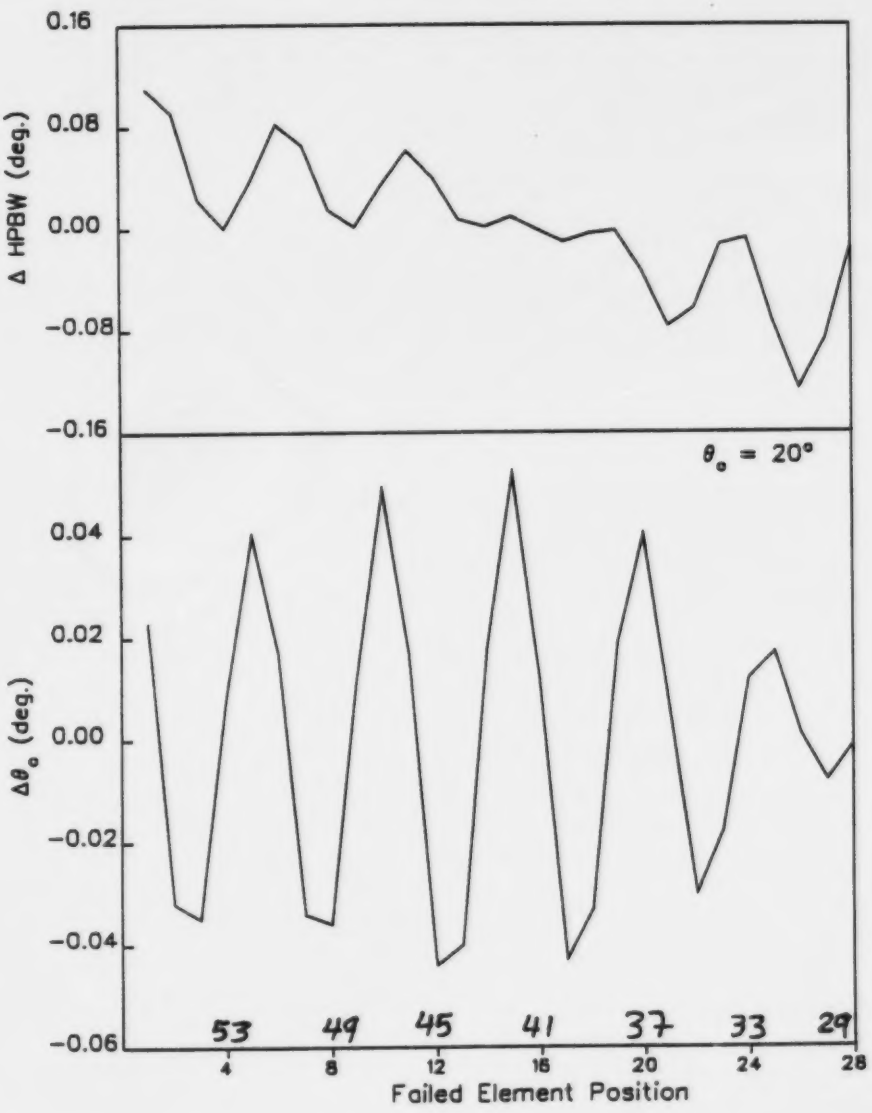

Fig. 7.9: Pointing and beam width errors due to two symmetrical phase shifters failure at 20 deg. scan angle.

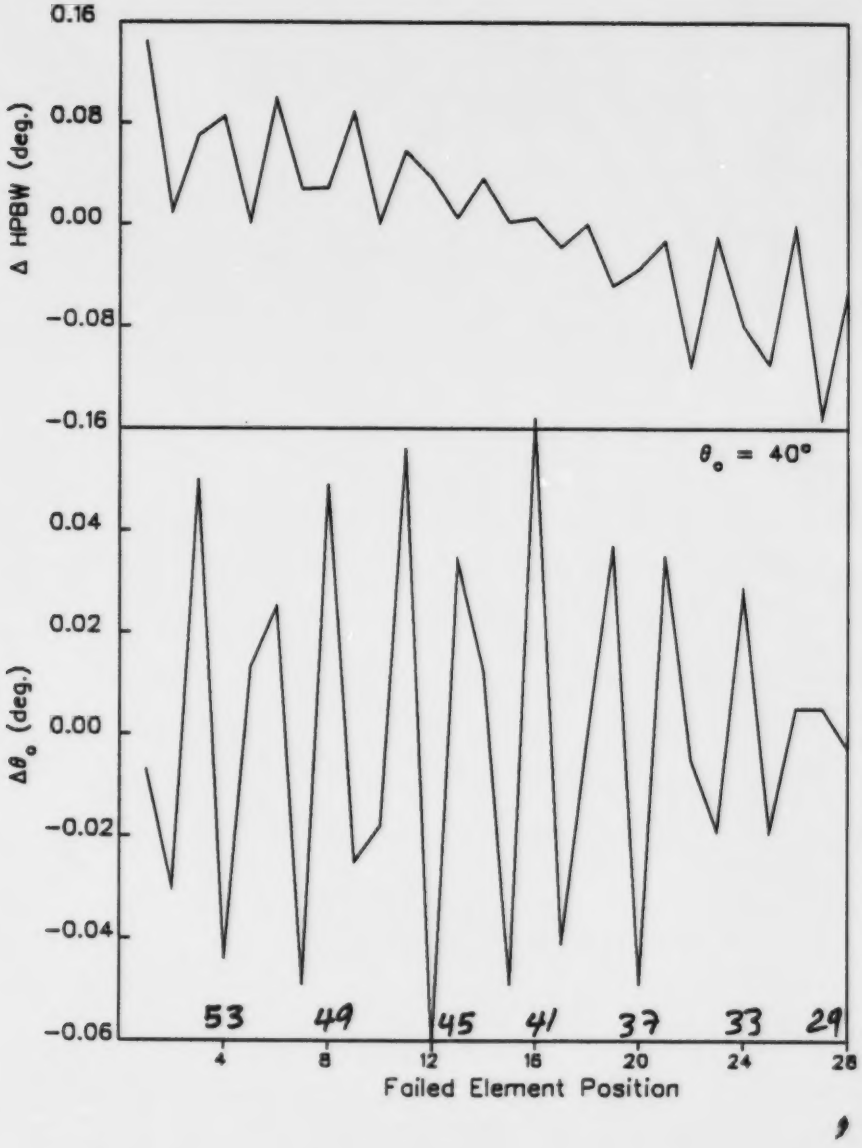

Fig. 7.10: Pointing and beam width errors due to two symmetrical phase shifters failure at 40 deg. scan angle.

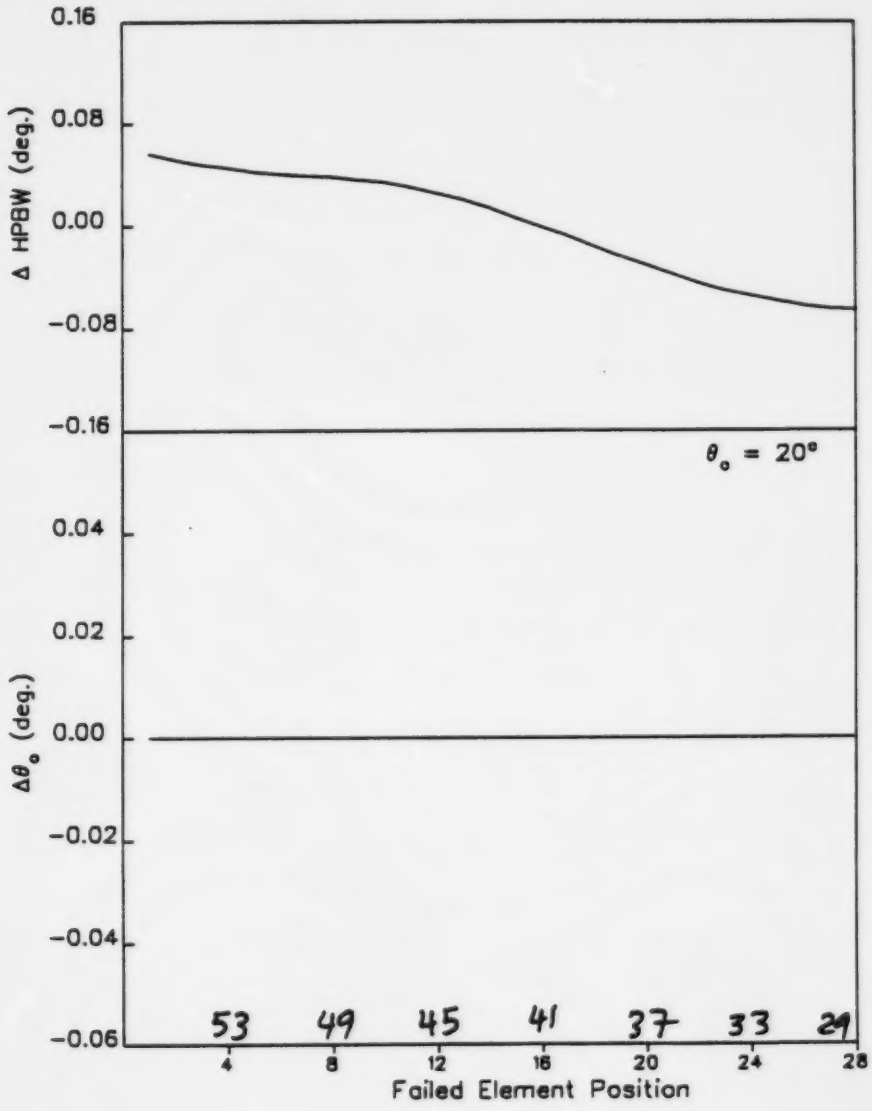

Fig. 7.11: Pointing and beam width errors due to two symmetrical amplifiers failure at 20 deg. scan angle.

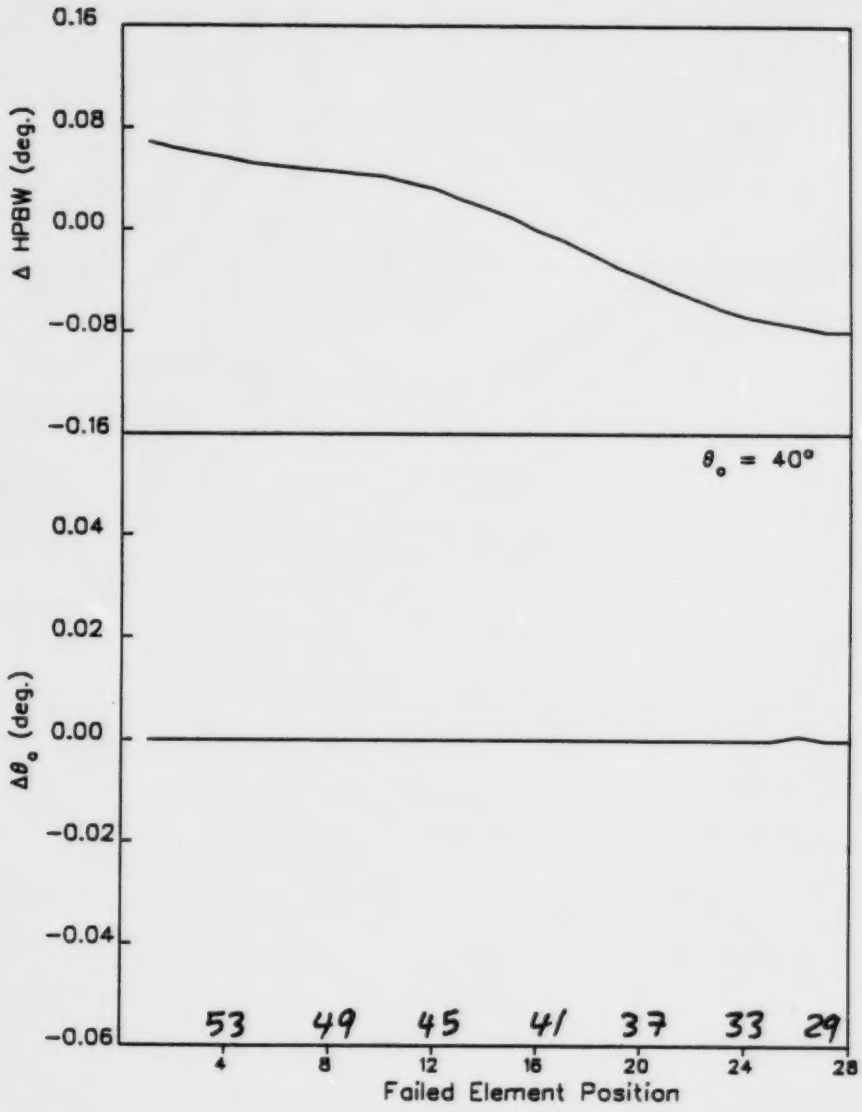

Fig. 7.12: Pointing and beam width errors due to two symmetrical amplifiers failure at 40 deg. scan angle.

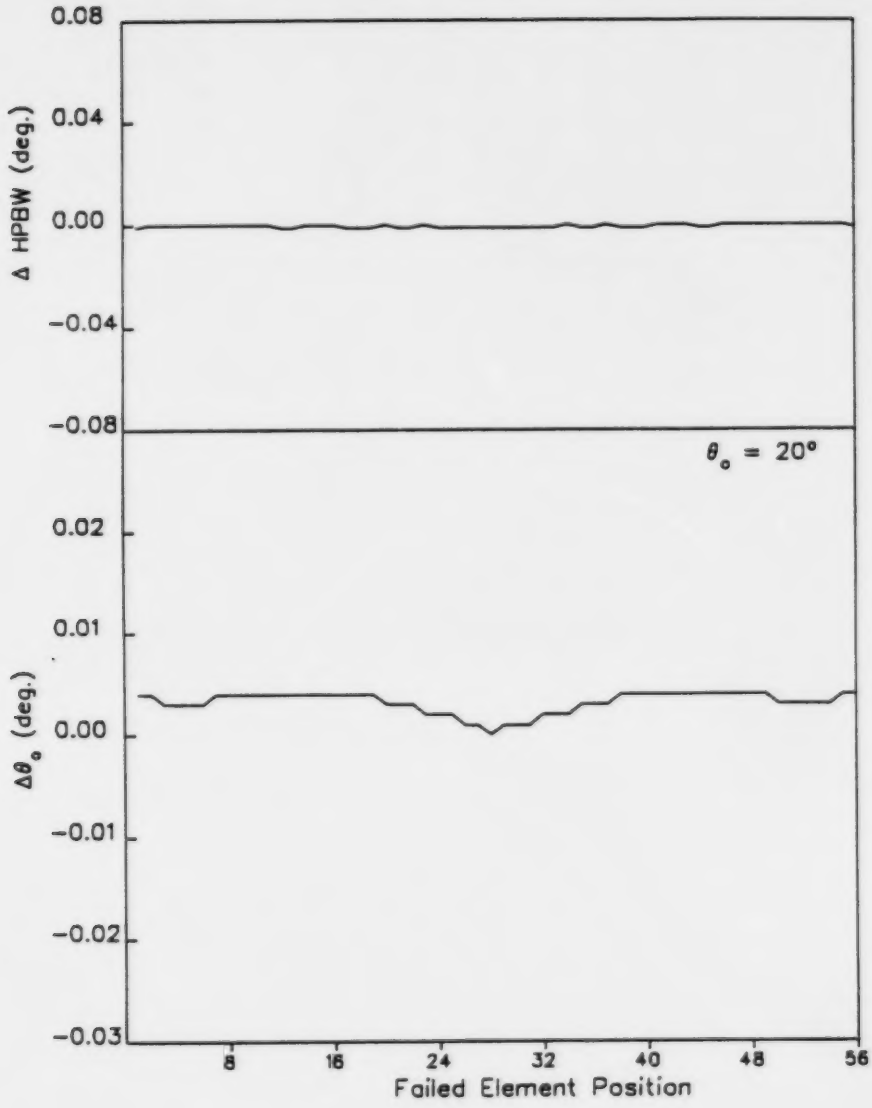

Fig. 7.13: Pointing and beam width errors due to a 10 deg. phase error added to each element (one at a time) at 20 deg. scan angle.

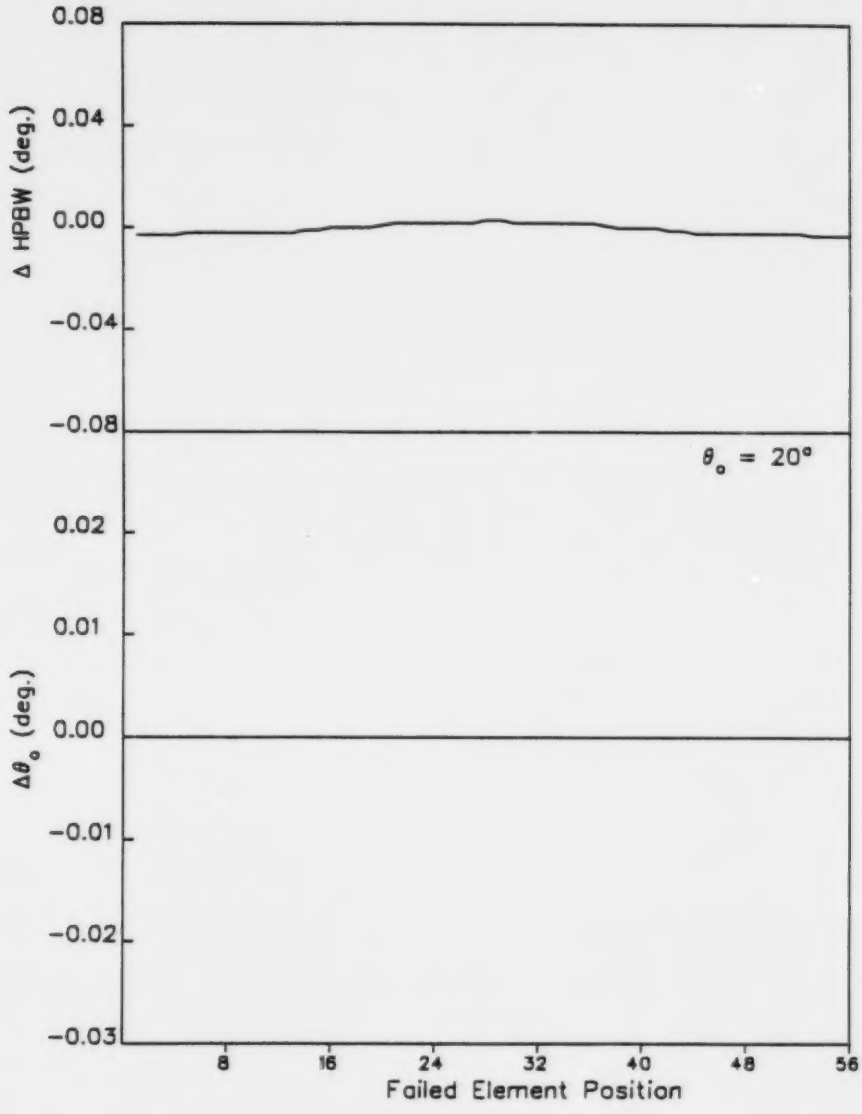

Fig. 7.14: Pointing and beam width errors due to a 10% amplitude error added to each element (one at a time) at 20 deg. scan angle.

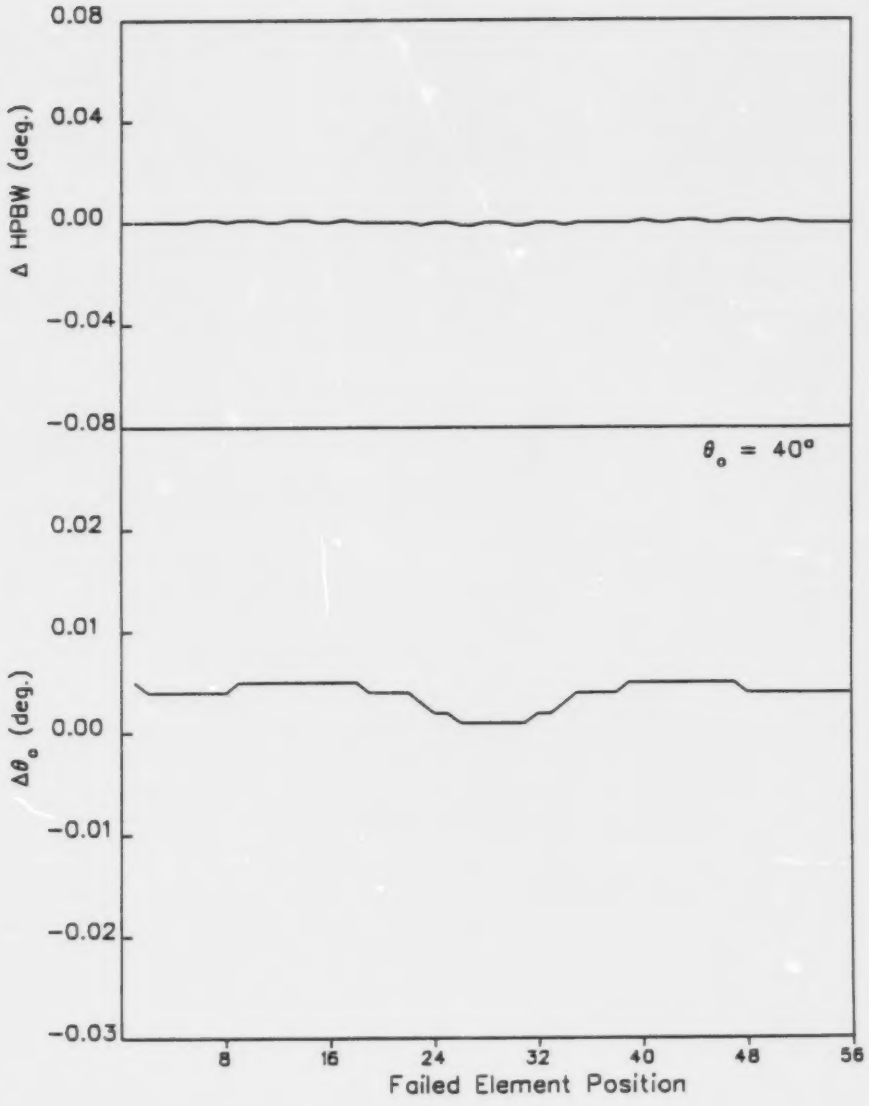

Fig. 7.15: Pointing and beam width errors due to a 10 deg. phase error added to each element (one at a time) at 40 deg. scan angle.

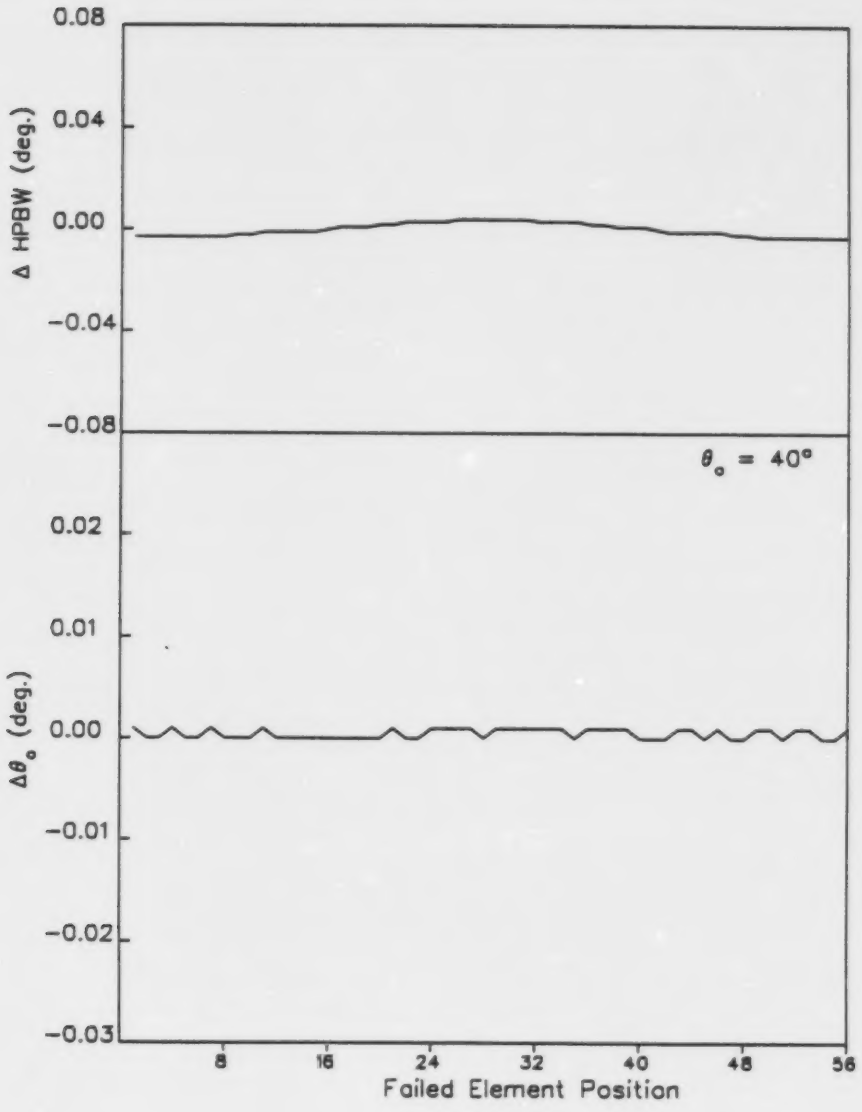

Fig. 7.16: Pointing and beam width errors due to a 10% amplitude error added to each element (one at a time) at 40 deg. scan angle.

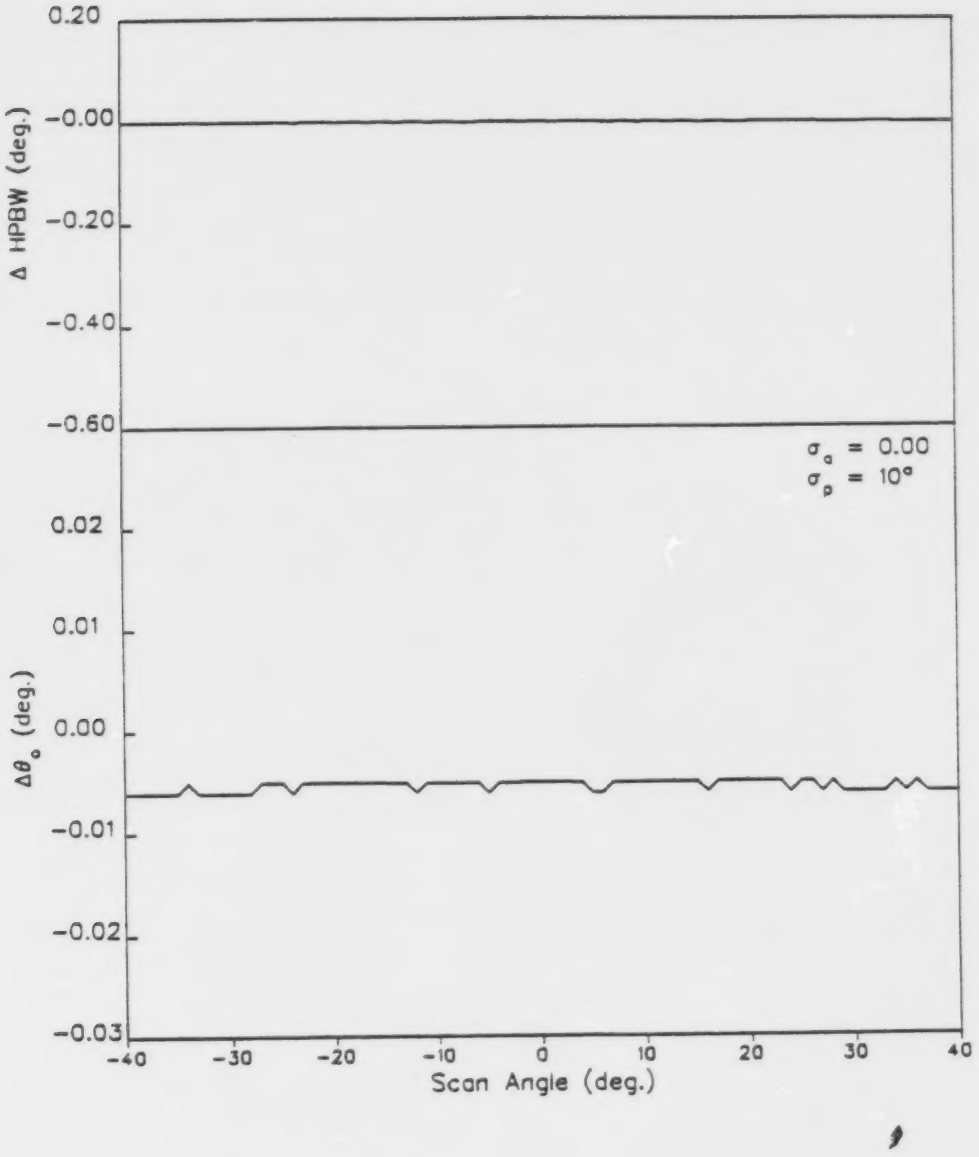

Fig. 7.17: Pointing and beam width errors due to random phase errors, with rms = 10 deg. across the array, added to all elements.

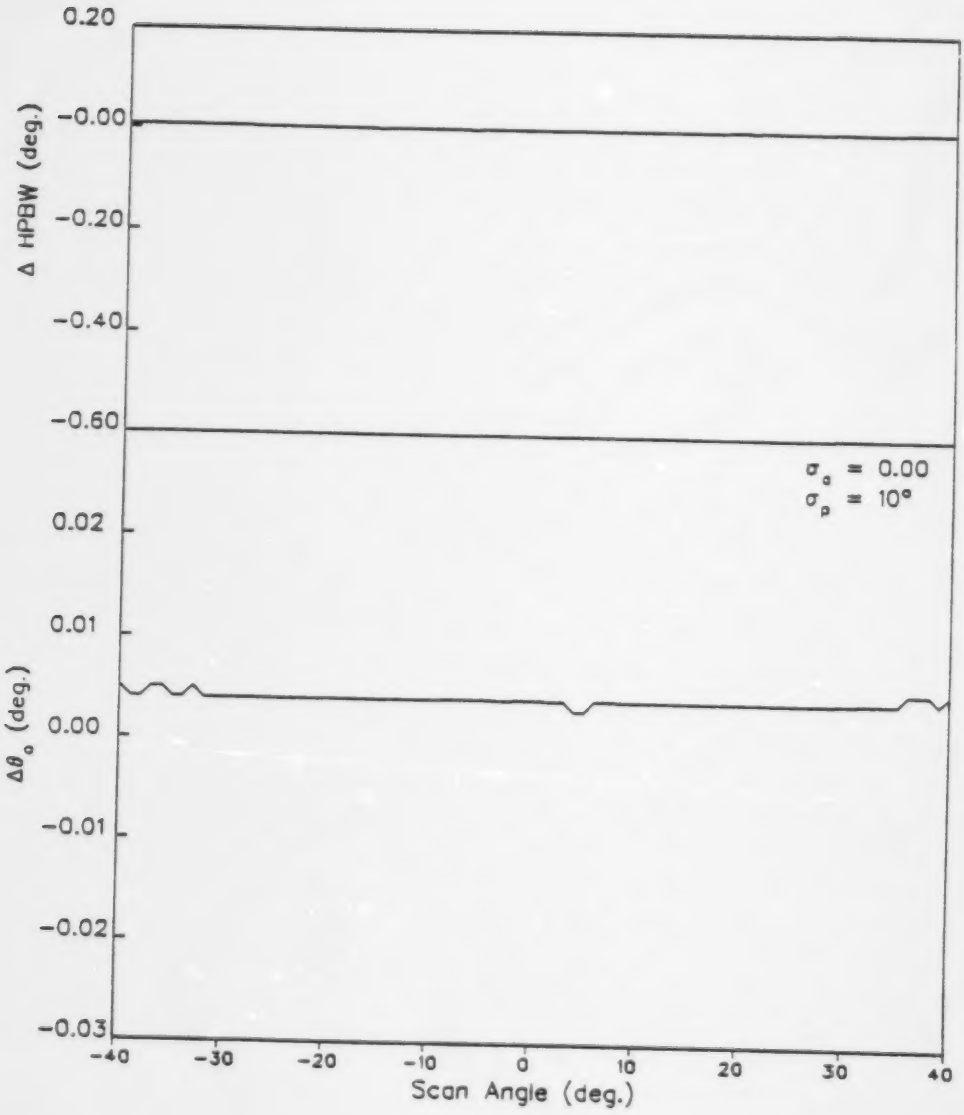

Fig. 7.18: Same as in Fig. 7.17, but with another set of random phase errors, with rms = 10 deg. across the array, added to all elements.

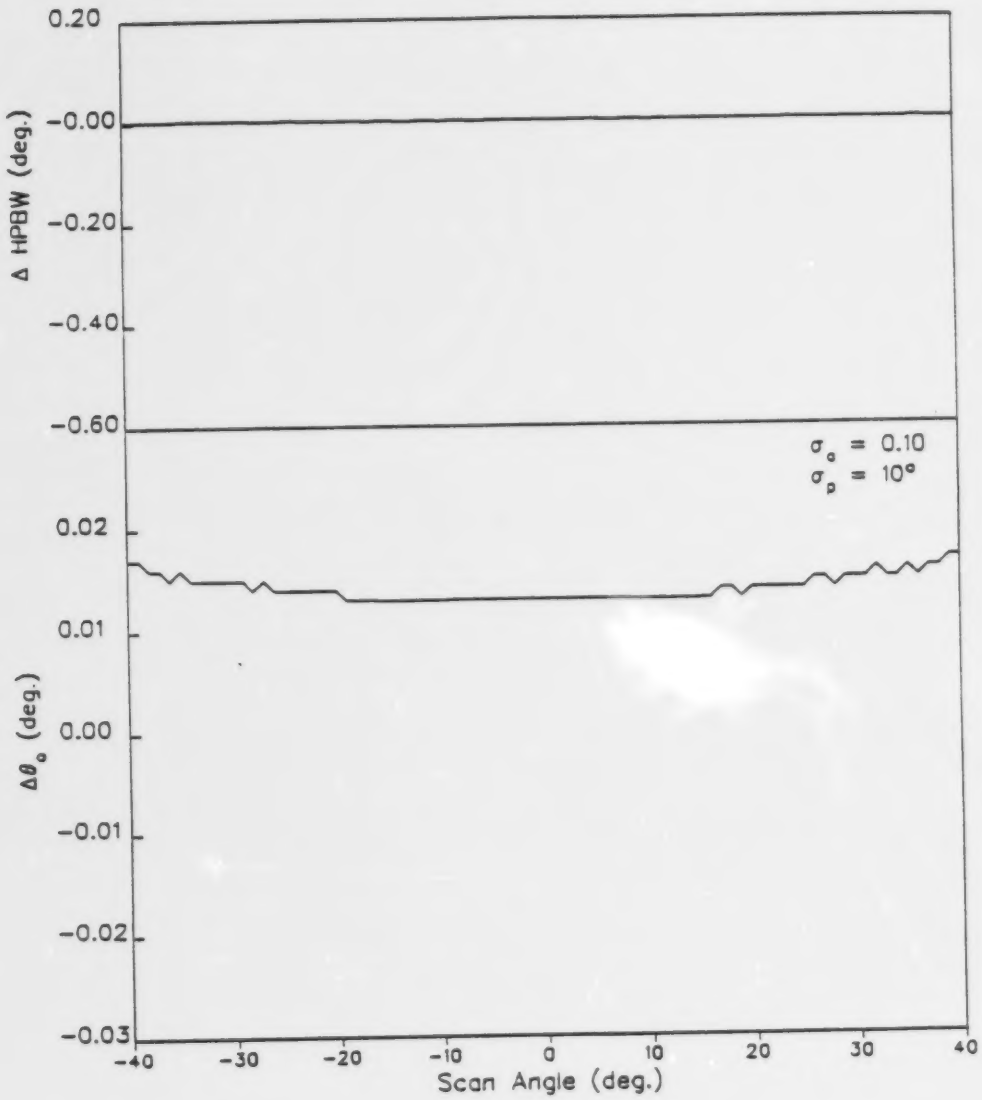

Fig. 7.19: Pointing and beam width errors due to combined random phase (rms = 10 deg) and amplitude (rms = 10%) errors add to all elements.

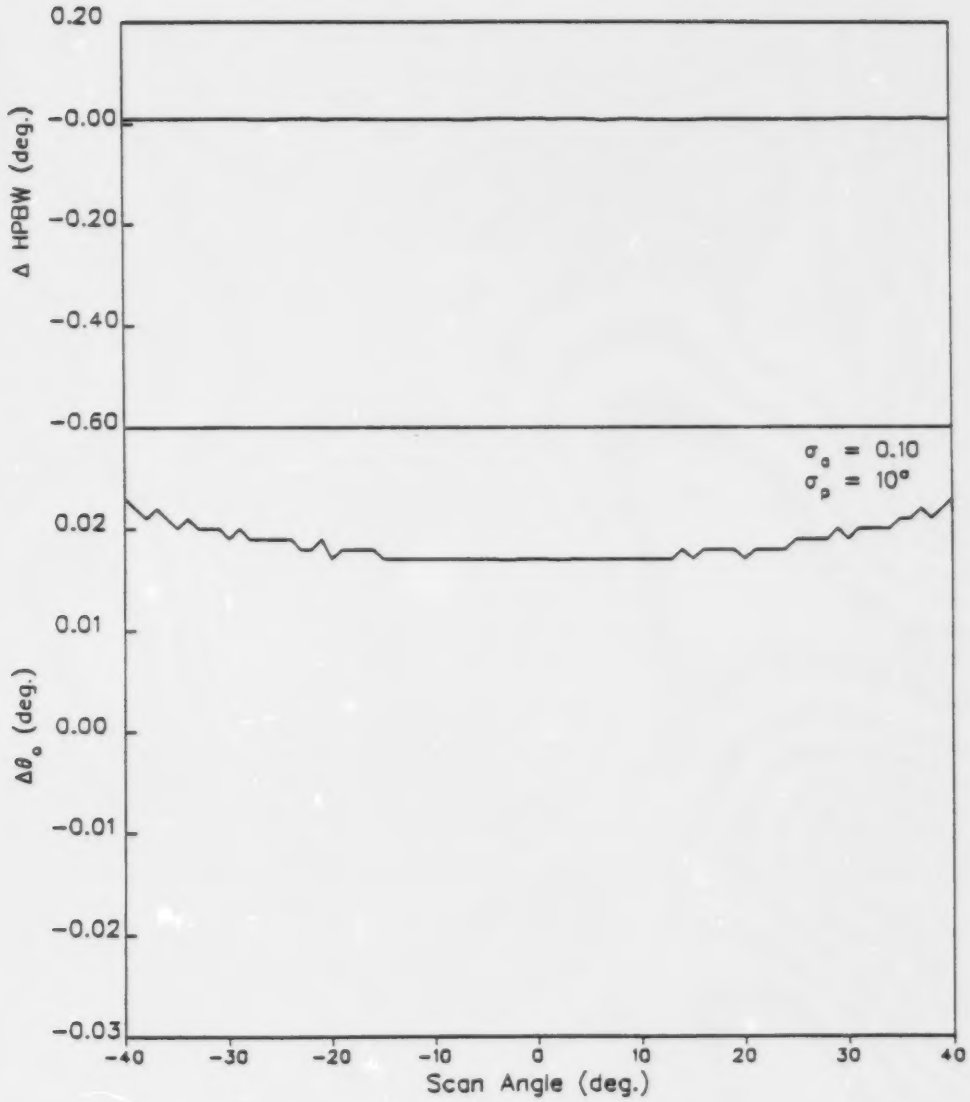

Fig. 7.20: Same as in Fig. 7.19, but with another set of combined random phase (rms = 10 deg) and amplitude (rms = 10%) errors add to all elements.

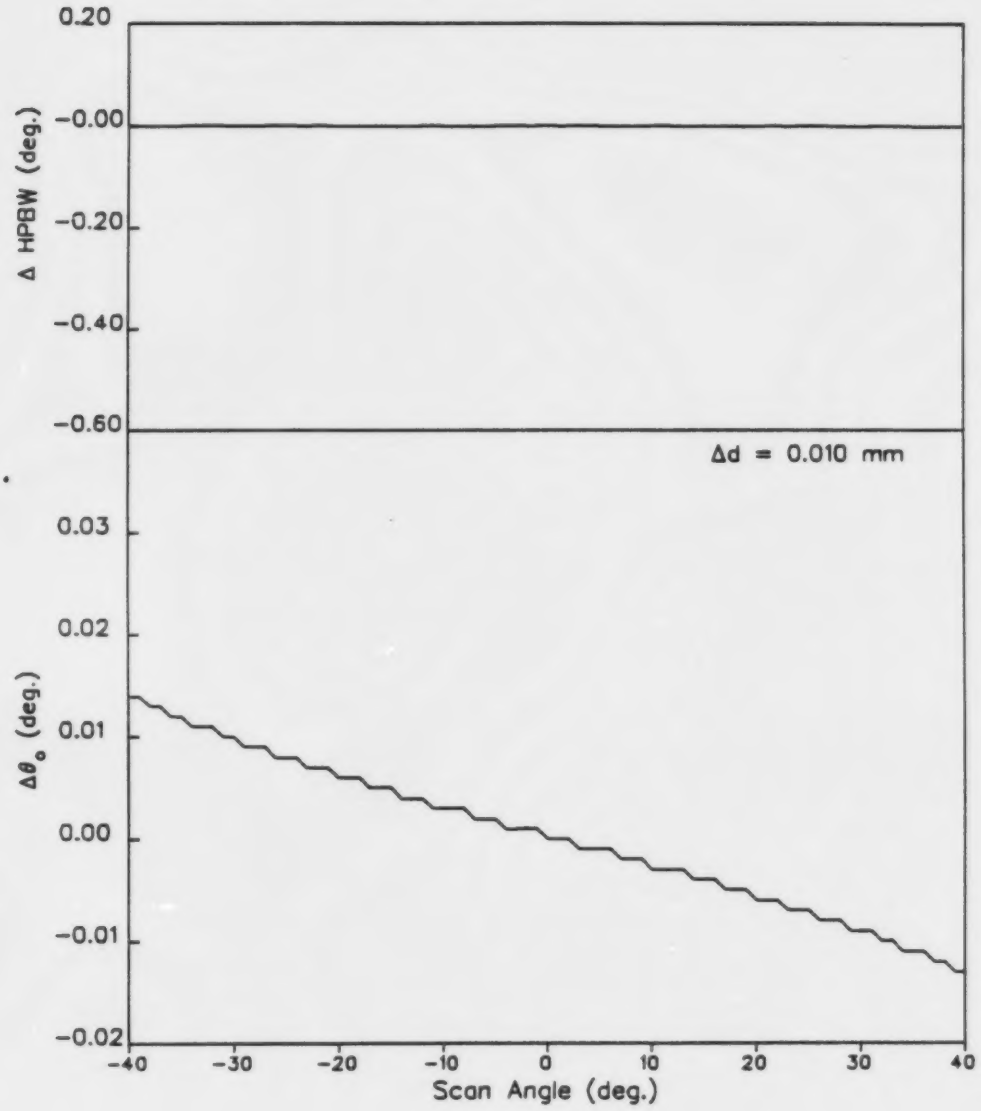

Fig. 7.21: Pointing and beam width errors due to a uniform thermal expansion of 0.01 mm per element spacing vs scan angle.

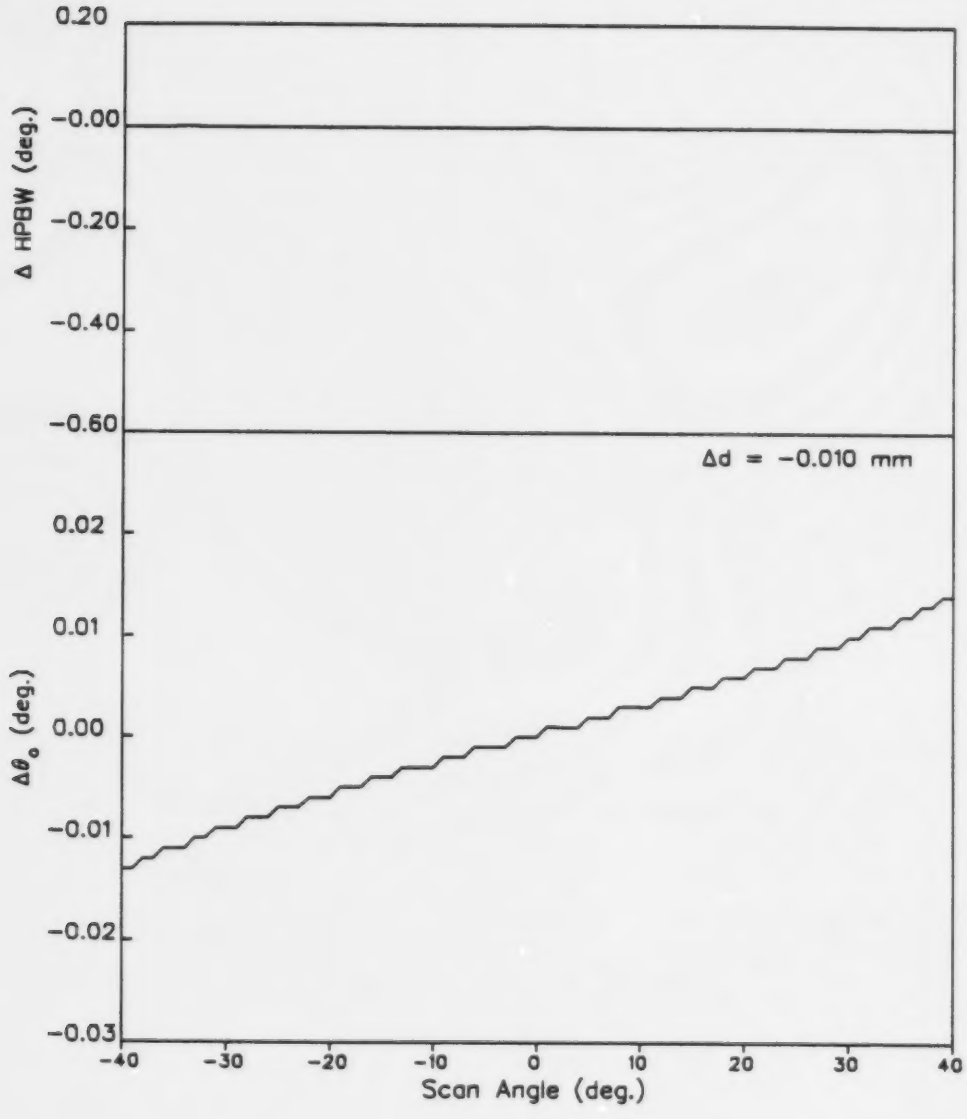

Fig. 7.22: Pointing and beam width errors due to a uniform thermal contraction of 0.01 mm per element spacing vs scan angle.

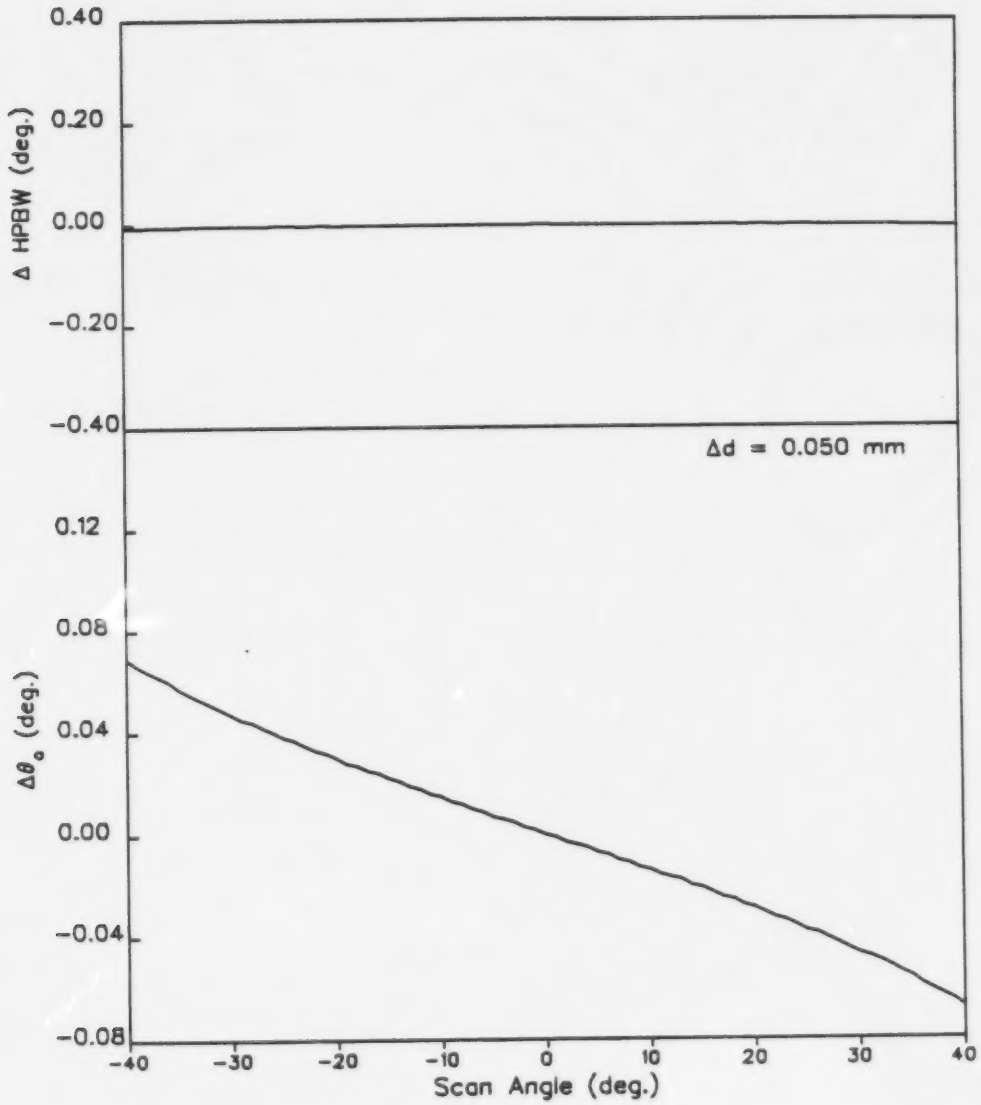

Fig. 7.23: Pointing and beam width errors due to a uniform thermal expansion of 0.05 mm per element spacing vs scan angle.

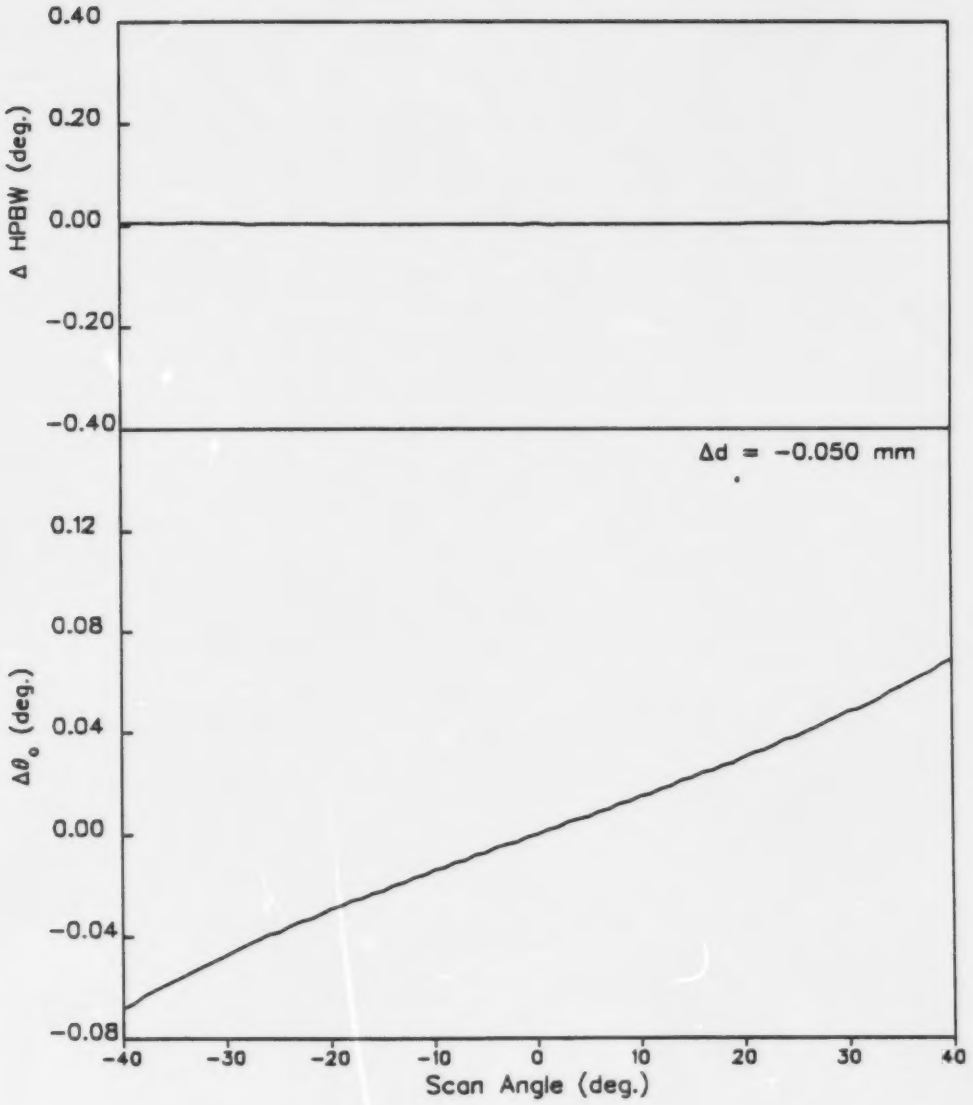

Fig. 7.24: Pointing and beam width errors due to a uniform thermal contraction of 0.05 mm per element spacing vs scan angle.

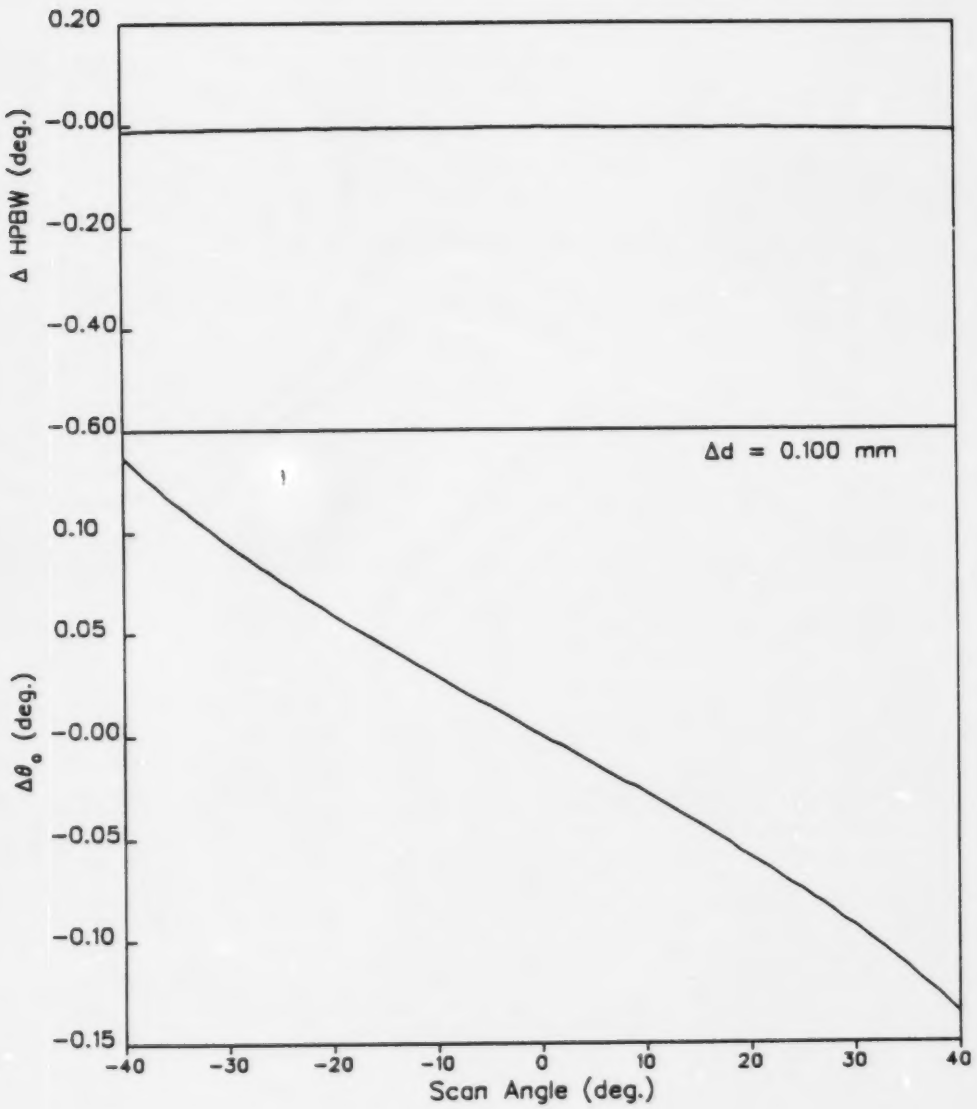

Fig. 7.25: Pointing and beam width errors due to a uniform thermal expansion of 0.1 mm per element spacing vs scan angle.

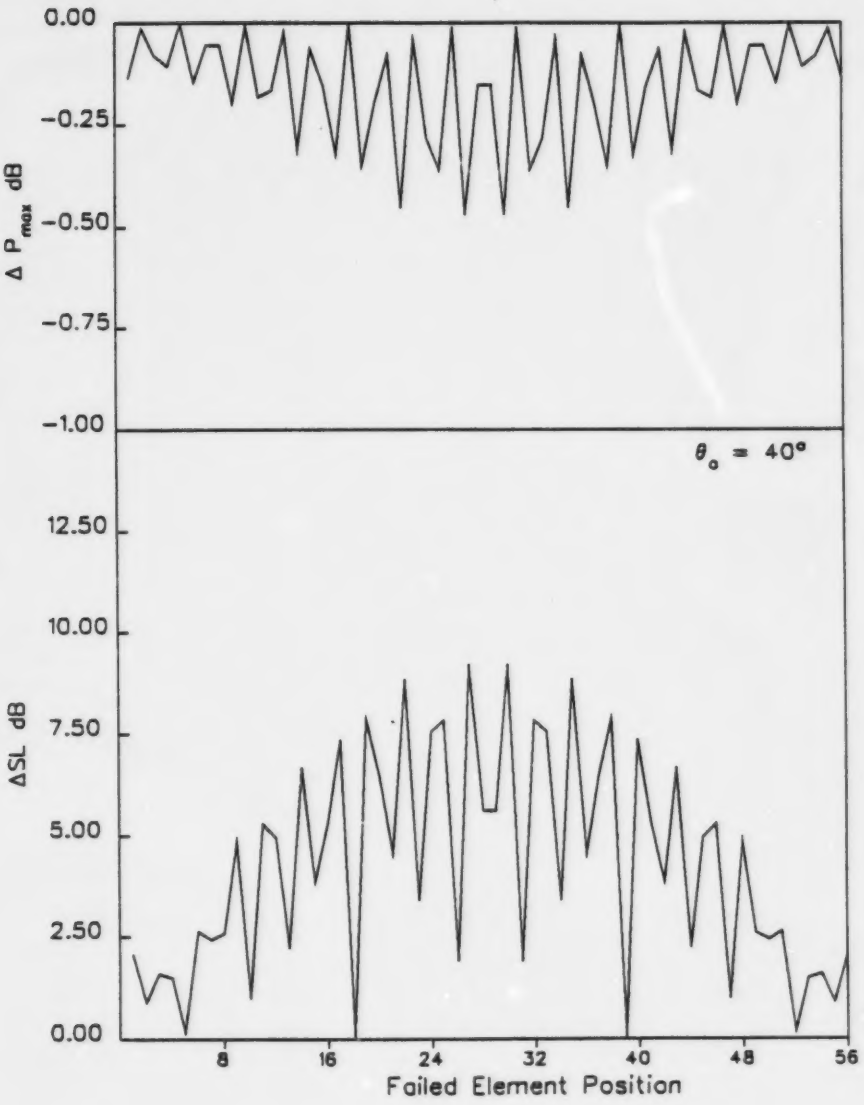

Fig. 7.26: The increase in the peak sidelobe and decrease in the maximum radiated power levels due to a single phase shifter failure.

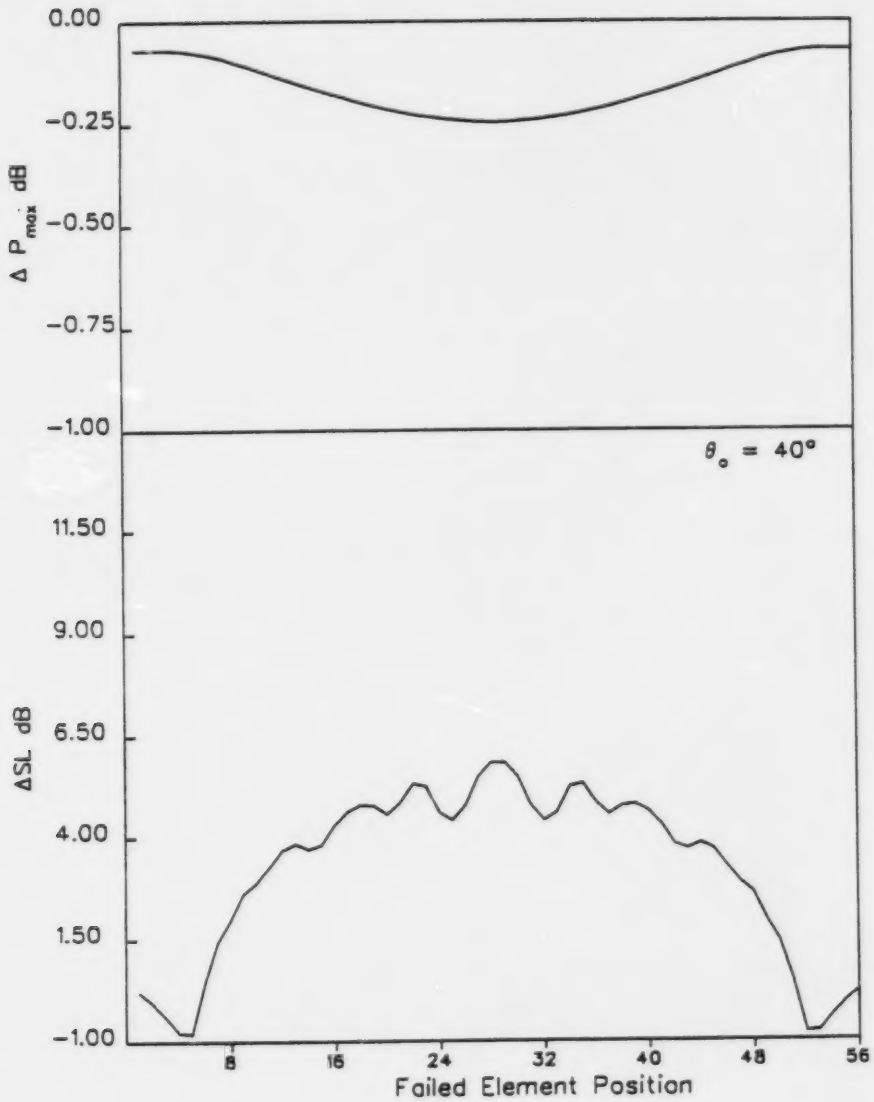

Fig. 7.27: The increase in the peak sidelobe and decrease in the maximum radiated power levels due to a single amplifier failure.

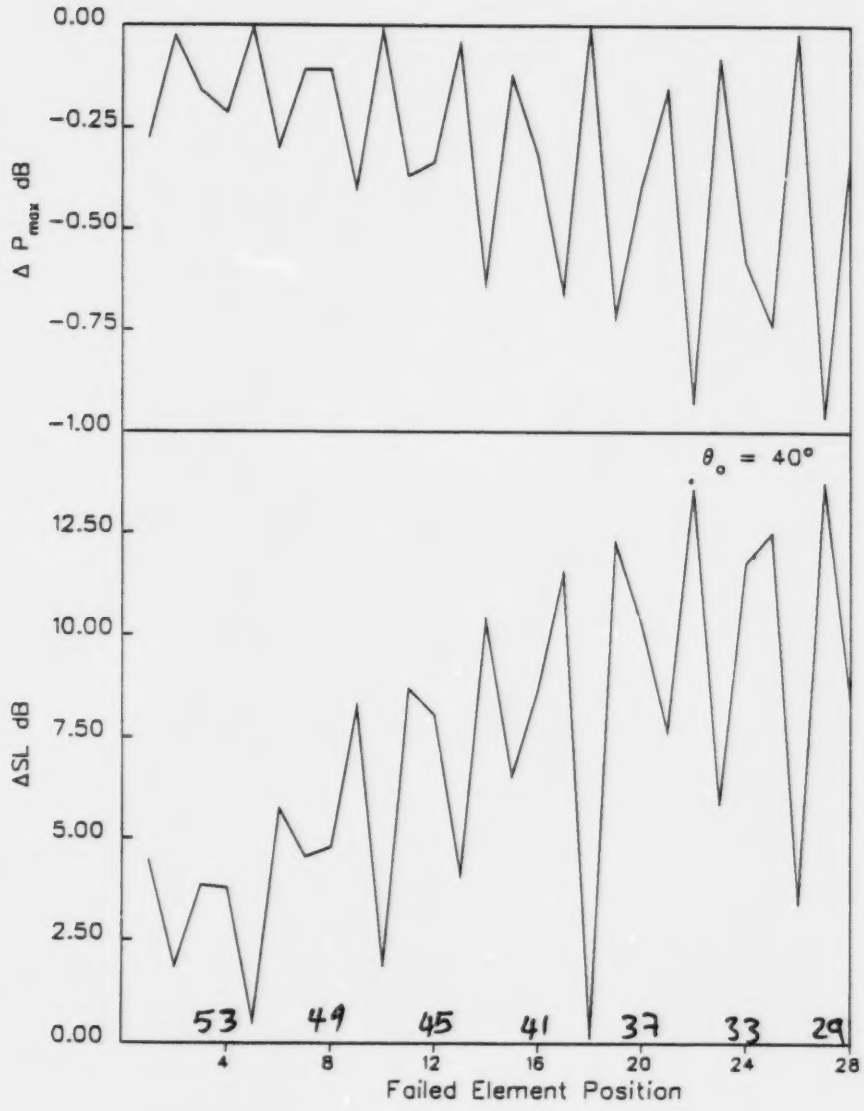

Fig. 7.28: The increase in the peak sidelobe and decrease in the maximum radiated power levels due to two symmetrical phase shifters failures.

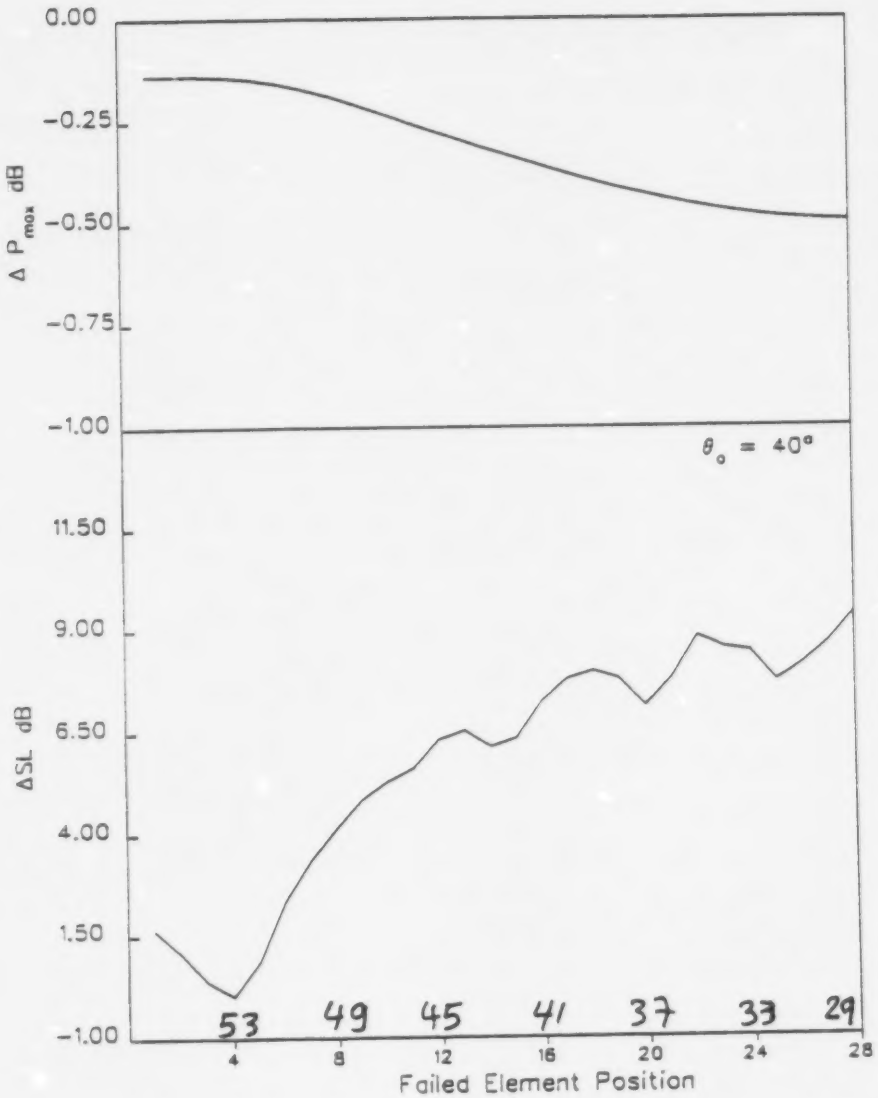

Fig. 7.29: The increase in the peak sidelobe and decrease in the maximum radiated power levels due to two symmetrical amplifiers failure.

Chapter 8
Conclusions and discussion

8.1 Conclusions

The principal aim of the present work was to develop a mathematical method to study the phase centre movement of the *MLS* azimuth antenna. The ideal *MLS* antenna is characterized by an aperture having the exact amplitude and phase distributions specified by the theory. In practice, no real antenna is free from errors, and irrespective of the cause, these errors have a significant effect on the amplitude and phase distributions across the array. In turn, the errors on the amplitude and phase distributions across a phased array can have great effects on the antenna phase centre location. Random errors, due to perturbations in the excitation coefficients, errors in the placement of antenna elements, mutual couplings, frequency variations in the signal, and manufacturing tolerances etc., also have a significant effect on the antenna far field data such as the beam width, pointing angles of the radiation patterns, and directivity. The purpose of this report was initially to investigate the effect of such errors on the antenna phase centre. The model was then extended to investigate the effects of ground reflection and thermal expansion and/or contraction on the phase centre movement.

Computer simulations were performed to investigate the effects of these errors on the antenna phase centre movement. The number of radiating elements, interelement spacing, and operating frequency were the input parameters for the error free case. Other information such as the number of failed amplitudes, the number of failed phase shifters, the seed number for the pseudo-random generator, and types of errors were input parameters for the simulation program. Data for computer runs were presented for both one- and two-dimensional array antennas. It was found that the recommended formulation was computationally efficient and required small computer times to perform calculations.

The technique was initially applied to a linear array of rectangular microstrip antennas, to investigate the contributions of mutual coupling between the patches. It was

found that the phase centre movement is generally less than 2.0%, when the mutual coupling is included. Next, the case of slotted waveguide array was considered. Neglecting the mutual coupling effects the contribution of random errors and element failures were investigated. It was found that the phase centre location is not unique and depends on the presence and types of errors. Also, the effects of phase shifter failures on the phase centre movement were more severe than those of amplitude failures. Generally, since the array distribution was tapered, the intermediate elements had more significant effects on the phase centre displacement. The variation in the phase centre coordinates was also found to be the scan angle dependent.

Finally, the effect of ground reflection and thermal contraction or expansion were studied. It was concluded that the phase centre movement is strongly dependent on the signal reflected by the ground. However, it was nearly independent of the thermal expansion and/or contraction.

Table 8.1 summarizes the simulated results of the phase centre displacement, for the selected input parameters.

Table 8.1

error type	x_p^t (λ)	x_p^m (λ)	y_p^t (λ)	y_p^m (λ)	z_p^t (λ)	z_p^m (λ)
Random phase error *	0.5	2.0	0.0	0.0	1.0	6.0
Random amplitude error *	0.01	0.1	0.0	0.0	0.01	0.08
Single amplitude failure	0.15	0.2	0.0	0.0	0.25	0.05
Multiple amplitude failure	0.5	1.1	0.0	0.0	0.1	0.2
Single phase failure	2.0	5.0	0.0	0.0	5.0	12.0
Multiple phase failure	4.0	6.5	0.0	0.0	5.0	50.0
Dry ground	0.0	0.0	1.5	3.0	4.0	6.0
Wet ground	0.0	0.0	0.5	1.0	3.5	4.0
Concrete	0.0	0.0	1.0	3.0	3.0	6.0
Thermal expansion	0.0	0.0	0.0	0.0015	0.0	0.0005
Thermal contraction	0.0	0.0	0.0	0.0015	0.0	0.0005

Table 8.1. Variations in the phase centre coordinates, x_p^t is a typical variation in the x-coord., x_p^m is the maximum variation in the x-coordinate.
* For the selected random numbers.

The tabulated results show the typical and also the maximum movement in the location of the phase centre. As discussed earlier, the worst possible case is, when there is a multiple phase shifter failure.

8.2 Experimental procedure

So far, all information on the *MLS* array phase centre that is provided in this report, has been based on computations. While, the concept used in determining the phase centre location is straightforward, nevertheless, there is a need for experimental verifications. This is primarily due to the fact that the input data for computations is selected using certain simplifying assumptions. For instance, the phase shift values for the beam scanning are computed and whenever the effect of their variation is studied, certain random errors are added to ideal quantities. In a practical situation, however, the phase values are provided by different phase shifters that usually operate with ac-

tive devices, and consequently, include design or quantization errors. Such uncertainties are present in almost all other input data and naturally affect the confidence level on the results. It is therefore essential that one verifies the phase centre location, and its subsequent effects on the beam deviation, for at least for a few selected beam locations.

To develop a satisfactory measurement procedure a number of meetings were held with staff of the David Florida Laboratory, *DFL*, that carries out the experimental work on Micronav antennas. One of error the sources in determination of the beam location at *DFL* is the finite size of the antenna range. This finite range distance, together with unequal transmitter and receiver heights, cause the antenna phase centre to trace a conical path and generate subsequent measurement errors.

To improve the measurement accuracy, a number of measurements should be carried out, after locating the antenna phase centre on the rotation axis of the turn table. Because of the large size of the *MLS* antenna this latter test can be a difficult job. Consequently, a new antenna holder, with adjustable arms in all x, y and z-coordinates must be fabricated. Recently, a meeting was held with *DFL* staff to explore their view on the possibility of using, such an antenna holder for phase centre study. Their response was positive. The phase centre study requires additional changes to the present set up and *DFL* staff saw no difficulties in corporating them. Actual designs and modification will be done whenever the experimental work is approved.

Experimental work on the phase centre determination has two important impact on the *MLS* antenna measurements. One is the verification of the computational work on the phase centre and its subsequent use for other antenna parameter computation. The second one is the use of the result to develop an error correction algorithm. With the antenna phase centre properly located on the turn table, one can minimize experimental errors. This can be used to validate the error correction algorithm, that in turn will help in eliminating the measurement errors of subsequent studies.

References

[1] L. Mania, "The antenna phase centre in satellite Radio-Doppler geodetic systems," IEEE Trans. Geosci. and Remote Sensing (USA), vol. Ge-20, no. 4, pp. 536-543, 1982.

[2] J. M. Tranquilla and S. R. Best, "Antenna phase centre movement in UHF radio positioning system," Can. Elect. Eng. J., vol. 12, no. 1, pp. 11-18, 1987.

[3] J. D. Dyson, "Determination of the phase centre and phase patterns of antennas," in Radio Antennas for Aircraft and Aerospace Vehicles, W. T. Blackband, Ed. Agard Conf. Proc., Slough, England : Technivision Services, no. 15, pp. 97-118, 1967.

[4] Y. Y. Hu, "A method of determining phase centres and its application to electromagnetic horns," Franklin Inst., vol. 271, no. 1, pp. 31-39, 1961.

[5] A. R. Vol'pert, "On the phase centre of antennas," Radio Eng. (U.S.S.R.), vol. 16, no. 3, pp. 1-17, 1961 (Translation).

[6] P. J. D. Gething, "Concept of phase centre of an array applied to elevation- angle measurement," Proc. Inst. Electr. Eng. (GB), vol. 120, no. 5, pp. 541-543, 1973.

[7] W. V. T. Rusch and P. D. Potter, "Analysis of Reflector Antennas," New York : Academic, pp. 145-152, 1970.

[8] P. S. Kildal, "Combined E- and H- plane phase centres of antenna feeds," IEEE Trans. Anten. Propag., vol. AP-31, no. 1, pp. 199-202, 1983.

[9] K. S. Rao and L. Shafai, "Phase centre calculations of reflector antenna feeds," IEEE Trans. Anten. Propag., vol. AP-32, no. 7, pp. 740-742, 1984.

[10] J. E. Evans, et. al, "Development and validation of model for MLS techniques, " Lincoln Lab., Report no. FAA-RD-79-21, vol. I, II, III, 1980.

[11] E. Capon, et. al, "Multipath parameter computations for the MLS simulation computer program, " Lincoln Lab. Report no. AtC-68, 1976.

[12] Y. Hu, "A method of determining phase centres and its application to electromagnetic horns," J. Franklin Inst., PP. 31-36. 1961.

[13] D. Carter, "Phase centres of microwave antennas," IRE Trans. Antenna Propagat., pp., 597-600, 1956.

[14] J. R. James, P. Hall and C. Wood, "Microstrip Antenna Theory and Design," Peter Peregrinus Ltd., 1981.

[15] I. J. Bahl and P. Bhartia, "Microstrip Antenna," Dedham, MA, Artech House, 1980.

[16] R. F. Harrington, "Time Harmonic Electromagnetic Fields," McGraw-Hill, N. Y., 1961.

[17] M. T. Ma, "Theory and Application of Antenna Arrays," John Wiley & Sons, Inc., USA, 1974.

[18] R.J. Ginnini, J.H. Gutman, "A cylindrical phased-array antenna for ATC interrogation," Microwave Journal, Oct. 1973.

[19] J. W. Ducan, "The effect of ground reflections and scattering on an interferometer direction finder," IEEE. Trans. Aerospace & Elec. Systems, vol. AES-3, no. 6, pp. 922-932, 1967.

[20] A. R. Lopez, "Scanning-beam microwave landing system - multipath errors and antenna design philosophy," IEEE. Trans. Ant. & Propag., vol. 25, no. 3, pp. 290-296, May 1977.

[21] W. D. White, "Low angle radar tracking in the presence of multipath," IEEE. Trans. Aerospace & Elec. Systems, vol. 10, no. 6, pp. 835-842, Nov. 1974.

[22] P. Beckmann, and A. Spizzichino, "The scattering of electromagnetic waves from rough surfaces," Artech House, 1987.

[23] M. W. Long, "Radar reflectivity of land and sea," second edition, Artech House, 1983.

[24] E. C. Jordan, and K. G. Balmain, "Electromagnetic waves and radiating systems," second edition, Prentice Hall, 1968.

[25] A. Sebak, L. Shafai, "The effect of random amplitude and phase errors on array performance," Final report, cont. no. 55SS.36001-7-3568, Done for communication research centre, Ottawa, Ont. K2H 8S2., March 1989.

Appendix
Application to MLS antenna

1. Introduction

In this appendix we present the generated results corresponding to the phase distributions furnished by Micronav Limited, for selected scan angles. Computer simulation runs are performed to determine the phase centre movement as well as pointing errors, for a specified failure and random errors. A -30 dB Taylor distribution is assumed through the linear array. The total number of elements is 56 with inter-element spacing of 3.509 cm (0.59185133 λ).

2. Phase Centre Movement

Figs. A.1 and A.2 show the phase centre location for the error free cases, using Micronav data. The results indicate that the input data for the beam algorithm is scan angle dependent, and causes the phase centre movement for the error free antenna. For the selected scan angles, the phase centre variation is about 3.3 λ in the z–coordinate and 1.9 λ in the x-coordinate. Figs. A.3 and A.4 show the phase centre movement, due to the phase random errors with $\sigma_p = 5$ degrees. Figs. A.5 and A.6 illustrate the amplitude failures at scan angles of 10^o and 30^o. For the selected scan angles, the movement in the phase centre coordinates are 7.0 λ and 2.0 λ in the z-coordinate and 1.1 λ, 1.0 λ in the x-coordinate, respectively. Fig. A.7 and A.8 show the output of the simulation runs for the phase shifter failures. For the selected scan angles of 10^o and 30^o, the results indicate the maximum coordinate variation of 5.0 λ and 8.5 λ in the z-coordinate and 2.5 λ and 5.0 λ in the x-coordinate.

3. Pointing Errors

In this section we consider the effect of one phase shifter failure, using the simulation program of Chapter 7, on the pointing angle. In the following results the order (location) of the array elements is as shown in Fig. 2.5.

The results for a complete phase failure, i.e. 0 degree phase with full input power, are shown in Figs. A.9-A.14 for optimal phase distribution (i.e. assuming analog phase shifters). The corresponding results using the data furnished by Micronav Ltd. are shown in Figs. A.15-A.20. From these figures, one may make the following

observations:

(1) The effect on the pointing angle is symmetric with respect to element locations for the case of optimal phase distributions, but it is not for the case of digital phase shifters. This is due to the asymmetry in the phase setting of the elements as provided by Micronav Ltd.

(2) The pointing errors are almost of the same order and of the same behavior for the same corresponding cases, except for the scan angle of 30.3138^o. For this particular scan angle, the magnitude of the peak pointing error is about 0.045 degree when Micronav Ltd. data is used. It should also be noted that, for the error-free cases considered here, the maximum phase centre movement occurs at the same scan angle.

Finally, the pointing error $\Delta\theta_o$ due to a uniform thermal expansion of Δd (mm) in spacing between array columns, is given in Table A.1 for selected values of the scan angle, θ_o using Micronav data. It is clear that an expansion of 0.1 mm (or equivalently, a displacement of the columns by 0.1 mm) results in a pointing error in the range of $0.093^o - 0.096^o$, which is about twice the allowable error in the pointing angle.

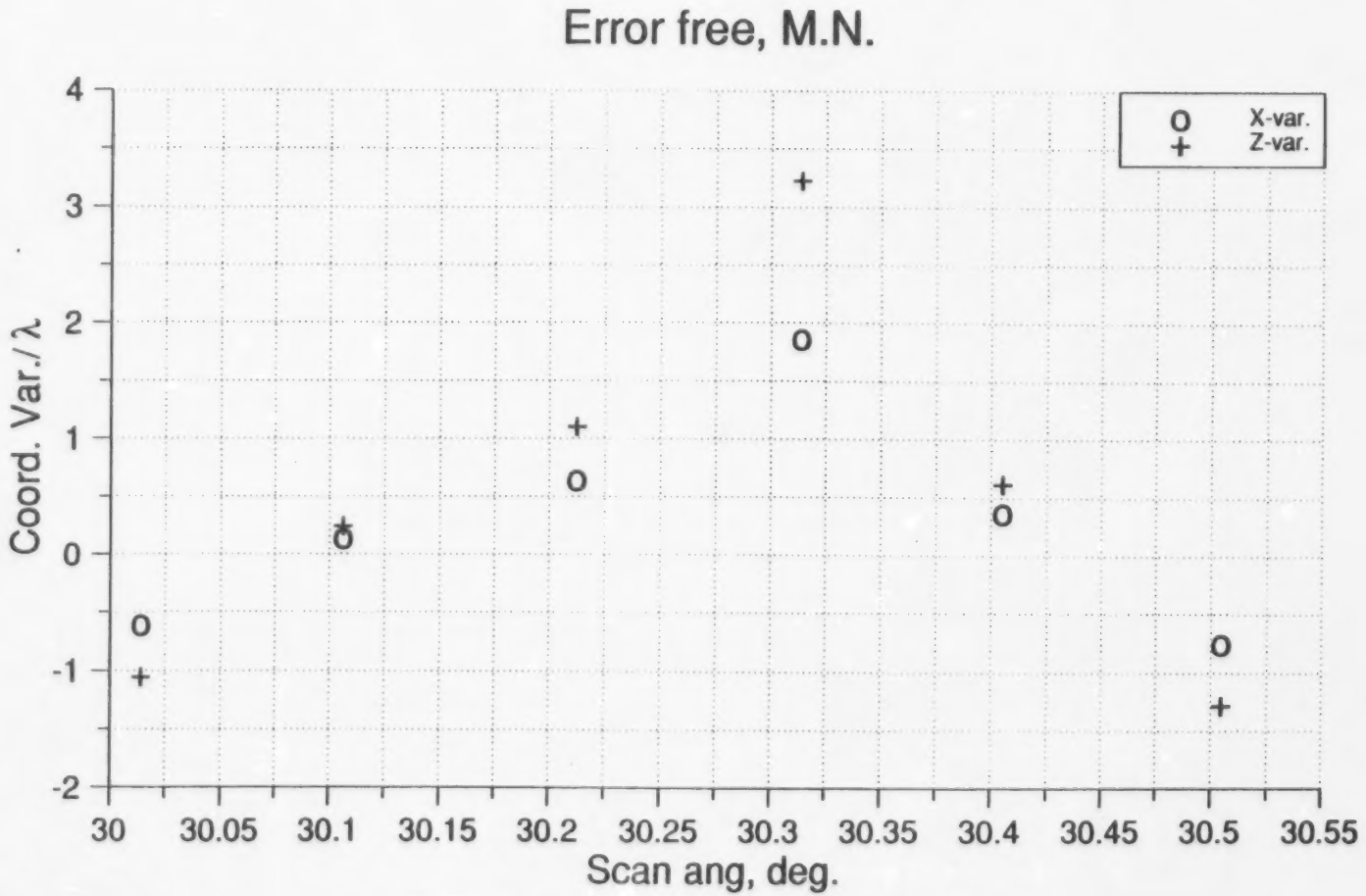

Fig. A.1 : Phase centre movement for the selected scan angles, error-free case

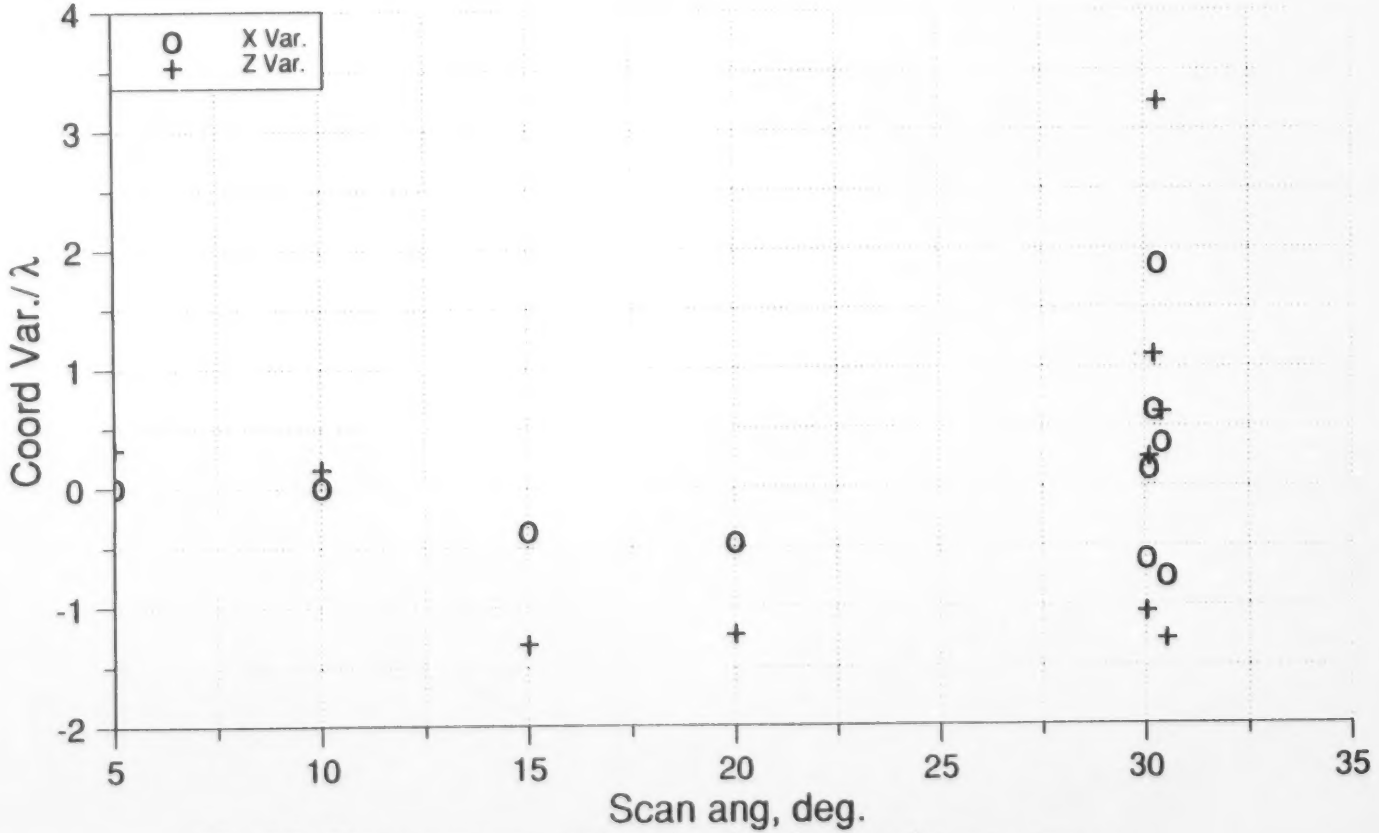

Fig. A.2 : Phase centre movement for the selected scan angles, error-free case

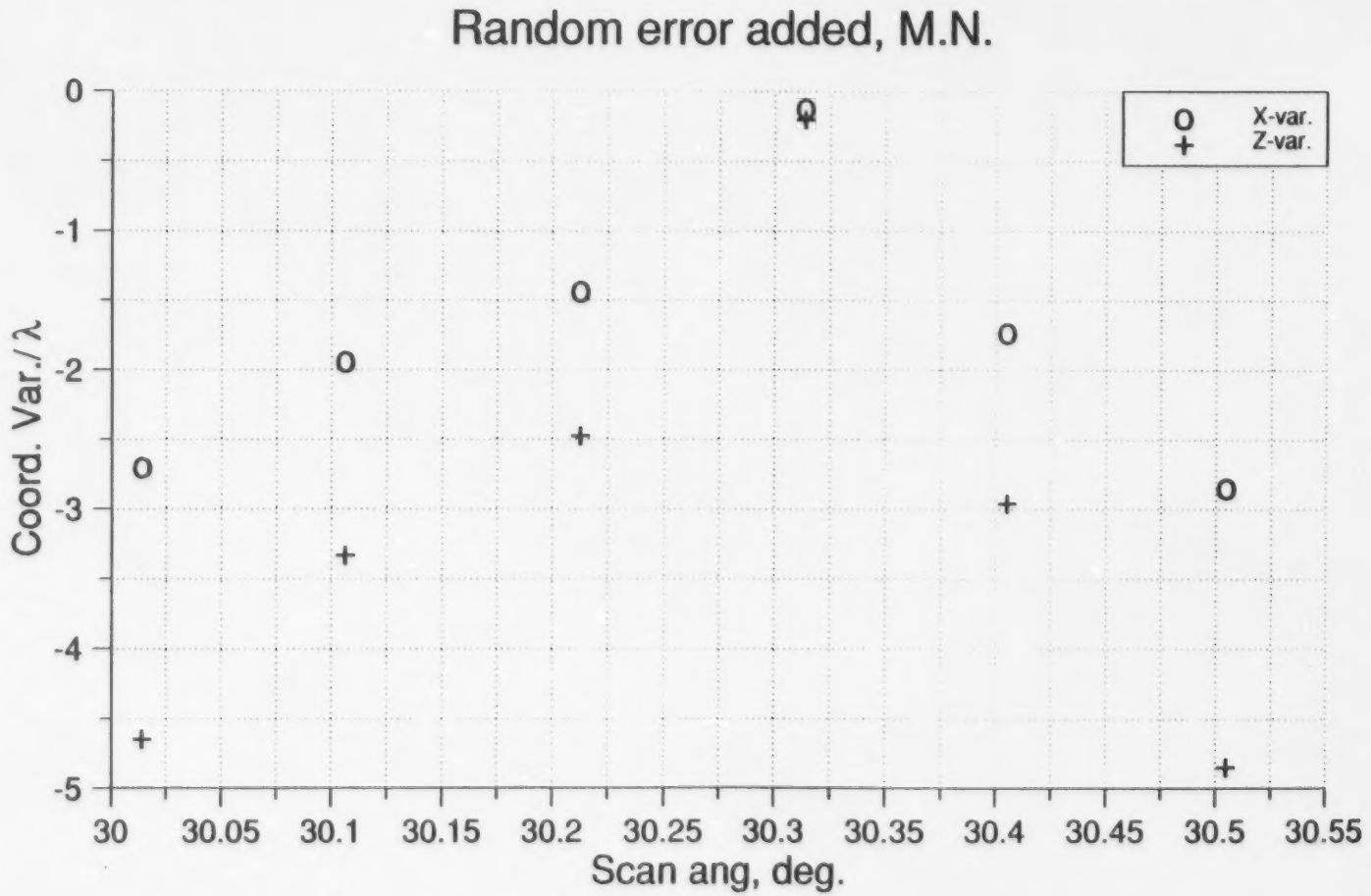

Fig. A.3 : Phase centre movement for the selected scan angles, random error added

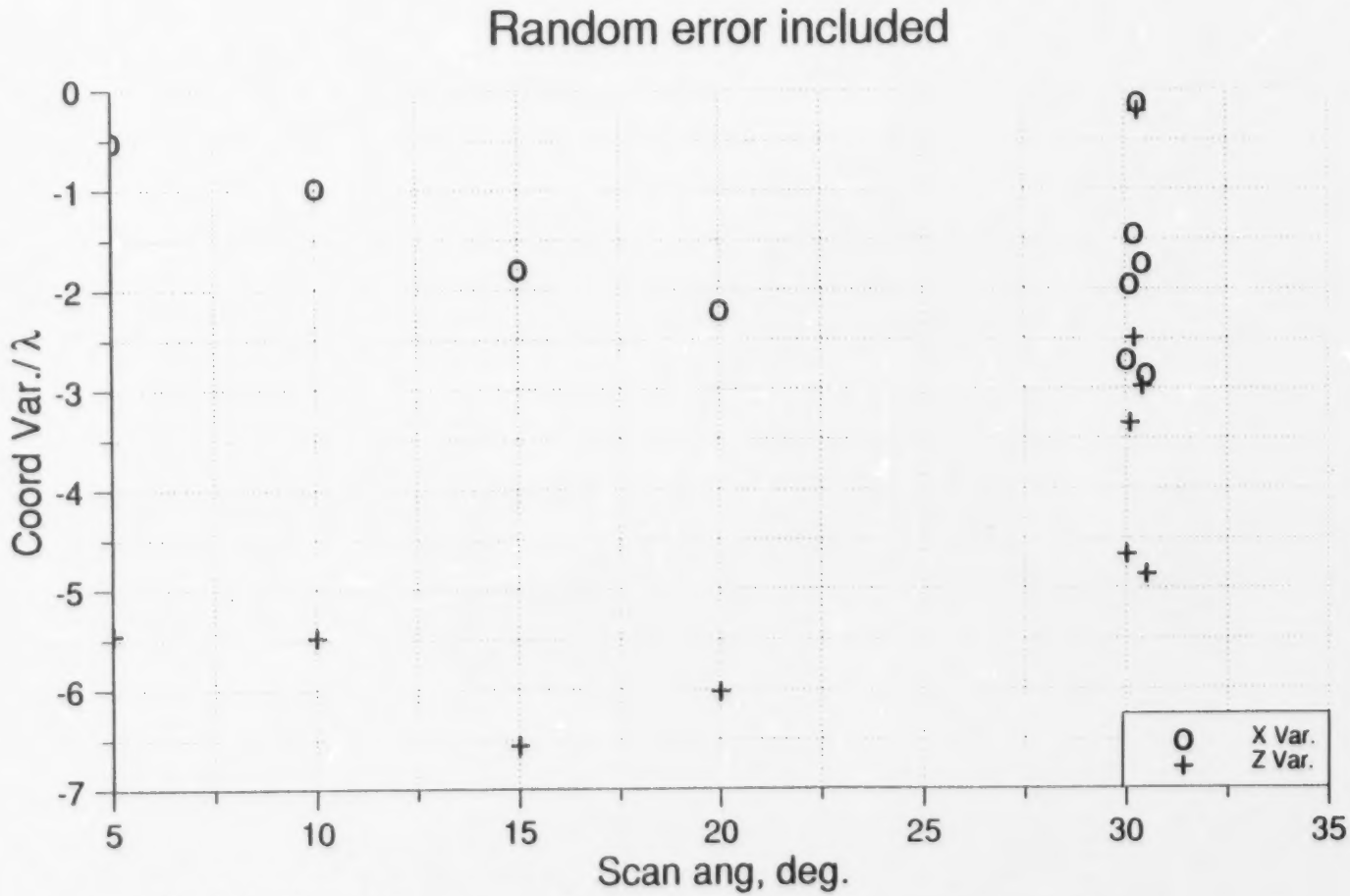

Fig. A.4 : Phase centre movement for the selected scan angles, random error added

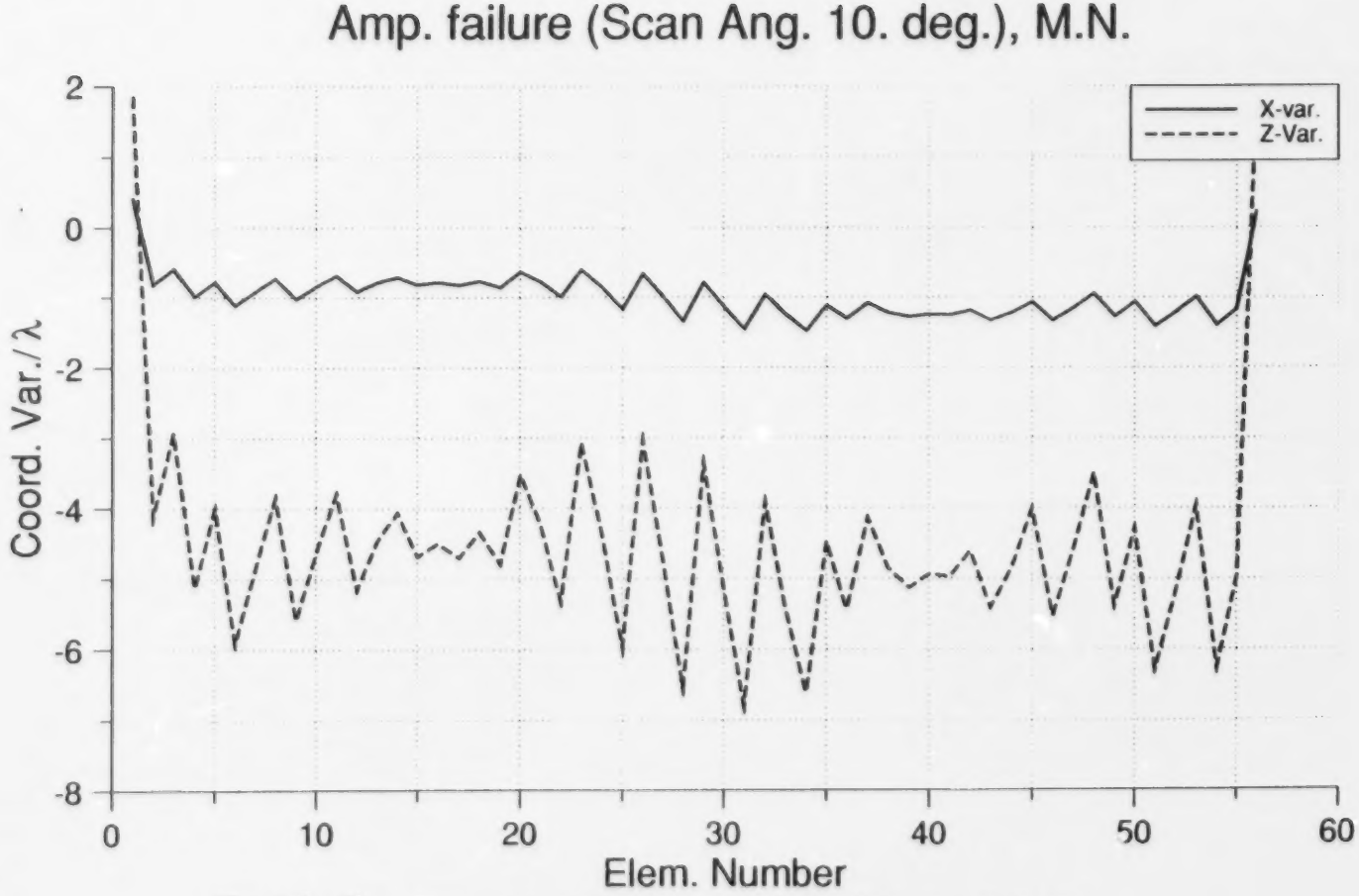

Fig. A.5 : Phase centre movement due to amplitude failure, θ_s = 10 degree.

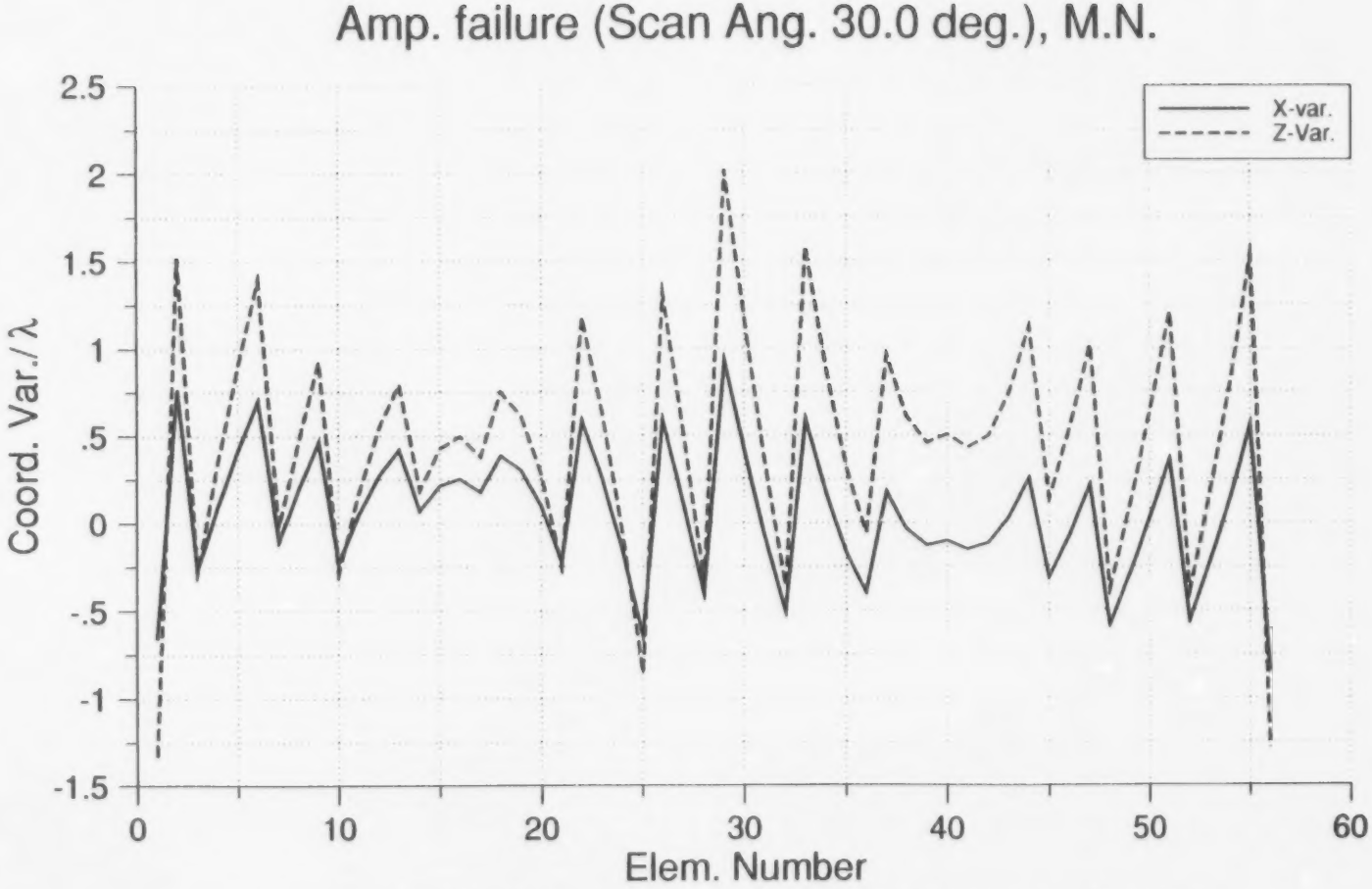

Fig. A.6 : Phase centre movement due to amplitude failure, θ_s = 30.014 degree.

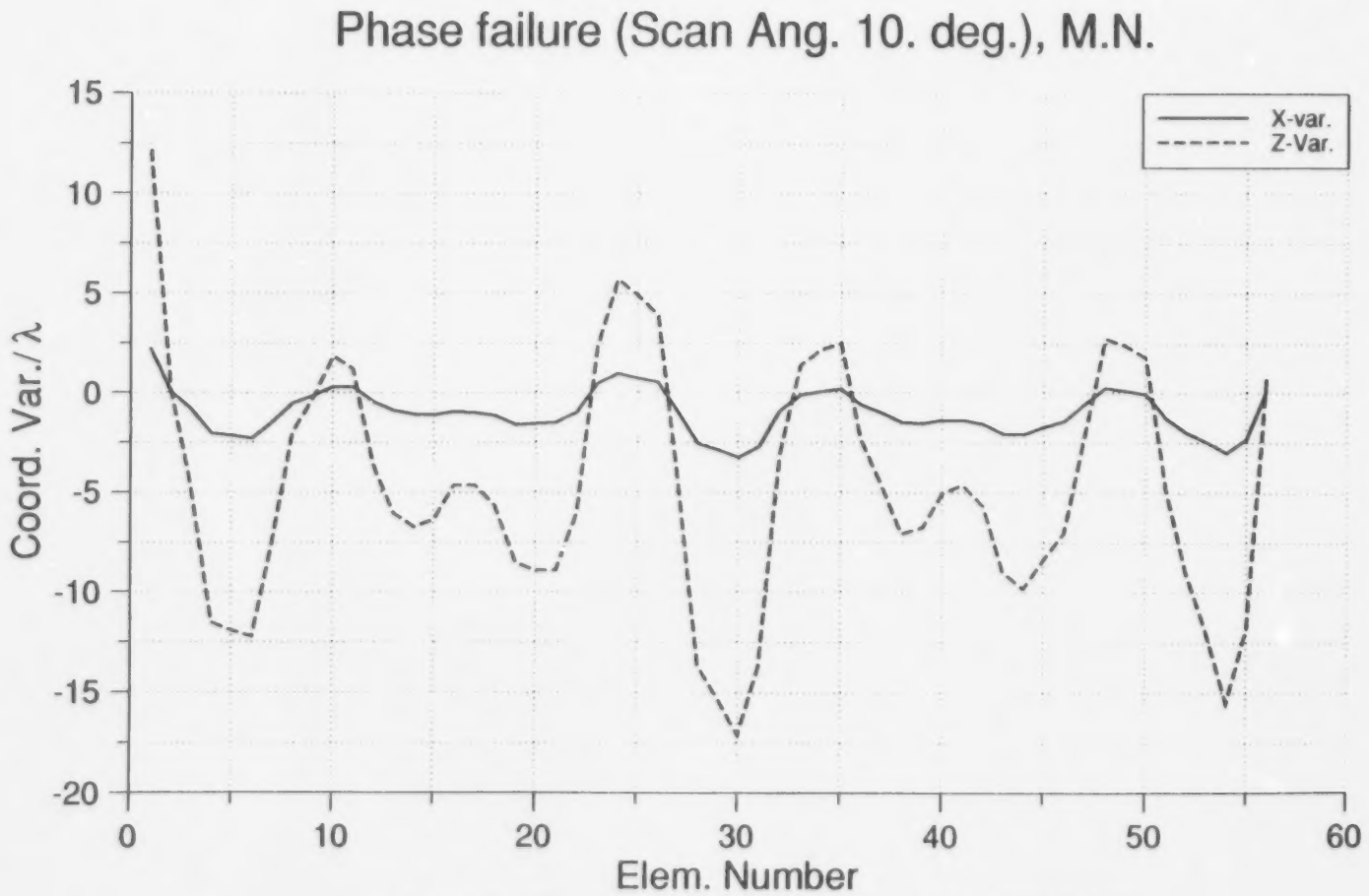

Fig. A.7 : Phase centre movement due to phase shifters failure,

θ_s = 10 degree

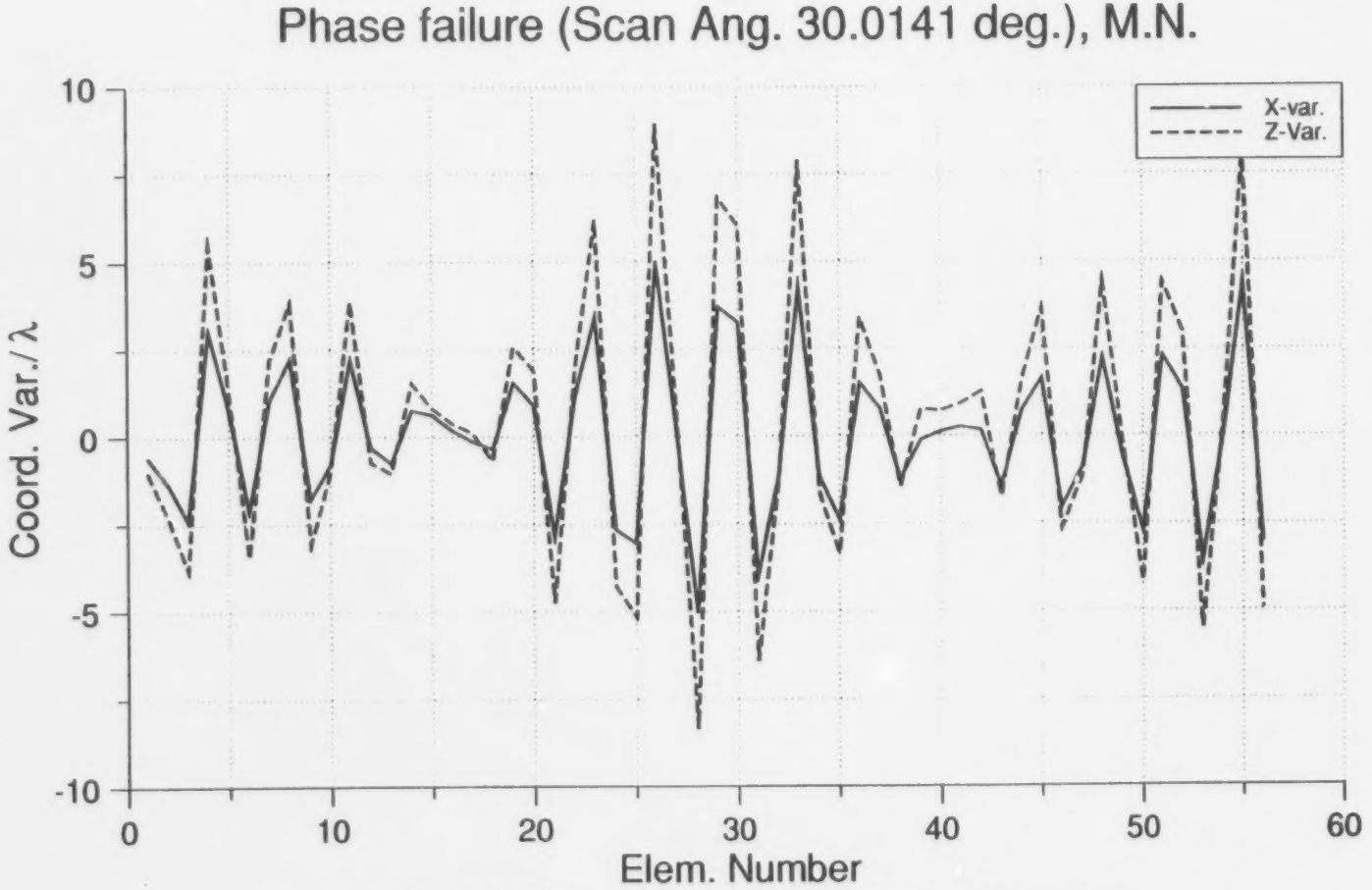

Fig. A.8 : Phase centre movement due to phase shifters failure,

θ_s = 30.014 degree

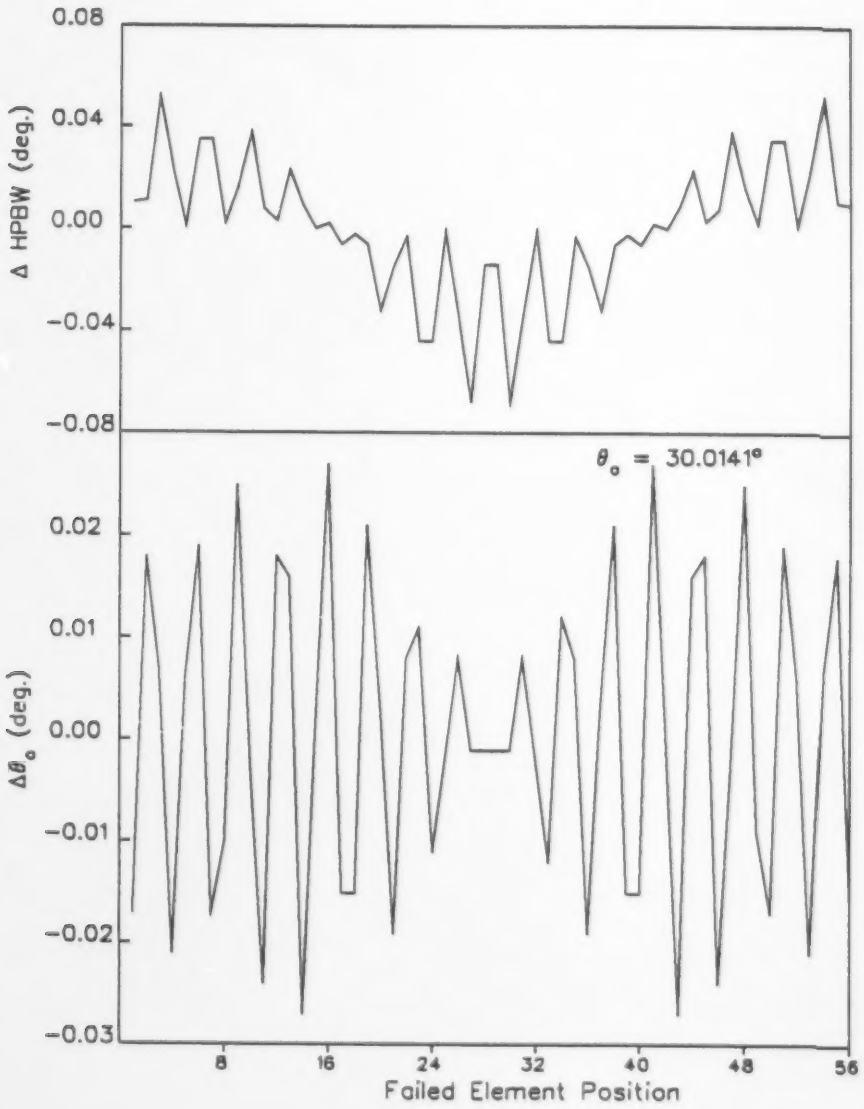

Fig. A.9: Pointing and beam width errors due to a single phase shifter failure at 30.0141 deg. scan angle and for optimal phase distributions.

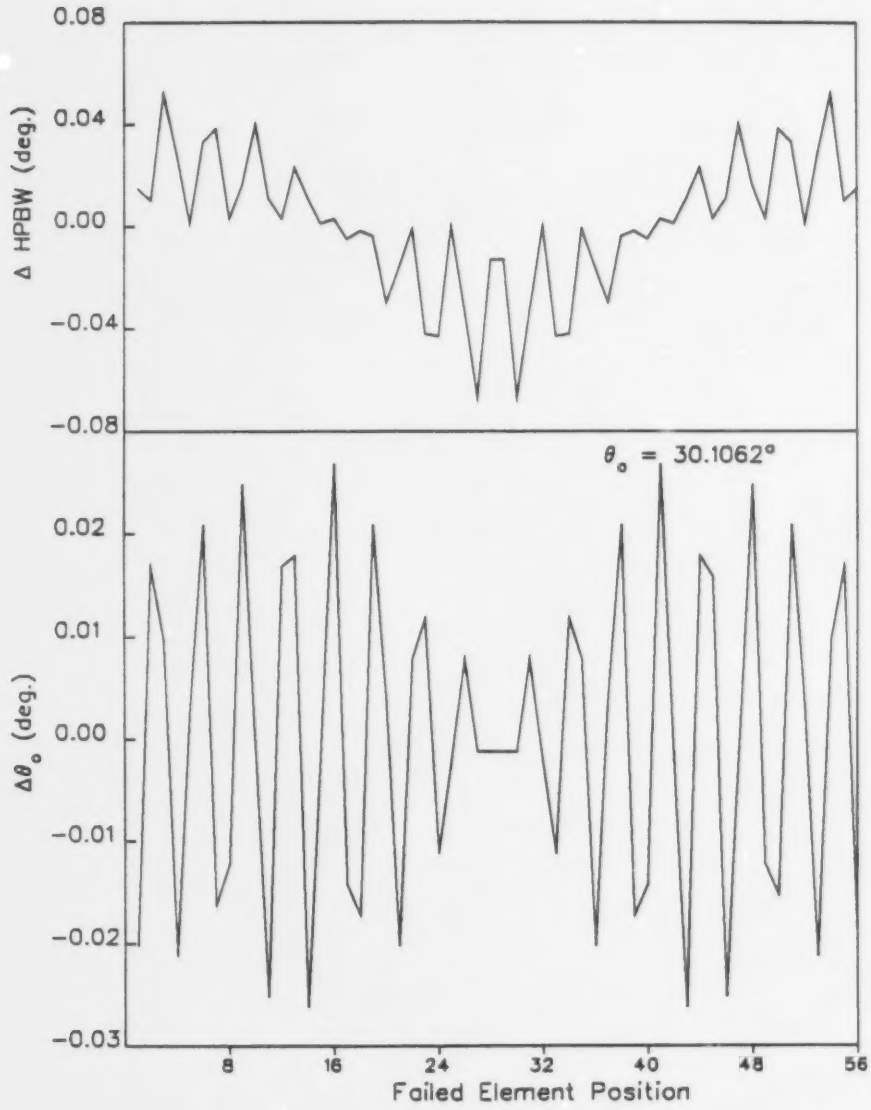

Fig. A.10: Pointing and beam width errors due to a single phase shifter failure at 30.1062 deg. scan angle and for optimal phase distributions.

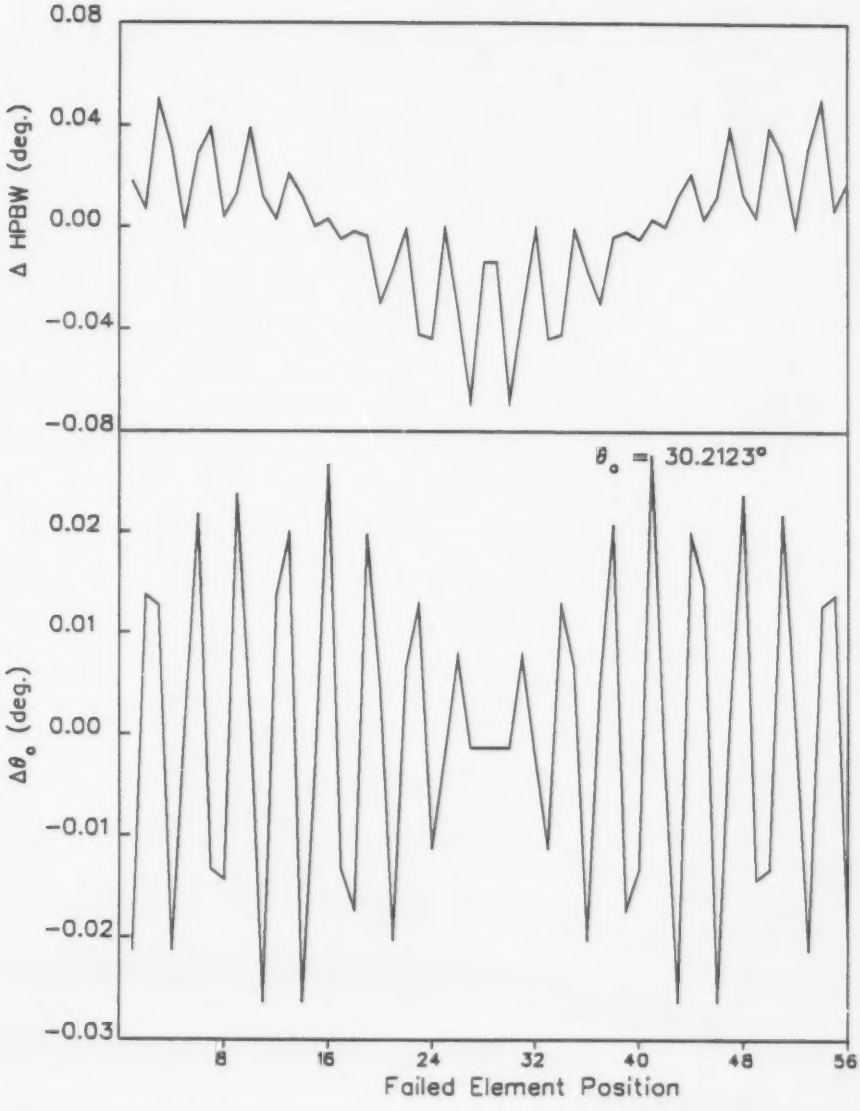

Fig. A.11: Pointing and beam width errors due to a single phase shifter failure at 30.2123 deg. scan angle and for optimal phase distributions.

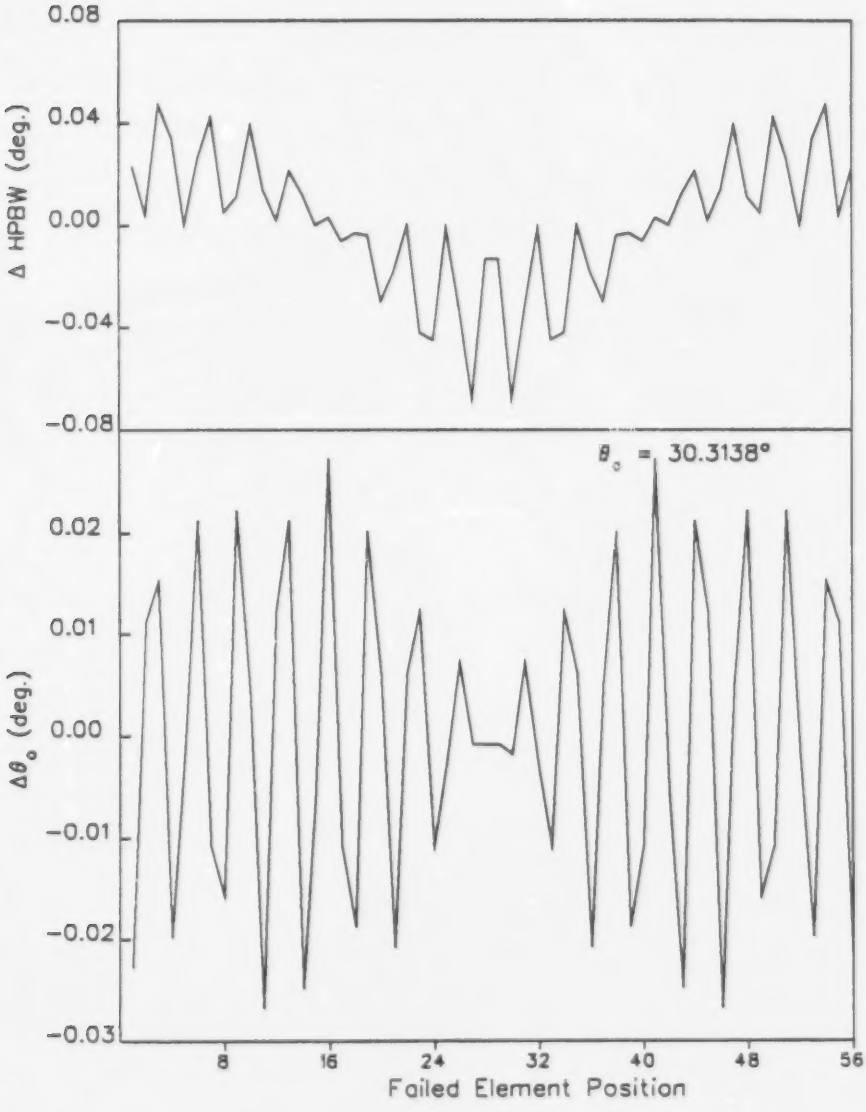

Fig. A.12: Pointing and beam width errors due to a single phase shifter failure at 30.3138 deg. scan angle and for optimal phase distributions.

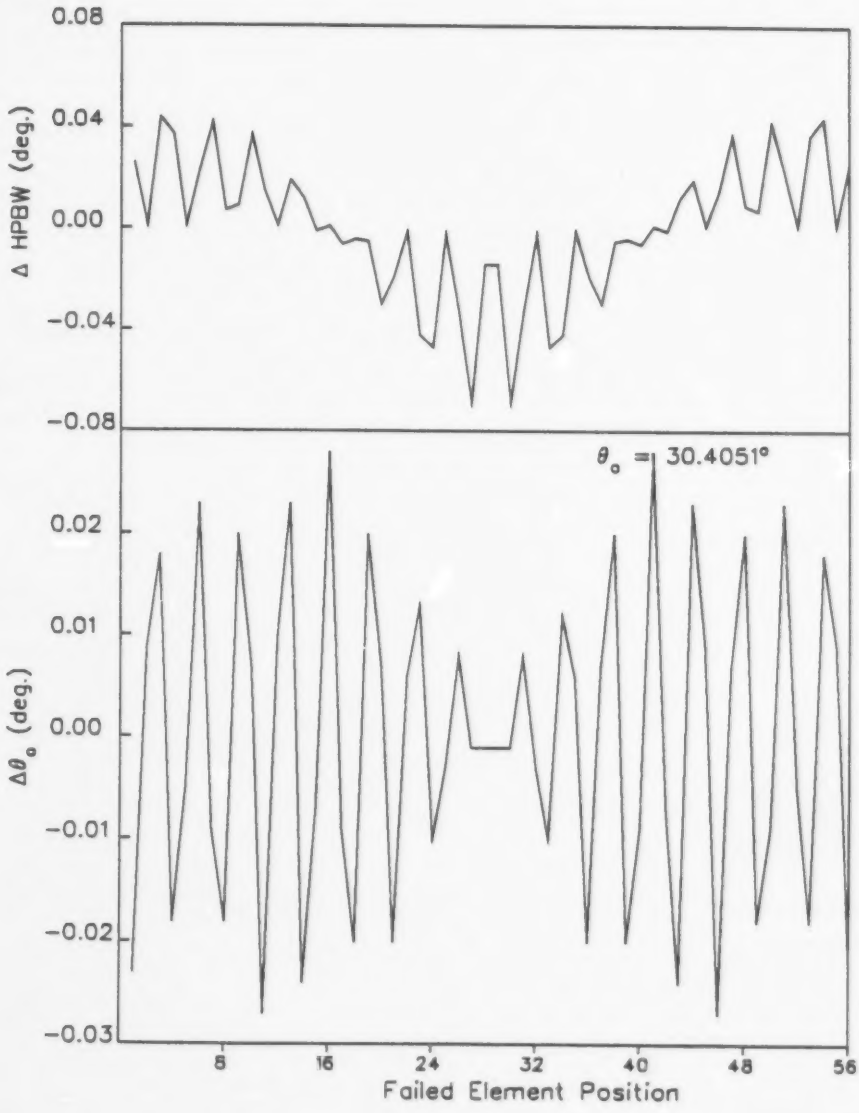

Fig. A.13: Pointing and beam width errors due to a single phase shifter failure at 30.4051 deg. scan angle and for optimal phase distributions.

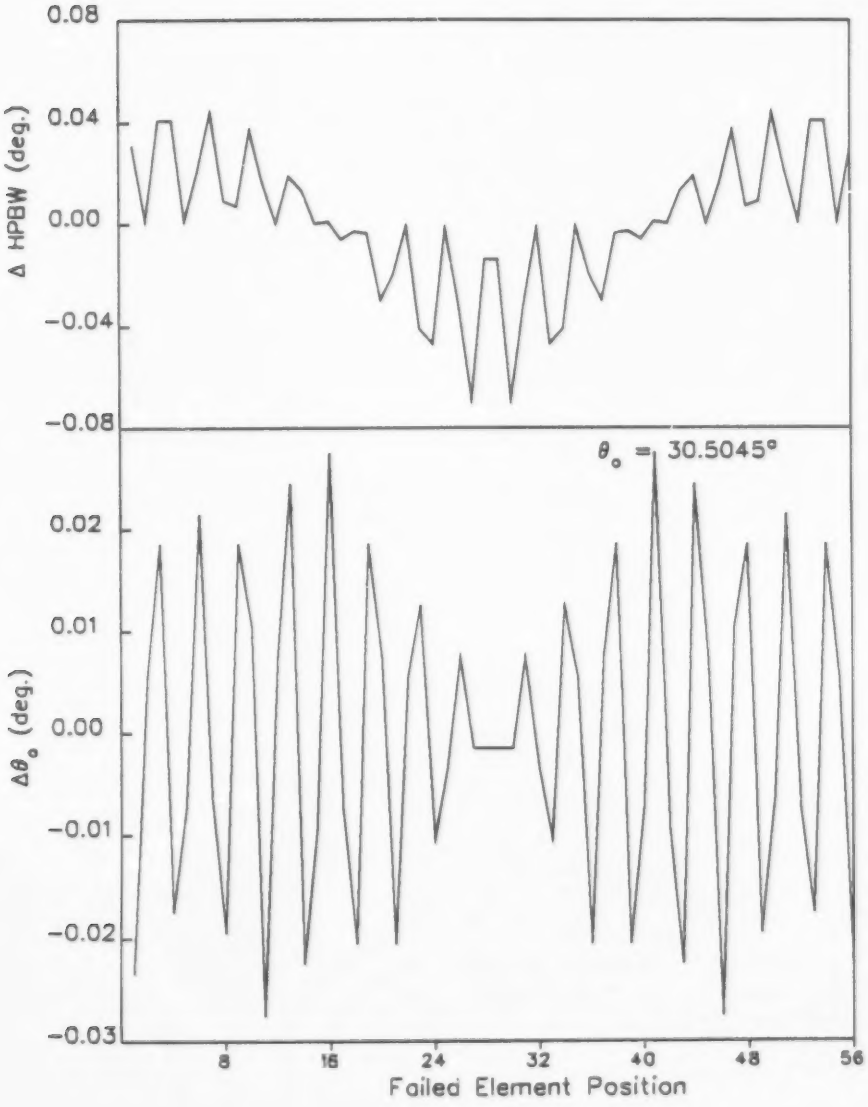

Fig. A.14: Pointing and beam width errors due to a single phase shifter failure at 30.5045 deg. scan angle and for optimal phase distributions.

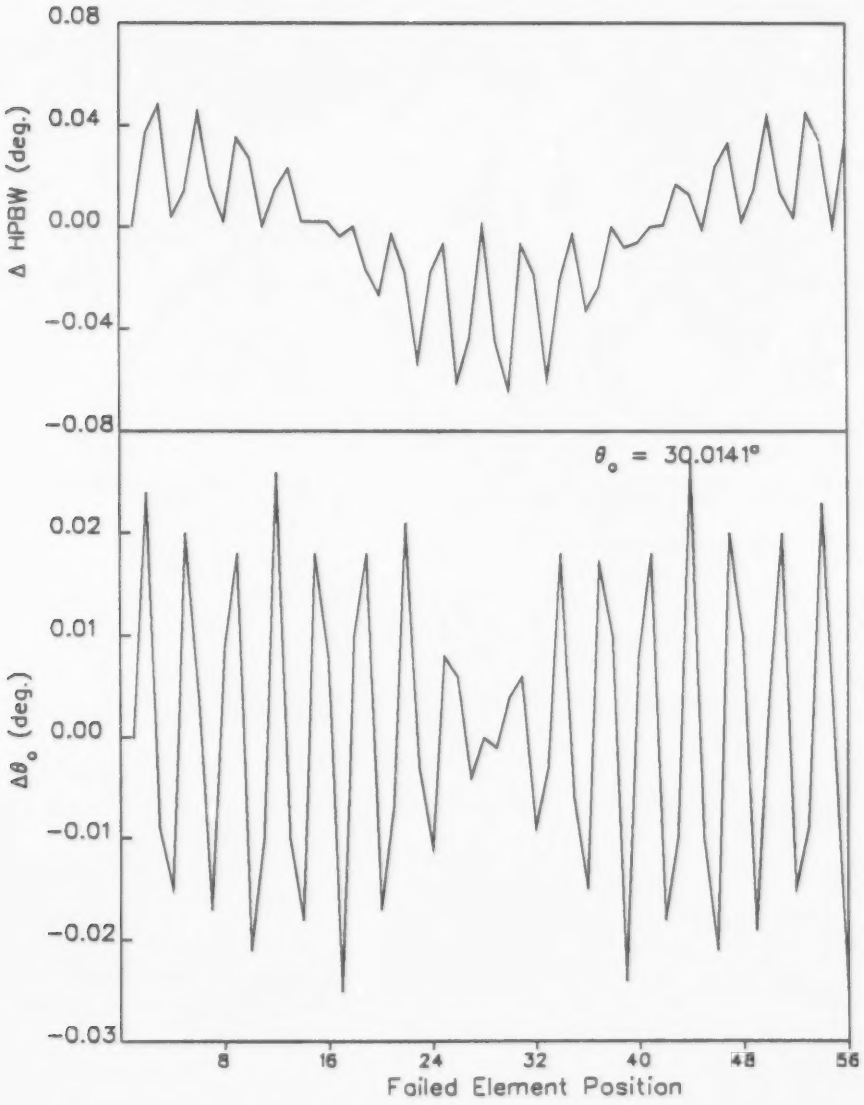

Fig. A.15: Pointing and beam width errors due to a single phase shifter failure at 30.0141 deg. scan angle and for Micronav phase distributions.

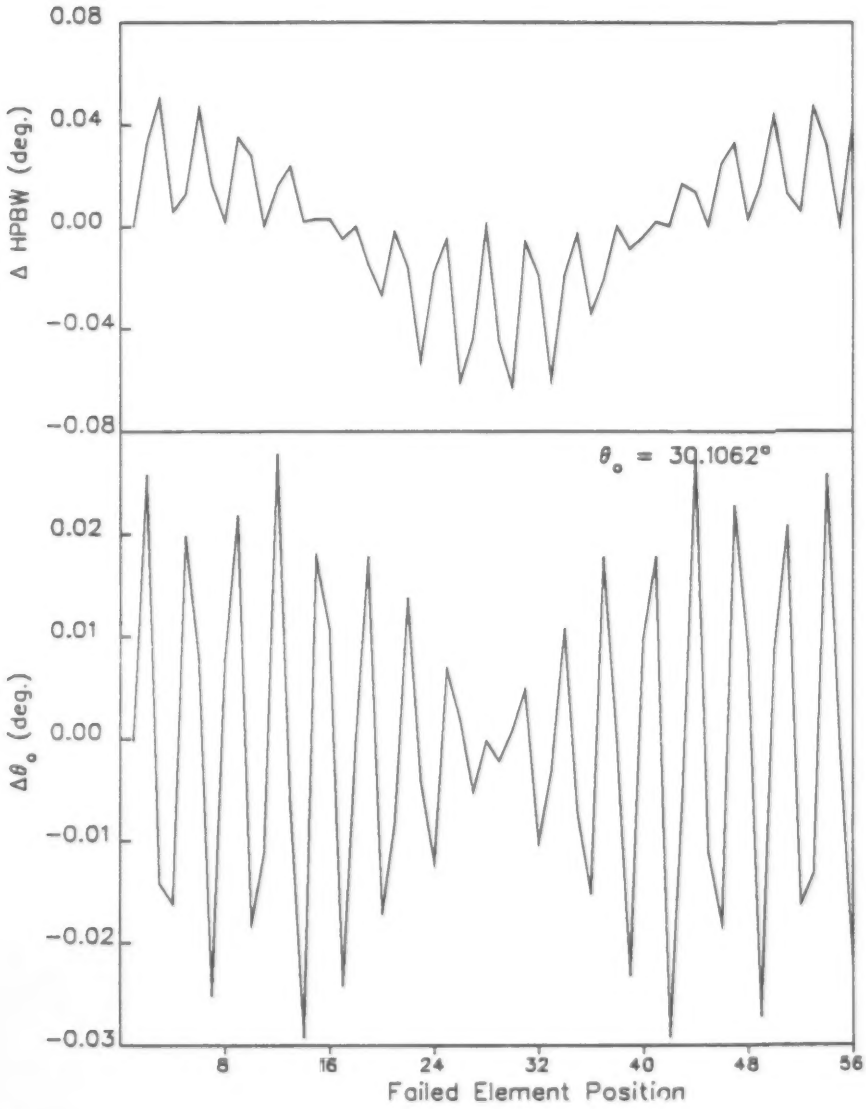

Fig. A.16: Pointing and beam width errors due to a single phase shifter failure at 30.1062 deg. scan angle and for Micronav phase distributions.

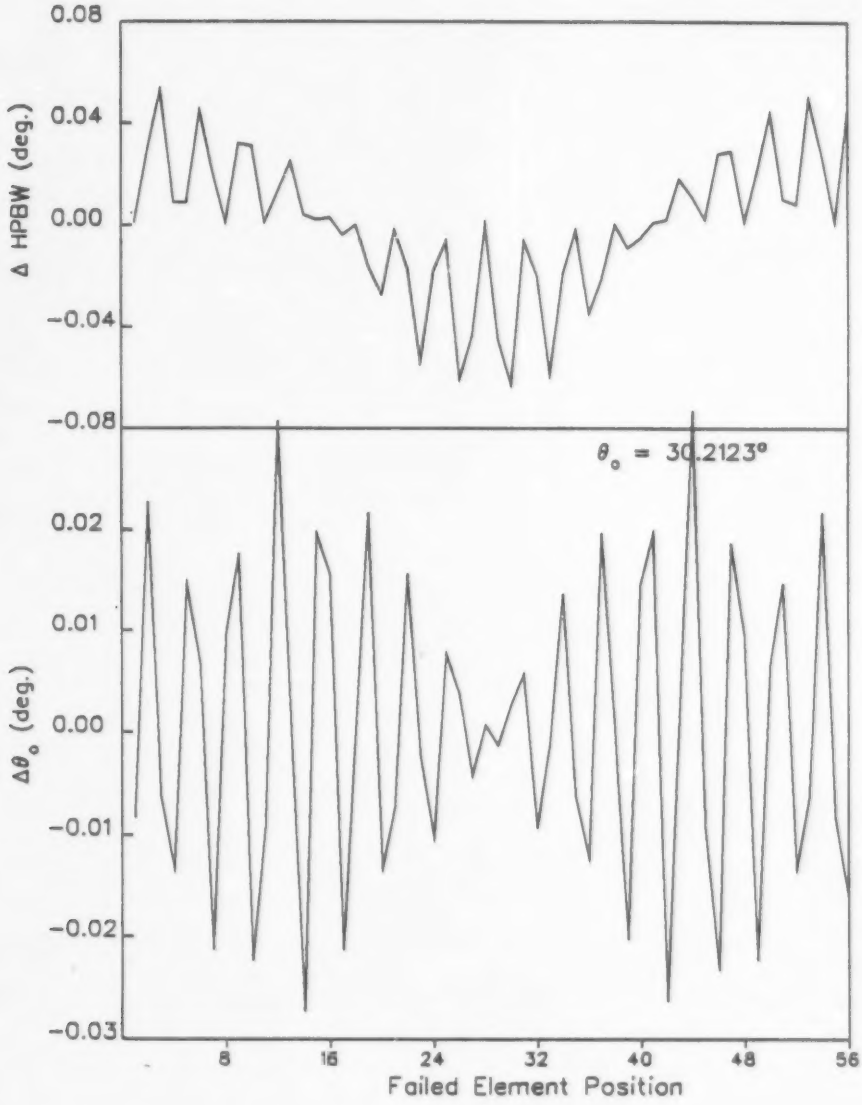

Fig. A.17: Pointing and beam width errors due to a single phase shifter failure at 30.2123 deg. scan angle and for Micronav phase distributions.

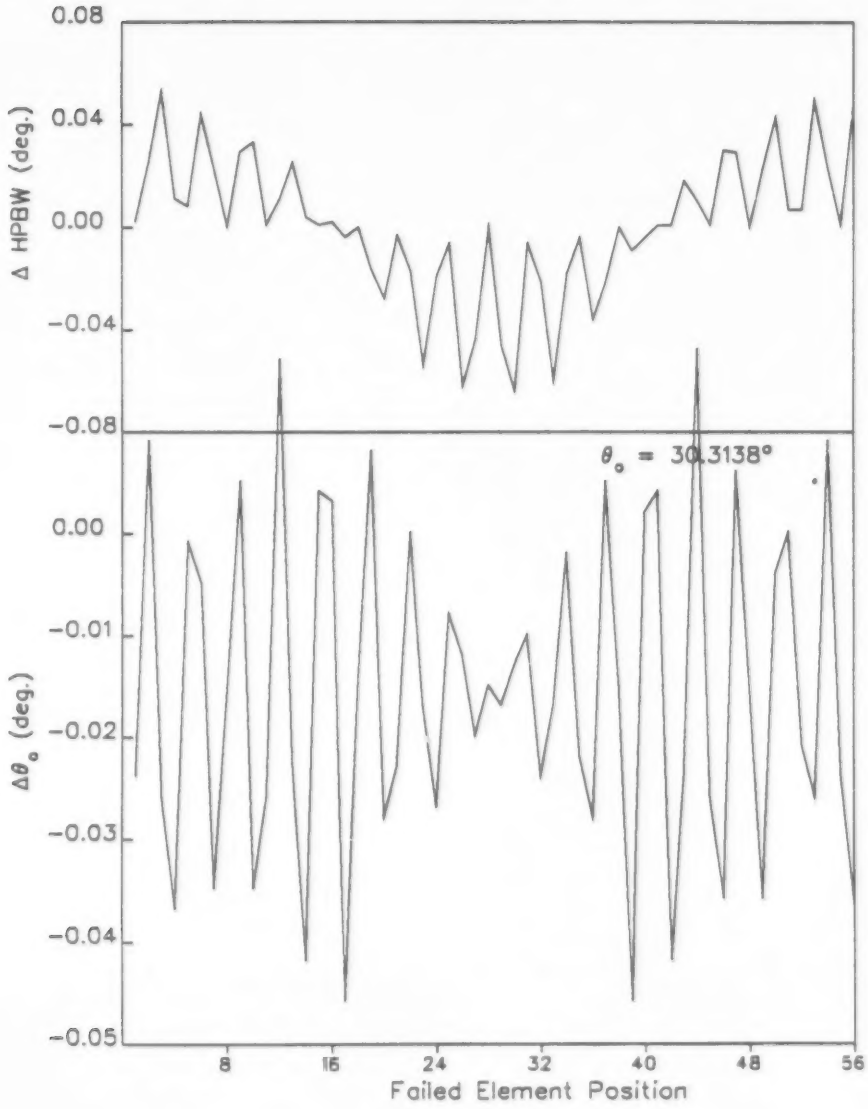

Fig. A.18: Pointing and beam width errors due to a single phase shifter failure at 30.3138 deg. scan angle and for Micronav phase distributions.

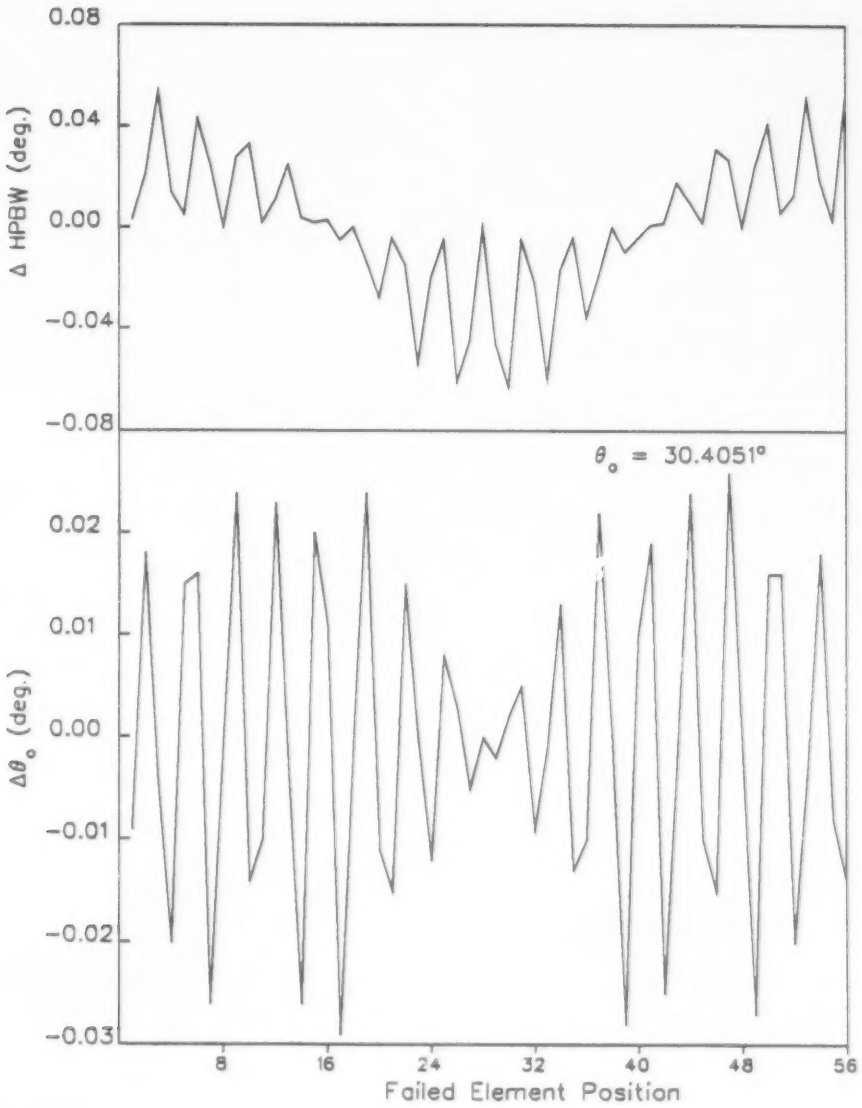

Fig. A.19: Pointing and beam width errors due to a single phase shifter failure at 30.4051 deg. scan angle and for Micronav phase distributions.

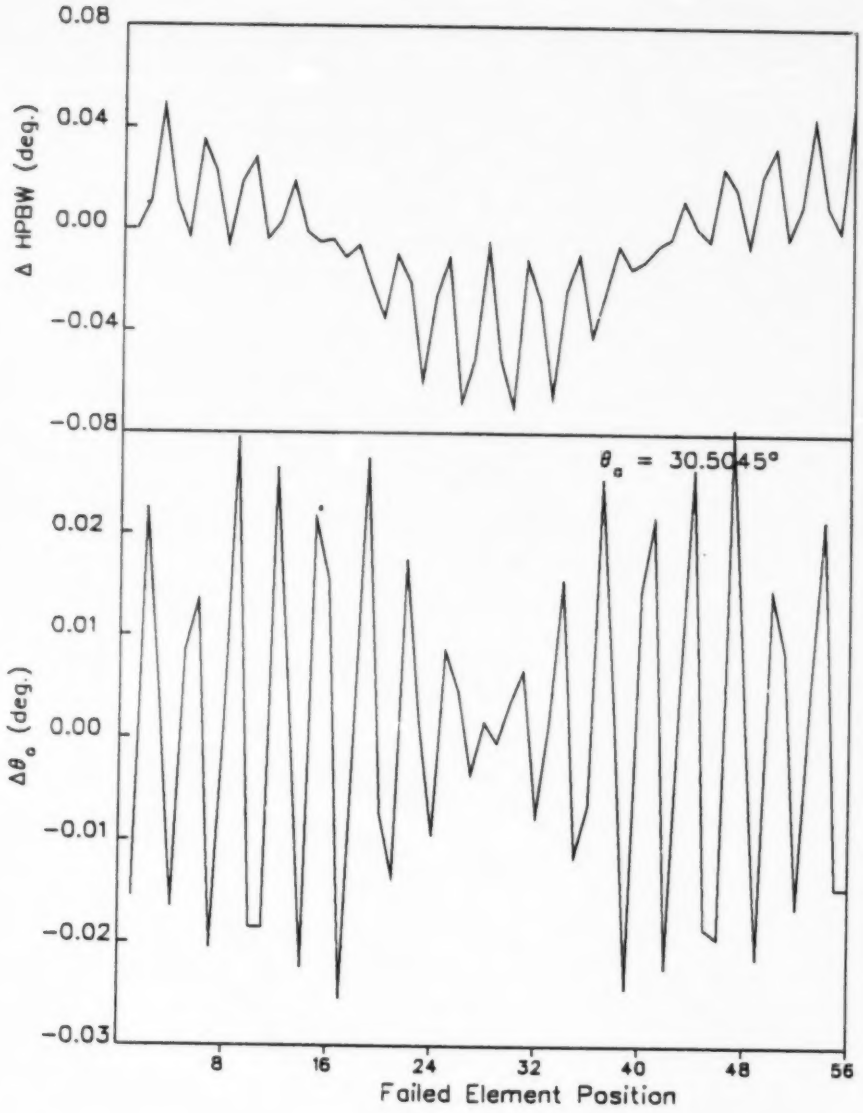

Fig. A.20: Pointing and beam width errors due to a single phase shifter failure at 30.5045 deg. scan angle and for Micronav phase distributions.

Table A.1

θ_o, *deg.*	Δd = 0.1 *mm*	Δd = 0.5 *mm*	Δd = 1.0 *mm*
30.0141	-0.0931	-0.4641	-0.9131
30.10624	-0.09524	-0.46624	-0.91724
30.2123	-0.0943	-0.4673	-0.9193
30.31383	-0.0948	-0.4698	-0.9238
30.40506	-0.0961	-0.4711	-0.9281
30.50446	-0.0945	-0.4715	-0.9295

Table A.1. Pointing errors (deg.) due to a uniform thermal expansion Δd (*mm*) spacing between columns for different scan angle θ_o, using Micronav data.